11-1-2011

# Development of Nano- and Microparticle Technologies for Targeted Gene Silencing through RNA Interference Manipulation of the Immune Response in Inflammatory Lung Disease

Ciara Kelly
*Royal College of Surgeons in Ireland*

# Development of Nano- and Microparticle Technologies for Targeted Gene Silencing through RNA Interference

## Manipulation of the Immune Response in Inflammatory Lung Disease


A thesis submitted to the
National University of Ireland for the
degree of Doctor of Philosophy

By

Ciara Kelly

Under the supervision of Dr. Sally-Ann Cryan
And co-supervised by Dr. Caroline Jefferies
November, 2011

I declare that this thesis, which I submit to RCSI for examination in consideration of the award of a higher degree Doctor of Philosophy, is my own personal effort. Where any of the content presented is the result of input or data from a related collaborative research programme this is duly acknowledged in the text such that it is possible to ascertain how much of the work is my own. I have not already obtained a degree in RCSI or elsewhere on the basis of this work. Furthermore, I took reasonable care to ensure that the work is original, and, to the best of my knowledge, does not breach copyright law, and has not been taken from other sources except where such work has been cited and acknowledged within the text.

Signed Ciara Kelly

Student Number 07209053

**Contents**

**Acknowledgements**

I would like to take this opportunity to thank all of those who have been involved in this project and to acknowledge their valuable contribution in getting me this far. I have been fortunate enough to meet so many wonderful people during my PhD and hopefully have included everybody.

First and foremost I would most like to thank my supervisor Dr. Sally-Ann Cryan for all her guidance, support and patience especially during the stressful times. And my co-supervisor Dr. Caroline Jefferies for all of her help, tissue culture training and immunology expertise. Also I would like to extend my appreciation to Dr. James Barlow for the synthesis of the mannosylated cholesterols and taking the time to explain it all as well as being my representation at CRS 2011. I also greatly appreciate the opportunity given by Dr. Cliff Taggart and Dr. Catherine Greene to work in their labs, in Queen's University Belfast (QUB) and the RCSI Education and Research Centre in Beaumont Hospital. I would also like to acknowledge the funding provided by the Health Research Board (HRB), without which none of this work would have been possible.

I especially want to thank Dr. Rosyln Cassidy (QUB), Dr. Tomás Carroll (Beaumont) and Dr. Joan Ní Gabhann for their excellent training and advice. And the students who have directly contributed to this project, Colin Burke (mannosylated cholesterol synthesis), Katie Nolan (preliminary siRNA microparticle work) and Christina Payne (liposome nebulisation) I greatly appreciate all your hard work. I would also like to thank all my friends and colleagues in RCSI and QUB for their help and just making everyday enjoyable, Neeraj, Sunday, Charlotte, Catherine, Peter, Awadh, Aileen, Claire, Danielle, Jim, Colin, Siobhán, Jen, Rebecca, Kevin, Ritesh, Ben, Cliona, Bernadette and last and certainly not least my two buddies Alan and Ciarán...I don't think I could have done it without you guys! Also, extra thanks to Alan Hibbitts for getting the soft bound thesis to RCSI...after being submitted from Washington DC.

Also my sincerest appreciation to Eimear Mallory for opening her home to me and making my stay in Belfast even more enjoyable. Finally I would like to thank my family and friends. A huge thank you to my parents for their continued support.

**Publications and Presentations**

**Publications** (*Abstract, **Review)

2011 The Effect of Liposome Encapsulation on the Pharmacokinetics of Recombinant Secretory Leukocyte Protease Inhibitor (rSLPI) Therapy after Local Delivery to a Guinea Pig Asthma Model. Gibbons A, Padilla-Carlin D, Kelly C, Hickey AJ, Taggart C, McElvaney NG and Cryan SA. Pharm Res 2011 28 (9) 2233-45

2011 Targeted Liposomal Drug Delivery to Monocytes and Macrophages. Kelly C, Jefferies C, Cryan SA. Journal of Drug Delivery. 2011;2011:727241 **

2011 Cellular Targeting And Trafficking Of Drug Delivery Systems For The Prevention And Treatment of MTb. Lawlor C, Kelly C, O'Leary S, O'Sullivan MP, Gallagher P, Keane J, Cryan SA. Tuberculosis 2011, 91 (1) 93-97**

2010 Development of a high throughput method for screening of novel nanotechnologies for siRNA transfection of airway cells using high content screening (HCS). Hibbitts A, Kelly C, Barlow J, Jefferies C, O'Brien F, Cryan SA. Drug Discovery Today 2010, 15, (23-24) 1107-1108 (CDTM*)

2010 Targeting Z-Alpha-1-antitryspin siRNA to primary macrophages using inhalable particulate technology. Nolan K, Sivadas N, Kelly C, Yadav AB, Carroll T, Thomas W, Greene C, Cryan SA. Irish journal of medical science 2010, 179 S299-S299*

2010 Mannosylated Liposomes for Targeted Delivery of siRNA to Alveolar Macrophages. Kelly C, Jefferies C, Barlow J and Cryan SA. Human Gene Therapy, 2010, 21 (4) (BSGT*)

2009 Respiratory Antivirals - Drugs, Vaccines and Novel Therapies. Cryan, SA, Shoyele, S and Kelly, C. RDD Europe 2009, Vol 1, pp 49-56 **

**Research Presentations** (Poster)

2011 Therapeutic Aerosol Bioengineering for Targeted Delivery of Anti-inflammatory siRNA to the Lungs. Kelly C, Nolan K, Yadav A, Sivadas N, Greene C, McElvaney NG, Jefferies C, Barlow J and Cryan SA
*American Association of Pharmaceutical Scientists (AAPS) Annuai Meeting and Exposition (Washington, DC)*

2011 Development of Mannosylated Liposomes for Targeted Delivery of siRNA to Alveolar Macrophages. Kelly C, McElvaney NG, Jefferies C, Barlow J and Cryan SA.
*The 37th Annual Meeting and Exposition of the Controlled Release Society (National Harbour, Maryland)*

2011 Targeting miRNA-based medicines to Cystic Fibrosis airway epithelial cells using nanotechnology. McKiernan P, Oglesby I, Boland E, Hibbitts A, Kelly C, Greene C, Cryan SA.
*18th Congress of International Society for Aerosols in Medicine (ISAM, Roterdam)*

2011 Nanoaerosols for siRNA Delivery to Alveolar Macrophages. Kelly C, McElvaney NG, Jefferies C, Barlow J and Cryan SA.
*All Ireland Pharmacy Conference, Royal College of Surgeons in Ireland*

2011 Nanoaerosols for siRNA Delivery to Alveolar Macrophages. Kelly C, McElvaney NG, Jefferies C, Barlow J and Cryan SA.
*Royal College of Surgeons in Ireland, Annual Research Day (RCSI)*

2010 Optimised manufacture of inhalable particles for targeted delivery of siRNA to alveolar macrophages. Lawlor C, Sivadas N, Kelly C, Yadav AB and Cryan SA.
*The 37th Annual Meeting and Exposition of the Controlled Release Society (Portland, Oregon)*

2010 Development of a high throughput method for screening of novel nanotechnologies for siRNA transfection of airway cells using high content screening (HCS). Hibbitts A, Kelly C, Barlow J, Jefferies C, O'Brien F, Cryan SA.
*3rd International Symposium "Cellular Delivery of Therapeutic Macromolecules" (CDTM, University of Cardiff)*

2010 Targeting Z-Alpha-1-antitrypsin siRNA to primary macrophages using inhalable particulate technology. Nolan K, Sivadas N, Kelly C, Yadav AB, Carroll T, Thomas W, Greene C and Cryan SA.
*Royal Academy of Medicine in Ireland, Section of Biomedical Sciences Annual Meeting (RCSI)*

2010 Mannosylated Liposomes for Targeted Delivery of siRNA to Alveolar Macrophages. Kelly C, Elias A, Jefferies C, Barlow J and Cryan SA.
*Royal College of Surgeons in Ireland, Annual Research Day (RCSI)*

2010 Mannosylated Liposomes for Targeted Delivery of siRNA to Alveolar Macrophages. Kelly C, Jefferies C, Barlow J and Cryan SA.
*7th Annual British Society for Gene Therapy Conference (BSGT, Royal Holloway, University of London)*

**Summary**

RNA interference (RNAi) allows specific and potent knockdown of target genes and interest now lies beyond its use as a molecular biology tool and in its potential as a therapeutic to mediate gene silencing in diseased cells. Targeted local delivery of small interfering RNA (siRNA) to the lungs via inhalation offers a unique opportunity to treat a range of previously untreatable or poorly controlled respiratory conditions. Alveolar macrophages are the first line of defence against inhaled toxins and pathogens and are essential for the initiation of the inflammatory response. Targeting these cells provides a means of manipulating the immune response of the lungs for the treatment of diseases such as chronic obstructive pulmonary disease (COPD), cystic fibrosis (CF) and asthma. However, macrophages are a difficult cell type to transfect. Consequently a delivery system that will enhance uptake as well as specifically target alveolar macrophages would be beneficial for the treatment of respiratory inflammatory conditions and has received notable attention in recent years. Herein we have developed targeted liposomes and microparticles (MP) suitable for inhalation for optimal siRNA delivery to alveolar macrophages.

Anionic and mannosylated liposomes and uncoated and gelatin coated poly(lactic-*co*-glycolic acid) (PLGA) microparticles targeted macrophages via scavenger receptors (SRs), mannose receptors (MRs) and size and charge related phagocytosis, respectively. Mannosylated cholesterol analogues Mann-C2-Chol, Mann-C4-Chol and Mann-C6-Chol, differing in linker lengths, were synthesised and incorporated into neutral liposomes. Formulations of liposomes and microparticles were optimised for efficient siRNA encapsulation and screened for uptake, toxicity and immunogenicity *in vitro* using high content cell analysis (HCA) methods that were specifically developed. HCA determined uptake of targeted anionic 1,2-dioleoyl-*sn*-glycero-3-phospho-L-serine (DOPS) and mannosylated (Mann-C6-Chol) composed liposomes between 200 and 400nm and uncoated PLGA microparticles to be optimal in macrophage cells.

Significant knockdown of tumour necrosis factor-alpha (TNFα) in lipopolysaccharide (LPS) stimulated cells was mediated via DOPS liposomes and uncoated PLGA microparticles. Additionally, mannosylated liposomes appeared to activate macrophage mannose receptors in a concentration and linker dependent manner and reduce inflammation. In general liposomes and microparticles were non-toxic and non-immunogenic compared to positive controls. However exceptions included high doses of DOPS liposomes which significantly reduced cell viability in RAW 264.7 cells, significantly increased nuclear factor kappa B (NFκB) activity and induced pro-inflammatory cytokines in differentiated THP-1 cells after 24 hours. However, mannosylated liposomes induced a potent inflammatory response *in vivo* but effects were localised to the lungs. *in vivo* reductions of TNFα in bronchoalveolar lavage fluid (BALF) following LPS challenge were observed in mice treated with TNFα targeted naked siRNA and encapsulated in mannosylated liposomes.

## Abbreviations

| | |
|---|---|
| 2'OMe | 2'-O-Methyl |
| AAV | adeno-associated virus |
| Ad5 | serotype 5 adenovirus |
| Ago2 | argonaute-2 |
| aiRNA | asymmetric interferring RNA |
| ALI | acute lung injury |
| Amp | ampicilin |
| ANOVA | analysis of variance |
| AP | ammonium persulfate |
| AP-1 | activator protein 1 |
| APC | antigen presenting cell |
| ARD | acute respiratory distress syndrome |
| AVP | artificial virus-like particles |
| β-AR | β-adrenergic receptor |
| BAL | bronchoalveolar lavage |
| BALF | bronchoalveolar lavage fluid |
| BCA | bicinchoninic acid |
| bm-RNAi | bacteria mediated RNA interference |
| bp | base pairs |
| BSA | bovine serum albumin |
| CD | cluster of differentiation |
| $CDCl_3$ | deuterised chloroform (chloroform-d) |
| cDNA | complementary DNA |
| CF | cystic fibrosis |
| CFTR | cystic fibrosis transmembrane conductance regulator |
| CHEMS | cholesteryl hemisuccinate |
| Choi | cholesterol |
| CINC-1 | cytokine-induced neutrophil chemoattractant-1 |
| CLSM | confocal laser scanning microscopy |
| $CO_2$ | carbon dioxide |
| COPD | chronic obstructive pulmonary disease |
| CPFX | ciprofloxacin |
| CR | cysteine rich |
| CTAB | cetyltrimethylammonium |
| CTLD | C-type lectin-like domains |
| d | doublet |
| DAOS | N-ethyl-N-(2-hydroxy-3-sulfopropyl)-3,5-domethoxyaniline |
| DAP | 1,2-diarachidonoyl-sn-glycero-3-phosphate |
| DCM | dichloromethane |
| DCP | dicetylphosphate |
| dd | doublet of doublets |
| DDAB | dimethyldioctadecylammonium |
| DEPC | diethylpyrocarbonate |
| Dex | dexamethasone |
| dH2O | deionised water |
| DMEM | dulbecco's modified eagle medium |
| DMPG | 1,2-dimyristoyl-sn-glycero-3-phospho-(1'-rac-glycerol) |
| DNA | deoxyribonucleic acid |
| DOPA | 1,2-dioleoyl-sn-glycero-3-phosphate |
| DOPC | 1,2-dioleoyl-sn-glycero-3-phosphocholine |
| DOPE | 1,2-dioleoyl-sn-glycero-3-phosphoethanolamine |
| DOPS | 1,2-dioleoyl-sn-glycero-3-phospho-L-serine |
| DOTAP | 1,2-Dioleoyl-3-trimethylammonium-propane |
| DOTMA | 1,2-Dioleoyl-3-trimethylammonium-propane |
| DPI | dry powder inhaler |
| DPPE | 1,2-dipalmitoyl-sn-glycero-3-phosphoethanolamine |
| DSPC | 1,2-distearoyl-sn-glycero-3-phosphocholine |
| dsRNA | double stranded RNA |
| DTT | Dithiothreitol |
| *E.coli* | *Escherichia coli* |
| EDTA | ethylenediaminetetraacetic acid |

| | |
|---|---|
| EE% | encapsulation efficiency |
| eGFP | enhanced green fluorescent protein |
| ELISA | enzyme-linked immunosorbant assay |
| EO | ethyleneoxy |
| EPC | egg phosphatidylcholine |
| exp5 | exportin 5 |
| FBS | foetal bovine serum |
| FDA | Food and Drug Administration |
| FITC | fluorescein isothiocyanate |
| fl-siRNA | fluorescein tagged siRNA |
| FN II | fibronectin type II |
| GAPDH | Glyceraldehyde 3-phosphate dehydrogenase |
| HBr | hydrogen bromide |
| HCA | high content cell analysis |
| HCl | hyrdrochloride |
| HEPES | 4-(2-hydroxyethyl)-1-piperazineethanesulfonic acid |
| HFDM | hydration of freeze-dried matrix |
| HFA | hydrofluoroalkane |
| HIF-1α | hypoxia inducible factor 1 alpha |
| HIV | human immunodeficiency virus |
| HRMS | high resolution mass spectroscopy |
| HRP | horseradish peroxidase |
| HSPC | hydrogenated soybean phosphotidyl choline |
| IFNy | interferon-gamma |
| IκB | Inhibitor of κB kinase |
| IL | interleukin |
| IP | intraperitoneal |
| IR | infrared |
| IRF3 | interferon Regulatory Protein 3 |
| KBr | postassium bromide |
| KC | keratinocyte-derived chemokine |
| LB | lysogeny broth |
| LDE | laser doppler electrophoresis |
| LOD | limits of detection |
| LPS | lipopolysaccharide |
| MAPK | mitogen activated protein kinase |
| MBSA | maleylated bovine serum albumin |
| MC2C (Mann-C2-Chol) | cholesten-5-yloxy-N-(2-((1-imino-2-α-thioglycosylethyl)amino) butyl)formamide |
| MC4C (Mann-C4-Chol) | cholesten-5-yloxy-N-(4-((1-imino-2-α-thioglycosylethyl)amino) butyl)formamide |
| MC6C (Mann-C6-Chol) | cholesten-5-yloxy-N-(6-((1-imino-2-α-thioglycosylethyl)amino) butyl)formamide |
| MCP-1 | monocyte chemotactic protein-1 |
| MHC | major histocompatibility complex |
| MIP-2 | macrophage inflammatory protein-2 |
| miRNA | microRNA |
| MLV | multi-lamellar vesicles |
| MMAD | mass median aerodynamic diameter |
| MMP | mitochondrial membrane potential |
| MMP-9 | matrix metallopeptidase 9 |
| MoMLV | Moloney murine leuckemia virus |
| MP | microparticle |
| MPO | myeloperoxidase |
| MPS | mononuclear phagocytic system |
| MR | mannose receptor |
| MS | mass spectrometry |
| MTP | muramyl tripeptide |
| N/P ratio | nitrogen/phosphate ratio |
| NaCl | sodium chloride |
| $NaHCO_3$ | sodium bicarbonate |
| NFκB | nuclear factor kappa B |
| NK | natural killer |

| | |
|---|---|
| NLC | nano-structure lipid carrier |
| NMR | nuclear magnetic resonance |
| NSAID | non-steroidal anti-inflammatory drug |
| NT | non-target |
| $O_2$ | oxygen |
| Oac | Acetoxy group |
| ODN | oligodeoxynucleotide |
| OEI-HD | hexanediol diacrylate cross-linked oligoethylenimine |
| O-SAP | O-steroly amplyopectin |
| PAZ | piwi-argonaute-zwille |
| PBS | phosphate buffered saline |
| PBST | phosphate buffered saline tween |
| PC | phosphatidylcholine |
| PDI | polydispersity index |
| PDMAEMA | poly(dimethylaminoethylmethacrylate) |
| pDNA | plasmid DNA |
| PE | phosphatidylethanolamine |
| PEG | polyethylene glycol |
| PEI | poly(ethyleneimine) |
| PE-Rhodamine | 1,2-dioleoyl-sn-glycero-3-phosphoethanolamine-N-(lissamine rhodamine B sulfonyl) |
| PG | phosphatidylglycerol |
| piRNA | piwi-interacting RNA |
| PIV | parainfluenza virus |
| PKC | protein kinase C |
| PKR | protein kinase R |
| PLGA | poly(lactic-co-glycolic acid) |
| PLL | poly-L-lysine |
| PMA | phorbol 12-myristate 13-acetate |
| pMDI | pressured meter dose inhaler |
| poi | polymerase |
| POPC | 1-palmitoyl-2-oleoyl-sn-glycero-3-phosphocholine |
| POPG | 1-palmitoyl-2-oleoyl-sn-glycero-3-phospho-(1'-rac-glycerol) |
| pre-miRNA | precursor miRNA |
| PS | phosphatidylserine |
| PTA | phosphotunstic acid |
| PTMAEMA | poly(trimethylaminoethyl-methacrylate) |
| PVA | poly vinyl alcohol |
| q | quartet |
| qRT-PCR | quantitative reverse transcriptase polymerase chain reaction |
| R8 | octa-arginine |
| RDS | respiratory distress syndrome |
| RGD | Arg-Gly-Asp |
| RIP-1 | receptor interacting protein-1 |
| RISC | RNA induced silencing complex |
| RNA | Ribonucleic acid |
| RNAi | RNA Interference |
| ROS | reactive oxygen species |
| rSLPI | recombinant secretory leukocyte protease inhibitor |
| RSV | Respiratory syncytial virus |
| s | singlet |
| SA | stearylamine |
| SD | standard deviation |
| SDS | sodium dodecyl sulfate |
| SEAP | secreted embryonic alkaline phosphatase |
| SEM | scanning electron microscopy |
| siRNA | small interfering RNA |
| sisiRNA | small internally segmented interferring RNA |
| SLE | systemic Lupus Erythematosus |
| SLN | solid lipid nanoparticles |
| SLPI | secretory leukocyte protease inhibitor |
| SM | sphingomyelin |
| SODD | silence of death domains |

| | |
|---|---|
| SPARC | secreted protein acidic and rich in cysteine |
| SR | scavenger receptor |
| STAT3 | Signal transducer and activator of transcription 3 |
| STREP-HRP | streptavidin-horseradish peroxidase |
| STR-R8 | stearylated octa-arginine |
| TAC | tetrameric antibody complexes |
| TACE | TNFα-converting enzyme |
| TAE | tris-acetate-EDTA |
| TBE | tris borate EDTA |
| *t*-Butanol | tertiary butanol |
| TE | tris-EDTA |
| TEM | transmission electron microscopy |
| TEMED | N,N,N',N'-Tetramethylethylenediamine |
| TGF-β1 | transforming growth factor beta-1 |
| tk-RNAi | transkingdom RNA interference |
| TLR | toll-like receptor |
| TNFα | tumour necrosis factor-alpha |
| TNFR | TNFα receptor |
| TRADD | TNF receptor-associated death domain |
| TRAF2 | TNFR-associated factor 2 |
| TRIM | tripartite motif-containing |
| TRITC | tetramethyl rhodamine isothiocyanate |
| TSI | twin stage impinger |
| UV | unilamellar vesicles |
| VCAM-1 | Vascular cell adhesion protein 1 |
| VEGF | vascular endothelial growth factor |
| W/o/w | water-oil-water |

# Chapter 1

# General Introduction

## 1.1 Introduction

Inhalation therapy has a long history stretching back thousands of years. Treatments for respiratory diseases such as asthma delivering drugs directly to the lungs via inhalation have been routinely used for decades. Systemic delivery of therapeutics via the lungs such as insulin has also achieved some success. However many conditions remain untreatable or difficult to treat such as inflammatory lung diseases. Gene therapy began with the development of recombinant DNA technology [1] and over the past few decades has been an area of intense research. This form of therapy sets out to insert genetic material into tissue with wide ranging applications including vaccination, gene replacement and gene silencing to treat numerous conditions such as genetic disorders, cancers and viral infections. In recent years the discovery of RNA interference (RNAi) has lead to a surge in interest into the use of small interfering RNA (siRNA) to mediate gene silencing. Above all, this could prove a useful therapeutic approach for previously difficult to treat conditions such as respiratory conditions including chronic obstructive pulmonary disease (COPD) and cystic fibrosis (CF).

## 1.2 Lung Anatomy and Physiology

The respiratory system can be divided into the upper and lower respiratory systems anatomically consisting of the nose, nasal cavity, paranasal sinuses and pharynx and larynx, trachea, bronchi, bronchioles and alveoli of the lungs, respectively [2] (Figure 1.1A). The complex architecture and interplay of specialised airway cells constitute the functional respiratory system which carries out a number of dedicated functions such as gaseous exchange at the alveolar level between the air and vascular system, the movement of air to and from the alveoli and the protection of pulmonary tissue against airborne pathogens and foreign particulates.

Air enters through the nose and mouth and continues through the conducting section of the respiratory system where it is filtered, warmed and humidified, through the trachea, bronchi, bronchioles and finally reaching the respiratory section, the alveoli, where gas exchange occurs [2] (Figure 1.1A and B). Morphometry of the human lung was first described in the Weibel Model [3] in the 1960s in which dichotomous branching of the airways were termed as generations initiating at generation 0, the trachea and terminating at generation 23, the alveoli (Figure 1.1C). Pulmonary branching is extensive and with each generation the airway dimensions narrow and particle deposition in these regions will occur either due to impaction, sedimentation or Brownian diffusion with decreasing channel diameter [4, 5].

The trachea branches to form the two primary bronchi which supply air to the right and left lung. Both the trachea and bronchi are supported with cartilaginous C-shaped rings [2]. From there the bronchi divide repeatedly to give rise to the bronchial tree of primary, secondary and tertiary bronchi. The amount of cartilage present in the bronchial walls decreases with subsequent branching and the relative amount of smooth muscle increases. Consequently smooth muscle

begins to play a more influential role in airway diameter and resistance to airflow. Further branching of tertiary bronchi leads to the formation of bronchioles, the walls of which no longer contain cartilage but are instead predominantly smooth muscle [2]. Bronchoconstriction of these airways leads to reduced airflow which can occur in allergic reactions and asthma. Alveolar ducts connect the bronchioles to alveolar sacs. Each alveolus is surrounded by an extensive network of capillaries and the basement membranes between the alveolar and endothelial capillary cells are fused to promote efficient gas exchange of oxygen ($O_2$) and carbon dioxide ($CO_2$) (Figure 1.3). During inflammation however the diffusion distance is increased and gas exchange is negatively affected [2].

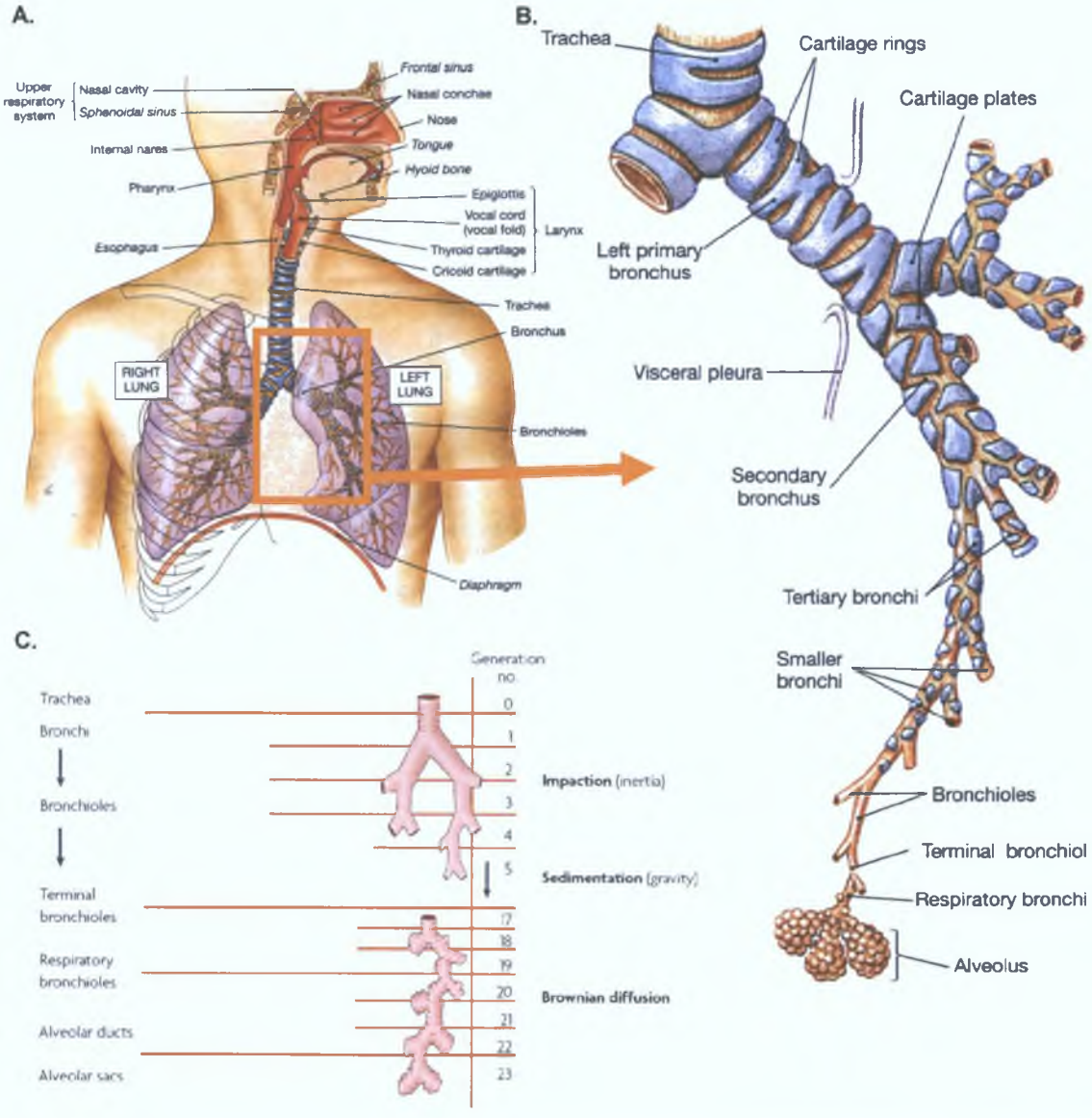


Figure 1.1: Illustration of (A) the anatomical structure and components of the respiratory system, (B) representation of bronchial branching and (C) the Weibel model of lung morphology showing generations 1 - 23 and corresponding particle sedimentation mechanisms (taken from [2] and [4])

The airway epithelium structure relates closely to function and varies in diameter and cell composition along the pulmonary system (Figure 1.2B). For instance the nasal cavity and bronchial epithelium is pseudostratified, ciliated and columnar containing secretory cells (such

as clara, goblet and serous cells), ciliated cells and brush cells [4, 6]. The respiratory epithelium is also supported by connective tissue known as the lamina propria which also varies depending on the respiratory region. Mucus glands are present in the lamina propria of the trachea and bronchi which secrete mucus onto the epithelium surface and can be increased in volume and consistency in certain diseases such as CF and COPD. This is also the location of smooth muscle for the conducting airways.

Aside from air conductance and gas exchange a major function of the pulmonary system is defensive. Secretory cells release mucins and molecules that are antimicrobrial, immunomodulatory and protective in nature such as lysozymes, cytokines and heregulin respectively [6]. By a process referred to as the mucocillary escalator, mucus and any insoluble particles deposited in the airways are propelled out of the lung towards the pharynx by ciliary beating at a velocity of 1mm per minute (fast phase removal, Figure 1.2A) [2, 4, 6]. Although particles deposited in the deep lung, non-ciliated regions, can remain for up to 24 hours (slow phase removal) [7] and are more likely cleared by macrophages [4].

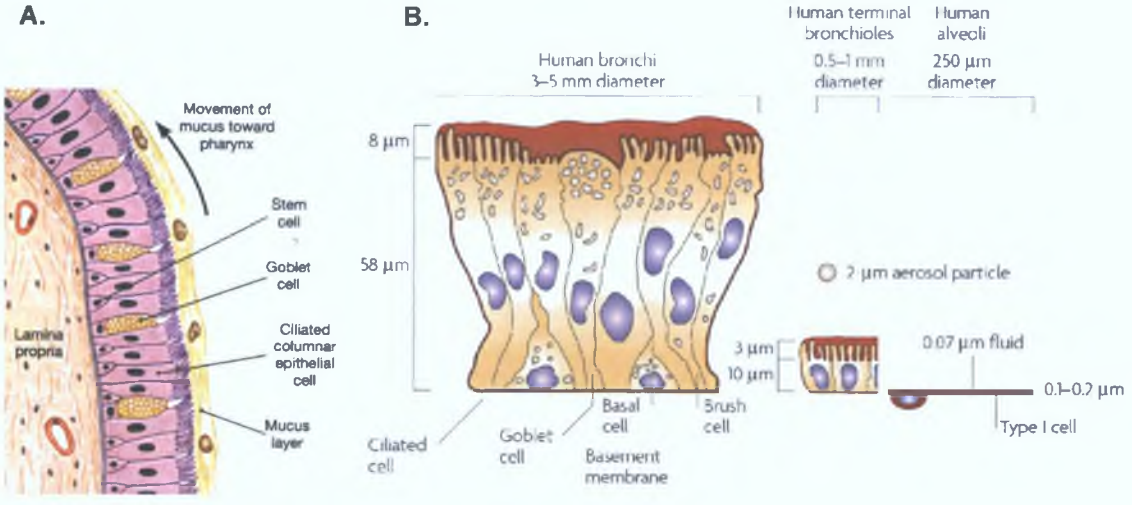


Figure 1.2: Structure of the human pulmonary epithelium. (A) shows the mucocilliary escalator action of the large airways and (B) the structure and relative sizes of the bronchial, brionchiole and alveolar epithelia (taken from [2] and [4]).

The epithelium of the alveolus is very different form the rest of the airways, no longer consisting of pseudostratified columnar cells but instead of a thin squamous monolayered epithelium consisting of alveolar Type I cells (Figure 1.2B and 1.3) covered in lung surfactant that is produced by alveolar Type II cells (Figure 1.3). Surfactant contains phospholipids and proteins which is important in reducing surface tension thereby preventing alveolar collapse [2]. There are approximately 5 x $10^8$ alveoli in the human lung, each of which is patrolled by 12 to 14 alveolar macrophages [4] in the interstitium which phagocytose particles that have evaded the preceding defence mechanisms.

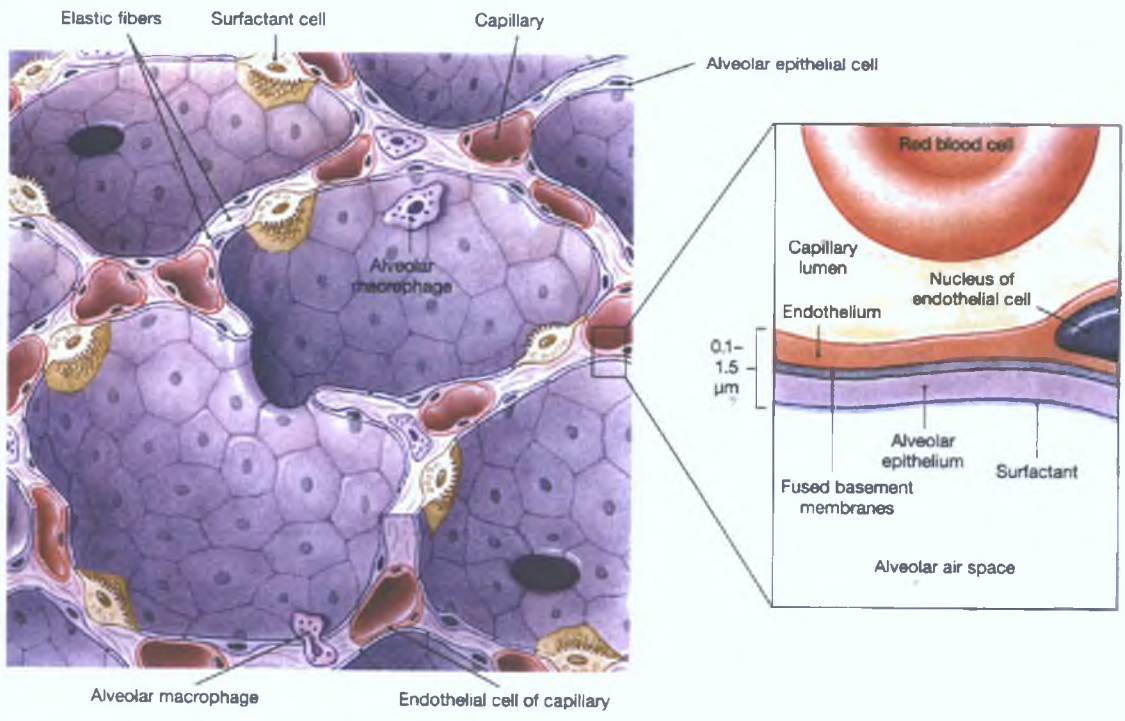


Figure 1.3: The structure of the alveoli consisting of a thin eptithelial monolayer of Type I cells, Type II surfactant cells and patrolling alveolar macrophages. The distance between the alveolar epithelium and capillary endothelia is very small promoting efficient gas exchange [2].

### 1.3 Drug Delivery to the Lungs

The anatomy and physiology of the lungs are designed for the efficient removal of inhaled particulates and consequently pulmonary drug delivery can be challenging. Apart from mucociliary clearance the action of delivered drugs can be impeded by the protective lung barriers including airway epithelium, alveolar epithelial tight junctions, surfactant, macrophages and enzymatic action [8]. In addition cilia, mucus and the complex architecture of the respiratory tree filters particles from inhaled air before they can even reach sites of action such as the alveoli. In order to effectively deliver aerosol therapeutics to the respirable regions of the lungs a number of interdependent factors must be taken into account including aerosol/particle characteristics such as size, size distribution, charge, shape, density and hygroscopicity, patient factors such as inspiratory flow rate, age or disease state and inhaler devices [9, 10]. Therefore targeting specific lung regions requires optimised particle/aerosol properties and modes of inhalation [10]. The fate of inhaled particles depends on many factors and can include removal by mucocilliary clearance, phagocytosis by macrophages or gaining access to the pulmonary epithelium and being locally or systemically absorbed [7].

Size has a critical effect on particle deposition in the lungs which can occur via various mechanisms including inertial impaction, sedimentation, diffusion, interception and electrostatic precipitation [9] (Figure 1.4). Large particles (>5µm) travelling at high velocity will generally impact in the upper airways where airflow direction changes rapidly. This is due to inertial impaction whereby aerosolised particles gain enough momentum to maintain their trajectory

rather than follow the path of airflow and collide with airway structures [7, 9]. Deposition of particles >10μm generally occurs in the oropharyngeal region. Sedimentation is the settling of particles in lungs due to gravity. It requires the slowing down of air velocity and usually occurs in the bronchioles and alveoli with particles <3μm in diameter. Aerosolised small particles <1μm undergo Brownian motion and tend to be deposited by diffusion but are more likely to be exhaled [9]. Slow deep inspiration followed by a breath hold may promote submicron particle diffusion [11]. Therefore, deep lung deposition is optimal in the 1 – 5μm size range [7]. Suspensions of hydrophobic drugs or nanoparticles can also be delivered by inhalation and deposition relies on aerosol droplet size rather than particle size (or aerodynamic size which also accounts for particle density) and can offer many advantages over dry powder inhalation such as higher bioavailability, increased lung retention, faster dissolution rates and better particulate homogeneity [11].

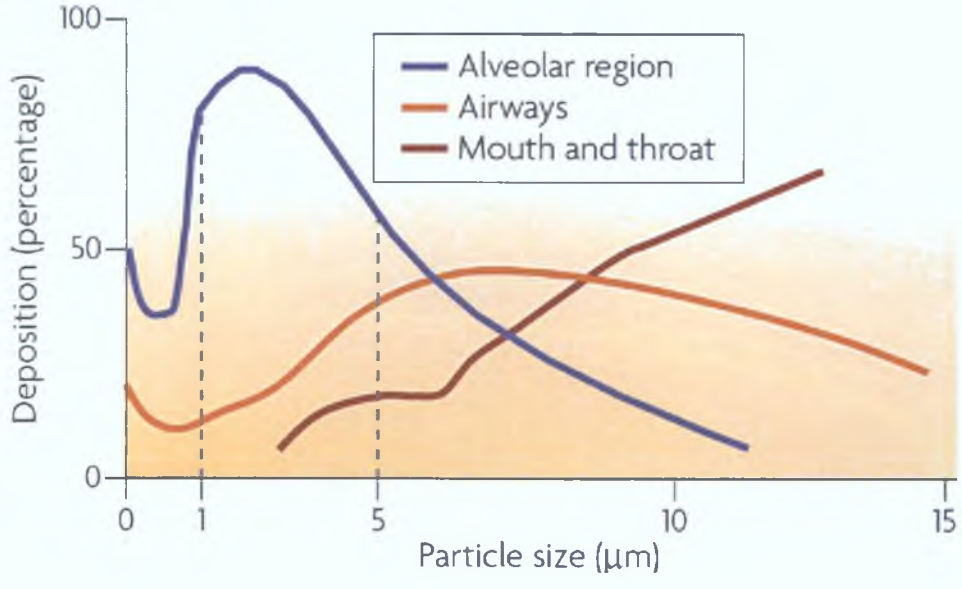


Figure 1.4: Deposition patterns of aerosolized monodisperse particles in the lungs related to particle size following a slow inhalation and short breath hold. Small particles (<1μm) can be exhaled, particles ranging from 1 – 5 μm can reach the alveolar region and large particles (>5μm) impact the mouth, throat and upper airways [4].

**1.4 Inflammatory Lung Diseases and Current Therapies**

Diseases associated with airway inflammation include COPD, asthma and CF [12-14], which involve a huge array of immune cells including mast cells, neutrophils, macrophages, eosinophils as well as epithelial cells [15-18]. The inflammatory process is a key driver of both disease progression as well as pathogenesis [19]. Features of these diseases include chronic inflammation, smooth muscle hyper-responsiveness and airway remodelling resulting in reduced airflow and lung function (Figure 1.5) [2, 20]. Pro-inflammatory cytokines such as TNFα and interleukin 1-beta (IL-1β) can lead to mucin production either indirectly or directly [6] and consequently chronic inflammation in the lung can lead to hypersecretion of mucus and is also associated with pulmonary lesions. Under normal healthy conditions mucus contains about

3% solids but hypersecretion can increase solid content up to 15% making the mucus more elastic and viscous [6]. Dehydrated viscous mucus is more difficult to clear from the lungs and is more adherent to the airway walls [6]. Characteristics of mucus vary between pulmonary diseases and can contain increased levels of mucin, plasma proteins, inflammatory cells, DNA and bacteria compared to the healthy state [6]. Mucus clearance is further hindered in CF due to mucocillary clearance dysfunction.

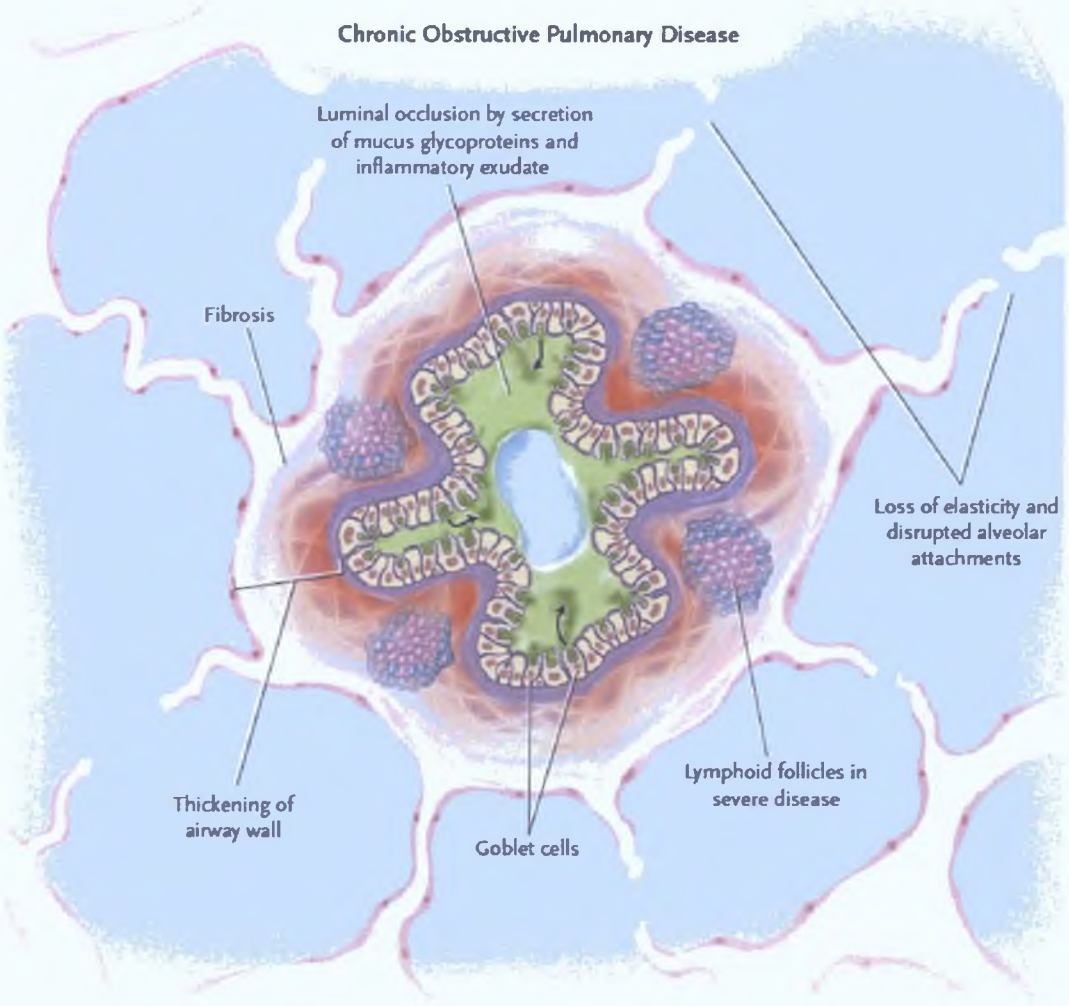


Figure 1.5 Characteristics of a Chronic Obstructive Pulmonary Disease (COPD) small airway obstruction [19, 21]

COPD is the fifth leading cause of death worldwide with a prevalence of 9 – 10% in adults over 40 years of age [22]. Drug development costs for COPD are high [22]. The Global Initiative for Chronic Obstructive Lung Disease (GOLD) defined COPD as "a preventable and treatable disease with some significant extrapulmonary effects that may contribute to the severity in individual patients. Its pulmonary component is characterized by airflow limitation that is not fully reversible. The airflow limitation is usually progressive and associated with an abnormal inflammatory response of the lung to noxious particles or gases" [23]. Risk factors associated with the disease include a genetic predisposition, exposure to inhaled noxious stimuli such as cigarette smoke (Figure 1.7), socioeconomic status, infection and gender [23]. COPD disease pathological changes include fibrosis and airway narrowing in the bronchi as well as fibrosis and

damage to the alveolar walls (emphysema) [19, 22] (Figure 1.5). Airway remodelling can occur due to repeated injury and repair [23]. COPD patients experience dyspnoea, cough, exercise intolerance and a lower quality of life in terms of health [22]. The roles of current therapeutic strategies are to prevent and control disease symptoms, decrease both the frequency and severity of exacerbations and improve quality of health but do not improve long term impaired lung function [23] and most commonly include inhaled bronchodilators and glucocorticosteroids (Table 1.1).

**Table 1.1: Common Medications for Chronic Obstructive Pulmonary Disease [23]**

| Medication | Inhaler (μg) | Solution for Nebulizer (mg/ml) | Oral | Vials for Injection (mg) | Duration of Action (h) |
|---|---|---|---|---|---|
| $\beta_2$-Agonists | | | | | |
| Short-acting | | | | | |
| Fenoterol | 100–200 (MDI) | 1 | 0.5% (syrup) | | 4–6 |
| Salbutamol (albuterol) | 100, 200 (MDI and DPI) | 5 | 5 mg (pill) 0.24% (syrup) | 0.1, 0.5 | 4–6 |
| Terbutaline | 400, 500 (DPI) | | | 0.2, 0.25 | 4–6 |
| Long-acting | | | | | |
| Formoterol | 4.5–12 (MDI and DPI) | | | | 12+ |
| Salmeterol | 25–50 (MDI and DPI) | | | | 12+ |
| Anticholinergics | | | | | |
| Short-acting | | | | | |
| Ipatropium bromide | 20, 40 (MDI) | 0.25–0.5 | | | 6–8 |
| Oxitropium bromide | 100 (MDI) | 1.5 | | | 7–9 |
| Long-acting | | | | | |
| Tiotropium | 18 (DPI) | | | | 24+ |
| Combination short-acting $\beta_2$-agonists plus anticholinergic in one inhaler | | | | | |
| Fenoterol/ipratropium | 200/80 (MDI) | 1.25/0.5 | | | 6–8 |
| Salbutamol/ipratropium | 75/15 (MDI) | 0.75/4.5 | | | 6–8 |
| Methylxanthines | | | | | |
| Aminophylline | | | 200–600 mg (pill) | 240 | Variable, up to 24 |
| Theophylline (SR) | | | 100–600 mg (pill) | | Variable, up to 24 |
| Inhaled glucocorticosteroids | | | | | |
| Beclomethasone | 50–400 (MDI and DPI) | 0.2–0.4 | | | |
| Budesonide | 100, 200, 400 (DPI) | 0.20, 0.25, 0.5 | | | |
| Fluticasone | 50–500 (MDI and DPI) | | | | |
| Triamcinolone | 100 (MDI) | 40 | | 40 | |
| Combination long-acting $\beta_2$-agonists plus glucocorticosteroids in one inhaler | | | | | |
| Formoterol/budesonide | 4.5/160, 9/320 (DPI) | | | | |
| Salmeterol/fluticasone | 50/100, 250, 500 (DPI) 25/50, 125, 250 (MDI) | | | | |
| Systemic glucocorticosteroids | | | | | |
| Prednisone | | | 5–60 mg (pill) | | |
| Methylprednisolone | | | 4, 8, 16 mg (pill) | | |

*Definition of abbreviation:* DPI = dry powder inhaler; MDI = metered-dose inhaler; SR = slow release.

Ireland has the highest incidence of CF in the world at 1 in 1353 [24]. CF is a genetic disease caused by mutations in a 175kD glycoprotein the cystic fibrosis transmembrane conductance regulator (CFTR) and mostly affects epithelial cells especially in exocrine glands [13]. The disease is associated with pancreatic insufficiency, high levels of sodium chloride in the sweat and COPD, the later being the main cause of morbidity and mortality [13]. The CF lung is associated with airway obstruction and maintains chronic bacterial infections and inflammation. Infections are usually caused by a number of bacteria including *S.aureus*, *H. influenzae*, and *P. aeruginosa* [13], hence antibiotics are an important part of CF therapy. Changes in the airway epithelium also occur including cilia loss and squamous metaplasia [13]. Aside from antibiotics, an anti-inflammatory approach to CF therapy has been the main focus to date via systemic and inhaled corticosteroids and non-steroidal anti-inflammatory drugs (NSAID) [13] such as ibuprofen. However, effects in terms of lung function improvement or reduction in inflammatory markers in the lungs have not been very successful using inhaled corticosteroids [13]. NSAIDs

on the other hand have shown positive results in CF patients but there are concerns over complications associated with NSAID therapy [13] such as venous thrombosis, pulmonary embolism, renal dysfunction, hypertension and damage to the gastrointestinal mucosa [25].

It is estimated that there are 300 million asthma sufferers globally and consequently asthma is a substantial economic burden [14]. Chronic inflammation of the airways, episodic and reversible airway obstruction, bronchial hyper-responsiveness and tissue remodelling are pathological hallmarks of asthma while clinical presentation includes breathlessness, wheeze and obstruction of airflow [14, 26]. A number of risk factors such as genetic predisposition, infection and inhaled allergen exposure are associated with asthma [14, 26]. Asthma is a heterogenous disorder with various distinct phenotypes, based on differences in drug responsiveness, long term outcomes such as lung tissue remodelling or irreversible loss of lung function, exacerbation frequency, severity and triggers which include allergens, exercise and aspirin and therefore targeted therapeutics are important [16, 26]. Asthma involves acute inflammatory episodes along with underlying chronic inflammation [14]. There is no cure for asthma, therapies simply provide symptomatic relief and again the gold standard therapeutics include bronchodialators and inhaled corticosteroids [14] alone or in combination with long acting β-agonists [27]. Inhaled corticosteroids fail to improve lung function in 30 - 45% of asthma sufferers [26] and steroid therapies are associated with many side effects and consequently poor patient compliance [14].

### 1.4.1 Macrophages and Inflammatory Lung Disease

Macrophages play a central role in the development, progression and resolution of inflammation in the lung [28]. Under inflammatory conditions circulating monocytes can be recruited to the site of infection or injury and once there, differentiate into macrophages. Monocytes differentiate from hematopoietic stem cells, specifically granulocyte/macrophage progenitors in the bone marrow; enter the periphery as circulating monocytes and various micro-environmental cues determine their fate which can lead to differentiation into macrophage and dendritic cells [29]. However under steady state conditions local proliferation maintains resident macrophages in the lungs.

The majority of lung macrophages are interstitial macrophages which are localised within the airway and alveolar walls. These cells may represent a stage in alveolar macrophage maturation of recruited peripheral monocytes [30]. Alveolar macrophages are found in the alveolar spaces and can secrete a wide variety of inflammatory mediators such as lipid mediators (e.g. leukotrienes and prostaglandins), chemokines (e.g. IL-8 for recruitment of monocytes, neutrophils and T-lymphocytes), cytokines (e.g. TNFα and IL-10), growth factors (e.g. transforming growth factor-β1 (TGF-β1)), proteases (such as matrixmetallo proteases) and reactive oxygen and nitrogen species [30]. Transcription factors such as NFκB are important in the enhanced expression of TNFα, IL-8 and monocyte chemotactic protein-1 (MCP-1) [30].

Following activation, macrophages become polarized into either classic (M1) or alternative (M2) macrophages [31-33]. M1 macrophage activation is induced mainly by microbial products such as LPS or cytokines like interferon-gamma (IFN-γ) and TNFα. M1 cells in a polarized response produce increased proinflammatory cytokines such as TNF-α, IL-12, IL-23, and proinflammatory mediators like nitric oxide (NO) and reactive oxygen intermediates (ROI). While, M2 macrophages are promoted by various signals such as IL-4, IL-13, glucocorticoids and IL-10. M2 cells function in inflammation resolution and tissue remodelling.

COPD patients experience poor lung function and eventual respiratory failure. A 5 – 10-fold increase in macrophage counts in the airways, lung parenchyma, bronchoalveolar lavage fluid (BALF) and sputum are found in COPD patients [30]. Furthermore, severity of COPD has been associated with the level of airway macrophage presence which may occur due to increased recruitment to the lung of peripheral monocytes represented by high levels of monocyte selective chemokine MCP-1 in COPD bronchoalveolar lavage (BAL) and expression by alveolar macrophages, prolonged macrophage survival and proliferation in the lung or an impaired macrophage clearance from the respiratory tract [30]. Macrophage secretory proteins such as TNFα, IL-8, IL-10 and TGF-β1 as well as activation of transcription factors such as NFκB are increased in COPD patients [30]. Traditional COPD treatments include anti-inflammatory agents such as corticosteroids and bronchodilators such as β-adrenergic receptor (β-AR) agonists which only treat immediate symptoms [19]. However, COPD macrophages have shown some resistance to corticosteroids [30]. Other potential therapeutics for inflammatory lung diseases include protease inhibitors such as secretory leukocyte protease inhibitor (SLPI), immunosuppressants, mucoregulators, NFκB inhibitors and inhibitors of specific inflammatory mediators such as TNFα.

The genetic defect in CF may have a direct link to IL-8 and other inflammatory mediator dysregulation leading to the large neutrophil influx found in BAL of CF patients [13]. IL-8 is produced by stimulated macrophages, neutrophils and epithelial cells in the CF lung and IL-1β, IL-6 and TNFα are also found in high concentrations in CF BALF [13]. The large presence of neutrophils which generally outnumber macrophages in the CF lung is associated with increased protease concentrations which may inhibit macrophage phagocytosis of apoptotic cells [13]. Asthma and COPD are becoming more prevalent mainly due to environmental changes such as increased exposure to cigarette smoke and particulates in the air [12] and alveolar macrophages play a central role in the inflammatory pathogenesis of these diseases. Thus strategies aimed at targeting alveolar macrophages and specifically inflammation are highly attractive. Due to its pivotal role in inflammation, the mononuclear phagocytic system (MPS) is an important target for drug delivery to treat disease. In general however these cells are reputed to be difficult targets [34] particularly where intracellular delivery of the active is required such as for gene delivery [35]. Therefore the development of delivery systems that can target monocytes/macrophages intracellularly is crucial and could potentially open up new treatment paradigms for a range of diseases.

### 1.4.2 Macrophage Mannose Receptor

The mannose receptor (MR, CD206) is a 180kDa type-I membrane protein and member of the MR family which forms part of the C-type lectin superfamily [36]. DEC-205, Endo-180 and the phospholipase $A_2$ receptor are also members of the MR family [37, 38]. The MR is highly expressed by macrophages and was first identified in rabbit alveolar macrophages in the late 1970s [36, 37]. Since then expression has also been identified in other cell types including monocyte-derived dendritic cells and lymphatic endothelial cells [36]. The MRs three extracellular domains include an *N*-terminal cysteine-rich (CR) domain involved in $qCa^{2+}$-independent binding to $SO_4$-3-Gal or $SO_4$-3/4-GalNAc terminating sulphated sugars [36], a fibronectin type II (FN II) domain capable of collagen binding [36, 37] and finally eight C-type lectin-like domains (CTLD) involved in $Ca^{2+}$-dependent binding to non-reducing sugars such as fucose, mannose, glucose and *N*-acetylglucosamine [36, 37] (Figure 1.6). MR also has a single transmembrane domain and a short cytoplasmic tail which mediates receptor internalisation and recycling [36, 37].

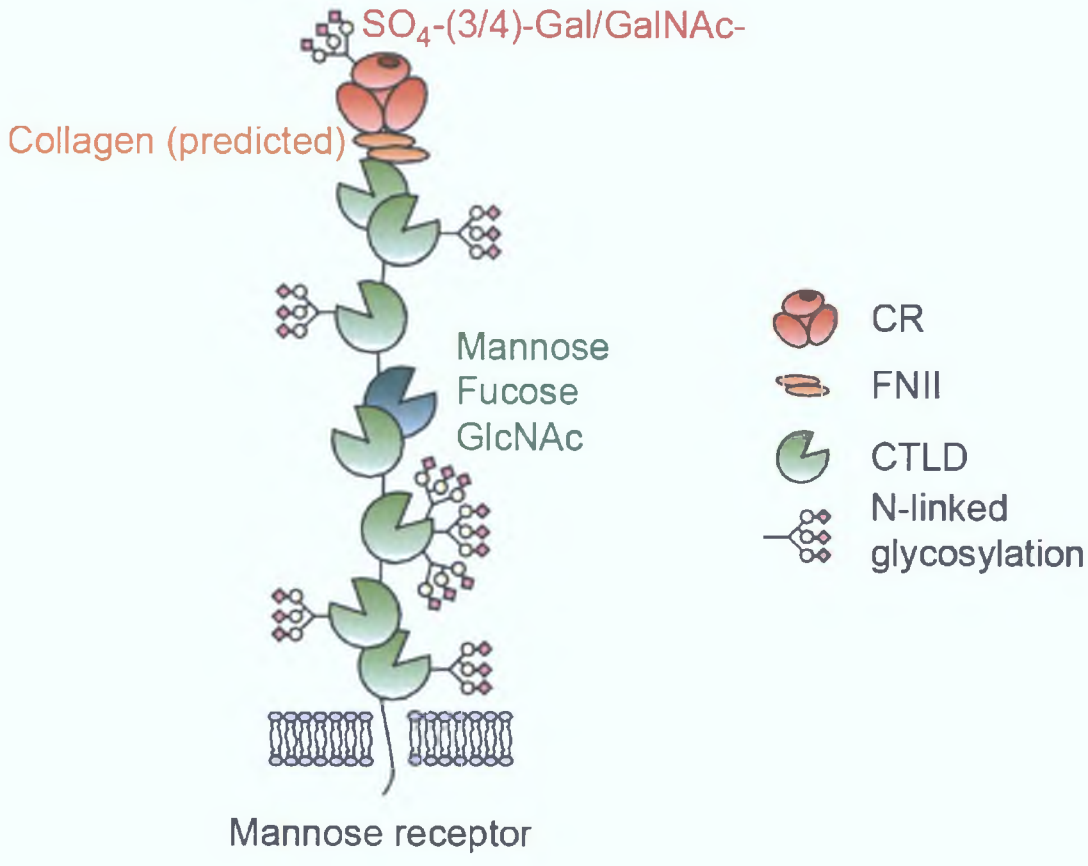


Figure 1.6: Structure of the mannose receptor (MR) (taken from [37]). The MR consists of an *N*-terminal cysteine-rich (CR) domain, fibronectin type II (FN II) domain, eight C-type lectin-like domains (CTLD), a transmembrane domain and a cytoplasmic domain. The extracellular domains are capable of binding sugar residues and collagen.

This receptor is involved in a range of processes including the recognition and internalisation of both foreign and self materials, antigen presentation and intracellular signalling [36]. MR

recognises and binds sugar residues found on gram negative and positive bacteria, fungi, parasites, virus infected cells, mycobacteria and yeasts [39, 40]. Additionally, MR is involved in the clearance of endogenous materials such as lysosomal hydrolases, pituitary hormones and tissue plasminogen activator [41, 42], many of which are secreted during inflammation. Therefore MR plays important roles in innate and adaptive immunity, homeostasis and the resolution of inflammation [36, 37, 43, 44]. Under steady state conditions only 10 – 30% of the MR is localised at the cell surface [36] and functions as an endocytic and/or phagocytic receptor [36]. The functional state and expression levels of MR are modulated by cytokines, pathogens and immunoglobulin receptors [40, 43], for instance IL-4 can enhance cell surface MR expression and MR endocytosis [40].

Internalisation of the receptor occurs via clathrin mediated endocytosis, MR enters endocytic pathways and is recycled back to the cell surface [36]. This mechanism is important for antigen presentation by both class I and class II major histocompatibility complex (MHC) molecules [36]. Additionally, the involvement of MR in phagocytic uptake of pathogens such as *Mycobacterium tuberculosis* has been shown [36, 43]. Phagocytosis is a type of endocytosis whereby a phagocytic cell will extend projections (or pseudopodia) around foreign material, the projections fuse surrounding the material and form a vesicle known as a phagosome and this vesicle can then enter the endocytic pathway [36].

### 1.4.3 Tumour Necrosis Factor-α (TNFα)

TNFα is a 17-kDa pro-inflammatory cytokine of the TNF super family [45, 46] secreted by a variety of cells but primarily by macrophages and other monocytic cells and is central to the innate immune system [27, 47]. The TNFα gene is found on human chromosome 6 and expression is regulated by the transcription factor NFκB [47]. It is expressed as a 27-kDa protein which anchors to the cell membrane and is proteolytically cleaved by a metalloprotease TNFα-converting enzyme (TACE) to produce the soluble 17-kDa TNFα (Figure 1.7) [47]. TNFα receptors (TNFR1 and TNFR2) bind TNFα with high affinity, leading to receptor activation, signal transduction through various pathways and induction of inflammatory mediators including TNFα, mainly via TNFR1 (Figure 1.7) [47]. The NFκB pathway can be activated via toll-like receptors (TLRs) as well as via TNFα-TNFR activation. Upon TNFα binding, the inhibitory protein silence of death domains (SODD) is released from the TNFR1 intracellular domain and an adaptor protein TNF receptor-associated death domain (TRADD) binds and recruits other adaptor proteins including receptor interacting protein-1 (RIP-1) and TNFR-associated factor 2 (TRAF2) [45, 47]. The TRADD-RIP-1-TRAF2 complex is released from TNFR1 and further proteins are recruited [47]. Inhibitor of κB kinase (IKK) complex is activated which phosphorylates IκB proteins leading to their ubiquintination and degradation and the release of NFκB subunits [47]. NFκB can then translocate to the nucleus and promote transcription of inflammatory genes. TRAF2 can also activate NFκB pathways [47].

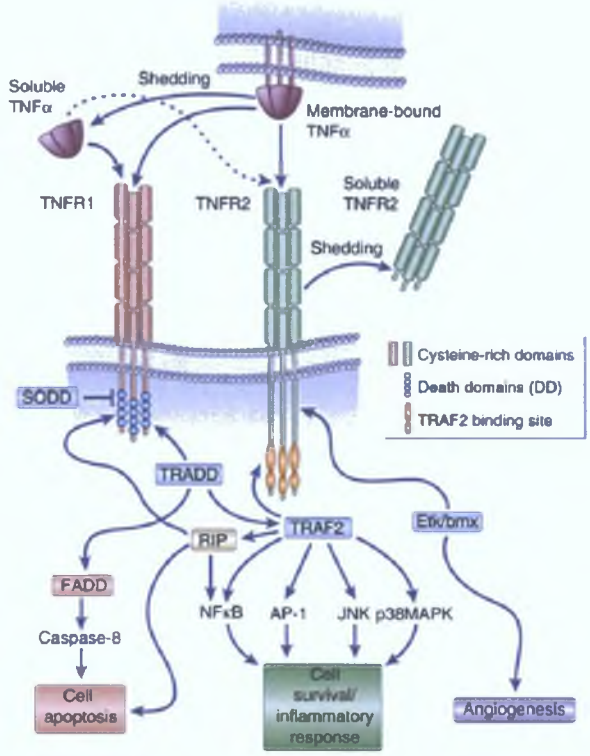


Figure 1.7: TNFα receptor signalling pathways (taken from [48]).

TNFα functions both directly and indirectly in the inflammatory response inducing a host of inflammatory mediators including IL-1, TNFα, IL-6, matrix metallopeptidase-9 (MMP-9) and -12, MCP-1 and p-selectin in a wide range of cells (Figure 1.8) [12]. In the lungs TNFα has also been associated with mucus hypersecretion, cytotoxicity and IFNγ receptor activation [12]. This potent cytokine is also involved in neutrophil recruitment leading to protease and reactive oxygen species (ROS) release.

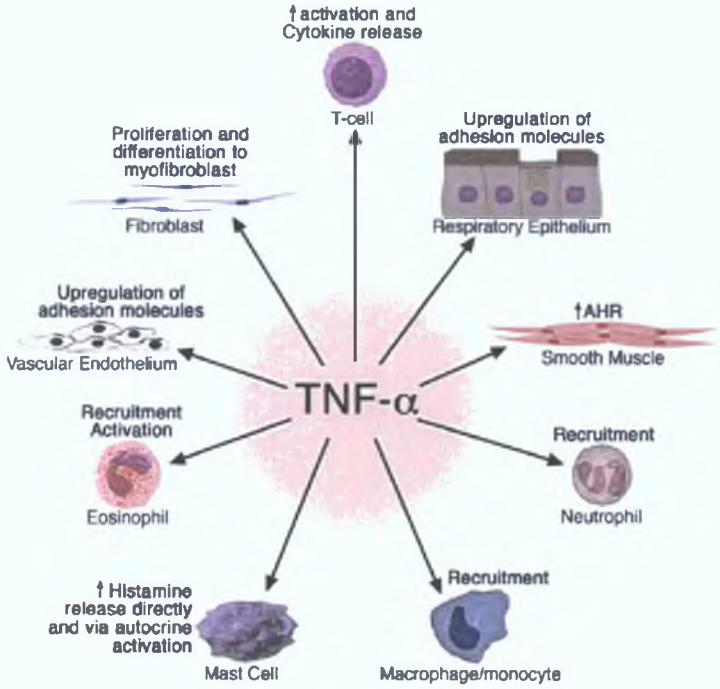


Figure 1.8: TNFα function in the inflamed lung [27]

Macrophages are the predominant cell type found in BALF recovered from COPD patients and unsurprisingly COPD patients show raised TNFα expression [12]. In CF TNFα induces changes in lipoprotein metabolism, increases neutrophil oxidative and secretory responses and may be involved in CF associated cachexia [13]. Increased TNFα has also been reported in asthmatic airways at both the protein and mRNA levels [27]. Additionally, inhalation of recombinant TNFα by normal subjects has resulted in airway hyper responsiveness and neutrophilia both features of asthmatic pathology [27]. TNFα is the key player in chronic inflammation and is associated with disease progression and pathogenesis (Figure 1.9). For instance overexpression of TNFα in mice can mediate increases in airspace, chest and lung cavity volume and collagen as well as small airspace loss [46]. Hence, TNFα poses a potential target for anti-inflammatory therapies and clinical trials have investigated this cytokine as a target for the treatment of asthma using strategies such as adalimumab (human antibody) and infliximab (chimeric mouse/humanized monoclonal antibody); with some positive results [27]

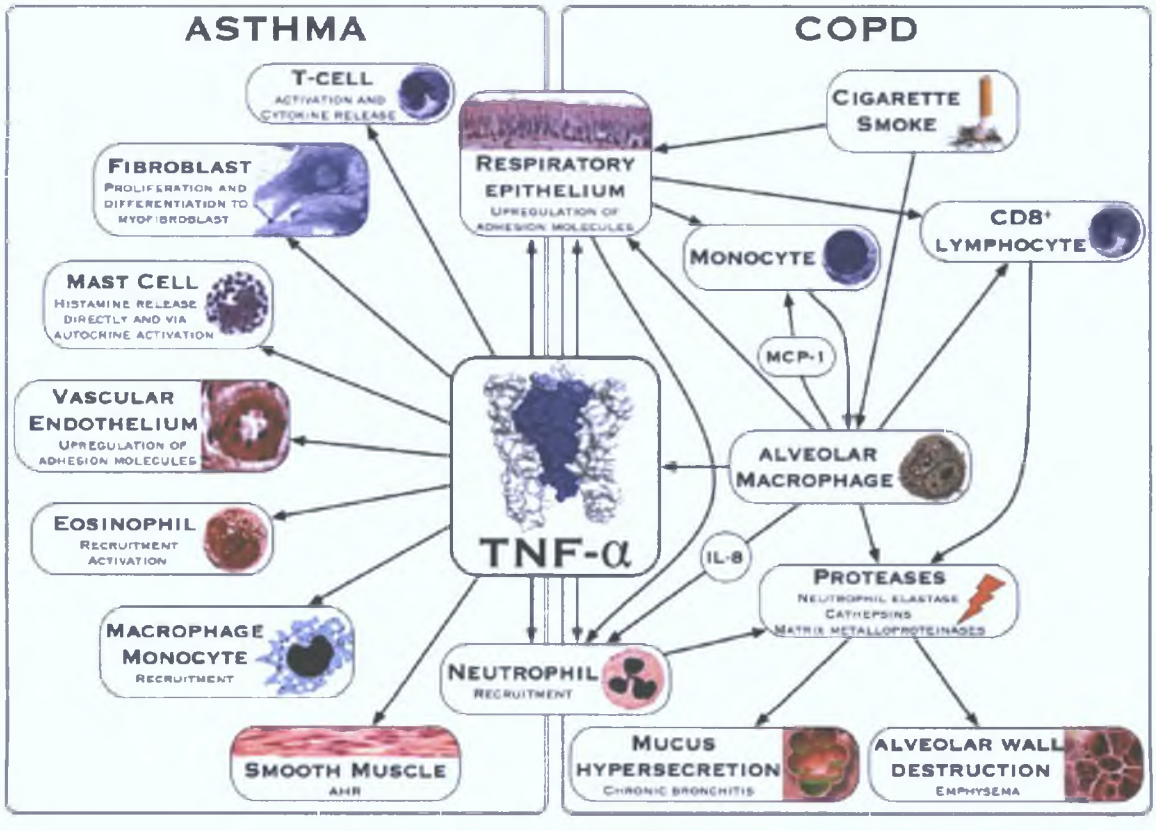


Figure 1.9: The central role of TNF-α in asthma and COPD pathogenesis [49].

### 1.5 New Treatments for Inflammatory Lung Disease

The ability to suppress chronic inflammation associated with lung diseases such as CF, asthma and COPD by the application of targeted siRNA presents an attractive therapeutic approach. Present therapies target inflammation such as glucocorticoids and smooth muscle such as bronchodilators and can be associated with many unwanted side effects [19].

### 1.5.1 RNA Interference

The term RNA interference was coined by Fire and Mello just over a decade ago to describe an endogenous cellular mechanism involved in gene regulation [50]. They discovered that specific down-regulation of gene expression could be achieved by the exogenous introduction of double stranded RNAs (dsRNA) into *C. elegans* (a nematode) [50] and were subsequently awarded the Nobel Prize for Physiology or Medicine in 2006. Initially similar observations were made in insects and plants but not in mammalian cells lines. Also in higher eukaryotes dsRNA greater than 30 base pairs (30bp) can potently induce an interferon response. It was not until 2001 that dsRNA 21 nucleotides in length (and therefore similar in length to the dicer processed dsRNA, siRNA) were found to silence genes in mammalian cells [51] and a new branch of gene therapy emerged.

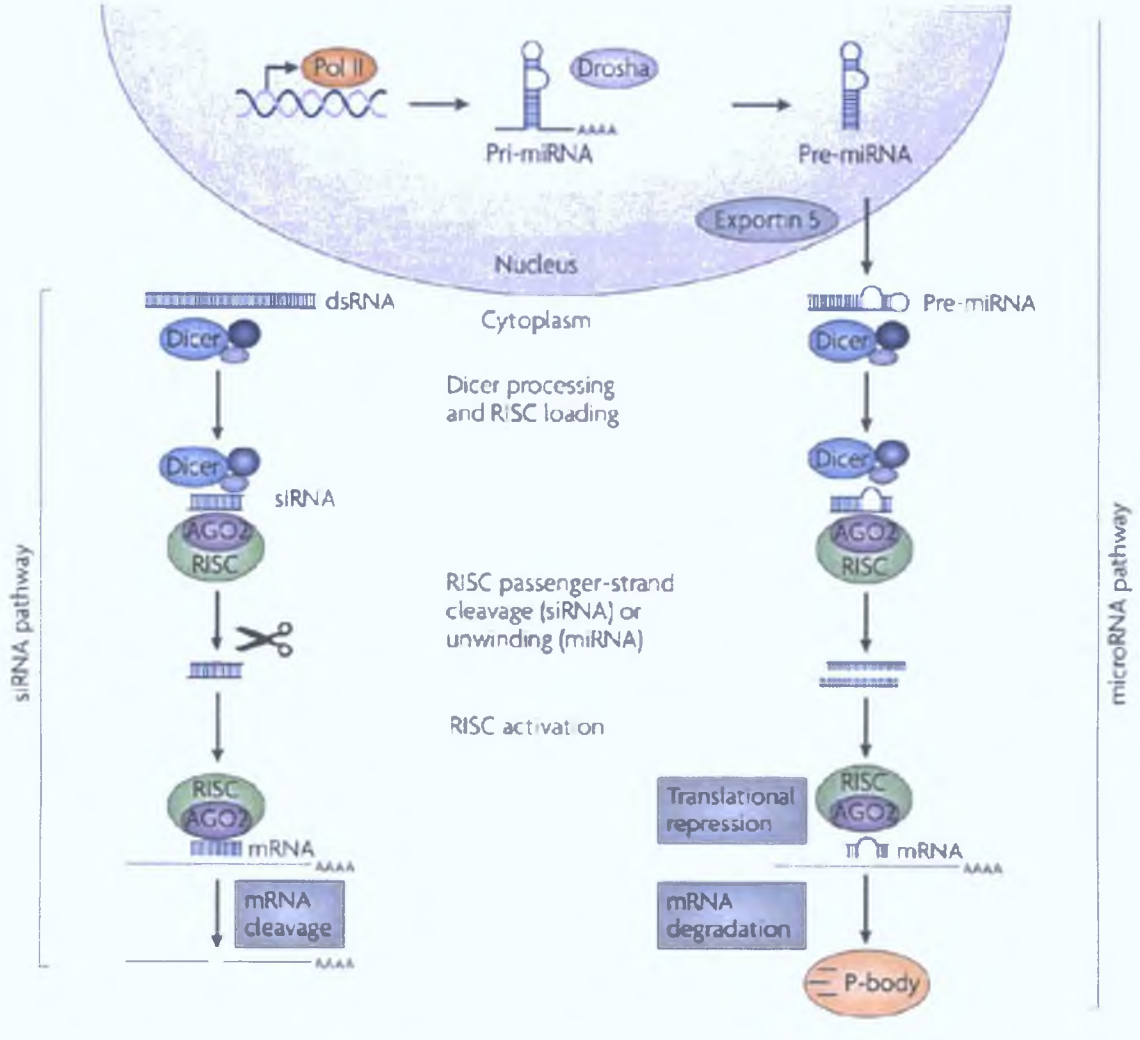


Figure 1.10: Endogenous Mammalian RNA Interference Pathway[52].

Endogenously the process of RNAi is very complex and is primarily guided by small RNAs such as microRNAs (miRNA), siRNA as well as the less elucidated piwi-interacting RNAs (piRNA) [53]. In general miRNA arises when long primary micro-RNAs (pri-mRNA) expressed in the nucleus are cleaved by the nuclear microprocessor Drosha (RNase III-like endoribonuclease) into shorter precursor miRNA (pre-miRNA) and transported to the cytoplasm via karyopherin

Exportin-5 (exp5) [54]. Once in the cytoplasm the pre-miRNA is processed along the microRNA pathway represented in Figure 1.10 in which translation of the target mRNA is prevented by the miRNA-RNA induced silencing complex (miRNA-RISC). Imperfect base-pairing exists between the miRNA and its target nucleic acid. The specificity of miRNA relies on a 6-7 base "seed region".

The origins of siRNA however can vary greatly but once present in cytoplasm, long, linear dsRNA is cleaved by Dicer, a ribonuclease III, into double stranded fragments of 21-23 perfectly paired nucleotides, known as siRNA. The siRNA complexes with a multi-protein complex that includes Argonaute-2 (Ago2) and RISC. The complex remains inactive while the siRNA duplex is unwound by RISC-mediated helicase activity [55], specifically by the protein Ago2 at its Piwi-Argonaute-Zwille (PAZ) domain [56]. The guide (antisense) strand is selected, the sense strand lost, and the RISC activated. Through RISC activation, the guide strand is hybridized to a perfect or near perfect complementary mRNA. Subsequently, the mRNA is cleaved by Ago2 between the complementary nucleotides of the guide strand nucleotides 10 and 11 (from the 5'-end) [52, 53]. Further degradation of these cleavage products by exonucleases has been observed in drosophila [57]. The guide strand disassociates from the RISC complex which can then complex with other siRNA.

It was believed that the role of miRNA was endogenous gene regulation while siRNA was defence of the genome against foreign or invasive nucleic acids such as viral nucleic acid or transposons ("jumping genes"). Following on from these roles miRNA appeared to be endogenous while siRNA chiefly exogenous possibly derived straight from a transposon, transgene or virus activator. However a range of other sources have since been observed including numerous endogenous genomic origins [53] indicating more diverse functions for these short RNA duplexes.

The potency and specificity of siRNA immediately attracted interest for its therapeutic potential. In short, plasmids or viral vectors expressing short hairpin RNA (shRNA) or synthetic siRNA duplexes can be introduced into cells to knockdown specific genes. In the case of shRNA, gene silencing can be longer lasting as expression of the shRNA persists within the cell while siRNA effects will only last a few days usually due to degradation [58]. However many concerns were raised over possible risks of introducing siRNA *in vivo* as well as difficulties in delivery. For instance, siRNA can target mRNA sequences of imperfect complementary likely causing undesired gene silencing or off-target effects [53] and so enter the miRNA pathway. A similar effect can be seen due to strand selection. The guide strand is selected based on the thermodynamic stability of its 5'- end, with the less stable (AU rich) terminus being preferred [53, 54]. While, thermodynamic symmetry grants each strand an equal opportunity of being selected [53] and therefore has a less predictable outcome. In addition, high concentrations of siRNA can induce an interferon response by the activation of protein kinase R (PKR; also triggered by dsRNA >30bp) as well as activating TLRs in particular TLR7 which recognizes dsRNA [52].

Another issue is associated with the stability of siRNA *in vivo*. In human plasma naked siRNA is degraded within minutes [52].

### 1.5.2 siRNA Delivery

#### 1.5.2.1 Naked Nucleic Acid

*In vivo* transfections with naked DNA have previously shown success using methods such as direct injection to muscle [59], electroporation to skin, muscle [60] and lungs [61], ultrasound and intravascular injection. However gene transfer of naked DNA is associated with low efficiency, variability [62] and has a serum half life of 10 minutes [63]. In addition mammalian DNA has methylated CpG sequences unlike bacterial DNA and plasmid vectors. Consequently immune activation occurs via TLR9 by the presence of unmethylated plasmid DNA (pDNA) [64]. Naked nucleic acids also lack cell target specificity [63].

Similarly siRNA is associated with many problems including toxicity, off-target effects and immune activation. In order to avoid these problems and to improve stability and potency modified siRNA duplexes are being developed. Synthetic siRNA typically is produced using phosphoramidite to form single-stranded oligonucleotides which are annealed into duplexes and can then be further modified. It is important that siRNA design also include bioinformatic and *in vitro* screening [52] for example "seed region" homology screening, however, this is not always effective and chemical alterations are also necessary [65]. To minimise off-target gene silencing (via the miRNA pathway) chemical modifications such as a single 2'-O-methyl (2'OMe) modification at nucleotide 2 [52] and substitution of DNA into "seed regions" have been successful. Immune activation can also be minimised by 2'-OMe modifications with ribose (r) U and rG modifications the most efficient [66]. siRNA modifications as simple as strand length changes can have substantial impact, for instance longer duplexes (up to 29bp) can be more potent and will be processed by Dicer while still avoiding the innate immune response [54]. Additionally to prevent TLR7 activation (an event that is sequence specific) GU-rich sequences should be avoided [52]. Other modifications include the synthesis of asymmetric siRNA with 3' 2-nt overhangs, small internally segmented interfering RNA (sisiRNA) with a guide strand and two shorter passenger strands and asymmetric interfering RNA (aiRNA) with minimally sized passenger strands (15bp) (Figure 1.11). A recent study by Bramsen *et al.* assessed the activity, stability and toxicity of 2160 different siRNA duplexes (with 21 types of chemical modifications) and found that 134 siRNA duplexes were more potent than standard siRNA [67].

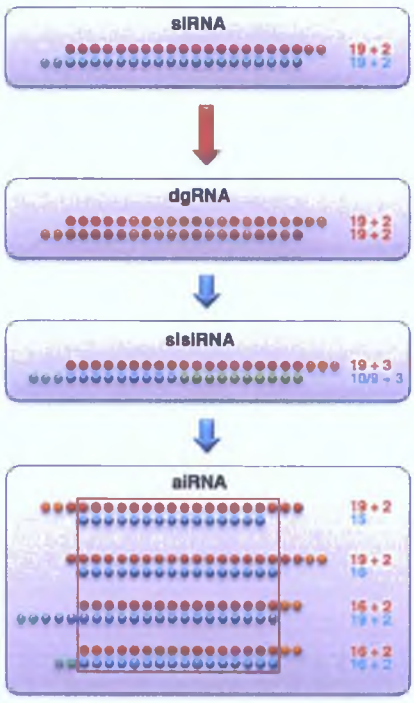


Figure 1.11: Some of the chemical modifications of siRNA duplexes to reduce unwanted effects while retaining functionality.[54]

Chemical modifications can lower these risks, however, a major obstacle still remains; inefficient transport across the cell membrane. The structure of siRNA, with a large molecular weight of over 13kDa and a polyanionic structure (almost 40 negative phosphate charges) [56] is not suitable for transfer across cellular membrane. Moreover naked siRNA has a half-life of minutes in human serum [68] as a result of degradation by serum nucleases [69]. The development of a pharmaceutical vehicle that can effectively deliver siRNA to the intracellular target, while also enhancing stability, is essential for the advancement of siRNA to a useful therapeutic. However modification of siRNA is still important particularly if the delivery system (such as cationic lipids) brings the siRNA into direct contact with various TLRs which are present in endosomes. A recent study by *Gao et al.* (2009) compared the stability, blood clearance and biodistribution of a range of chemically modified siRNA and siRNA nanoparticles in mice [70]. It was found that modifications to siRNA increased *in vivo* stability nevertheless nanoparticle formulations such as siRNA complexes with cationic polymers and polyethylene glycolated (PEGylated) liposomes improved blood stability and biodistribution compared to naked siRNA.

### 1.5.2.2 siRNA Vectors

In order to overcome the numerous barriers to siRNA delivery such as off-target effects, nuclease siRNA degradation, non-specific accumulation, toxicity, cell internalisation and poor endosomal escape [71] vectors or carriers can be developed. These vectors are generally categorised as viral or non-viral. Viruses such as lentiviruses and adenoviruses can be harnessed for efficient delivery of siRNA in the form of a viral genome but their use has been

limited by the difficulties associated with large-scale manufacture and possible mutagenic and immunogenic effects [71]. The need for an alternative to viral based delivery systems arose from the serious adverse effects associated with the use of viruses [1]. The most frequently used non-viral vectors are polymers and liposomes which are very versatile carriers allowing modification to improve cell specific targeting, overcoming many of the previously mentioned barriers.

Cationic polymers and lipids are usually ionically complexed with negatively charged nucleic acids to form polyplexes and lipoplexes respectively [72]. While not as efficient as virally based delivery systems these vectors are somewhat safer. Also non-viral vectors can be synthesised in larger quantities to be more readily prepared and chemical improvements e.g. PEGylation targeting more easily incorporated. Commonly used polymers include poly(ethyleneimine) (PEI), poly-(l-lysine) (PLL), chitosan, gelatin, poly(dimethylaminoethylmethacrylate) (PDMAEMA) and poly(trimethylaminoethyl-methacrylate) (PTMAEMA) [72]. Many polymers can offer various advantages for nucleic acid delivery including biocompatibility, protection of siRNA against nucleases [73] and can be biodegradable. Many polymers are also strongly cationic. This characteristic helps in the formation of polyplexes with a net positive charge but can have biological consequence *in vivo*.

Non-viral vectors such as liposomes have been shown to enhance pharmacokinetics and decrease toxicity associated with siRNA therapy [74, 75]. Liposomes are versatile delivery systems that can incorporate components to enhance cell fusion, targeting and control the pharmacokinetics of the siRNA *in vivo*. Cationic liposomes tend to be toxic and have lower transfection efficiency *in vivo*. To address these shortcomings neutral targeted liposomes are being explored which encapsulate rather than bind with RNA [75, 76].

#### 1.5.2.3 siRNA Delivery to the Lungs

Inhalation offers the means of direct delivery of siRNA to the target organ, the lungs. It also offers many advantages over systemic delivery such as decreased systemic toxicity, immediate availability, local and non-invasive delivery [75]. *In vivo* studies have administered siRNA naked [77-81], complexed with polymers or lipids [82, 83] or encapsulated in liposomes [84, 85] but to date there are no siRNA based therapeutics available as commercial products for lung disease. Clinical studies are currently underway for treatment of diseases including of wet neovascular age-related macular degeneration and respiratory syncytial virus (RSV) currently at clinical trial phase III and IIb respectively [75, 76]. Delivery of siRNA to the lungs must overcome the pulmonary barriers discussed in 1.3 as well as maintain stability following formulation and inhalation and in the respiratory environment which can be achieved through siRNA modification and/or the use of carriers [75]. Therefore both formulation and the inhaler device used are very important for successful siRNA delivery to the lungs [75].

### 1.6 Overall Aims

- To prepare and develop biocompatible siRNA liposomal and polymeric particles targeted to alveolar macrophages
- To develop high content screening methods to enable comprehensive, high throughput methods to compare cellular delivery and toxicity of siRNA carriers
- To determine siRNA-carrier ability to faciltate TNFα knockdown in LPS-stimulated macrophages *in vitro* and in LPS stimulated mice *in vivo*

# Chapter 2

# Alveolar Macrophage Targeted siRNA Liposomes for Inhalation

## 2.1 Introduction

Alveolar macrophages reside in the alveolar region of the lung and rapidly phagocytose foreign particles. Targeting of alveolar macrophages via inhalation avoids many of the barriers associated with delivery to other pulmonary targets such as the epithelium and vasculature including mucus and enzymatic degradation. One strategy to target siRNA to alveolar macrophages via inhalation is liposome delivery. Lipid based formulations form a major branch of non-viral gene therapy. A variety of lipid based formulations have been described including micelle structures, solid lipid nanoparticles (SLN) and nano-structure lipid carriers (NLC) but the most extensively investigated for gene delivery are liposomes and cationic lipid nucleic acid complexes (lipoplexes) [86]. Liposomes have been evaluated for decades as drug carriers due in part to their versatility. They boast a great number of benefits over other drug carrier systems such as the capability of entrapping a wide range of drugs, biocompatibility and low toxicity [87]. Furthermore, phospholipids have a long history in relation to pulmonary drug delivery, being used in the treatment of respiratory distress syndrome (RDS) in newborns for over 40 years [87].

### 2.1.1 Liposomes

A liposome is a lipid vesicle in which natural or synthetic lipids are arranged in one or more concentric lipid bilayers with an inner aqueous volume [88]. First described to entrap solutes as early as 1965, liposomes have since established themselves as extremely versatile drug carrier systems with the added advantage for inhalation that their composition can utilize lipids endogenous to the lungs such as those found in the lung surfactant [89, 90] potentially bestowing biocompatibility. Consequently liposomes will undergo uptake, processing and recycling by alveolar type II cells similar to endogenous surfactant [90]. Phospholipids consist of polar or hydrophobic head groups and hydrophilic fatty acid tails which in aqueous solution will spontaneously rearrange to form structures such as lipid bilayers or micelles (Figure 2.2). The variation in lipid properties (Figure 2.1) including self assembly characteristics lends itself to preparation of liposomes with diverse qualities. Depending on the target (such as tumour, specific organ or cell type), the drug to be incorporated and method of delivery, liposome composition can be tailored, using a vast array of lipids and the incorporation of ligands and/or chemical modifications. Liposome physicochemical properties include variations in size, surface charge, encapsulation efficiency, drug release profiles and bilayer fluidity [90] optimised for their therapeutic end goal.

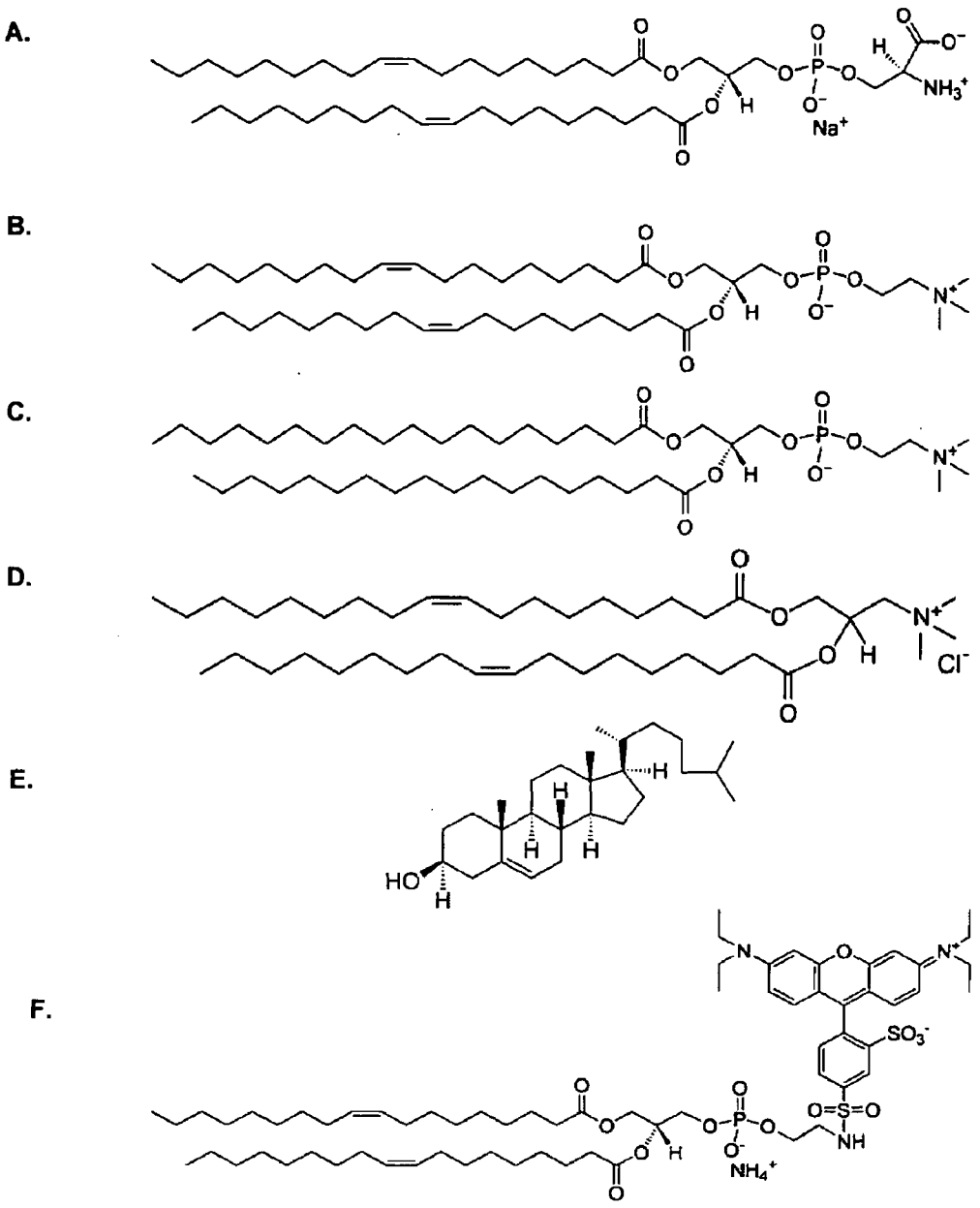


Figure 2.1: Structure of commonly used synthetic lipids (A) 1,2-dioleoyl-*sn*-glycero-3-phospho-L-serine (DOPS), (B) 1,2-dioleoyl-*sn*-glycero-3-phosphocholine (DOPC), (C) 1,2-distearoyl-*sn*-glycero-3-phosphocholine (DSPC), (D) ,2-Dioleoyl-3-trimethylammonium-propane (DOTAP), (E) cholesterol and (F) 1,2-dioleoyl-*sn*-glycero-3-phosphoethanolamine-N-(lissamine rhodamine B sulfonyl) (PE-rhodamine) (Avanti Polar Lipids Inc.)

Using various techiques liposomes are formed normally as large multi lamellar vesicles (MLV) and re-sized to unilamellar vesicles (UV) of a predetermined diameter via sonication, extrusion, reverse-phase evaporation or solvent injection [86]. Liposomes by virtue of their structure can entrap hydrophobic, hydrophilic and amphiphilic drugs within the lipid bilayer, the aqueous compartment and at the bilayer interface respectively [90] and encapsulation efficiencies can be maximised using a number of strategies. Release of drug can also be controlled by the formulation with the capability of internal or external triggers such as pH, enzymes, light, heat or a magnetic field [86].

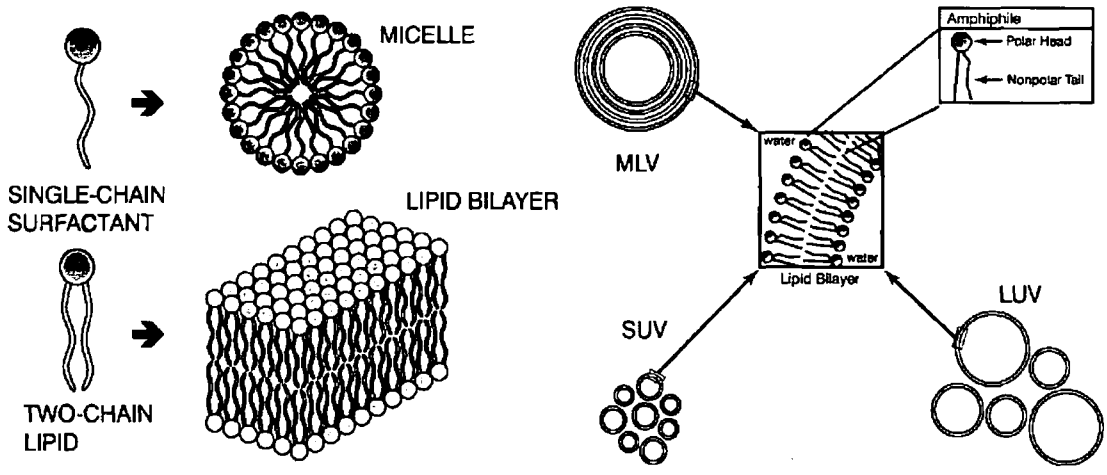


Figure 2.2: Lipid and liposome structures. Lipids are amphiphiles with a polar head and non-polar tail. Lipid structure dictates resulting self-assembly such as micelle or lipid bilayer formation. Liposomes formed are usually large multilamellar vesicles (MLV) or can be resized via sonication or extrusion to form small or large unilamellar vesicles (SUV or LUV respectively). [91]

### 2.1.2 Liposomes as siRNA Carriers in Gene Therapy

The encapsulation of nucleic acids into liposomes of neutral naturally occurring lipids was first described in the late 1970s [92]. Nucleic acids including pDNA and siRNA are highly negatively charged which is one of many barriers to cell internalisation and hence the need for a carrier system. This feature however allows nucleic acids to be complexed through electrostatic interactions to cationic lipids such as 1,2-Dioleoyl-3-trimethylammonium-propane (DOTAP) and 1,2-di-O-octadecenyl-3-trimethylammonium propane (DOTMA) to form lipoplexes. Although cationic lipoplexes enable efficient nucleic acid encapsulation and *in vitro* cell uptake and transfection they are associated with cytotoxicity most likely due to interaction with enzymes such as protein kinase C (PKC) [93] and proteoglycans on the cell surface (Chapter 3) that often results in toxicity and poor transfection efficiencies *in vivo* [92]. Consequently, interest has turned to the use of more biocompatible neutral and anionic lipids sometimes with ligands for intracellular targeting. However efficient encapsulation of siRNA is a major obstacle in neutral and anionic liposome preparations.

Various strategies have been developed to encapsulate nucleic acids in non-cationic liposomes including passive, ethanol drop method, ethanol destabilisation, ethanol dilution, reverse phase evaporation and hydration of freeze-dried matrix (HFDM) [92, 94, 95]. A summary of the methods for the encapsulation of nucleic acids into liposomes composed of neutral and/or anionic lipids in the absence of cationic lipids is shown in Table 2.1. The most commonly used method for liposome preparation is dry film hydration where lipids are dissolved and mixed in a solvent such as chloroform. The solvent is removed leaving a dry lipid film which is then hydrated with an aqueous buffer. Passive encapsulation of siRNA simply involves the rehydration of the lipid film with an aqueous siRNA solution. This generally leads to poor encapsulation efficiency particularly if cationic lipids are completely absent from the formulation. To improve loading of siRNA one strategy has been used most frequently, the pre-complexation

of siRNA with cationic reagents such as protamine, octa-arginine (R8) and PLL achieving encapsulation efficiencies greater than 80% [96-98]. Nakamura *et al.* (2007) condensed siRNA using PLL, stearylated R8 (STR-R8) and protamine for encapsulation into anionic 1,2-dioleoyl-sn-glycero-3-phosphoethanolamine:cholesteryl hemisuccinate (DOPE:CHEMS) liposomes [98]. STR-R8 siRNA complexes showed the most efficient condensation (with particle sizes less than 100nm) and were encapsulated in liposomes at an efficiency of 87.8 ± 8%. Additionally, luciferase activity in HeLa cells was knocked down by 80% 24 hours following transfection with these liposomes.

**Table 2.1 Strategies for Nucleic Acid Encapsulation in Liposomes Composed Anionic and/or Neutral Lipids**

| Lipid Components | Preparation Method | Nucleic Acid | Encapsulation Method | EE% | Ref. |
|---|---|---|---|---|---|
| POPC:DDAB, DSPE-PEG, DSPE-PEG-MAL | thin film hydration | siRNA | Freeze thaw 6x in liquid ntirogen | 3 | [99] |
| EPC, DMPG,DSPE-PEG | thin film hydration | ODN | ODN pre-complexed with PEI (N/P ratio 8) | 80 | [100] |
| DOPE,Choi, PS, PC | thin film hydration | pDNA | DNA complexed with protamine | - | [101] |
| DOPE:DOPA:Chol | - | siRNA | siRNA pre-complexed with protamine and calf thymus DNA | - | [96] |
| PC:DPPE:Chol | thin film hydration | siRNA | siRNA pre-complexed with protamine | - | [97] |
| PE:Chol:CHEMS | reverse phase method | siRNA | Via liposome preparation method | 10 - 12 | [102] |
| POPC:POPG:Chol:DSPE-PEG | thin film hydration | ODN | ODN pre-complexed with PEI (N/P 6) | 95 | [103] |
| EPC:DSPE-PEG | thin film and reverse phase | ODN | ODN pre-complexed with DOTAP mixed with PC lipids in ethanol | up to 97 | [104] |
| DOPC, DAP | thin film hydration | siRNA | 7 freeze thaw cycles | 19 | [105] |
| DOPE:CHEMS | thin film hydration | siRNA | siRNA pre-complexed with STR-R8 | 88 | [98] |
| PE:CHEMS:Chol | reverse phase | siRNA | Via liposome preparation method | 10 -14 | [106] |
| DOPC | freeze-dried matrix hydration | siRNA | Via liposome preparation method | 65 | [94] |

### 2.1.3 Liposomes for Macrophage Targeting

Targeting of liposomes to specific locations or cell type can be determined to some extent by the liposome physicochemical properties including size, surface charge and the incorporation of ligands such as proteins, peptides, antibodies, polysaccharides, glycolipids, glycoproteins and lectins. Macrophages are notoriously difficult to transfect and although their location and phagocytotic nature are advantages in terms of alveolar macrophage targeting and pulmonary delivery, strategies that enhance cellular uptake are important. A number of strategies have been developed to target liposomes to macrophages/monocytes (Figure 2.3 and Table 2.2).

Uptake of small liposomes (< 100nm) by phagocytic cells has been reported [107] however many other studies have shown liposome uptake to be improved with increased size [108-110]. Surface charge may also promote macrophage targeting. Negatively charged lipids such as phosphatidylserine (PS) and phosphatidylglycerol (PG) are preferentially recognised by macrophages [107]. Chono *et al* (2006) evaluated the uptake of anionic liposomes loaded with ciprofloxacin (CPFX), composed of hydrogenated soybean phosphatidylcholine (HSPC), cholesterol (chol) and the anionic lipid dicetylphosphate (DCP) at five different sizes 100, 200, 400, 1000 and 2000 nm by rat alveolar macrophages [108]. Following pulmonary administration efficiency of CPFX delivery to alveolar macrophages was improved with increasing liposome size from 100 – 1000nm and became constant over 1000nm. PS and phosphatidylethanolamine (PE) are located in the inner membrane leaflet of eukaryotic cells [111-113] which is exposed on the outer cell surface during apoptosis. It is believed that PS targets scavenger receptors (SRs) on macrophages.

In addition to controlling the physicochemical properties of liposomes, ligands such as lectins, antibodies and peptides can be incorporated into liposome formulations for improved macrophage targeting and uptake via lectin recpectors, Fc receptors and integrins respectively. The MR, a C-type lectin receptor [43, 114], is constitutively highly expressed by immune cells including alveolar macrophages, peritoneal macrophages, monocyte-derived dendritic cells and Kupffer cells. Ligands of the MR can be incorporated into liposome formulations for macrophage targeting such as mannosylated cholesterol (Mann-C4-Chol) [115]. MRs are involved in antigenic recognition, endocytosis and presentation as well as in homeostatic maintenance, inflammation and immune responses [36, 116]. Consequently MR can identify and engulf pathogens such as *Mycobacterium turberculosis* and *Leishmania donovani* via surface sugar antigens.

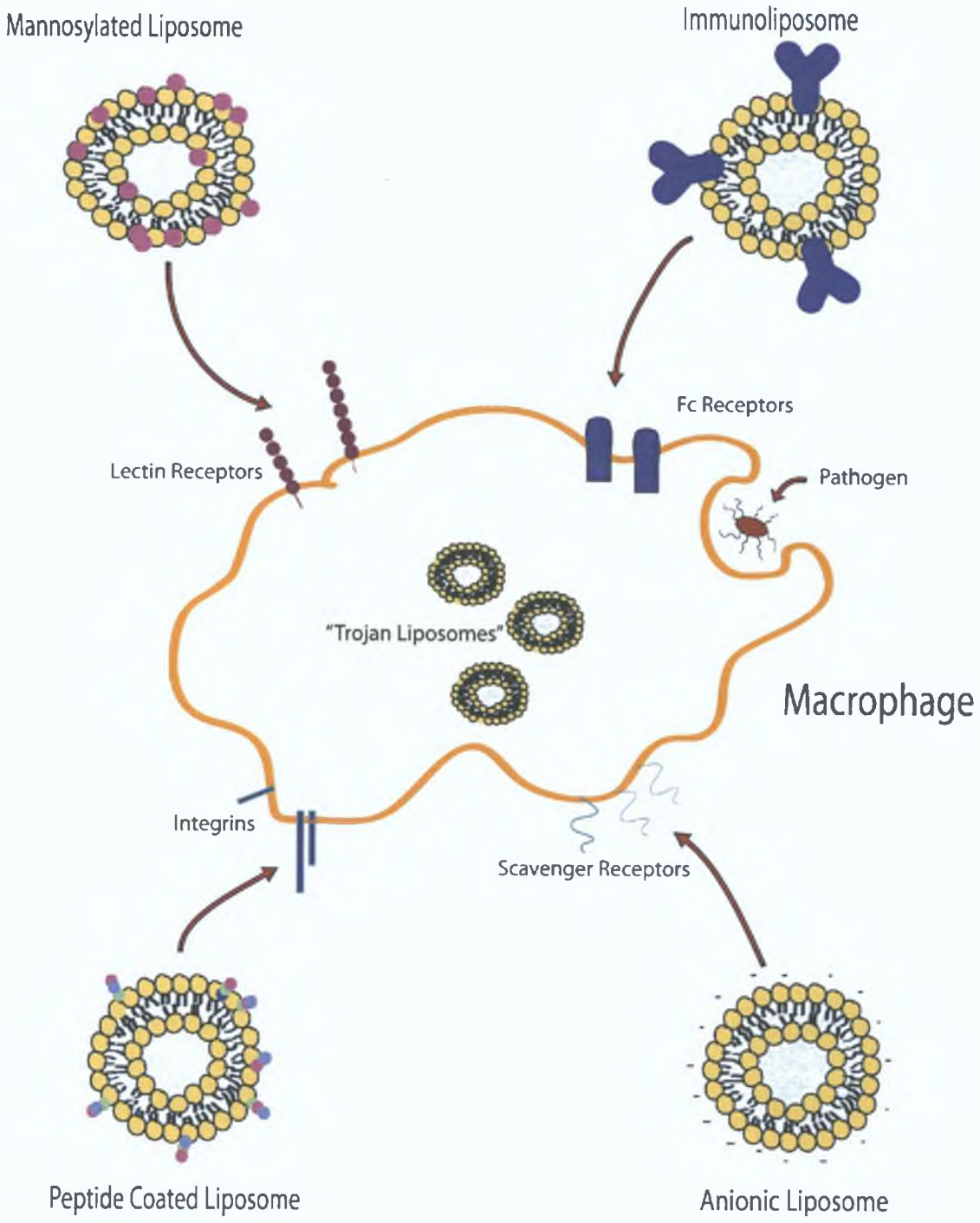


Figure 2.3: Summary of liposomal targeting strategies to macrophages [117]

**Table 2.2 Summary of Ligand Based strategies for Monocyte/Macrophage Liposomal Targeting**

| Ligand | Active | Disease | Reference |
|---|---|---|---|
| **Anionic Lipids** | Dexamethasone | Atherosclerosis | [118] |
| | SLPI | Inflammatory Lung Disease | [119] |
| | Bisphosphonates | Restinosis | [120] |
| | Rifampicin | Tuberculosis | [121] |
| | Dideoxycytidine-5'-triphosphate | HIV | [122] |
| | Clarithromycin | Mycobacterium avium infection | [123] |
| **Peptides** | | | |
| Muramyl tripeptide (MTP) | MTP-phosphotidylethanolamine | Osteosarcoma | [124] |
| Arg-Gly-Asp (RGD) | diclofenac sodium (model drug) | Cerebrovascular disease | [125] |
| **Antibodies** | | | |
| Anti-VCAM-1 | Prostaglandins | Atherosclerosis | [126] |
| Anti-CC52 | - | Colon Cancer | [127] |
| anti-CC531 | - | Colon Adenocarcinoma | [128] |
| Anti-CD11c/DEC-205 | tumour antigen (OVA) | Cancer | [129] |
| **Lectins** | | | |
| Mann-C4-Chol | dexamethasone palmitate | Inflammatory Lung Disease | [130] |
| $Man_2DOG$ | - | - | [131] |
| Aminophenyl-α-D-mannopyranoside doxorubicin | | experimental visceral leishmaniasis | [132] |
| | Ciprofloxacin | respiratory infection | [133] |
| Man3-DPPE | OVA | | [134] |
| | - | Gastric cancer | [135] |
| **Other Ligands** | | | |
| Maleylated bovine serum albumin (MBSA) | | | [121] |
| *O*-steroly amylopectin (*O*-SAP) | | | [121] |
| Fibronectin | | | [107] |
| Galactosyl | | | [107] |

### 2.1.4 Liposome Nebulisation

A means of effective *in vivo* targeting is critical. Liposomes have been used in the pulmonary delivery of antioxidants, anti-microbial compounds, proteins, peptides and DNA in animals and humans [89] but there are no products on the market. For effective pulmonary delivery it is necessary to attain a high respirable fraction (i.e. the amount of drug reaching the deep lungs). In order to achieve this, various device technologies are available including metered dose inhalers (MDI), dry powder inhalers (DPI) and nebulisers. Other factors affecting deep lung deposition include particle size (or aerodynamic diameter), patient inhalation pattern, oral or nasal inhalation, airflow obstruction and patient disease severity [136].

Pressurized MDIs (pMDIs) contain drug in suspension or solution in a liquefied propellant such as hydrofluoroalkanes (HFAs) which forms a high velocity aerosol when actuated [136] and are the most widely used inhalers for asthma and COPD [136]. Phospholipids are poorly soluble in HFA propellants [89]. DPIs deliver a fine powder and can be breath actuated but liposome formulations must be prepared as dry powders [89] involving increased development time and manufacturing complexity. Nebulisers such as air-jet, ultrasonic and vibrating mesh nebulisers on the other hand, deliver liquid suspensions in the form of a mist or aerosol which can vary in droplet size suitable for liposome aerosolisation. The particulate aerodynamic diameter and droplet size are crucial for efficient deep lung deposition of powdered and liquid based formulations respectively. *Ex vivo* testing of aerosol delivery can be carried out in lung models including twin-impinger systems [89], cascade impactors [137] and mathematical [138, 139] models as *in vivo* predictors of drug deposition patterns, respirable doses, formulation stability and device efficiency. Table 2.3 summarises the main types of nebulisers currently available.

Although nebulisation appears to be the simplest method of liposome delivery to the lungs from a formulation perspective, damage to nucleic acids and liposome destabilisation has been reported [89]. To date nebulisation of liposomes encapsulating DNA [140-144], isoniazid [145], salbutamol sulphate [146, 147], rSLPI [119], peptides [148], insulin [149] and rifampicin [150] have been assessed for inhalation but as of yet, siRNA loaded liposomes have not been evaluated. However nebulisation of particles associated with siRNA including hexanediol diacrylate cross-linked oligoethylenimine (OEI-HD) [151], chitosan [152] and polyesters [153] have been assessed. Recently, Steele *et al.* (2011) nebulized anti-luciferase siRNA complexed with OEI-HD at various weight ratios with an AeroNeb nebuliser and noted significant changes in polyplex size at certain weight ratios [151]. Furthermore *in vitro* knockdown via these polyplexes was used to determine siRNA functionality following nebulisation as nebulisation has the potential to cause siRNA nicking, polyplex re-organisation or splitting of the siRNA duplex post-nebulisation [151].

**Table 2.3: Comparison of the main types of nebulisers** [136]

| | Jet | Ultrasonic | Vibrating mesh |
|---|---|---|---|
| ***Features*** | | | |
| Power source | Compressed gas or electrical mains | Electrical mains | Batteries or electrical mains |
| Portability | Restricted | Restricted | Portable |
| Treatment time | Long | Intermediate | Short |
| Output rate | Low | Higher | Highest |
| Residual Volume | 0.8 - 2.0 ml | Variable but low | ≤ 0.2 ml |
| ***Environmental contamination*** | | | |
| Continuous use | High | High | High |
| Breath-activated | Low | Low | Low |
| Performance variability | High | Intermediate | Low |
| ***Formulation characteristics*** | | | |
| Temperature | Decreases | Increases | Minimum change |
| Concentration | Increases | Variable | Minimum change |
| Suspensions | Low efficiency | Poor efficiency | Variable efficiency |
| Denaturation | Possible | Probable | Possible |
| Cleaning | Required, after single use | Required, after multiple use | Required, after single use |
| Cost | Very low | High | High |

### 2.1.5 Chapter Aims

siRNA targeting to alveolar macrophages using liposomes provides both anatomical (nebulisation) and cellular targeting using DOPS and mannosylated liposomes. DOPS liposomes can target macrophage SRs. DOPS liposome targeting to alveolar macrophages has been previously shown in work by us [154]. Mannosylated liposomes provide alveolar macrophage targeting via the macrophage mannose receptor. Therefore, this chapter aims to:

- synthesise mannosylated cholesterols
- prepare and characterise a range of liposomes (anionic and mannosylated) for alveolar macrophage targeting
- optimise encapsulation of siRNA by neutral, anionic and mannosylated liposomes
- determine siRNA-liposome suitability for inhalation using nebulisers

## 2.2 Materials

1,2-Dioleoyl-3-trimethylammonium-propane (DOTAP), M.W. 698.542, Avanti Polar Lipids Inc.
1,2-dioleoyl-sn-glycero-3-phosphocholine (DOPC), M.W. 786.15, Avanti Polar Lipids Inc.
1,2-dioleoyl-sn-glycero-3-phosphoethanolamine-N-(lissamine rhodamine B sulfonyl) (PE-rhodamine), M.W. 1319.753, Avanti Polar Lipids Inc.
1,2-dioleoyl-sn-glycero-3-phospho-L-serine (DOPS), M.W. 810.025, Avanti Polar Lipids Inc.
1,2-distearoyl-sn-glycero-3-phosphocholine (DSPC), M.W. 790.145, Avanti Polar Lipids Inc.
2% bisacrylamide, Sigma Aldrich
40% acrylamide, Sigma Aldrich
Acetic anhydride, Sigma Aldrich
Acetone, Sigma Aldrich
AeroNeb® Pro, Aerogen
AllStar Negative Control siRNA, AlexaFluor 488 (Qiagen)
Ammonium persulfate (AP), Sigma Aldrich
Anhydrous magnesium sulphate, Sigma Aldrich
Avanti ® Mini-Extruder, Avanti Polar Lipids Inc.
Blue/orange 6x loading dye, Promega
Celite, Sigma Aldrich
Centristart spin filters 100,000 MW, Sartorius
Charcoal, Sigma Aldrich
Chloroacetonitrile, Sigma Aldrich
Chloroform, Fisher Scientific
Cholesterol, M.W. 386.66, Avanti Polar Lipids Inc.
Dichloromethane (DCM), Sigma Aldrich
Disposable Capillary Cells, Malvern
D-Mannose, Sigma Aldrich
Drain disc polyethylene 10mm, Whatman
Ethylenediaminetetraacetic acid (EDTA), Sigma Aldrich
Filter circle nucleopore 0.1, 0.2, 0.4 and 1µm polycarbonate membrane 19mm, Whatman
Filter circle nucleopore 0.2µm polycarbonate membrane 25mm, Whatman
G:BOX, Syngene
GelStar, Lonza
GIBCO PBS, Invitrogen
Iodine, Sigma Aldrich
LabAssay (TM) Cholesterol, Wako Pure Chemical Industries, Ltd.
LabAssay (TM) Phopholipid C, Wako Pure Chemical Industries, Ltd.
Labconco Freeze Drier, Labconco
Lipex 10ml Thermo-barrel Extruder, Northern Lipids
Methanol, Fisher Scientific
Methanol, Sigma Aldrich
N,N,N',N'-Tetramethylethylenediamine (TEMED), Fluka

NanoDrop 1000 Spectrophotometer

PARI Air-Jet Nebuliser, PARI

Phosphate buffered saline (PBS), GIBCO

Polyethylenimine (PEI), average MW 25kDa, Sigma Aldrich

Potassium bicarbonate, Sigma Aldrich

Protamine sulphate, for biochemistry, Merck

Pyridine, Sigma Aldrich

Quant iT RiboGreen Assay, Invitrogen

Rotary Evaporator, Büchi Rotavapor R200

siRNA (siCONTROL non-targeting and siGLO RISC-free) Dharmacon

siRNA marker, New England Biolabs

siRNA, Dharmacon

Sodium bicarbonate, Sigma Aldrich

Sodium bisulfite, Sigma Aldrich

Sodium Chloride (NaCl), Sigma Aldrich

Sodium methoxide, Sigma Aldrich

Sodium sulphate, Sigma Aldrich

Sodium thiosulphate, Sigma Aldrich

Solid-glass beads borosilicate, diameter 1 mm, Sigma Aldrich

Sorvall Discovery M120SE Centrifuge, Sorvall

Tertiary-Butanol (t-Butanol), Fluka

Thiourea, Sigma Aldrich

Triethylamine, Sigma Aldrich

Trifluoroacetic acid, Sigma Aldrich

Triton X-100, Sigma Aldrich

Ultrapure TBE buffer, Invitrogen

Wallac Victor2 1420 Multilabel Counter (Perkin Life Sciences)

## 2.3 Methods

### 2.3.1 Synthesis of Mannosylated Cholesterol Derivatives

Cholesten-5-yloxy-*N*-(4-((1-imino-2-α-thioglycosylethyl)amino)butyl)formamide (Mann-C4-Chol) and its C2 and C6 derivatives were synthesized in house by Colin Burke supervised by Dr. James Barlow. Briefly 2-imino-2-methoxyethyl-1-thio-α-D-mannopyrannoside was synthesized from mannose in a five step procedure (Figure 2.4) while cholesterol chloroformate was reacted with N-Boc spacers in a two-step reaction (Figure 2.5). Cholesterol chloroformate and 2-imino-2-methoxyethyl-1-thio-α-D-mannopyrannoside were then reacted to give Mann-Cn-Chol (Figure 2.6). Melting points were obtained using a Stuart Scientific SMP10 apparatus, and are uncorrected. Infrared Spectroscopy (IR) of test samples was performed on a Bruker Tensor 27 FTIR. Nuclear Magnetic Resonance (NMR) Spectroscopy was performed using a Bruker DPX400 instrument, at 400.13 MHz for proton ($^1$H) magnetic resonance and 100.61 MHz for carbon ($^{13}$C). All NMR samples were prepared in deuterised chloroform (chloroform-d). High Resolution Mass Spectroscopy (HRMS) was performed using a Micromass LCT instrument ($ES^+$ mode).

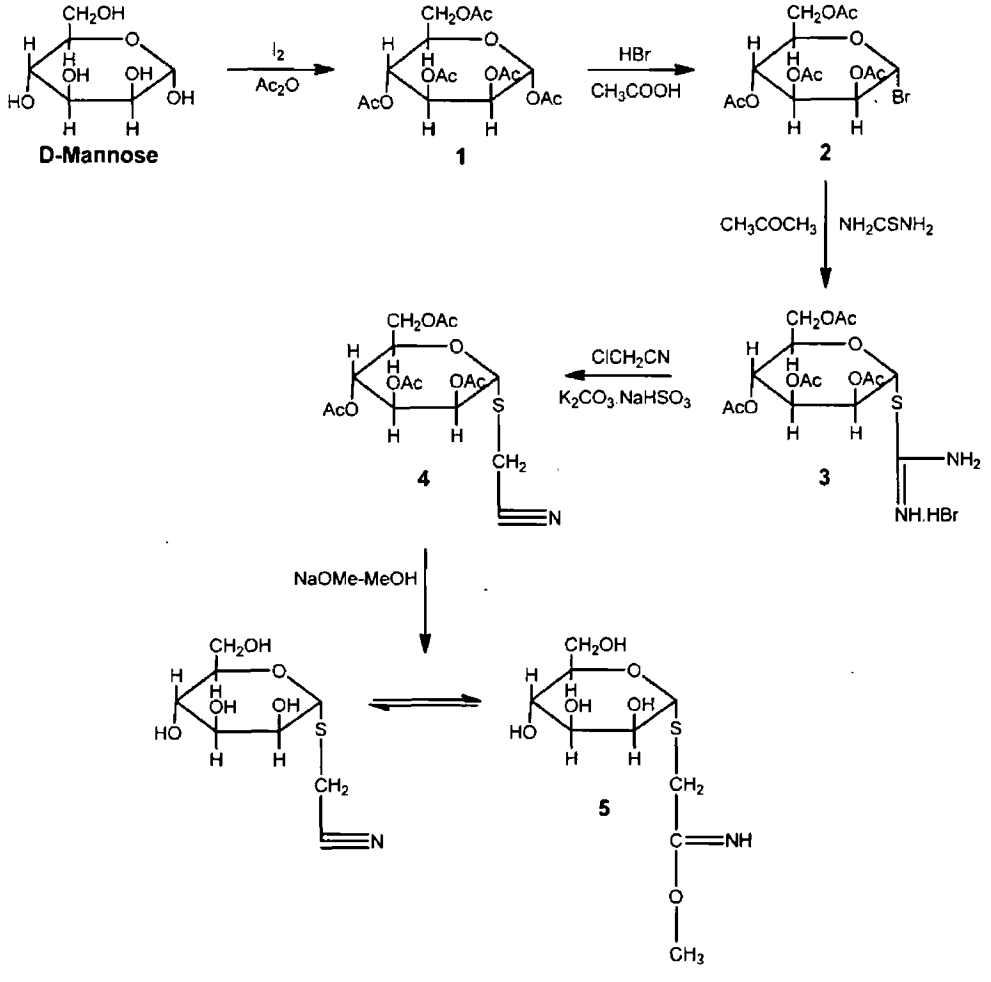


Figure 2.4: Schematic of the 5 step synthesis of the methyl imidate 2-imino-2-methoxyethyl-1-thio-α-D-mannopyrannoside (compound 5).

### 2.3.1.1 Synthesis of 2-imino-2-methoxyethyl-1-thio-α-D-mannopyrannoside

*D-Mannose Penta-acetate (1)*

D-Mannose (10g, 55 mmol) was dissolved in acetic anhydride (40ml, 423 mmol). Iodine (0.5g, 2 mmol) dissolved in acetic anhydride (2ml, 2 mmol) was added dropwise. The reaction was stirred under an argon atmosphere in an ice bath for 3.5 hours. Dichloromethane (DCM) was added and the mixture was washed twice with sodium thiosulphate (10% w/v). The organic layer was collected and washed twice with sodium bicarbonate (20% w/v). The organic layer was then collected, washed with saturated brine and dried with anhydrous magnesium sulphate. This was then concentrated *in vacuo* to D-mannose penta-acetate. Yield 83%; IR (potassium bromide (KBr), v) 3474, 2967, 2257 $cm^{-1}$. $^1H$ NMR: $\delta_{ppm}$ = 6.11 (d, *J*=1.7Hz, 1H), 5.35 (m, 2H), 5.28 (m, 1H), 4.30 (dd, *J*=4.8 and 12.3Hz, 1H), 4.12 (dd, *J*=2.5 and 12.4Hz, 1H), 4.07 (m, 1H), 2.20 (s, 3H, OAc), 2.19 (s, 3H, OAc), 2.12 (s, 3H, $OacCH_3$), 2.07 (s, 3H), 2.03 (s, 3H).

*2,3,4,6-tetra-O-acetyl-α-D-mannopyranosyl Bromide (2)*

Compound 1 (17.99g, 46 mmol) was dissolved in anhydrous DCM (40ml, 620 mmol) and 33% hydrogen bromide (HBr) in acetic acid (30ml, 167 mmol) was added. The reaction was stirred under an argon atmosphere at room temperature for 24 hours. The completed reaction was diluted with DCM (40ml) and washed with cold water, sodium bicarbonate 20% twice and cold water. The organic layer was dried with anhydrous magnesium sulphate and concentrated *in vacuo* to an oil. Yield 64%; $^1H$ NMR: $\delta_{ppm}$ = 6.23 (brs, H1), 5.65 (dd, *J*=3.5 and 10.1Hz, 1H), 5.38 (dd, *J*=3.5 and 1.5Hz, 1H), 5.31 (t, *J*=10.3Hz, H-4, 1H) 4.27 (dd, *J*=12.5 and 4.7hz, 1H), 4.16 (ddq, *J*=10.2, 4.8, 2.2Hz, 1H), 4.07 (dd, *J*=12.2 and 2.1Hz, 1H), 2.11 (s, 3H), 2.05 (s, 3H), 2.01 (s, 3H), 1.95 (s, 3H).

*2-S-(2,3,4,6-tetra-O-acetyl-α-D-mannopyranosyl)-2-thiopseudourea Hydrobromide (3)*

Compound 2 (12.65g, 30 mmol) was dissolved in dry acetone (25ml) and mixed with 1.1 equivalents of thiourea (2.48g, 30 mmol). The reaction was boiled and refluxed under an argon atmosphere for 2 hours. The resulting crude mixture was concentrated *in vacuo*.

*Cyanomethyl 2,3,4,6-tetra-O-acetyl-1-thio-α-D-mannopyrannoside (4)*

Compound 3 (13.65g, 27 mmol) was dissolved in a 1:1 (v/v) water:acetone mixture (25ml). To a stirred solution, chloroacetonitrile (6.83ml, 108 mmol, 4 equivalents) was added dropwise, then sodium bisulfite (4.37g, 42 mmol, 2 equivalents) and finally potassium bicarbonate (4.49g, 32.5 mmol, 1.2 equivalents) were added. The solution was stirred at room temperature for 2 hours at which point 100ml of ice water was added to the reaction mixture and stirred for a further 2 hours. The resulting precipitate was suction filtered. The air-dried filtrate was dissolved in a minimum of boiling methanol. The methanolic solution was stored at 4°C overnight to promote

crystallisation. The crystals formed were then filtered off and vacuum dried. In some instances little precipitate crystallised out of the methanolic solution and the following purification was performed. The methanolic solutions were mixed with water. The water methanol mix was washed with chloroform (60ml) three times. The chloroform layers were combined and washed with 1M NaCl twice. The chloroform layers were then dried with sodium suphate and decolourised with charcoal. The solution was then vacuum filtered through celite. The solution dried using rotary evaporation. The resulting solid was dissolved in boiling methanol. The resulting crystals were filtered off and dried by rotary evaporation. The cyanomethyl crystals were stored at -10°C. Yield: 44% to 27.4%. IR (KBr, v) 3454, 2970, 2931, 2852, 2257 $cm^{-1}$. $^{1}H$ NMR: $\delta_{ppm}$ = 5.40 (d, *J*=1.2Hz, 1H), 5.27 – 5.32 (m, 2H, 2 x C**H**), 5.13 (dd, *J*=10.0, 3.2Hz, 1H, CH), 4.24 -4.32 (m, 2H), 4.10 (dd, *J*=12.0Hz, 1.4Hz, 1H), 3.25 (d, *J*=17.1Hz, 1H, H of $CH_2$), 3.41 (d, *J*=17.1Hz, 1H, H of $CH_2$) 2.13 (s, 3H), 2.05 (s, 3H), 2.00 (s, 3H), 1.94 (s, 3H). $^{13}C$ NMR: $\delta_{ppm}$ = 169.6, 169.7, 169.8, 170.6 (**C**=O), 115.6 (**C**N), 82.4, 70.0, 69.6, 69.3, 65.8, 62.0 (**C**H), 62.0 (**C**$H_2$O), 20.83, 20.76, 20.69, 20.6 (**C**$H_3$), 15.5 (S**C**$H_2$). Melting Point: 136°C.

*2-imino-2-methoxyethyl-1-thio-α-D-mannopyrannoside (5)*

Compound 4 (0.1M) was dissolved in anhydrous methanol and reacted with 0.01M sodium methoxide solution under an argon atmosphere at room temperature. The mix was reacted for 48 hours and then concentrated *in vacuo* and stored at -10°C. $^{1}H$ NMR (400MHz, $CDCl_3$, 25°C): $\delta_{ppm}$ = 5.35 (d, 1H, *J*=0.4Hz, OCHS), 5.18 (d, *J*=0.74Hz, OCHS).

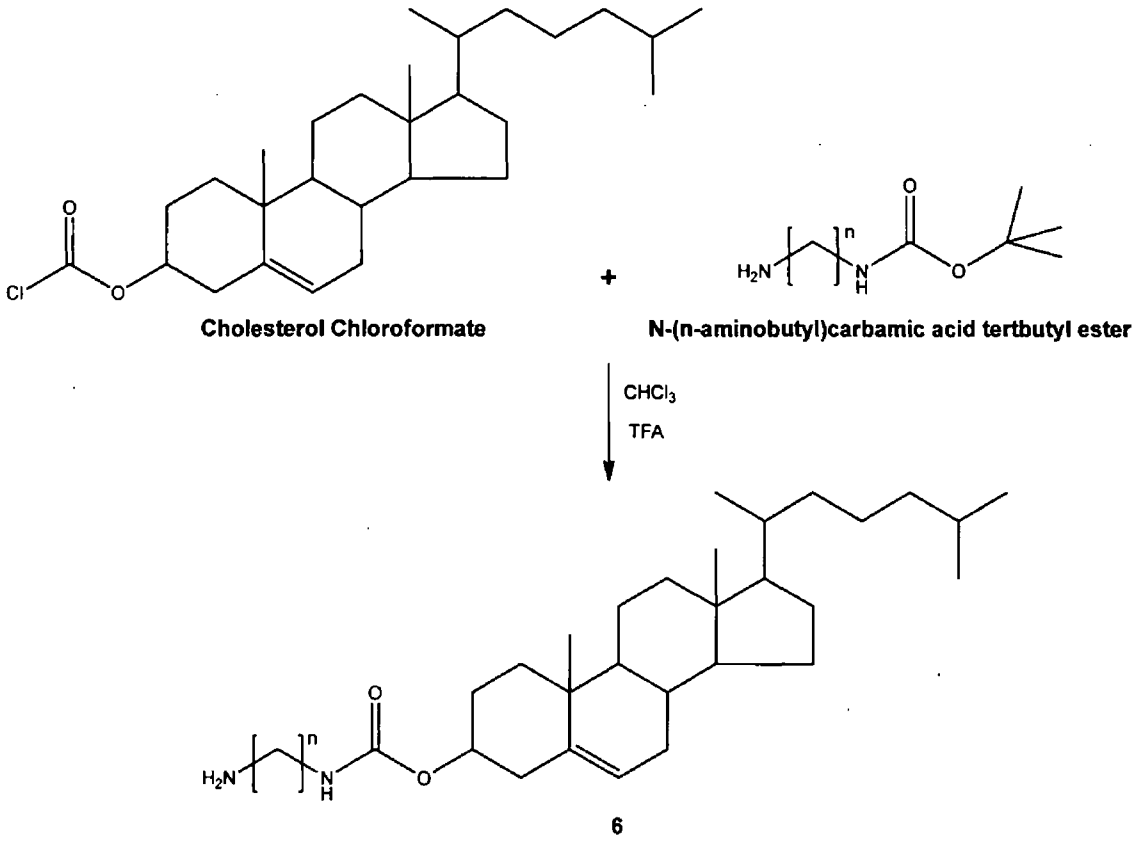


Figure 2.5: Schematic of *N*-(n-aminobutyl)-(cholesten-5-yloxy)formamide synthesis (compound 6). Cholesteryl chloroformate is reacted with *N*-(n-aminobutyl)carbamic acid tertbutyl ester (where n = 2, 4 or 6)

### 2.3.1.2 Synthesis of N-(4-aminobutyl)-(cholesten-5-yloxy)formamide, N-(2-aminobutyl)-(cholesten-5-yloxy)formamide and N-(6-aminobutyl)-(cholesten-5-yloxy)formamide

*N-(4-aminobutyl)-(cholesten-5-yloxy)formamide (6a)*

Cholesteryl chloroformate (2.64g, 5.8 mmol) was reacted with a 1.1 equivalent of *N*-(4-aminobutyl)carbamic acid tertbutyl ester (6.4 mmol) in anhydrous chloroform (10ml) for 24 hours at room temperature under an argon atmosphere. This was then purified using column chromatography. The purified intermediate produced a 42.4% yield. IR (KBr, v) 3330, 2948, 2853, 2719, 2356 $cm^{-1}$. $^1H$ NMR (400MHz, $CDCl_3$, 25°C): $\delta_{ppm}$ = 5.30 (m, H-1 C=CH), 4.61, 4.52 (broad s, 1H, NH), 4.44 (m, 1H, OCH), 3.15 (m, 4H, 2x$NCH_2$), cholesterol skeleton (2.34 -0.59). $^{13}C$ NMR (100.61 MHz, $CDCl_3$) $\delta_{ppm}$ = 156.1 (C=O), 156.0 (C=O), 122.5 (C), 74.5 (CH), 56.6 (CH), 56.1 (CH), 49.8 (CH), 42.3 (C), 41.2 (C), 39.7 ($CH_2$), 39.5 ($CH_2$), 37.0 ($CH_2$), 36.6 (C), 36.2 (C), 35.8 (CH), 31.9 ($CH_2$), 31.8 (CH), 28.4 ($CH_3$), 28.2 ($CH_2$), 28.1 ($NCH_2$), 28.0 (CH), 24.3 ($CH_2$), 23.8 ($CH_2$), 22.5 ($CH_3$), 21.0 ($CH_2$), 19.3 ($CH_3$), 18.7 ($CH_3$), 11.8 ($CH_3$). Anal Calc. for $C_{37}H_{64}N_2O_9$ C, 73.95. H, 10.73. N, 4.66. Found: C, 72.18, H, 10.56. N, 4.33. Melting point: 112°C. The intermediate was deprotected using an excess of trifluoroacetic acid (1.6ml, 21.5 mmol) in anhydrous chloroform for 24 hours at room temperature under an argon atmosphere and then concentrated *in vacuo*.

*N-(2-aminobutyl)-(cholesten-5-yloxy)formamide (6b)*

Cholesteryl chloroformate (3.5g, 7.8 mmol) was reacted with *N*-(2-aminobutyl)carbamic acid tertbutyl ester (8.6 mmol). The intermediate was purified using column chromatography. The purified intermediate produced a 51.4% yield. $^{1}$H NMR (400MHz, $CDCl_3$, 25°C): $\delta_{ppm}$ = 5.31 (m, H-1 C=CH), 4.88, 4.77 (broad s, 1H, NH), 4.42 (m, 1H, OCH), 3.22 (m, 4H, 2x$NCH_2$), cholesterol skeleton (2.32 -0.6). $^{13}$C NMR (100.61 MHz, $CDCl_3$) $\delta_{ppm}$ = 122.5 (C), 74.1 (CH), 56.6 (CH), 56.1 (CH), 49.8 (CH), 42.3 (C), 41.2 (C), 39.7 ($CH_2$), 39.5 ($CH_2$), 37.0 ($CH_2$), 36.6 (C), 36.2 (C), 35.8 (CH), 31.9 ($CH_2$), 31.8 (CH), 28.4 ($CH_3$), 28.2 ($CH_2$), 28.1 ($NCH_2$), 28.0 (CH), 24.3 ($CH_2$), 23.8 ($CH_2$), 22.5 ($CH_3$), 21.0 ($CH_2$), 19.3 ($CH_3$), 18.7 ($CH_3$), 11.8 ($CH_3$). Anal Calc. for $C_{35}H_{60}N_2O_4$ C, 73.38 H, 10.56. N, 4.89. Found: C, 73.74, H, 10.66. N, 4.92. Melting point: 152°C.

The intermediate was deprotected using an excess of trifluoroacetic acid (1.6ml, 21.5 mmol) in anhydrous chloroform for 24 hours at room temperature under an argon atmosphere and then concentrated *in vacuo*.

*N-(6-aminobutyl)-(cholesten-5-yloxy)formamide (6c)*

Cholesteryl chloroformate (2g, 4.5 mmol) was reacted with *N*-(6-aminobutyl)carbamic acid tertbutyl ester (4.9 mmol) and this intermediate was then purified using column chromatography producing a 63.7% yield. $^{1}$H NMR (400MHz, $CDCl_3$, 25°C): $\delta_{ppm}$ = 5.39 (m, H-1 C=CH), 4.65, 4.54 (broad s, 1H, NH), 4.50 (m, 1H, OCH), 3.15 (m, 4H, 2x$NCH_2$), cholesterol skeleton (2.4 - 0.67). $^{13}$C NMR (100.61 MHz, $CDCl_3$) $\delta_{ppm}$ = 156.1 (C=O), 156.0 (C=O), 122.5 (C), 74.0 (CH), 56.7 (CH), 56.1 (CH), 42.3 (C), 40.7 ($CH_2$), 39.7 ($CH_2$), 39.6 ($CH_2$), 36.9 ($CH_2$), 36.5 (C), 36.2 (C), 35.8 (CH), 31.9 ($CH_2$), 31.8 (CH), 28.4 ($CH_3$), 28.2 ($CH_2$), 28.1 ($NCH_2$), 28.0 (CH), 24.3 ($CH_2$), 23.8 ($CH_2$), 22.5 ($CH_3$), 21.0 ($CH_2$), 19.3 ($CH_3$), 18.7 ($CH_3$), 11.8 ($CH_3$). Anal Calc. for $C_{39}H_{68}N_2O_4$ C, 73.47. H, 10.90. N, 4.45. Found: C, 73.98, H, 10.92. N, 4.27. Melting point: 63°C.

The intermediate was deprotected using an excess of trifluoroacetic acid (1.6ml, 21.5 mmol) in anhydrous chloroform for 24 hours at room temperature under an argon atmosphere and then concentrated *in vacuo*.

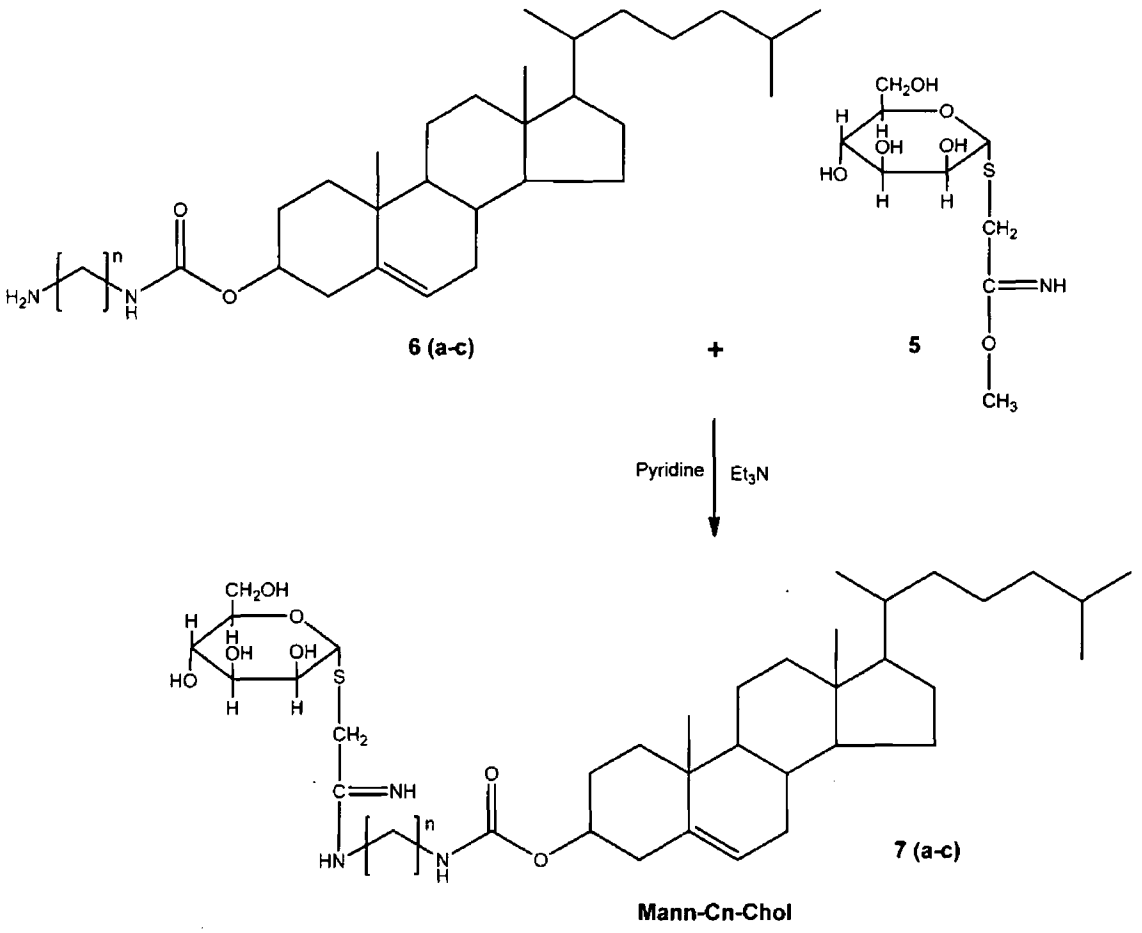


Figure 2.6: Schematic of the reaction of *N*-(n-aminobutyl)-(cholesten-5-yloxy)formamide (compound 6) and 2-imino-2-methoxyethyl-1-thio-α-D-mannopyrannoside (compound 5) to yield Mann-Cn-Chol (where n = 2, 4 or 6)

### 2.3.1.3 Synthesis of Cholesten-5-yloxy-N-(4-((1-imino-2-α-thioglycosylethyl) amino) butyl) formamide (Mann-C4-Chol) (7a)

Compound 5 (0.75g, 3.7 mmol, 2.5 equivalents) was dissolved in pyridine containing triethylamine (1.5mmol). Compound 6a (1g, 2mmol) was added and the solution was reacted for 24 hours at room temperature under an argon atmosphere. The reaction mixture was concentrated in vacuo. Mann-C2-Chol and Mann-C6-Chol were synthesised in a similar manner with *N*-(2-aminobutyl)-(cholesten-5-yloxy)formamide (compound 6b) and *N*-(6-aminobutyl)-(cholesten-5-yloxy)formamide (compound 6c) respectively replacing *N*-(4-aminobutyl)-(cholesten-5-yloxy)formamide (compound 6a) in the reaction.

### 2.3.1.4 Purification and Characterisation of Mannosylated Cholesterol Derivatives

Mann-C2-Chol (compound 7b), Mann-C4-Chol (compound 7a) and Mann-C6-Chol (compound 7c) were dialyzed for 48 hours. Briefly, dialysis tubing was prepared to remove glycerol and sulphur compounds by placing cut tubing in bicarbonate solution (2% w/v sodium bicarbonate ($NaHCO_3$) and 1mM ethylenediaminetetraacetic acid (EDTA), pH 8.0) at 70°C for 10 minutes and rinsed with distilled water ($dH_20$). The tubing was placed in 1mM EDTA (pH 8.0) at 70°C for 10 minutes followed by rinsing in $dH_20$. Mann-C2-Chol, Mann-C4-Chol and Mann-C6-Chol were

suspended in $dH_20$ and dialyzed against $dH_20$ for 48 hours. Water was replaced with fresh $dH_20$ after 24 hours. The compounds were then lyophilized for 48 hours and underwent analysis by IR spectroscopy, MS and NMR, to confirm synthesis and determine purity. IR spectra were recorded as KBr discs on a Mattson Genesis II CSI FTIR spectrometer in the 4000-400 $cm^{-1}$ region. NMR spectra were acquired with a Bruker Advance DPX-400 instrument.

Mann-C2-Chol: IR (KBr, v): 3354, 2936, 2868 $cm^{-1}$. $^1$H-NMR (400 MHz, $CDCl_3$): 0.6–1.9 (m, cholesteryl skeleton), 2.2-2.3 (m, N-$CH_2$), 3.2 (s, N-$CH_2$). HR-ESI-MS *m/z* ($[M-H]^+$): calculated for $C_{38}H_{65}N_3O_7S$ 708.00 found 708.4645. Mann-C4-Chol: IR (KBr, v): 3351, 2933, 2868 $cm^{-1}$. $^1$H-NMR (400 MHz, $CDCl_3$): 0.6–2.0 (m, cholesteryl skeleton), 3.0 (broad s, N-$CH_2$). HR-ESI-MS *m/z* ($[M-H]^+$): calculated for $C_{40}H_{69}N_3O_7S$ 736.49 found 736.5215. Mann-C6-Chol: IR (KBr, v): 3345, 2933, 2868 $cm^{-1}$. $^1$H-NMR (400 MHz, $CDCl_3$): 0.6–1.9 (m, cholesteryl skeleton), 2.2 (s, N-$CH_2$), 3.0 (broad s, N-$CH_2$). HR-ESI-MS *m/z* ($[M-H]^+$): calculated for $C_{42}H_{73}N_3O_7S$ 764.11 found 764.5182.

### 2.3.2 siRNA Condensation and Complex Characterisation

siRNA was complexed with DOTAP, 25kDa PEI and protamine at various weight or nitrogen/phosphate (N/P) ratios in order to condense the siRNA prior to encapsulation and improve siRNA encapsulation efficiency by liposomes. N/P ratio is calculated using the formula in Table 2.4 with repeating units of 698.55g/mol and 43.1g/mol for DOTAP and PEI respectively. Each repeating unit corresponds to one mole of nitrogen. Protamine sulphate was of unknown molecular weight. Consequently weight ratios were used to prepare siRNA protamine complexes.

**2.4: Table: N/P ratio calculation**

$$\frac{[N]}{[P]} = \frac{\text{Number of moles of Nitrogen in DOTAP or PEI}}{\text{Number of moles of Phosphate in siRNA}}$$

For optimisation of siRNA condensation, complexes were prepared by diluting 1µg siRNA in diethylpyrocarbonate (DEPC)-treated RNase free water up to a final volume of 25µl. The cationic component was prepared separately in 25µl of RNase free water. Following a 5 minute incubation at room temperature siRNA and the cationic reagent were mixed by pipetting up and down at least 5 times and incubated at room temperature for 20 minutes.

For protamine and PEI, stock solutions of 1mg/ml in DEPC-treated RNase free water was prepared and diluted appropriately in 25µl of RNase free water. DOTAP liposomes were prepared by dehydration rehydration with 10mg of DOTAP dissolved in Folch and rehydrated in 1ml of RNase free water following solvent evaporation (Liposome Preparation 2.3.3). DOTAP

suspensions were then passed 10 times through 100nm pore filters using an Avanti® syringe mini-extruder. DOTAP liposomes were then diluted appropriately in RNase free water.

An alternative method for siRNA-DOTAP complexation was also used. 1mg/ml DOTAP solutions were prepared by dissolving the lipid in tertiary-butanol. A suitable amount of DOTAP was added to a fresh tube and brought up to 200µl with *tertiary*-butanol (*t*-butanol). Separately 1µg siRNA was diluted in RNase-free water and brought up to a final volume of 200µl. Diluted siRNA was added dropwise and mixed with DOTAP in *t*-butanol. Mixtures were frozen at -80°C and then lyophilized overnight. The lyophilised pellet was rehydrated in 50µl of RNase free water with vortexing.

#### 2.3.2.1 Particle size and Zeta Potential

Complex size was determined by dynamic light scattering. Zeta potential was measured by laser Doppler electrophoresis (LDE) using the Smoluchowski theory. Complexes were diluted 50 times in ultrapure water and 1ml was loaded into a disposable capillary cell. Sizes and zeta potentials were determined using a zetasizer (nanoseries, Malvern) with 5 measurements acquired per sample.

#### 2.3.2.2 Gel Retardation Assay

Gel retardation assays were used to determine the minimum amount of cationic reagent necessary to form neutralised complexes. A 20% non-denaturing polyacrylamide (19:1 acrylamide:bisacrylamide) Tris-borate-EDTA (TBE) gel was prepared with 30% polyacrylamide, TBE buffer, 10% ammonium persulfate (AP), de$H_2O$ and *N,N,N',N'*-Tetramethylethylenediamine (TEMED) with a 4% stacking gel using the recipe in Table 2.5. The stacking gel was prepared with 30% polyacrylamide, 10x TBE buffer, 10% AP, de$H_2O$ and TEMED. Blue/orange 6x loading dye (Promega) was used to track gel migration. Loading dye contains 0.4% orange G, 0.03% bromophenol blue, 0.03% xylene cyanol FF, 15% Ficoll® 400, 10mM Tris-hydrochloride (HCl) (pH 7.5) and 50mM EDTA (pH 8). In a 20% polyacrylamide gel bromophenol blue migrates equivalent to 12bp double stranded DNA (dsDNA) while xylene cyanol migrates to the same point as 45bp dsDNA. Complexed siRNA is retarded in the wells and unable to enter the gel. 100ng of siRNA marker, free siRNA and complexed siRNA were mixed with loading dye and loaded onto 20% polyacrylamide TBE gels and run at 100V for 90 minutes. Gels were post-stained with GelStar and visualisation was obtained using a GBox.

**Table 2.5: 20% Polyacrylamide TBE gel recipe**

| Ingredient | 4% Stack Gel Total volume 8 ml | 20% Running Gel Total volume 20 ml |
|---|---|---|
| **30% Polyacrylamide** | 800 µl | 4.75ml |
| **10x Ultrapure TBE buffer** | 800 µl | 2 ml |
| **10% Ammonium Persulfate** | 36 µl | 200 µl |
| **Deonized Water** | 6 ml | 7.8 ml |
| **TEMED** | 8 µl | 10 µl |

#### 2.3.2.3 Fluorescence Quenching Assay

Standard curves were prepared by diluting fluorescent siRNA (AlexFluor488-siRNA) in TE buffer to give a curve from 0 to 50ng/ml. 100µl of fluorescein tagged siRNA (fl-siRNA) at 0, 2, 10, 50 and 100ng/ml was added to wells of a black 96 well plate in triplicate. 5µl of complexes prepared in DEPC RNase free water with 1µg of siRNA and PEI were added to wells in triplicate in black 96 well plates and brought up to 100µl with TE buffer pH 7.5 or pH 12. Fluoresence was detected at 485nm excitation and 535nm emission wavelengths using a Wallac multiplate reader. Free siRNA was set as 100% fluorescence.

#### 2.3.2.4 RNA Quantification

Ribogreen RNA quantitation uses a fluorescent RNA stain that can provide 200- and 1000-fold greater sensitivity than ethidium bromide and ultraviolet based detection. Ribogreen reagent binds to RNA and fluoresces with maximum excitation and emission wavelengths of 500nm and 525nm respectively. Fluorescence can be detected at fluorescein wavelengths with detection as low as 1ng/ml RNA [155]. Briefly, 100µl of appropriately diluted samples and standards in TE buffer (10nM Tris-HCl, 1mM EDTA, pH 7.5) were added to wells of black 96 well plates in triplicate. Ribogreen reagent was diluted 1 in 2000 in TE buffer. 100µl of diluted ribogreen reagent was added to each well and protected from the light until read at fluorescein excitation and emission settings on a multiplate reader. Fluorescence of blank reagent was subtracted from sample and standard readings as recommended by the manufacturer.

Standard curves were prepared using ribosomal RNA (rRNA) standard supplied or siRNA of known concentration to give a curve from 0 to 50ng/ml. rRNA (16S and 23S rRNA from *Escherichia coli* (*E. coli*)) or siRNA was diluted in TE buffer and 100µl at 0, 2, 10, 50 and 100ng/ml was added to wells of a black 96 well plate in triplicate. 5µl of complexes prepared with 1µg of siRNA were added to wells in triplicate in black 96 well plates and brought up to 100µl with TE buffer. Ribogreen reagent was diluted 1 in 2000 and 100µl was added to each well. Fluoresence was detected at 485nm excitation and 535nm emission wavelengths using a Wallac multiplate reader. Free siRNA was set as 100% fluorescence.

TE buffer was adjusted to pH 12 and used to dilute ribogreen reagent in order to disrupt siRNA/PEI complexes [156-158] while 0.2% Triton-X100 and 1% sodium dodecyl sulfate (SDS) was added to wells after initial fluorescence detection and used to disrupt siRNA/DOTAP and siRNA/protamine complexes respectively [105, 159].

### 2.3.3 Liposome Preparation

Liposomes containing phospholipids, mannosylated cholesterol and cholesterol were formed by dehydration-rehydration. The liposome components (Table 2.11 and 2.12) were dissolved in a minimal volume of Folch (Chloroform:Methanol; 2:1 (v/v)) and mixed in a round bottomed flask. PE-Rhodamine (0.1% of mole ratio) was added to fluorescently label liposomes.

Solvents were evaporated at 40°C using a rotary evaporator (Büchi Rotavapor R200) and the lipid film was rehydrated in pH 7.4 Phosphate Buffered Saline (PBS; GIBCO). Following agitation or mixing with an equivalent mass of glass beads (1mm diameter) the system was allowed to hydrate overnight at 4°C resulting in large multi-lammellar liposome formation.

Passive encapsulation of siRNA was achieved by the rehydration of the thin lipid film with siRNA (0.5μM) or siRNA condensed with DOTAP, PEI or protamine (1pM) in PBS. Size reduction of rehydrated lipids was achieved by extrusion using a LIPEX™ Thermobarrel Extruder or Avanti® Mini-Extruder 10 times through a polycarbonate membrane filter with 200nm or 400nm pores. Two polycarbonate membrane filters were used for thermobarrel extrusions and one membrane with 4 drain discs or filter supports were used in syringe extrusions. Extrusion was carried out at 60°C for DSPC containing formulations and a room temperature for all other formulations.

### 2.3.4 Characterisation of Liposomes

#### 2.3.4.1 Particle Size and Zeta Potential

Liposome particle size and zeta potential were measured as described in 2.3.2.1.

#### 2.3.4.2 Transmission Electron Microscopy

For transmission electron microscopy (TEM) studies copper thin bar 200-mesh grids were coated with pioloform. Liposomes (2pl) were placed on the grid for 1 minute and blotted. The grid was negatively stained with a drop of (2% w/v) phosphotunstic acid (PTA) for 1 minute and again blotted followed by washing with deionized water. The grids were viewed the same day using a Hitachi H-7650 TEM.

#### 2.3.4.3 Liposome Quantification

Liposome quantification was determined by cholesterol assay (WAKO) and/or phospholipid assay according to the manufacturers' instructions, using a cholesterol oxidase and choline oxidase N-ethyl-N-(2-hydroxy-3-sulfopropyl)-3,5-domethoxyaniline (DAOS) method. A blue pigment is produced and absorbance measured. Standards and samples were prepared in triplicate using a clear 96-well plate.

##### 2.3.4.3.1 Cholesterol Assay

A cholesterol standard curve was prepared by adding a diluted cholesterol standard to wells to give 0, 1, 2, 4, 8 and 12 µg/well. Fluorescent and unlabelled liposomes (8µl) were added to wells in triplicate. 300µl of Chromagen reagent was added to each well. Chromagen reagent contains cholesterol esterase (1.6 units/ml), cholesterol oxidase (0.31 units/ml), peroxidise (HRP; 5.2 units/ml), DAOS (0.95 mmol/ml), 4-aminoantipyrin (0.19 mmol/ml) and ascorbate oxidase (4.4 units/ml). The plate was incubated at 37°C for 5 minutes. Cholesterol oxidase oxidises cholesterol producing hydrogen peroxide. In the presence of hydrogen peroxide oxidative condensation of DAOS and 4-aminoantipyrine occurs catalysed by peroxidise producing a blue pigment. Absorbance was read at 572nm using a Wallac multiplate reader.

##### 2.3.4.3.2 Phospholipid Assay

A phospholipid standard curve was prepared by adding provided phosopholipid standard (choline chloride) to wells to give 0, 2, 3, 6, 12 and 24 µg/well. Fluorescent and unlabelled DOPC containing liposomes (3µl) were added to wells in triplicate. 300µl of Chromagen reagent was added to each well. Chromagen phospholipid reagent contains phospholipase D (0.47 units/ml), choline oxidase (250 units/ml), peroxidise (POD; 4.2 units/ml) DAOS (0.77 mM), 4-aminoantipyrine (0.24 mM) and ascorbate oxidase (3.9 units/ml) in 50mM 2-(*N*-

morpholino)ethanesulfonic acid (MES) buffer (pH 7.5). The plate was incubated at 37°C for 5 minutes and absorbance read at 572nm using a Wallac multiplate reader.

#### 2.3.4.4 Encapsulation Efficiency

To determine siRNA encapsulation efficiency a number of methods were applied. Firstly, siRNA was quantified in liposome preparations before and after liposome disruption by triton-X using a Ribogreen assay. Standard curves were prepared as described in 2.3.2.4. Liposomes were diluted to give a maximum of 100ng/ml siRNA. 100µl of diluted liposomes was added to wells of a black 96-well plate in triplicate. 100µl of a diluted ribogreen reagent was added to each well and fluorescence was detected as previously described. 4µl of 10% Triton-X100 was added to each well. Plates were incubated for 20 minutes at room temperature followed by repeated fluorescence detection. Secondly, unencapsulated free or condensed siRNA was removed by ultracentrifugation or by ultrafiltration. To determine siRNA encapsulation efficiencies in condensed siRNA liposome preparation unencapsulated free and condensed siRNA was quantified by Quant-iT ribogreen assay. Liposome preparations were centrifuged three times at 45,000rpm for 40 minutes (DOPS liposomes) or 2 hours (DOPC and DSPC liposomes) under vacuum at 4°C using a Sorvall Discovery M120SE Centrifuge and S100 AT4 rotor. Supernatants were collected and pelleted liposomes gently resuspended in fresh PBS. Thirdly, using inverted centrifugal spin filters (*Centrisart* I, 100.000 MWCO), 500µl of liposome preparation was brought up to 2ml with PBS. Diluted siRNA-liposome preparations were placed in the spin filter outer tube and left to stand at room temperature for 5 minutes to wet the filters. Spin filters were centrifuged at 5000 rpm for 30 minutes at 4°C. Filtrate was collected from the inner chamber (Figure 2.7). Centrifugation was repeated until less than 500µl remained in the inner tube. siRNA complexes were disrupted using 0.2% TritonX, pH 12 TE buffer and 1% SDS for DOTAP, PEI and protamine respectively and siRNA quantified by Ribogreen assay.

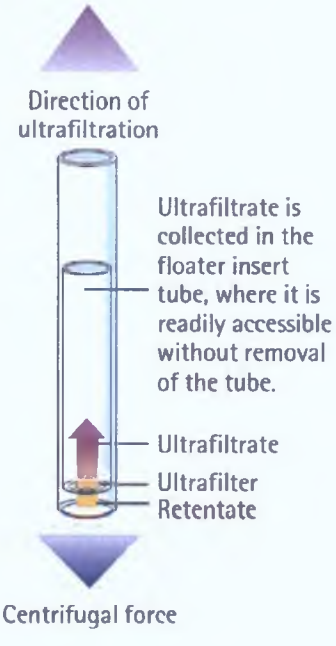


Figure 2.7: Centrisart I spin filters

### 2.3.5 Aerosolisation of siRNA and Liposomes

Formulations of 10µg/ml of siRNA in PBS were prepared. The formulations (10ml) were aerosolized into a glass twin stage impinger (TSI) (Figure 2.8A) at 60 liters per minute with either an AeroNeb® Pro nebulizer or PARI air jet nebulizer (pressure set to 2 bars) (Figure 2.8). PBS was added to the upper (3 ml) and lower (10 ml) stages. Washes were collected and concentrations were determined for each stage. Percentage respirable fraction and emitted doses were calculated (Table 2.6). Initially, 400nm liposomes at various concentrations 1, 2.5 and 4.5mg/ml were nebulized with an AeroNeb® Pro nebulizer. Nebulized vapour was collected in a 15ml tube and percentage output of liposomes at each concentration was calculated. The amount of liposomes collected was determined by cholesterol and lipid assays described in 2.3.4.3 and output was calculated as a percentage of the liposome amount loaded onto the nebulizer. Similarly to siRNA nebulisation, 5ml of liposomes (4.5mg/ml) were aerosolised into the impinger.

Air-jet nebulisers such as PARI produce aerosols when compressed air enters the nebulizer unit at a high velocity breaking the liquid formulation into very small droplets. While the vibrating mesh or micropump nebulisers such as the AeroNeb® Pro nebulizer uses an OnQ technology (or electronic micropump) to produce an aerosol. This micropump consists of a vibrational element surrounding a domed aperture plate that contains as much as 1000 holes. When an electric current is applied to a vibrational element it contracts and expands therefore causing the mesh to move, vibrating about 100,000 times per second. The holes act as micropumps as the mesh vibrates bringing the liquid formulation through and generating an aerosol.

**Table 2.6:**

$$\%\ \text{Emitted Dose} = \frac{\text{Upper Impinger Dose} + \text{Lower Impinger Dose}}{\text{Dose Loaded into the Nebuliser}} \times \frac{100}{1}$$

$$\%\ \text{Respirable Fraction} = \frac{\text{Lower Impinger Dose}}{\text{Emitted Dose}} \times \frac{100}{1}$$

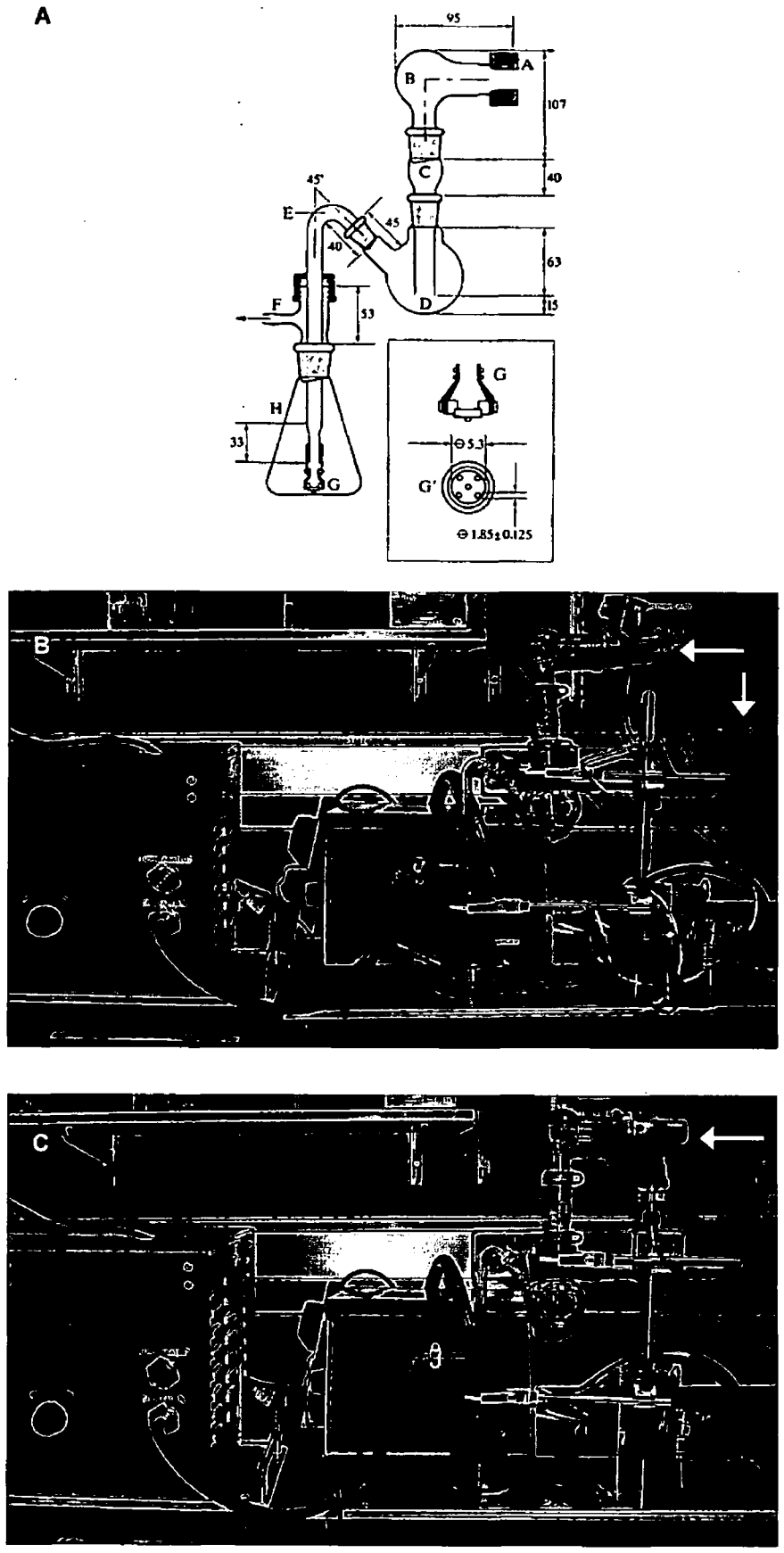


Figure 2.8: Set up of the (A) glass impinger apparatus with (B) AeroNeb® Pro vibrating-mesh and (C) PARI air jet nebulizer.

#### 2.3.5.1 Aerosolised siRNA and Liposome Characterisation

siRNA concentration was determined using a NanoDrop 1000 Spectrophotometer. Initially, a series of dilutions was prepared giving siRNA concentrations of 266 (stock, 20pM), 100, 50, 25, 12.5, 6.25, 3.125, 2 and 1 ng/µl to determine the limits of detection (LOD) of siRNA with a NanoDrop 1000 Spectrophotometer. 5 measurements were taken per dilution at 260nm. Liposome size and zeta potential were measured as described in 2.3.2.1. Liposome concentration was determined by cholesterol and phospholipid assays as described in 2.3.4.3.

#### 2.3.5.2 Polyacrylamide Gel Electrophoresis

siRNA integrity post-nebulisation was assessed by gel electrophoresis. A 20% non-denaturing polyacrylimide (19:1 acrylamide:bisacrylamide) TBE gel was prepared as described in 2.3.2.2. Samples (30µl) and a siRNA marker (New England Biolabs) were loaded and the gels were run in 1x TBE buffer at 100V for 45 minutes followed by post-staining with GelStar (Lonza) for 30 minutes. Visualization was obtained by UV transillumination (G:BOX, Syngene).

### 2.3.6 Statistics

Results are expressed as means ± standard deviation (SD). One way or two way analysis of variance (ANOVA) was used to test for differences between treatments with $p$-values $< 0.05$ considered significant, $< 0.01$ very significant and $< 0.001$ highly significant.

## 2.4 Results

### 2.4.1 Characterisation of Mannosylated Cholesterols

Synthesis of intermediate products was confirmed by NMR, IR and elemental analysis and was carried out by Colin Burke under the supervision of Dr. James Barlow. The final Mann-C2-Chol, Mann-C4-Chol and Mann-C6-Chol products were dialysed and lyophilized. IR spectroscopy showed very similar spectra for each compound. Theoretical masses for Mann-C2-Chol, Mann-C4-Chol and Mann-C6-Chol are 708.5, 736.5 and 764.5 g/mol respectively. ESI-MS shows mass peaks at 708.5, 736.5 and 764.5 amu for Mann-C2-Chol (Figure 2.9A), Mann-C4-Chol (Figure 2.9B) and Mann-C6-Chol (Figure 2.9C) respectively.

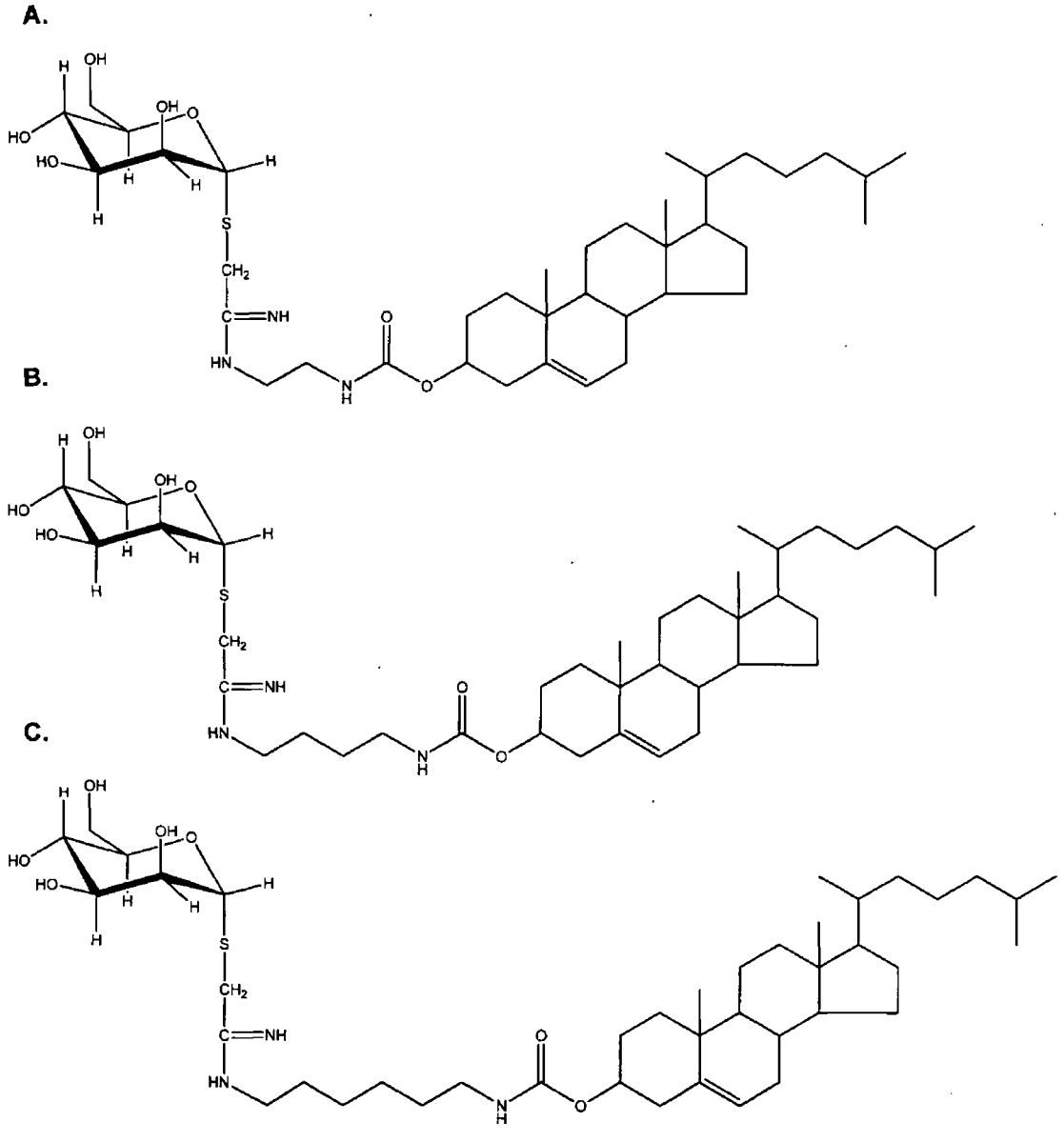


Figure 2.9 Structure of (A) Mann-C2-Chol, (B) Mann-C4-Chol and (C) Mann-C6-Chol

### 2.4.2 siRNA Complexation

To improve encapsulation efficiency of siRNA in neutral liposomes siRNA was first condensed by complexation with DOTAP, protamine and PEI. Complexes were characterised by size and zeta potential. Additionally, complexes were electrophoresed to determine complexation efficiency. Only free or uncomplexed siRNA can run through the gel therefore a stronger band corresponds to a greater amount of free or uncomplexed siRNA and no band indicating complete complexation. Characterization was used to determine the optimal N/P or weight ratios to provide maximum siRNA encapsulation while attaining a small nano-scale size suitable for encapsulation by 200-400nm liposomes and minimizing the positive charge introduced to the liposome preparations. Therefore the optimal ratios used the minimum amount of cationic reagent whilst achieving high encapsulation, low zeta potential and a particle size less that 400nm.

DOTAP/siRNA complexes prepared with extruded DOTAP suspension (100% DOTAP liposomes) formed complexes less than 400nm with zeta potentials ranging from -39 ± 3 mV to 59 ± 11 mV (Table 2.7 and Figure 2.10A). However gel retardation assays showed low siRNA encapsulation even at N/P ratios up to 8 (Figure 2.11A). DOTAP-siRNA complexes prepared by lyophilisation of lipid and nucleic acid components in *t*-butanol showed improved siRNA complexation from N/P ratios of 5 and higher while sizes were more variable and polydisperse (Table 2.8). DOTAP siRNA complexes produced positive zeta potentials at N/P ratios above 3 (Figure 2.10B). DOTAP siRNA complexes of N/P ratio 4 prepared by lyophilisation were selected for liposome encapsulation. Lyophilisation preparation showed improved siRNA condensation over DOTAP liposome complexation as well as lower zeta potentials. N/P ratio of 5 gave a very positive zeta potential and therefore a ratio below this was chosen for liposome encapsulation.

Protamine siRNA complexes had sizes less than 400nm at weight ratios of 3 and 4 (Protamine/siRNA (w/w)) (Table 2.9) and positive zeta potentials at and above a weight ratio of 3 (Figure 2.10C). Gel retardation assays repeatedly showed maximum complexation achieved at a weight ratio of 4 (Figure 2.11C). Consequently the weight ratio of protamine:siRNA of 4 was determined the optimum ratio for use in liposome encapsulation.

Negative zeta potentials of PEI-siRNA complexes were observed below N/P 7 (Figure 2.10D). At N/P 7 small sized (115.3nm and polydispersity index (PDI) 0.249) and positively charged (17.5 ± 5 mV) complexes were attained (Table 2.10 and Figure 2.10D). Gel retardation assay also confirmed optimal complexation of siRNA at N/P 7 (Figure 2.11D) and this ratio was used for liposome siRNA encapsulation.

**Table 2.7: Sizes of DOTAP liposome-siRNA complexes** (means ± SD, n = 3)

| Complex Ratio | Average Diameter (nm) | PDI |
|---|---|---|
| 0:1 | 135.2 | 0.254 |
| 1:1 | 298.9 | 0.246 |
| 2:1 | 154.6 | 0.224 |
| 3:1 | 351.8 | 0.173 |
| 4:1 | 205.8 | 0.131 |
| 5:1 | 300.9 | 0.237 |
| 6:1 | 156.8 | 0.091 |
| 7:1 | 216.4 | 0.174 |
| 8:1 | 212.9 | 0.276 |
| 10:1 | 148.7 | 0.137 |

**Table 2.8: Sizes of DOTAP-siRNA complexes prepared by lyophilisation.** (means ± SD, n = 3).

| Complex Ratio | Average Diameter (nm) | PDI |
|---|---|---|
| 1:1 | 4431.3 | 1 |
| 5:1 | 584.9 | 0.515 |
| 7.5:1 | 297.7 | 0.354 |
| 10:1 | 1473 | 0.709 |
| 12.5:1 | 721.5 | 0.618 |
| 15:1 | 339.5 | 0.627 |

**Table 2.9: Sizes of Protamine-siRNA complexes** (means ± SD, n = 3)

| Complex Ratio | Average Diameter (nm) | PDI |
|---|---|---|
| 1:1 | 491.7 | 0.267 |
| 2:1 | 415.4 | 0.376 |
| 3:1 | 272 | 0.297 |
| 4:1 | 386.9 | 0.401 |
| 6:1 | 550.7 | 0.365 |

**Table 2.10: Sizes of PEI complexes.** (means ± SD, n = 3)

| Complex Ratio | Average Diameter (nm) | PDI |
|---|---|---|
| 1:1 | 235.6 | 0.414 |
| 3:1 | 146.5 | 0.23 |
| 5:1 | 356.1 | 0.189 |
| 7:1 | 115.3 | 0.249 |
| 10:1 | 721.1 | 0.216 |

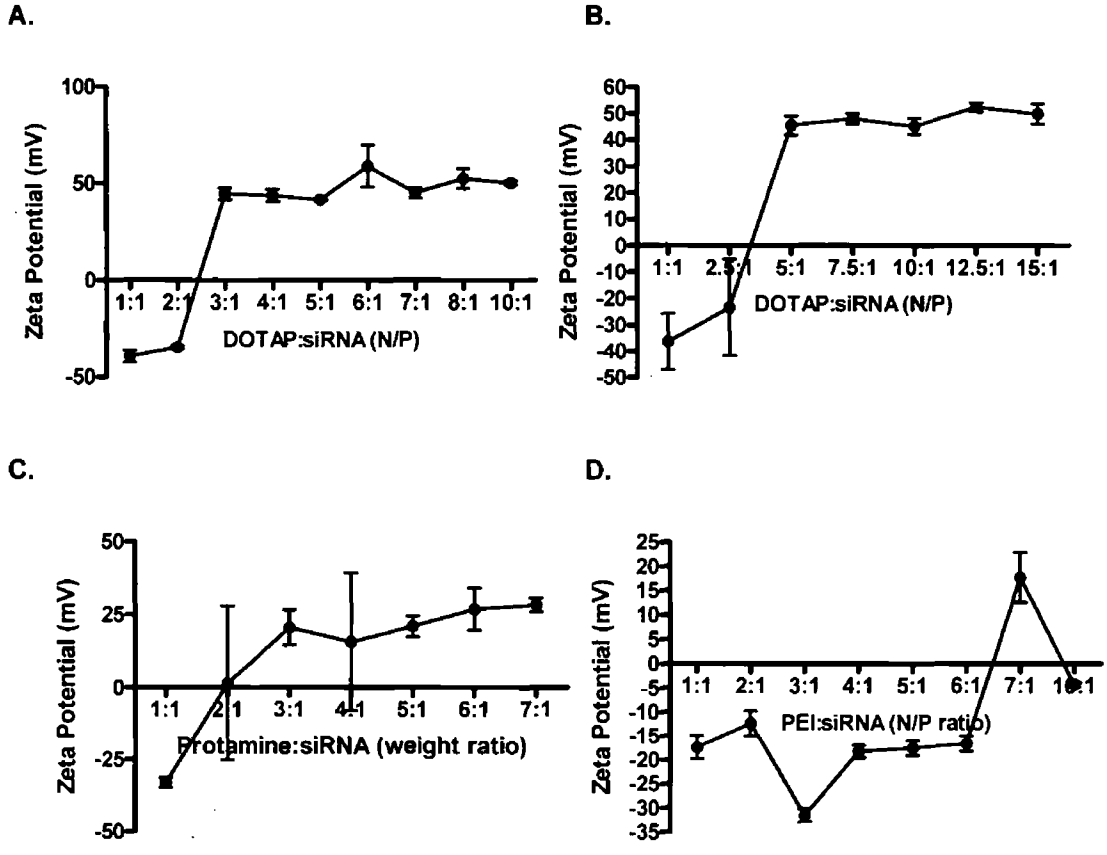


Figure 2.10: Zeta potentials of (A) DOTAP liposome siRNA complexes, (B) DOTAP-siRNA complexes prepared by lyophilisation, (C) protamine:siRNA complexes and (D) PEI:siRNA complexes at a range of N/P or weight ratios.
Data expressed as means ± SD (n = 3)

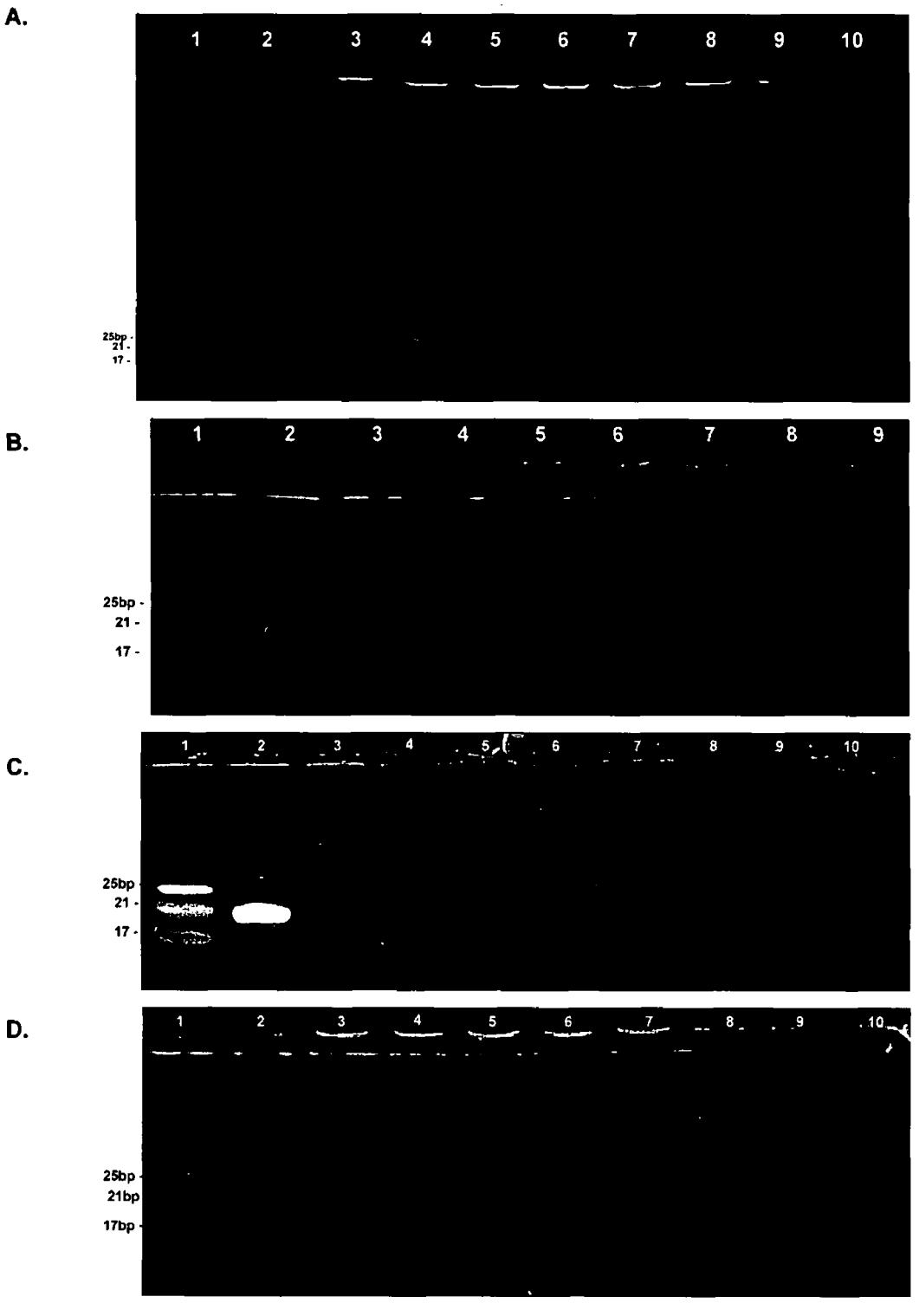


Figure 2.11: 20% non-denaturing polyacrylamide gels loaded with 100ng siRNA per well. Gel A shows the siRNA marker (Lane 1), siRNA stock (Lane 2) and DOTAP liposome siRNA complexes at N/P ratios of 1, 2, 3, 4, 5, 6, 7 and 8 (Lanes 3 – 10). Gel B shows the siRNA marker (Lane 1), siRNA stock (Lane 2) and DOTAP siRNA complexes rehydrated after lyophilisation at N/P ratios of 1, 2.5, 5, 7.5, 10, 12.5 and 15 (Lanes 3 – 9). Gel C shows the siRNA marker (Lane 1), free siRNA stock (Lane 2) and Protamine siRNA complexes at N/P ratios of 2, 3, 3.75, 4, 4.25, 4.5, 4.75 and 5 (Lanes 3 – 10). Gel D shows the siRNA marker (Lane 1), siRNA stock (Lane 2) and PEI siRNA complexes at N/P ratios of 1, 2, 3, 4, 5, 6, 7 and 10 (Lanes 3 – 10).

Free or uncomplexed siRNA was quantified using Ribogreen assay. This is an ultrasensitive assay, detecting RNA concentrations as low as 1ng/ml. Free siRNA was undetectable at all weight ratios of protamine-siRNA complexes (Figure 2.12A). Gel retardation assays as well as zeta potentials at low N/P ratios (below 4) indicate the presence of uncomplexed siRNA. Therefore protamine must be interfering with the assay resulting in fluorescence intensities just above background fluoresence in each sample.

As was observed by gel retardation assay PEI-siRNA complexes at and above N/P ratio of 7 achieve maximum encapsulation of siRNA with little or no free siRNA detectable (Figure 2.12B - D). At pH 12 PEI-siRNA complexes should disassociate which has previously been reported by Merkel *et al.* (2009) [158]. Figure 2.12C shows little disruption of the complexes at pH 12 compared to pH 7.5. Assays were preformed in triplicate three times. However samples using fluorescently tagged siRNA were diluted in pH 12 TE buffer and complete disassociation was observed (Figure 2.12D). Additionally as the N/P ratio increased above 5 the fluorescence intensity began to rise again. This has previously been observed in other studies [158, 160] and is attributed to a rearrangement of the nucleic acid within the complexes at higher N/P ratios.

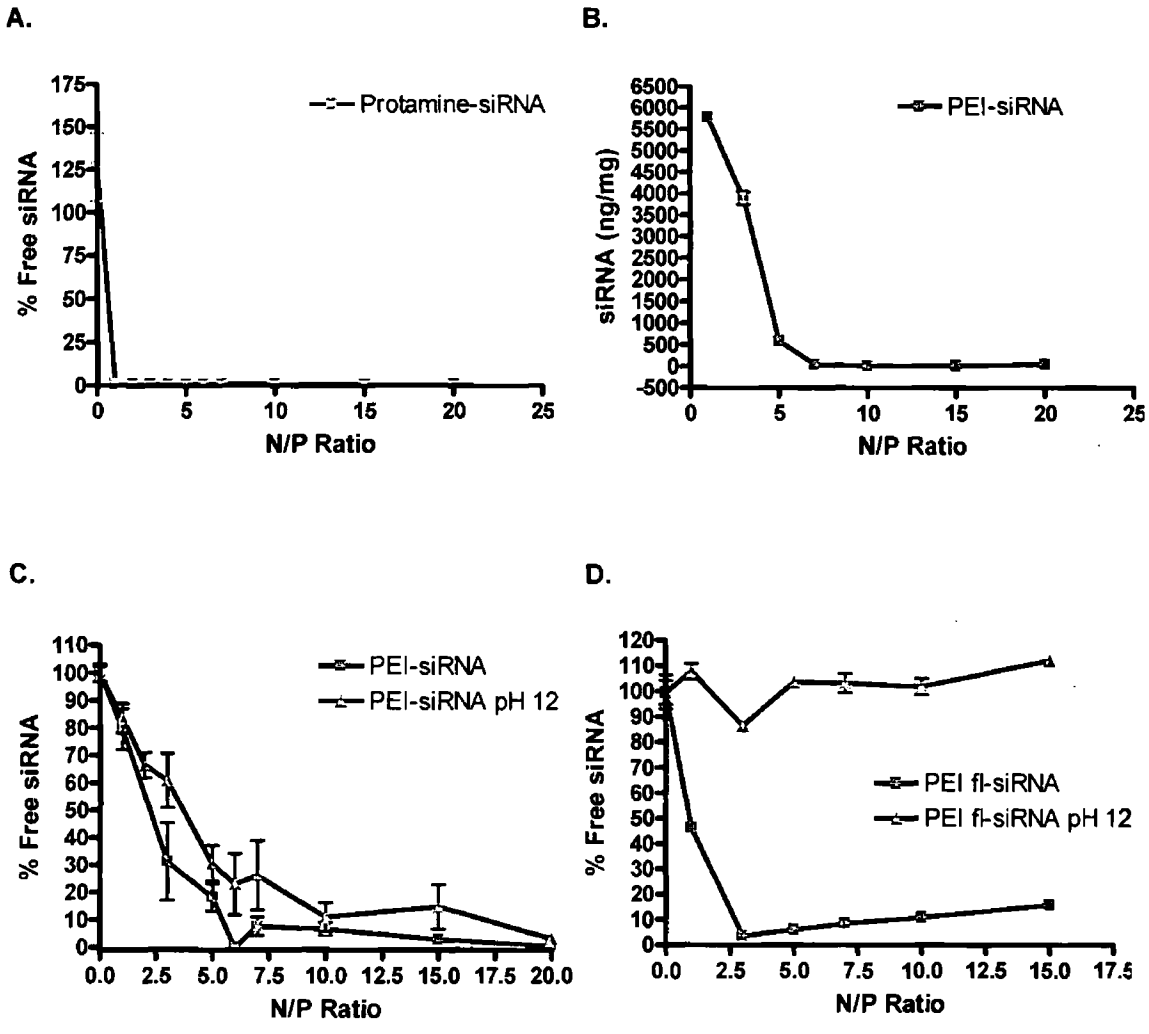


Figure 2.12: Fluorescent binding assays quantifying free siRNA following siRNA complexation. Quant iT ribogreen assay shows the percentage of free siRNA following complexation with (A) protamine (n =1) at a range of weight ratios and (B – C) with PEI (n = 3) at various N/P ratios at pH 7.5 and pH 12. Fluorescently tagged siRNA (n = 1) complexed with PEI at various N/P ratios was also quantified at pH 7.5 and pH 12.
Data represented as means ± SD

### 2.4.3 Liposome Preparation and Characterisation

A range of non-mannosylated and mannosylated liposomes containing DOPS, DOTAP, DOPC, DSPC, Mann-C2-Chol, Mann-C4-Chol, Mann-C6-Chol and cholesterol in the molar ratios shown in Tables 2.11 and 2.12 were prepared. DOPS is an anionic lipid that could offer an advantage for targeting macrophages while DOPC or DSPC and DOTAP liposomes act as its neutral and cationic comparisons respectively. DOPC liposomes were used as a control for the mannosylated systems.

**Table 2.11: Non-mannosylated Liposomes Prepared**

| Liposome Nomenclature | Molar Ratios of Constituent Lipids | | | | |
|---|---|---|---|---|---|
| | DOPC | DOPS | DSPC | DOTAP | Chol |
| *DOPS* | - | 70 | - | - | 30 |
| *DSPC* | - | - | 60 | - | 40 |
| *DOPC* | 70 | - | - | - | 30 |
| *DOTAP* | 30 | - | - | 50 | 20 |

**Table 2.12: Mannosylated Liposomes Prepared**

| Liposome Nomenclature | Molar Ratios of Constituent Lipids | | | | |
|---|---|---|---|---|---|
| | DSPC or DOPC | Chol | Mann-C2-Chol | Mann-C4-Chol | Mann-C6-Chol |
| *MC2C-2.5* | 60 or 70 | 37.5 or 27.5 | 2.5 | - | - |
| *MC2C-5* | 60 or 70 | 35 or 25 | 5 | - | - |
| *MC2C-7.5* | 60 or 70 | 32.5 or 22.5 | 7.5 | - | - |
| *MC4C-2.5* | 60 or 70 | 37.5 or 27.5 | - | 2.5 | - |
| *MC4C-5* | 60 or 70 | 35 or 25 | - | 5 | - |
| *MC4C-7.5* | 60 or 70 | 32.5 or 22.5 | - | 7.5 | - |
| *MC6C-2.5* | 60 or 70 | 37.5 or 27.5 | - | - | 2.5 |
| *MC6C-5* | 60 or 70 | 35 or 25 | - | - | 5 |
| *MC6C-7.5* | 60 or 70 | 32.5 or 22.5 | - | - | 7.5 |

Cholesterol quantification was used to determine total liposome concentration after extrusion. Total loss of liposomes due to extrusion was less than 50% and 15% by thermo-barrel extrusion and syringe extrusion respectively. In the case of DOPC containing liposomes a phospholipid assay for phosophatidylcholine was also used for quantification.

### 2.4.3.1 Encapsulation efficiency

Encapsulation efficiencies of free siRNA in neutral and mannosylated liposomes ranged from 0 to 10%. With the incorporation of a small proportion of cationic lipid DOTAP into the liposome this encapsulation efficiency was improved to ~30% but was not reproducible. Additionally, as DOTAP is associated with toxicity the use of DOTAP in the liposome structure is undesirable. Consequently, condensation of siRNA was achieved by complexation with DOTAP, PEI and protamine prior to encapsulation in liposomes. To measure encapsulation efficiency unencapsulated (free and condensed) siRNA was separated from liposomes by ultracentrifugation or ultrafiltration. However, quantification of siRNA encapsulated was unsuccessful. Ultracentrifugation separated free and condensed siRNA from liposomes (determined by dynamic light scattering). Ultrafiltration separated free siRNA from condensed

siRNA and siRNA encapsulated in liposomes. Formulations showed encapsulation efficiencies up to 98% however this did not take into account condensed siRNA that could not be detected by this technique. Various methods were used to disrupt complexes but either interfered with the RNA quantitation assay or complete disruption of the complexes could not be achieved. Both protamine and SDS interfered with the RiboGreen assay. Increased pH did not disassociate PEI-siRNA complexes (Figure 2.12C). And DOTAP condensation of siRNA produced very variable encapsulation results.

#### 2.4.3.2 Particle Size and Zeta Potential

Particle size was recorded for each batch of liposomes prepared to assess the effectiveness of size reduction and liposome stability. Average sizes for non-mannosylated liposomes extruded through 200nm pore filters were below 200 nm with PDI between 0.066 and 0.254 (Table 2.13).

**Table 2.13: Non-mannosylated liposome particle sizes**

| Liposome | Average Size ($d_{50}$ nm) | Polydispersity Index (PDI) |
|---|---|---|
| ***DOPS*** | 150 ± 2 | 0.101 |
| ***DSPC*** | 196 ± 37 | 0.254 |
| ***DOPC*** | 168 ± 1 | 0.118 |
| ***DOTAP*** | 137 ± 5 | 0.066 |

Mannosylated liposomes showed higher average diameters and PDI compared to non-mannosylated liposomes (Table 2.14). Size reduction appeared to be less problematic using DOPC than DSPC.

**Table 2.14: Mannosylated liposome particle sizes**

| Liposome | Lipid | Average Size ($d_{50}$ nm) | Polydispersity Index (PDI) |
|---|---|---|---|
| ***MC2C-2.5*** | DSPC | 165 ± 6 | 0.16 |
| | DOPC | 173 ± 3 | 0.119 |
| ***MC2C-5*** | DSPC | 203.6 | 0.351 |
| | DOPC | 167 ± 2 | 0.126 |
| ***MC2C-7.5*** | DSPC | 266 ±14 | 0.39 |
| | DOPC | 146 | 0.15 |
| ***MC4C-2.5*** | DOPC | 176 ± 3 | 0.139 |
| ***MC4C-5*** | DSPC | 2073.7 | 0.476 |
| | DOPC | 173 ± 6 | 0.133 |
| ***MC4C-7.5*** | DOPC | 179 ± 34 | 0.08 |
| ***MC6C-2.5*** | DOPC | 171 ± 3 | 0.126 |
| ***MC6C-5*** | DOPC | 169 ± 1 | 0.124 |
| ***MC6C-7.5*** | DOPC | 164 ± 4 | 0.095 |

Size distribution showed single peaks for most extruded liposomes (Appendix). Multiple peaks were observed in DSPC composed mannosylated liposomes. Increasing the concentration of mannose incorporated corresponded with more variable size distribution [115]. However, DOPC based liposomes did not exhibit this problem. Consequently liposomes composed with DOPC were used in *in vitro* studies. Anionic, neutral and cationic liposomes stored at 4°C were stable for up to one month (see Appendix).

Optimum condensation of siRNA by the cationic reagents generally produced complexes greater than 200nm in size (with the exception of PEI siRNA complexes). Cell uptake studies (3.4.2) showed optimal size for liposome uptake to be between 200 and 400nm. Consequently following passive encapsulation of condensed siRNA, liposomes were extruded through polycarbonate filters with 400nm pores. Zeta potentials of liposomes composed of 50% cationic lipid DOTAP were recorded and ranged from 37.6 to 39.7 mV. Anionic liposomes had a surface charge of - 45mV and mannosylated liposomes incorporating 10% DOTAP had a zeta potential of 19mV.

Electron micrographs were also used to confirm liposome size. Figure 2.13 shows DOPS liposomes visualised by TEM using the negative stain PTA. Liposomes appear spherical and of about 200nm in diameter confirming sizes determined by dynamic light scattering. Alternative staining could be used such as uranyl acetate (2% w/v) to increase contrast. This stain is typically used for imaging liposomes. Some fusion can also be seen (Figure 2.13B).

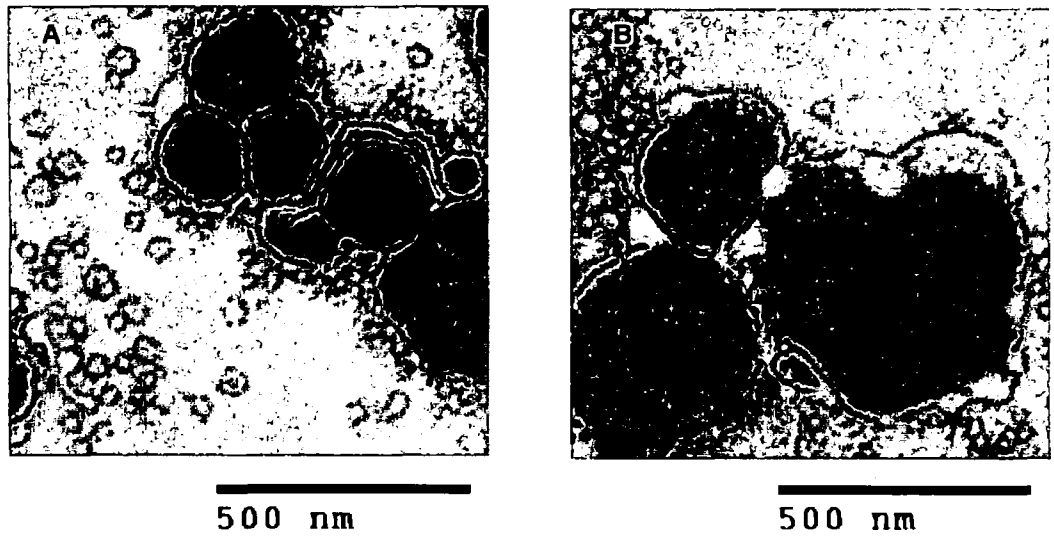


Figure 2.13: Transmission electron microscopy images of DOPS:Chol (7:3) liposomes at 100 kV high voltage and 50,000x magnification negatively stained with 2% phosphotunstic acid (PTA).

### 2.4.4 Aerodynamic Study of siRNA Aerosolised Using Nebulisers

For local siRNA delivery to the lung the siRNA must be aerosolised. In order to conserve stock siRNA, due to its expense, it was necessary to determine the lowest concentration that could be detected using the NanoDrop 1000 spectrophotometer and from this work out the minimum amount to be loaded into the impinger system (that could still be detected later after further dilutions). At this point a RiboGreen assay was not available. According to the NanoDrop manufacturer, detection of nucleic acids range from 2 to 100ng/µl (± 2ng/µl) and siRNA as dilute as 2ng/µl was detectable although accuracy became quite low below concentrations of 6.25ng/µl (Appendix). The TSI was set up with a minimum volume of buffer in each of the stages. Washings were also collected with just 5ml of PBS to minimise further dilutions of the siRNA.

#### 2.4.4.1 Twin Stage Impinger (TSI) Deposition of Aerosolised siRNA

Formulations of siRNA (100µg in 10ml) were aerosolised using a PARI air jet nebuliser or AeroNeb vibrating mesh nebuliser device into a glass impinger. The time taken to aerosolise the 10ml formulation for each device was 135 and 28 minutes for the PARI and AeroNeb devices respectively. The amount of siRNA deposited in the devices, "throat" section, stage A and stage B of the twin impinger was determined. The deposition patterns represented in Figure 2.14 show the percentage of deposited siRNA of total loaded siRNA detected.

The highest level of siRNA in the PARI impinger system remained in the device (79.7% ± 2.3) with low quantities detected in the throat (8.4% ± 0.4), stage A (3.9% ± 0.6) and stage B (8.1% ± 2.1). The AeroNeb nebuliser shows the higher percentage of siRNA being deposited at stage B (64.2 % ± 5.1) while stage A (12.2% ±1.1), throat (12.3%±1.2) and the device (12.3%±1.5) contain similar low levels of siRNA deposition.

Respirable and emitted doses of siRNA with each nebuliser were calculated (Table 2.15). The AeroNeb nebuliser showed a higher respirable fraction (63.2% ± 3.4), respirable dose (50.7µg ± 4.8) and emitted dose (87.7% ± 1.5 and 70.4µg ± 4.8) than the PARI nebuliser (8.1% ± 2.1, 10.1µg ± 2.8, 20.3% ± 2.3 and 25.4µg ± 3.2 respectively).

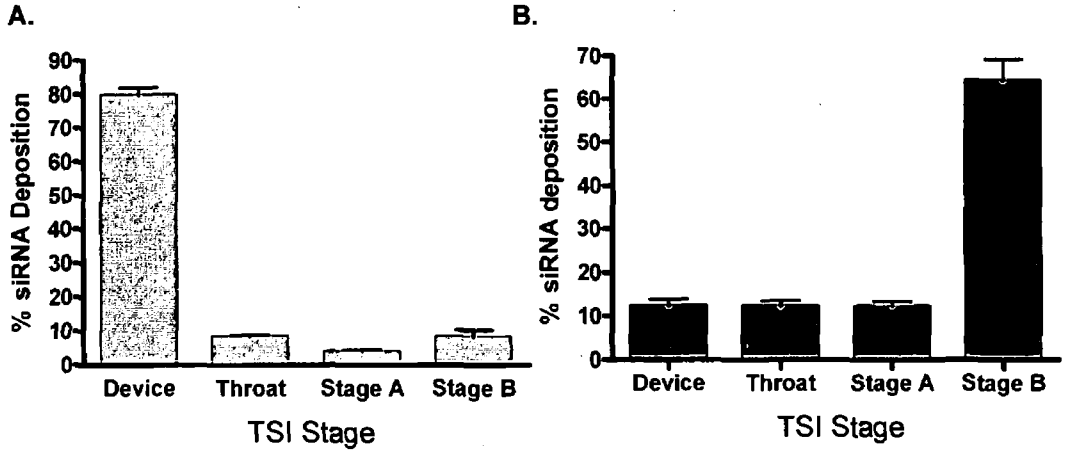


Figure 2.14: Deposition patterns of siRNA by the (A) PARI air jet and (B) AeroNeb vibrating mesh nebulisers. Data represented as mean percentages of total siRNA ± SD.

**Table 2.15: Respirable and Emitted Doses of siRNA** Data represented as means ± SD. (n = 3)

| Device | Respirable Fraction (%) | Respirable Dose (µg) | Emitted Dose (%) | Emitted Dose (µg) |
|---|---|---|---|---|
| PARI | 8.1 ± 2.1 | 10.1 ± 2.8 | 20.3 ± 2.3 | 25.4 ± 3.2 |
| AeroNeb | 63.2 ± 3.4 | 50.7 ± 4.8 | 87.7 ± 1.5 | 70.4 ± 4.8 |

### 2.4.4.2 Post-Aerosolisation Stability

To assess siRNA integrity after dilution in PBS and aerosolisation, samples from the impinger were electrophoresed on a 20% non-denaturing polyacrylamide gel [161-163]. A siRNA marker containing siRNA of 17, 21 and 25bps in length was loaded as a control. The level of the loaded samples corresponds to 21bp the length of siRNA used. One band was visualised per lane (Figure 2.15). Relative band intensities are consistent with quantities detected by spectrophotometry with the AeroNeb Stage B and PARI device samples having the highest intensity (and highest % deposition). Smearing can be seen in lanes due to siRNA degradation particularly following nebulisation (Figure 2.15).

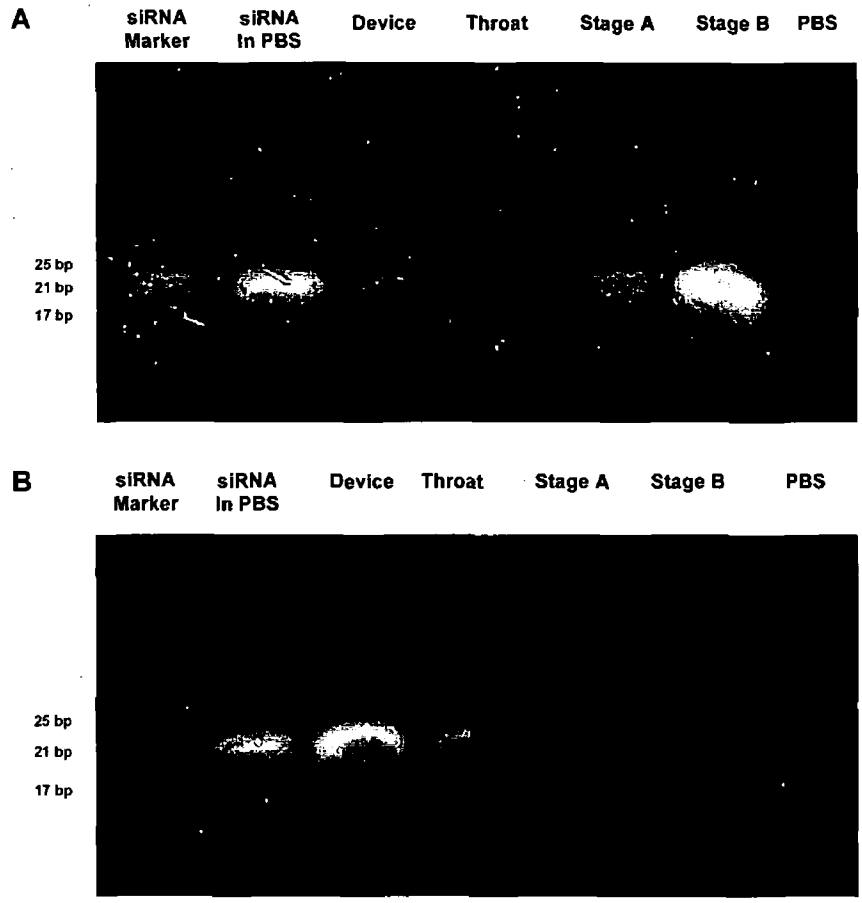


Figure 2.15: siRNA integrity post-nebulisation assessed using 20% non-denaturing polyacrylamide gels. The gels show the siRNA marker (lane 1), PBS alone (lane 7), siRNA diluted and stored in PBS (lane 2) and siRNA collected after aerosolisation (lanes 3 – 6) by AeroNeb Nebuliser (Gel A) and by the PARI air-jet nebuliser (Gel B).

### 2.4.5 Aerodynamic Study of Liposomes Aerosolised Using Nebulisers

#### 2.4.5.1 TSI Deposition of Aerosolised Liposomes

Liposomes were aerosolised using a PARI air jet nebuliser or AeroNeb vibrating mesh nebuliser device into a glass impinger. The time taken to aerosolise 1 ml of liposomes for each device was 7.98 ± 4 minutes and 2.05 ± 0.2 minutes for the PARI and AeroNeb devices respectively. The amount of liposomes deposited in the devices, "throat" section, stage A and stage B of the twin impinger was determined by assay. The deposition patterns represented in Figure 2.16 show the percentage of deposited liposomes of total liposomes loaded. Overall liposomes nebulised via the air jet PARI nebuliser remained in the device or stage B of TSI whilst aerosols generated by the AeroNeb deposited predominantly in Stage B of TSI with minimal residual volume in the device. Furthermore little of the liposome preparation was lost during aerosolisation by the AeroNeb nebuliser with almost all loaded liposome being recovered from the system post-nebulisation (determined by assay). However, over 50% of loaded preparations escaped the twin impinger system during nebulisation by the PARI air jet

nebuliser. This also highlights the efficiency of the vibrating mesh nebuliser over the air jet device for liposome lung delivery.

Nebulisation via the PARI nebuliser resulted in the highest proportion of DOPS liposome preparations remaining in the device (Figure 2.16A). The vibrating mesh nebuliser was more efficient delivering 35.7 ± 23.9 % DOPS liposomes to TSI Stage B (the deep lung) but also depositing 25.7 ± 17.1 % in TSI Stage (Figure 2.16B). Consequently, the emitted dose by the AeroNeb device was 89.3 ± 0.4 % with a respirable fraction of 46.4 ± 26.4 % (Table 2.16). Deposition patterns for DOPC and mannosylated MC6C liposomes were similar to DOPS liposome preparations but with greater respirable doses and reduced loss of liposome preparation from the system following PARI air jet nebulisation. Deposition (Figure 2.16C) of neutral DOPC liposomes was greatest in stage B with 18.3 ± 18.2 %. AeroNeb nebulisation lead to 56.3 ± 3.4 % deposition of DOPC liposome preparation in Stage B (Figure 2.16D). Emitted doses of 56.9 ± 22.4 % and 90.5 ± 2.1 % and respirable fractions of 45.8 ± 24.9 % and 69.2 ± 18.6 % were determined for DOPC liposome nebulisation via PARI and AeroNeb devices respectively (Table 2.16).

Mannoyslated liposomes composed with 7.5% Mann-C6-Chol were also aerosolized and 17.6 ± 4.7 %, 3.6 ± 1.7 % and 13.4 ± 9.1 % were deposited in the device, Stage A and Stage B via the PARI device respectively (Figure 2.16E and F). The AeroNeb nebulizer resulted in 2.8 ± 1.5 %, 13.7 ± 10.7 and 55.5 ± 20.4 % deposition of Mannosylated liposomes in the Throat stage, Stage A and Stage B respectively. 5.5 ± 1.1 % of mannosylated liposome preparations remained in the device. The liposome doses emitted from the PARI and AeroNeb devices were 48.7 ± 17.8 % and 92.8 ± 2.1 % with 37.6 ± 22.9 % and 70.6 ± 19.8 % respirable respectively (Table 2.16).

Minimal liposome escape from the TSI system was obtained with AeroNeb device while over 50% of liposome formulations were lost via PARI nebulisation. Additionally, the AeroNeb device was more efficient at delivering liposome formulations to TSI Stage B with least residual volume in the device. Deposition patterns of anionic, neutral and mannosylated liposomes also differed with mannosylated liposomes achieving the highest respirable fraction via the AeroNeb device.

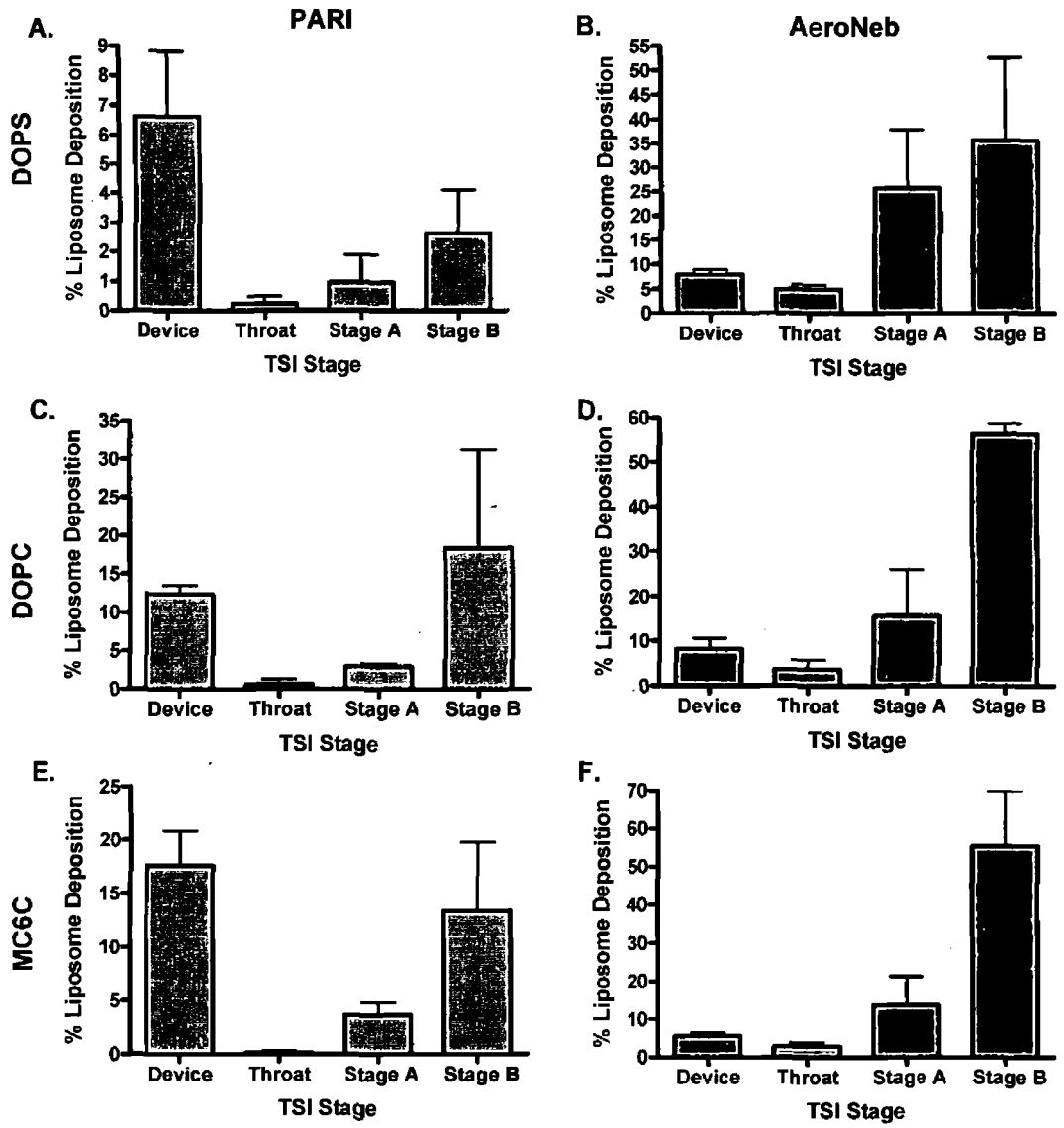


Figure 2.16: Twin Stage Impinger (TSI) Liposome Deposition Patterns by PARI air jet and AeroNeb nebulisers. DOPS liposome deposition by (A) PARI and (B) AeroNeb nebuliser, DOPC liposome deposition by (C) PARI and (D) AeroNeb nebuliser and MC6C liposome deposition by (E) PARI and (F) AeroNeb nebuliser represented as percentage of total loaded liposomes.

**Table 2.16: Respirable and Emitted Doses of DOPS Liposomes**

| Liposome | Device | Respirable Fraction (%) | Respirable Dose (μg) | Emitted Dose (%) | Emitted Dose (μg) |
|---|---|---|---|---|---|
| DOPS | PARI | 23.8 ± 4.3 | 2.6 ± 2.1 | 31.6 ± 15.3 | 3.8 ± 3.8 |
| | AeroNeb | 46.4 ± 26.4 | 35.7 ± 23.9 | 89.3 ± 0.4 | 66.3 ± 8.1 |
| DOPC | PARI | 45.8 ± 24.9 | 18.3 ± 18.2 | 56.9 ± 22.4 | 21.8 ± 19.7 |
| | AeroNeb | 69.2 ± 18.6 | 56.3 ± 3.4 | 90.5 ± 2.1 | 75.6 ± 14.2 |
| MC6C | PARI | 37.6 ± 22.9 | 13.4 ± 9.1 | 48.7 ± 17.8 | 17.2 ± 7.6 |
| | AeroNeb | 70.6 ± 19.8 | 55.5 ± 20.4 | 92.8 ± 2.1 | 72.1 ± 8.2 |

### 2.4.5.2 Effect of Nebulisation of Liposome Properties

In studies following nebulisation liposomes are generally evaluated for changes in size, zeta potential and morphology through TEM and drug release. It is important that liposomes are not only delivered to the deep lung efficiently for alveolar macrophage targeting but also reach their destination intact to reduce drug loss. Consequently the characterisation of liposomes deposited in Stage B is most important. Nebulisation greatly affected size and surface charge of empty liposomes both of which are good indicators of particle stability. Changes were different for anionc, neutral and mannosylated liposomes and different for each device.

Anionic (DOPS) liposomes increased in size following deposition within the impinger system. Liposomes remaining in the device showed a marginal decrease in size. Nebulisation via the AerNeb device resulted in an increase in size almost two-fold from pre-nebulised DOPS liposomes reaching TSI Stage B ($p < 0.001$). The increase was higher than PARI aerosolised DOPS liposomes. Zeta potential of DOPS liposomes aerosolised by AeroNeb nebuliser remained unchanged (Figure 2.17).

DOPC liposomes showed altered mean diameter following PARI air-jet nebulisation with less dramatic effects brought on by AeroNeb nebulisation (Figure 2.17). Stage B deposited DOPC liposomes aerosolised by the AeroNeb device were equivalent to pre-nebulised liposomes while PARI aerosolisation increased size from 623.6 ± 301 nm to 893.4 ± 501.2 nm. Overall for DOPC liposomes sizes between batches and runs were variable. Zeta potentials were all negative but close to neutrality of 0 mV. PARI aerosolised liposomes recovered from the device and Stage B showed the greatest degree of difference in zeta potential to pre-nebulised liposomes ($p < 0.001$).

Mannosylated liposomes were most affected by nebulisation via the vibrating mesh AeroNeb device (Figure 2.17). Liposome size was increased in all stages whereas PARI aerosolised liposomes reaching Stage B showed little difference in size compared to pre-nebulised liposomes. More significantly nebulisation affected surface charge ($p < 0.001$). Mannoslyated liposomes were composed of neutral lipid DOPC (70%), cholesterol (22.5%) and Mann-C6-Chol (7.5%). The addition of the mannosylated cholesterol to the formulation changed the particle charge from neutral to positive. The decrease in zeta potential of the mannosylated liposomes particularly in Stage A and Stage B of the impinger system suggests alteration and perhaps loss of the liposome mannosylated coating.

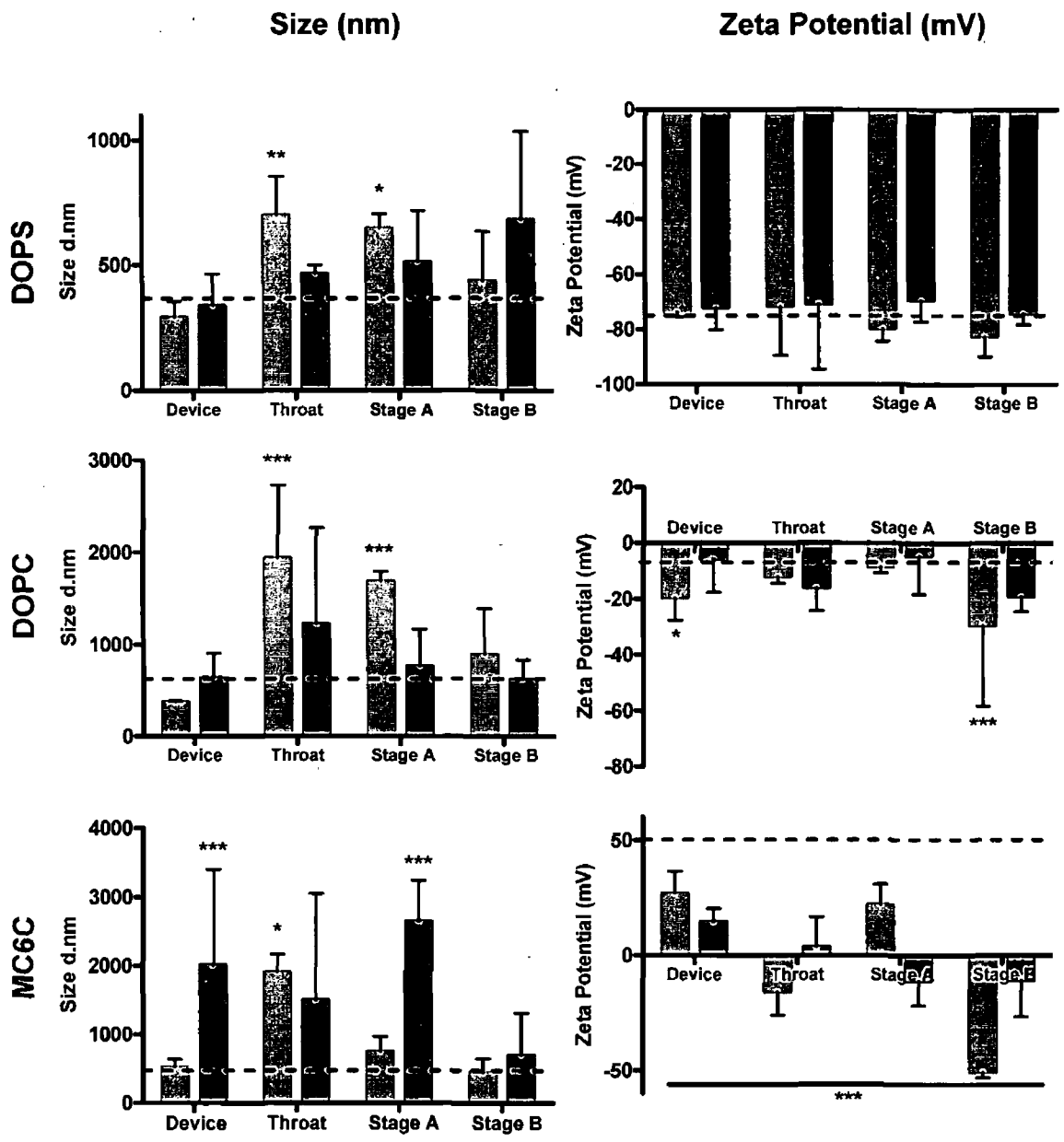


Figure 2.17: Size and zeta potentials of nebulised liposomes. Anionic (DOPS), neutral (DOPC) and mannosylated (MC6C) liposomes were nebulised using either an air-jet PARI ( ■ ) or vibrating mesh AeroNeb ( ■ ) nebulising device into a twin-stage impinger (TSI). Liposomes were recovered from the devices and each stage of the impinger corresponding to "Throat", upper lung (Stage A) and lower lung (Stage B) post-nebulisation and characterised by size (nm) and zeta potential (mV). A dashed line indicates the size or zeta potential of corresponding pre-nebulised liposomes. Data represented as means ± SD. Statistical significance was determined by two-way ANOVA vs pre-nebulised liposomes (* $p < 0.05$, ** $p < 0.01$, *** $p < 0.001$)

Liposomes encapsulating siRNA were also assessed but not coupled with the twin stage impinger. DOPS, DOPC and mannosylated liposomes encapsulating PEI/TNFα siRNA complexes were nebulised using an AeroNeb vibrating mesh nebuliser. These liposomes were selected as the siRNA-liposome model for nebulisation as they showed good *in vitro* transfection efficiencies (Chapter 3) and the effect of nebulisation would be more relevant. Liposomes encapsulating siRNA showed little change in size or zeta potential pre- and post-nebulisation particularly compared to empty liposomes (Figure 2.17). siRNA liposomes were not impinged due to limited size of volume preparation, difficulty in determining encapsulation efficiency and siRNA expense. Liposomes were nebulised using the AeroNeb nebuliser and immediately collected. Changes in size and surface charge were not significant. The mean diameter of anionic siRNA DOPS liposomes decreased from 403.7 ± 5.4 nm to 382.7 ± 3.6 nm with an increase in surface charge from -73.7 ± 1.7 mV to -69.9 ± 1.4 mV. DOPC liposomes encapsulating siRNA showed the least stability with an increase in size from 620.7 ± 13.3 nm to 792.5 ± 35.4 nm. Zeta potential of siRNA DOPC liposomes also increased 1.5 ± 0.3 mV to 4.5 ± 0.2 mV. Mannosylated liposomes encapsulating siRNA also showed an increase in size but not as substantial as uncoated DOPC liposomes. Mean diameter increased to 352 ± 2.2 nm from 310 ± 3.7 nm while zeta potential decreased from 56.8 ± 0.9 mV to 54.1 ± 1.5 mV.

Previously, gel electrophoresis of nebulised naked siRNA showed signs of degradation (Figure 2.15) with single yet smeared bands per lane following nebulisation by the PARI and AeroNeb devices. DOPS, DOPC and MC6C liposomes encapsulating PEI/siRNA complexes were also assessed by gel electrophoresis with the dual purposes of evaluating encapsulated siRNA integrity and to give an indication if nebulisation is associated with siRNA leakage or release from the liposomes. Before nebulisation a very faint band of 21 bp corresponding to siRNA can be visualised from the DOPS liposomes. siRNA is not detected following treatment with 1% SDS (or 0.3% Triton X, data not shown). The presence of siRNA in the pre-nebulised and post-nebulised DOPS sample in Figure 2.18A could be due to liposome instability. Following nebulisation siRNA was detected only in lanes loaded with DOPS liposomes. This suggests DOPC and mannosylated liposomes are more stable formulations than the siRNA encapsulating DOPS liposomes and therefore more suitable for nebulisation.

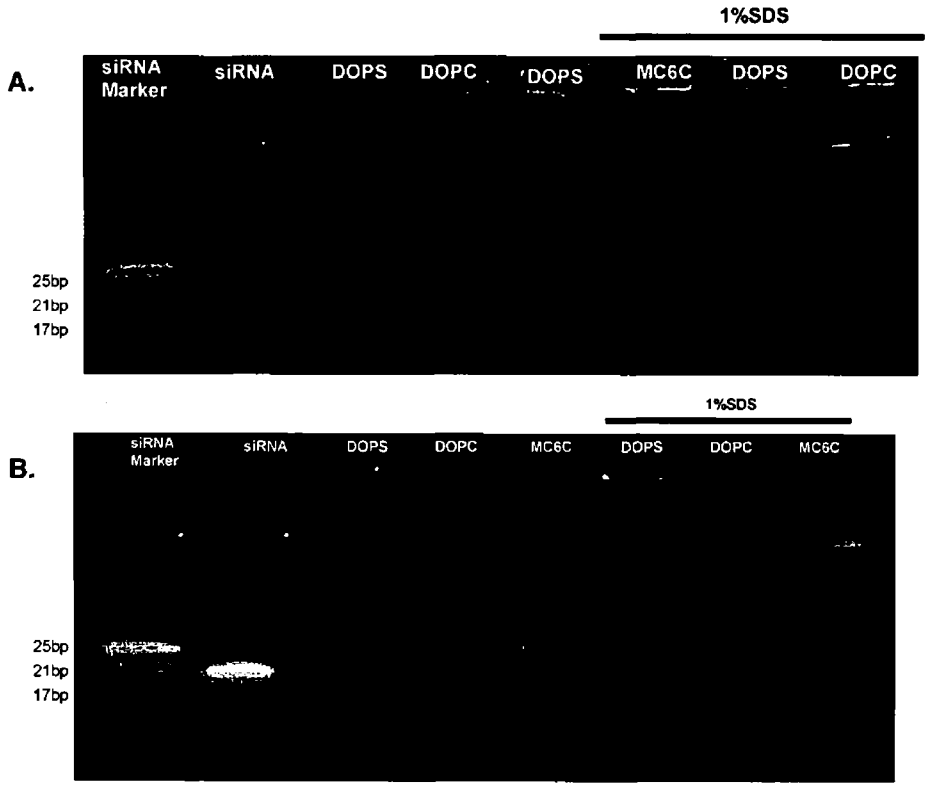


Figure 2.18: Polyacrylamide gels. DOPS, DOPC and mannosylated (MC6C) liposomes encapsulating siRNA complexed with PEI were nebulised using an AeroNeb Pro nebuliser. (A) show liposomes pre-nebulisation and (B) show formulations post-nebulisation. Liposomes were lysed using 1% SDS.

## 2.5 Discussion

Liposomes have been used to entrap molecules for almost half a century [86] and have since developed into carriers for drug delivery offering improved dosing, controlled release, targeting and biocompatibility over free drug and many other types of carriers. A carrier system for siRNA therapy is essential as siRNA can not cross the cell membrane due to its size and charge. Cationic liposomes have been the most extensively researched for siRNA and other nucleic acid delivery in the form of lipoplexes. However toxicity, immune activation and poor *in vivo* transfection have led to a need for alternative neutral and anionic lipid formulations for siRNA delivery to provide safe, non-toxic and biocompatible formulations. Inhalation as a therapeutic route allows rapid clinical response with minimal system side-effects as therapeutics can be delivered in low doses directly to the target organ [136].

A range of control (DOPC, DSPC and DOTAP) and targeted (DOPS and mannosylated) liposomes were prepared (Tables 2.11 and 2.12). Non-mannosylated liposomes particularly those composed of DOPC and DOPS were very reproducible to manufacture with each batch differing only by a few nm in mean diameter and having low PDI. A low PDI indicates uniformity. High PDI could signify aggregation, contamination or inefficient sizing [164].

Initially mannosylated liposomes included the lipid DSPC as a constituent. Use of this lipid has been applied in previous mannosylated liposome studies [115, 165]. DSPC is a neutral lipid with a high phase transition temperature (60°C). Characteristic phase transition temperatures ($T_c$) are reliant on both the length and saturation of the lipids fatty acid chains generally ranging from -20°C to 90°C [90]. Lipids tend to be rigid and ordered below their $T_c$ (gel phase) and in a liquid crystalline state (fluid phase) above the $T_c$ [90]. Therefore a benefit of a high $T_c$ which is above physiological temperature (37°C) is reduced bilayer fluidity and consequently a less leaky liposome and higher stability *in vivo* [166]. As a result hydration and extrusion must be carried out above this temperature. Sizing of DSPC liposomes gave mean diameters less than 200nm with PDI as high as 0.254. In all cases more than one peak was present, typically a second peak over 1000nm.

Size reduction of mannosylated liposomes containing DSPC was difficult. Extrusions were increased but multiple peaks and high PDI were still recorded. In many cases, higher concentrations of mannosylated cholesterol in the preparation meant sizing measurements were more variable and the PDI higher. Mean sizes per reading ranged from 165nm to 2074nm with PDI from 0.16 to 0.467. This suggests aggregation is occurring and is most likely due to the presence of mannosylated cholesterol. The addition of Mann-C4-Chol and Mann-C2-Chol made uniform size reduction more difficult. Wijagkanalan, *et al.* (2008) reported PDI of similar mannosylated liposomes ranging from 0.14 to 0.35 [115]. It is possible the high temperatures required for DSPC may also be having an effect on the mannosylated cholesterol. Liposomes were subsequently prepared substituting DOPC [167] for DSPC to eliminate any problems caused by temperature. Reproducible formulations were prepared with sizes less than 200nm

and low PDI using DOPC. Thus mannosylated DOPC based liposomes were assessed *in vitro* in Chapter 3. Although the $T_c$ of DOPC is -20°C the incorporation of cholesterol, which greatly affects bilayer fluidity, at a molar percentage of 30% can compensate for a low phase transition to form liposomes with better stability and reduce leakiness [90] *in vivo*. High temperatures may also have negative effects on siRNA stability.

Liposomes were loaded with free siRNA and encapsulation efficiencies determined. Cationic formulations are generally used for nucleic acid delivery as high encapsulation can be achieved by the complexation of positively charged lipids and negatively charged nucleic acid [92]. Encapsulation of free siRNA was low and irreproducible. However the incorporation of a small percentage of (10%) DOTAP [168] into the liposome itself improved the encapsulation efficiency up to 30%. It would be preferable to avoid the use of a cationic surface charge on the liposomes therefore pre-complexation or condensation of siRNA with a cationic lipid or polymer was carried out to decrease possible toxicity and improve encapsulation efficiency in targeted liposomes.

Three different cationic reagents were evaluated for siRNA condensation; DOTAP, protamine and PEI. Through size, zeta-potential and electrophoresis analysis optimal condensation parameters were found and condensed siRNA was encapsulated into liposomes. Studies have used triton X-100 disruption in combination with ribogreen assay to determine encapsulation efficiencies of liposomes loaded with protamine siRNA complexes [169] reporting 90% encapsulation efficiency. Huang *et al.* (2009) also incorporated calf thymus DNA into complexes with protamine:siRNA weight ratio of 1.2 [169]. However, repeated ribogreen assays of protamine siRNA complexes showed protamine interfered with the assay at all weight ratios. Additionally triton X-100 and SDS did not disassociate complexes. Other studies have used fluorescently tagged siRNA to determine encapsulation efficiencies by simply detecting fluorescence intensities in formulations before and after disruption by for example triton X-100 or separated from liposomes by filtration, ultracentrifugation or size exclusion columns [98, 170, 171]. Figure 2.12D shows fl-siRNA complexed with PEI disassociates at pH 12. Merkel *et al.* (2009) found at higher N/P ratios that fluorescence intensity increased and was not representative of the amount of free or uncomplexed fl-siRNA present [158]. Consequently a method to determine encapsulation efficiency of siRNA by liposomes could not be optimised.

Targeting to alveolar macrophages involves both cellular and anatomical targeting by means of inhalation. Aerosolisation of formulations is required for local delivery to the lungs and was characterised in advance of *in vivo* testing. The nebulisers evaluated represent the early and more recent products available for aerosolisation. AeroNeb® Micropump nebulisers are claimed not to disrupt or damage the molecular integrity of formulations and can aerosolise a wide range of formulations (Aerogen Ltd.). Liposome nebulisation has frequently been assessed using the TSI system coupled with jet nebulisers such as PARI LC plus [140, 146], or ultrasonic/mesh/electronic nebulisers including AeroNebPro-4 and -8 [146, 147], and Omron NE U07B [143]. To date, while mannosylated liposomes and siRNA liposomes have been

aerosolised for direct delivery to animal models, no aerosolisation data has been published. AeroNeb Pro nebuliser has been used to evaluate aerosolisation of siRNA polyester nanoparticles [153]. Additionally, Vyas *et al.* (2003) characterized anionic (incorporating DCP) and mannosylated (MBSA coated) liposome aerosols using a pressurized packed system [121].

siRNA is expensive and labile and therefore an efficient means of delivering it is critical. Overall the AeroNeb nebuliser was shown to be more efficient than the PARI device for aerosolising naked siRNA and a range of liposomes. Over 50% of liposome preparations were not recovered from the TSI system following aerosolisation by the PARI Air-jet device. During set up of naked siRNA aerosolisation via PARI nebuliser one side of the T –piece was attached to the "mouth" of the twin impinger and the other side sealed with parafilm to prevent escape of the aerosol. The omission of this step would explain the difference in the amount of loaded preparation recovered post nebulisation between naked siRNA and empty liposomes. Mannosylated liposomes deposited in TSI Stage B showed good stability in terms of size but a change in zeta-potential from positive to negative indicating damage to the mannosylated coating following nebulisation.

Gel electrophoresis showed slight leakage of siRNA from DOPS liposomes which was increased following AeroNeb nebulisation. Release of siRNA from DOPC or mannosylated liposomes was not detected pre- or post-nebulisation. This indicates DOPS liposome instability both pre- and post-nebulisation. Nebulised DNA encapsulating liposomes have been assessed in various studies and collected directly in glass tubes [140, 143], using a reflux reservoir [141], Anderson casade [143] or nebulised directly onto cells [144]. Nebulisation has previously been reported to damage naked DNA with liposomes affording some protection to maintain functional nucleic acids post-nebulisation. A comparison study between air-jet and ultrasonic nebulisation of PEGPEI-DNA complexes determined ultrasonic nebulisation to be a milder method for aerosolisation [172]. Nguyen *et al.* (2008) nebulised siRNA encapsulating polyester nanoparticles using an AeroNeb Pro nebuliser and noted changes in particle size and transfection efficiencies due to nebulisation which was dependent on the formulation [153].

A range of liposomes designed to target alveolar macrophages were prepared including DOPS and mannosylated liposomes targeting macrophage scavenger and mannose receptors respectively. Mannosylated cholesterol derivatives Mann-C2-Chol, Mann-C4-Chol and Mann-C6-Chol, differing in the cholesterol mannose linker length, were synthesized and incorporated into liposomes composed of neutral (DOPC) lipid and cholesterol. Differences in linker length have previously been assessed and may influence interaction with the mannose receptor [173, 174]. Various strategies for efficient encapsulation of siRNA into anionic and neutral liposomes were evaluated. Optimal siRNA liposomal systems were finally nebulised and assessed for stability and deep lung delivery. Nebulisation of empty liposomes showed some instability perhaps due to liposome fusion and damage to mannosylated coating. In conclusion, targeted liposomes were manufactured and a means of encapsulating siRNA was developed. Targeted siRNA liposomes could be aerosolised effectively.

**Key Findings**

- Synthesis of mannosylated cholesterols
- Preparation and characterisation of targeted liposomes
- Optimised method for maximal liposome encapsulation of siRNA
- Liposome formulation capable of nebulisation and therefore suitable for inhalation

# Chapter 3

# Liposomes for Targeted siRNA Delivery to Alveolar Macrophages

### 3.1 Introduction

Mononuclear phagocytes such as monocytes, macrophages and dendritic cells play a central role in innate immunity. The chief role of these cells is phagocytosis whereby cells will engulf and destroy apoptotic cells, pathogens and other targets generally by opsonin receptor-dependent mechanisms via complement- and Fc-receptors or opsonin receptor –independent mechanisms via lectin-receptors, SRs, stearylamine (SA) receptors or CD14 [111]. Liposomes are the most extensively explored delivery system for phagocyte-targeted therapies and offer many benefits such as low immunogenicity, biocompatibility, cell specificity and drug protection. However, liposomal drug carriers are also associated with poor scale-up and shelf-life, high cost and in some cases toxicity. The majority of studies have focused on the development of delivery formulations that avoid monocyte/macrophage clearance to enhance and prolong systemic circulation. Liposomal delivery systems targeting other cell types outside the MPS are modified to evade phagocytosis for instance "stealth liposomes" include poly-ethylene-glycol (PEG) into their formulation to shield the liposomes from the MPS and increase their circulation times [175]. Consequently there is now a greater understanding of the mechanisms of binding and uptake that can be harnessed for drug targeting to monocyte/macrophage cells.

#### 3.1.1 Liposomal Targeting to Macrophages

Liposome drug delivery systems can be formulated to exploit the physiological role of macrophages to provide specific targeting and enhance drug efficacy. Mononuclear phagocytes have key roles in metabolism such as cholesterol and bilirubin metabolism and pathogen clearance [28]. For this reason, specialised cell surface receptors are expressed, for example SRs, which allow the identification and uptake of materials. These receptors can also be targeted for drug delivery. Targeting of liposomes to monocytes and macrophages can be achieved through various strategies including modification of lipid composition and physicochemical properties such as size and charge and by the inclusion of surface ligands including peptides such as Arg-Gly-Asp (RGD) [125], antibodies for example anti-CC531 antibodies [128], polysaccharides such as O-stearyl amylopectin (O-SAP) [121], glycolipids such as Man3-DPPE [134, 135] and Mann-C4-Chol [130] and glycoproteins for example fibronectin [107]. Our strategies use anionic phosphatidylserine composed liposomes to target macrophage SRs and mannosylated liposomes composed of neutral lipids for macrophage MR targeting (Figure 3.1).

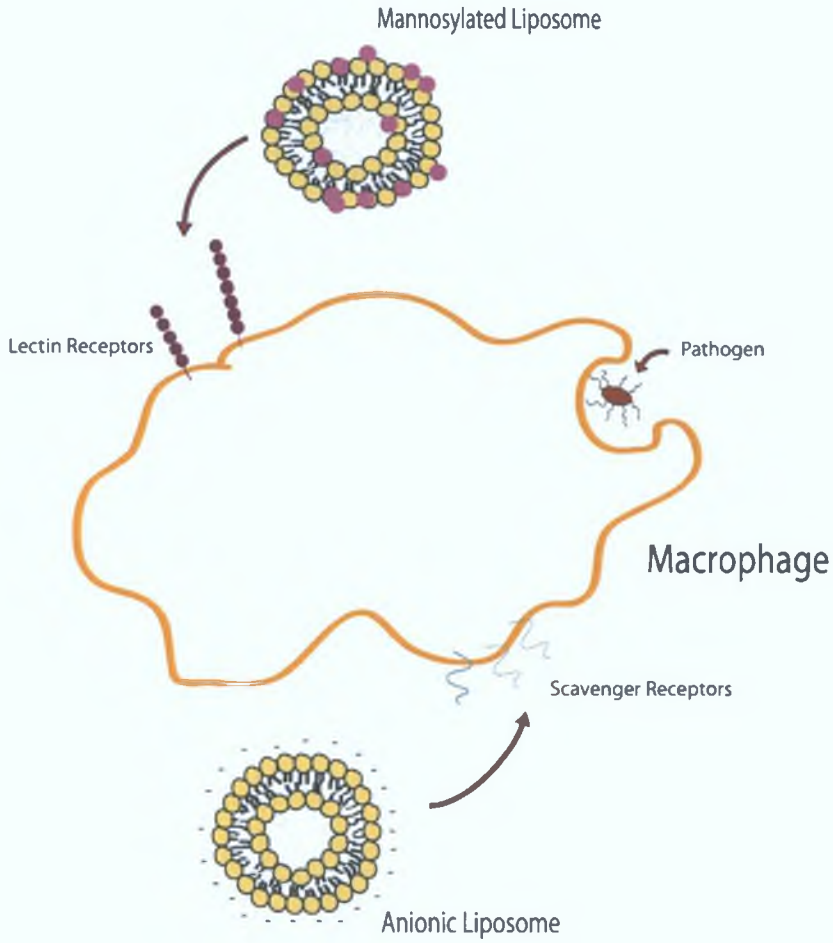


Figure 3.1: Liposomal targeting strategies to alveolar macrophages

#### 3.1.1.1 Anionic Liposomes

Cationic liposomes are associated with efficient cellular delivery of drug cargoes and routinely applied for *in vitro* gene delivery [176]. Electrostatic interactions between positively charged liposomes and the negatively charged cell membranes and cell surface proteoglycans [177] facilitates cell uptake. Unfortunately, cationic liposomes can cause cytotoxicity limiting their safety for clinical use [93]. In RAW264.7 macrophages cationic liposomes containing SA have previously been shown to induce apoptosis through mitochondrial pathways generating ROS, releasing cytochrome C, caspase-3 and -8 and more recently activating PKCδ possibly by cell surface proteoglycan interaction [178-181]. Consequently interest has turned to neutral and anionic liposomes for drug delivery applications. Currently there are several FDA approved liposomes available for the delivery of drugs such as amphotericin B (AmBisome®, ABELCET® and Amphocil) and doxorubicin (Doxil®) [86]. Although there are a number of amphotericin B liposome therapeutics available the liposome formulations of each differ considerably in terms of lipid composition, shape, size, stability, pharmacokinetics and toxicity [182]. The lipid compositions do not include cationic lipids but consist of hydrogenated soy phosphatidylcholine, cholesterol and distearoyl-phophatidylglycerol (DSPG); dimyristoyl phosphatidylcholine and dimyristoyl phosphatidylglycerol and cholesteryl sulfate for AmBisome®, ABELCET® and Amphocil respectively [182].

Anionic lipids such as PS and PG are preferentially recognised by macrophages [107]. Comparison studies between PC (neutral) and PS composed liposomes have long established the enhanced macrophage internalisation of negative liposome formulations [183]. Negative charge can also be achieved by the incorporation of DCP [109]. Vyas *et al.* (2004) showed a 3.4-fold increase in rifampicin lung retention in rats when rifampicin was encapsulated in negatively charged DCP, PC and cholesterol composed liposomes compared to free drug after aerosol administration [121]. Furthermore work by us to deliver recombinant SLPI (rSLPI) encapsulated in DOPS:Chol (7:3 molar ratio) liposomes has shown enhanced monocyte/macrophage uptake of liposomes both *in vitro* and *in vivo* [154]. Detection of rSLPI in BALF was decreased when rSLPI was delivered encapsulated in anionic liposomes (Figure 3.2A). Additionally BAL cell internalisation of the intratracheally instilled rSLPI was greater when rSLPI was encapsulated in anionic liposomes compared to free rSLPI in guinea pigs 48 hours post-administration (Figure 3.2B) [154]. Monocytes were the most abundant cell type present in the BALF of these animals indicating monocyte targeting which was also confirmed *in vitro* [154].

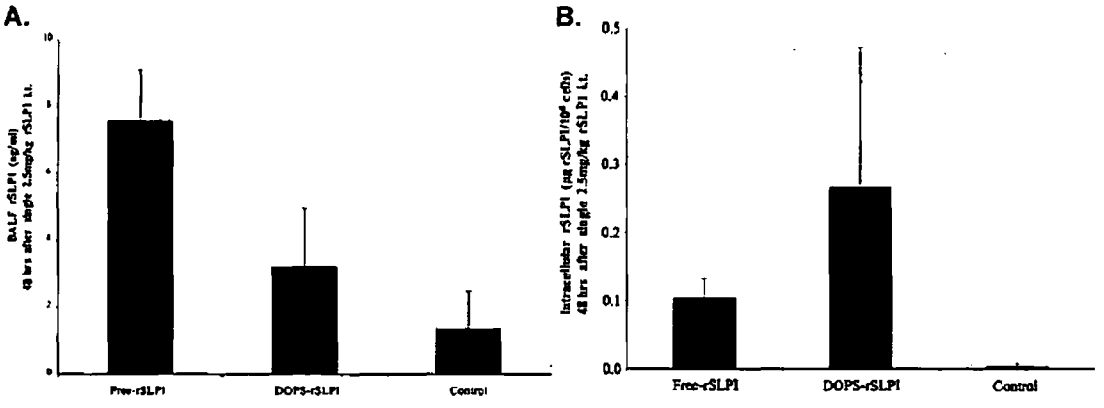


Figure 3.2: (A) rSLPI concentration present in bronchoalveolar lavage fluid (BALF) of single prophylactic dose to guinea pigs. BALF was collected 48 hrs following a single 2.5 mg rSLPI/kg dose by intratracheal instillation. (free-rSLPI n=3; DOPS-rSLPI n=5; Control (DOPS-Empty or PBS) n=3). (B) rSLPI concentration in BALF cells taken from single prophylactic dosed guinea pigs. Cell lysates were collected 48 hrs following a single 2.5 mg rSLPI/kg dose by intratracheal administration. (free-rSLPI n=3; DOPS-rSLPI n=5; Control [DOPS-Empty or PBS] n=9; ± S.D.) Data represented as means ± SD. [154]

The composition of the inner membrane leaflet of eukaryotic cells [111] consists of PS and phosotidylethanolamine (PE) with an outer layer of PC and sphingomyelin (SM) [112, 113]. Apoptosis results in PS being exposed on the outer cell surface and the induction of monocytic phagocytosis. It is believed that PS target SRs on macrophages. What is more, PS can activate complement and associate with plasma apolipoproteins such as ApoE and therefore promote phagocytosis by macrophages [184]. There are six classes of SRs with A, B and D as the most likely participants in liposome recognition [184]. Previously, liposomes composed of DOPS, DOPE and cholesterol at a molar ratio 1:1:1 have been mixed with siRNA pre-complexed with PEI to form artificial virus-like particles (AVPs) [185]. These AVPs were shown

to mediate gene silencing *in vitro* in primary neurons with a reduction in cytotoxicity compared to commercial cationic transfection reagent Lipofectamine 2000™ [185].

### 3.1.1.2 Mannosylated Liposomes

A multitude of ligands are currently being assessed which make use of mononuclear phagocytes characteristic receptor expression and phagocytic innate processes. Using a ligand targeting strategy for liposome drug delivery has many advantages including increasing target specificity and avoiding the need for cationic lipids to trigger intracellular delivery. Immune cells including alveolar macrophages, peritoneal macrophages, monocyte-derived dendritic cells and Kupffer cells constitutively express high levels of the MR. Macrophages can therefore be targeted via mannosylated nanoparticles (Figure 3.1). The MR is a C-type lectin type I transmembrane protein [43, 114] whose ligands possess a terminal non-reducing sugar such as mannose, glucose, *N*-acetylglucosamine and fucose [186, 187]. These receptors play numerous roles in immune function and inflammation [36, 116]. Moreover MR activation has been linked to the initiation of an anti-inflammatory immunosuppressive programme in cells [188] and impaired NFκB activation [189]. Hence, MR has the potential to be exploited for targeted drug delivery to macrophages but also as a therapeutic target. Herein we aimed to explore mannosylated liposomes with an anti-inflammatory cargo such as anti-inflammatory siRNA as dual acting therapeutics.

Mannosylated liposomes have repeatedly been shown to preferentially target macrophages and DCs attaining enhanced cellular uptake both *in vitro* and *in vivo* with better *in vitro/in vivo* correlation than for non-ligand containing liposomes [110, 115, 116, 130-135, 165, 174, 183, 190-193]. Mannosylation has been achieved by the incorporation of ligands such as alkyl mannosides [174], Cholesten-5-yloxy-*N*-(4-((1-imino-2-α-thioglycosylethyl)amino)butyl) formamide (Mann-C4-Chol) [130, 165, 193, 194], Mann-His-C4-Chol [194], $Man_2DOG$ [131], 4-aminophenyl-a-D-mannopyranoside [133, 190] and manntriose (Man3)-DPPE [134, 135, 191] into the liposome formulations or by liposome coating with *p*-aminophenyl-α-D-mannopyranoside [132].

Over the past decade Hasida and colleagues have led the way in the development of mannosylated liposomes targeted to macrophages and DCs for the delivery of anti-inflammatory agents such as dexamethasone palmitate (dex) [130] and NFκB decoy and anti-cancer agents including CpG oligonucleotides and DNA [195]. Intratracheally administered Man-C4-Chol liposomes were shown to be preferentially taken up by alveolar macrophages which was mediated via MR endocytosis as revealed by inhibition studies. Mannosylation and the extent of this mannosylation significantly improved liposome internalisation by macrophages [115]. The ability of these liposomes to efficiently deliver their load has been the focus of a more recent study in which the use of bubble liposomes and ultrasound in combination with mannosylated liposomes to deliver plasmid DNA to mouse peritoneal macrophages was assessed [192]. To date, mannosylated liposome delivery has not been applied to siRNA.

### 3.1.2 Chapter Aims

The focus of this chapter is to evaluate a range of targeted liposomes *in vitro* in terms of uptake, cytotoxicity, immunogenicity and knockdown ability. In order to achieve this high throughput screening assays were developed.

- To assess targeted liposome uptake by macrophages
- To determine knockdown in LPS stimulated macrophages via targeted liposomes using anti-inflammatory siRNA
- To evaluate toxicity and immunogenicity of targeted liposomes *in vitro*

### 3.2 Materials

10-Plex TH1/TH2 Human, Mesoscale Discovery

12 well plate, Grenier Bio One

Alexa Fluor® 488 Goat anti-Rabbit IgG (H+L), Invitrogen

BCA assay, Pierce

bisBenzimide H 33342 trihydrochloride (Hoescht), Sigma Aldrich

Bovine serum albumin (BSA), Sigma

Cellomics® Multiparameter Cytotoxicty 3 kit, Thermo

CELLSTAR® 96well plate, Grenier Bio One

Confocal Laser Scanning Microcope, Zeiss LSM 510

DAKO fluorescent mounting medium (DakoCytomation S3023), DAKO

EDTA, Amresco

FBS, BioSera

Ficoll-Paque Plus

Fluorescent Microscope, Nikon Eclipse 90i

Goat anti-rabbit secondary antibody Alexa Fluor® 488, Invitrogen

Hoechst 33342, Sigma

IN Cell Analyzer 1000, GE Healthcare

Lab-Tek™ Chamber Slides, Nunc

Lipofectamine 2000$^{TM}$, Invitrogen

LS 50B Fluorescence Spectrometer, Perkin Elmer

MACS Columns, Miltenyi Biotec

MACS MicroBead Kit, Miltenyi Biotec

MACS® Separator for MicroBeads, Miltenyi Biotec

Mannose Receptor Rabbit Polyclonal Antibody, Abcam

Micro BCA™ Protein Assay Kit, Thermo Scientific Pierce

PBS, GIBCO

Phalloidin-FITC, Sigma Aldrich

Phalloidin-TRITC, Sigma Aldrich

Phorbol myristate acetate (PMA), Sigma Aldrich

Rabbit polyclonal mannose receptor antibody, Abcam

RPMI 1640, BioSera

siGENOME Non-Targeting siRNA #2, Dharmacon

siGLO Lamin A/C Control siRNA (Human), Dharmacon

Silencer® Select Pre-designed TNFα siRNA, Ambion

THP-1 cell line. ATCC

THP1-XBlue cell line, Invivogen

TNFα ELISA, Biolegend

### 3.3 Methods

#### 3.3.1 siRNA

siGENOME Non-Targeting siRNA #2 (Dharmacon) is designed to target firefly luciferase mRNA (U47296) with at least 4 mismatches to human, mouse or rat genes serving as a non-target negative control to provide a baseline cellular response to siRNA transfection. siGLO Lamin A/C Control siRNA (Human) is a fluorescent siRNA that targets Lamin A/C and is chemically modified with a DY-547 fluorophore. The sequences of siGENOME non-targeting #2 and siGLO siRNA were 5'-UAAGGCUAUGAAGAGAUAC-3' and 5' ACCAGGUGGAGCAGUAUAA 3' respectively. Three *Silencer*® Select Pre-designed siRNA sequences, sequence 1 (siRNA ID # s14249) sense 5'-GCGUGGAGCUGAGAGAUAAtt-3' and anti-sense 5'-UUAUCUCUCAGCUCCACGAca-3', sequence 2 (siRNA ID # s14248) sense 5'-GACCUCACCUAGAAAUUGAtt-3' and antisense 5'-UCAAUUUCUAGGUGAGGUCtt-3' and sequence 3 (TNFα 3; siRNA ID # s14247) sense 5'-AGGCGGUGCUUGUUCCUCAtt-3' and anti-sense 5'-UGAGGAACAAGCACCGCCUgg-3' targeted to TNFα (Ambion). siRNAs for *in vitro* studies were reconstituted with nuclease-free buffer (Dharmacon) or water (Ambion) to a concentration of 20μM (non-targeting and siGLO siRNA) or 100μM (TNFα siRNA).

#### 3.3.2 Cell Culture

##### 3.3.2.1 THP-1 Cells

THP-1 cells a human acute monocytic leukemia cell line derived from a 1 year old male infant were maintained in RPMI 1640 (BioSera) supplemented with 10% heat inactivated fetal bovine serum (FBS, BioSera) from passage 4 – 20 in a humidified atmosphere at 37°C and 5% $CO_2$. THP-1 cells were differentiated by the addition of 100nM phorbol myristate acetate (PMA) and incubated at 37°C for 72 hours.

##### 3.3.2.2 Primary Blood Monocyte Isolation

Ethical approval was obtained from the Research Ethics Committee (REC), Royal College of Surgeons in Ireland (REC651). Human monocytes were isolated from blood collected from healthy donors using Ficoll-Paque Plus density gradient separation and MACs colloidal super-paramagnetic MicroBeads conjugated with monoclonal mouse anti-human CD14 antibodies. 60ml of blood was collected with 10% Na citrate and transferred to 50 ml tubes. Blood was diluted 1:1 with PBS and carefully layered onto Ficoll-Paque Plus (volume ratio PBS:blood:Ficoll-Paque of 1:1:1). Tubes were centrifuged at 300xg for 30 minutes with no brake. Following centrifugation a distinct band is formed at the blood/Ficoll-Paque interface. This fraction was carefully aspirated using a sterile pasture pipette into fresh 50ml tubes. The volumes per tube were adjusted to 50ml with PBS and tubes were centrifuged at 400xg for 5 minutes with the brake on to pellet cells. If red blood cells were present the pellet was

resuspended in 5ml red cell lysis buffer, the volume per tube brought up to 50ml and centrifugation at 400xg for 5 minutes repeated. Supernatants were discarded and pellets resuspended in RPMI and combined. A cell count was taken using a haemocytometer. Cells were centrifuged at 300xg for 10 minutes and supernatants were discarded. The cell pellet was resuspended in buffer (0.5% FBS and 2mM EDTA in PBS pH 7.2) 80µl per $10^7$ cells. MACS CD14 magnetic microbeads were added (20µl per $10^7$ cells), mixed and incubated for 15 minutes at 4°C. Cells were washed with buffer by adding 10 times the labelling volume of buffer, centrifuging at 300xg for 10 minutes and resuspending in 500µl of buffer. A MACS LS column was placed in the MACS Multistand magnetic separator and equilibrated by adding 3ml of buffer. Once buffer has eluted from the LS column cell suspension was loaded. CD14 positive monocytes were retained on the column. The column was washed by loading 3ml of buffer on to the column and allowing buffer and negative cells to elute. Washes were repeated twice more. The column was removed from the magnetic separator. 5ml of buffer was loaded onto the column and monocytes were flushed using the supplied plunger. Cells were collected and counted.

#### 3.3.2.3 THP1-XBlue™ cells

THP1-XBlue™ cells are stably transfected THP-1 cells expressing secreted embryonic alkaline phosphatase (SEAP) gene which is induced by the transcription factors NF-κB and activator protein-1 (AP-1). Cells were maintained in RPMI 1640 supplemented with 10% heat inactivated FBS and 200µg/ml of selection marker Zeocin™. TLR stimulation induces NFκB and AP-1 production which in turn leads to expression of the reporter protein SEAP. THP1-XBlue™ cells were differentiated by the addition of 100nM PMA and incubated at 37°C for 72 hours.

### 3.3.3 Immunofluoresence Microscopy to Determine Mannose Receptor Expression

THP-1 cells were seeded at $1x10^5$ cells/ml in 96-well plates, differentiated and fixed with 4% paraformaldehyde for 20 minutes. Cells were incubated in 1% bovine serum albumin (BSA) in PBS tween (PBST) for one hour and then for another hour at room temperature with 0, 1 or 2 µg/ml rabbit polyclonal MR antibody (Abcam). Cells were then washed with PBS three times with 5 minute incubations per wash and were subsequently incubated with goat anti-rabbit secondary antibody Alexa Fluor® 488 (1/200, 1/500 and 1/1000 dilutions) for 1 hour and counterstained with Hoechst 33342 (5 minutes) and phalloidin-tetramethyl rhodamine isothiocyanate (TRITC) (45 minutes). Images were acquired using an INCELL 1000 cell analyser.

### 3.3.4 *In Vitro* Uptake Studies

#### 3.3.4.1 Fluorescence Spectroscopy

THP-1 cells were differentiated at $1x10^5$ cells/ml in 12 well plates and incubated for 2 hours with anionic, neutral and mannosylated liposomes at 0, 100 and 300μM (Table 3.1). Liposomes were either unlabelled or fluorescently tagged with rhodamine. Media was removed and cells were washed three times with warmed PBS. Cells were lysed with 200μl 0.1% Triton X-100 in PBS and centrifuged at 2000rpm for 5 minutes to remove cell debris. 150μl of lysed cells were brought up to 500μl with PBS and fluorescence was measured using a fluorescence spectrometer (LS 50B) at 550nm excitation and 590nm emission wavelengths.

**Table 3.1: Liposome composition for differentiated THP-1 cell uptake assessment by Spectrofluorimetry**

| Liposome Nomenclature | Lipid Components Molar Ratio | | | | | |
|---|---|---|---|---|---|---|
| | DOPC | DOPS | Choi | MC2C | MC4C | MC6C |
| DOPS | - | 70 | 30 | - | - | - |
| DOPC | 70 | - | 30 | - | - | - |
| MC2C-2.5 | 70 | - | 27.5 | 2.5 | - | - |
| MC2C-5 | 70 | - | 25 | 5 | - | - |
| MC2C-7.5 | 70 | - | 22.5 | 7.5 | - | - |
| MC4C-2.5 | 70 | - | 27.5 | - | 2.5 | - |
| MC4C-5 | 70 | - | 25 | - | 5 | - |
| MC4C-7.5 | 70 | - | 22.5 | - | 7.5 | - |
| MC6C-2.5 | 70 | - | 27.5 | - | - | 2.5 |
| MC6C-5 | 70 | - | 25 | - | - | 5 |
| MC6C-7.5 | 70 | - | 22.5 | - | - | 7.5 |

Fluorescently labelled siRNA (siGLO) was encapsulated in MC4C-7.5 liposomes with or without the incorporation of 10% DOTAP into the liposome formulation. THP-1 cells differentiated at $1x10^5$ cells/ml in 12 well plates were incubated for 2 hours with naked siGlo or siGlo encapsulated in MC4C liposomes (Table 3.2). THP-1 cells were washed three times with warmed PBS, lysed with 200μl 0.1% TritonX100 and centrifuged at 2000rpm for 5 minutes to remove cell debris. 150μl of lysed cells were brought up to 500μl with PBS and fluorescence was measured using a fluorescence spectrometer (LS 50B) at 550nm excitation and 590nm emission wavelengths.

**Table 3.2: siRNA-Liposome composition for differentiated THP-1 cell uptake assessment by Spectrofluorimetry**

| Liposome Nomenclature | siRNA | Liposome Components Molar ratio | | | |
|---|---|---|---|---|---|
| | | DOPC | DOTAP | Choi | MC4C |
| siGLO | siGLO | - | - | - | - |
| MC4C siGLO | siGLO | 70 | - | 22.5 | 7.5 |
| MC4C/DOTAP siGLO | siGLO | 60 | 10 | 22.5 | 7.5 |

Total protein levels were determined using a bicinchoninic acid (BCA) assay and used to normalise the fluorescence levels per well. BCA assay was carried out as per the manufacturers instructions using a clear 96-well plate and Wallac mulitplate reader. Briefly, BSA standard curve was prepared ranging from 0µg/ml to 100pg/ml. Diluted albumin standard (150µl) or 75µl of diluted cell lysates were added to a 96 well plate in triplicate. Volumes per well were brought up to 150µl. Working reagent (150µl) was added to each well. Plates were incubated for 2 hours at 37°C and absorbance was read at 562nm.

### 3.3.4.2 High Content Cell Analysis (HCA)

A HCA method was developed for analysis of uptake to enable high throughput studies. Cells were differentiated at a density of $1x10^5$ cells/ml in 96-well plate. Anionic, neutral and mannosylated liposomes were incubated with cells in triplicate according to Table 3.3. Additionally 200nm liposomes were incubated with cells for 2 hours at 4°C at 100, 200 and 300µM. Liposomes were either unlabelled or rhodamine-tagged. Cells were washed three times with warmed PBS, fixed with 4% paraformaldehyde and stained with phalloidin-fluorescein isothiocyanate (FITC) and Hoescht 33342. 150µl of PBS was added to each well and plates were stored at 4°C in the dark until analysed.

**Table 3.3: Liposome treatments for differentiated THP-1 cell uptake assessment by HCA**

| | Size (nm) | Concentration (µM) | Time (hours) |
|---|---|---|---|
| **Size** | Unextruded, 100, 200, 400, 1000 | 200 | 2 |
| **Concentration** | 200 | 0, 50, 100, 200, 300 , 1000 | 2 |
| **Time** | 200 | 200 | 0.5, 1, 2, 4, 24 |

HCA was carried out using INCELL 1000 analyser. Images were acquired in three channels, 5 fields per well and analysed using INCELL1000 analyser software. Multi target analysis module was used with nuclei, cells and organelles inputted as objects to be measured and assigned wavelengths for nuclei, cells and liposomes respectively. Parameters for segmentation analysis were then inputted. Nuclei were identified using Top Hat. A minimum area was inputted based on the images required and sensitivity generally set to 80%. Multi-scale top hat was used to identify cells. A minimum area based on representative images acquired was inputted and sensitivity set to 70%. Organelles (or liposomes) were identified using mulit-target analysis method. A minimum and maximum size was specified and a scale number selected. Scales can be set from 1 to 10 depending on the range of sizes to be detected. Scale was set to 10. It was necessary to acquire images for liposome uptake at least at a magnification of 200x to identify liposomes at the minimum end of the size range. A sensitivity level of 30% was used.

Detection of liposomes was specified in cells only. Input values and sensitivity settings were adjusted for each experiment until all parameters were correctly assigned and identified (Figure 3.3).

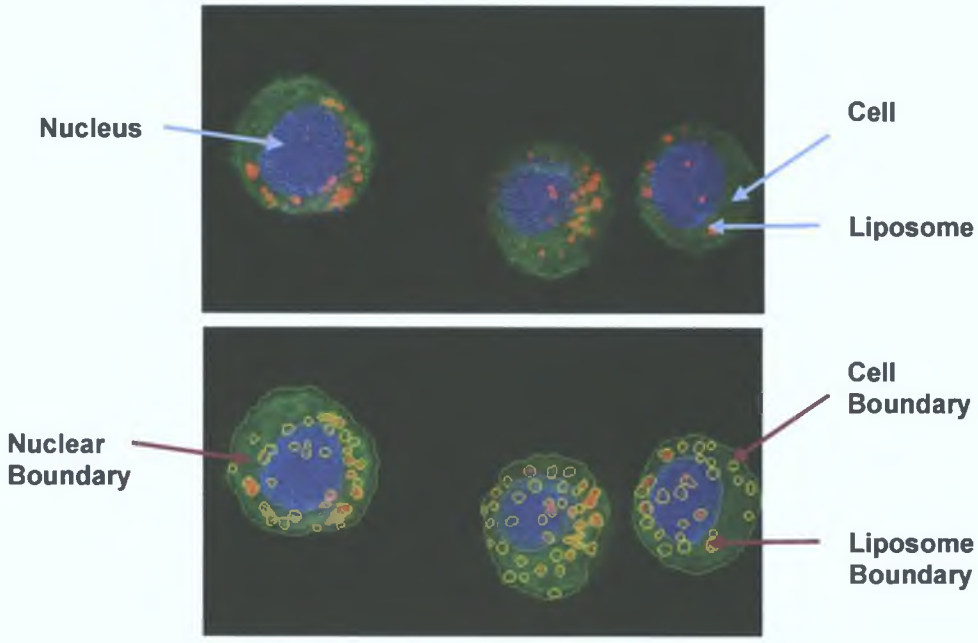


Figure 3.3: INCELL cell analysis. Images acquired at 3 excitation/emission wavelengths 360/480 blue (nuclei; hoescht), 480/535 green (cells; phalloidin-FITC) and 535/620 (red; liposomes). Minimum area of nuclei, average are of cells and minimum and maximum size of liposomes was inputted into software. Images of each wavelength was analysed and nuclei, cells and liposomes were segmented. Fused images show each component circled. The number of liposomes in cell regions only were counted.

### 3.3.5 Toxicity

Cellomics® Multiparameter Cytotoxicty 3 kit and an INCELL 1000 analyser were used to determine cytotoxicity following liposome treatment and optimised for differentiated THP-1 cells. THP-1 cells were differentiated at $1.5x10^5$ cells/ml in a flat-blottomed 96-well plate (CellStar, Grenier) for 72 hours. Media was replaced with fresh media and cells were treated with liposomes at concentrations of 0, 100 or 300μM in triplicate and incubated at 37°C for 23.5 hours. Cells were also treated with valinomycin (120μM) for 23.5 hours as a positive toxicity control. 50μl of Live Staining Solution (2.1μl permeability dye and 21μl mitochondrial membrane potential dye in 6ml complete RPMI) was added to each well and cells were incubated at 37°C for 30 minutes. Media and staining solution was removed and the wells were washed with PBS. To fix cells, 4% paraformaldehyde (100μl) was added to each well and incubated at room temperature for 20 minutes. The wells were washed twice with PBS and 100μl of permeablisation buffer (0.1% Triton X-100 in PBS) was added to each well and incubated for 10 minutes protected from the light. Washing was repeated and 100μl of blocking buffer was added to each well and incubated at room temperature for 15 minutes. Blocking buffer was aspirated and 50μl of primary antibody solution (15μl cytochrome c primary antibody

in 6ml of blocking buffer) was added to each well and incubated at room temperature for 60 minutes protected from the light. Wells were washed three times with PBS followed by the addition of 50µl of a secondary antibody/staining solution (0.6µl Hoechst dye and 12µl DyLIght 649 Goat anti-mouse antibody in 6ml of blocking buffer) to the wells. Cells were incubated for 60 minutes at room temperature protected from the light followed by three washes with PBS. 150µl of PBS was added to each well and the plate was stored at 4°C protected from light until analysis.

Images were acquired by an INCELL 1000 analyser within 24 hours in 4 fields per well using 4 wavelengths; excitation/emission wavelengths of 360/460nm (Hoechst dye), 480/535nm (Permeability dye), 535/600nm (Mitochondrial Membrane Potential dye) and 620/700nm (DyLight 649). Cell loss, nuclear area, nuclear intensity, cytochrome c release, mitochondrial membrane potential and cell permeability were determined using INCELL analysis software using multiparameter target analysis and the settings in Table 3.4. Region growing method was used to identify nuclei as nuclei size was more variable. Segmentation of cells was performed using the collar method. This sets up a ring-shaped region around the nucleus using a specified average cell radius value to assign this region as the cell. Mitrochondrial membrane potential, cytochrome c and cell permeability were set as references and measurements were detected in cells. Intensities of each reference in cells were compared between treatments. Images were acquired at 10x magnification to include a larger number of cells in the analysis. Input values and sensitivity settings were adjusted for each experiment until all parameters were correctly assigned.

**Table 3.4: Representative Parameters for HCA Analysis of Liposome Toxicity in THP-1 Cells**

| Parameters | Wavelength (Ex/Em wavelengths, nm) | Analysis Settings |
|---|---|---|
| **Nucleus** | 360/460 | Region growing; min. area 33.2µm$^2$ |
| **Cell** | - | Collar; 11µm |
| **Permeability** | 480/535 | Reference; In Cell |
| **Mitochondrial Membrane Potential** | 535/600 | Reference; In Cell |
| **Cytochrome c** | 620/700 | Reference; In Cell |

### 3.3.6 *In Vitro* Knockdown Studies

#### 3.3.6.1 Targeted Knockdown of TNFα Expression in Differentiated THP-1 Cells

THP-1 cells were seeded $2\times10^5$ cells/well in a 96 well culture plate and differentiated. Cells were treated with an equal amount of siRNA complexed with lipofectamine 2000 or encapsulated in mannosylated (MC4C) liposomes for 3 hrs and media was replaced. Cells

were stimulated with 100ng/ml LPS and supernatants were collected 24 and 48 hours post-transfection 3 hours following LPS stimulation. TNF-α production was estimated by enzyme linked immunosorbant assay (ELISA; 3.3.6.3).

### 3.3.6.2 Targeted Knockdown of TNFα Expression in Primary Monocytes

Isolated primary monocytes were seeded at $3x10^4$ cells per well in 96 well plates and incubated at 37°C 5% $CO_2$ overnight. Media was changed leaving adherent macrophages. siRNA transfections were mediated by a commercial transfection reagent Lipofectamine 2000 and various liposome formulations listed in Table 3.5. Non-target or three TNFα targeted siRNAs were diluted in serum free RPMI while 1µl of lipofectamine 2000 was diluted separately in serum free RPMI. Diluted siRNA and lipofectamine 2000 were mixed and incubated at room temperature for 20 minutes to allow complexation. siRNA lipofectamine 2000 complexes were added dropwise to wells in triplicate. 4.5µl of each liposome preparation (~50ng siRNA) was added to wells in triplicate. Cells were incubated with liposomes at 37°C. Cells were stimulated with 100ng/ml LPS for 3 hours prior to each media collection time point of 24 and 48 hours. TNFα expression levels were determined by ELISA (3.3.6.3).

**Table 3.5: Liposome Formulations for *In Vitro* Transfection of Primary Monocytes**

| siRNA Liposome Nomenclature | Liposome | N:P or Weight Ratio | Cationic Complexing Reagent | siRNA |
|---|---|---|---|---|
| DOPS DOTAP/NT | DOPS | 4 | DOTAP | Non-Target |
| DOPS PEI/NT | DOPS | 7 | PEI | Non-Target |
| DOPS Protamine/NT | DOPS | 4 | Protamine | Non-Target |
| DOPS DOTAP/NT | DOPS | 4 | DOTAP | TNFα |
| DOPS PEI/NT | DOPS | 7 | PEI | TNFα |
| DOPS Protamine/NT | DOPS | 4 | Protamine | TNFα |
| DOPC DOTAP/NT | DOPC | 4 | DOTAP | Non-Target |
| DOPC PEI/NT | DOPC | 7 | PEI | Non-Target |
| DOPC Protamine/NT | DOPC | 4 | Protamine | Non-Target |
| DOPC DOTAP/NT | DOPC | 4 | DOTAP | TNFα |
| DOPC PEI/NT | DOPC | 7 | PEI | TNFα |
| DOPC Protamine/NT | DOPC | 4 | Protamine | TNFα |
| MC6C DOTAP/NT | MC6C | 4 | DOTAP | Non-Target |
| MC6C PEI/NT | MC6C | 7 | PEI | Non-Target |
| MC6C Protamine/NT | MC6C | 4 | Protamine | Non-Target |
| MC6C DOTAP/NT | MC6C | 4 | DOTAP | TNFα |
| MC6C PEI/NT | MC6C | 7 | PEI | TNFα |
| MC6C Protamine/NT | MC6C | 4 | Protamine | TNFα |

#### 3.3.6.3 TNFα Enzyme Linked Immunosorbant Assay (ELISA)

Media was collected from transfected cells 3 hours following LPS stimulation and frozen at -80°C until assayed. An ELISA was carried out as per manufacturer's instructions. TNFα capture antibody was diluted 1/200 in provided coating buffer and 100µl was added to each well of a NUNC Maxisorp™ 96 MicroWell plate. The plate was sealed and incubated at 4°C overnight. The plate was washed 4 times with wash buffer (PBS and 0.05% Tween-20, pH 7.4) and blotted dry. 200µl of assay diluent was added to each well and plates were sealed and shaken for 1 hour at room temperature to block non-specific binding. Washing was repeated. Mouse TNFα standard curve was prepared from provided stock solution and diluted in assay diluent to give 500, 250, 125, 62.5, 31.3, 15.6 and 7.8 pg/ml of mouse recombinant TNFα. 100µl of standards and appropriately diluted samples were added to wells in duplicate and incubated for 2 hours at room temperature in sealed plates with shaking. Washing was repeated and 100µl of Avidin-horseradish peroxidise (HRP) was added to each well, the plated sealed and incubated at room temperature for 30 minutes with shaking. Washing was repeated allowing the wash buffer to soak for up to 1 minute for each wash to lower background readings.

Finally 100µl of TMB substrate solution was added to each well and incubated for at least 10 minutes in the dark. The reaction was stopped by the addition of 100µl 2N $H_2SO_4$ stop solution per well. Absorbance was read at 450nm.

### 3.3.7 Liposome Immunogenicity Screening

#### 3.3.7.1 NF-κB Induction in THP-1 Blue Cells

THP-1 Blue cells (NF-κB/AP-1 Reporter Monocytes) were differentiated for 72 hours at $1x10^6$ cells/ml in a 96 well plate. PMA free media (100µl) was replaced daily for a further 5 days to remove residual PMA. Liposomes were added to cells in fresh media at 0, 100, 200 and 300µM final concentration in triplicate. Cells were stimulated with 100ng/ml LPS as a positive control. After 24 hours 20µl of media was removed and was added to 180µl of QUANTI-Blue™. After a 4 hour incubation absorbance measured at 630nm using a mulitplate reader to determine SEAP activity.

#### 3.3.7.2 10-Plex TH1/TH2 Assay

MesoScale Discovery multiplex assays allow the detection and quantitation of multiple analytes simultaneously over a wide range of concentrations using as little as 10µl of sample. Human TH1/TH2 10-plex assay simultaneously detects IFNγ, IL-1β, IL-2, IL-4, IL-5, IL-8, IL-10, IL-12p40, IL-13 and TNFα key effectors in the TH1/TH2 inflammatory response. The surface of each well contains 10 discrete capture antibody coated electrodes or "spots". Each spot is coated with a different capture antibody arranged in a characteristic pattern (Figure 3.4). Analytes in samples are bound to specific capture and detection antibodies. Detection antibodies are labelled with SULFO-TAG™, an electrochemiluminescent compound. When a voltage is applied to the plate using the SECTOR Imager instrument light is emitted by the SULFO-TAG™ label and the intensity detected.

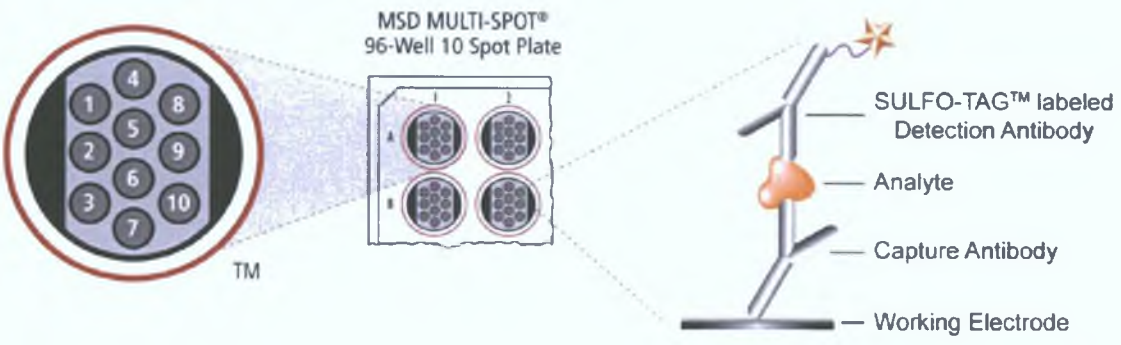


Figure 3.4: Meso Scale Discovery multiplex assay. MSD multiplex or multispot 96-well plates have a carbon electrode plate surface onto which each capture antibody is coated onto one of ten electrodes or spots. The assay works as a sandwich immunoassay where the analyte is bound to the capture and detection antibody. MSD detection antibodies are labelled with SULFO-TAG™, an electrochemiluminescent compound, which emits light when voltage is applied to the electrodes. The light intensity is measured by the analyser and allows quantification of each analyte. (Image taken from MSD Multispot manual)

THP-1 cells were differentiated in 24 well plates at $1x10^5$ cells/ml. Cells were incubated in fresh complete media (untreated), RPMI supplemented with 100ng/ml LPS or empty DOPS, DOPC, MC2C, MC4C or MC6C liposomes at 100μM or 300μM for 24 hours. Media was harvested and stored at -80°C until assayed.

MSD mutilplex assay was carried out according to the manufacturers' instructions. Briefly, the plate was blocked for 1 hour at room temperature with 150μl of 1% (w/v) Blocker B solution (blocking was recommended to improve the sensitivity of IFNγ and IL-12p40 detection). Wells were washed with wash buffer (0.05% Tween20 in PBS (PBST)) three times and blotted dry with absorbent paper. A 4-fold serial dilution of mouse TH1/TH2 9-Plex Calibrator (10ng/ml to 2.4pg/ml) was prepared in Diluent 1 (RPMI supplemented with 10% FBS). Standards and cell supernatants (25μl) were added in triplicate to wells and the plate was sealed and incubated over night at 4°C. The plate was washed 3 times with PBS-T followed by the addition of 25pl of 1X detection antibody solution (50X stock diluted in Diluent 100 containing monoclonal antibodies to each analyte). The plate was resealed and vigorously shaken at room temperature for 2 hours. Washing 3 times in PBS-T was repeated. 150pl of 2X Read Buffer T (4X Read Buffer T diluted in de$H_2O$) was added to each well and the plate was immediately analysed on a SECTOR Imager. Read buffer provides a suitable chemical environment for electrochemiluminescence. Standard curves were produced and concentrations of analytes for each sample determined using the MSD DISCOVERY WORKBENCH® software.

### 3.3.8 Statistics

In general results are expressed as means ± SD. One way or two way ANOVA was used to test for differences between treatments with *p*-values $< 0.05$ considered significant, $< 0.01$ very significant and $< 0.001$ highly significant.

## 3.4 Results

### 3.4.1 THP-1 cells as a Macrophage Cell Model: Mannose Receptor Expression

THP-1 cells are differentiated into a macrophage-like cell [196]. To confirm use of this cell line as an appropriate *in vitro* model for mannosylated liposome targeting immunofluoresence was carried out to determine MR expression. Figure 3.5 shows MR expression in differentiated THP-1 cells.

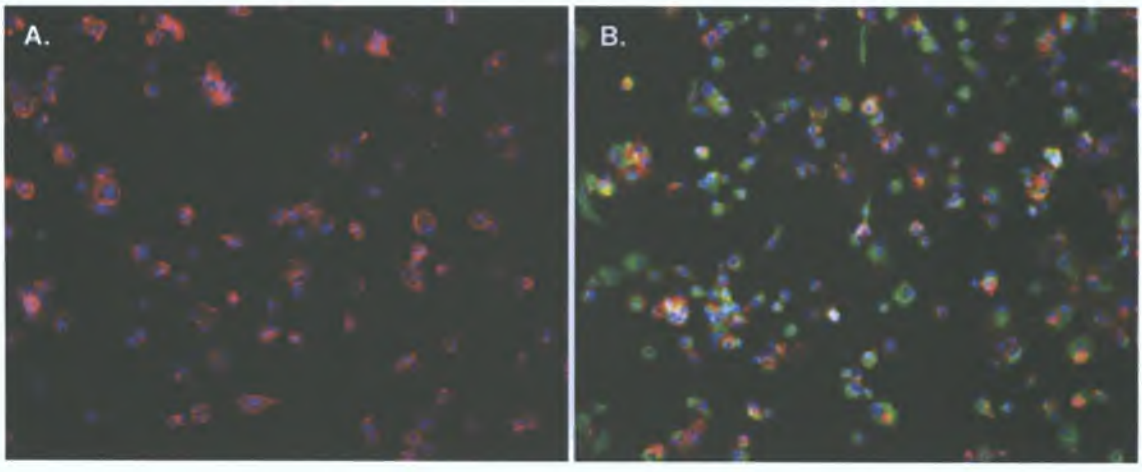


Figure 3.5: Immunofluorescence to determine the expression of mannose receptor by differentiated THP-1 cells. Fixed cells were incubated 1% BSA for 1 hour followed by incubation with (A) 1% BSA or (B) polyclonal mannose receptor antibody (1µg/ml) for 1 hour. Cells were then incubated with secondary Alexa Fluor 488 antibody (green) for 1 hour followed by staining with Hoechst (nuclei; blue) and phalloidin-TRITC (T-Actin; Red). Images were acquired using an INCELL 1000 analyser at 100x magnification.

### 3.4.2 Cell Uptake Studies

#### 3.4.2.1 Spectrofluorimetric Assessment of Liposome Uptake

Cell uptake is the first stage of transfection and can be difficult to achieve particularly with macrophages [35]. The aim of this set of experiments was to optimise and compare cell uptake of anionic liposomes and mannosylated liposomes in differentiated THP-1 cells. To quantify liposome uptake by THP-1 cells fluorescently tagged anionic, neutral and mannosylated liposomes (composed of 0.1% PE-Rhodamine) at 100 and 300μM were incubated with differentiated THP-1 cells for 2 hours. The cells were then washed, lysed and fluorescence was measured using spectrofluorimetry and normalised to per mg protein. Significant increases in ($p < 0.001$) cell association of anionic DOPS (Figure 3.6A) and mannosylated (Figure 3.6B) liposomes was found in comparison with neutral uncoated (DOPC) liposomes. There was a 5.3 fold increase in the association of negatively charged DOPS liposomes compared to neutral DOPC liposomes.

Liposome composition for this experiment is described in Table 3.1. Mannosylated liposomes were prepared using DOPC (70%), cholesterol (22.5, 25 and 27.5%) and either mann-C2-chol (MC2C), mann-C4-chol (MC4C) or mann-C6-chol (MC6C) (2.5, 5 and 7.5%). Hence, mannosylated liposomes ranged in their degree of mannosylation (from 0 to 7.5% of the liposome molar composition) and in the mannosylated cholesterols. Three mannosylated cholesterol analogs were used, differing on the linker length between the mannose and cholesterol. The greater the extent of mannosylation the higher the level of cell uptake observed (Figure 3.6B) with all 7.5% mannosylated liposome formulations showing significantly increased cell uptake compared to unmannosylated DOPC liposomes ($p < 0.01$, MC2C-7.5 and MC6C-7.5; $p < 0.001$, MC4C-7.5). Additionally uptake was increased with higher concentrations of liposomes. MC4C-7.5 liposomes exhibited the most significant level of uptake by THP-1 cells ($p < 0.001$). Therefore uptake appears to be dependent on liposome concentration, mannosylated cholesterol linker length and the extent of liposome mannosylation with MC4C-7.5 as the optimal formulation.

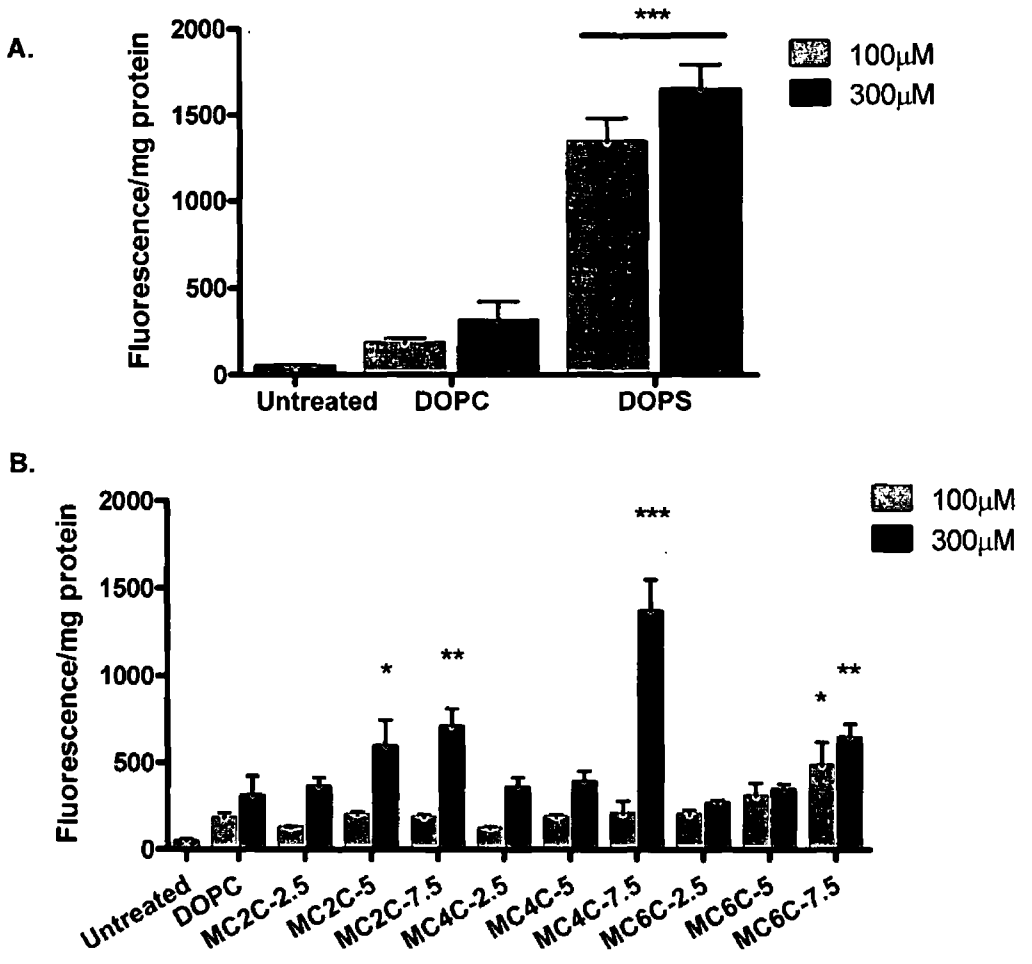


Figure 3.6: Uptake of liposome formulations by differentiated THP-1 cells determined by spectrofluorimetry. Cells were incubated for 2 hours with 100μM or 300μM rhodamine-labelled liposomes (A) anionic or (B) mannosylated, washed and lysed. DOPC liposomes were the neutral or uncoated controls for anionic DOPS liposomes or mannosylated liposomes respectively. Fluorescence intensities of cell lysates at 550nm excitation and 590nm emission were measured and normalised to total protein. Data represented as means ± SEM (n = 6). Statistical differences were determined by two-way ANOVA with Bonferrini's post-hoc test (* $p < 0.05$, ** $p < 0.01$, *** $p < 0.001$) vs. DOPC liposome treated counterparts.

### 3.4.2.2 Spectrofluorimetric Assessment of siRNA-Liposome Uptake

Additionally, the spectrofluorimetric method was used to determine the effect of liposome encapsulation on siRNA uptake into differentiated THP-1 cells. Initial studies to enhance siRNA encapsulation incorporated low percentages of DOTAP into the liposome formulations which later was optimised by encapsulation of pre-complexed siRNA. As shown in chapter 2 encapsulation efficiency of free siRNA was low, usually <10%. In order to compare and quantify uptake of naked siRNA and liposome encapsulated siRNA a fluorescent siRNA (siGlo) was used (excitation/emission 560nm/590nm). From the previous uptake studies mannosylated liposomes composed of 7.5% Mann-C4-Chol were optimal for cell internalisation and were used for siGlo encapsulation. Fluorescent siRNA (siGlo) encapsulated in mannosylated liposomes showed increased uptake by differentiated THP-1 cells compared to free siGlo (Figure 3.7). Enhancement of siGlo uptake was significant when encapsulated in mannosylated liposomes (7.5%MC4C) incorporating DOTAP compared to siGlo alone ($p < 0.01$) and to siGlo encapsulated in mannosylated liposomes (7.5%MC4C) without DOTAP ($p < 0.05$). Encapsulation efficiencies were low and therefore fluorescence intensities were low however it is clear that liposome encapsulation enhances uptake of siRNA.

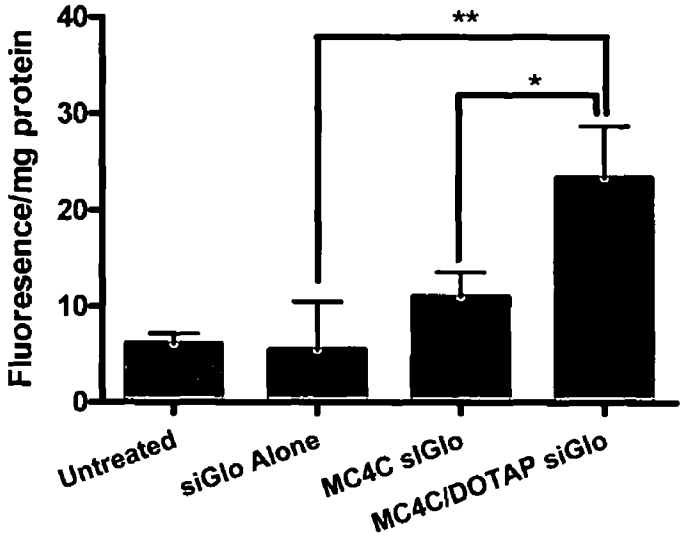


Figure 3.7: Uptake of liposome formulations by differentiated THP-1 cells determined by spectrofluorimetry. Cells were incubated for 2 hours with naked fluorescent siRNA (siGlo) or liposome encapsulated siGlo, washed and lysed. siGlo was encapsulated in 7.5% MC4C liposomes with or without DOTAP incorporated into the liposome formulation. Fluorescence intensities of cell lysates at 550nm excitation and 590nm emission were measured and normalised to total protein. Data represented as means ± SEM (n = 6).
Statistical differences were determined by one-way ANOVA with Bonferrini's post-hoc test (* $p < 0.05$, ** $p < 0.01$)

Following uptake assessment of liposomes and liposomes encapsulating siRNA (siGlo) by spectrofluorimetry MannC4Chol (7.5%) liposomes including 10% DOTAP in their formulation was selected to encapsulate TNFα targeted siRNA. MC4C liposomes empty and encapsulating non-target or TNFα siRNA were used to transfect differentiated THP-1 cells. TNFα expression by THP-1 cells was determined 48 and 72 hours post transfection following a 3 hour LPS stimulation (100ng/ml). TNFα targeted siRNA encapsulated in MC4C liposomes composed with

10% DOTAP reduced TNFα expression by 20.8 ± 7% and 21.4 ± 4% 48 and 72 hours post transfection respectively compared to untransfected stimulated cells. Furthermore a commercial transfection reagent Lipofectamine 2000 was used as a positive transfection control but yielded negligible changes in TNFα gene expression in LPS stimulated THP-1 cells (Appendix). In order to further optimise formulations to enhance knockdown a HCA method was developed to quantify liposome uptake in a high throughput format.

### 3.4.2.3 High Content Cell Analysis (HCA) Assessment of Liposome Uptake

A method was developed to quantify liposome uptake in differentiated THP-1 cells using HCA technology. Previous approaches to quantify liposome cellular internalisation have included spectrofluorimetry [197] and flow cytometry [115], both of which rely on fluorescent intensity measurements as indications of the extent of liposome cell uptake and are usually coupled with microscopy to confirm liposome internalisation and localisation. HCA combines imaging and quantitative analysis in a high throughput format to determine liposome cell uptake consequently providing more detail and accuracy than former techniques. HCA permits a visual assessment of uptake and liposome per cell count which can be defined by a number of parameters including particle size exclusion and localisation. Further information can be extrapolated such as uptake distribution pattern (homogenous or heterogenous), localisation and cell viability. Additionally techniques such as flow cytometry require cells to be in suspension. This could be problematic with adherent cells such as macrophages which cannot be trypsinised and cell detachment can potentially cause damage and bias the results [198].

Uptake of anionic DOPS, neutral DOPC and 7.5% mannosylated MC2C, MC4C and MC6C liposomes by differentiated THP-1 cells was determined by HCA. This high throughput assessment also showed an improvement by anionic surface charge and mannosylation (Figure 3.8 – 3.11) as was found by spectrofluorimetry (Figure 3.6). However using HCA several conditions could be evaluated including a range of liposome sizes (100nm to >1μm in diameter), concentrations (0 to 1mM), incubation times (0.5 to 24 hours) and temperatures (4 or 37°C).

Size can contribute greatly to liposome cell uptake efficiency. Liposomes were extruded to 100nm, 200nm, 400nm or 1000nm or unextruded (>1000nm) and incubated with differentiated THP-1 cells for 2 hours at 200pM. With increasing size of anionic DOPS liposomes uptake increased (Figure 3.8G) while neutral DOPC and MC2C and MC4C mannosylated liposomes showed a similar pattern up to 200nm but uptake decreased with liposomes ≥ 400nm in diameter. DOPS and DOPC uptake was not significantly altered by size reduction when compared to unextruded counterparts. The most significant increase was of MC4C 200 and 400nm ($p < 0.001$) and MC6C 200nm ($p < 0.001$). Overall DOPS and MC6C liposomes showed the greatest level of cell internalisation with DOPS uptake size dependent and MC6C uptake size independent in the 100 - 1000nm range. Furthermore the longer the linker length of the mannosylated cholesterols used the greater the cell uptake.

In general the higher the concentration of liposome treatments the greater the number of liposomes internalised by THP-1 cells after 2 hours. Significant increase in targeted liposome uptake was found compared to concentration matching non-target DOPC liposomes. DOPS liposomes showed significant enhanced uptake at 100μm ($p < 0.01$), 200μM ($p < 0.001$) and 300μM ($p < 0.01$) compared to DOPC liposomes. MC6C liposomes also showed highly significant uptake at 100 and 200μM ($p < 0.001$) and very significant uptake at 300μM and 1mM ($p < 0.01$) to compared to DOPC control. MC4C liposomes also showed significant increase in uptake over DOPC liposomes but not as enhanced as MC6C liposomes.

Incubation time of liposomes with differentiated THP-1 cells was also assessed for 30 minutes to 24 hours. A trend of increasing uptake over time was observed but for DOPC, MC2C and MC4C liposomes major changes in uptake over time were not detected. DOPS liposomes showed significant increase in uptake after 0.5 hour ($p < 0.01$), 1 hour ($p < 0.05$) and 2 hours ($p < 0.01$) compared to corresponding DOPC liposomes and decreased at 24 hours. Uptake of MC6C liposomes was very significant following treatment times of 0.5 and 1 hour ($p < 0.01$) and highly significant beyond 1 hour ($p < 0.001$) compared to DOPC liposome counterparts (Figure 3.10G).

HCA assessment of liposome uptake in differentiated THP-1 cells showed overwhelming confirmation of DOPS and MC6C liposomes as lead delivery platforms. Additionally uptake of DOPS, MC4C and MC6C liposomes was impeded at 4°C with high significance ($p < 0.001$) suggesting an active uptake process (Figure 3.11).

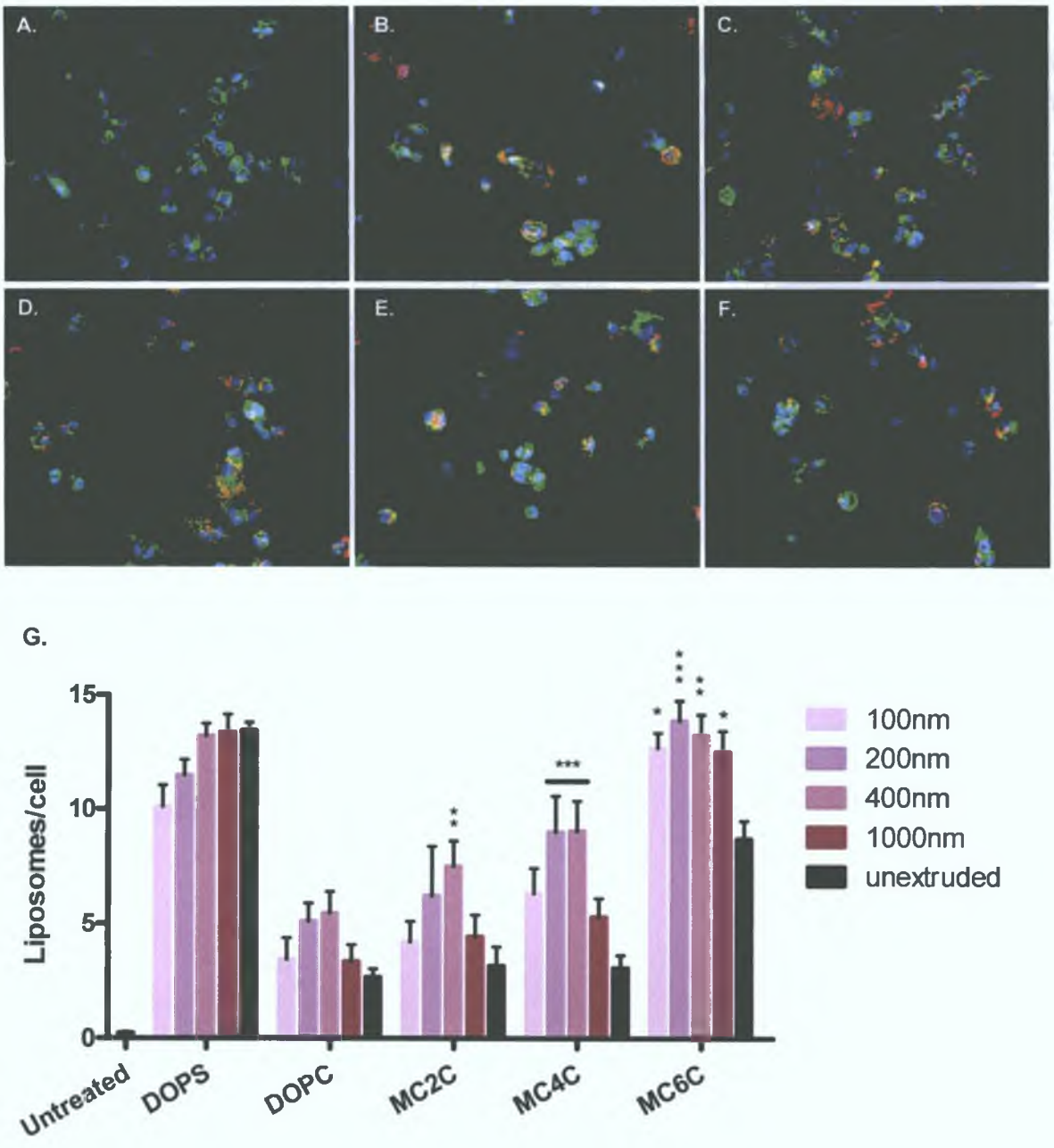


Figure 3.8: Uptake analysis by INCELL HCA of rhodamine labelled liposomes ranging in size by differentiated THP-1 cells. Cells were incubated without liposomes (untreated) or with fluorescently tagged (rhodamine; red) anionic (DOPS), non-mannosylated neutral (DOPC) and mannosylated liposomes (7.5% MC2C, MC4C and MC6C) unextruded or sized to 100nm, 200nm, 400nm or 1000nm in diameter by extrusion at 200μM and 37°C for 2 hours. Cells were fixed and stained for nuclei (hoescht; blue) and F-Actin (phalloidin-FITC; green). Representative images show (A) untreated cells or uptake of MC6C mannosylated liposomes sized to (B) 100nm, (C) 200nm, (D) 400nm, (E) 1000nm and (F) unextruded. Images were acquired by an INCELL 1000 cell analyser and (G) liposomes were counted per cell using INCELL 1000. Data represented as means ± SD (n = 6)
Statistical differences were determined by two-way ANOVA with Bonferrini's post-hoc test (* $p < 0.05$, ** $p < 0.01$) vs. unextruded liposome treated counterparts

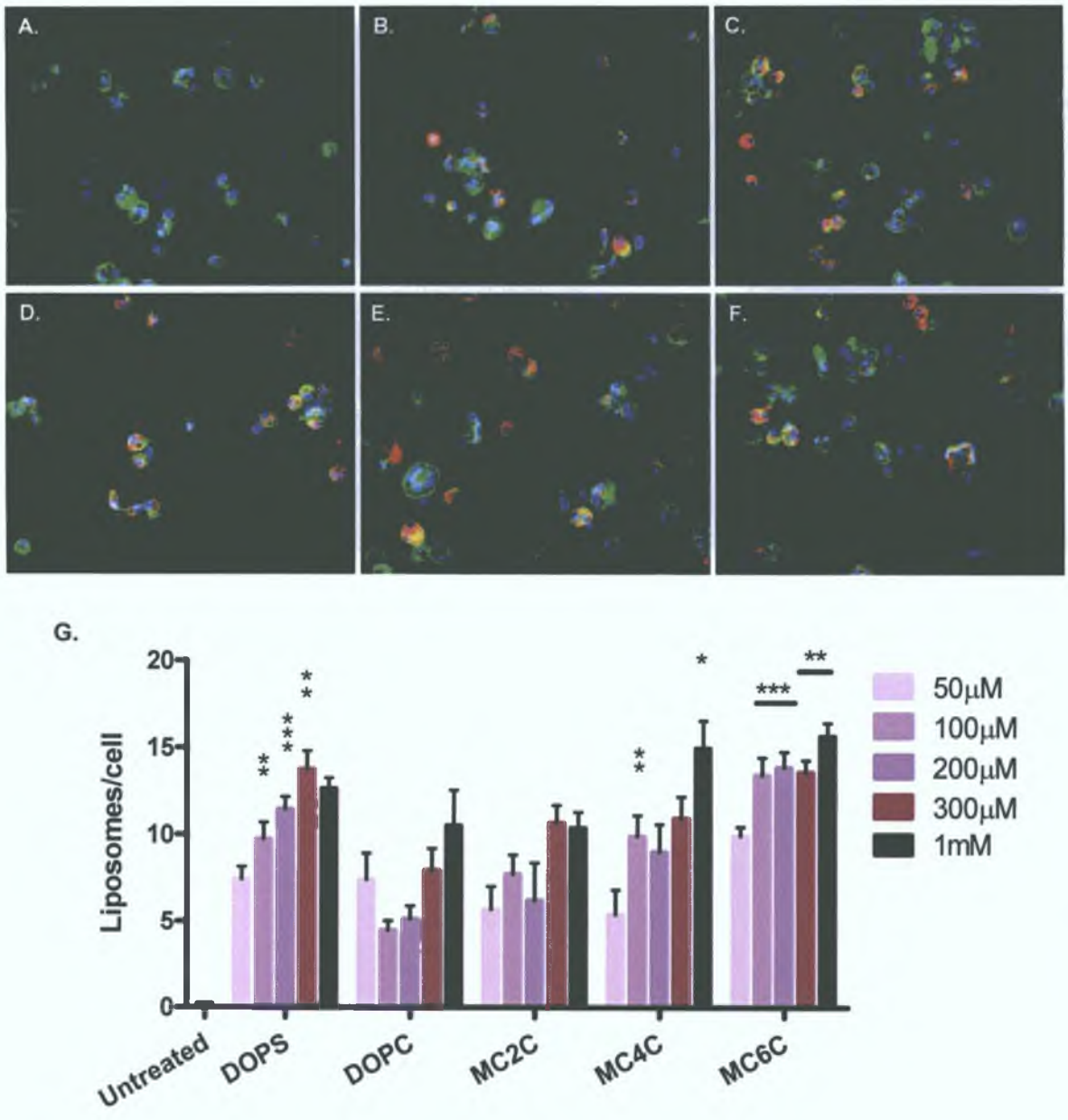


Figure 3.9: Uptake analysis by INCELL HCA of rhodamine labelled liposomes over a range of concentrations by differentiated THP-1 cells. Cells were incubated without liposomes (untreated) or with 200nm fluorescently tagged (rhodamine; red) anionic (DOPS), neutral non-mannosylated (DOPC) and mannosylated (7.5% MC2C, MC4C and MC6C) liposomes at 50, 100, 200, 300 and 1000 μM for 2 hours at 37°C. THP-1 cells were fixed and stained for nuclei (hoescht; blue) and F-actin (phalloidin-FITC; green) and images were acquired at 20x magnification using an INCELL 1000 cell analyser. Representative images show (A) untreated cells and cells treated with 200nm DOPS liposomes at concentrations of (B) 50, (C) 100, (D) 200, (E) 300 and (F) 1000μM for 2 hours. Images were analysed and liposomes counted per cell (G). Data represented as means ± SD (n = 6)
Statistical differences were determined by two-way ANOVA with Bonferrini's post-hoc test (* $p < 0.05$, ** $p < 0.01$, *** $p < 0.001$) vs. neutral (DOPC) liposome treated counterparts

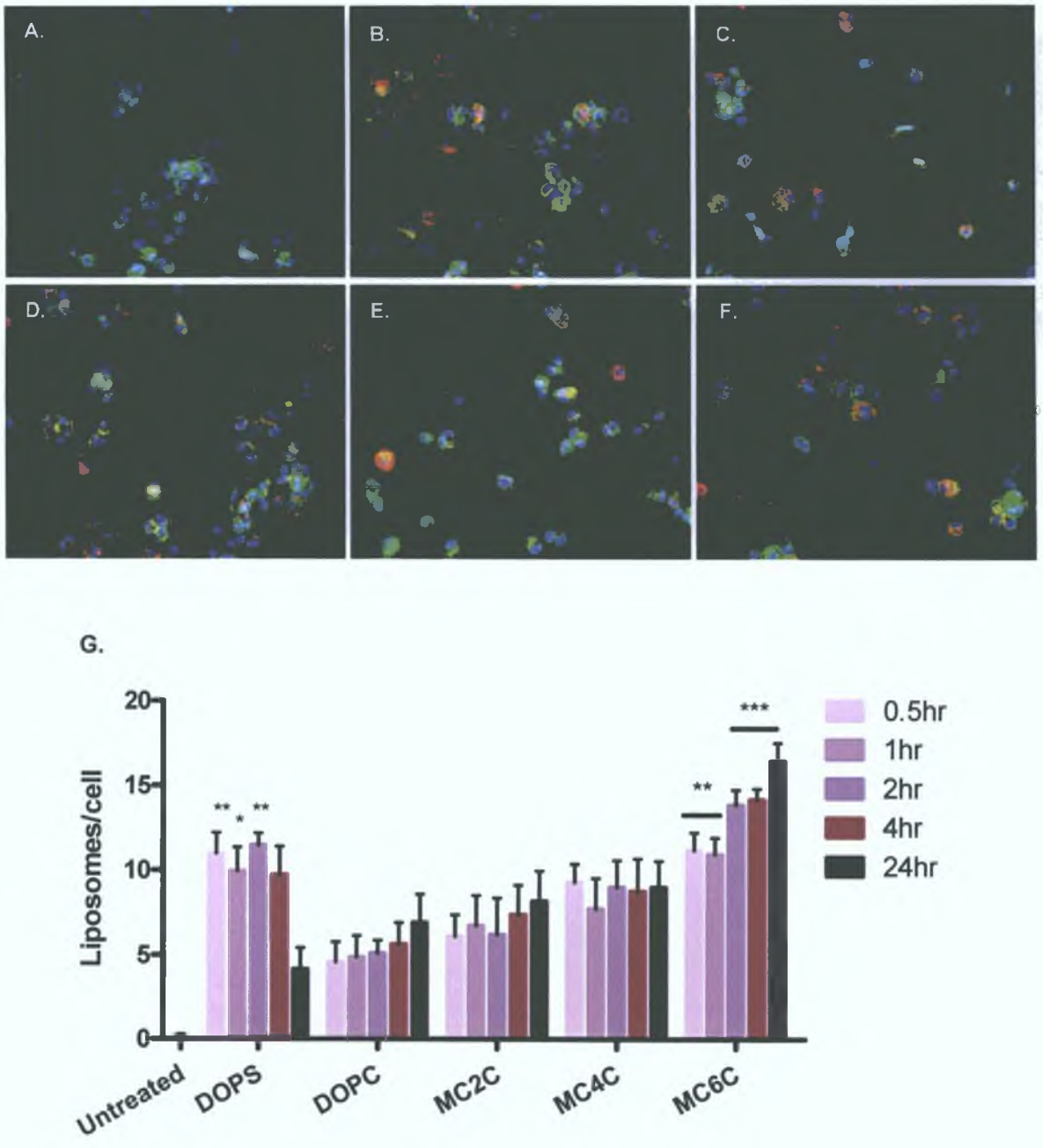


Figure 3.10: Uptake analysis by INCELL HCA of rhodamine labelled liposomes by differentiated THP-1 cells at various time points. Cells were incubated without liposomes (untreated) and 200nm fluorescently tagged (rhodamine; red) anionic (DOPS), neutral non-mannosylated (DOPC) and mannosylated (7.5% MC2C, MC4C and MC6C) liposomes at 200 μM for 0.5, 1, 2, 4 and 24 hours at 37°C. THP-1 cells were fixed and stained for nuclei (hoescht; blue) and F-actin (phalloidin-FITC; green) and images were acquired using an INCELL 1000 cell analyser. Representative images show (A) untreated cells and cells treated with 200μM of 200nm MC6C liposomes for (B) 0.5, (C) 1, (D) 2, (E) 4 and (F) 24 hours. Images were analysed and liposomes counted per cell (G). Data represented as means ± SD (n = 6)
Statistical differences were determined by two-way ANOVA with Bonferrini's post-hoc test (* $p < 0.05$, ** $p < 0.01$, *** $p < 0.001$) vs. DOPC liposome treated counterparts

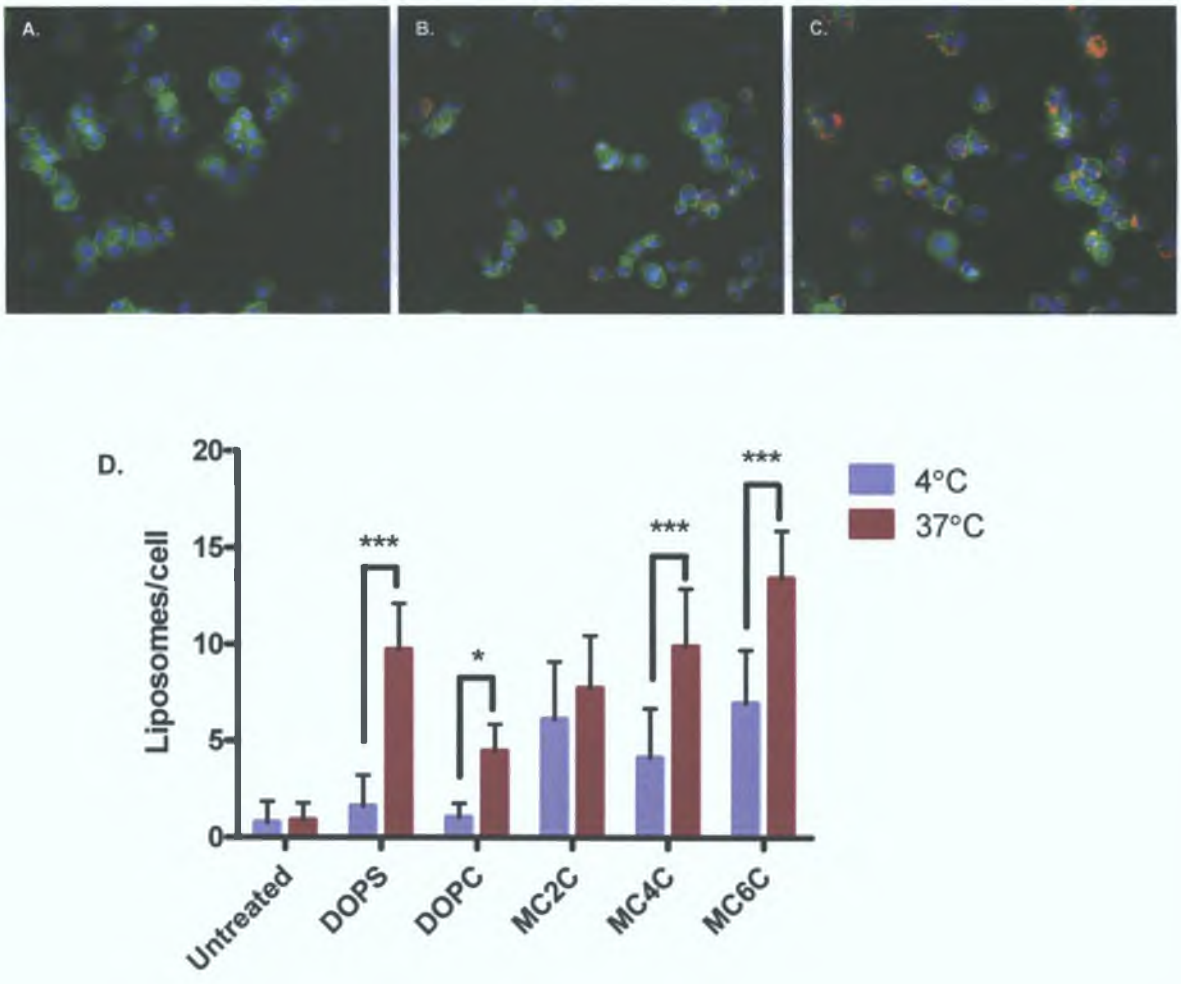


Figure 3.11: Uptake analysis by INCELL HCA of rhodamine labelled liposomes by differentiated THP-1 cells at 4°C and 37°C. Cells were incubated without liposomes (untreated) or with 100μM 200nm fluorescently tagged (rhodamine; red) anionic (DOPS), neutral non-mannosylated (DOPC) and mannosylated (7.5% MC2C, MC4C and MC6C) liposomes at 4 and 37°C for 2 hours. THP-1 cells were fixed and stained for nuclei (hoescht; blue) and F-actin (phalloidin-FITC; green) and images were acquired using an INCELL 1000 cell analyser. Representative images show (A) untreated cells and cells treated with 100μM of 200nm MC6C liposomes at (B) 4°C and (C) 37°C for 2 hours. Images were analysed and liposomes counted per cell (G). Data represented as means ± SD (n = 6)
Statistical differences were determined by two-way ANOVA with Bonferrini's post-hoc test (* $p < 0.05$, ** $p < 0.01$, *** $p < 0.001$)

### 3.4.3 *In vitro* TNFα Knockdown

Transfection using lipofectamine 2000 targeting TNFα expression was carried out in LPS stimulated isolated primary human monocytes/macrophages (Figure 3.12). Primary monocytes/macrophages showed a better LPS response and so were used here for knockdown studies. Interestingly the commercially available transfection reagent induced high levels of TNFα after 24 hours returning to levels below untransfected LPS stimulated control cells after 48 hours. There was no significant knockdown of target TNFα as seen in THP-1 cells (Appendix).

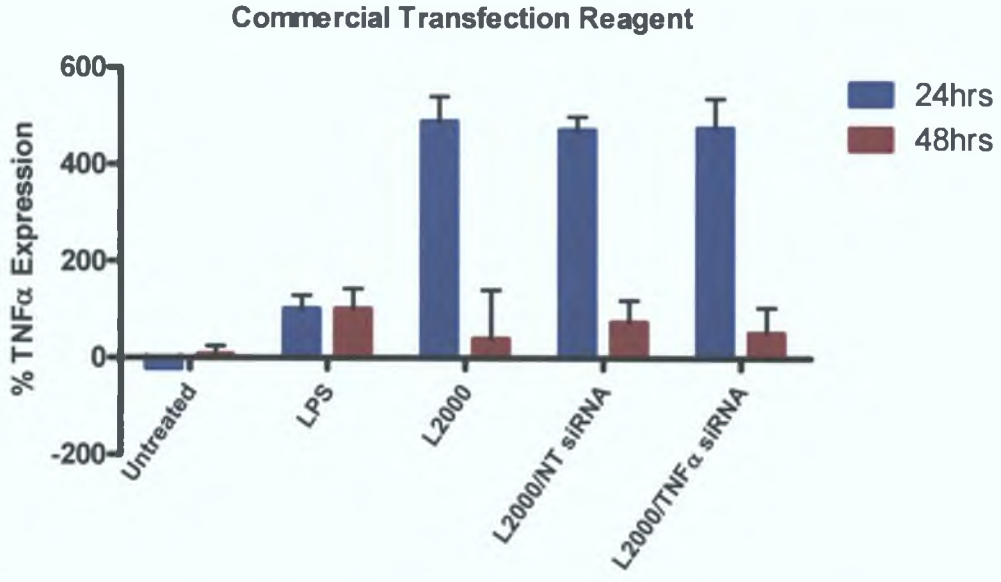


Figure 3.12: TNFα modulation in primary blood derived monocytes by TNFα targeted siRNA complexed with commercially available transfection reagent. Cells were transfected using lipofectamine 2000 and non-target (NT) or TNFα siRNA and stimulated with LPS 3 hours prior to supernatant collection at 24 and 48 hours. TNFα secretion was determined by ELISA. Data represented as means ± SD vs non-target counterparts (n = 3)

Optimal formulations based on HCA uptake were composed of DOPS:Chol (70:30), DOPC:Chol (70:30) and DOPC:Chol:MC6C (70:22.5:7.5) for anionic, neutral and mannosylated liposomes. Non-target and TNFα targeted siRNA complexed with DOTAP, PEI and protamine was encapsulated into these liposome formulations (as described in 2.3.3) and knockdown via liposomal delivery was evaluated in primary cells. DOPC liposomes served as a neutral control for anionic DOPS liposomes and an unmannosylated control for mannosylated liposomes. Primary monocytes were transfected with 50ng of siRNA encapsulated in liposomes. Neutral DOPC liposomes encapsulating TNFα siRNA complexed with DOTAP or protamine did not result in TNFα suppression but induced TNFα expression was slightly reduced (not significantly) when PEI/TNFα siRNA complexes were transfected encapsulated in DOPC liposomes clearly showing that using targeted systems enhanced knockdown (Figure 3.13).

DOPS liposomes caused a slight increase in TNFα expression compared to untransfected controls. However relative to non-target counterparts all DOPS formulations delivering TNFα targeting siRNA mediated significant knockdown which was dependent on the siRNA complexation agent used and time (Figure 3.13A). Significant suppression of TNFα ($p < 0.01$) was mediated via DOPS liposomes encapsulating PEI/TNFα siRNA complexes by 88 ± 28.7 % and 100 ± 16.2 % after 24 and 48 hours respectively while DOPS liposomes encapsulating protamine/TNFα siRNA reduced expression by 95.9 ± 3.3 % after 24 hours (Figure 3.13A).

Mannosylated (MC6C) liposomes encapsulating DOTAP/TNFα complexes reduced TNFα expression by 87.1 ± 46.6 % 24 hours post-transfection. PEI/TNFα siRNA and Protamine/TNFα siRNA complexes encapsulated in mannosylated liposomes 48 hours following transfection suppressed TNFα expression by 81.1 ± 16.4 % and 64 ± 45.3 %, respectively, compared to non-target siRNA counterparts (Figure 3.13C). Although knockdown was observed it was not significant.

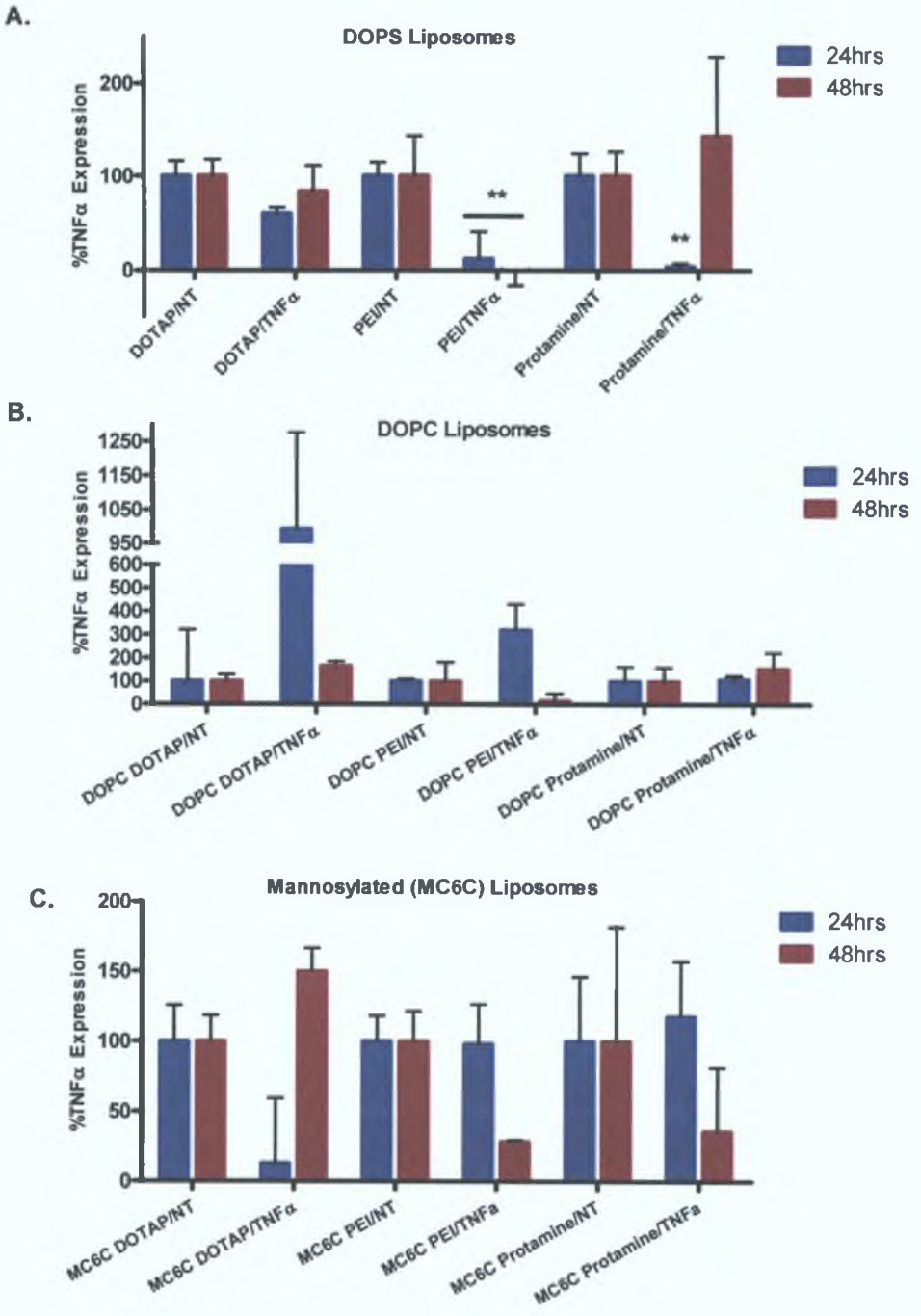


Figure 3.13: TNFα modulation in peripheral blood derived monocytes by TNFα targeted siRNA encapsulated in anionic, neutral or mannosylated liposomes. Isolated monocytes were transfected using non-target (NT) or TNFα targeted siRNA was complexed with DOTAP (N/P ratio 4), PEI (N/P ratio 7) or protamine (weight ratio 4) and encapsulated in (A) DOPS (anionic),(B) DOPC (neutral) or (C) mannosylated (MC6C) liposomes. Primary cells were transfected with liposomes and stimulated with LPS 3 hours prior to supernatant collection at 24 and 48 hours. TNFα secretion was determined by ELISA. Data represented as means ± SD vs non-target counterparts (n = 3) Statistical significance was determined by two-way ANOVA with Bonferini's Post-hoc test (* $p < 0.05$, ** $p < 0.01$, *** $p < 0.001$)

### 3.4.4 Toxicity

Differentiated THP-1 cells were used to assess the affects of liposome treatment on cell viability. Drug carriers are not always inert and therefore monitoring of carriers alone in terms of toxicity and immunogenicity is an essential step in the development of successful and safe drug delivery systems. Anionic (DOPS), neutral (DOPC) and mannosylated (MC2C, MC4C and MC6C) liposomes were incubated at 100μM and 300μM with differentiated THP-1 cells for 24 hours, fixed and stained. The concentrations required for transfection experiments generally fell between these concentrations.

As positive toxic controls cells were treated with 120μM valinomycin (Figure 3.14) or cationic (DOTAP) liposomes at 100pM or 300μM. Negative controls were incubated under normal conditions and served as the healthy cell comparison for other treatments. HCA was used to acquire and analyse images based on staining for nuclei, cell permeability, mitochondrial membrane potential (MMP) and cytochrome c (Figures 3.14 – 3.16). Cell loss, nuclear size, total nuclear intensity, cell permeability, mitochondrial membrane potential and cytochrome c release were measured as the parameters of cytotoxicity.

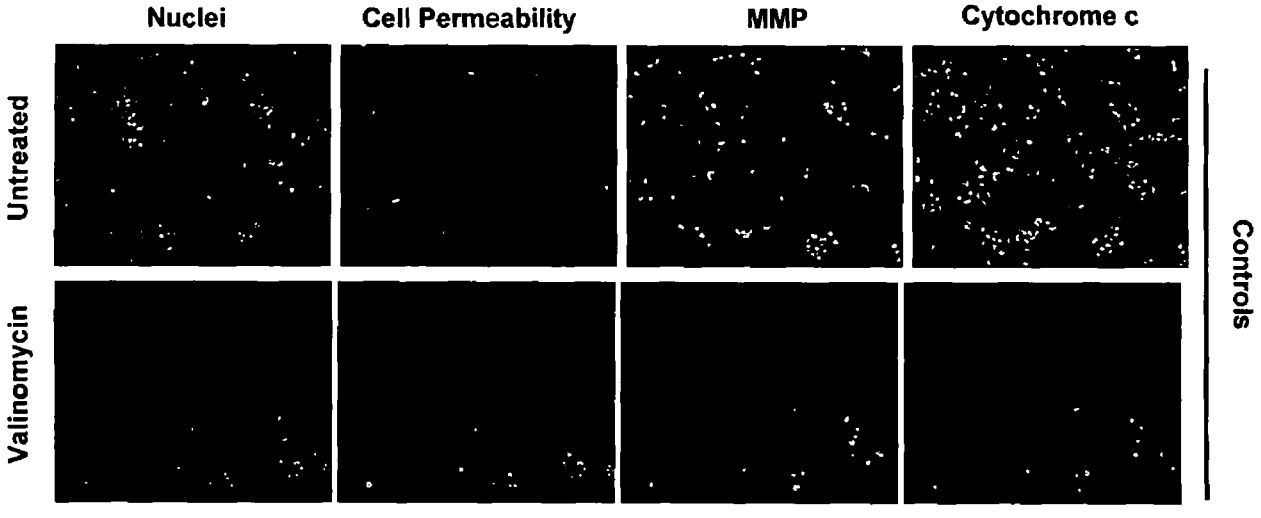


Figure 3.14: High content cell assessment of liposome associated cytotoxicity in differentiated THP-1 cells. Fluorescent images were acquired by an INCELL 1000 analyser in 4 channels and show control treatments with cells treated with complete media as a negative control or 120μM valinomycin as a positive control.

Overall cell counts between replicate assays were variable. Positive control valinomycin induced significant cell loss ($p < 0.001$) (Figure 3.13 and Figure 3.17A) as did DOTAP liposome treatments at 100μM and 300μM ($p < 0.05$) (Figure 3.15, 3.16 and 3.17A). DOTAP liposomes were composed with 50% DOTAP and were used as a liposome positive toxic control. DOTAP is a cationic lipid that is regularly used in lipoplex formation for gene transfections but has been shown to cause toxicity in macrophages [199, 200]. Significant cell loss was also found following 300μM treatments of mannosylated liposomes (Figure 3.16 and 3.17A). Valinomycin

showed the most toxic effect in differentiated THP-1 cells while DOTAP liposomes were the most toxic liposome formulation. DOTAP liposomes significantly reduced cell numbers ($p < 0.05$), increased cell permeability, reduced MMP and lead to significant cytochrome c release indicating the induction of both necrosis and apoptosis in these cells.

Chromatin condensation is associated with apoptosis which can be monitored by changes in nuclear size and intensity. No significant changes in nuclear size were found but valinomycin treatment did decrease the mean nuclear area. Valinomycin also increased the total nuclear intensity but not significantly. However, 300μM MC2C liposomes significantly ($p < 0.01$) increased nuclear intensity (Figure 3.17C).

Increased cell permeability occurs during necrosis and therefore was determined in differentiated THP-1 cells following liposome treatment. DOTAP liposomes showed increased permeability at both 100μM and 300μM concentrations however no significant elevation in permeability was determined following any treatment (Figure 3.17D).

A fall in MMP in associated with apoptosis and is linked with cytochrome c release. No significant changes in MMP were observed following any treatments in differentiated THP-1 cells. However mean MMP intensities do decrease from untreated healthy cell level most notably after treatment with 120μM valinomycin and 300μM DOTAP, DOPS and MC2C liposomes. Cytochrome c intensity was significantly ($p < 0.05$) reduced compared to healthy control cells following 300μM DOTAP liposome treatment indicative of cytochrome c release. A reduction was also found following valinomycin and 100μM DOTAP liposome treatments but was not significant.

Of the targeted liposomes MC2C liposomes at 300μM caused the most significant effect leading to apoptosis in THP-1 cells after 24 hours with a highly significant cell loss ($p < 0.001$), a significant increase in nuclear intensity ($p < 0.01$) and a decrease in MMP. Liposome concentrations required for transfection were <300μM.

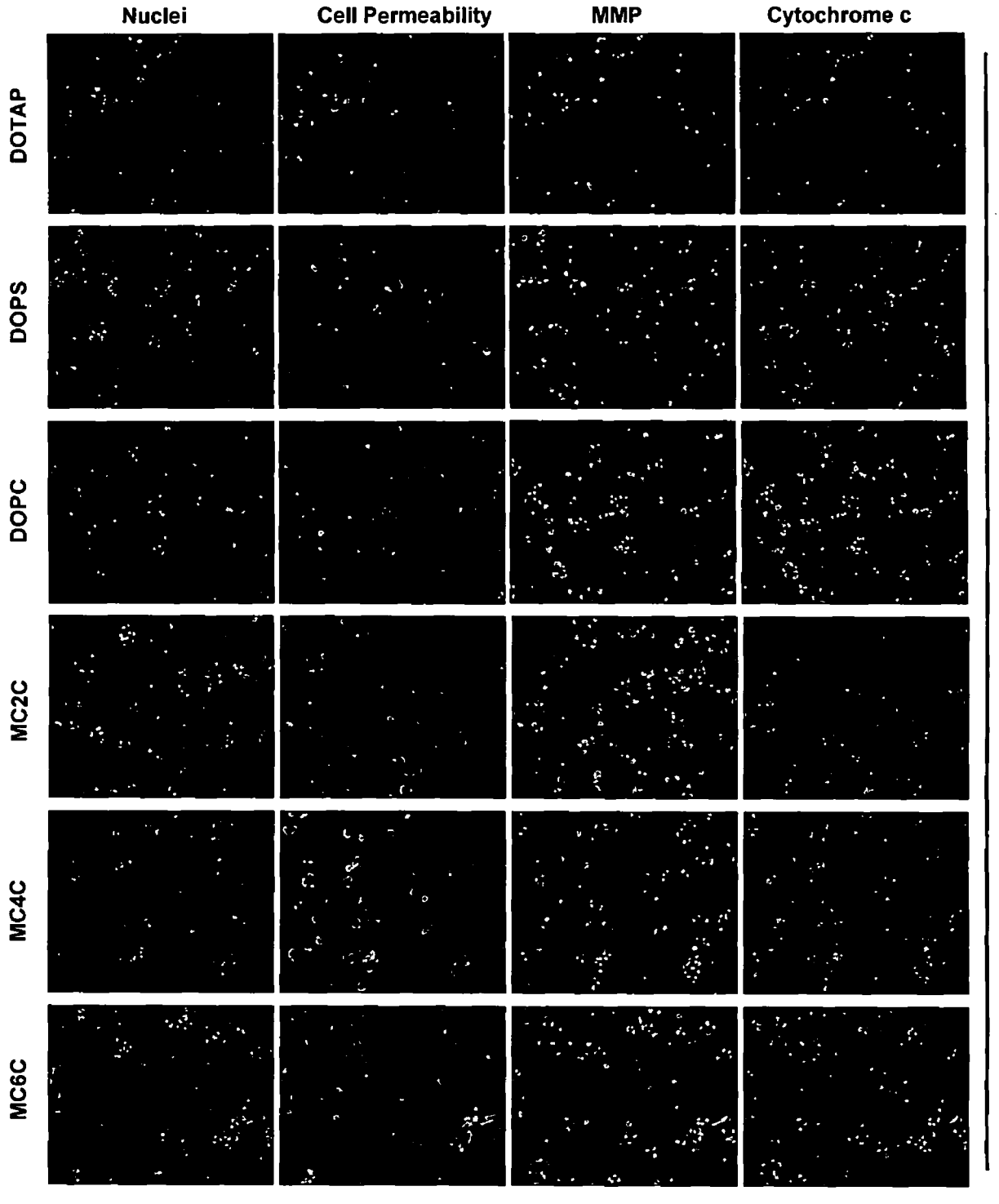


Figure 3.15: High content cell assessment of liposome associated cytotoxicity in differentiated THP-1 cells. Fluorescent images were acquired in 4 channels by an INCELL 1000 analyser and show cells treated with 100µM liposomes in complete media for 24 hours.

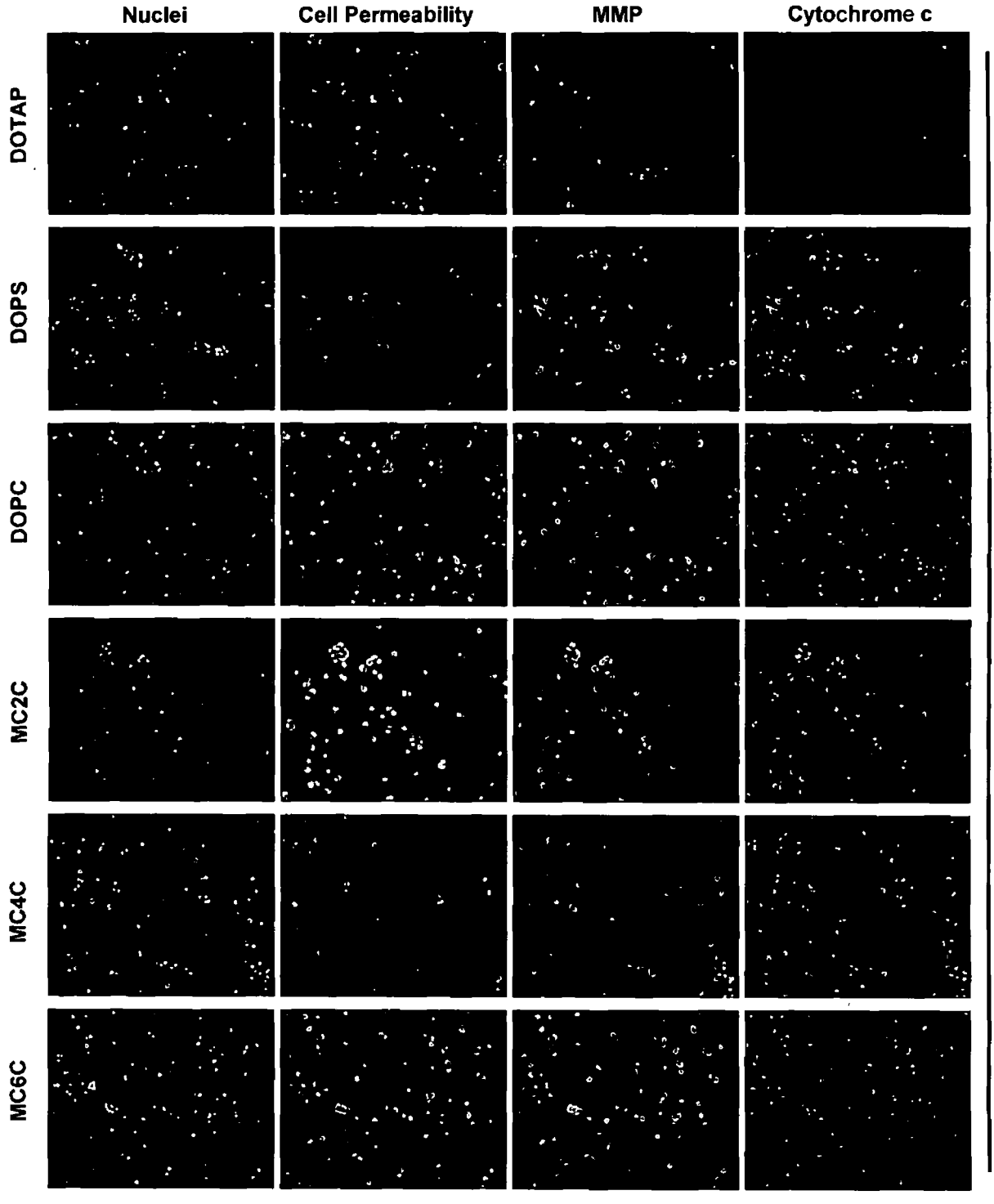


Figure 3.16: High content cell assessment of liposome associated cytotoxicity in differentiated THP-1 cells. Fluorescent images were acquired in 4 channels by an INCELL 1000 analyser and show cells treated with 300µM liposomes in complete media for 24 hours.

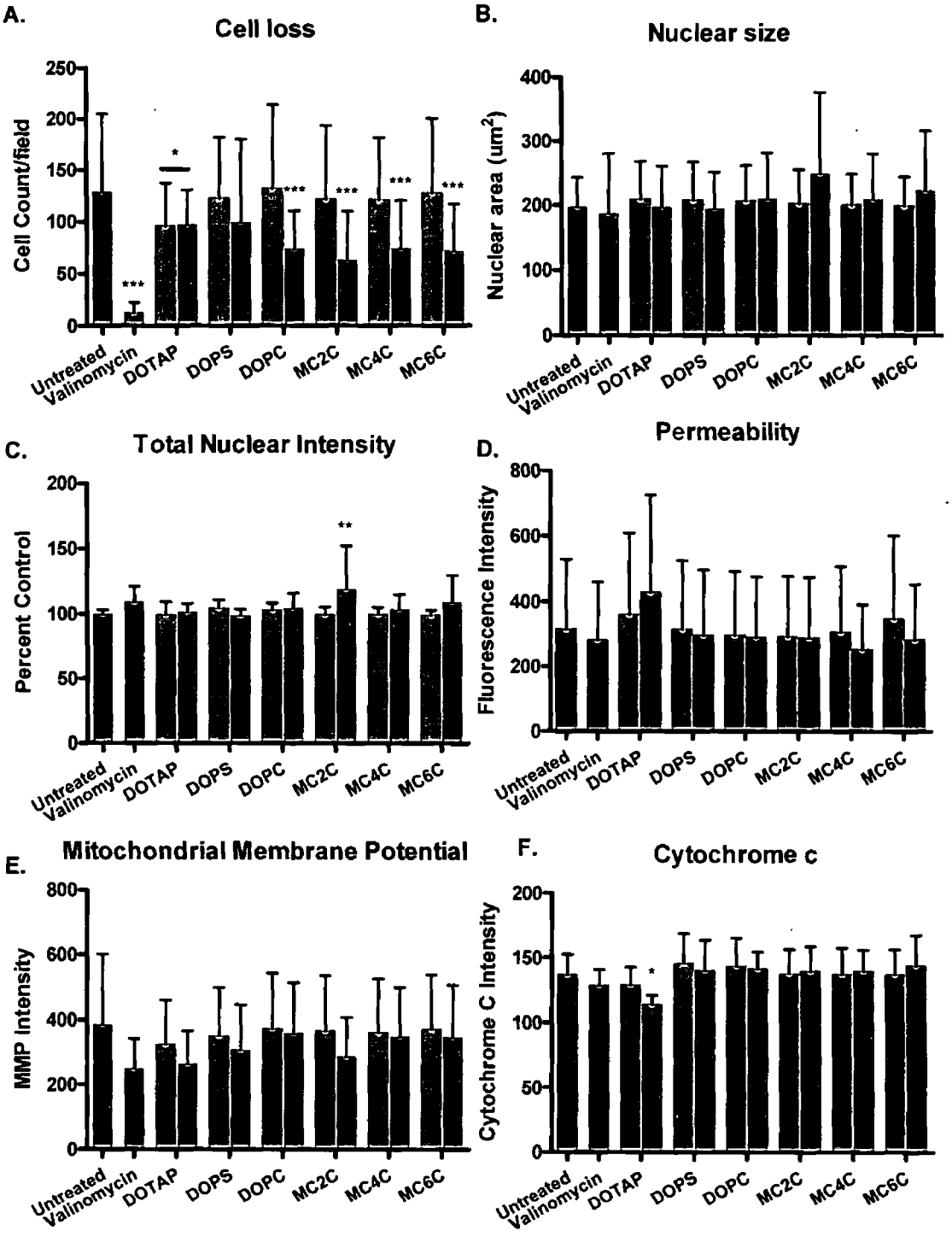


Figure 3.17: High content cell assessment of toxicity in differentiated THP-1 cells induced by liposomes. Differentiated THP-1 cells were treated with 100μM ■ or 300μM ■ anionic (DOPS), neutral (DOPC) or mannosylated (MC2C, MC4C and MC6C) liposomes. Positive controls were treated with 120μM valinomycin or 100 or 300 μM cationic (DOTAP) liposomes. Cells were treated for 24 hours, fixed and stained. Images were acquired and analysed using an INCELL 1000. Cell loss, nuclear size and intensity, MMP, cytochrome c release were measured (A-F). Data represented as means ± SD (n = 9). Statistical significance was determined by two-way ANOVA vs untreated controls (* $p < 0.05$, ** $p < 0.01$, *** $p < 0.001$)

### 3.4.5 Liposome Immunogenic Effects in a Macrophage Cell Model

#### 3.4.5.1 NFkB Activity Induction by Liposome Treatment

To develop a successful drug delivery system it must have low toxicity and not lead to immune activation. Liposomes were incubated with THP-1 Blue cells and NFκB activation was determined. NFκB is a transcription factor that is activated by various stimuli and has a central role in inflammation [201]. A significant increase in NFκB activation compared to untreated cells was found following 24 hour treatment with the positive control LPS ($p < 0.001$) (Figure 3.18). NFκB activation by DOPS liposomes was concentration dependent and 300μM DOPS liposomes ($p < 0.01$) induced significant NFκB activation. NFκB was also significantly activated by 100μM DOPC liposomes ($p < 0.05$).

However, mannosylated liposome treatment showed no significant difference in NFκB activation compared to untreated cells but in comparison to unmannosylated DOPC liposome treatment at equal concentrations NFκB activation was significantly lower following 200μM MC4C ($p < 0.01$), 300μM MC4C ($p < 0.05$), 200μM MC6C ($p < 0.05$) and 300μM MC6C ($p < 0.05$) liposome treatment. Activation of MR has previously been shown to have an anti-inflammatory effect with impaired NFκB activation [188, 189]. Mannosylated liposomes have reduced NFκB activation in differentiated THP-1 cells compared to unmannosylated DOPC liposomes in a concentration and mannosylated cholesterol linker dependent manner.

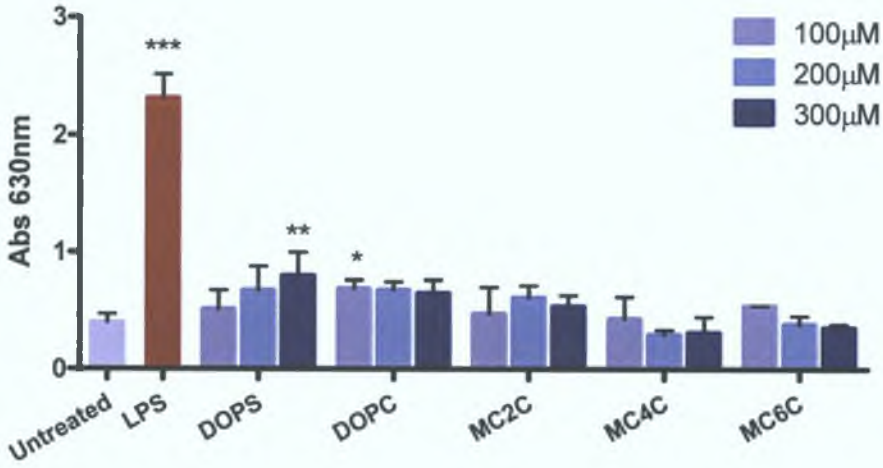


Figure 3.18: Liposome induced NFkB Activation in THP-1 Blue Cells. Data represented as means ± SD (n = 3)

### 3.4.5.2 TH1/TH2 Cytokine Response

NFκB can induce transcription of many pro-inflammatory genes such as TNFα, IL-1β, IL-6 and IL-8 [201]. In order to assess these downstream effects the production of a range of cytokines were determined including cytokines associated with a TH1 response such as TNFα, IL-1β, IL-2, IL-12p70, IFNγ and IL-8 (Figure 3.19) and a TH2 response such as IL-2, IL-4, IL-5, IL-10 and IL-13 (Figure 3.20).

As part of the TH1 response TNFα was significantly induced by LPS ($p < 0.05$), further validation of inflammatory macrophage cell model used for *in vitro* transfections. DOPS liposomes at 300μM also induced TNFα production but not significantly. All other liposome treatments did not induce a TNFα response above untreated control cells. The pro-inflammatory cytokine IL-1β was increased above baseline levels following LPS, DOTAP (100μM and 300μM) and DOPS (300μM) liposome treatments but was not significantly induced in differentiated THP-1 cells by any treatment. IL-2 was induced by LPS, DOPS (300μM) MC2C (100 and 300μM) and MC6C (100μM) liposomes but decreased following treatment with DOPC (100 and 300μM), MC4C (100 and 300μM) and MC6C (300μM) liposomes. IL-12p70 was only slightly elevated following LPS stimulation. Induction of IL-12p70 was brought about by DOPC (300μM) and MC2C (100μM) liposomes but not significantly. No significant changes in IFNγ expression were detected. However, elevated IFNγ was measured following LPS, DOTAP (100μM), DOPS (300μM), MC2C (100μM) and MC4C (100μM) liposome treatments. DOPC (100 and 300μM), MC4C (300μM) and MC6C (100 and 300μM) decreased IFNγ levels compared to untreated control cells. IL-8 is an important chemokine for neutrophil recruitment and therefore is upregulated during inflammation. Significant induction of IL-8 ($p < 0.05$) followed 24 hour treatment with 300μM DOPS liposomes. LPS also increased IL-8 production in THP-1 cells while mannosylated liposomes showed levels of IL-8 below untreated control cells.

The TH2 response is most reliant on IL-4 [202] which was increased in differentiated THP-1 cells following treatment with LPS and 300μM DOPS liposomes. IL-5 levels were elevated above levels of untreated cells by LPS, DOPS (300μM), MC2C (100μM) and MC6C (300μM) liposomes (Figure 3.20). IL-10 was also induced by LPS, DOPS (300μM), MC2C (100μM) and MC6C (100μM) liposomes. IL-13 was induced by all treatments except MC4C (100μM). Induction of IL-13 by 300μM MC6C liposomes was significant ($p < 0.05$).

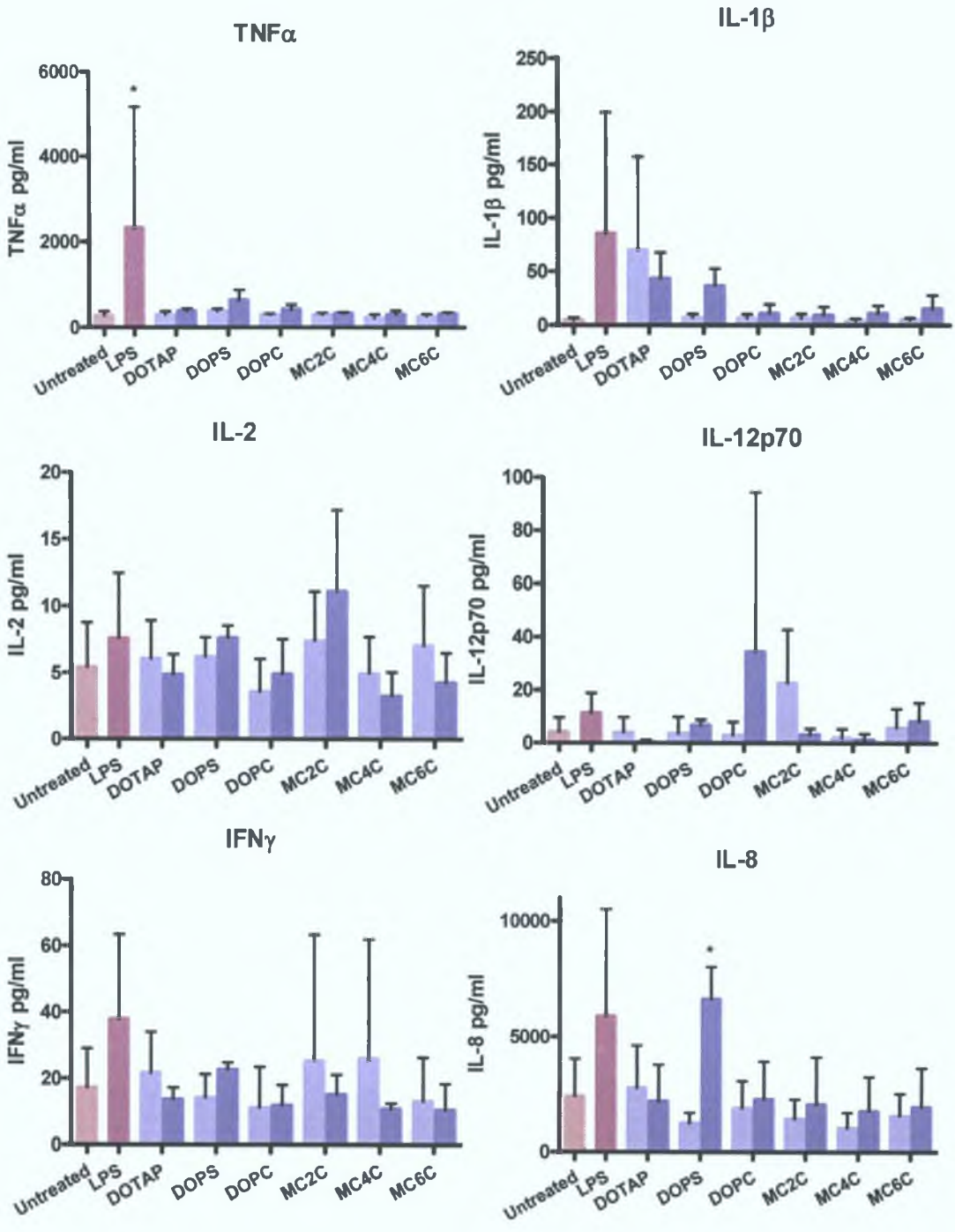


Figure 3.19: TH1 response in differentiated THP-1 cells following 24 hour liposome treatment. Differentiated THP-1 cells were incubated for 24 hours with complete media (negative control), 100ng/ml LPS (positive control) or DOTAP (liposome positive control), DOPS (anionic), DOPC (neutral), mannosylated (MC2C, MC4C, MC6C) liposomes at 100μM ( ) or 300μM ( ). Supernatants were analysed using a MSD 10-plex cytokine assay and TNFα, IL-1β, IL-2, IL-12p70, IFNγ and IL-8 concentrations were determined.
Data represented as means ± SD. (n = 3) Statistical significance was determined by two-way ANOVA with Bonferini's Post-hoc test (* $p < 0.05$, ** $p < 0.01$, *** $p < 0.001$)

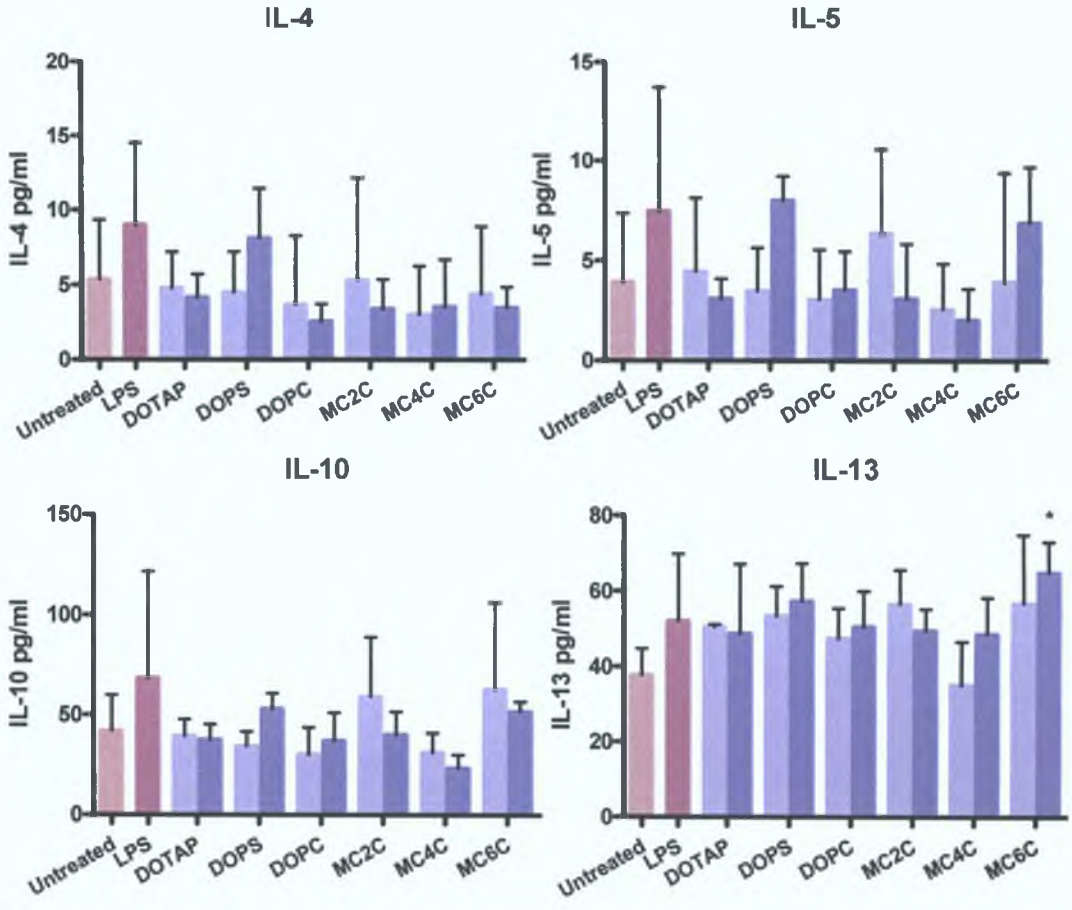


Figure 3.20: TH2 repsonse in differentiated THP-1 cells following 24 hour liposome treatment. Differentiated THP-1 cells were incubated for 24 hours with complete media (negative control), 100ng/ml LPS (positive control) or DOTAP (liposome positive control), DOPS (anionic), DOPC (neutral), mannosylated (MC2C, MC4C, MC6C) liposomes at 100μM ( ) or 300μM ( ). Supernatants were analysed using a MSD 10-plex cytokine assay and IL-4, IL-5, IL-10 and IL-13 concentrations were determined.
Data represented as means ± SD. (n = 3) Statistical significance was determined by two-way ANOVA with Bonferini's Post-hoc test (* $p < 0.05$, ** $p < 0.01$, *** $p < 0.001$)

### 3.5 Discussion

Previous strategies for liposomal gene delivery have centred on cationic formulations. However limitations due to toxicity have focused interest in alternative non-toxic biocompatible formulations. Neutral lipids have received FDA approval for use in liposome delivery of many drugs such as amphotericin B (Ambisome®) [182]. Consequently neutral and anionic lipids are currently being explored for siRNA delivery. Here we have formulated a range of liposomes based on neutral and/or anionic lipids specifically to target alveolar macrophages. These liposomes were composed with phosphatidylserine to target macrophage SRs or mannosylated cholesterols to target the macrophage MR. Both of these strategies have previously been shown to provided specific macrophage targeting and enhance cell uptake but neither formulations have been harnessed for siRNA delivery.

An essential step in targeted delivery is internalization of the carrier system by the target cells. Cell uptake of liposomes has been studied using a range of techniques such as flow cytometry, confocal microscopy and spectrofluorimetry [115, 197, 198]. We have developed a more powerful method for uptake analysis using HCA to combine imaging and uptake quantification, from single cells to cell populations, in a high throughput format [198, 203]. From both spectrofluorimetry and HCA uptake data DOPS and mannosylated liposomes showed significantly better cellular uptake compared to untargeted DOPC controls. Spectrofluorimetry determined the greatest degree of cellular uptake by differentiated THP-1 cells of 7.5% MC4C liposomes while MC6C liposomes were repeatedly the most significantly internalized liposome formulations determined by HCA. Spectrofluorimetry relies on the fluorescence intensities of lysed cells that have previously been treated with fluorescent liposomes. This technique does therefore not distinguish between liposomes associated with cells or the culture plate and those internalized. HCA can add further levels of precision. The protocol was established to count liposomes per cell. Cells could be identified and consequently liposomes counted in the cell only. This could explain the difference in the relative uptake levels of MC4C and MC6C liposomes determined using spectrofluorimetry and HCA.

HCA also enabled multiple, parallel experiments to be carried out to optimize the liposome formulation for siRNA delivery to macrophages. Optimal sizes ranged from 200 to 400nm, concentrations were above 100μM and incubation times >2 hours for the leading DOPS and MC6C liposomes. Uptake of mannosylated liposomes also appeared to be linker dependent with uptake of liposomes composed with mann-C6-chol greater than those composed with mann-C4-chol which both facilitated higher uptake than MC2C liposomes. Engel *et al.* (2003) investigated the influence of spacer length between alkyl mannosides and liposome surface, on liposome interaction with phagocytic cells [174]. Spacers were 0 to 8 ethyleneoxy units long (Man0 - Man8) with longer spacers mannosylated liposome uptake by MR expressing cells was more enhanced [174]. Furthermore Gal-C6-Chol composed liposomes were previously shown to mediate a higher DNA transfection efficiency than Gal-2-Chol and Gal-C4-Chol liposomes [173].

Strategies to encapsulate siRNA included the incorporation of a small percentage of DOTAP into the liposome formulation [168] and the condensation of siRNA using various cationic reagents [98]. The first strategy yielded low and variable encapsulation and transfection efficiency in THP-1 cells. Whereas, encapsulation of DOTAP, PEI and protamine condensed siRNA in DOPS liposomes yielded significant knockdown in primary monocytes. PEI and protamine formulations were the most effective. Depending on the liposome and complexation agent knockdown was observed either at 24 or 48 hours. DOPS liposomes appeared to have a more rapid effect than MC6C liposomes with knockdown of TNFα detected after 24 hours using DOTAP, PEI and protamine as condensing agents. DOPS/PEI/TNFα liposomes also showed very significant ($p < 0.01$) knockdown after 48 hours. MC6C liposomes mediated TNFα gene suppression at 48 hours with PEI and protamine siRNA complexes while DOTAP/siRNA formulations decreased TNFα at 24 hours. Additionally, TNFα expression was increased by commercial reagent lipofectamine 2000 after 24 hours and failed to illicit knockdown. This highlights the importance of avoiding cationic liposomes in the treatment of inflammatory conditions. Previously, Jing *et al.* (2008) delivered TNFα targeted siRNA encapsulated in anionic liposomes composed of phosphatidyl ethanolamine (PE), CHEMS and cholesterol (PE:CHEMS:Chol 7:4:2) to primary rat kupffer cells (resident macrophages of the liver) [102]. Significant knockdown of TNFα following LPS stimulation was found up to 4 days following transfection ranging from 50 to 70% relative to non-target siRNA liposome controls [102]. Furthermore, a study using cationic liposome formulations to deliver anti-TNFα siRNA reported 27-32% TNFα suppression in J774.1 murine macrophages following LPS stimulation [204].

Drug delivery systems are not always inert and therefore toxicity screening is important particularly relating to nanotoxicology. Nanoparticle induced toxicity is connected to particle size and surface chemistry and especially important in the lungs [205]. Smaller liposomes can be more toxic than larger liposomes [206]. HCA and the Cellomics Multiparameter Cytotoxicity kit allowed the screening of multiple parameters in differentiated THP-1 cells following liposome treatment for 24 hours. For these assays the ionophor valinomycin served as a positive control and validated the assay in terms of detection of changes in cell number, nuclear morphology, cell permeability, MMP and cytochrome c release in a toxic event. Usually assays such as MTT are used to assess cell viability but this method enables more subtle changes in cell health to be detected with more detail. Aside from toxicity, drug delivery systems can also induce immune responses, the extremes of which have been witnessed in clinical trials and in some cases have been fatal [1]. To assess the effects of the liposome carriers on the immune response in differentiated THP-1 cells we looked at NFκB activation and at cytokine/chemokine induction following 24 hours treatment with liposomes. NFκB can be activated through various receptors including TLRs and TNF receptors. NFκB is a transcription factor that regulates the transcription of numerous genes including TNFα, IL-8 and IL-1β [201].

Cationic liposomes have previously exhibited cytotoxic effects, particularly in macrophages [200] and consequently were avoided in the formulation of our siRNA liposomes. Additionally a study compared the toxicity of liposomes composed of cationic (SA and cardiolipin), anionic

(phosphatidylglycerol and phosphatidylserine) or neutral (phosphatidylcholine or dipalmitoylphosphatidylcholine) lipids [206]. Toxicity was determined at 200μM, 130-3000μM and 3000-4000μM for cationic, anionic and neutral liposome formulations in a range of human cell lines [206]. Cationic DOTAP liposomes however were used as positive toxic liposome controls in toxicity and immunogenicity assays. DOTAP liposomes induced significant cell loss while increasing cell permeability, decreasing MMP and promoting cytochrome c release at 100 and 300μM indicative of both apoptosis and necrosis. DOTAP liposomes also induced a more predominantly TH1 response in the macrophage-like cells with increases in IL-1β, IL-2 and IFN-γ and decreases in IL-4. DOTAP has been shown to suppress TNFα synthesis in activated macrophages [200] and therefore the lack of TNFα induction following DOTAP liposome treatment was expected.

Anionic liposomes were composed of DOPS which targets macrophage SRs by mimicking apoptotic cells. At the higher concentration of 300μM DOPS liposomes were found to reduce cell number and MMP, a sign of induced apoptosis. Furthermore, NFκB activity was significantly induced ($p < 0.001$) at 300μM and related cytokines induced including TNFα, IL-1β and IL-8. IL-8 was significantly induced ($p < 0.05$). DOPS liposomes were the most potent inducer of cytokines and chemokines in THP-1 cells with all measured immune mediators induced except IL-12p70.

Neutral DOPC liposomes were not completely inert either. Cell loss resulted from 300μM treatments of DOPC liposomes in THP-1 cells however other signs of apoptosis or necrosis were not observed. Interestingly NFκB was significantly ($p < 0.05$) activated following 24 hour DOPC liposome treatment at 100μM and IL-12p70 was induced by a 300μM dose of DOPC liposomes. In general DOPC liposome treatment in THP-1 cells resulted in reduction of immune mediators compared to untreated control cells.

Activation of the MR can have immunosuppressive effects and inactivate NFκB [188, 189]. A decrease in NFκB activity was observed in differentiated THP-1 cells following 24 hour incubation with MC4C and MC6C liposomes in a concentration dependent manner. Inactivation of NFκB associated with mannosylated liposome treatments at 200μM and 300μM was significant compared to DOPC unmannosylated liposome treatments. In general this non-immunogenic effect was corroborated in cytokine screens. MC2C liposomes which did not significantly alter NFκB activation induced increased synthesis of IL-12p70 (to a lesser extent than DOPC liposomes), IFNγ (at 100μM, similar to MC4C) and IL-2 and IL-13, IL-5 and IL-10 in a TH2 response. MC2C liposomes at 300μM induced significant cell loss ($p < 0.001$) and showed increased nuclear intensity ($p < 0.01$) and a drop in MMP all signs of apoptosis.

On the other hand MC6C liposomes composed of mannosylated cholesterols with longer linker length at 300μM induced significant cell loss but all other measures of cell health were comparable with untreated control cells. A significant inactivation of NFκB was induced by MC6C liposomes at 200 and 300μM with induction of TH2 cytokines in cells including IL-5, IL-10

and IL-13 ($p < 0.05$). MC6C liposomes were also lead to IFNγ and IL-8 suppression compared to untreated control levels. Previously, TNFα, IL-1β and cytokine-induced neutrophil chemoattractant-1 (CINC-1) levels have been monitored *in vitro* in alveolar macrophages and *in vivo* in rat lungs following mannosylated liposome delivery of dex [130]. However, the immune response to mannosylated liposomes alone has not been investigated.

Overall, a range of liposomes were prepared that successfully targeted macrophages with DOPS and mannosylated 7.5% MC6C liposomes as the leading formulations. A range of macrophage targeting liposomes were prepared and HCA was applied to study their uptake into macrophage cells. DOPS and MC6C liposomes showed the most significant cellular internalization. The ability of liposomes to mediate gene silencing of a therapeutic inflammatory target TNFα was also assessed. Anionic DOPS and mannosylated liposomes encapsulated siRNA and mediated significant knockdown of an inflammatory cytokine in primary monocytes. At the lower concentration range suitable for *in vitro* transfection liposomes were non-toxic however DOPS liposomes caused immune activation particularly an inflammatory response in differentiated THP-1 cells. Although knockdown via MC6C liposomes was not as significant as DOPS formulations MC6C liposomes showed immunosuppressive characteristics such as a hampering of NFκB activation and reduced IL-8 and IFNγ production. Hence, MC6C liposomes have the potential of mediating a dual anti-inflammatory effect via MR activation and delivery of anti-TNFα siRNA.

**Key Findings**

- Targeting (via DOPS and mannosylated cholesterols) significantly enhanced liposome uptake by macrophages
- Targeted liposomes mediated significant TNFα knockdown via delivery of TNFα targeted siRNA in LPS stimulated macrophages
- At higher doses targeted liposomes induced some cytotoxicity
- DOPS liposomes induced an inflammatory response while mannosylated liposomes showed immunosuppressive characteristics in differentiated THP-1 cells

# Chapter 4

# Microparticles for siRNA Delivery to Alveolar Macrophages

### 4.1 Introduction

Gene transfer by non-viral vectors has also been investigated using naturally occurring or synthetic polymers such as poly(ethyleneimine) (PEI), chitosan, gelatin, silica, PLL, polylactic acid (PLA) and PLGA [207, 208]. PLA and PLGA are the most extensively studied for general polymeric drug delivery. Polymer-based particles of less than 1000nm in diameter are generally referred to as nanoparticles while microparticles have diameters ranging between 1 and 250μm [209]. However, these designations are not widely agreed upon. Polymers allow encapsulation of a wide variety of drug types both small molecules and a range of macromolecules including proteins, antigens, vaccines and nucleic acids and can be designed to promote cell uptake [209, 210]. PLGA microparticles have been engineered by our group to specifically target macrophages and enhance uptake using HCA [198]. siRNA has previously been incorporated into PLGA particles with favourable *in vitro* efficacy (Table 4.1). Development of macrophage targeting PLGA microparticles loaded with TNFα targeted siRNA allows comparison between a lipid (Chapter 3) and polymer based non-viral delivery of siRNA in terms of stability, uptake, toxicity and immunogenicity in order to determine the most suitable delivery system for *in vivo* applications.

#### 4.1.1 PLGA Microparticles

PLGA microparticles allow controlled release of the loaded drug over periods extending to days and months [209]. This offers the advantage of sustained delivery perhaps negating the need for repeated dosing. Other advantageous qualities of PLGA include biocompatibility, low immunogenicity, low toxicity and biodegradability. For nucleic acid application PLGA microparticles allow high loading capacity, improved formulation stability and macrophage targeting [198] however nucleic acid stability during particle preparation could be an issue. PLGA *in vivo* is hydrolysed to form lactic acid and glycolic acid which are removed through the citric acid cycle [211]. The rate of biodegradation is dependent on the PLGA composition [209] but is slow, consequently these biocompatible degradation products do not interfere with normal cell function [211]. It has also been reported that PLGA encapsulated drugs achieve sustained cytoplasmic delivery with rapid endo-lysosomal escape. This is due to their ability to change surface charge in the acidic endo-lysosomal environment, a property that makes PLGA microparticles suitable for gene delivery. PLGA has established use in humans [212] with numerous FDA approved PLGA-based microparticle therapies [209].

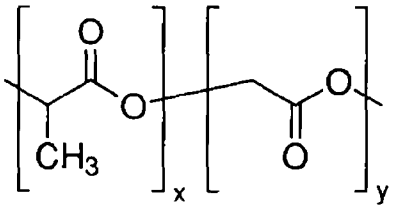


Figure 4.1: Structure of poly(D,L-lactide-*co*-glycolide) (PLGA). X represents the lactic acid component and Y represents the glycolic acid component

Polymeric microparticles contain uniformly distributed interstitial spaces between polymer chains. Hydrophobic drugs which are miscible with PLGA tend to fill these spaces [213]. Nucleic acids such as DNA and siRNA are generally encapsulated by polymeric particles using double emulsion methods. The double emulsion method provides improved encapsulation efficiency over single emulsion methods as the nucleic acids and polymer tend not to be soluble in the same solvents [213]. Consequently distribution of encapsulated nucleic acid is not evenly dispersed through the particle usually accommodating voids within the particle rather than interstitial spaces. This leads to large initial burst release. In order to reduce or control the initial burst, formulations can be altered to improve the miscibility of the drug and polymer such as complexation of the nucleic acid with a cationic reagent such as PEI, use of co-solvents or chemical modifications of the drug including esterification and PEGylation or of PLGA [211]. Alternatively nucleic acids can be complexed with PLGA particles rather than encapsulated by coating the PLGA particle in a cationic surfactant such as cetyltrimethylammonium bromide (CTAB) [214]. However CTAB preparation has been associated with decreased *in vitro* DNA release [215].

### 4.1.2 PLGA Microparticle Preparation

Difficulties can arise in efficiently encapsulating hydrophilic nucleic acids such as DNA and siRNA in hydrophobic polymeric microparticles. Therefore approaches such as double emulsion water-oil-water (w/o/w) solvent evaporation are used to encourage encapsulation [208]. Hydrophilic nucleic acids generally require double emulsion preparations as the drug is not soluble in the polymer solvent, usually an organic solvent such as DCM or ethyl acetate leading to poor encapsulation efficiency by single emulsion methods [213].

PLGA microparticles can be prepared using a diverse range of methods that have been optimised over the past few decades to produce particles with specific characteristics including size, morphology, surface charge, cell specific targeting, controlled release profiles and specific drug loading or encapsulation. In general polymers are dissolved in an appropriate solvent typically ethyl acetate or DCM and the drug solution such as an aqueous pDNA or siRNA solution is added. The organic and aqueous solutions are mixed by homogenisation to form an emulsion (water in oil (w/o)), in the case of double emulsion methods this is the primary emulsion. Emulsions are then transferred to an emulsifying solution mostly commonly a polyvinyl alcohol (PVA) solution and homogenized to form the secondary emulsion which is added to another emulsifying solution, solvent is removed and particles isolated and dried [215]. Parameters required for preparation are polymer and cargo dependent. Alternatively polymeric-drug emulsions can be added to a hardening agent or spray dried to promote particle formation (Figure 4.2).

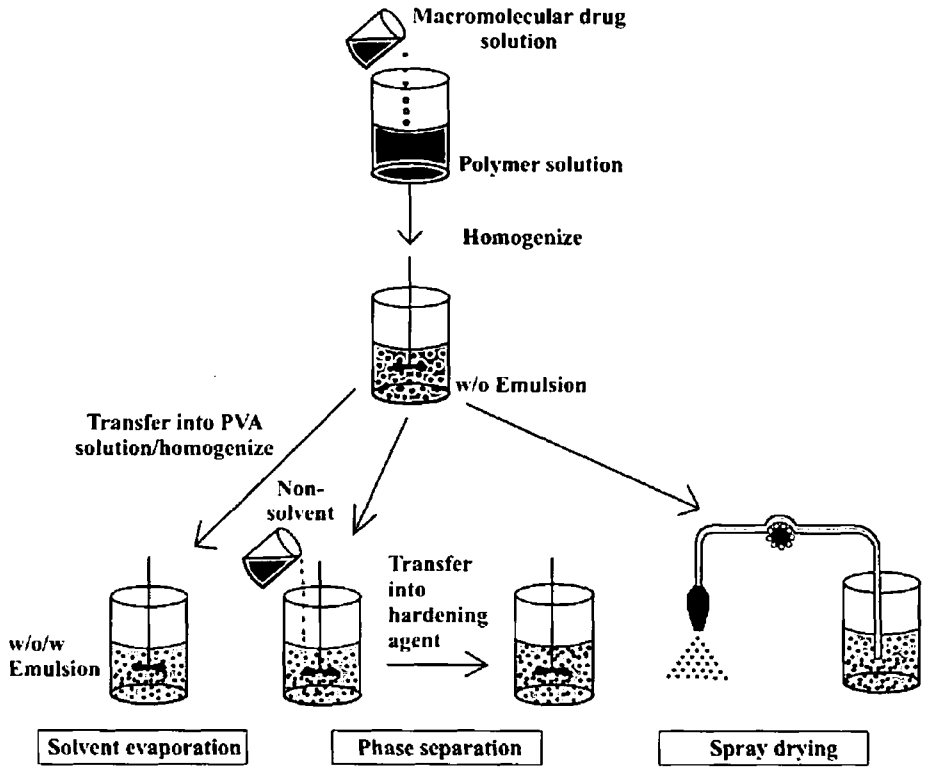


Figure 4.2: Polymer-based microparticle preparation techniques for encapsulating macromolecular drugs [209]

Each step in the preparation process will determine the characteristics of the particles formed. The properties and scale of the drug being encapsulated determine the optimal method for encapsulation such as double emulsion for nucleic acids. Size can be determined by various means such as homogenisation speed and the percentage PVA used as an emulsifier [208, 215]. Surface charge and targeting can be altered by modifications to PLGA or later coating of the particles [213]. Drug release from PLGA particles occurs by diffusion and/or particle erosion and usually involves an initial burst release followed by sustained release over days and months [213]. The initial burst refers to drug that is released prior to polymer erosion-related release [213]. To create more predictable and reproducible release profiles, modification of particle preparation methods are key. Drug release is dependent on various factors including drug solubility and distribution within the particle and the presence of channels or pores [213].

PVA is a non-toxic and non-mutagenic polymer and is the most commonly used emulsifying agent in PLGA microparticle formulation [215]. It is used to stabilize the emulsion as it is associated with the formation of relatively small particles with uniform size distribution [216] but is also a limiting factor in PLGA based gene delivery [207]. PVA is used up to 10% (w/v) in aqueous solution and the greater the percentage PVA the smaller the particles. Residual PVA remains following aqueous washes during particle preparation as it forms an interconnected network with the polymer at the interface [217]. The amount of residual PVA is related to the % PVA solution used to stabilize the emulsion and the organic solvent used during particle preparation. Residual PVA can affect many physicochemical properties of the particles including drug release, zeta potential, encapsulation efficiency and surface hydrophobicity as

well as cell uptake [217]. Sahoo *et al.* (2002) found reduced cell uptake by human arterial smooth muscle cells of PLGA nanoparticles associated with increased residual PVA [217].

PLGA particle preparation techniques however involve mechanical, thermal and chemical stresses which could damage the drug being encapsulated [209]. DNA damage can be caused by sonication, homogenisation, high percentage PVA solutions, high interfacial surface tension at the oil water interface, acidic conditions during formulation due to the presence of PLGA and freeze drying [215]. Furthermore the amassing of oligomers due to degradation of DNA within the particles can produce an acidic environment leading to inactivation of the encapsulated DNA [215]. Various measures can be taken to minimize denaturation or inactivation of nucleic acids such as complexation with cationic agents to protect the nucleic acid or the addition of a buffering solution which can lower the deleterious effects of sonication and acidic environments [215].

### 4.1.3 siRNA-Microparticles

To date most studies have focused on the formulation of pDNA loaded polymeric particles but with an increased requirement for non-viral, biocompatible siRNA delivery systems these findings and formulations are being applied to siRNA polymer encapsulation and delivery. Double emulsion solvent evaporation is the most commonly used technique for siRNA microparticle preparations (Table 4.1) and produces solid particles with low encapsulation efficiencies. To overcome poor encapsulation and transfection efficiencies cationic reagents such as PEI [156, 218], DOTAP [219], chitosan and polyamines have been incorporated into formulations. Recently Lee et al took a more novel approach to PLGA siRNA particle formulation by the preparation of self-assembling siRNA-PLGA conjugate micelles [220]. siRNA was conjugated to PLGA via cleavable disulfide bonds at the 3' end of siRNAs. These conjugate in aqueous solution spontaneously formed 20nm micelle structures which were then coated with linear PEI to form 30nm cationic particles.

**Table 4.1 Summary of PLGA delivery of siRNA**

| siRNA Target | Method | Particle Diameter | EE % | Effect | Ref. |
|---|---|---|---|---|---|
| TNFα | siRNA/PEI complexed<br>Double emulsion solvent evaporation<br>Lyophilisation | 26 -32pm | ≤ 77% | siRNA/PEI polyplex burst release | [156] |
| eGFP<br>Luciferase | DOTAP mixed with PLGA in chloroform<br>Double emulsion solvent evaporation<br>Spray drying | 207.7 – 261.1 nm | - | Significant eGFP knockdown in H-1299 cells | [219] |
| eGFP | Double emulsion solvent evaporation<br>Spray drying | | 60% | | [221] |
| GFP | siRNA conjugated to PLGA<br>Self-assembly followed by PEI coating | 30nm | - | Successful knockdown of GFP | [220] |
| eGFP | Double emulsion solvent evaporation<br>Freeze dried | ~250nm | ~70% | Release profile shows initial burst followed by slow release. Optimised formulation parameters. siRNA functional after encapsulation | [222] |
| STAT3 | siRNA complexed with PEI or PEI-StA<br>Double emulsion solvent evaporation<br>Freeze dried | 351/392nm<br>(w/PEI or PEI-StA) | 26.31/43.98 %<br>(w/PEI or PEI-StA) | Three phase release profile with burst release within 24hrs, sustained release up to 6 days,increased until 8 days. Up to 77% reduction in pSTAT3 compared to naked siRNA treated cells | [218] |
| TNFα | siRNA/DOTAP complexes<br>Single emulsion | 709 nm | ~31% | After 24 hours significant TNFα suppression in LPS activated macrophages | [223] |
| Luciferase | siRNA/DOTAP complexes (also chitosan modified particles)<br>Emulsion solvent diffusion<br>Freeze dried | 317nm | 28.3% | Chitosan modified nanospheres showed higher uptake and knockdown ability than unmodified PLGA nanospheres | [224] |
| VEGF | siRNA complexed with arginine or PEI<br>Double emulsion solvent evaporation | 35 -45 μm | Arg:64.3%<br>PEI:80.3% | Sustained siRNA release for one month<br>Effect on tumour growth | [225] |
| EGFR | Double emulsion deposition | 10 – 20 μm | | | [226] |

### 4.1.4 Microparticles for Targeted Delivery to Alveolar Macrophages

Microparticles can be prepared over a wide range of sizes; larger sized microparticles are advantageous when targeting macrophages, as size is an important factor in cell uptake. It has been shown that particle size ranging from 1 to 10μm are preferentially internalised by antigen presenting cells (APCs) such as macrophages and dendritic cells which is an advantageous feature in DNA vaccine development [215]. Previously, uptake of PLGA microparticles ranging in size were assessed by us in primary alveolar macrophages and differentiated THP-1 cells and microparticles of 2.1μm in diameter showed the greatest cell uptake [198]. The optimal mass median aerodynamic diameter (MMAD) of particles for efficient pulmonary delivery ranges from 1μm to 5μm [153]. Consequently, PLGA microparticles loaded with siRNA can be bioengineered for both inhalation and alveolar macrophage targeting.

Previously it has been shown that gelatin coating can promote macrophage uptake possibly via opsonisation. Gelatin is a natural polymer and is derived from collagen [227]. It is widely used in various clinical applications and is noted for its safety *in vivo*. Similarly to PLGA, gelatin is biodegradable and can be used to load biomolecules for controlled release delivery to cells. The surface charge of gelatin is determined by the conditions used for extraction from collagen [227] and a change in zeta potential or surface charge can dramatically affect cell internalisation efficiency. Recently our group has shown the uptake of PLGA microparticles by differentiated THP-1 cells to be significantly ($p < 0.05$) enhanced by gelatin coating [198].

### 4.1.5 Chapter Aims

This chapter sets out to bioengineer microparticles specifically for siRNA delivery to alveolar macrophages.

- Development of a method for efficient siRNA encapsulation in PLGA microparticles of optimal size for macrophage uptake
- Assess macrophage cell uptake of PLGA microparticles loaded with siRNA
- Determine transfection efficiency using TNFα siRNA

**4.2 Materials**

1,2-Dioleoyl-3-trimethylammonium-propane (DOTAP), M.W. 698.542, Avanti Polar Lipids Inc.

1x Saline

AllStars negative control siRNA, Qiagen

Chloroform, Sigma Aldrich

DCM, Sigma Aldrich

DEPC, Sigma Aldrich

EasySep CD14 kit, StemCell Technologies

EasySep magnet, StemCell Technologies

Ethanol, Sigma Aldrich

FreeZone 4.5, Labconco

Gelatin, Sigma Aldrich

HBSS, Invitrogen

Isopropanol, Sigma Aldrich

LightCycler 480 PCR system, Roche

LSM510 Meta laser scanning confocal microscope, Zeiss

Lymphoprep, Axis Shield

Malvern Mastersizer 2000, Malvern Instruments

Nanoseries Zetasizer, Malvern

Nucleofector® Device, Lonza

Nucleofector® Kit V for THP-1, Amaxa

Oligonucleotide primers, MWG Biotech

Poly(lactic-co-glycolic acid) (PLGA) 503, Boehringer Ingelheim

Quantitect Reverse Transcription kit, Qiagen

RPMI, BioSera

siGENOME Non-Targeting siRNA #2, Dharmacon

Silencer® Select Pre-designed siRNA, Ambion

siPORT$^{TM}$ NeoFXTM Transfection Reagent, Applied Biosystems

SYBRgreen master mix, Roche
t-butanol, Sigma

Tescan Mira XMU Variable Pressure Field Emission Scanning Electron Microscope

(VPFESEM), Tescan USA Inc. USA

TRI Reagent, Sigma Aldrich

Vectashield, Vector Laboratories

## 4.3 Methods

### 4.3.1 siRNA

siGENOME Non-Targeting siRNA #2 (Dharmacon) and *Silencer*® Select Pre-designed TNFα siRNAs are described in 3.3.1. AllStars negative control siRNA (Qiagen) was modified with Alex Fluor 488 (fl-siRNA) and has no homology to any known mammalian gene. *Silencer*® Select Pre-designed siRNA were also targeted to glyceraldehyde 3-phosphate dehydrogenase (GAPDH). siRNAs were reconstituted with nuclease-free water to a concentration of 50 or 100μM.

### 4.3.2 Cell Culture

THP-1 cells were maintained as described in Chapter 3.

#### 4.3.2.1 Isolation of Monocytes/Macrophages from peripheral blood

Primary blood monocytes were isolated using Ficoll-Paque™ Plus and MACS CD14 kit as described in 3.3.2.2 or Lymphoprep and EasySep CD14 kit. For EasySep CD14 purification primary monocytes were isolated from heparinized venous peripheral blood obtained from volunteers. Whole blood was collected from patients in Lithium-Heparin serum tubes. Blood was immediately transferred to 50ml tubes and mixed gently with an equal volume of 0.9% NaCl (1x saline). Diluted blood was then carefully layered over Lymphoprep in fresh 50ml tubes (volume ratio 2:1 blood:Lymphoprep) for density gradient centrifugation. Tubes were centrifuged at 800g for 10 minutes at room temperature with the brake off. Following centrifugation a distinct band of mononuclear cells is formed at the blood/lymphoprep interface (the buffy coat). The mononuclear cell layer was carefully aspirated using a pasture pipette and washed in HBSS (10 – 20ml). Cells were pelleted by centrifugation at 1500 rpm for 5 minutes with the brake on. Monocytes were purified using the EasySep Human CD14 Selection Cocktail. Briefly cell pellets were resuspended in 1ml EasySep recommended medium (PBS containing 2% FBS and 1 mM EDTA) and transferred to a polystyrene tube. EasySep positive selection cocktail 100μl per ml of cell suspension was added, mixed gently and incubated at room temperature for 15 minutes. Positive seclection cocktail consists of monoclonal antibodies bound in bispecific tetrameric antibody complexes (TAC) directed against CD14 and dextran in PBS. EasySep magnetic particles (magnetic dextran iron particles in water) were added to the cell suspension (50μl/ml of cells) and mixed followed by 10 minute incubation at room temperature. The cell suspension volume was brought up to 2.5ml with recommended medium and mixed. The tube was placed into the EasySep magnet and incubated for 5 minutes at room temperature. The magnet and tube were inverted in one continuous motion and held inverted for 2 seconds. The tube was removed from the magnet and cells (adhered to the tube sides) were resuspended in 2.5ml of recommended media and the washing step repeated twice more for a total of 3 washes. Finally cells were resuspended in 1ml of 10% RPMI and transferred to a

polypropelene tube. Cells were counted, plated and maintained in RPMI 1640 containing 10% FBS in a 5% $CO_2$ atmosphere at 37°C.

### 4.3.3 Preparation of siRNA loaded Poly(lactic-co-glycolic acid) Microparticles

Microparticles containing fl-siRNA, GAPDH or TNF-α siRNA were prepared using a double emulsion (w1/o/w2). To improve encapsulation efficiency siRNA was condensed with a cationic lipid DOTAP at a N:P ratio of 4:1 (Table 2.4) using a HFDM method adapted from Wu *et al.* (2009) [228]. HFDM was shown previously to produce lipid particles in the nanometer range with very high siRNA encapsulation efficiencies at N/P ratio 4 [228]. DOTAP and PEI have also been used in a number of studies to promote siRNA loading into PLGA partilces [156, 218, 219, 223-225]. Naked siRNA and siRNA PEI complexes were also assessed but gave negligible siRNA encapsulation.

For a 50mg PLGA preparation, 100nmoles of siRNA was diluted in 200µl of DEPC-treated RNase-free water (the equivalent of 24.2 nmoles of phosphate). 96.8nmoles of DOTAP (67.62µg) was dissolved in 200µl of *t*-butanol. The siRNA solution was added dropwise to the lipid mixture, mixed and lyophilised overnight (Figure 4.3). 50mg of PLGA 503 (Boehringer Ingelheim) was dissolved in 1.75ml DCM (2.9% w/v) and vortexed. Lyophilised siRNA/DOTAP was resuspended in 50µl of RNase-free water and 1ml of the PLGA solution and vortexed vigorously. The remaining 750µl of PLGA solution was added and the mixture was manually probe sonicated for 30 seconds at an output level of 1 to form the primary (w/o) emulsion. The primary emulsion was added dropwise to a 5% (w/v) PVA solution (12.5ml) homogenizing over an ice-bath at 13,500 rpm (or level 3) to form a secondary or multiple w/o/w emulsion. This emulsion was added to 25 ml 1% (w/v) PVA and gently stirred for 4 hours or overnight at room temperature to allow DCM evaporation. Microparticles were recovered by centrifugation at 5,000 rpm for 15 min at 4 °C, washed three times with water to remove residual PVA, resuspended in 1.5ml d $dH_2O$ and then lyophilized (Labconco, FreeZone 4.5). For gelatin coating, after centrifugation the final pellet was resuspended in gelatin solution (1mg/ml gelatin Type A in de$H_2O$ to give a PLGA:Gelatin weight ratio of 1:3) and stirred gently for 4 hours. The coated particles were centrifuged at 5,000rpm for 15 min at 4 °C three times and washed with $dH_2O$ to remove excess gelatin. The final pellet was resuspended in 1.5ml $dH_2O$ and lyophilized.

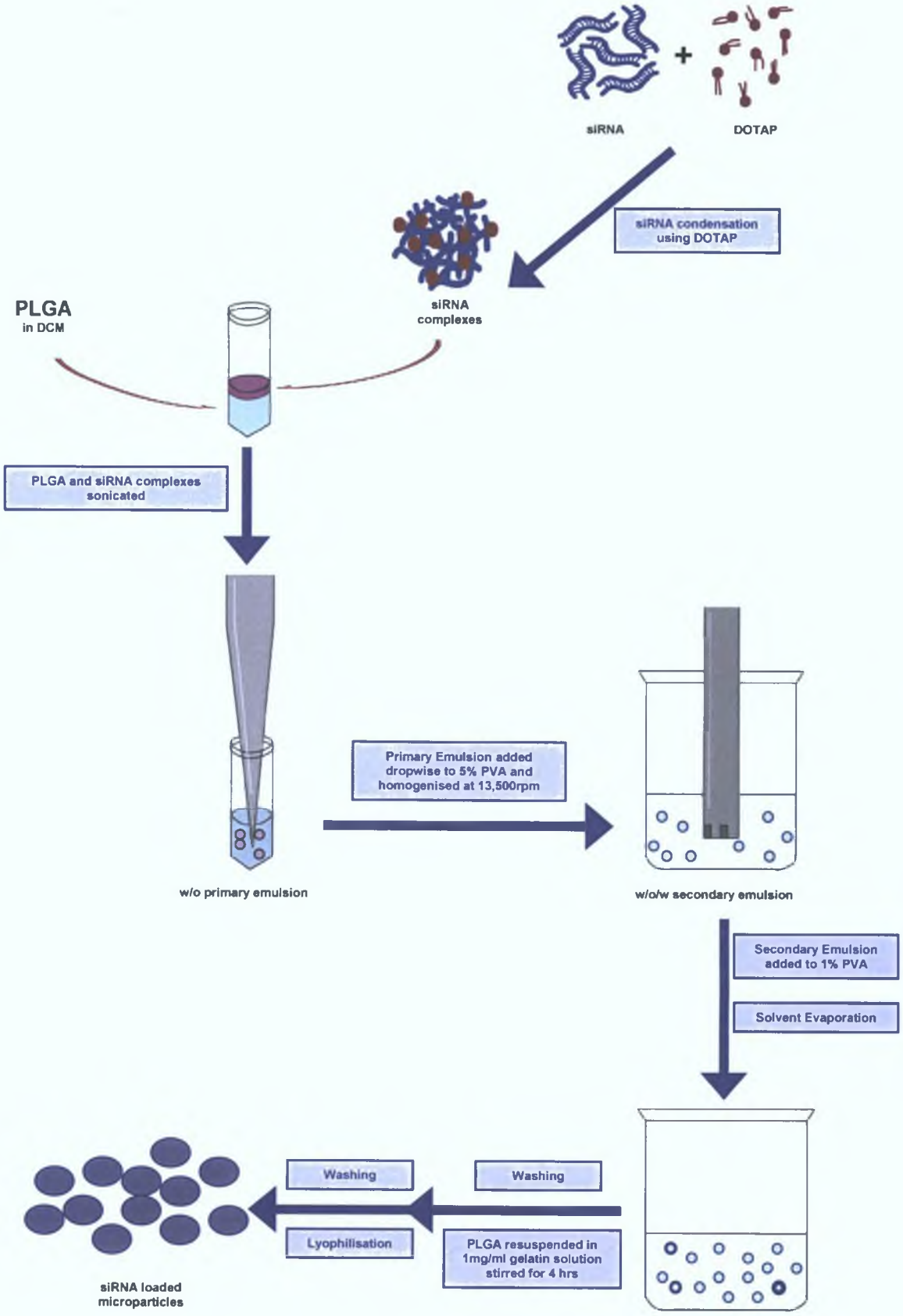


Figure 4.3: Schematic of siRNA-microparticle preparation by double emulsion solvent evaporation method.

### 4.3.4 Microparticle Characterisation

#### 4.3.4.1 Particle Size

Microparticle size was determined by laser diffraction using a Malvern Mastersizer 2000 (Malvern Instruments, UK). Lyophilized microparticles (5mg) were resuspended in 1 ml of $dH_2O$ and sonicated. Particle sizes were recorded in triplicate for each batch of microparticles.

#### 4.3.4.2 Zeta Potential of microparticles

Zeta potentials of microparticles were measured in disposable capillary cells using a nanoseries Zetasizer (Malvern) to determine surface charge. Lyophilized microparticles (5mg) were resuspended in 1 ml of $dH_2O$ and sonicated. Zeta potential for each batch was acquired five times and means were calculated.

#### 4.3.4.3 Surface morphology by scanning electron microscopy (SEM)

Microparticle size and surface morphology was assessed by scanning electron microscopy (SEM) using a Tescan Mira XMU Variable Pressure Field Emission Scanning Electron Microscope (VPFESEM) (Tescan USA Inc. USA). Lyophilized particles were mounted onto aluminium stubs with double sided adhesive tape and coated in a vacuum with a thin layer of gold to impart electrically conductivity using a Polaron SC500 Gold Sputter Coater (Quotum technologies). The coated specimen was then examined under the microscope operated at an acceleration voltage of 5kV.

#### 4.3.4.4 Encapsulation Efficiency

Lyophilised microparticles encapsulating siRNA (1mg) were dissolved in 50µl of chloroform. To this 50µl of nuclease free water was added and the mixture was vortexed for 15 minutes followed by centrifugation at 10000 rpm for 5 minutes. The upper aqueous layer was collected and the centrifugation step was repeated twice more after the addition of another 50µl of TE buffer. Collected aqueous layers were pooled and the nucleic acid concentrations determined. siRNA quantification was estimated using a ribogreen assay (as described in 2.3.2.4) or in the case of fl-siRNA fluorescent intensities were measured using fluorescent spectroscopy at 485nm and 520nm excitation and emission wavelengths respectively. Fl-siRNA concentration was determined using a prepared calibration curve.

#### 4.3.4.5 Release Profile of siRNA

siRNA release from PLGA microparticles was assessed over 7 days at 37°C [229] and measured by RiboGreen assay. Lyophilised microparticles encapsulating siRNA (5mg) were suspended in 1ml TE buffer (pH 7.4) and incubated at 37° C under gentle shaking. At specific

time points, the microparticle suspensions were centrifuged at 10000 rpm for 10 min. Supernatants were collected and stored at -80°C until analysis. Microparticle pellets were re-suspended with 1ml fresh TE buffer and incubated at 37°C. siRNA in supernatants for each time point was determined using RiboGreen assay as described in 2.3.2.4. Cumulative siRNA release was calculated.

#### 4.3.4.6 Integrity of encapsulated nucleic acids

siRNA integrity was evaluated by gel electrophoresis using a 20% polyacrylamide (19:1 acrylamide:bisacrylamide) TBE gel as described in 2.3.2.2. Blue/orange 6x loading dye (Promega) was used to track gel migration. Nucleic acids were extracted from microparticle preparations by aqueous and solvent phase separation as described in 4.3.4.4. Extracted siRNA, stock siRNA and a siRNA marker were loaded and the gels were run in 1x TBE buffer at 100V for 45 minutes followed by post-staining with GelStar for 30 minutes. Visualization was obtained by UV transillumination.

### 4.3.5 Functional Activity of encapsulated siRNA

TNFα siRNA was extracted from microparticle preparations by aqueous/solvent phase separation as described in 4.3.4.4. THP-1 cells ($1x10^6$) were electroporated with 50ng of unprocessed TNFα or 50ng of microparticle extracted TNFα siRNA using Nucleofector® Device (Lonza) and Nucleofector® Kit V for THP-1 (Amaxa). Briefly, $1x10^6$ cells per replicate were centrifuged and resuspended in 100µl Nucleofector® Solution. For siRNA transfections, 50ng of unprocessed TNFα siRNA or extracted microparticle TNFα siRNA was added to the cell suspensions. Each cell suspension was transferred to a cuvette and the cuvette cap was closed. The cuvettes were placed into the Nucleofector® Cuvette Holder and programme V001 selected. Cuvettes were removed from the device and 500µl of supplemented RPMI was added. Cell suspensions were transferred to 24 well plates and differentiated with the addition of 100nM PMA. After 21 and 45 hours cells were stimulated with 100ng/ml LPS for 3 hrs. Media was harvested 24 and 48 hours following electroporation and TNFα expression was determined by ELISA.

### 4.3.6 *In Vitro* Uptake of siRNA-Microparticles

#### 4.3.6.1 Confocal Microscopy

Primary monocytes were isolated and seeded at $1x10^5$ cells/well in 8-well chamber slides. Cells were incubated with fresh media, fl-siRNA alone (28ng), fl-siRNA complexed with commercially available transfection reagent NeoFx, NeoFx alone, unloaded gelatin-coated and uncoated microparticles and fl-siRNA-loaded gelatin-coated and uncoated microparticles for 2 and 24 hours. For NeoFx fl-siRNA complexation, 28ng of fl-siRNA was diluted in optiMEM up to 25µl while 1µl NeoFx was diluted up to 25µl with optiMEM. Diluted siRNA and NeoFx were added

together and mixed and incubated at room temperature for 10 minutes to allow complexation. Cells were washed with warmed PBS and stained with phalloidin-TRITC (45 minutes) and hoescht (5 minutes). Following a washing step, cells were mounted in Vectashield and visualised using a LSM510 Meta laser scanning confocal microscope (Zeiss, Germany).

#### 4.3.6.2 Flow Cytometry

THP-1 cells were seeded at a density of $2x10^5$ cells/well and differentiated in a 24-well plate. Differentiated THP-1 cells were incubated for 3 hrs with fl-siRNA alone, fl-siRNA-loaded microparticles, or fl-siRNA complexed with lipofectamine 2000. Cells were then washed with PBS, detached from wells, suspended in PBS and analyzed using Cell Quest Pro software.

#### 4.3.6.3 High Content Cell Analysis

Primary monocytes were seeded in 96-well plates at a density of $1x10^5$cells/ml. Cells were incubated with fresh media, fl-siRNA alone, fl-siRNA complexed with commercially available transfection reagent NeoFx, unloaded gelatin-coated and uncoated microparticles and fl-siRNA-loaded gelatin-coated and uncoated microparticles for 2 and 24 hours. Varying amounts of 1mg/ml microparticle preparations were added to the cells (50µl, 100µl and 250µl). Cells were washed three times with warmed PBS and counterstained with phalloidin-TRITC and Hoescht. 150µl of PBS was added to each well and plates were stored at 4°C in the dark. HCA was carried out using INCELL 1000 analyser. Images were acquired in three channels with excitation/emission wavelengths 360/460nm, 480/535nm and 565/620nm and 5 fields per well. Images were analysed using INCELL analyser software as described in 3.3.4.2 with parameters adjusted accordingly.

### 4.3.7 Toxicity

THP-1 cells were seeded at $1x10^5$ cells/ml in 96-well plates and incubated with microparticles or 120µM valinomycin (positive control) for 23.5 hours. Microparticles were suspended in RPMI at 1, 3 or 5mg/ml. 20 or 50µl of microparticle suspension was added to wells in triplicate and the final volume per well was brought up to 100µl with supplemented media. The Cellomics Multiparameter Cytotoxicity assay was performed as described in 3.3.5.

### 4.3.8 Microparticle Mediated siRNA Knockdown in Macrophage Cell Models

#### 4.3.8.1 Targeted Knockdown of GAPDH Expression in Primary Monocytes

Primary monocytes were seeded at 2.5 - $5x10^5$ cells per well in 24 well plates immediately following isolation and incubated overnight to allow adherence to the wells. Media was replaced with fresh supplemented RPMI. All transfections were performed in triplicate with 99ng siRNA per well. The commercially available transfection reagent NeoFx was used as a positive

transfection control. Briefly, 7.5µl of siRNA was brought up to 25µl with optiMEM while separately 1µl of NeoFX transfection reagent was brought up to 25µl with optiMEM and incubated at room temperature 10 minutes. Diluted siRNA and NeoFx were mixed and incubated room temperature for a further 10 minutes. The mixture was added dropwise to cells and plates were moved back and forth to mix. Microparticles empty or encapsulating non-target, GAPDH targeted siRNA were suspended in media at a concentration dependent on encapsulation efficiency. 250µl of microparticle suspension was added to wells. After 48 hours cells were lysed for GAPDH gene expression analysis by real time PCR.

#### 4.3.8.2 Targeted Knockdown of TNFα Expression in Differentiated THP-1 Cells

THP-1 cells were seeded $2\times10^5$ cells/well in a 96 well culture plate and differentiated. Cells were treated with an equal amount of siRNA complexed with lipofectamine 2000 or encapsulated in MPs for 3 hrs and media was replaced. Cells were stimulated with 100ng/ml LPS and supernatants were collected 24 and 48 hours post-transfection 3 hours following LPS stimulation. TNFα production was estimated by ELISA described in 3.3.6.3.

#### 4.3.8.3 Targeted Knockdown of TNFα Expression in Primary Monocytes

Isolated primary monocytes were seeded at $3x10^4$ cells per well in 96 well plates and incubated at 37°C 5% $CO_2$ overnight. Media was changed leaving adherent macrophages. siRNA transfections were mediated by a commercial transfection reagent Lipofectamine 2000 and microparticles. Non-target or three TNFα targeted siRNAs were diluted in serum free RPMI while 1µl of lipofectamine 2000 was diluted separately in serum free RPMI. Diluted siRNA and lipofectamine 2000 were mixed and incubated at room temperature for 20 minutes to allow complexation. siRNA lipofectamine 2000 complexes were added dropwise to wells in triplicate. Microparticles were suspended in serum-free RPMI (2 and 5mg/ml). Media was replaced with microparticle suspensions. 100µl of 2mg/ml empty and siRNA (non-target and TNFα targeted) encapsulating microparticles were added to wells in triplicate. 200µl of 5mg/ml TNFα siRNA encapsulating microparticles were also added to wells in triplicate. Cells were incubated with microparticles at 37°C for 2 – 3 hours and media was replaced with fresh supplemented RPMI. Cells were stimulated with 100ng/ml LPS for 3 hours prior to each media collection time point of 48 and 72 hours. TNFα induction was determined by ELISA described in 3.3.6.3.

### 4.3.9 RNA Extractions

Total RNA was isolated from primary cells using TRI-reagent (Sigma-Aldrich) according to the manufacturer's instructions. Following supernatant collection from transfected primary monocytes, 500µl of TRI-reagent was added to each well of the 24 well plates and pipetted up and down to lyse cells and form a homogenate cell lysate. Cell lysates were transferred to microtubes and were allowed to stand at room temperature for 5 minutes. 100µl of chloroform was added to each sample and tubes were shaken vigorously. Following a 2 minute incubation

at room temperature samples were centrifuged at 12,000xg for 15 minutes at 4°C. This results in phase separation with a lower red organic layer (protein), an interphase (DNA) and an upper aqueous layer (RNA). The upper layer was transferred to a fresh tube and 250pl of isopropanol was added and mixed. Samples were incubated at room temperature for 5 minutes and centrifuged at 12,000xg for 10 minutes at 4°C. Supernatants were discarded and the RNA pellet was washed by adding 500µl of 75% ethanol, vortexing and centrifuging at 12,000xg for 5 minutes at 4°C. The supernatants were carefully removed so as not to disturb the RNA pellets. Samples were briefly allowed to air-dry and dissolved in 20µl 0.1% DEPC water. RNA yields and purity were determined spectrophotometrically using a NanoDrop8000. RNA samples were stored at -80°C.

### 4.3.10 cDNA Synthesis

Quantitect Reverse Transcription kit (Qiagen) was used to reverse transcribe 300ng of total RNA. RNA samples were thawed on ice. To eliminate genomic DNA (gDNA) 300ng of each sample template RNA was added to nuclease free reaction tubes. 2µl of gDNA wipeout buffer (7x) was added to each reaction and brought up to a final volume of 14pl with RNase-free water. Reaction tubes were incubated at 42°C for two minutes (PTC Thermocycler) and immediately placed on ice. To each reaction tube containing 300ng total RNA reverse-transcription reaction mixtures were added consisting of 1µl Quantiscript Reverse Transcriptase (RT), 4µl Quantiscript RT buffer and 1µl RT primer mix and incubated for 30 minutes at 42°C followed by 3 minutes at 95°C. cDNA samples were stored at -20°C until analysed by real time PCR.

### 4.3.11 Real time PCR

Quantitative PCR was preformed in 20 µl reactions containing 2 µi template cDNA, 2x SYBR green master mix (Roche) and 10 pmol of oligonucleotide primer (MWG Biotech). Reaction components were added to the wells of a white 96 well PCR plate (1µl reverse primer, 1µl forward primer, 10µl SYBR green and 6µl sterile water). Plates were sealed and centrifuged at 2000rpm for 2 minutes. Primers used were GAPDH (NM_002046) (Forward Primer CATGAGAAGTATGACAACAGCCT, Reverse Primer AGTCCTTCCACGATACCAAAGT) or β-actin (F Oligo, 0.01scale 5'-GGACTTCGAGCAAGAGATGG-3', R Oligo, 0.01scale 5'-AGGAAGGAAGGCTGGAAGAG-3'). Amplification was performed using a LightCycler 480 PCR system (Roche) set at 57°C for 55 cycles. Gene expression was calculated relative to β-actin expression giving an RQ value ($2^{-\Delta\Delta Ct}$, where CT is the threshold cycle).

### 4.3.12 Statistical Analysis

In general results are expressed as means ± SD. One way or two way ANOVA was used to test for differences between treatments with $p$-values < 0.05 considered significant, < 0.01 very significant and < 0.001 highly significant.

## 4.4 Results

### 4.4.1 Characterisation of Microparticles

#### 4.4.1.1 Size

Particle size is important to ensure particles were optimal for macrophage targeting and uptake. in the development of a drug delivery system especially for inhalation. 2.1μm PLGA microparticles were previously determined as optimal size for alveolar macrophage uptake [198]. Each microparticle was sized and mean diameters were found to be between 2 and 3.2 μm (Table 4.2), fitting into the size range for effective pulmonary delivery. Gelatin coating and siRNA/DOTAP complex encapsulation increased particle size.

**Table 4.2: Microparticle Average sizes (mean ± SD)**

| PLGA Microparticle | Average Size ($d_{50}$ μm) |
|---|---|
| **Gelatin Coated Empty** | 3.209 ± 0.126 |
| **Uncoated Empty** | 2.387 ± 0.034 |
| **Uncoated siRNA/DOTAP loaded** | 2.882 ± 0.416 |

#### 4.4.1.2 Zeta Potential

Zeta potential is a measure of particle surface charge and has been associated with system stability and transfection efficiency. A colloidal system is stable when the zeta potential is within the -30 to +30mV range. Surface charge can also greatly affect cell internalisation. Overall zeta potentials of uncoated microparticles were negative and greater than -30mV (Table 4.3) while gelatin coating increased the charge to 11.2 mV a property that could effect cell uptake.

**Table 4.3: Microparticle Zeta Potentials (mean ± SD)**

| PLGA Microparticle | Zeta Potential (mV) |
|---|---|
| **Gelatin coated Empty** | 11.2 ± 2.34 |
| **Empty** | -2.3 ± 0.17 |
| **Uncoated siRNA/DOTAP loaded** | -26.1 ± 2.39 |

#### 4.4.1.3 Encapsulation Efficiency

To accurately assess nucleic acid dosing and concentrations the amount of siRNA encapsulated into the microparticles using DOTAP pre-condensation was determined. PLGA microparticle encapsulation efficiencies of siRNA on average were found to be 56.5 ± 12.9% for uncoated microparticles (Table 4.4). Encapsulation efficiencies confirmed the reproducibility and the versatility of this method for a range of siRNAs including non-target, GAPDH and TNFα targeted siRNA. However, gelatin-coated particles had much lower siRNA encapsulation efficiencies averaging 12.3 ± 7% perhaps due to the additional wash steps.

**Table 4.4: Summary of % Encapsulation Efficiency of PLGA Microparticles (means ± SD)**

| PLGA Microparticle | Average Encapsulation Efficiency (%) |
|---|---|
| **Empty** | 0 |
| **Gelatin Coated siRNA/DOTAP** | 12.3 ± 7 |
| **Uncoated siRNA/DOTAP** | 56.5 ± 12.9 |

#### 4.4.1.4 Scanning Electron Microscopy (SEM)

SEM was used to examine morphology, size and particle size distributions of microparticles. SEM and laser diffraction established microparticle size to be with the optimal size range for successful pulmonary delivery and alveolar macrophage targeting. SEM also confirmed the homogeneity of microparticle size distribution showing smooth spherical particles (Figure 4.4).

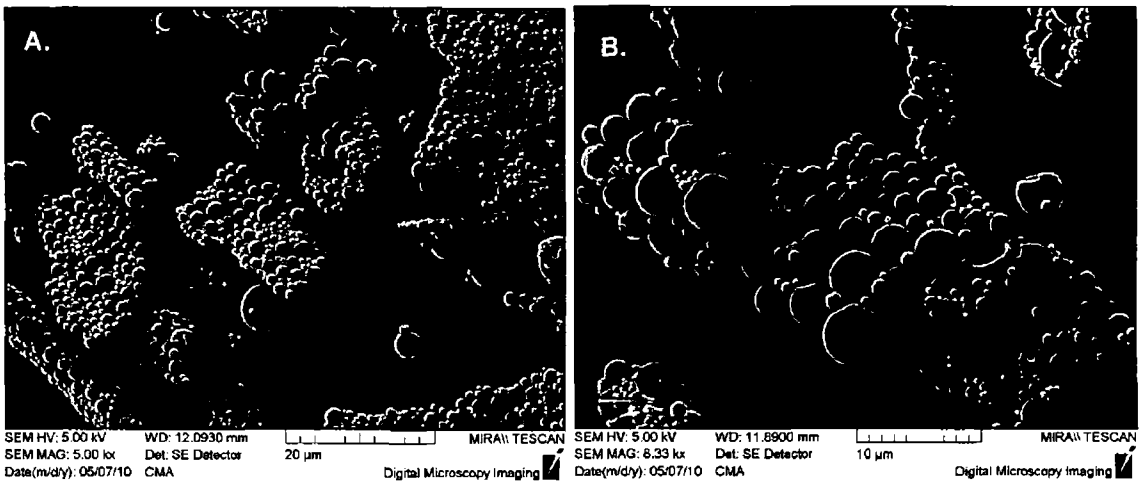


Figure 4.4: Microparticle morphology, particle size and particle size distribution was examined using SEM. (A) GAPDH loaded PLGA at 5.00 kx magnification and (B) fl-siRNA loaded PLGA microparticles at 8.33 kx magnification

#### 4.4.1.5 Microparticle siRNA Release

It has previously been reported that PLGA microparticles show a drug release profile that consists of an initial burst followed by slow release extending for days or months including PLGA particle release of siRNA [225]. Microparticles encapsulating siRNA were incubated at 37°C in pH 7.4 TE buffer and the amount of released siRNA determined after 0.5, 1 and 3 hours and 1, 2, 3, 5 and 7 days which was carried out by Dr. Awadh Yadav. An initial burst of siRNA release from PLGA microparticles was observed with 12.6 ± 1.2 % siRNA released by 3 hours followed by slow controlled release with 20.5 ± 1.2 % released after 7 days (Figure 4.5). The extended siRNA release also shows the stability of the system at physiological conditions.

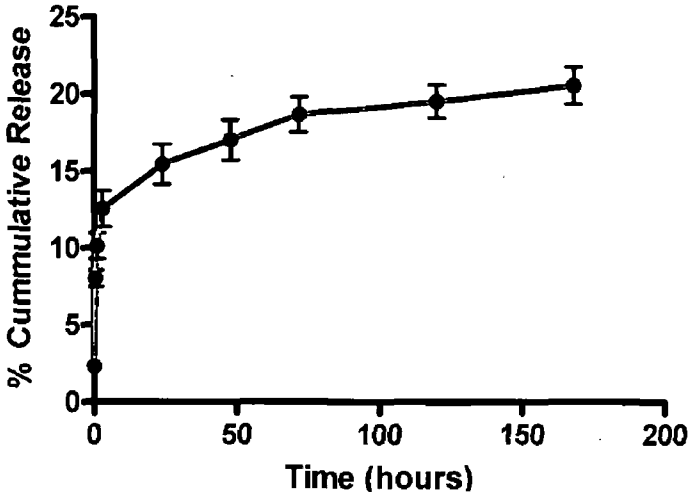


Figure 4.5: Microparticle siRNA release profile. Microparticles encapsulating siRNA were incubated at 37°C under gentle shaking at pH 7.4. Released siRNA was determined at 0.5, 1, 3, 24, 48, 72, 120 and 168 (7 days) hours. Data is represented as means ± SD (n = 4)

#### 4.4.1.6 Nucleic Acid Integrity

The microparticle preparation procedure involves the use of stresses such as sonication, homogenisation and low temperatures increasing the possibility of degradation and functional loss to the loaded nucleic acids. To address this issue the integrity of loaded nucleic acids was assessed by gel electrophoresis. The presence of a single band of appropriate size showed no degradation or structural damage to extracted siRNA (Figure 4.6).

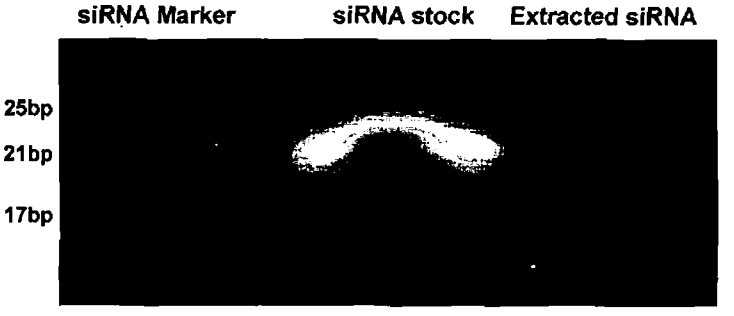


Figure 4.6: 20% polyacrylamide gel. The 20% polyacrylamide gel shows the siRNA marker (45ng), siRNA stock (1.1µg) and microparticle extracted siRNA (18.5ng).

#### 4.4.1.7 Functionality of Microparticle Encapsulated siRNA

Due to the stresses involved in microparticle preparation siRNA is susceptible to degradation. Gel electrophoresis showed single bands representing siRNA extracted from microparticles (Figure 4.6), however while this indicates intact siRNA it does not confirm functionality of the extracted siRNA. Therefore the ability of siRNA extracted from microparticles to mediate RNAi was compared to unprocessed siRNA in THP-1 cells and was carried out by Dr. Awadh Yadav (Figure 4.7). TNFα siRNA was extracted from microparticles and using nucleofection THP-1 cells were transfected with TNFα siRNA. TNFα siRNA was most effective at mediating knockdown at 48 hours. Greater knockdown was observed by 50ng of unprocessed siRNA (61.6 ± 13% TNFα expression ($p < 0.01$)) but only marginal compared to extracted siRNA (77.4 ± 1% TNFα expression). Extracted siRNA also showed some functionality at 24 hours with 92 ± 12% TNFα expression. Overall TNFα siRNA following the stresses of microparticle encapsulation remains largely functional.

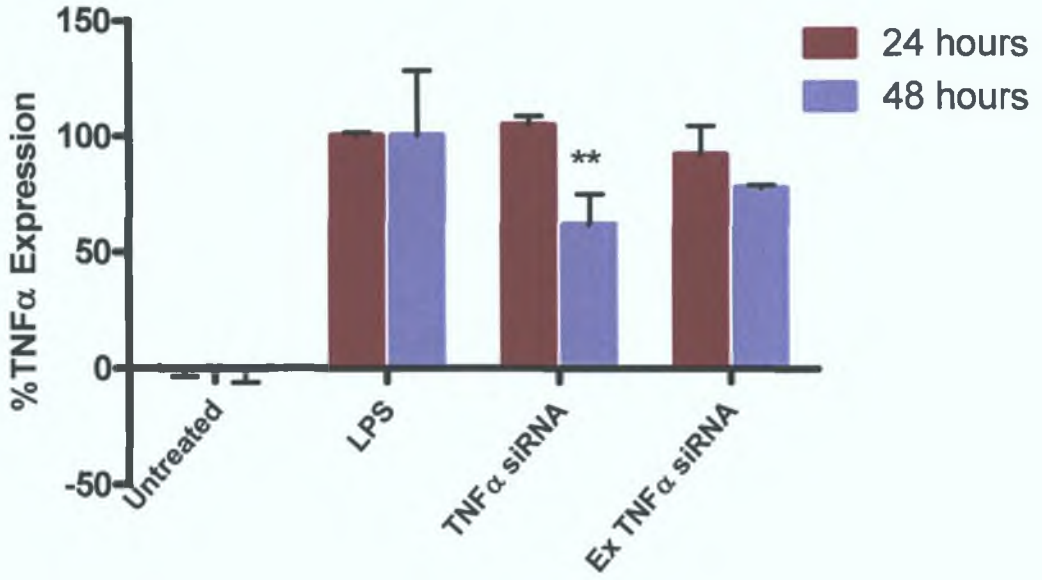


Figure 4.7: Functionality of microparticle encapsulated TNFα siRNA in THP-1 cells. TNFα siRNA was encapsulated in PLGA microparticles by the double emulsion evaporation method followed by lyophilisation. THP-1 cells were electroporated with 50ng of unprocessed TNFα siRNA (TNFα siRNA) or 50ng of TNFα siRNA extracted from microparticles (Ex TNFα siRNA). Cells were stimulated for 3 hours with LPS 24 and 48 hours following electroporation and TNFα expression determined. Data expressed as means ± SD (n = 3)
Statistical significance was determined by two-way ANOVA followed by Bonferroni Post hoc test (*$p < 0.05$, ** $p < 0.01$, *** $p < 0.001$) vs untransfected stimulated cells

### 4.4.2 Cell Uptake Studies

In order to achieve transfection, efficient uptake by cells of the microparticle delivery system is necessary. Microparticles were loaded with fl-siRNA for flow cytometric analysis and uptake determined by confocal laser scanning microscopy (CLSM) and HCA. Confocal microscopy, flow cytometry and HCA were used to determine internalisation and the extent of uptake respectively of a range of carrier systems into THP-1 cells and primary monocytes/macorphages.

#### 4.4.2.1 *Internalisation* by Differentiated THP-1 Cells

In order to quantify the percentage of differentiated THP-1 cells transfected fl-siRNA was quantified using flow cytometry by Dr. Awadh Yadav. The increase of fl-siRNA uptake was highly significant ($p < 0.001$) when loaded in uncoated microparticles compared to all other treatments including fl-siRNA dose and fl-siRNA transfected with Lipofectamine 2000 (Figure 4.8).

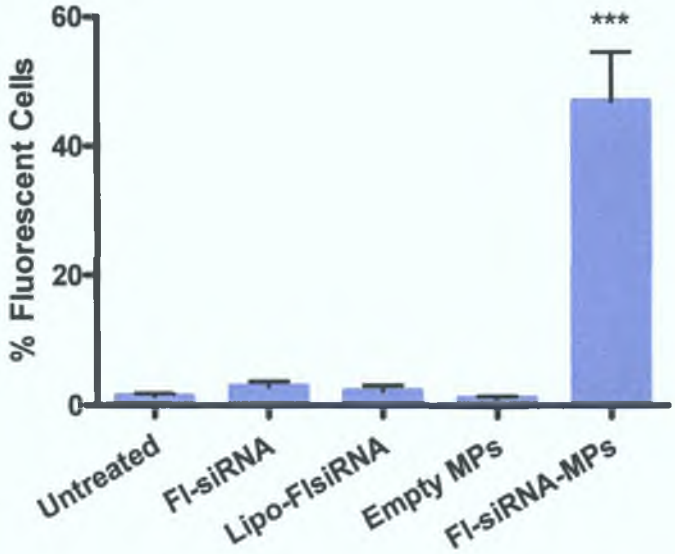


Figure 4.8: Microparticle uptake by differentiated THP-1 cells assessed using flow cytometry. Cells were untreated or treated with, fl-siRNA alone, fl-siRNA/lipofectamine 2000 (Lipo-FlsiRNA), empty uncoated microparticles (MPs) or fl-siRNA loaded uncoated microparticles (Fl-siRNA-MPs). Data represented as means ± SD (n = 3). Statistical significance was determined by one-way ANOVA followed by Dunnett's Post hoc test (*$p < 0.05$, ** $p < 0.01$, *** $p < 0.001$)

#### 4.4.2.2 Internalisation by Primary Monocytes

Primary macrophages were treated with uncoated and coated fl-siRNA loaded microparticles and fl-siRNA/NeoFx as a positive control for 2 hours and 24 hours. CLSM and Z-stack analysis carried out by Katie Nolan and Warren Thomas confirmed microparticle uptake into the cells at 24 hr for both gelatin-coated and uncoated microparticles (Figure 4.9). Coated and uncoated microparticle treatment showed increased fl-siRNA cell uptake at both time points in comparison to fl-siRNA alone and the positive control fl-siRNA/ NeoFx treatments. In addition cell loss was observed following 24 hour NeoFX treatments at concentrations recommended by the manufacturers.

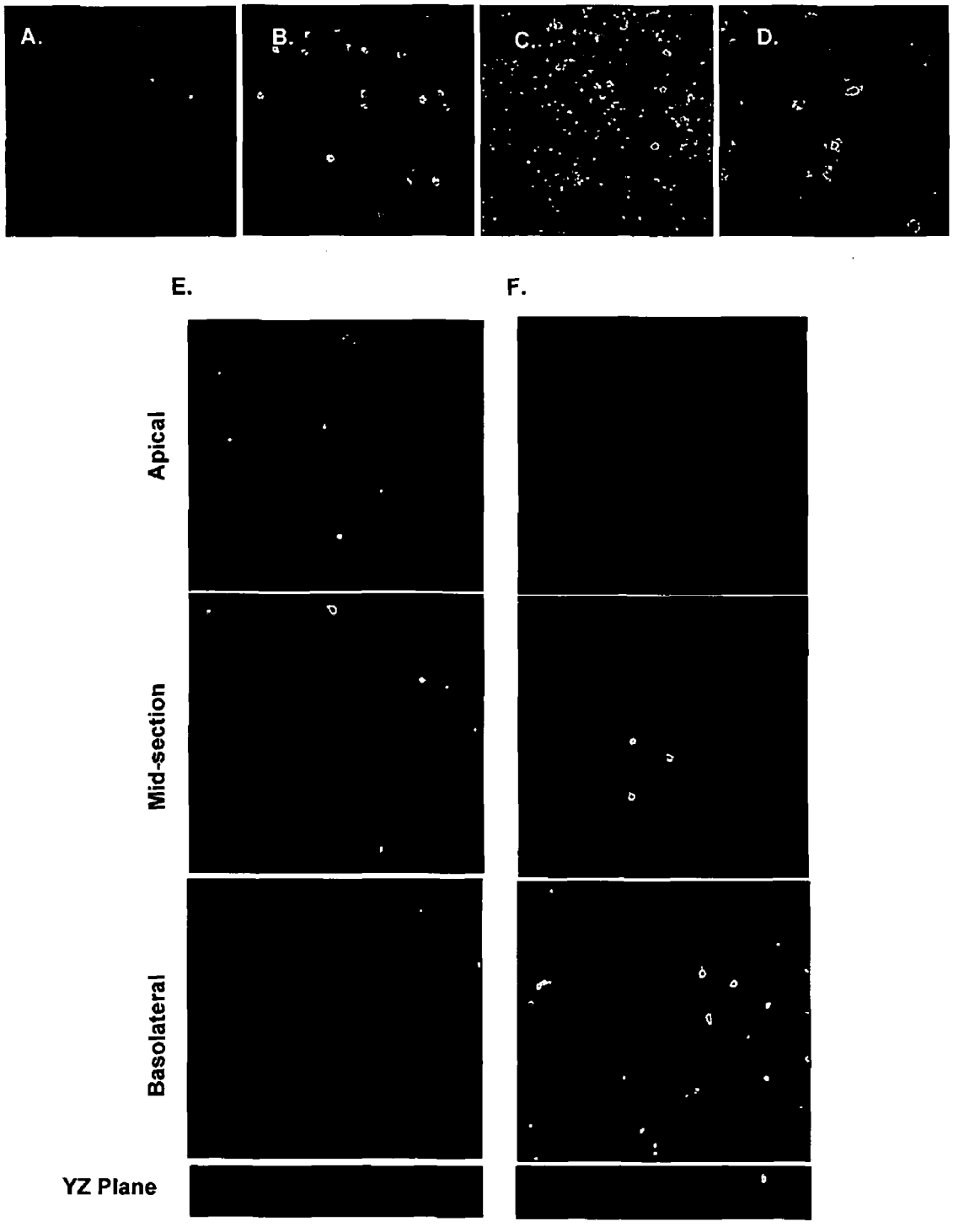


Figure 4.9: Confocal images of primary monocytes (A) untransfected or transfected with (B) fluorescently tagged siRNA (fl-siRNA, green) complexed with siPORT NeoFx, fl-siRNA encapsulated in (C) uncoated PLGA microparticles and (D) gelatin-coated PLGA microparticles. Z-stack analysis of (E) uncoated fl-siRNA loaded PLGA microparticle uptake in primary macrophages at 24 hours and (F) gelatin coated fl-siRNA loaded PLGA microparticle uptake in primary macrophages at 24 hours.

Quantification of fl-siRNA loaded microparticles and fl-siRNA/NeoFx positive control uptake was determined using high content screening with corresponding treatment to confocal analysis at 2 hr and 24 hr. Treatment at 24 hours with siRNA/NeoFx showed cell loss and the presence of cells without nuclei indicative of cytotoxicity as was observed by confocal uptake assessment. siPORT NeoFX siRNA complexes appeared more diffuse and not defined particles (Figure 4.10B). Hence, fl-siRNA/NeoFX complexes were not picked up in the particle count by the analysis software.

Uncoated and coated fl-siRNA loaded microparticle uptake at 50µg, 100µg and 250µg was significantly enhanced compared to untreated controls and cells transfected with the commercial transfection reagent NeoFx. Empty microparticles both coated and uncoated however showed slight autofluoresence. Uptake of 100µg and 250µg uncoated and 250µg gelatin coated fi-siRNA loaded microparticles was highly significant ($p < 0.001$) after 2 hours in comparison to empty uncoated and coated microparticles respectively (Figure 4.10E). Uptake of uncoated and gelatin coated fl-siRNA microparticles was greater at 2 hours than 24 hours most likely due to fl-siRNA release from microparticles. Confocal microscopy confirmed internalisation of microparticles (Figure 4.9).

Uncoated microparticles showed higher encapsulation efficiency of siRNA and greater uptake by primary macrophages than gelatin coated microparticles. siRNA leached from PLGA microparticles during the coating process leading to reduced siRNA encapsulation. Gelatin coating also added further complexity to manufacture, increasing the risk of contamination. Consequently all further studies were carried out using uncoated PLGA microparticles.

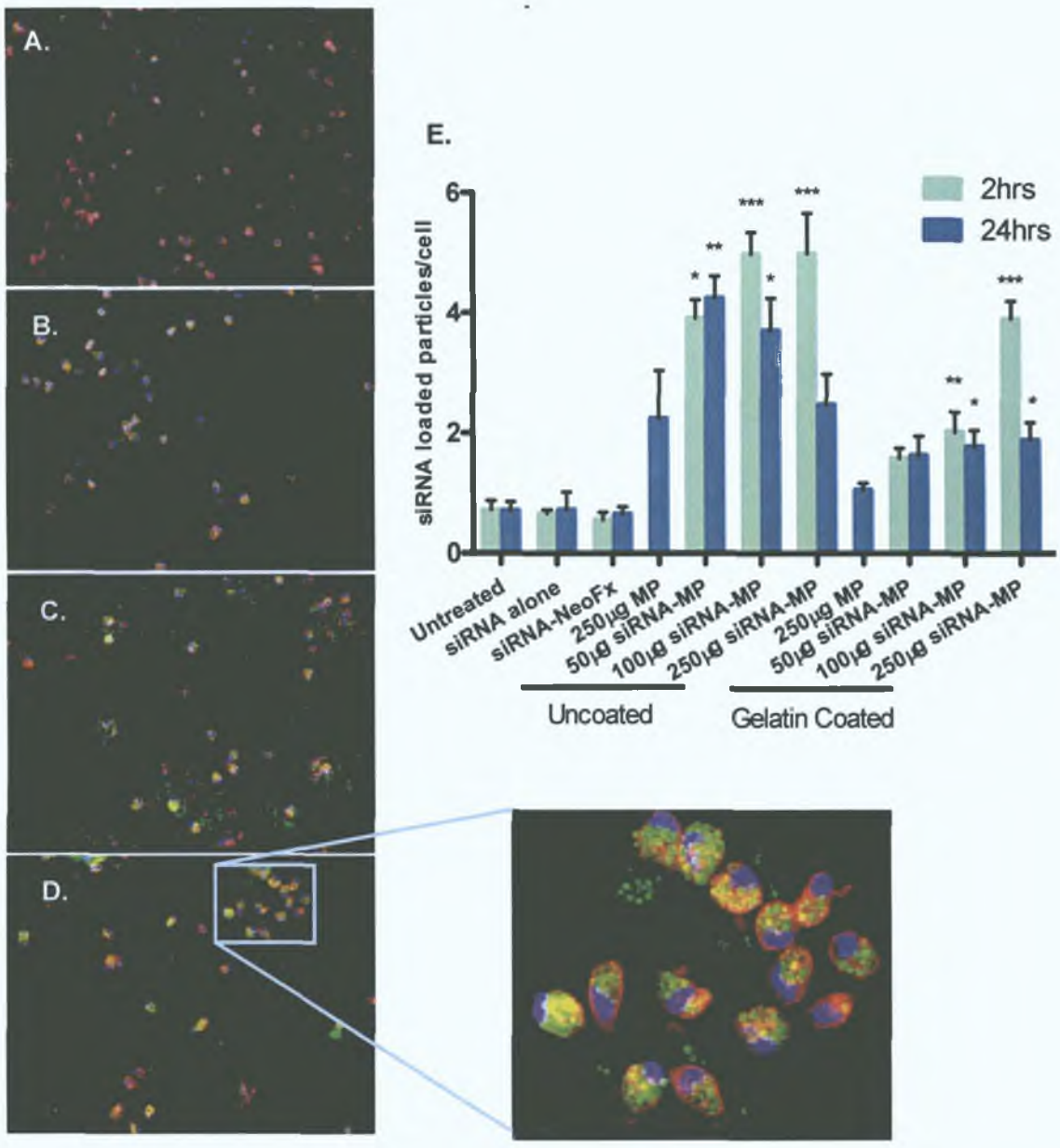


Figure 4.10: High content cell of siRNA microparticle uptake by primary macrophages. Human *monocytes* were isolated and allowed to adhere to 96 well plates. Cells were transfected with empty microparticles (MP) or fluorescently tagged siRNA alone (AlexaFluor 488, green), complexed with NeoFx or encapsulated in uncoated or gelatin coated microparticles (siRNA-MP). Following 2 or 24 hour incubation cells were fixed and counterstained with phalloidin-TRITC (F-actin, red) and Hoecsht (nucleus, blue). Images were acquired at 10x using an INCELL 1000 showing (A) untreated cells, (B) cells transfected with fl-siRNA/NeoFX, (C) cells treated with uncoated Fl-siRNA-MPs and (D) gelatin-coated siRNA-MPs after 2 hours. The number of fl-siRNA particles was counted per cell (E) using INCELL 1000. Data represented as mean ± SD (n = 3) Statistical significance was determined by two-way ANOVA followed by Bonferroni Post hoc test (*$p < 0.05$, ** $p < 0.01$, *** $p < 0.001$) vs empty microparticle counterparts

### 4.4.3 Toxicity

Differentiated THP-1 cells were treated with PLGA microparticles empty or encapsulating siRNA at various concentrations for 24 hours in order to assess cell viability following microparticle treatment. As a positive control cells were treated with a toxic agent, valinomycin (120μM), while negative controls were left untreated and incubated in complete media. Cells were treated with two doses of 1mg/ml empty or siRNA-microparticles (Figure 4.11 and 4.12).

To assess a dose response higher concentrations of 3mg/ml and 5mg/ml microparticles encapsulating TNFα were also used for comparison with later GAPDH transfections. In general transfections used 1 – 1.5mg/ml concentrations. Following 24 hour treatment cells were stained and fixed. Images (Figure 4.11) and quantitative analysis (Figure 4.12) were acquired using an INCELL 1000 cell analyser and cell loss, nuclear size and intensity, cell permeability, *mitochondrial membrane potential* and cytochrome c were determined.

Cell loss was significant following valinomycin treatment (Figure 4.11 and 4.12A) but not after microparticle treatment. Cell count however was variable within treatment groups and a loss although not significant was observed in the 100μg TNFα microparticle (100μl of 1mg/ml) treatment group. *Apoptosis is associated with chromatin condensation* and consequently nuclear morphological changes were monitored i.e. size and intensity. Positive controls again showed significant changes compared to untreated healthy cells. Nuclear size was significantly decreased following valinomycin ($p < 0.001$) and 100μg NT microparticles ($p < 0.05$) treatment (Figure 4.12B). While total nuclear intensity was significantly increased by valinomycin ($p < 0.001$) and 300μg and 500μg TNFα microparticles treatments (100μl of 3mg/ml and 5mg/ml) (Figure 4.12C).

Cell permeability is linked with necrosis and was increased following valinomycin and all higher dose microparticle treatments with 100μg TNFα microparticles significantly ($p < 0.001$) increasing permeability (Figure 4.12D). MMP decrease is associated with apoptosis and related to cytochrome c release. Valinomycin treatment decreased MMP as did 50μl of all 1mg/ml microparticle treatments but not significantly. Increased MMP was found following the higher dose of all microparticles treatments (Figure 4.12E). In general cytochrome c levels did not deviate significantly from those of healthy cells except following 20μg and 100μg TNFα microparticle (1mg/ml) treatment ($p < 0.05$) (Figure 4.12F).

Overall microparticles do not impair cell viability. At all concentrations there is no significant cell loss. Microparticles at the higher doses encapsulating siRNA caused changes in nuclear size. MMP and a small increase in cell permeability suggesting some toxicity induced through both apoptosis and necrosis. Additionally, the higher concentrations of TNFα microparticles 3mg/ml and 5mg/ml significantly increased nuclear intensity and MMP while cell loss was unaffected. The lower concentrations are therefore more suitable for *in vitro* transfection.

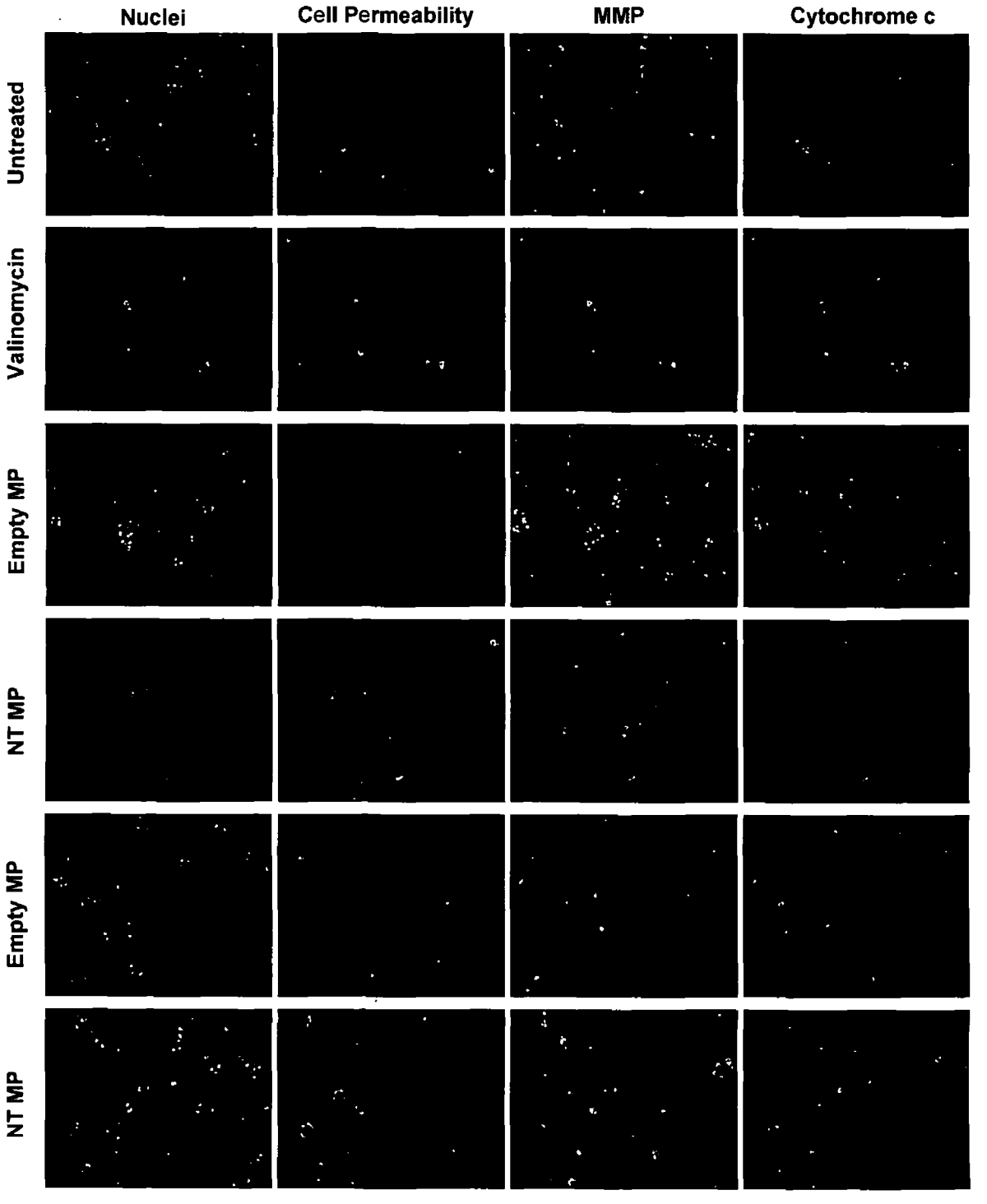


Figure 4.11: High content cell assessment of toxicity in differentiated THP-1 cells induced by microparticles. Differentiated THP-1 cells were treated with either 20 or 100μg empty microparticles (MP) or microparticles encapsulating non-target siRNA (NT MP). Negative controls were healthy cells incubated in complete media. Positive controls were treated with 120pM valinomycin. Cells were treated for 24 hours, fixed and stained for nuclei (hoescht), cell permeability, mitochondrial membrane potential (MMP) and cytochrome c release. Images were acquired and analysed using an INCELL 1000.

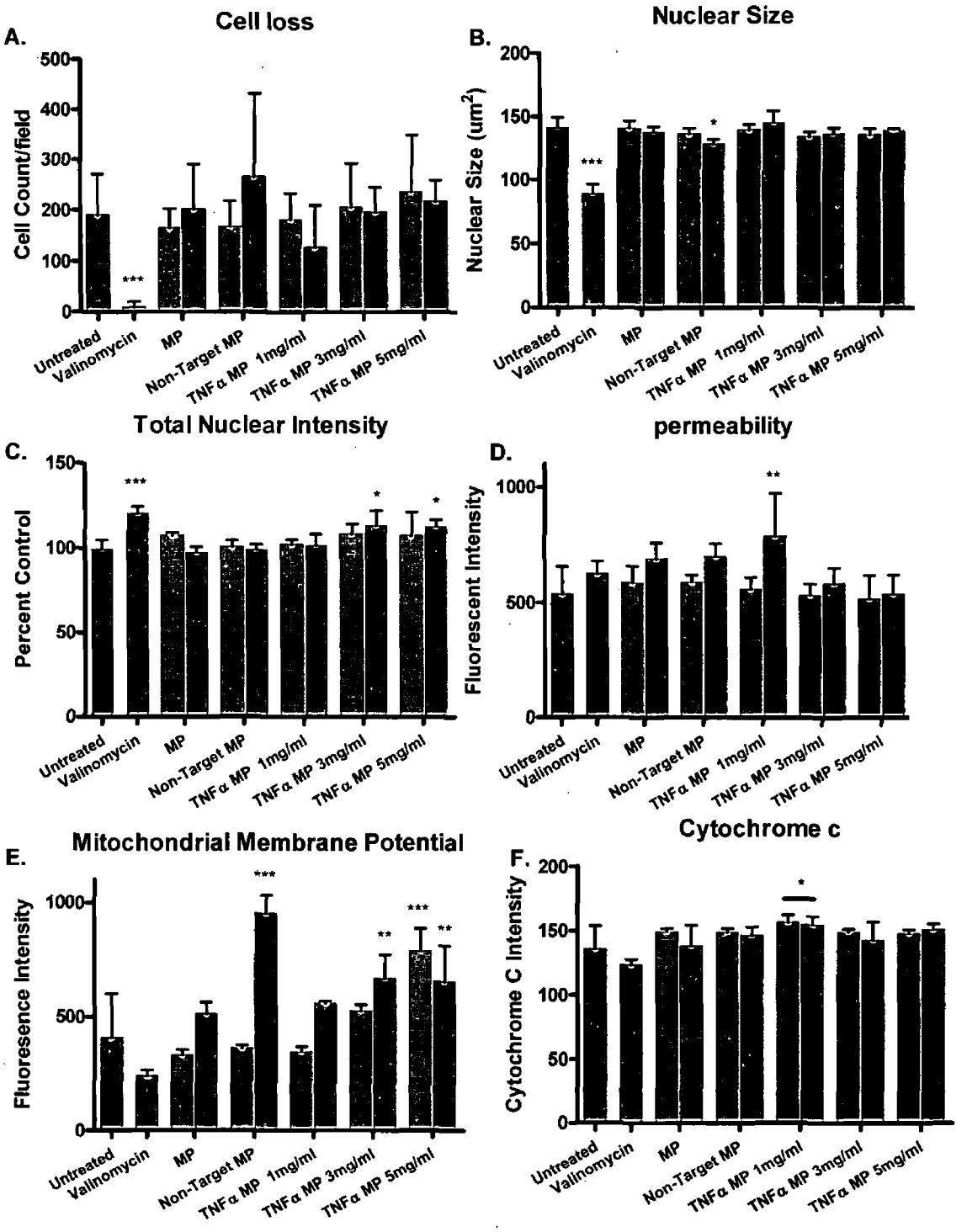


*Figure* 4.12: High content cell assessment of toxicity in differentiated THP-1 cells induced by PLGA microparticles. Differentiated THP-1 cells were treated with either 20µl ■ or 100µl ■ of 1mg/ml empty microparticles (MP) or microparticles encapsulating non-target siRNA (Non-Target MP) or TNFα targeted siRNA (TNFα MP). TNFα MP treatments were also at 3mg/ml and 5mg/ml. Positive controls were treated with 120pM valinomycin. Cells were treated for 24 hours, fixed and stained. Images were acquired and analysed using an INCELL 1000. Cell loss, nuclear size and intensity, MMP, cytochrome c release were measured (A-F). Data represented as means ± SD. Statistical significance was determined by two-way ANOVA vs untreated controls (* $p < 0.05$, ** $p < 0.01$, *** $p < 0.001$)

### 4.4.4 Microparticle siRNA Transfections

#### 4.4.4.1 GAPDH Knockdown in Primary Monocytes

Initially knockdown of an endogenously expressed house keeping gene GAPDH was evaluated in isolated primary monocytes by qRT-PCR. Compared to non-target siRNA transfections NeoFX/GAPDH siRNA reduced GAPDH expression by 26.4 ± 36.3 % while an equivalent amount of GAPDH siRNA delivered via microparticles suppressed GAPDH expression by 31.1 ± 60.1 % (Figure 4.13). Microparticle GAPDH siRNA transfections also showed a dose dependent knockdown (data not shown). In order to acquire a sufficient amount of RNA for qRT-PCR analysis a large amount of cells were required and results between experiments were somewhat variable in the extent of knockdown. However, an optimised microparticle transfection method in primary monocytes was established.

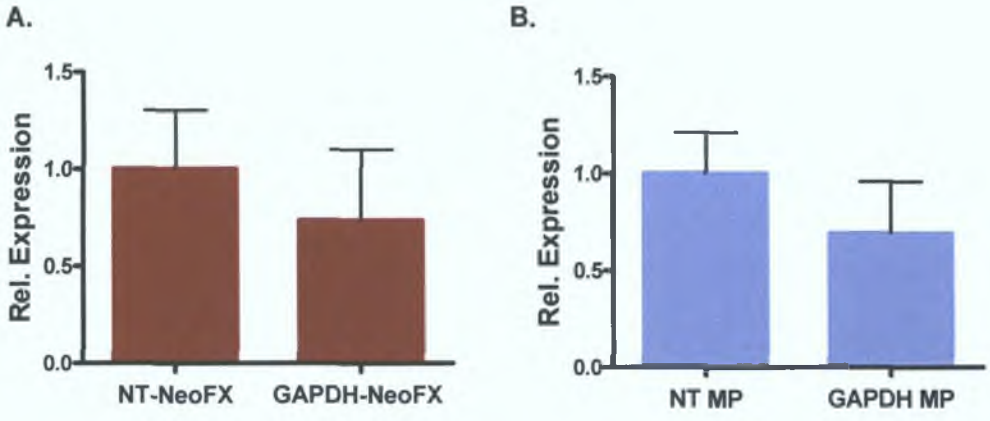


Figure 4.13: Modulation of GAPDH expression in primary blood derived monocytes by GAPDH targeted siRNA delivered using siPort NeoFX transfection reagent and PLGA microparticles. Isolated primary monocytes were transfected with 99ng of GAPDH targeted siRNA delivered using (A) siPORT NeoFX commercial transfection reagent or (B) uncoated PLGA microparticles. Cells were transfected and harvested 48 hours later for qRT-PCR analysis. Data is represented as means ± SD (n = 3) normalised to non-target siRNA transfected counterparts.

#### 4.4.4.2 TNFα Knockdown in LPS Stimulated THP-1 and Primary Monocyte Cells

Following knockdown of endogenously expressed GAPDH, microparticles were used for inflammatory gene knockdown in differentiated THP-1 cells. In LPS stimulated cells TNFα is greatly induced and therefore the need for high cell numbers to detect gene expression changes in this model is reduced offering a sensitive and potentially therapeutic target for knockdown. Also cytokine production can be determined by ELISA enabling sensitive detection of gene expression. Using another commericial transfection reagent LipoFectamine 2000 and siRNA-microparticles differentiated THP-1 cells were transfected with non-target and TNFα targeted siRNA. TNFα production was determined 3 hours following LPS stimulation at a number of time points following transfection. TNF-α expression was reduced by 44.8 ± 3.4 % and 39.6 ± 4.9 % after 48 and 72 hours respectively using microparticles. The commercial reagent Lipofectamine 2000 led to little or no knockdown (Figure 4.14). Lipofectamine 2000 however caused TNFα induction in primary monocytes (Chapter 3 Figure 3.12).

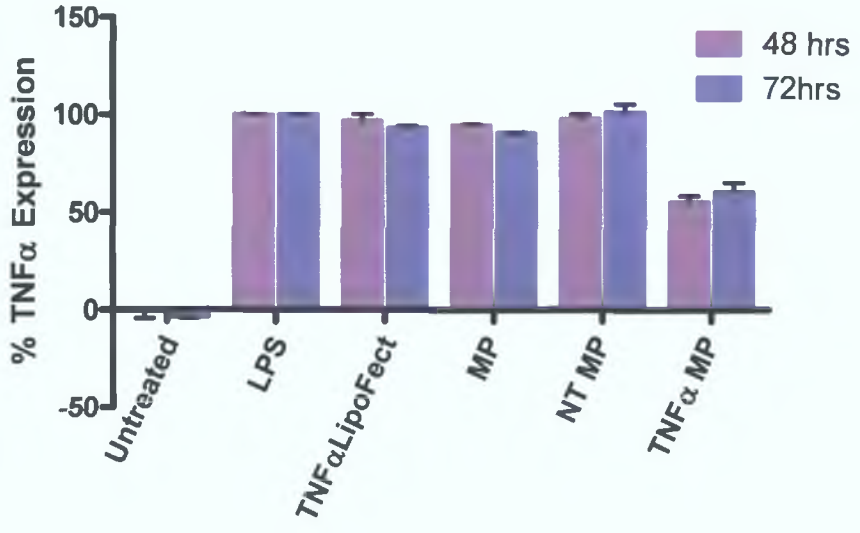


Figure 4.14: Modulation of TNF-α expression in LPS-stimulated differentiated THP-1 cells following transfection. Transfected cells were treated with empty microparticles (MP), non-target or TNFα directed siRNA either complexed with commercial transfection reagent Lipofectamine™ 2000 (TNFαLipoFect) or encapsulated in microparticles (NT MP or TNFα MP). TNFα expression was determined by ELISA 48 and 72 hours post transfection following a 3 hour LPS-stimuation. Data represented as means ± SD (n=2).

Knockdown of TNFα in LPS stimulated primary monocytes was also assessed after 48 and 72 hours. Monocytes were isolated from venous blood of 6 healthy donors and allowed to adhere to 96 well plates overnight. Cells were transfected with non-target or TNFα targeted siRNAs via Lipofectamine 2000 (data not shown) and PLGA microparticles. LipoFectamine 2000 mediated transfection decreased LPS stimulated TNFα expression by 52.8 and 49.7% at 48 and 72 hours respectively compared to untransfected stimulated cells. Levels of knockdown varied between donors as was observed in GAPDH transfections. However microparticles encapsulating TNFα siRNA on average decreased TNFα expression in LPS stimulated primary monocytes compared to non-target controls (Figure 4.15) at 48 and 72 hours. Knockdown was dose and time dependant with the 150μg dose significantly decreasing TNFα expression after 72hours ($p < 0.05$).

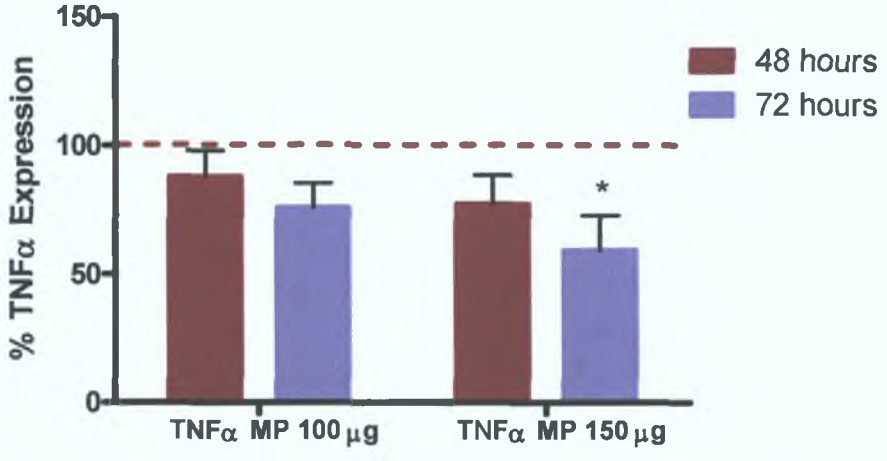


Figure 4.15: Modulation of TNFα expression by PLGA microparticles encapsulationg TNFα targeted siRNA in LPS stimulated primary monocytes. Primary blood derived monocytes from 6 healthy donors were transfected with 100μg or 150μg microparticles encapsulating non-target or TNFα targeted siRNA. After 48 and 72 hours TNFα expression was determined following a 3 hour stimulation with 100ng/ml LPS. Data is represented as percentage mean of non-target siRNA transfected counterpart. Statistical significant was determined by one-way ANOVA vs non-target siRNA transfected counterparts (* $p < 0.05$) with Dunnett's post hoc test

## 4.5 Discussion

A method was developed for preparation of siRNA loaded gelatin coated and uncoated PLGA microparticles using the double emulsion solvent evaporation method. The central objectives were to achieve a high level of nucleic acid encapsulation into microparticles and to monitor the uptake of these loaded microparticles by macrophage cell lines and primary cells. Microparticles formulated were optimised for pulmonary delivery and alveolar macrophage targeting. Particle sizes were in the range of 2 – 3 μm an optimal size for pulmonary delivery and phagocytic uptake by alveolar macrophages. In addition uncoated microparticles showed negative surface charge most likely due to underivatised lactic and glycolic acid in PLGA 503. This characteristic could also promote uptake by macrophages.

Low encapsulation of nucleic acids by microparticles has previously been reported [230]. Various strategies have been used to improve siRNA loading into PLGA particles including siRNA conjugation to PLGA [220] but pre-complexation of siRNA with cationic reagents including DOTAP [223, 224], PEI [156, 218, 225] and arginine [225] is the most common method used. Previously TNFα siRNA has been encapsulated in PLGA microparticles as siRNA/PEI polyplexes and in PLGA nanoparticles as siRNA/DOTAP lipoplexes achieving up to 77% and 31% encapsulation efficiencies respectively [156, 223]. However in our hands PEI condensation of siRNA did not increase siRNA encapsulation over encapsulation of uncomplexed siRNA. DOTAP was instead complexed with siRNA using a method by Wu et al. (2009) with modifications. At N/P ratio of 4 siRNA/DOTAP lipid particles could be formed with high siRNA encapsulation (>90%) and a nanoscale size (<200nm) [228]. Loading of these siRNA lipid particles into PLGA microparticles achieved encapsulation efficiencies of 56.5 ± 12.9%. During coating with gelatin however siRNA appeared to leach out of the particles reducing the encapsulation efficiency to 12.3 ± 7%. An encapsulation efficiency of PEI/siRNA complexes in PLGA microparticles was negligible but this may have been a method issue as found with liposome encapsulation efficiency determination. The siRNA quantification assay requires the siRNA to be accessible for binding of the reagent which may not be possible if it is still complexed. On the other hand the method used mixes the microparticle formulations in chloroform and water. Both DOTAP and PLGA separate into the organic phase while siRNA remains in the aqueous phase. It is less likely that siRNA is still complexed to DOTAP which is soluble in non-polar solvents such as chloroform and so siRNA can be detected. Therefore it is likely PEI/siRNA encapsulation results gave a false negative as this technique was unsuitable for the determination of encapsulation efficiency when PEI is the cationic condensing reagent.

Release of siRNA from uncoated microparticles at pH 7.4 and 37°C was monitored over 7 days. A release profile emmerged similar to that found by Lee *et al.* (2011) at pH 7.4, in a study which also evaluated siRNA release from polymeric microparticles at an acidic (phagosomal) pH. Lee *et al.* (2011) found at pH 5 almost complete siRNA release from particles at 48 hours with 50% after just 7 hours, showing the difference in particle stability and hence siRNA release for

different pH environments. This indicates microparticles remain stable at physiological pH 7.4 but upon entering an acidic intracellular environment the siRNA load will be released.

To visualise and confirm uptake of microparticles by macrophage cell models, particles were loaded with fluorescent siRNA. Confocal analysis of transfected differentiated THP-1 cells and primary macrophages with fl-siRNA loaded microparticles at 2 and 24 hours showed particle cell association and intracellular delivery was confirmed by Z-stack analysis. Commercial transfection reagent NeoFx complexed with fl-siRNA was used as a positive control however little uptake was observed at 2 hours and after 24 hours was cytotoxic which was represented by cell loss and the presence of cells with absent nuclei.

Quantification of cell uptake was determined by flow cytometry and HCA. Flow cytometry determined uptake of fl-siRNA by THP-1 cells to be significantly higher when encapsulated in microparticles. However, this method is not the most suitable for analysing differentiated monocytes as it requires cells to be in suspension and this is difficult to achieve once cells have differentiated into macrophages. HCA is a far more suitable technique for analysis of these adherent cells and was subsequently used for primary cell uptake assessment. HCA of primary macrophages transfected with fl-siRNA loaded microparticles for 2 and 24 hours showed significant enhancement of uptake of fl-siRNA in uncoated microparticles compared to fl-siRNA alone, complexed with NeoFx or encapsulated in coated particles. Furthermore images obtained again showed cell loss and the presence of cells without nuclei at 24 hours with fl-siRNA/NeoFx treatment.

Differentiated THP-1 cells were assessed for toxicity induced by a range of doses of empty and DOTAP/siRNA loaded uncoated microparticles by HCA. Cytotoxcity screens determined changes in total nuclear intensity, cell permeability, mitochondrial membrane potential and cytochrome C release of DOTAP/siRNA loaded microparticles particularly of DOTAP/TNFα loaded microparticles at 1mg/ml. However there was no significant cell loss associated with microparticle treatment. Wilson *et al.* (2010) evaluated cytotoxicity in macrophages treated with increasing doses of PLGA particles loaded with DOTAP/TNFα siRNA from 1mg/ml up to 6mg/ml [223]. Toxicity assessed by MTT assay was not detected up to a dose of 5mg/ml [223]. Observed toxicity could be associated with the presence of the cationic lipid DOTAP and siRNA sequence. Synthetic siRNA can induce sequence specific immune responses which could be associated with presence of GU dinucleotides [231, 232]. Three siRNA sequences targeted at TNFα were pooled and used for *in vitro* studies. Two of these sequences contained two pairs GU nucleotides while the third contained one GU dinucleotide. The TNFα siRNA sequence therefore could have brought about the toxic effects determined following treatment with DOTAP/TNFα loaded microparticles.

Furthermore, a TH1/TH2 cytokine profile in response to 24 hour coated and uncoated microparticle treatment in differentiated THP-1 cells revealed no significant TH1 or TH1 cytokine induction (Lawlor *et al.*, unpublished). Levels of IL-1β and IL-8 were slightly increased above

control untreated cells following microparticle treatment particularly with gelatin coated microparticle treatment. Additionally, PLGA microparticles particularly gelatin coated particles caused significant NFκB induction in differentiated THP-1 Blue cells (Lawlor *et al.*, unpublished). Although microparticles are not inert carriers, inflammatory cytokine induction is non-significant in differentiated THP-1 cells and most importantly the target cytokine TNFα is not affected by PLGA microparticle treatment.

Knockdown of an endogenous house keeping gene GAPDH was mediated via NeoFX transfection reagent and uncoated microparticles encapsulating GAPDH siRNA in primary monocytes. However gene suppression was variable and consequently not significant. Additonally high cell numbers were necessary to generate adequate cDNA for qRT-PCR analysis which can be an issue when using primary cells. Although ubiquitously expressed, the level of GAPDH mRNA in monocytes was low and consequently changes in expression were more challenging to decipher. Disease states are generally associated with abnormal gene expression such as elevated levels of TNFα in COPD patients [233]. Hence, targeted gene suppression of an inducible protein, TNFα, in response to an inflammatory stimulator, LPS, was a more suitable and valid approach to determine siRNA knockdown efficiency using macrophages. Differentiated THP-1 cells and adherent primary monocytes were stimulated with LPS to induce high levels of the target pro-inflammatory cytokine TNFα, a key mediator in the inflammatory response. Microparticle delivery of anti-inflammatory siRNA to inflammatory macrophage cell models showed significant knockdown after 48 and 72 hours (Figure 4.14). Previously significant TNFα knockdown in activated macrophages has been shown with similar particle formulations [223]. DOTAP/TNFα siRNA microparticles mediated almost 50% knockdown in stimulated differentiated THP-1 cells (Figure 4.14) while suppression levels were more variable in primary monocytes but none aimed at alveolar macrophages.

Lipofectamine 2000 was used as the positive control transfection reagent and showed no effect in differentiated THP-1 cells. However, in primary monocytes lipofectamine 2000 transfection with TNFα siRNA decreased TNFα expression in activated cells by 52.8 and 49.7% at 48 and 72 hours respectively. In Figure 3.12 lipofectamine 2000 was shown to induce high levels of TNFα in LPS stimulated primary monocytes after 24 hours. It appears that lipofectamine 2000 initially induces an inflammatory response in primary monocytes, not observed in THP-1 cells, but disappears by 48 hours. This emphasises that siRNA vectors are not always inert and the use of non-target siRNA as negative controls is essential to show the specificity of the target siRNA in cells that have undergone analogous processes.

PLGA is an FDA approved polymer. PLGA microparticles were bioengineered to efficiently encapsulate siRNA with a range of gene targets. These siRNA loaded microparticles also possessed beneficial physicochemical and biopharmaceutical properties such as biocompatibility, low cytotoxcity, low immunogenicity, sustained siRNA release at physiological pH and a size suitable for inhalation which is also optimal for targeting alveolar macrophages. Ultimately microparticles were used to knockdown TNFα expression in inflammatory

macrophage cell models leading to significant TNFα gene suppression in primary monocytes. In conclusion, siRNA/DOTAP loaded microparticles as non -viral delivery vectors for siRNA *in vitro* are stable, biocompatible, non-toxic, non-immunogenic and efficient.

**Key Findings**

- Optimised method for maximal encapsulation of siRNA in PLGA microparticles
- Uncoated microparticles were optimal for macrophage uptake and delivery of siRNA
- Significant knockdown of TNFα in LPS stimulated primary cells via PLGA microparticles encapsulating TNFα targeted siRNA

# Chapter 5

# Microparticles for Intracellular Delivery of shRNA Expressing Plasmids

### 5.1 Introduction

Following on from the discovery of RNAi, siRNA was developed to specifically knockdown genes with high potency yet avoid innate immune activation initiated by dsRNA. However siRNA transfection is typically transient and efficiency can be low. Additionally synthesis is costly and delivery can be difficult. In 2002 Yu *et al.* first described using vectors to express siRNA and hairpin siRNA in the hopes of overcoming the aforementioned problems [234]. Herein, the microparticles developed in Chapter 4 were harnessed for short hairpin RNA (shRNA) delivery. shRNA is expressed, generally by a polymerase III promoter such as U6 small nuclear RNA (U6) or human RNase P RNA H1 (H1) promoters, from a viral or non-viral DNA plasmid transfected into cells and consists of a base-paired stem and loop (Figure 5.1). shRNA utilizes miRNA machinery to be transported to the cytoplasm where it is processed to siRNA (Figure 5.2 and 5.3) and can mediate RNAi. Elucidation of the miRNA pathway has been greatly utilized in shRNA vector development for RNAi.

#### 5.1.1 Short Hairpin RNA (shRNA) RNA Interference

There are three main approaches in the construction of shRNA vectors. The majority of shRNA constructs are synthesised by annealing complementary oligonucleotides but can also be assembled using a PCR method with hairpin containing primers or primer extension of hairpin templates [235]. For shRNA synthesis vectors containing an oligonucleotide for a shRNA sequence simply need to express a single strand of RNA (50 – 100bp) specifically designed to fold back on itself with complimentary segments annealing and a mismatched segment forming a stem-loop (Figure 5.1). This requires a promoter (generally a polymerase III promoter), followed by oligonucleotide sequences for the sense strand (at least 19 nt), loop (4 – 10 nt), anti-sense strand and lastly 4 – 6 terminating uracils [236].

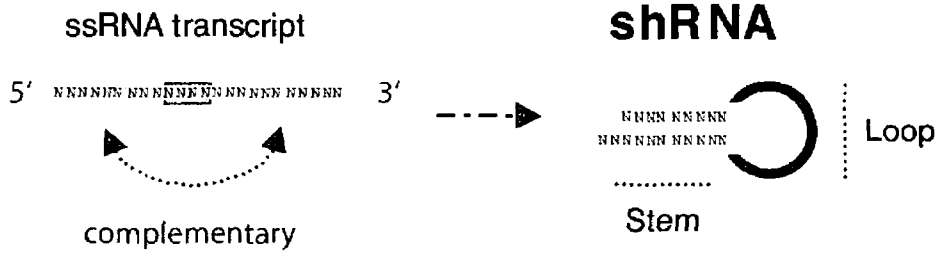


Figure 5.1: Short hairpin RNA (shRNA). shRNA is initially expressed as single stranded RNA (ssRNA) in which complimentary segments anneal and a stem-loop formation arises. (Modified from [235])

Conventional shRNAs are expressed in this manner using a U6 promoter (and RNA polymerase III) and are transported via exp5 from the nucleus to the cytoplasm [237] where they are processed by dicer into a functional siRNA. However shRNA can also be designed to resemble pri-miRNA (using RNA polymerase II (pol II) or pol III promoters) and once in the cytoplasm enter the miRNA pathway. miRNA-like shRNA is transcribed by RNA polymerases (pol II) and

processed to pre-shRNA in the nucleus by a complex containing the RNase III enzyme Drosha into shRNAs with 2 nt 3' overhangs [238]. Pre-shRNA is transported by the nuclear export factor exp5 to the cytoplasm where it is processed by another RNase III complex containing Dicer [238, 239]. The RNase III enzyme dicer binds to the 2nt 3' overhang and cleaves the terminal loop leaving a 2nt 3' overhang resulting in a double-stranded siRNA with 2nt 3' overhangs [239]. This siRNA product is then incorporated into RISC with Ago2 [238, 239] and can mediate sequence specific mRNA degradation as described in Chapter 1 (Figure 5.2).

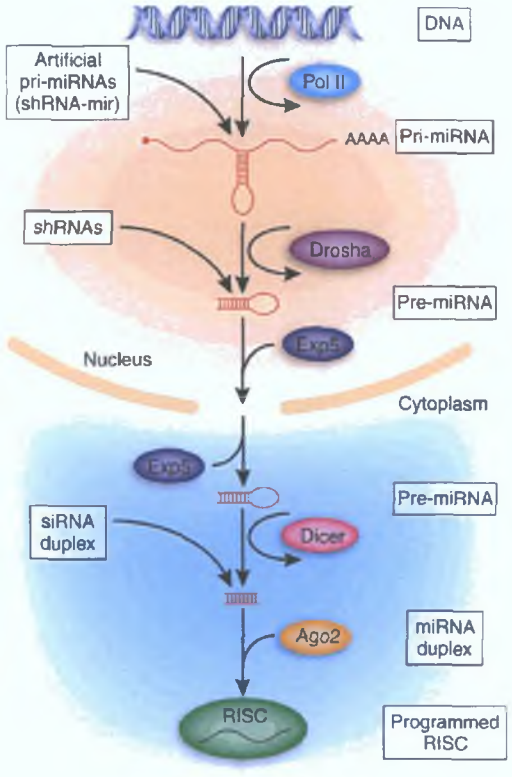


Figure 5.2: RNA interference mediated by shRNA or siRNA [239]. shRNA is transcribed in the nucleus as an artificial pri-miRNA and processed by Drosha or as a shRNA structure. shRNA is exported to the nucleus by exportin 5 (Exp5) and processed by Dicer into a RNA duplex capable of mediated RNA interference. Synthetic siRNA is introduced into the cell cytoplasm where it enters the RISC complex mediating gene silencing.

### 5.1.2 Advantages and Problems of shRNA in RNA Interference

shRNA boasts many advantages over siRNA particularly in terms of long term gene suppression. As part of a plasmid or viral vector shRNA will be expressed by a cell once its vector has successfully inserted into the host cell genome and can be expressed for long periods of time. This is advantageous in the establishment of stable cell lines and for long term suppression of disease related genes. Also shRNA tends to be more potent than siRNA for mediating gene silencing [240, 241] and less susceptible to enzymatic degradation. Furthermore it is possible to deliver multiple shRNA sequences using for example polycistronic expression vectors [58, 242] or long hairpin RNAs (lhRNA) [243]. This is beneficial especially in the treatment of viral infections with high mutation rates such as human immunodeficiency virus (HIV) [243]. Also these shRNAs can target multiple regions of the same gene thereby

decreasing overall shRNA dose requirements while maintaining gene suppression. Expression of several shRNA sequences by multiple promotors or vectors could lead to varied levels of expression of each shRNA which can be eliminated using polycistronic expression vectors. shRNA although long (>50bp) do not induce an interferon response.

shRNA expression vectors are also suitable for viral transfection which are very efficient delivery systems but as previously discussed can have immunogenic problems and vectors must be carefully designed to avoid the production of viral particles capable of replication. The necessity of genome insertion for shRNA production means that shRNA vectors must be delivered to the nucleus unlike siRNA which must only reach the cytoplasm to mediate RNAi. It has been estimated that as little as one in 1000 – 5000 cytosolic DNA plasmids penetrates the nuclear envelope and is transcribed [236, 244]. Additionally plasmids are much larger than siRNA (approximately 20bp siRNA compared to >2000bp DNA plasmid). This large size may hamper nucleocytoplasmic transport [244].

Unfortunately shRNA transfection is associated with similar side effects as that of siRNA (described in chapter 1) such as off-target effects and immune responses. In the case of shRNA these unwanted effects could be further amplified due to the extended expression of shRNA compared to siRNA. Pol III expressed shRNAs have been found to induce an interferon response [245]. However comparison studies of siRNA and a pol III expressed shRNA *in vitro* have found endogenously processed shRNA not to initiate an interferon response [246].

Moreover a major problem of shRNA vectors is over expression and consequently the possibility of over saturating intracellular miRNA machinery such as exp5, Dicer and RISC [245]. Several studies have found toxicity and morbidity due to this over expression [58]. Grimm *et al.* (2006) constructed a range of shRNA expressing vectors based on duplex-DNA-containing adeno-associated virus type 8 (AAV8) targeting luciferase, α1AT and four other genes in mice. Although targeted luciferase and α1AT gene suppression was maintained for over one month and one year respectively toxicity and morbidity were associated with a majority of the 49 vectors assessed [247]. Toxicity was not accompanied by interferon response but was with high shRNA doses. Moreover competition studies with various shRNA vectors and over expression of exp5 showed an over saturation of miRNA machinery were linked to fatality in shRNA delivery [247]. shRNA as a therapy could be more suitable for retroviral transfections when the expression level will remain low and PLGA microparticles where shRNA release can be controlled. Over expression can also be overcome by designing shRNA that utilize RNA polymerase III (pol III) or pol II promoters and therefore will be processed similar to miRNA. Conventional shRNA use U6 or H1 promoters which express large quantities of shRNA whereas pol II promoters will express shRNA at a similar level to the endogenous miRNA [58]. Depending on the level of expression required shRNA vectors and their delivery systems need to be adjusted. It is also possible to design conditional expressing vectors [247].

### 5.1.3 shRNA Delivery

A wide range of delivery vectors both viral and non-viral based have been investigated for DNA and shRNA delivery (Figure 5.3). The need for vector systems has been driven by molecular biology and more recently drug delivery. These vectors must efficiently deliver their load, allowing lysosomal/endosomal escape of the nucleic acid as well as achieve delivery for their cargo to the nucleus. A major advantage of shRNA and DNA plasmid based therapeutics is their suitability for viral mediated delivery. Viral based vectors are very efficient delivery vehicles. However the down side is the associated oncogenicity and safety concerns. Consequently interest in non-viral delivery systems including the use of neutral or cationic polymer and lipid based nanoparticles as well as proteins and peptides has grown. Proteins used in gene delivery are usually viral proteins which can bind DNA and mediate nuclear transport while peptides include histone and protamine derivatives [236]. Additionally bacteria can be used for shRNA vector delivery as shown in Figure 5.3. Transkingdom RNAi (tkRNA) involves the use of bacteria that have been altered to produce shRNA to infect cells and consequently lead to specific gene suppression. Alternatively, bacteria can be used simply to deliver shRNA expressing plasmids, a process known as bacteria mediated RNAi (bm-RNAi) [248].

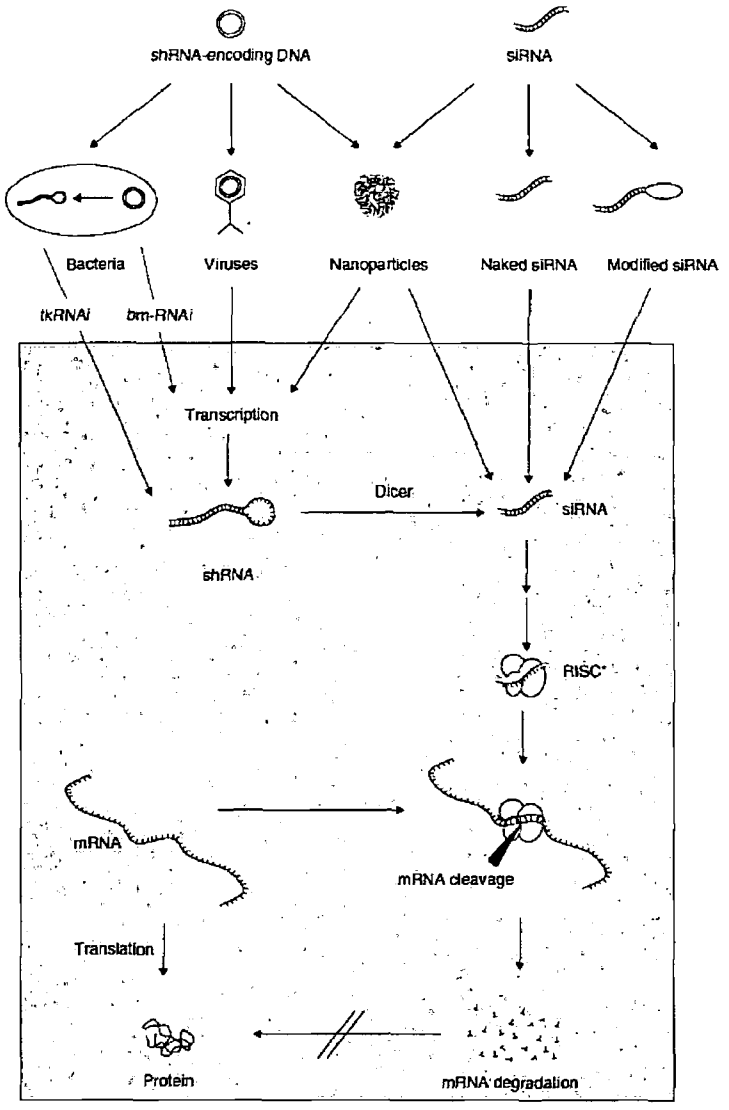


Figure 5.3: Schematic representation of delivery strategies for shRNA and siRNA mediated RNA interference [248]. shRNA is expressed by specially designed vectors which can be delivered to cells via bacteria, viruses or synthetic particles. Once transcribed in the cytoplasm shRNA is processed by Dicer into siRNA. Synthetic siRNA duplexes can also be delivered directly to cells. Naked siRNA is often delivered *in vivo* but for enhanced delivery and protection from degradation siRNA can be encapsulated in micro- or nanoparticles or undergo chemical modification. siRNA will then complex with RISC and direct sequence specific mRNA degradation.

#### 5.1.3.1 Viral Vectors

The major advantage of viral vectors in gene delivery is their efficiency but this is for the most part outweighed by safety risks. Although the viral vectors used are modified to be replication-deficient (Figure 5.4) there are still some concerns associated with their use in patients [1] particularly oncogencity and immune activation. Also the need to produce large quantities of these vectors and their limitations in transgene loading capacity could be problematic. Adenoviruses (for example serotype 5 adenovirus (Ad5)), AAV, retroviruses (such as Moloney murine leuckemia virus (MoMLV) and lentiviruses) and Herpes Simplex virus are among the viral vectors being used in therapies today [1, 249].

Adenoviruses (*Adenoviridae Mastadenovirus*) possess many advantageous attributes including the ability to transduce dividing and non-dividing cells [1, 250], produce high-titers of recombinant viruses and to package large transgenes [250]. Ad5 vectors do not integrate into host chromosomes avoiding potential oncogenecity. However, Ad5 vectors strongly activate a host immune response as was evidenced by the death of a clinical trial patient Jesse Gelsinger in 1999 due to an immune reaction following the administration of a modified Ad5 vector delivering the ornithine decarboxylase gene [1]. Other disadvantages of adenoviral vectors include long production time, pre-existing immunity and off-target cell transduction [250]. Despite this adenoviruses are the most commonly used shRNA viral vectors for *in vitro* use and are available commercially [251].

AAV (*Parvoviridae Dependovirus*) are non-pathogenic and not associated with any human disease. Furthermore long-term gene expression in a wide range of cells types has been seen *in vivo* by AAV transduction. AAV delivery of shRNA to specific cells or tissues is possible [251]. Similarly to adenoviruses AAV vectors can transduce off-target cells and pre-existing immunity can exist. These vectors also have a limited transgene capacity and only permit DNA-based material to be loaded [63] however up to 8 individual shRNA cassettes can be loaded [251]. Repeated administration of the same serotype of AAV in mice has shown gene expression to be decreased [252].

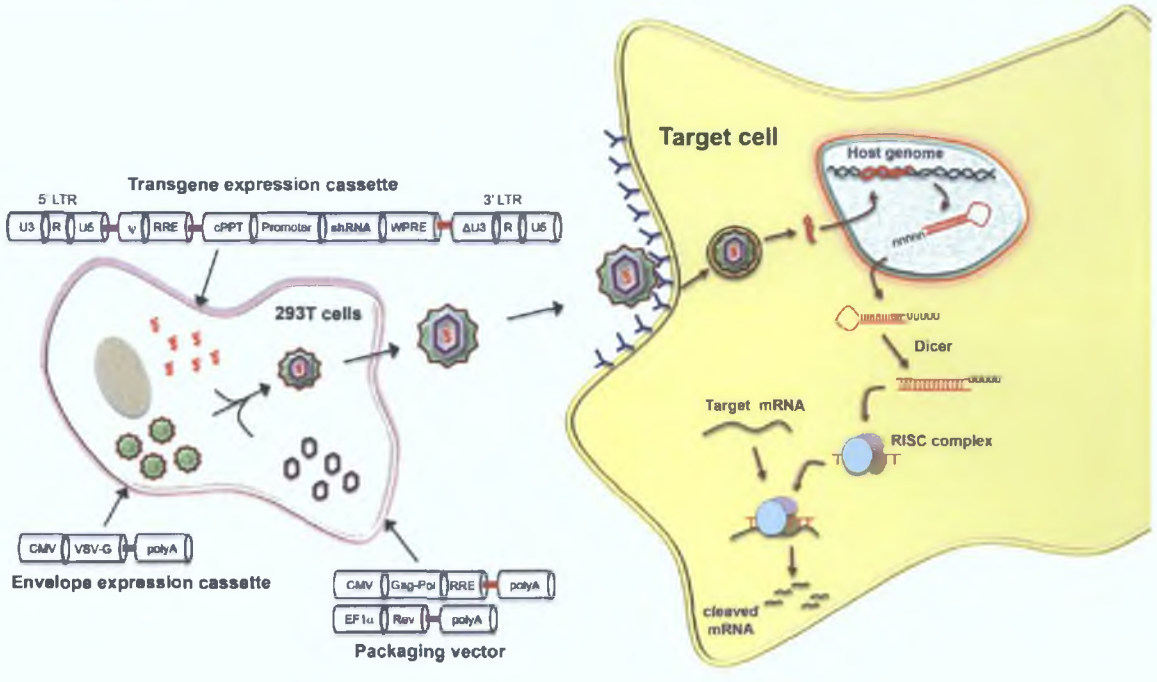


Figure 5.4: Diagrammatic representation of non-replicating lentiviral vector transduction [58]. The viral particles are constructed in a host cell line (such as human 293T cells). The host cells are transfected with various viral elements expressed on different plasmids including envelope expression cassette, packaging vector and transgene expression cassette (expressing shRNA). Target cells are infected with the lentivirus and the transgene integrated into the host genome. shRNA is expressed and enters the siRNA pathway. Only the transgene cassette is inserted into the host genome allowing shRNA expression but not replication of an infectious virus.

Retroviruses such as MLV target dividing cells and can integrate into the chromosome of these cells resulting in stable and extended transfections [250]. Unfortunately this means limitations in target cell types and possible mutagenic events. Retroviruses were among the first used viral vectors for shRNA cassette delivery [251]. Lentiviruses, unlike retroviruses such as MoMLV, can enter the nucleus of dividing, non-dividing and differentiated cells [58, 250] and generally integrate distally from promoters in introns which could reduce the possibility of oncogenicity [253]. Typically HIV-1 based vectors are used as HIV-1 replication is the most comprehensively characterised. Further safety precautions are taken when using HIV-1 including the removal of cis elements (essential for viral replication) from the packaging vector, deletion of accessory genes, dividing packaging genes into different plasmids and avoiding homology between the various plasmids [58]. These viruses are also very suitable for shRNA transfections (Figure 5.4) however the side effects associated with siRNA such as immune activation and off-target effects are enhanced with the long-term expression of shRNA. Recent advances in this area stem from the development of specially engineered viral vectors that can avoid immune stimulation while retaining high efficiency as well as the development of viral-like particles [63, 254] and bacteriophage vectors [63].

#### 5.1.3.2 Non-Viral Polymer Based Delivery

Non-viral vectors have the added benefits of storage stability, scale up and enhanced quality control [255]. DNA delivery has been extensively explored while only in recent years is non-viral technology being applied to shRNA expressing vector delivery. shRNA expressing plasmids can be encapsulated in a wide variety of polymer based particles such as PEI [256-258], chitosan [259], PLL and PLGA for improved transfection efficiency. However compared to viral vectors these delivery systems tend to show low transfection and poor tissue penetration [236].

Each polymer type shows promise as well as associated problems for successful shRNA plasmid delivery. For instance, PEI has been used to prepare transferrin (Tf) coated nanoparticles for shRNA plasmid delivery for cancer therapies [257, 258]. Tf-PEI complexed with hypoxia-inducible factor-1α (HIF-1α) expressing shRNA-vectors in mice delivering shRNA to target cells and reducing tumor growth [258] nevertheless PEI is not biodegradable and can cause necrotic and apoptotic toxicity [236]. On the other hand chitosan is biodegradable, biocompatible and of low immunogenicity and toxicity. Chitosan has also recently acted as a carrier for a cancer targeting shRNA expression vector in rhabomycosarcoma cells [259].

PLGA as discussed in chapter 4 is biocompatible and biodegradable polymer with low toxicity and immunogenicity. PLGA has also received approval for clinical use by the US FDA [260] though not for inhalation and biodegradable particles encapsulating DNA have entered clinical trials [261]. It has been extensively investigated for DNA delivery but only recently have shRNA expressing plasmids been incorporated into PLGA nanoparticles [249, 262]. Along with the biocompatibility advantages, PLGA particles also potentially protect DNA from degradation,

allow sustained release and possible control over dosing. PLGA particle uptake is size dependent with larger microparticles phagocytosed by for example macrophages or target APCs (a feature advantageous for DNA vaccine delivery) [255] and smaller nanoparticles taken up via endocytosis. Particles cause swelling and rupture of endosomes and/or lysosomal compartments leading to their release into the cytoplasm. Cohen *et al.* (2000) monitored uptake of a fluorescently tagged pDNA and found PLGA nanoparticle encapsulated pDNA in the cytoplasm while released pDNA localised in the cytoplasm and around and in the nucleus [263] confirming the capability of nuclear delivery via these polymeric platforms.

### 5.1.4 shRNA Gene Targets

#### 5.1.4.1 Interferon Regulatory Protein 3 (IRF3)

Interferon regulatory protein 3 (IRF3) is a transcription factor central in Type I IFN transcriptional regulation which is key in the response to bacterial and viral infection. IRF3 is expressed constitutively in all cells and in its inactivated form is present in the cell cytoplasm [264]. Activation of IRF3 can occur through various pathways. Briefly, following immune stimulation for example via TLRs (Figure 5.5) IRF3 is phosphorylated, dimerizes and translocates to the nucleus where it binds to its consensus sequence in target genes (such as the type I IFNs) and drives gene expression [264].

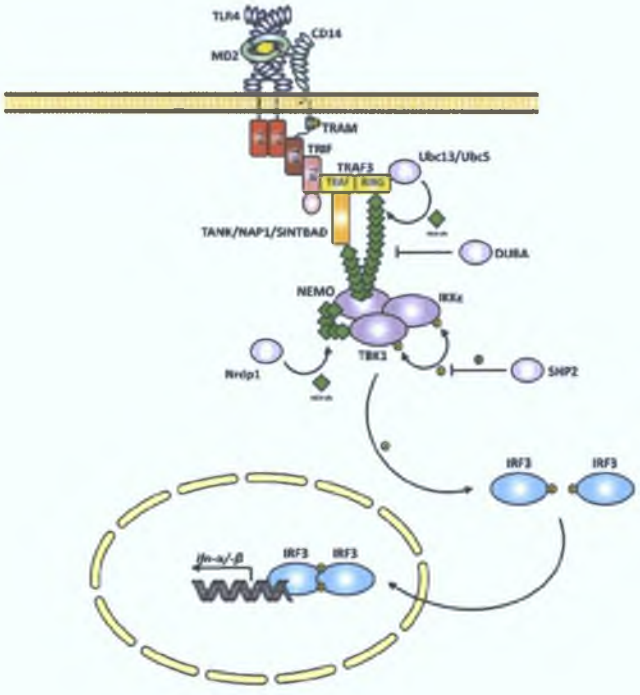


Figure 5.5: Interferon regulatory protein-3 (IRF3) activation via toll like receptor (TLR) activation [265].

IL-23 is a cytokine consisting of p19 and p40 subunits. It plays an important role in inflammation and auto-immunity and is highly expressed by macrophages. For this reason IL-23 represents an important target in therapeutic development. Clinical trials are investigating

monoclonal antibodies against IL23 for psoriasis, psoriatic arthritis and Crohn's disease [266]. From studies carried out by Dr. Jefferies' group, it is possible that IRF3 is involved in IL-23p19 production. In order to decipher if the role played by IRF3 is central to IL-23p19 induction it will be knocked down and IL-23p19 secretion determined in monocytes stimulated with Poly I:C a TLR3 agonist.

#### 5.1.4.2 Tripartite motif-containing 68 (TRIM68 or SS-56)

Tripartite motif-containing 68 (TRIM68 or SS-56) is an ubiquitin E3 ligase similar in structure to TRIM21 (Ro52) and a member of the superfamily of TRIM proteins [267]. It has been shown that TRIM68 is an auto-antigen in Systemic Lupus Erythematosus (SLE) and Sjögren's syndrome [268, 269] as well as playing a role in prostate cancer [270] however little is known of TRIM68 function. Unpublished data from Dr. Jefferies' group have shown that TRIM68 activity is regulated by tyrosine phosphorylation and negatively regulates IFNβ production a role that is blocked by TRIM68 tyrosine residue mutations. Additionally TRIM68 is highly expressed by natural killer (NK) cells. Association between NK cells and SLE has been reported with SLE patients having a lower proportion of NKT cells [271] and NK cells producing high levels of IFNγ [272].

As NK cells are altered in SLE and could be involved in SLE pathogenesis through IFN production TRIM68 may play a key role in this disease. The involvement of TRIM68 in NK cell TLR-responses and NK cell activity need to be elucidated. Consequently the knock down of TRIM68 in NK cells would allow the activation, cytokine release and activity of NK cells to be assessed in the absence of TRIM68.

### 5.1.5 Chapter Aims

- To harness microparticle technology developed in chapter 4 for shRNA delivery to macrophages
- To optimise microparticle development and transfection with microparticles loaded green fluorescent protein (GFP) expressing plasmids
- To compare PLGA microparticle systems for macrophage transfection with commercial non-viral and lentiviral based transfections
- To assess targeted gene transfections using shRNA loaded microparticles

**5.2 Materials**

10kb DNA ladder
10x Ultrapure TBE buffer, Invitrogen
30 % Acrylamide/Bisacrylamide (37.5:1) solution, Bio-Rad
Afl II restriction enzyme, New England Biolabs
Agarose, Sigma Aldrich
α-Lactose, Sigma Aldrich
Ammonium persulphate (AP), Sigma Aldrich
Ampicillin, Sigma Aldrich
Anti- α-actinin, Santa Cruz
Anti-IRF3 (polyclonal goat), Santa Cruz
Anti-TRIM68, Sigma Aldrich
Aprotinin, Sigma Aldrich
BCA Protein Assay, Pierce
Black 96 well plates, Fisher scientific
Blue/orange 6x loading dye, Promega
BSA, New England Biolabs
Cellstar flat-bottomed 96 well plates, Grenier
Chloroform, Fisher scientific
Competent DH5α cells, Invitrogen
DEPC-treated RNase DNase free water, Fisher
Dicholoromethane (DCM), Reagent grade, Fisher Scientific or Sigma Aldrich
Dithiothreitol (DTT), Sigma Aldrich
DMEM, BioSera
EDTA, Amresco
EndoFree Plasmid Maxi Kit, Qiagen
Ethidium bromide, Sigma Aldrich
Foetal Bovine Serum, BioSera
Freeze Drier FreeZone 4.5, Labconco
Fuji SuperRX film, FujiFilm Ireland Ltd.
G:BOX, Syngene
Glycerol 99.99%, Sigma Aldrich
Hoescht, Sigma Aldrich
Ika homogenizer, IKA
Immobilon Western HRP Substrate, Millipore
INCELL1000 Cell Analyser, GE Healthcare
Iodoacetamide, Sigma Aldrich
Kanamycin, Sigma Aldrich
LB broth, Sigma Aldrich
LB-Agar, Sigma Aldrich
Leupeptin, Sigma Aldrich

Malvern Mastersizer 2000, Malvern Instruments

Metafectene pro, Biontex

Metafectene, Biontex

Methanol, Sigma Aldrich

Mission® Interferon Regulatory Factor 3 (IRF3) shRNA Plasmid DNA, Sigma Aldrich

Mission® Non-Target Control Vector shRNA, Sigma Aldrich

Mission® Tripartite Motif-containing 68 (TRIM68) shRNA Plasmid DNA, Sigma Aldrich

MoFlo High Performance Cell Sorter, Dako

N,N,N',N'-Tetramethylethylenediamine (TEMED), Sigma Aldrich

Nanodrop1000, Thermo Scientific

Nanoseries Zetasizer, Malvern

NE Buffer 4, New England Biolabs

Nucleobond® Endotoxin Free Maxi Prep Kit, Machery-Nagel

Paraformaldehyde, Sigma Aldrich

pCDF1-MCS2-EF1-copGFP, System Biosciences, SBI

pGIPz GFP

Phalloidin-FITC, Sigma Aldrich

Phenylmethanesulfonyl fluoride (PMSF), Sigma Aldrich

Phosphate Buffered Saline (PBS), BioSera and GIBCO (Invitrogen))

PLGA, Resomer RG503, 50:50, poly( lactide-co-glycolide), Boehringer Ingelheim

pmaxGFP, AMAXA

Polybrene, Millipore

polyethylene glycol (PEG) MW8000, Sigma Aldrich

Polyvinyl Alcohol (PVA), Mw 31,000 – 50,000, 87-89% hydrolyzed, Sigma Aldrich

Ponceau S Solution, Sigma Aldrich

Potassium Chloride (KCl) , Sigma Aldrich

Potassium phosphate (KH2PO4), Sigma Aldrich

Precast 1% Agarose Gel, Sigma Aldrich

Precision Plus Protein™ Dual Color Standard, Bio-Rad

Probe sonicator, Branson

Propan-2-ol (isopropanol), VWR International Ltd.

Quant-iT PicoGreen Assay, Invitrogen

Rotina 35 R centrifuge, Hettich

RPMI-1640 w/stable L-Glutamine, BioSera

Sodium Azide, Sigma Aldrich

Sodium Chloride, Sigma Aldrich

Sodium dodecylsulphate (SDS), Sigma Aldrich

Sodium Orthovanidate, Sigma Aldrich

Sodium phosphate dibasic (Na2PHO4) , Sigma Aldrich

Tescan Mira XMU Variable Pressure Field Emission Scanning Electron Microscope (VPFESEM), Tescan USA Inc. USA.

Tris-acetate-EDTA (TAE), Sigma Aldrich

Triton X-100, Sigma Aldrich

Trizma Base, Sigma Aldrich

Tween® 20, Sigma Aldrich

Victor Wallac Multiplate Reader, Wallac

## 5.3 Methods

### 5.3.1 DNA and shRNA Plasmids

pmaxGFP is a 3486bp plasmid expressing copGFP (Evrogen) inserted into a pMCV1.4 backbone (Mologen) (Figure 5.6A). copGFP gene is derived from copepod plankton (Panalina sp.). This plasmid contains 35 unique restriction sites and kanamycin resistance. pCDF1-MCS2-EF1-copGFP and pGIPz-GFP are lentiviral vectors expressing GFP with ampicillin (Amp) resistance and 6,771bp and >11,688bp in size, respectively (Figure 5.6B and C). pCMV-VSV-G (6363bp) and pCMV-HIV1 lentiviral vectors are envelope and packaging plasmids respectively.

Mission® shRNA plasmid DNA express shRNA targeted to human IRF3 and TRIM68 (or SS-56) genes inserted into a pLKO.1 vector backbone (Figure 5.7B). IRF3 is involved in interferon-α/β (IFNα/β) gene expression regulation. TRIM68 is an E3 ubiquitin ligase [270] as well as an auto-antigen for SS and SLE [269]. Mission® non-target control vector was used as a negative control or "scrambled" sequence (Figure 5.7A). shRNA plasmids are both Amp and puromycin resistant for bacterial and mammalian selection respectively.

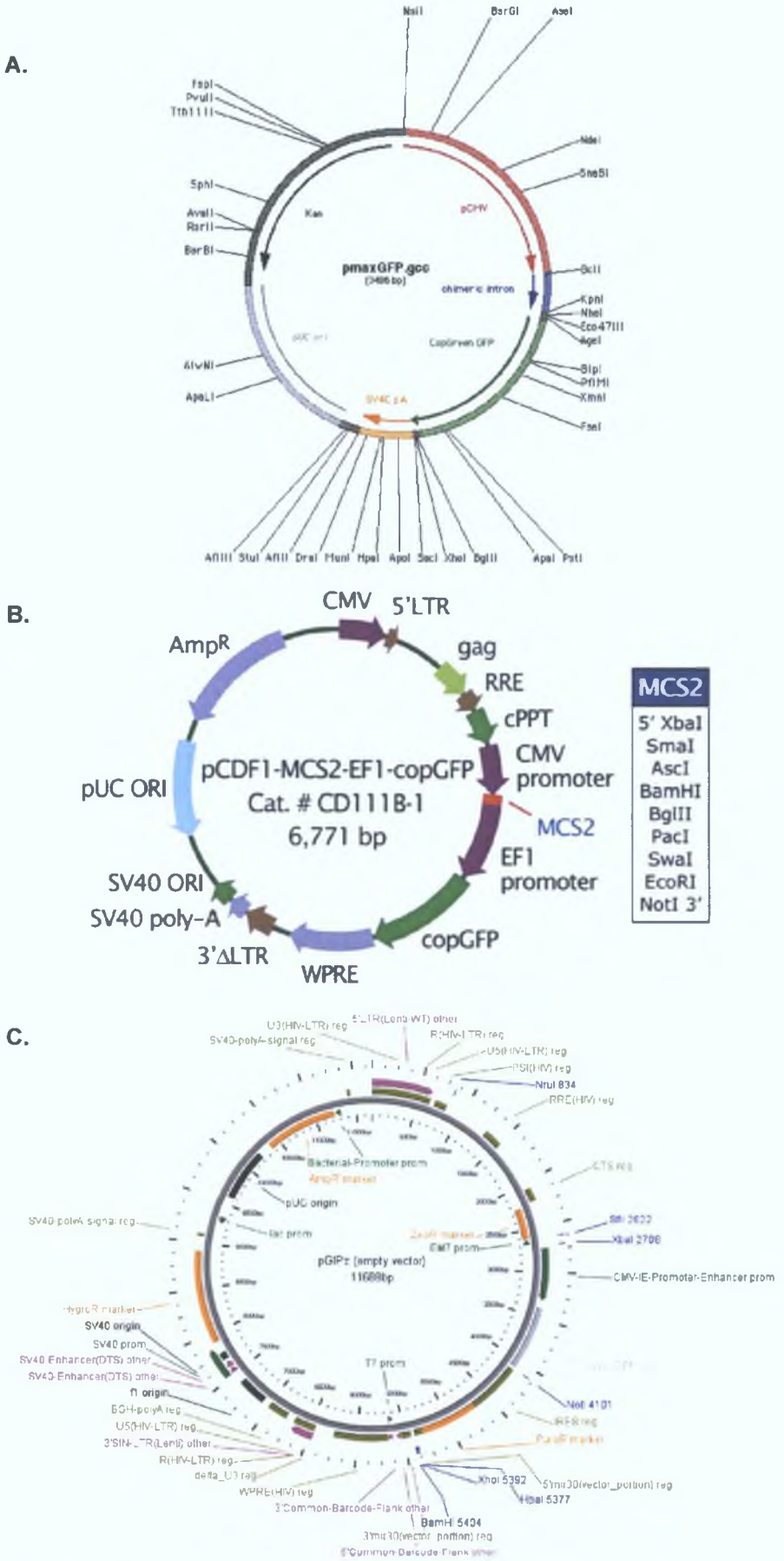


Figure 5.6: GFP vector maps of (A) pmaxGFP, (B) pcdf1-mcs2-ef1-copGFP and (C) pGIPz (empty vector) plasmids.

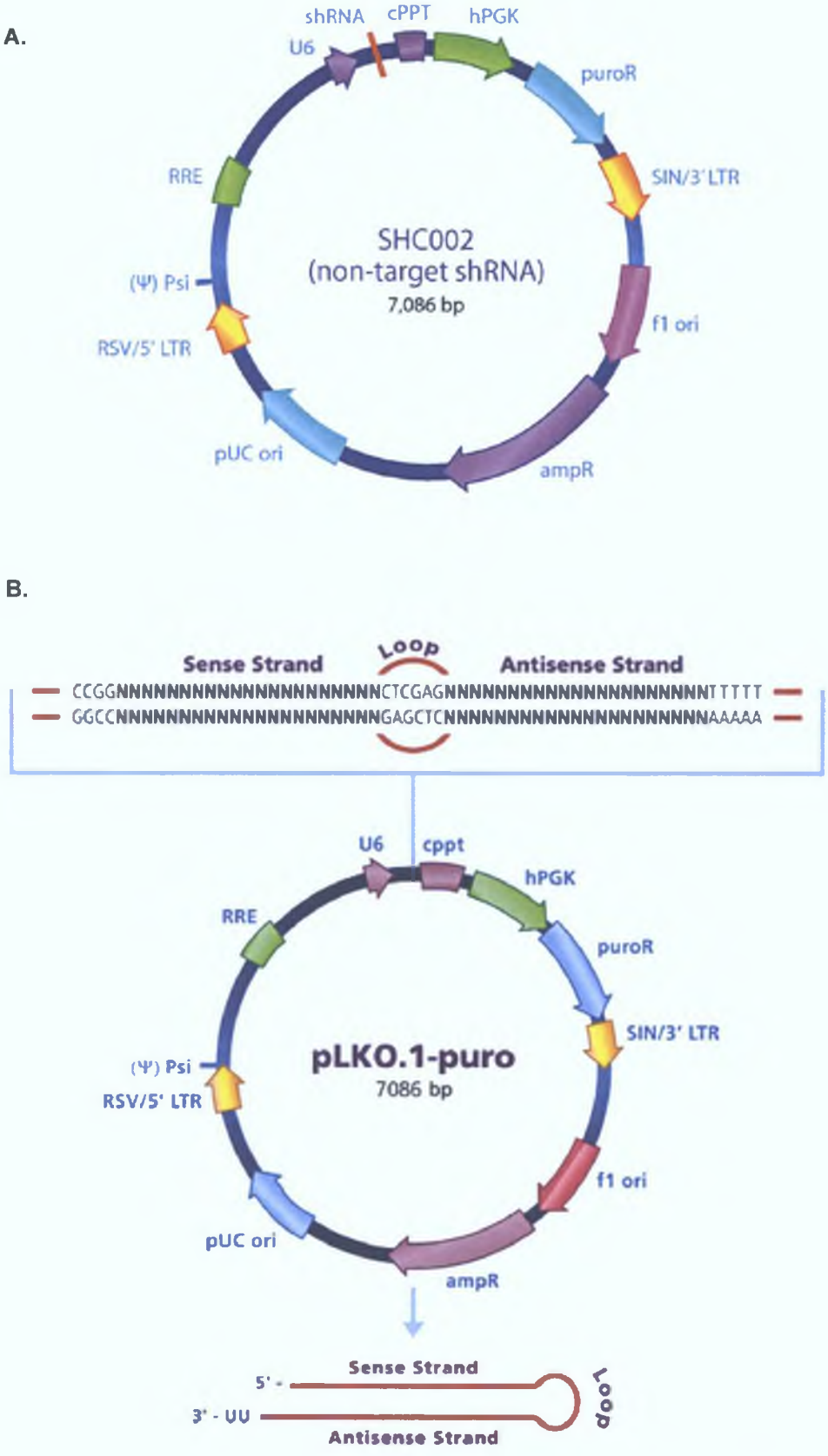


Figure 5.7: Mission® shRNA plasmid DNA. (A) Non-target shRNA vector and (B) pLKO.1 vector backbone and shRNA gene insert and expression. (Sigma Aldrich)

#### 5.3.1.1 Plasmid Transformations

Plasmid vectors were transformed in competent DH5α cells. Briefly, 200µl of DH5α cells were added to 1µl of plasmid stock and incubated on ice for 20 – 30 minutes. Controls contained no plasmid. The cells were heat shocked for 2 minutes at 43°C followed by cooling on ice for 1 – 2 minutes. The cells were then transferred to 1ml of lysogeny broth (LB) at room temperature (RT) and shaken for 1 hour at 37°C. Kanamycin (pmaxGFP) and Amp agar plates were prepared with 35g/L of autoclaved LB-agar supplemented with 100µg/ml of antibiotic. 50µl of cells were plated onto pre-warmed plates and incubated at 37°C for 15 - 16 hours. Plates were then stored at 4°C.

#### 5.3.1.2 Plasmid Maxi Preps

Single colonies were selected and grown in sterile LB broth (25mg/ml) containing antibiotic (1µg/ml) overnight shaken at 250 rpm at 37°C. Plasmids were isolated using maxi prep kits according to the manufacturer's protocols. Concentration and DNA integrity was assessed by spectroscopy (NanoDrop) and gel electrophoresis. For gel electrophoresis pmaxGFP plasmid was linearised by digestion with Afl II restriction enzyme. The reaction mixture (50µl) contained BSA (5µl), NE Buffer 4 (5µl), pmaxGFP plasmid (0.5µg), TE buffer (32.02µl) and Afl II (0.5 units). The control did not contain the restriction enzyme. Reaction mixtures were heated for 1 hour at 37°C and 20 minutes at 65°C. DNA was analysed by gel electrophoresis (1% agarose gel stained with ethidium bromide) tris-acetate-EDTA (TAE) for 40 minutes at 110V. Visualization was obtained by UV transillumination (Appendix).

### 5.3.2 Cell Culture

THP-1 cells were cultured and differentiated as described in 3.3.2. Human monocytes were isolated and maintained as described in 3.3.2.2 and 4.3.2.1. HEK-293T cells are a human embryonic kidney cell line and were maintained in dulbecco's modified eagle medium (DMEM) supplemented with 10% FBS, 0.1% Amphotericin B and 0.1% gentamicin. Natural killer (NK92MI) cells derived from peripheral blood mononuclear cells of a 50 year old Caucasian male with rapidly progressive non-Hodgkins lymphoma were maintained in suspension in RPMI media supplemented with 10% FBS in a humidified atmosphere at 37°C and 5% $CO_2$.

### 5.3.3 Preparation of pDNA and shRNA-loaded PLGA Microparticles

Microparticles containing pDNA or shRNA were prepared using a double emulsion (w1/o/w2) solvent evaporation method (Figure 5.8). pDNA was either encapsulated alone or complexed with DOTAP using the method described in 4.3.3 with an N/P ratio of 4 and 40µg of pDNA. 50mg of PLGA 503 was dissolved in 1.75ml DCM (2.9% w/v) in a glass test tube and vortexed. A mixture of 30µl of pDNA-DOTAP complexes rehydrated in RNase free water or pDNA or shRNA with a nucleic acid concentration of at least 1mg/ml and 32µl of $dH_2O$ containing 300mM

lactose and 1mM EDTA was added to the PLGA solution and the mixture was manually probe sonicated with four pulses at an output level of 4 to form the primary w/o emulsion. The primary emulsion was added dropwise to a 5% (w/v) PVA solution containing 300mM lactose and 0.2M NaCl (12.5ml) homogenizing over an ice-bath at 13500 rpm (or level 3) to form a secondary or multiple w/o/w emulsion. This emulsion was added to 25ml 1% (w/v) PVA containing 300mM lactose and 0.2M NaCl and gently stirred for at least 4 hours at room temperature to allow DCM evaporation. Microparticles were recovered by centrifugation at 5,000rpm for 15 min at 4 °C, washed three times with water to remove residual PVA, resuspended in 1.5ml d $dH_2O$ and lyophilized for 18 hours.

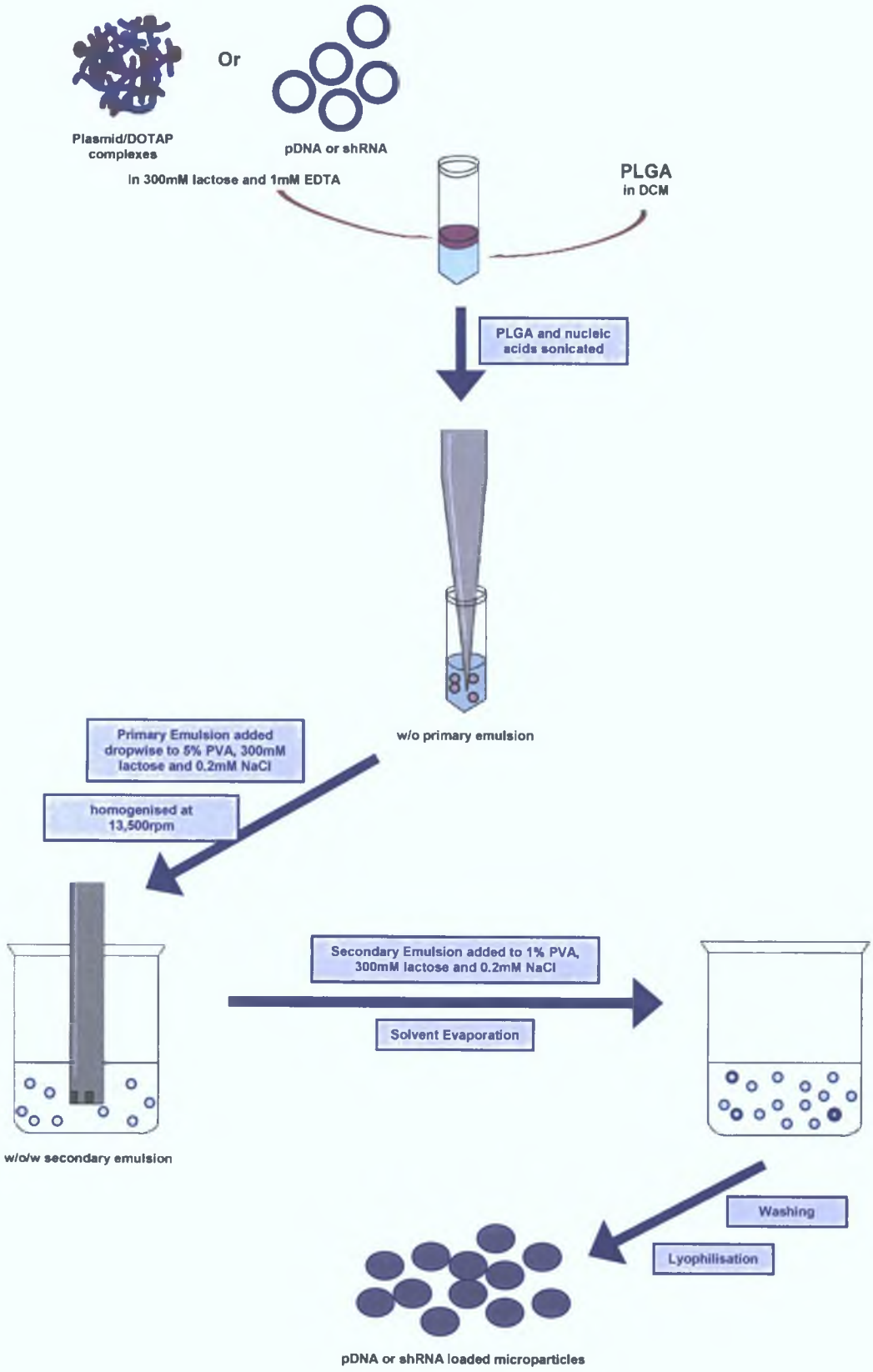


Figure 5.8. Schematic of pDNA or shRNA microparticle preparation by double emulsion solvent evaporation method.

### 5.3.4 Microparticle Characterisation

#### 5.3.4.1 Particle Size

Microparticle size was determined as described in 4.3.4.1.

#### 5.3.4.2 Zeta Potential of microparticles

Zeta potentials of microparticles were measured as described in 4.3.4.2.

#### 5.3.4.3 Surface morphology by scanning electron microscopy (SEM)

Microparticle size and surface morphology was assessed by SEM as described in 4.3.4.3.

#### 5.3.4.4 Encapsulation Efficiency

Lyophilised pDNA or shRNA-loaded microparticles (1mg) were dissolved in 50µl of chloroform. To this 50µl of nuclease free water was added and the mixture was vortexed for 15 minutes followed by centrifugation at 10000 rpm for 5 minutes. The upper aqueous layer was collected and the centrifugation step was repeated after the addition of another 50µl of TE buffer. Collected aqueous layers were pooled and the nucleic acid concentrations determined. pDNA and shRNA concentration was determined using a Quant-iT PicoGreen assay. This assay uses a fluorescent nucleic acid stain for double-stranded DNA (dsDNA) that allows detection of dsDNA at concentrations as low as 25pg/ml.

A standard curve was prepared using stock pDNA or shRNA diluted with TE buffer (200mM Tris-HCl, 20mM EDTA, pH 7.5) to give 0, 1, 10, 100 and 1000ng/ml final concentration. 100µl of diluted pDNA or shRNA was added in triplicate to wells of a black 96 well plate. 5µl of extracted nucleic acid was added in triplicate to wells. The volume per well was brought up to 100µl. PicoGreen reagent was diluted 1 in 200 and 100µl was added per well. Fluorescence was detected at 485nm excitation and 535nm emission wavelengths using a Wallac multiplate reader. To correct for background fluorescence, readings of blank wells was subtracted from samples.

#### 5.3.4.5 Integrity of Encapsulated Nucleic Acids

shRNA integrity was assessed by gel electrophoresis using a pre-cast 1% TBE-agarose gel with 0.5µg/ml ethidium bromide. Blue/orange 6x loading dye (Promega) was used to track gel migration. shRNAs were extracted from microparticle preparations by aqueous and solvent phase separation as described in 5.3.4.4 50ng of stock and extracted shRNA were loaded per well and the gels were run in 1x TBE buffer at 100V for 1 hour. Visualization was obtained by UV transillumination (G:BOX, Syngene).

### 5.3.5 Lipid Based DNA Transfection

#### 5.3.5.1 Metafectene Transfection

THP-1 cells were seeded in 6 well plates and incubated overnight. 2µg of pmaxGFP was added to serum free RPMI brought to a final volume of 700µl. 8µl of metafectene or metafectene pro was added to 692µl of serum free media and incubated at room temperature for 5 minutes. The diluted metafectene was added and gently mixed with the diluted DNA and incubated at RT for 20 minutes. The mixture was added dropwise to the media covering the cells. The cells were incubated at 37°C for 24 hours and transfection was accessed by fluorescent microscopy and flow cytometry. Transfected cells were selected by fluorescence associated cell sorting (FACS).

#### 5.3.5.2 Flow Cytometry and Fluorescence Associated Cell Sorting

THP-1 cells transfected with pmaxGFP/metafectene and pmaxGFP/Metafectene Pro were pooled. Wash buffer (2ml) was added to pmaxGFP (1ml) and untransfected (500µl) THP-1 cells and centrifuged at 1500 rpm for 5 minutes. The supernatant was discarded. Cells were resuspended in 300µl of wash buffer and stored on ice. Flow cytometry determined transfection efficiency. Cells were maintained at 37°C for one week to increase cells numbers and sorted with a MoFlo High Performance Cell Sorter (Dako). Sorted cells were maintained at 37°C in 1ml of fresh media supplement with 20% FBS.

### 5.3.6 Lentiviral Transfection

HEK-293T cells were seeded at $2.5x10^6$/ml in 10cm culture dishes in a total of 10ml of DMEM supplemented with 10% FBS. After 24 hours the media was replaced with 9ml of fresh media and the cells were further incubated for 1 – 2 hours under tissue culture conditions.

10µg of transfer plasmid (pGIPz-GFP), 3 µg of envelope plasmid (pCMV-VSV-G) and 6.5 µg of packaging plasmid (pCMV-HIV1) were diluted in sterile water to a final volume of 295pl. 55 µl of 2M calcium chloride ($CaCl_2$) was added and mixed gently by pipetting. 350 µl of 2x HEPES (4-(2-hydroxyethyl)-1-piperazineethanesulfonic acid) Buffered Saline (HeBS, pH 7.5 (280mM NaCl, 10mM KCl, 1.5mM $Na_2HPO_4$, 12mM D+Glucose and 50mM HEPES)) was added dropwise whilst bubbling the mixture and incubated at room temperature for 30 minutes. The mixture was added to the media covering cells dropwise. Cells were incubated for 4 hours at 37°C. The media was removed and the cells were washed once with warm PBS. The cells were shocked with 3ml per plate of 15% glycerol in PBS (v/v) for 60 seconds at 37°C. The glycerol was removed and the cells were washed twice with warm PBS. Fresh media was added and cells were incubated at 37°C for 24 hours.

The cells were washed once with PBS and 10ml of 20% FBS DMEM was added. Transfection was confirmed by fluorescent microscopy. A few hours later the media was replaced with 6ml of

20% RPMI and incubated overnight at 37°C. THP-1 cells were seeded in 6 well plates at $2.5x10^5$ cells in 3ml and incubated overnight.

The media was harvested off the transfected HEK-293T cells and replaced with 6ml of fresh 20% FBS RPMI. A few hours later the second media was collected. Harvested media was centrifuged at 1500rpm for 5 minutes and filtered (0.45µm filter). Supernatants were transferred to sterile 50ml tubes and 1 volume of cold 1X PEG (MW8000, pH 7.2) solution was added. The solution was incubated at 4°C for at least 12 hours and then centrifuged at 1500xg for 30 minutes. The supernatant was removed and residual PEG solution was spun down at 1500xg for 5 minutes. All trace of liquid was removed by pipette. The lentiviral pellet was resuspended in 1/10 or 1/100 of the original volume using cold sterile PBS.

THP-1 cell media was replaced with fresh media supplemented with 10% FBS. Polybrene (5µg/ml) was added to each well. Concentrated lentiviral supernatant (0 – 200µl) was added dropwise to the wells, mixed and incubated at 35°C. After 24 hours the media was replaced with fresh media and the cells were incubated for 48 hours at 35°C.

### 5.3.7 Microparticle mediated pDNA Transfection

#### 5.3.7.1 Flow Cytometry

$2x10^5$ THP-1 cells were differentiated per well in 24 well plates. Microparticles were suspended in RPMI to give a final concentration of 1mg/ml. Differentiated THP-1 cells were untreated or treated with 100µg or 200µg empty microparticles, microparticles encapsulating pmaxGFP plasmid or pmaxGFP plasmid complexed with DOTAP at N/P ratio of 4 for 3 to 4 hours. Treatments were preformed in triplicate. Media was replaced by fresh media and cells were incubated for 24 hours. Cells were washed with warmed PBS and collected in 500µl of PBS and centrifuged at 8000rpm in a microcentrifuge for 2 minutes. Supernatants were discarded and cells were resuspended in 500µl of PBS and analysed using a flow cytometer. Cells were divided into two populations based on fluorescence intensity and GFP expression determined from 5000 cells per replicate.

#### 5.3.7.2 High Content Cell Analysis

THP-1 cells were differentiated at a density of $1x10^5$ cells/ml in 96 well plates. Microparticles were resuspended at 1mg/ml in RPMI. Cells treated with media alone, 20µl (20µg) empty microparticles or microparticles encapsulating pmaxGFP plasmid or pmaxGFP plasmid complexed with DOTAP (N/P ratio 4) for 3 hours. GFP expression was monitored by fluorescent microscopy. 72 hours following microparticle treatment cells were fixed with 4% paraformaldehyde for 20 minutes at room temperature. Cells were washed with PBS three times and nuclei were stained with hoescht for 5 minutes at room temperature. PBS washes were repeated and 150µl PBS was added to each well. Plates were stored at 4°C protected

from the light until analysed. Images were acquired by an INCELL 1000 cell analyser at 10x magnification in 5 fields per well. GFP was detected at 480nm excitation and 535nm emission wavelengths and nuclei were detected at 360nm excitation and 460nm emission wavelengths.

Multi target analysis module was used with nuclei, cells and a reference inputted as objects to be measured and assigned wavelengths for nuclei, cells and green fluoresence respectively. Parameters for segmentation analysis were then inputted. Nuclei were identified using Top Hat. A minimum area was inputted based on the images required and sensitivity generally set to 80%. Segmentation of cells was performed using the collar method. This sets up a ring-shaped region around the nucleus using an inputted average cell radius value assigning this region as the cell. The reference was detected in cells and cell intensity of the reference per cell above background fluorescence was used as the measure of GFP expression. Input values and sensitivity settings were adjusted for each experiment until all parameters were correctly assigned.

### 5.3.8 Microparticle mediated shRNA Transfection

#### 5.3.8.1 shRNA Transfection

The functionality of microparticle encapsulated IRF3 and TRIM68 shRNA was assessed in isolated human monocytes and NK92MI cells respectively. IRF3 shRNA transfections were carried out by Siobhán Smith and TRIM68 shRNA transfections were carried out by Claire Wynne. Microparticles were suspended in media at 1mg/ml and cells were either untreated or treated with empty microparticles or microparticles encapsulating scrambled, IRF3 or TRIM68 shRNA for 24, 48 and 72 hours. As a positive control NK92MI cells were transfected with TRIM68-FLAG. Protein expression was assessed by western blot analysis.

#### 5.3.8.2 Western Blot Analysis

At each endpoint plates were spun down at 1600rpm for 5 minutes and supernatants removed. 100µl of 1X sample loading buffer with protease inhibitors was added to the wells and cells were scraped and collected. Sample loading buffer contained 10% (v/v) glycerol, 2% (w/v) SDS, 0.1% (w/v) Bromophenol blue, 5% (v/v) Tris HCl (1M, pH 6.8) and 100mM DTT. The protease inhibitors phenylmethylsulfonyl fluoride (PMSF; 1mM), sodium orthovanadate ($Na_3VO_4$; 1mM) and potassium fluoride (KF; 1mM) were added to the sample loading buffer. Samples were then boiled for 5 minutes at 95°C followed by sonication for 15 seconds and centrifugation at 13,000rpm for 5 minutes.

Ladders and samples (40µg) were loaded onto a stacking gel and electrophoresed on 8% or 12% polyacrylamide Tris-HCl resolving gel (IRF3 and TRIM68 respectively) at 60mA in SDS running Tris-glycine buffer (25mM Tris, 92mM glycine and 0.1% SDS). Protein was transferred to PVDF membrane at 200mA for 1 hour in transfer buffer (25mM Tris, 192mM glycine and 20%

(v/v) methanol). Membranes were rinsed in TBS-0.1% Tween and blocked for up to 5 hours at room temperature with blocking solution (5% milk in TBS-0.1% Tween). Membranes were then incubated with primary antibody, IRF3 goat polyclonal antibody (1:500), TRIM68 antibody or positive control actin primary antibodies at 4°C for 1-5 hours or overnight. Following incubation membranes underwent three 5 minutes washes in TBS-0.1% Tween. Membranes were incubated for 1-3 hours with HRP conjugated secondary antibody (anti-goat antibody 1:10000 dilution for IRF3) followed by three 5 minute washes in TBS-0.1% Tween. Membranes were covered in ECL reagent and incubated for 1 minute in the dark followed by exposure to film in a cassette.

### 5.3.9 Statistical Analysis

In general results are expressed as means ± SD. One way or two way ANOVA was used to test for differences between treatments with $p$-values $< 0.05$ considered significant, $< 0.01$ very significant and $< 0.001$ highly significant.

## 5.4 Results

### 5.4.1 Plasmid Preparation

Various plasmids were transformed, replicated, isolated and purified with good yields. Spectrophotometry showed products with 260/280 ratio of about 1.8 and 260/230 ratio of 2.2 indicating high purity. Yields ranged from 115 to 661µg. Gel electrophoresis also confirmed purity as well as integrity (Appendix).

### 5.4.2 Characterisation of pGFP-loaded Microparticles

#### 5.4.2.1 Size

The geometric sizes of the prepared microparticles were between 2 and 3µm (Table 5.1) fitting into the size range for effective pulmonary delivery. However, microparticles encapsulating GFP plasmid DNA complexed with DOTAP were greater than 6µm.

**Table 5.1: Average sizes of Microparticle Encapsulating DNA Plasmids (n = 3, ± SD)**

| Microparticle | Average Size ($d_{50}$ µm) |
|---|---|
| ***Empty*** | 2.387 ± 0.034 |
| ***GFP*** | 3.209 ± 0.297 |
| ***GFP-DOTAP*** | 5.866 ± 1.293 |

#### 5.4.2.2 Zeta Potential

Overall zeta potentials were negative. Empty particles had a surface charge of -2mV while following encapsulation of pDNA zeta potential decreased to greater than -37mV (Table 5.2).

**Table 5.2: Zeta Potentials of Microparticle encapsulating plasmid DNA (n=3, ± SD)**

| Microparticle | Zeta Potential (mV) |
|---|---|
| ***Empty*** | -2.33 ± 0.174 |
| ***GFP pDNA*** | -37.4 ± 0.522 |
| ***GFP pDNA-DOTAP*** | -9.89 ± 0.514 |

### 5.4.2.3 Encapsulation Efficiency

To accurately assess nucleic acid dosing and concentrations the amount of pDNA encapsulated into the microparticles was determined. Encapsulation efficiency of pDNA was >83%. Encapsulation efficiency of pDNA was decreased by 70% by pre-complexation of pDNA with DOTAP.

**Table 5.3: Summary of % DNA Encapsulation Efficiency of PLGA Microparticles (n=5, ± SD)**

| Microparticle | Average Encapsulation Efficiency (%) |
|---|---|
| ***Empty*** | 0 |
| ***GFP pDNA*** | 83.33 ± 10.90 |
| ***GFP pDNA-DOTAP*** | 13.26 ± 2.88 |

### 5.4.2.4 Scanning Electron Microscopy (SEM)

SEM was used to examine morphology, size and particle size distributions of microparticles. The electron micrographs also displayed the range of microparticle size distribution and showed smooth spherical empty particles (Figure 5.9A) and pDNA loaded particles (Figure 5.9B).

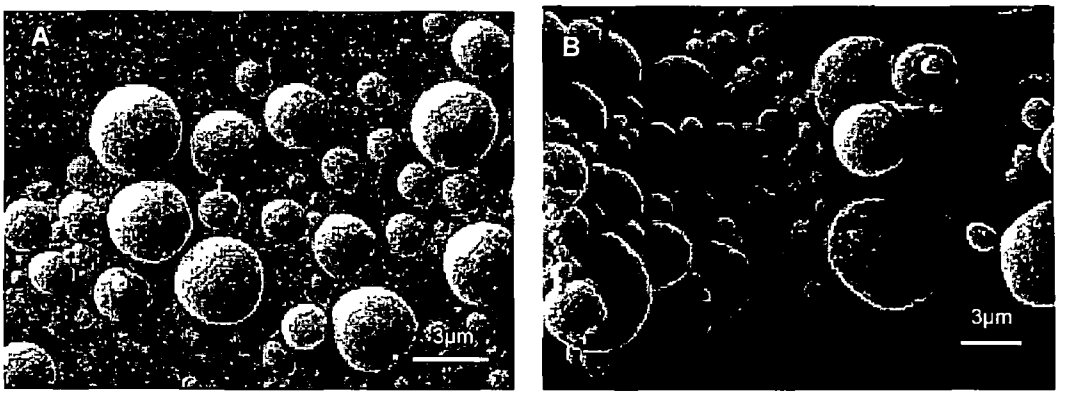


Figure 5.9: Morphology, particle size and particle size distribution of pDNA loaded microparticles was examined using SEM. (A) shows unloaded PLGA microparticles and (B) PLGA microparticles encapsulating pDNA at 5.00 kx magnification

### 5.4.3 Metafectene GFP Plasmid Transfections

To determine a suitable GFP expression vector for microparticle pDNA transfections and to compare the efficiency of transfection by commercial reagents and microparticles THP-1 cells were transfected with a range of GFP plasmids using commercially available pDNA transfection reagents Metafectene and Metafectene Pro. THP-1 cells were transfected at a low efficiency with pmaxGFP. The efficiency assessed visually was improved using Metafectene Pro over Metafectene (Figure 5.10A and B). GFP could not be visualised by fluorescent microscopy in cells transfected with lentivectors. Flow cytometry of THP-1 cells transfected with pmaxGFP showed 43% transfection efficiency (Figure 5.10C). GFP positive THP-1 cells were collected by FACS. Low numbers of positive cells were collected ($1x10^3$ cells) from the pmaxGFP transfected cells. FACS showed less than 20% GFP positive cells in the transfected cell groups (Figure 5.10E) compared with the untransfected cells (Figure 5.10D). Sorted cells did not express GFP after one week.

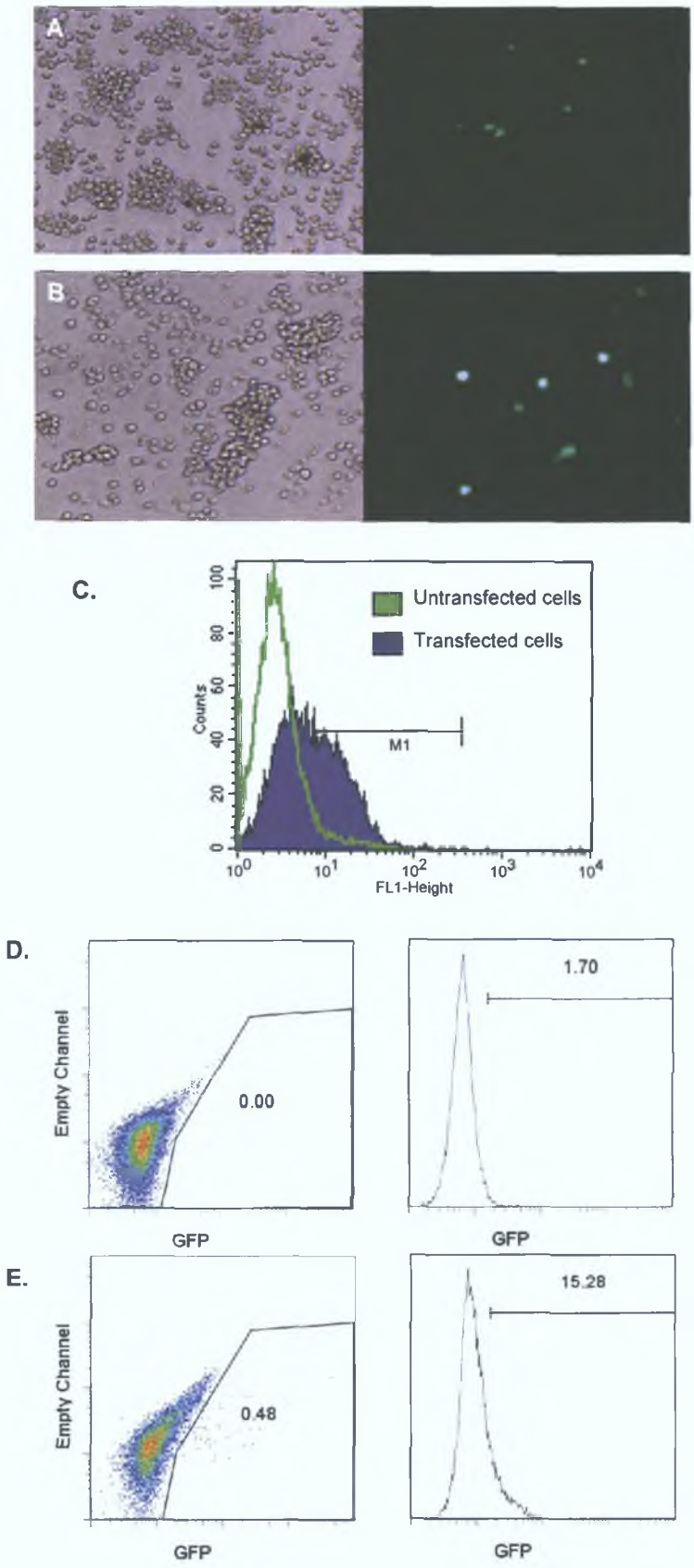


Figure 5.10: Bright field and fluorescent images of pmaxGFP THP-1 transfection with Metafectene (A) and Metafectene Pro (B) after 24 hours. (C) Flow cytometry histogram of pmaxGFP transfected THP-1 cells. Fluorescent associated cell sorting (FACS) showing dot plots and histograms of (D) control untransfected THP-1 cells and (E) pmaxGFP transfected THP-1 cells.

### 5.4.4 Lentiviral Transfections

Lentiviruses are very well suited for stable transductions and have been used previously to stably transduce THP-1 cells [62, 273] and other monocytes [59, 61]. The viral particles are constructed in a host cell line (such as human 293T cells which can be easily transfected). The host cells are transfected with various viral elements expressed on different plasmids including envelope, packaging and transgene (for example a GFP gene) expression vectors. Target cells are infected or transduced with the viral particles and the GFP gene will be integrated into the host genome (Figure 5.11).

The transfection efficiency of the HEK-293T cells with the lentiviral plasmids was almost 100% as shown in Figure 5.11. Media was harvested from these cells and viral particles were concentrated with a PEG solution. Subsequent transfections with the concentrated viral particles yielded no expression of GFP in THP-1 cells.

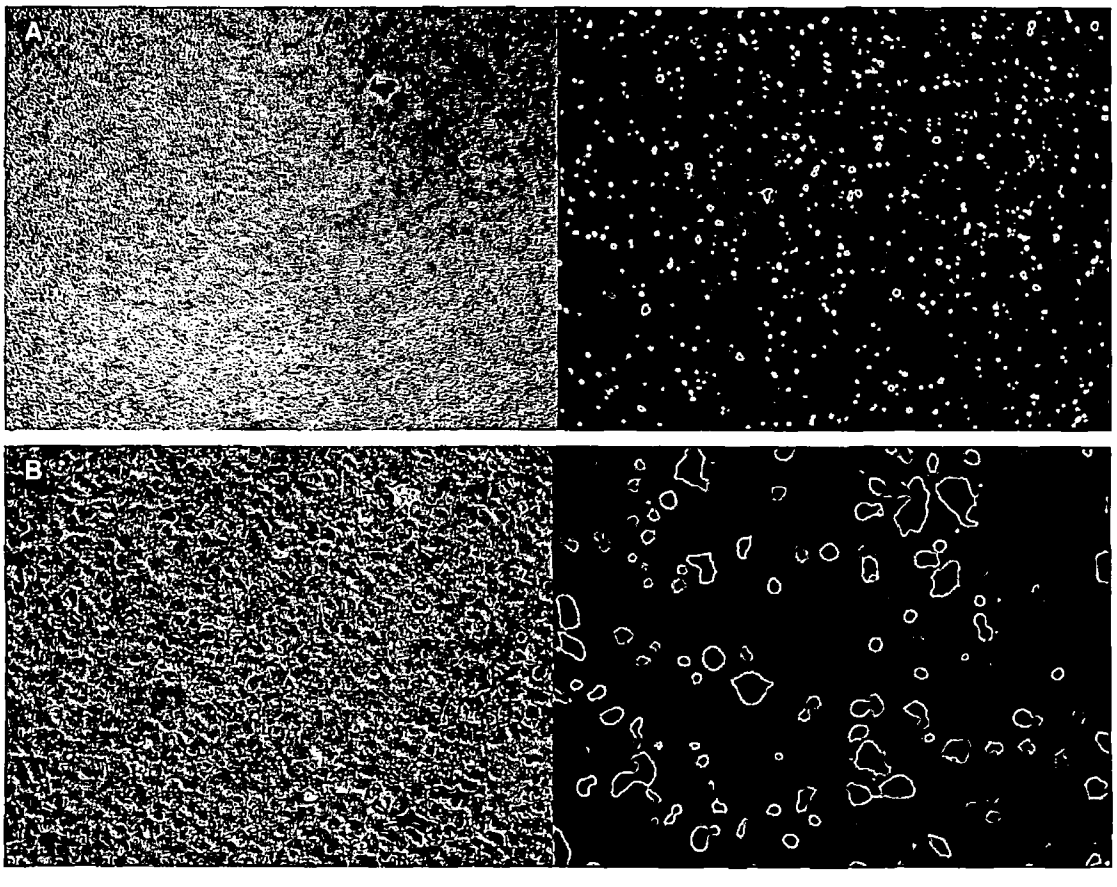


Figure 5.11: Bright light and fluorescent images of HEK-293T cells 48 hours after calcium phosphate transfection with pGIPZ-GFP, pCMV-VSV-G and pCMV-HIV-1 at 40x (A) and 200x (B)

### 5.4.5 Microparticle GFP Plasmid Transfections

#### 5.4.5.1 Flow Cytometry

Differentiated THP-1 cells were transfected with pmaxGFP plasmid delivered by microparticles and assessed by flow cytometry and HCA. Through metafectene transfections pmaxGFP was chosen as the most suitable GFP plasmid. Although encapsulation efficiency by microparticles of pmaxGFP alone was significantly greater than pmaxGFP complexed with DOTAP, GFP expression was significantly enhanced after transfection by microparticles encapsulating pmaxGFP plasmid complexed with DOTAP. Flow cytometry carried out by Dr. Awadh Yadav showed a 69.6% increase in GFP positive cells (Figure 5.12) while HCA showed a 4-fold increase in GFP fluorescence intensity by the incorporation of DOTAP into formulations (Figure 5.13). It should also be noted that a significant level of fluorescence was detected by flow cytometry and HCA following treatment with empty PLGA microparticles suggesting the particles exhibit auto-fluorescent properties.

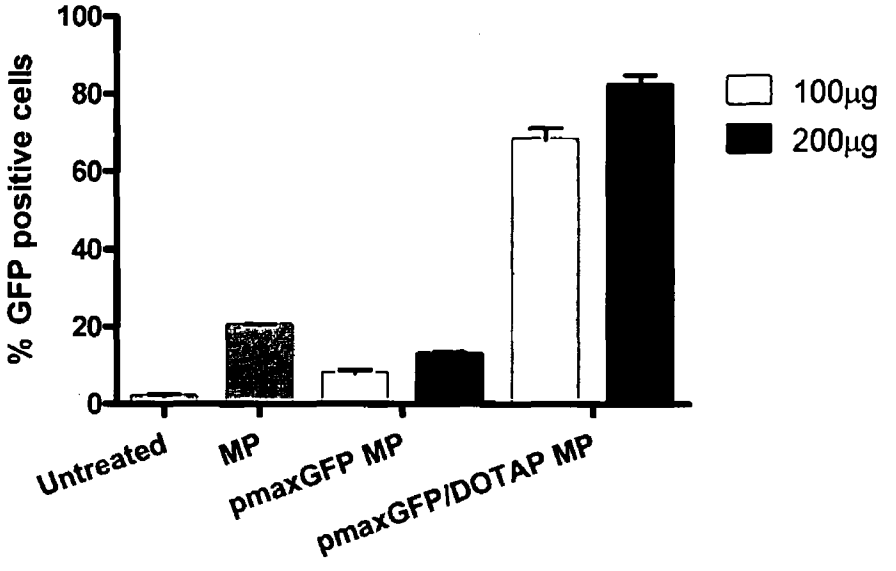


Figure 5.12: Flow cytometry analysis of pmaxGFP-microparticle transfected differentiated THP-1 cells. Cells were treated with empty microparticles (MP), 100µg or 200µg of 1mg/ml microparticles encapsulating pmaxGFP plasmid DNA (pmaxGFP MP) or pmaxGFP complexed with DOTAP at N/P ratio of 4 (pmaxGFP/DOTAP MP).
Data represented as means ± SD (n = 2)

#### 5.4.5.2 High Content Cell Analysis

Differentiated THP-1 cells are resistant to trypsin treatment however some reagents such as accutase I [274] are recommended for detachment. Flow cytometry requires a high number of cells in suspension. The process of resuspending differentiated THP-1 cells can be stressful and cause cell damage. Additionally not all cells will detach successfully and consequent cell analysis may not be an accurate representation of the entire cell population. Therefore a method that avoids cell resuspension leaving cells *in situ* is preferable. HCA was used to assess copGFP expression in differentiated THP-1 cells (Figure 5.13). Cells could be imaged and analysed adhered to wells. Fewer cells are required and can be fixed or imaged live.

HCA showed a high level of fluorescence after treatment with empty microparticles (also observed by FACS analysis) suggesting microparticles autofluoresce at these wavelengths. GFP expression by microparticle transfected cells visually was not as intense or definite as observed in metafectene/GFP transfected cells. Expression appeared to be more diffuse in the pmaxGFP microparticle transfected cells but with a greater number of cells expressing GFP.

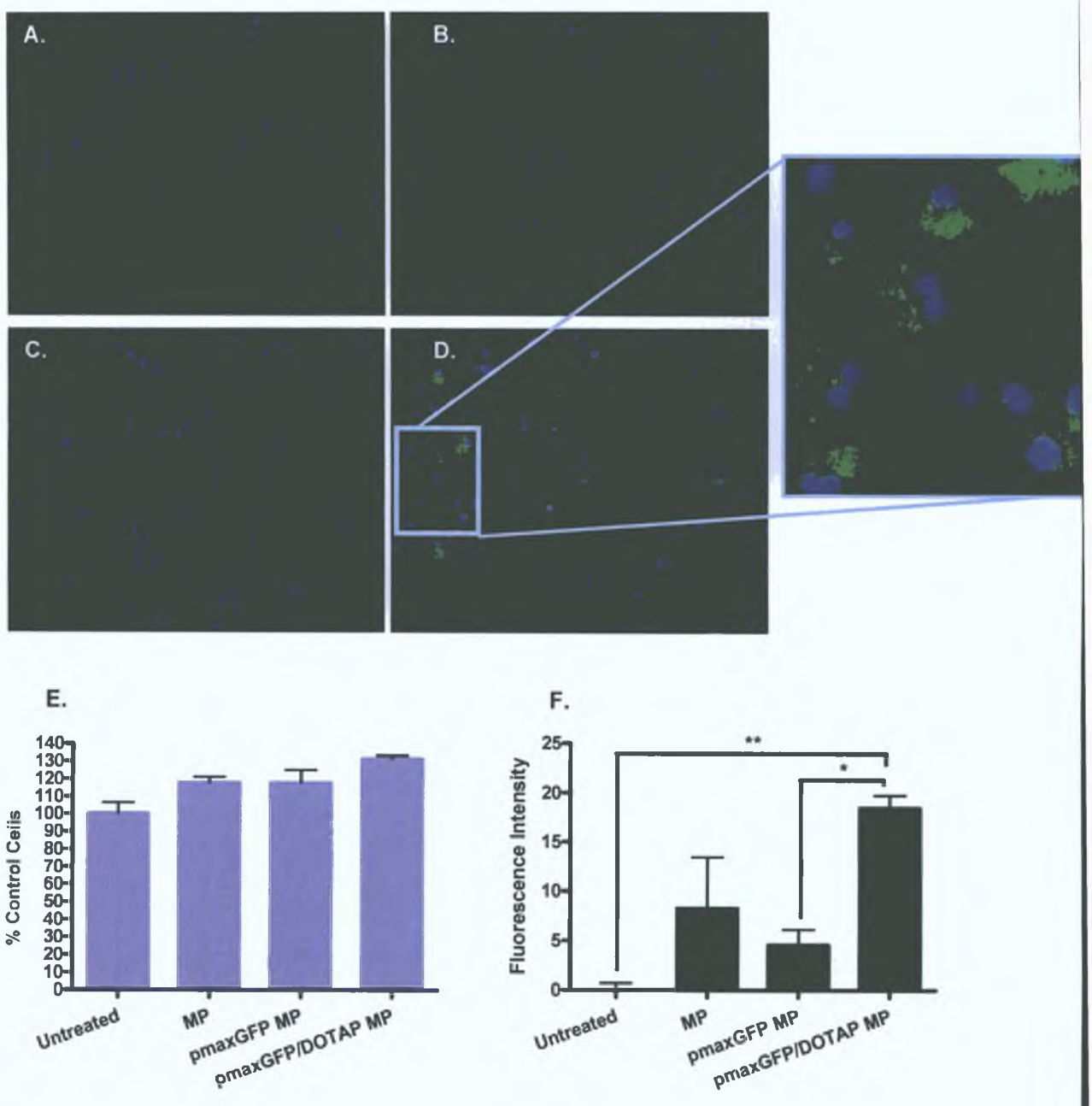


Figure 5.13: High content cell analysis of GFP expression by differentiated THP-1 cells (A) untreated, treated with 20µg of (B) empty microparticles, (C) pmaxGFP encapsulated microparticles and (D) pmaxGFP-DOTAP encapsulated microparticles. Cells were fixed and stained with hoescht (nuclei; blue). (A-D) Images were acquired at 100x magnification and analysed for cell number (E) and GFP fluorescence intensity (F) (GFP fluorescence intensity was corrected for background fluorescence). Data expressed as means ± SD (n = 3)
Statistical differences were determined by one-way ANOVA with Bonferroni's Post-hoc test. *$p < 0.05$, ** $p < 0.01$ and *** $p < 0.001$

### 5.4.6 Characterisation of shRNA-loaded Microparticles

#### 5.4.6.1 Size

The sizes of the prepared microparticles encapsulating shRNA plasmids were on average 2.9μm (Table 5.4).

**Table 5.4: Average sizes of Microparticle Encapsulating shRNA (n = 3, ± SD)**

| Microparticle | Average Size ($d_{50}$ μm) |
|---|---|
| ***Empty*** | 2.91 ± 0.036 |
| ***Scrambled shRNA*** | 2.853 ± 0.38 |
| ***IRF3 shRNA*** | 2.941 ± 0.04 |
| ***TRIM68 shRNA*** | 2.936 ± 0.03 |

#### 5.4.6.2 Zeta Potential

Zeta potentials were negative. Loaded particle zeta potentials ranged from -22 to -32mV (Table 5.5).

**Table 5.5: Zeta Potentials of Microparticles Encapsulating shRNA (n=3, ± SD)**

| Microparticle | Zeta Potential (mV) |
|---|---|
| ***Empty*** | -2.33 ± 0.174 |
| ***Scrambled shRNA*** | -31.28 ± 0.622 |
| ***IRF3 shRNA*** | -21.5 ± 0.711 |
| ***TRIM68 shRNA*** | -31.9 ± 0.663 |

#### 5.4.6.3 Encapsulation Efficiency

Encapsulation efficiencies of shRNA plasmids were found to be >43% (Table 5.6). Stock concentrations of scrambled, IRF3 and TRIM68 shRNA were 0.863mg/ml, 1.217mg/ml and 1.906mg/ml. For optimal encapsulation efficiency shRNA loading concentrations of at least 1mg/ml were required.

**Table 5.6: Summary of % shRNA Encapsulation Efficiency of Microparticles (n=5, ± SD)**

| Microparticle | Average Encapsulation Efficiency (%) |
|---|---|
| ***Empty*** | 0 |
| ***Scrambled shRNA*** | 42.68 ± 4.59 |
| ***IRF3 shRNA*** | 79.11 ± 52.43 |
| ***TRIM68 shRNA*** | 62.91 ± 1.41 |

#### 5.4.6.4 Scanning Electron Microscopy (SEM)

SEM assessing morphology and particle size showed smooth spherical particles of non-homogenous size distribution (Figure 5.14). Particles sizes concurred with laser diffraction data.

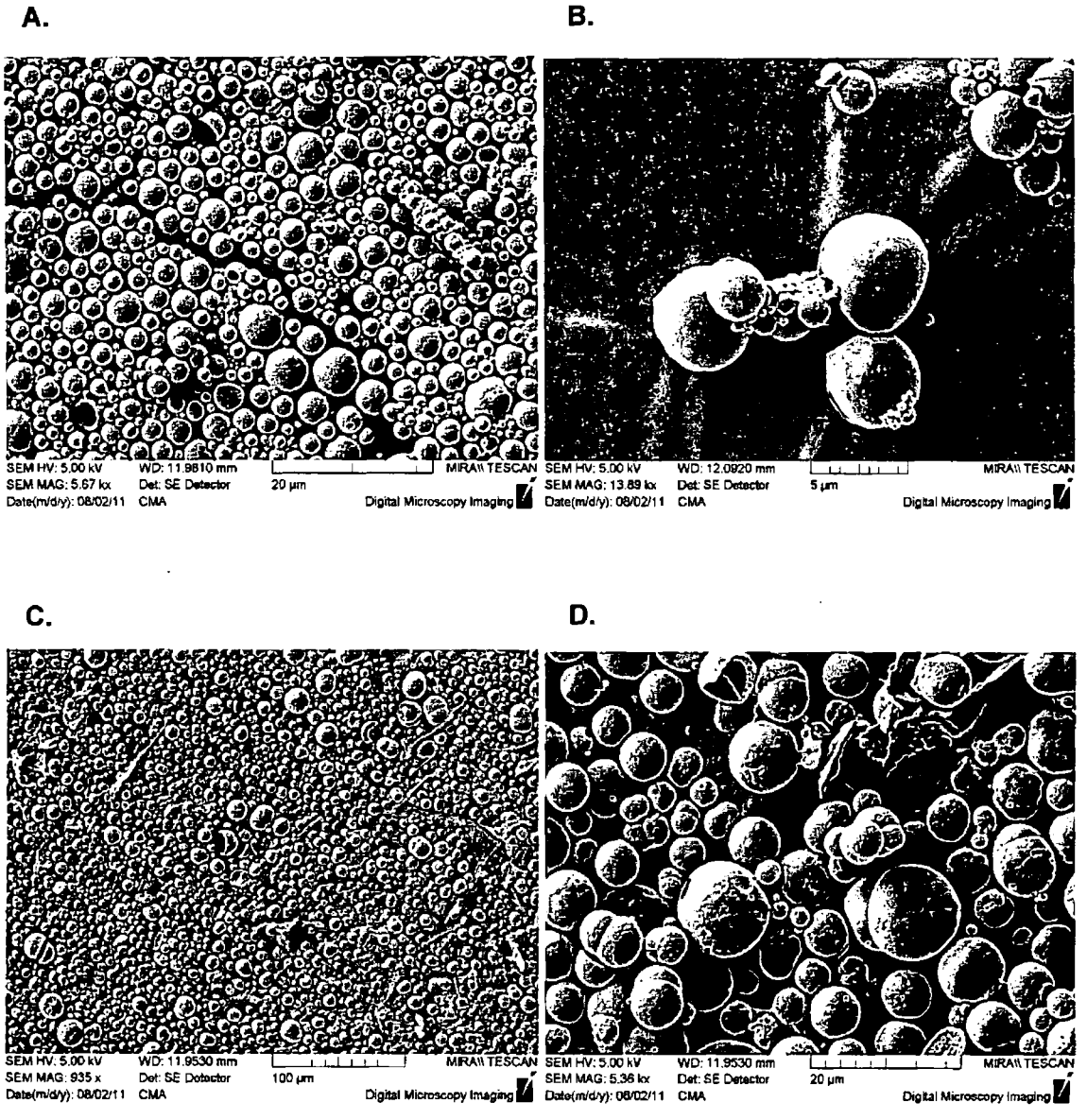


Figure 5.14: Morphology, particle size and particle size distribution of pDNA loaded microparticles was examined using SEM. (A and B) show PLGA microparticles encapsulating scrambled shRNA and (C and D) PLGA microparticles encapsulating TRIM68 shRNA at 5.67, 13.89, 9.35 and 5.36 kx magnification respectively.

#### 5.4.6.5 shRNA plasmid Integrity

Microparticle preparation involves stresses such as sonication, homogenisation, low temperatures and exposure to organic solvents increasing the possibility of damage and subsequently functional loss of the loaded nucleic acids [255, 275]. To address this issue the structural integrity of loaded nucleic acids was assessed by gel electrophoresis.

The presence of a single band of appropriate size would signify no degradation or structural damage to extracted pDNA and shRNA. Comparison of shRNA prior to and following microparticle encapsulation shows some degradation by the visualisation of a second band in each of the extracted shRNA samples (Figure 5.15). The second bands are of smaller size and appear to be the same size in each sample. The presence of strong bands representing the intact shRNA indicates the bulk of the shRNA has evaded degradation. Although shRNA extracted from microparticles appears to undergone some degradation this may not correspond to functional loss.

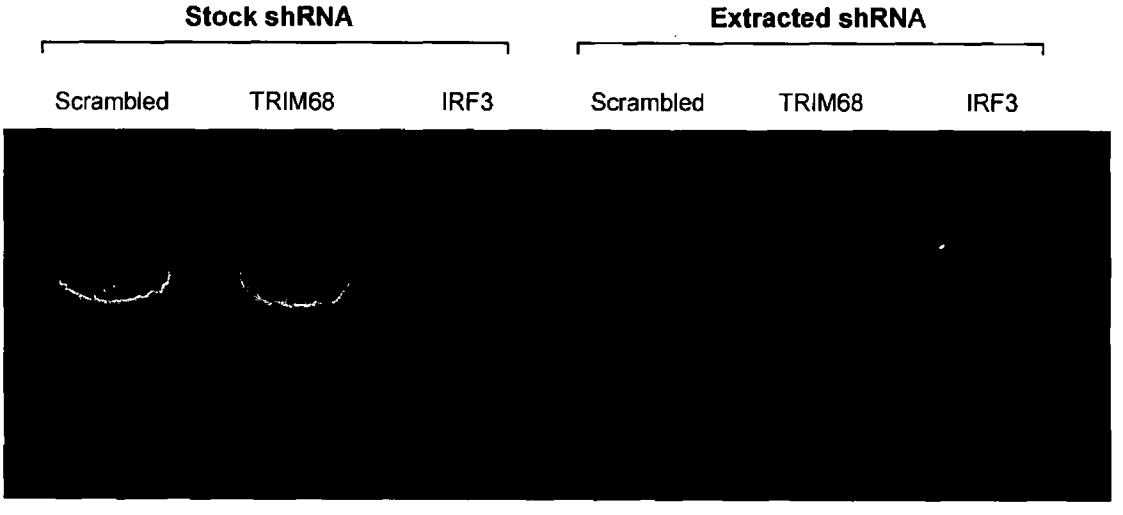


Figure 5.15: 1% ethidium bromide agarose gel showing the supercoiled stock scrambled, TRIM68 and IRF3 shRNAs (Lanes 1 – 3) and scrambled, TRIM68 and IRF3 targeted shRNA extracted from microparticles (lane 4 - 6). 50ng of shRNA was loaded per well.

### 5.4.7 Micrparticle Mediated IRF3 and TRIM68 shRNA Knockdown

IRF3 and TRIM68 expression was assessed in human monocytes and NK92NI cells respectively and was carried out by Siobhán Smith and Claire Wynne. Cells treated with microparticles encapsulating IRF3 and TRIM68 targeted shRNA showed knockdown of both genes at 48 and 72 hours (Figure 5.16A and 5.16B respectively). Endogenous control actin expression remained constant for each treatment.

A.

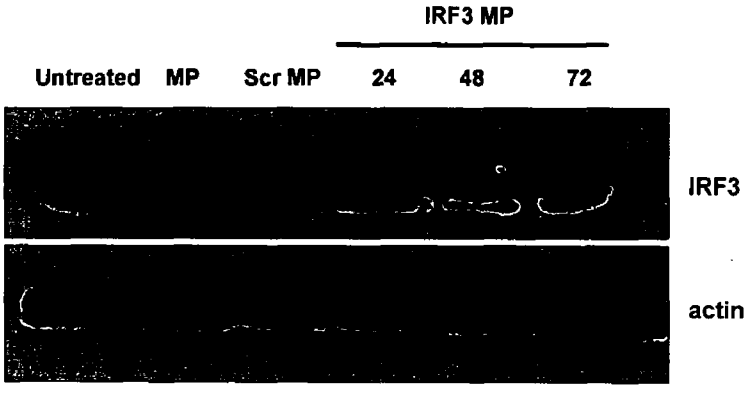


B.

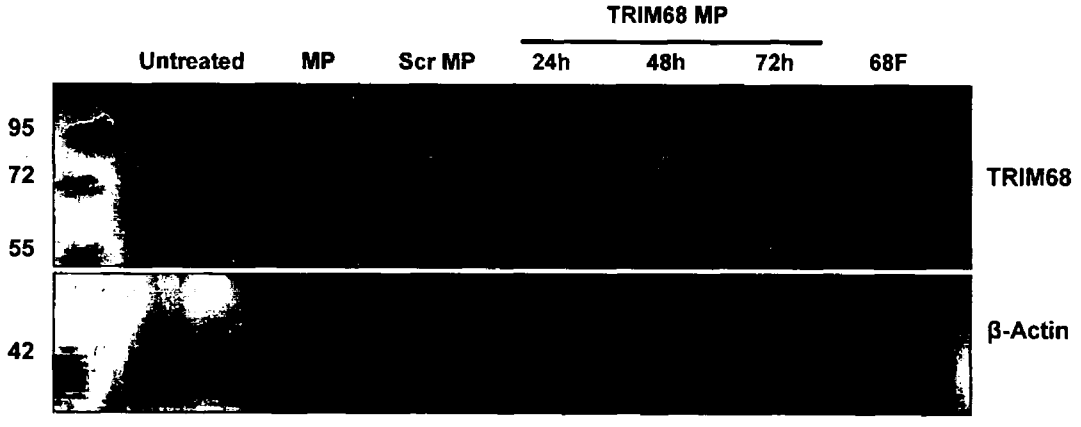


Figure 5.16: Western Blot analysis of IRF3 and TRIM68 knockdown by microparticles encapsulating shRNA. (A) shows IRF3 expression in isolated human monocytes treated with microparticles empty (MP) or encapsulating scrambled (scr) or IRF3 shRNA and (B) shows TRIM68 expression in NK92NI cells following treatment.

### 5.5 Discussion

DNA based therapeutics have been of great interest for the last three decades. The discovery that transfected DNA plasmids expressing antigens could activate specific humoral responses, lead to the development of DNA vaccines [276]. DNA vaccination or gene immunization is an intensely researched area and consequently improvements for therapeutic approaches mainly via DNA plasmid delivery are heavily investigated. Meanwhile over the last decade advances in RNAi and the understanding of endogenous RNAi pathways have brought about DNA vectors expressing shRNA as well as siRNA to mediate gene suppression with high potency and sustained effects. Similar approaches for delivery of pDNA and shRNA expressing vectors can be employed. Viral vectors show high efficiency but also severe safety risks. Non-viral vectors are wide ranging but the most successful and investigated are liposomes and polymers. One such polymer is PLGA boasting a good safety profile, biodegradability as well as FDA approval for use in humans. PLGA particles for DNA delivery have been studied extensively however to date very few studies have combined PLGA microparticles and shRNA expressing vectors.

Similar to siRNA microparticles, pDNA and shRNA encapsulating microparticles formulated were optimised for pulmonary delivery. PVA is the most commonly used emulsifier in PLGA microparticle formulation as it is associated with the formation of relatively small particles with uniform size distribution [216]. pDNA microparticle sizes were in the range of 2 – 3 μm an optimal size for pulmonary delivery and phagocytic uptake by alveolar macrophages. In addition microparticles showed negative surface charge most likely due to underivatised lactic and glycolic acid in PLGA 503.

Low encapsulation of nucleic acids by microparticles has previously been reported [230]. In order to enhance encapsulation efficiency of pDNA/shRNA the osmotic balance during preparation was altered. 0.2M NaCl was added to the external aqueous phase (PVA solution) for osmotic balance [277] changing the tonicity of the solution. Various PGLA 503 concentrations were initially examined and it was found increasing PLGA concentration improved encapsulation efficiencies of up 83%. This method however was not transferable to siRNA encapsulation perhaps due to its small size resulting in very low encapsulation efficiency. Conequently, siRNA was pre-complexed with the cationic lipid DOTAP. Optimal N:P ratios of 4:1 were found for DOTAP:siRNA condensation and microparticle siRNA encapsulation. Conversely application of complexation of pDNA with DOTAP prior to microparticle encapsulation lead to decreased encapsulation compared to pRNA loaded alone. This did not however translate to a functional loss or decreased transfection efficiency as shown by microparticle mediated GFP transfections.

GFP transfections were initially performed using commercially available transfection reagents. Lentiviral vectors can integrate into the host cell genome more readily and give a high level of transfection [58]. However these vectors are very large in size and therefore difficult to deliver. Methods such as calcium phosphate transfection can be more effective but are not suitable for

all cell types. pmaxGFP/metafectene successfully transfected THP-1 cells with a 43% efficiency while metafectene delivered GFP expressing viral vectors showed 0% transfection efficiency. An optimised calcium phosphate transfection was used to transfect HEK-293T cells with transfer, envelope and packaging lentiviral plasmids. The transfer plasmid expressed GFP and almost all cells expressed this protein after 48 hours with high levels (over 50%) after 24 hours. Despite this little or no viral particles were recovered and later infections of THP-1 cells yielded no GFP expressing cells. Lentiviral transfections are often used to establish stable cells lines as high efficiency can be achieved [61, 62, 273].

For microparticle GFP transfections pmaxGFP was selected. This allowed direct comparison between commercial reagent metafectene and microparticle transfection. Intensity of GFP expression was visually greater by metafectene transfection however the number of GFP expressing cells was lower (43% compared to 69.6% with microparticle treatment). GFP transfections could be used to develop a stable GFP THP-1 cell line as a reporter system for screening siRNA transfection. However, pmaxGFP does not contain a mammalian antibiotic selection marker.

Gel electrophoresis of shRNA before and after microparticle encapsulation gave an indication of the structural integrity of the plasmids. Intact unprocessed plasmids appeared as one clear band however those extracted from microparticles having undergone sonication, homogenisation and temperatures as low as -80°C bore two bands (Figure 5.15). Typically plasmids are represented by two bands in agarose gel electrophoresis one nicked circles and the other is supercoiled. These will not correspond to sizes of a DNA ladder only linear DNA will and therefore the ladder was omitted from the figure. Nicked circles can be faintly visualised above the strong bands in lanes 1 – 3 (Figure 5.15). The higher molecular weight band corresponded to the intact plasmid. The second band is unlikely to represent nicked circles as it has travelled further in the gel and are not present in the unprocessed shRNA. This lower molecular weight band is more likely to be plasmid fragments although the presence of only one band suggests all fragments to be of one size. For plasmid integrity damage multiple bands would be expected.

pmaxGFP microparticle transfections not only allowed formulation optimisation but also confirmed the prepared formulations facilitated transfection prior to shRNA transfections. Initially microparticles were prepared with uncomplexed shRNA and assessed in primary monocytes and NK92NI cells targeting IRF3 and TRIM68. IRF3 knockdown was greatest after 48 hours. Almost complete knockdown of TRIM68 was shown after 48 and 72 hours in NK92NI cells. This is due to slow release of the nucleic acid by the microparticles, a property that as has been repeatedly observed by *in vitro* release assays [278, 279].

Consequently the incorporation of DOTAP was not deemed necessary. Precomplexation also increases preparation time, reagent costs and potentially introduces DOTAP to cells. DOTAP has been widely associated with toxicity. Although gel electrophoresis suggests a high

proportion of shRNA did not maintain its structural integrity knockdown studies have shown the system to work effectively with high potency. IRF3 and TRIM68 are important proteins in the study of immune signalling and auto-immune disease. It is planned for future work to further elucidate the roles and pathways these proteins are involved in particularly TRIM68 as little is known of its function.

shRNA expressing vectors can easily be designed and synthesised and offer the huge advantage of stock replenishment by replication in competent cells similar to plasmid DNA reducing the cost of synthesis. DNA is also less susceptible to degradation than siRNA and will have longer lasting knockdown with the possibility of stable selection making use of the mammalian selection marker. Additionally many manufacturers have pre-made shRNA targeting a wide range of genes readily available including shRNA targeting TNFα and many other pro-inflammatory genes. A possible direction for future work could focus on shRNA delivery for knockdown over siRNA. Here, we developed a potentially useful tool for delivery of shRNA to immune cells for molecular biology and *in vivo*. PLGA microparticles were harnessed for shRNA loading with good encapsulation efficiencies. Preparation and transfection methods were optimised using pGFP and transfection efficiencies compared with commercial non-viral transfection reagents and lentiviral transfections in macrophages. Microparticles mediated the most efficient transfection. The developed shRNA loaded microparticles also knocked down two target genes IRF3 and TRIM68 in immune cells.

**Key Findings**

- Achieved high encapsulation of pDNA and shRNA in microparticles
- Microparticles more efficiently transfected macrophage cells with GFP expressing pDNA than commercial transfection reagents and lentiviral transfection in macrophages
- shRNA loaded microparticles mediated efficient knockdown of targeted genes *in vitro*

# Chapter 6

## *In Vivo* Assessment of siRNA Delivery via Mannosylated Liposomes

## 6.1 Introduction

RNAi could prove to be a powerful therapeutic tool for a wide range of diseases boasting superior specificity and potency over other forms of therapy. It shows promise to treat previously untreatable or difficult to treat diseases and has the potential to be used prophylactically and therapeutically. However, RNAi therapy is still in its infancy. Clinical trials are ongoing for conditions including cancer, neovascular age-related macular degeneration (AMD) [280] and viral infections. Concerns over off-target effects, immunogenicity and toxicity remain due to the adverse effects witnessed during previous gene therapy trials [1]. In addition due to its chemical nature as has been discussed previously in Chapter 1 it is necessary to encapsulate siRNA in a carrier vector such as a viral vector, liposome or microparticle for protection against nucleases and delivery efficiency. These delivery systems are not always inert and also may act differently *in vivo* than *in vitro*.

### 6.1.1 Pulmonary Delivery

Success of a therapeutic is greatly dependent on the target tissue, disease type and severity as well as the characteristics of the therapeutic agent. Pulmonary drug delivery presents many challenges such as the presence of mucus and other alveolar fluids [281]. Additionally, many chronic obstructive diseases such as CF and asthma are associated with mucus hypersecretion and severe inflammation [281]. Efficiency of delivery is important and dependent on a suitable drug, nanoparticle carrier and inhaler/nebuliser combination. The therapeutic system must reach the desired lung section and once there be protected from degradation or expulsion. Unfortunately nanoparticles can be captured by mucus mainly due to steric, hydrophobic or electrostatic interactions and removed from the lung by coughing [281]. Due to its specificity and potency of siRNA low doses can be used with inhalation offering the benefit of direct delivery to the target organ. Also specific cell targeting to alveolar macrophages allows off target effects to be minimized. Additionally alveolar macrophages are situated in the surfactant film and therefore more accessible to inhaled particles than endothelial cells due to the presence of the mucus layer barrier.

### 6.1.2 siRNA Therapy *In Vivo*

To date no siRNA based therapeutics has been approved as commercial products with all studies only reaching the clinical trial stage. However some success has been reported by Alnylam with an anti-RSV N gene siRNA, ALN-RSV01, reaching the Phase II clinical stage. Alnylam reports ALN-RSV01 to be safe and well tolerated with significant antiviral activity. A Phase IIb clinical trial is currently underway. Reports from animal studies have shown more success (Table 6.1). For instance, Bitko *et al.* (2005) showed very promising results using siRNA targeted at P proteins of both RSV and parainfluenza virus-3 (PIV-3) in infected mice [282] The Bitko group determined that intranasally administered siRNA alone or complexed with TransIT-TKO prior to RSV or PIV challenge inhibited viral proliferation, reduced infection

and prevented disease. In addition, when administered after viral inoculation the siRNA had a curative effect [282].

Pulmonary drug delivery in humans generally involves the use of inhalers or nebulisers (Chapter 2). Prior to clinical testing, drug formulations must be assessed in suitable *in vivo* models to examine efficacy, toxicity and immunogenicity and siRNA therapies are no different. The most common routes for pulmonary drug administration particularly in rodents are intratracheal, intranasal and inhalation [283]. A recent study by Gutbier *et al.* (2010) compared intracheal, intranasal and intravenous administration of siRNA both naked and complexed with cationic liposomes in C57BL/6 mice [85]. Intratracheal instillation of fluorescently tagged naked siRNA was efficiently distributed throughout the lung while a higher dose was necessary to reach a similar level of siRNA delivery via the intranasal route with non-uniform distribution resulting. Although knockdown of E-cadherin was observed following intratracheal E-cadherin targeted naked siRNA administration, siRNA rapidly entered the systemic circulation and was detected in the kidneys. Interestingly siRNA cationic lipid (AtuFECT01) lipoplexes caused an inflammatory response characterized by a leukocyte influx in the lungs following intratracheal administration however following intravenous administration, lipoplexes mediated significant targeted gene knockdown in lungs devoid of pulmonary inflammation.

In rodents intratracheal administration can offer many benefits over other routes of pulmonary administration due to their smaller anatomy such as increased dose reaching the smaller airways [284]. It can give more reproducible and higher deliverable dose than inhalation and improved pulmonary distribution compared to intranasal administration. Inhalation will lead to variable respired doses between animals which will depend on the animal model being used and may lead to exposure, for example of the eyes, to aerosolized drug formulations. Also stable and functional siRNA formulations for inhalation are complex to develop [283]. Intratracheal administration is invasive. It requires the animal to be anesthetized and formulations to be instilled via a tube surgically inserted between the tracheal rings or the endotracheal insertion of a tube through the mouth (without surgery and therefore less invasive) [283, 284]. Intratracheal administration works best for proof of concept work and due to its invasive nature it is not routinely used in humans and also does not require the assessment of aerosol droplet or particle size. Inhaled delivery in animals cannot be extrapolated to humans due to differences in anatomy and immunology.

**Table 6.1 Summary of non-viral siRNA delivery to the lungs *in vivo* via intratrachael administration**

| siRNA Target | siRNA Dose | Delivery Carrier | Animal Model | Effect | Ref. |
|---|---|---|---|---|---|
| GRP78 | 50, 100, 500mM | Naked siRNA | BALB/C mouse OVA induced asthma model | Decreased GRP78 in lung parenchyma, eosinophils in BAL and bronchial hyper-responsiveness in a dose dependent manner | [77] |
| eGFP<br>siGL3 | 35µg | PEI | C57BL/6J-Tg(Bos/GFP)CaBa-Bii011Dcm mice | Successful knockdown of target genes and non-specific knockdown | [82] |
| β-catenin | ~21µg | Naked siRNA | Pulmonary Fibrosis induced in C57BL/6N mice | Significant reduction in β-catenin expression and induced pulmonary fibrosis | [78] |
| siGLO Green<br><br>SPARC<br>Ctgf | 3µg | DharmaFect (lipid based transfection reagent) | Pulmonary Fibrosis induced in C57BL/6 mice | siRNA detected in bronchi and bronchioles<br><br>Reduced collagen content in the lungs | [83] |
| Cy3-tagged<br>VE-Cadherin<br>E-Cadherin | 9.3,/125µg<br>50/250µg | naked, stabilized siRNA (AtuRNAi)<br>Cationic liposomes | C57BL/6 mice | Efficient distribution of siRNA in lung parenchyma | [85] |
| XCL1 | 5, 10, 15 µg | Naked | C57BL/6 mice | Significant knockdown of XCL1 gene | [79] |
| siGLO red | ~37µg | Cationic liposomes | Athymic nu/nu mice | Longer siRNA retention in the lungs compared to systemic delivery | [84] |
| eGFP | 35µg | PEI | C57BL/6 Tg(CAG-EGFP)1Osb/J mice | 42% decrease in eGFP expression | [80] |
| p38<br>MAP kinase | 1, 10, 50nmol<br>(~0.75, 7.5, 37.5 mg/kg) | Naked siRNA<br>Cholesterol<br>Peptides | BALB/c mice | Acute 30 -45% p38 MAPkinase knockdown extended by cholesterol conjugation | [285] |
| GFP<br>Fas<br>Caspase-8 | 100µg | Naked siRNA | C57BL/6-TgN(ACTbEGFP)1Osb mice<br>C3H/HeN mice | GFP expression decreased. Fas and Caspase-8 expression significantly reduced. | [81] |
| GFP<br>KC<br>MIP-2 | 75pg | Naked siRNA | C57BL/6-TgN and C3H/HeN mice | Lung GFP expression suppressed. Lung KC and MIP-2 expression significantly decreased in a hemorrhage/sepsis mouse model | [286] |

### 6.1.3 LPS Mouse Models

For proof of concept of anti-inflammatory siRNA in the lung the establishment of an inflammatory animal model was required. Therein we used a LPS mouse model. LPS is an endotoxin of the outer membrane on gram-negative bacteria [287] that is used in the establishment of a variety of animal models including sepsis, acute lung injury (ALI) and acute respiratory distress syndrome (ARD) [288]. LPS is most commonly derived from different serotypes of *E. coli* and consists of a hydrophobic lipid (lipid A) and a hydrophilic polysaccharide

which is composed of a core region and an O-specific chain [287]. LPS structure is mainly serotype dependent with some being more suitable than others in the establishment of an inflammatory model for instance LPS from rough *E.coli* colonies tend to be more pyrogenic [289]. LPS can be administered systemically (as a model of sepsis) or directly to the lungs via inhalation, intranasal or intratracheal administration to produce models for lung inflammation [290]. Mice such as C57BL/6 are frequently used [291]. In general animal models such as mice [289, 290] and dogs [288] are not as sensitive to LPS and doses necessary to achieve an adequate inflammatory response are usually quite high (mg/kg in some mouse strains). An inflammatory lung model is used to model respiratory diseases such as COPD and asthma to carry out early pre-clinical testing of novel therapeutics.

Once administered LPS can induce acute inflammation via the induction of TLR-4 and CD14 signalling cascades which involve MyD88 and the activation of the mitogen-activated protein kinase (MAPK) signalling cascade. This in turn leads to cytokine secretion and bronchoconstriction as well as chemokine production and neutrophil infiltration as p38 MAPK is pivotal in TNFα transcription regulation and chemotaxis of neutrophils [292]. Jeyaseelan *et al.* (2004) generated a temporal gene expression profile of the inflamed mouse lung. C57BL/6 mice received aerosolised 0.3mg/ml LPS and the transcriptional profile from 1 to 24 hours was determined using an oligonucleotide microarray. 71 inflammatory related genes were up-regulated with maximal expression levels at 2 hours [293].

In the normal healthy lung, residential macrophages are present in the interstitium and the alveoli within the pulmonary surfactant film which is produced by type II alveolar epithelial cells (Figure 6.1A). If activated for example by LPS or other inhaled pathogens or toxins pro-inflammatory cytokines such as TNFα [291] or IL-1 and chemokines including keratinocyte-derived chemokine (KC or chemokine (C-X-C motif) ligand 1 (CXCL1)) and macrophage inflammatory protein-2 (MIP-2) [290] are released. In response further chemokines are produced by respiratory epithelial cells subsequently leading to neutrophil migration and infiltration [291] into the interstitium and alveolar space (Figure 6.1B). Neutrophils are the first cells recruited during an inflammatory response [294] the process of which is illustrated in Figure 6.1B. Neutrophils are a type of polymorphonuclear cells which can neutralise LPS by the release of antimicrobial cationic proteins that bind to the endotoxin rendering it inactive or degrade it (and lipid A) enzymatically [287]. If the inflammatory response persists, or is substantial, damage to the epithelium can occur which is characterised by an influx of protein rich fluid along with other macromolecules into the alveolar space [294]. The central role played by TNFα in the inflammatory response makes it an attractive target for anti-inflammatory siRNA therapies.

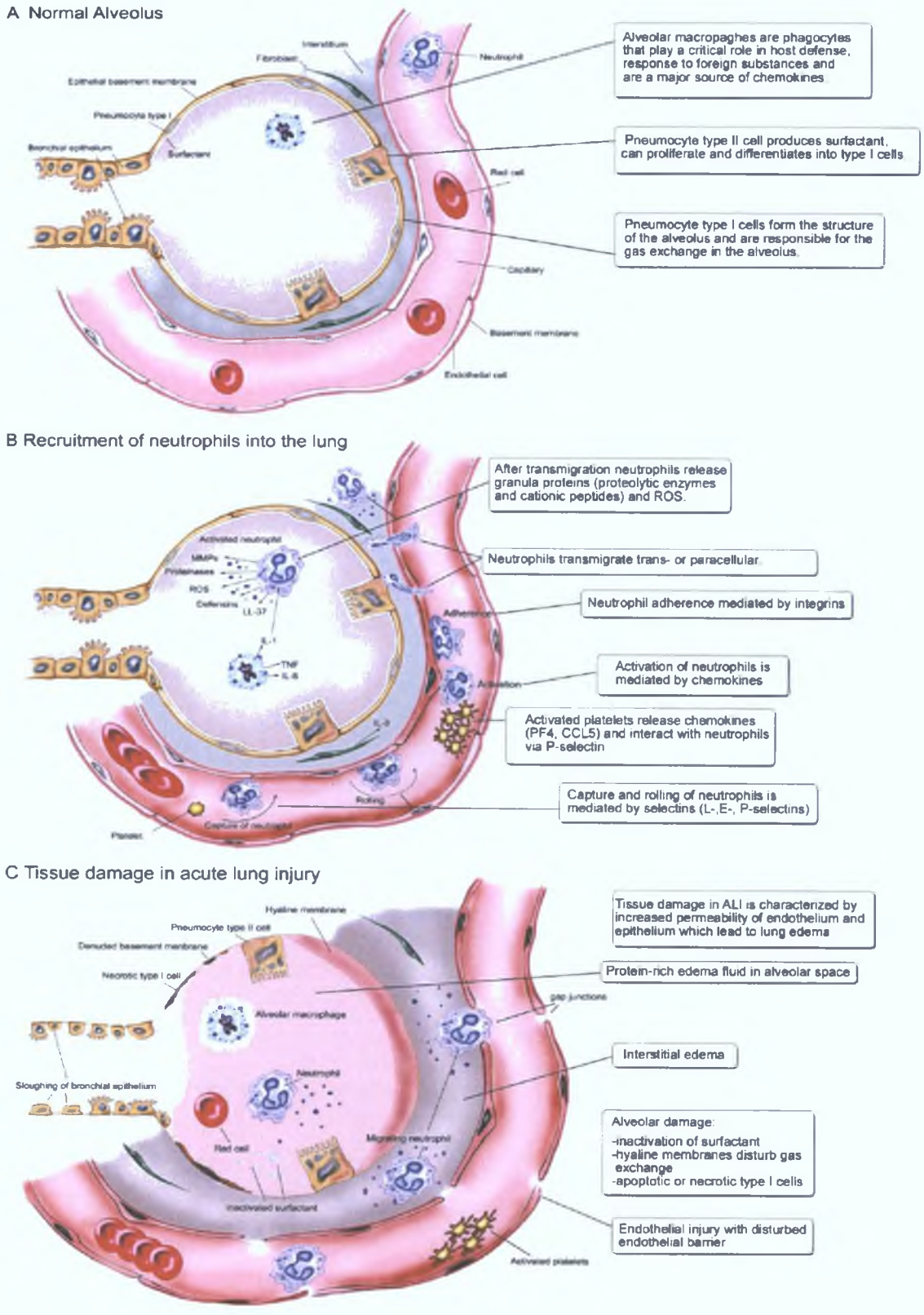


Figure 6.1: Structure of the alveolus under normal and inflammatory conditions [294].

### 6.1.4 Mannoslyated Liposomes *In vivo*

As has been previously discussed cationic lipids are most commonly used for non-viral siRNA delivery both *in vitro* and *in vivo*. This is due to both the high encapsulation and transfection efficiencies associated with nucleic acid cationic lipid formulations. Toxicity is a problem (Chapter 3) and the use of neutral or negatively charged lipids which avoid this toxic effect but lack the high encapsulation and transfection rates of cationic counterparts are becoming more attractive. Macrophages are the first line of defense against inhaled toxins and pathogens due to their location in the lungs [295]. These monocyte-derived phagocytes are situated within the pulmonary surfactant film in the interstitium and the alveoli. The MR is highly expressed by this cell type and has been studied widely for macrophage drug targeting by the mannosylation of carriers with ligands including alkyl mannosides [174], palmitoyl mannose [296], Cholesten-5-yloxy-*N*-(4-((1-imino-2-α-thioglycosylethyl)amino)butyl)formamide (Mann-C4-Chol) [130, 165, 193, 194, 297], Mann-His-C4-Chol [194], $Man_2DOG$ [131], 4-aminophenyl-a-D-mannopyranoside [133, 190] and manntriose (Man3)-DPPE [134, 135, 191] in liposome formulations or by liposome coating with *p*-aminophenyl-α-D-mannopyranoside [132].

Delivery using mannosylated liposomes of anti-inflammatory agents such as dex [130] and NFκB decoy as well as anti-cancer agents CpG oligonucleotides and DNA [195] targeting macrophages and DCs have been extensively explored by Hasida and colleagues. Intratracheally administered Man-C4-Chol liposomes were shown to be preferentially taken up by alveolar macrophages in rats which was mediated via MR endocytosis as revealed by inhibition studies [115]. These liposomes were also reasonably stable in lung microenvironment with increased levels of uptake and hence targeting associated with higher degrees of mannosylation [115]. Wijagkanalan *et al.* (2008) showed dex encapsulated in neutral Mann-C4-Chol liposomes was localised in alveolar macrophages and undetectable systemically following intratrachael instillation in Wistar rats whereas systemic distribution of free drug was detected within 30 minutes [130]. In addition co-administration of LPS and mannosylated liposomes containing dex showed significantly enhanced anti-inflammatory effects including suppression of the inflammatory cytokines TNFα, IL-1β and CINC1 (rat homolog to murine KC) in BAL and lung tissue as well as decreased neutrophil infiltration and myeloperoxidase (MPO) activity in lungs via mannoyslated liposome delivery of dex compared to co-administration of dex alone or dex in non-mannosylated liposomes. This effect was blocked in the presence of an excess of mannan (a MR competitive ligand).

To date the literature indicates that mannosylated liposomes have not been used for siRNA delivery but a few studies have assessed DNA [194] and oligonucleotide delivery [297, 298]. A NFκB decoy encapsulated in a cationic mannosylated liposome however has successfully decreased inflammation in a rat LPS-induced lung inflammatory model following intratracheal instillation [298]. This is an oligonucleotide with a sequence analogous to the binding site of the transcription factor NFκB and therefore competes for NFκB binding and modulates NFκB related gene expression. More recently Singodia *et al.* (2011) compared the delivery capability

of mannosylated liposomes and liposomes coated with another MR ligand sulfated-N–acetylgalactosamine (4-SO4GalNAc) carrying Amphotericin B. Male wistar rats received liposomes by IV administration and a significant enhancement of drug localisation in spleen and liver cells in coated liposome treated groups compared to uncoated liposomes was observed [296].

Overall mannosylated liposomes *in vivo* have been shown to specifically target macrophages, deliver their drug load efficiently and be safe and well tolerated [190]. Although as of yet siRNA delivery via mannosylated liposomes has not been published. Zhao *et al.* (2008) are currently investigating chemically modified siRNAs for MR targeting [299]. This group has synthesised mannosylated oligoribonucleotides with the intention of further investigation into mannosylated siRNA synthesis. Recently mannosylated pegylated PEIs were synthesised and complexed with siRNA to mediate knockdown of luciferase and hypoxanthine-guanine phosphoribosyl transferase (HGPT) in RAW264.7 cells with up to 42 and 62% knockdown respectively [300].

### 6.1.5 Chapter Aims

This chapter set out to assess the efficacy, immunogenicity and toxicity of mannosylated liposomes as siRNA delivery systems in a mouse model.

- To assess mannosylated liposome uptake and cytotoxicity in a murine macrophage cell line
- To determine suitable siRNA sequences for TNFα knockdown *in vitro*
- To assess immunogenic and therapeutic effects of empty and siRNA loaded mannosylated liposomes *in vivo*

**6.2 Materials**

20 GA I.V. Catheter, BD Insyte

24 GA I.V. Catheter, BD Insyte

ABTS Chromogen/Substrate Solution for ELISA, Invitrogen

Biolegend Mouse TNFα ELISA MAX™ Deluxe set

Bovine serum albumin (BSA), Sigma Aldrich

Cellomics Multiparameter Cytotoxicity kit 3, Thermo Scientific

DPX, Sigma Aldrich

Duoset Mouse CXCL1/KC Immunoassay, R & D Systems

Duoset Mouse CXCL2/MIP-2 Immunoassay, R & D Systems

Duoset Mouse IL-1β Immunoassay, R & D Systems

Eosin Y, Dye content ~99%, MW 647.89, Sigma Aldrich

Formaldehyde 38% Solution, GPR, BDH

Hematoxylin Solution, Harris Modified, Sigma Aldrich

Heparin Sodium Preservative Free, 1000 units in 1ml, Wockhardt®

HistoChoice® Clearing Agent, Sigma Aldrich

INCELL 1000 Analyser, GE Healthcare

Ketaset

LPS from E.coli 055:B5, Sigma Aldrich

Magnesium Sulphate, Sigma Aldrich

Magnum T microscope with Si 3000 camera, CETI

Mouse Intubation Platform, Penn Century

Paraformaldehyde, Sigma Aldrich

PBS tablets, GIBCO

Potassium Bicarbonate, Sigma Aldrich

Pro-lab Diagnostics Immersion Oil (R.I. 1.517)

RNAlater Solution, Ambion

Shandon Cytospin 2

Shandon double cytoslide, microscope slides for Shandon Cytospin (coated), Thermo Scientific

Shandon Filter Cards Thick (white), Thermo Scientific

siGENOME Non-Targeting siRNA #2, MW 13,400 g/mol, Dharmacon

Silencer® Select Pre-designed In Vivo Ready siRNA, MW 13,400 g/mol, Ambion,

Silencer® Select Pre-designed siRNA TNFα Targeting, MW 13,400 g/mol, Ambion

Small Animal Laryngoscope, Model LS-2, Penn Century

Speedy DIFF, Clin-Tech Ltd.

Synergy HT Multi-Mode Microplate Reader, Bio-Tek

Tween-20, Sigma Aldrich

## 6.3 Methods

### 6.3.1 siRNA

siGENOME Non-Targeting siRNA #2 (Dharmacon) is described in 3.3.1. Three *Silencer*® Select Pre-designed siRNA sequences (sequence 1 (mTNFα 1; siRNA ID # s75248) sense 5'-GCCGAUUUGCUAUCUCAUAtt-3' and anti-sense 5'-UAUGAGAUAGCAAAUCGGCtg-3', sequence 2 (mTNFα 2; siRNA ID # s75250) sense 5'-CAAUCUGCCCAAGUACUUAtt-3' and antisense 5'-UAAGUACUUGGGCAGAUUGac-3' and sequence 3 (mTNFα 3; siRNA ID # s202295) sense 5'-CGUCGUAGCAAACCACCAAtt-3' and anti-sense 5'-UUGGUGGUUUGCUACGACGtg-3' targeted to murine TNFα. *Silencer*® Select Pre-designed *In Vivo* Ready siRNA (sequence 1) is targeted to murine TNFα and negative control #1 has no significant rat, mouse or human gene sequence similarities. *In vivo* ready siRNA have undergone extra purification in the manufacturing process. siRNAs for *in vitro* studies were reconstituted with provided ambion nuclease-free water to a concentration of 20μM. *In vivo* ready siRNAs were reconstituted with nuclease-free water to a concentration of 500μM.

### 6.3.2 Cell Culture

RAW 264.7 cells an Abelson murine leukemia virus transformed macrophage cell line derived from ascites of a male BALB/c mouse were maintained in RPMI 1640 supplemented with 10% heat inactivated FBS from passage 2 – 12 in a humidified atmosphere at 37°C and 5% $CO_2$.

### 6.3.3 Animals

Female C57BL/6 mice were purchased from Harlan Laboratories UK and housed in the Biological Resource Unit (BRU) at Queen's University Belfast. Mice were maintained in a specific pathogen free unit with 10 mice per cage and permitted water and food *ad libitum*. Experiments were performed using 20g mice between 8 and 12 weeks in accordance with Animals (Scientific Procedures) Act 1986 and local ethics approval.

### 6.3.4 *In Vitro* Mannose Receptor (CD206) Expression

RAW 264.7 cells were seeded at $5x10^4$ cells/ml in 96 well plates and incubated overnight. Cells were treated as described in 3.3.3.

### 6.3.5 *In Vitro* Uptake Studies by High Content Cell Analysis

RAW 264.7 cells were seeded at a density of $5x10^4$ cells/ml in 96-well plates and incubated at 37°C overnight. 200nm anionic, neutral and mannosylated liposomes at 0, 100, 200 and 300 μM were incubated with unstimulated or LPS stimulated cells for 2 hours at 4°C or 37°C. Cells were washed three times with warmed PBS and fixed with 4% paraformaldehyde for 20 minutes

and counterstained with phalloidin-FITC and Hoescht. 150µl of PBS was added to each well and plates were stored at 4°C in the dark. HCA was carried out using INCELL 1000 analyser as described in 3.3.4.2. Images were acquired in three channels, 5 fields per well and analysed using INCELL analyser software with parameters shown in Table 6.2.

**Table 6.2 Representative High Content Cell Analysis Uptake Assay Parameters**

| Parameters | Wavelength (Ex/Em wavelengths, nm) | Analysis Settings | Sensitivity |
|---|---|---|---|
| **Nucleus** | 360/460 | Top Hat; min. area 39.6 $\mu m^2$ | 70% |
| **Cell** | - | Top Hat; min. area 93.2 $\mu m^2$ | 93% |
| **Liposomes** | 535/600 | Organelle; In Cell<br>Scales: 10<br>Min. 0.2 µm (3 pixels) - Max. 2.26 µm (7 pixels) | 30% |

### 6.3.6 *In Vitro* Toxicity

Cellomics® Multiparameter Cytotoxicty 3 kit and an INCELL 1000 analyser were used to determine toxicity in RAW 264.7 cells following liposome treatment. Liposomes were prepared as described in 2.3.3. RAW 264.7 cells were seeded at $5x10^4$ cells/ml in a flat-blottomed 96-well plate (CellStar, Grenier) and incubated overnight at 37°C and 5% $CO_2$. Media was replaced with fresh RPMI and cells were treated with liposomes at concentrations of 0, 100 or 300µM in triplicate and incubated at 37°C for 23.5 hours. Cells were also treated with valinomycin (120µM) for 23.5 hours as a positive control. Staining and analysis was carried out as described in 3.3.5. Cell loss, nuclear area, nuclear intensity, cytochrome c release, mitochondrial membrane potential and cell permeability were determined using INCELL analysis software using multiparameter target analysis and the settings in Table 6.3.

**Table 6.3 Representative High Content Cell Analysis Toxicity Assay Parameters**

| Parameters | Wavelength (Ex/Em wavelengths, nm) | Analysis Settings |
|---|---|---|
| **Nucleus** | 360/460 | Region growing; min. area 42.02 $\mu m^2$ |
| **Cell** | - | Collar; 6.75 µm |
| **Permeability** | 480/535 | Reference; In Cell |
| **Mitochondrial Membrane Potential** | 535/600 | Reference; In Cell |
| **Cytochrome c** | 620/700 | Reference; In Cell |

### 6.3.7 siRNA Transfection of RAW 264.7 cells

Transfection of RAW 264.7 cells was carried out using HiPerFect transfection reagent as per the manufacturer's recommendations. RAW 264.7 cells were seeded at $2x10^5$ cells per well of a 24 well plate in 100µl of complete medium and incubated at 37°C until transfection. Transfections were performed in triplicate with untreated, HiPerFect transfection reagent and non-target siRNA/HiPerFect complexes as controls. Non-target and TNFα siRNAs were diluted separately to 375ng in 100µl of serum free RPMI (per well). 6µl of HiPerFect transfection reagent was added to the diluted siRNA and vortexed. The mixtures were incubated for 10 minutes at room temperature to allow complexation and then added drop wise to the cells. Plates were gently swirled and incubated at 37°C for 6 hours. Media was replaced and cells were incubated overnight. 24, 48 and 72 hours following transfection cells were stimulated with 100ng/ml LPS for 3 hrs. Bright field images were acquired 24 and 48 hours post-transfection at 10x and 40x magnification prior to LPS stimulation. Supernatants were collected. Mouse TNFα ELISAs were preformed to determine TNFα expression as described in 3.3.6.3.

### 6.3.8 Acute *In Vivo* Study

#### 6.3.8.1 *In Vivo* Liposome Preparation

Mannosylated liposomes were prepared using DOPC, cholesterol and Mann-C6-Chol (70:22.5:7.5 molar ratio) by dehydration rehydration as described in 2.3.3 with modification. Liposome components were dissolved in Folch in sterile autoclaved glassware and solvents were evaporated using a rotary evaporator. Briefly, for 1ml liposome preparations 600µg of *in vivo* ready siRNA was diluted in RNase free sterile water and mixed with 548.5µg PEI dissolved in RNase free sterile water (N/P ratio 7). *In vivo* ready siRNA and PEI were allowed to complex at room temperature for 20 minutes in a sterile environment. RNase free water was not DEPC treated. The thin lipid film was rehydrated with siRNA/PEI complexes brought up to 1ml with sterile PBS and agitated. Final liposome concentration was 2.5 times more concentrated than *in vitro* preparations with a final concentration of 17mg/ml. Rehydrated lipid suspensions were stored at 4°C overnight and extruded using an Avanti mini extruder and 400nm pore polycarbonate filters. Size and zeta potential was determined as described in 2.3.4.1.

#### 6.3.8.2 Endotrachael Intubation

Mice received 100µl of intraperionteal (I.P.) administered recovery anaesthetic (2ml Ketaset, 9.2ml Saline and 2ml Rhompin) and were returned to their home cage until anaesthetic took effect. A tail or toe pinch was used to assess the depth of anaesthesia. Anaesthetised mice were positioned supine on an inclined mouse intubation platform suspended from front incisors (Figure 6.2A). The tongue was extended and moved to one side using forceps. A small animal laryngoscope was used to illuminate the vocal cords, epiglottis and opening to the trachea as well as to hold the tongue in place (Figure 6.2B). The needle tip from a 24-gauge IV catheter

(similar to Figure 6.2C) was cut and placed back into the flexible tubing of the catheter to provide rigidity during intubation. The blunted catheter was carefully inserted between the vocal chords and into the trachea and the needle was quickly removed from the catheter and liquid formulations administered.

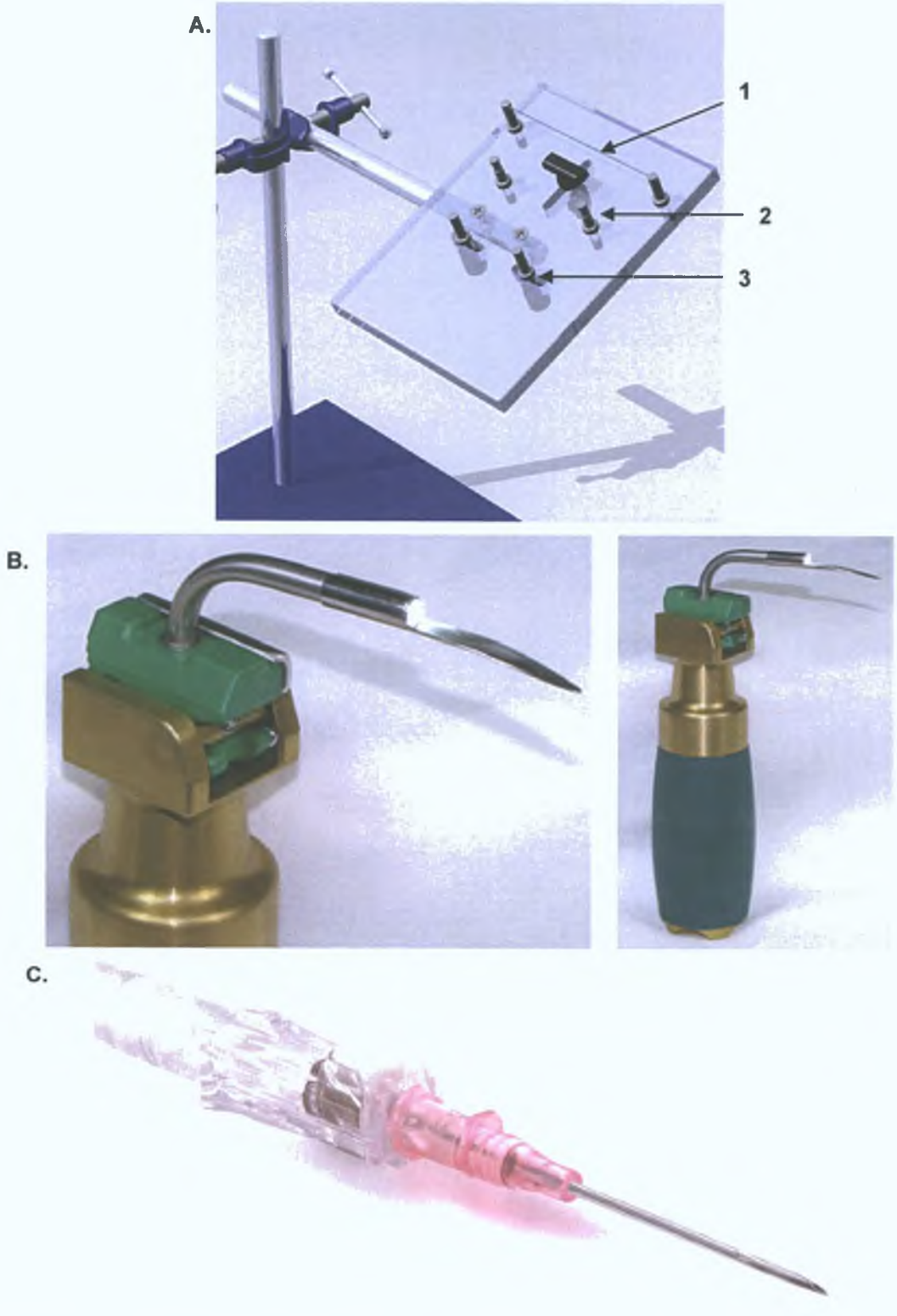


Figure 6.2: *In vivo* endotracheal intubation and BAL collection components. (A) Penn Century Mouse Intubation Platform, (B) Penn Century small animal laryngoscope (LS-2) and (C) 20 gauge catheter including syringe (BD Insyte). Mice are suspended by front incisors from part 1 and immobilised (parts 2 and 3).

#### 6.3.8.3 Intratrachael siRNA/Liposome Administration

Prior to endotrachael intubation, saline, LPS, siRNA or liposomes (50µl) were loaded into 1ml syringes such that an air pocket (200µl in volume) remained behind the leading liquid load. Following endotrachael intubation of mice and the removal of the needle from the catheter a 1ml syringe loaded with saline, 30µg NT or TNFα targeted siRNA or mannosylated liposomes empty or loaded with 30µg siRNA complexes (NT or TNFα targeted) was securely attached to the catheter and the plunger depressed expelling the 50µl of liquid followed by a volume of air. The catheter was immediately removed and mice were placed on their sides on a heated mat and then moved to a room with constant temperature set at 37°C for 24 hours with access to food and water *ad libitum*. 24 hours following the initial treatment mice underwent intratracheal administration of either 50µl saline or 0.4mg/ml LPS (from *E.Coli* 055:B5) by the same procedure. After 3 hours mice were administered 100µl ketaset (100mg/ml) by IP injection for terminal anaesthesia. A set of control mice were administered 2% Evan's Blue to confirm the accuracy of lung delivery.

#### 6.3.8.4 *In Vivo* Tissue Harvesting

Mice were administered 100µl IP injection of ketaset and placed in their cages until anaesthesia took effect. A tail or toe pinch was used to assess depth of anaesthesia. Once mice were anaesthetised and pain free the thoracic cavity was opened to expose the heart. Blood was collected directly from the heart using a 23 gauge needle and 1ml syringe pre-washed with heparin. Blood was stored on ice and centrifuged at 13,000rpm for 15 minutes at 4°C. Supernatant (plasma) was collected and stored at -80°C.

The lungs and heart were excised *en bloc*. One bronchus was clamped to allow BAL collection from one side of the lungs only. 200µl of saline was added to one side of the lung through the trachea using a 20 gauge catheter with the needle removed (Figure 6.2C) and a 1ml syringe. Saline was collected and a further 200µl of fresh saline was added. This procedure was repeated until the lung had been washed with 1ml of saline. The remaining lobes were collected for PCR and histological analysis in 1ml of RNase later and 1ml 4% paraformaldehyde respectively.

#### 6.3.8.5 Bronchoalveolar Lavage (BAL) Differential Cell Count

BAL was collected from mouse lungs and centrifuged at 1xg for 10 minutes at 4°C. Supernatants were collected as BALF and stored at -80°C. Cell pellets were resuspended in 1ml of red cell lysis buffer and centrifuged at 1xg for 10 minutes at 4°C. Supernatants were discarded and cell pellets resuspended in 100µl of saline. 10µl of cell suspension was mixed with 90µl of trypan blue and total cell counts taken using a haemocytometer. 90µl of cell suspension was spun for 5 minutes at 500rpm onto Shandon coated microscope slides using Shandon filter cards and Shandon cytospin 2. Cells were fixed and stained using Speedy-Diff

cell stain kit. Briefly, slides were immersed for a few seconds in speedy-diff fixative (coloured methanol) five times then immersed for a few seconds in Speedy-Diff A (buffered Eosin Y) at least 5 times followed by blotting and washing in PBS and finally immersed in Speedy-Diff B (buffered azur/methylene blue) at least 5 times, blotted and washed. Slides were allowed to dry and differential cell counts were obtained using a CETI light microscope at 100x magnification under oil immersion. Macrophages and neutrophils were counted in 5 random fields and total differential cell counts calculated.

### 6.3.9 *In Vivo* Cytokine Expression

#### 6.3.9.1 Enzyme Linked Immunosorbant Assay

TNFα, IL-1β, KC and MIP-2 (or CXCL2) levels were determined in BALF by ELISA. TNFα ELISAs were carried out as described in 3.3.6.3. IL-β, CXCL1/KC and CLXCL2/MIP-2 were performed according to the manufacturer's protocol with some modifications. Briefly, 96 well ELISA plates were coated overnight at room temperature with 100µl per well capture antibody (rat anti-mouse IL-1β, KC or MIP-2) diluted in PBS to 4µg/ml (IL-1β) or 2µg/ml (KC and MIP-2). Capture antibody was aspirated and plates were washed 3 times with wash buffer (PBS with 0.05% Tween-20) and blotted with absorbent paper. Plates were blocked with 300µl of assay diluent (1% BSA in PBS) for 1 hour with shaking. Standard curves were prepared using provided IL-1β, KC and MIP-2 standards and assay diluent from 0 up to 500 or 1000 pg/ml. Washing and blotting was repeated. 100µl of diluted standards and BALF samples were added to the wells, plates were sealed and incubated at room temperature for 2 hours with shaking. Plates were washed 4 times and blotted. IL-1β, KC or MIP-2 biotinylated goat anti-mouse detection antibodies (100µl) were added to each well at working concentrations of 2.5µg/ml, 200ng/ml and 75ng/ml in assay diluent respectively. Plates were sealed and shaken at room temperature for 2 hours. Washing and blotting steps were repeated and 100µl of streptavidin conjugated to horse radish peroxidise (strep-HRP) diluted 1 in 200 in assay diluent was added to the wells for 20 minutes with shaking at room temperature out of direct light. Strep-HRP was aspirated and plates were washed and blotted. 100µl of ABTS substrate solution was added to each well and plates were incubated at room temperature in the dark unsealed until a green colour developed (15 – 30 minutes). Absorbance was measured at 405nm using a Synergy HT Multi-Mode Microplate reader and Gen5™ software.

#### 6.3.9.2 Mouse TH1/TH2 9-plex Assay

The MesoScale Discovery multiplex assay is described in 3.3.7.2. Mouse TH1/TH2 9-plex assay simultaneously detects IFNγ, IL-1β, IL-2, IL-4, IL-5, KC, IL-10, total IL-12 and TNFα key effectors in the TH1/TH2 inflammatory response. Capture antibodies for all analytes are rat monoclonal antibodies except the IL-1β capture antibody which is a mouse monoclonal antibody. Briefly, 25µl of provided Diluent 4 was added to each well and the plate was sealed and incubated at room temperature for 30mins. A 4-fold serial dilution of mouse TH1/TH2 9-

Plex Calibrator (1µg/ml to 2.4pg/ml) was prepared in Diluent 4 (for plasma calibration) or 1% BSA in PBS (for BALF calibration). BALF samples were mixed with 1% BSA to reduce protein adherence to the microtubes. Standards, plasma and BALF (25µl) were added in duplicate to wells and the plate was sealed and incubated over night at 4°C. The plate was washed 3 times with PBS-T followed by the addition of 25µl of 1X detection antibody solution (50X stock diluted in Diluent 5 containing either rat or goat monoclonal antibodies to each analyte). The plate was resealed and vigorously shaken at room temperature for 2 hours. Washing 3 times in PBS-T was repeated. 150µl of 2X Read Buffer T (4X Read Buffer T diluted in de$H_2O$) was added to each well and the plate was immediately analysed on a SECTOR Imager. Read buffer provides a suitable chemical environment for electrochemiluminescence. Standard curves were produced and concentrations of analytes for each sample determined using the MSD DISCOVERY WORKBENCH® software.

#### 6.3.9.3 Histopathology

Fixed lung tissue was embedded in paraffin and sections mounted onto slides. Paraffin was removed by immersing slides in HistoChoice® Clearing Agent for at least 30 minutes. Tissue sections were hydrated by immersing for a few seconds in 100% ethanol followed by 90%, 70% and 50% ethanol and finally d$H_2O$. After hydration sections were stained with haematoxylin for 15 minutes followed by rinsing in d$H_2O$. Sections were differentiated in 1% acid alcohol to remove excess haematoxylin by immersing for a few seconds in 50% ethanol, then 70% ethanol followed by acid alcohol (1% concentrated hydrochloric acid in 70% ethanol (v/v)). Sections were then immersed in 70% ethanol followed by rinsing in d$H_2O$. Sections were immersed in alkaline ammonia water (0.2% potassium bicarbonate and 2% magnesium sulphate) and rinsed by running under tap water for 10 minutes. Following rinsing sections were stained with eosin (5 minutes) and then immersed for a few seconds in d$H_2O$. Sections were then dehydrated by immersing for a few seconds in 50%, then 70%, 90% and finally 100% ethanol followed by a short immersion in HistoChoice® Clearing Agent. Coverslips were mounted onto slides with DPX mounting medium. Lung sections were examined by a pathologist Dr Joseph Cassidy for inflammation by light microscopy with up to 4 mice per treatment group. The degree of neutrophil-rich inflammation was scored as – (absent), +/- (very mild), + (mild) or ++ (moderate). Scores were then assigned per treatment group. Photomicrographs were acquired for each "score" using a Nikon Eclipse E600 microscope.

### 6.3.10 Statistics

Data was analysed using one or two-way ANOVA. If any statistically significant difference was found, *post hoc* comparisons were performed using Bonferroni's test. Data was deemed significant when $p < 0.05$ and expressed as group means with standard errors.

## 6.4 Results

### 6.4.1 Mannose Receptor Mediated Mannosylated Liposome Uptake in RAW 264.7 cells

Mouse macrophage RAW 264.7 cells were assessed for MR expression by immunofluorescence similarly to differentiated THP-1 cells in chapter 3. RAW 264.7 cells were fixed and stained for MR expression with primary MR antibody and secondary Alexa Fluor-488, nucleus (hoescht; blue) and F-Actin (phalloidin-TRITC; red). Representative images are shown in Figure 6.3 and show ubiquitous MR expression by RAW 264.7 cells.

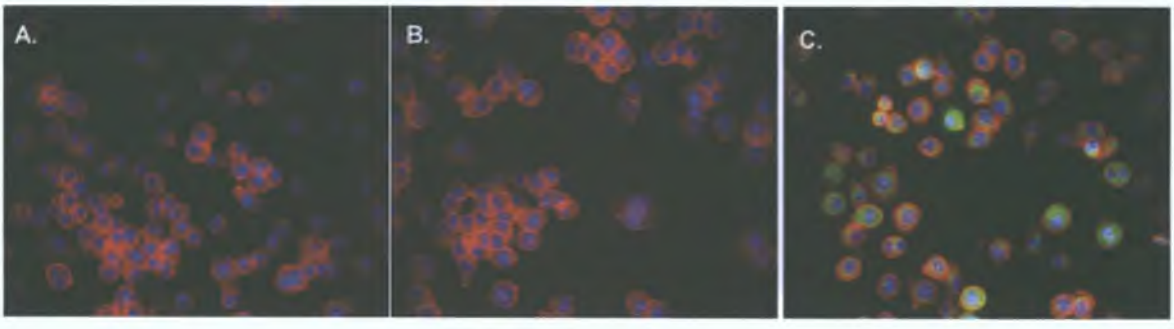


Figure 6.3: High content cell analysis of mannose receptor expression by RAW264.7 cells. Cells were fixed and stained for mannose receptor expression with primary mannose receptor antibody (1µg/ml) and secondary Alexa Fluor-488 (1/1000 dilution), nucleus (hoescht; blue) and F-Actin (phalloidin-TRITC; red). Images were acquired by an INCELL 1000 analyser (A) shows cells incubated without primary mannose receptor or secondary antibodies, (B) shows cells incubated without primary mannose receptor antibody only and (C) shows cells stained using primary mannose receptor antibody and 1/1000 AlexFluor488 secondary antibody.

Uptake of rhodamine labelled anionic, neutral and mannosylated liposomes was determined by HCA in order to assess the impact of liposome composition on uptake into RAW 264.7 cells and to compare this uptake with human differentiated THP-1 cells. Liposome uptake of DOPS, DOPC and mannosylated (7.5% MC2C, MC4C, MC6C) liposomes was assessed at 0, 100, 200 and 300µM concentrations after 2 hours and showed highly significant uptake ($p < 0.001$) of DOPS liposomes at all concentrations and MC6C liposomes at 300µM (Figure 6.4). This is in accordance with uptake assessment in human differentiated THP-1 cells.

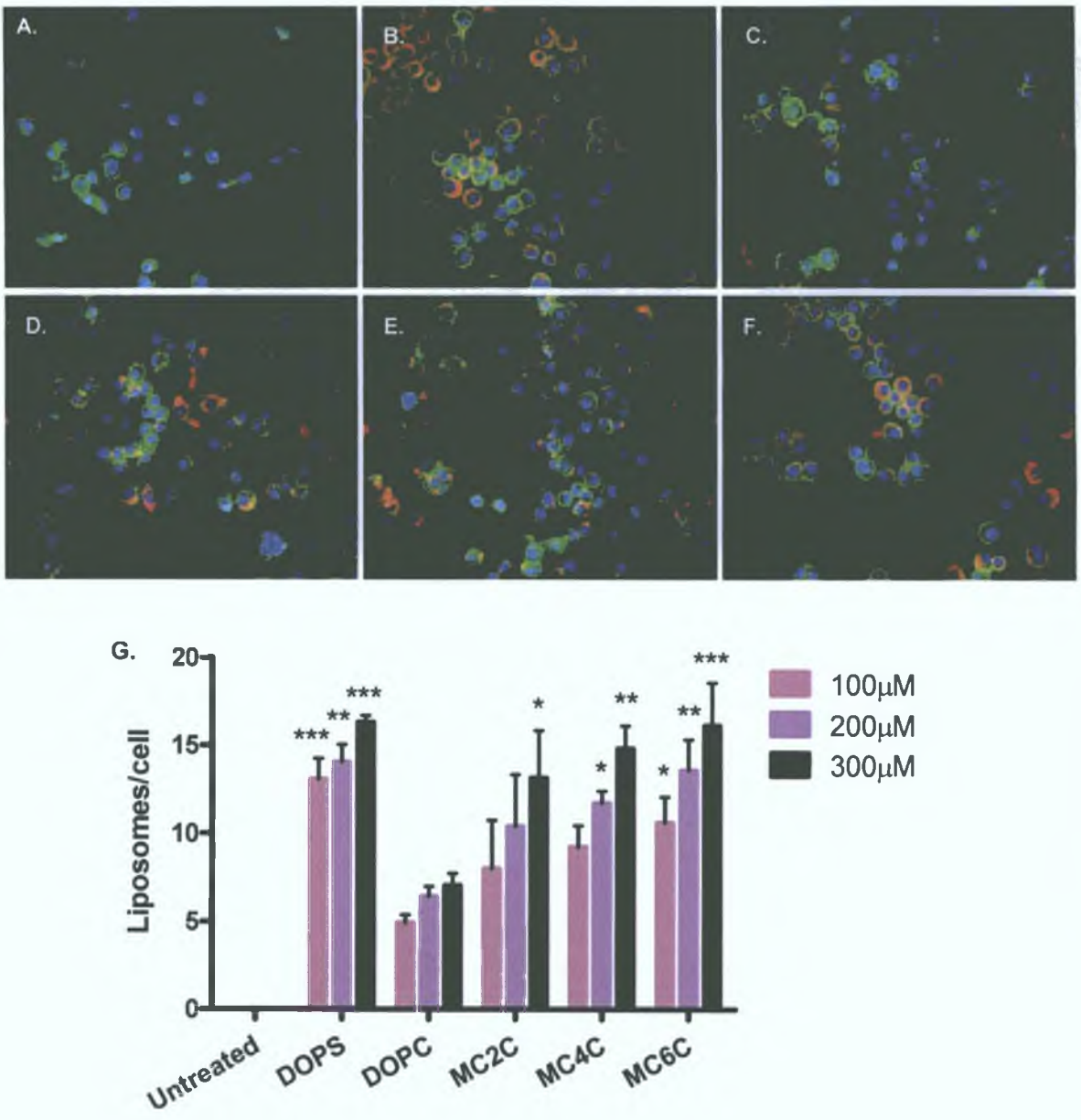


Figure 6.4: Assessment of liposome uptake by RAW 264.7 cells by high content cell analysis. RAW 264.7 cells were incubated with 0, 100, 200 or 300μM rhodamine (red) tagged anionic (DOPS), neutral (DOPC) or mannosylated (MC2C, MC4C or MC6C) liposomes for 2 hours at 37°C, fixed and counterstained with hoescht (nucleus; blue) and phalloidin-FITC (F-Actin; green). Images were acquired using an INCELL 1000 cell analyser in 5 fields per well. Images show (A) untreated cells, cells treated with (B) DOPS, (C) DOPC, (D) MC2C, (E) MC4C and (F) MC6C liposomes at 200μM for 2 hours. All images were analysed and liposomes per cell counted (G).
Statistical significance was determined by a two-way ANOVA.
* $p < 0.05$, ** $p < 0.01$, *** $p < 0.001$ vs. DOPC treated counterparts (Bonferrioni's test)
Data represented as means ± SD (n = 6)

Uptake of 0, 100, 200 and 300μM liposomes was also assessed by HCA at 4°C, with the lower temperature impeding uptake in all but DOPS and DOPC treated cells. This suggests an active uptake process is involved in mannosylated liposome uptake. Mannosylated liposome uptake is receptor mediated and co-incubation with MR ligands such as mannan has been previously shown to inhibit mannosylated liposome uptake [115, 130]. MC2C liposomes showed the most significant decrease ($p < 0.001$) in uptake due to the low temperature (Figure 6.5D).

To develop liposome formulations for delivery to the lung the liposomes must be capable of aersolisation. Uptake of liposomes at 100, 200 and 300μM pre- and post-nebulisation via an AeroNeb Pro nebuliser was measured by HCA (Figure 6.6) in order to determine the impact of nebulisation on cell interaction. Overall there was a decrease in uptake following nebulisation. MC6C liposomes showed significant reduction in liposome association following 100 and 200μM treatments ($p < 0.05$) (Figure 6.6D). Mannosylated liposome stability may have been affected during nebulisation resulting in decreased uptake by RAW 264.7 cells.

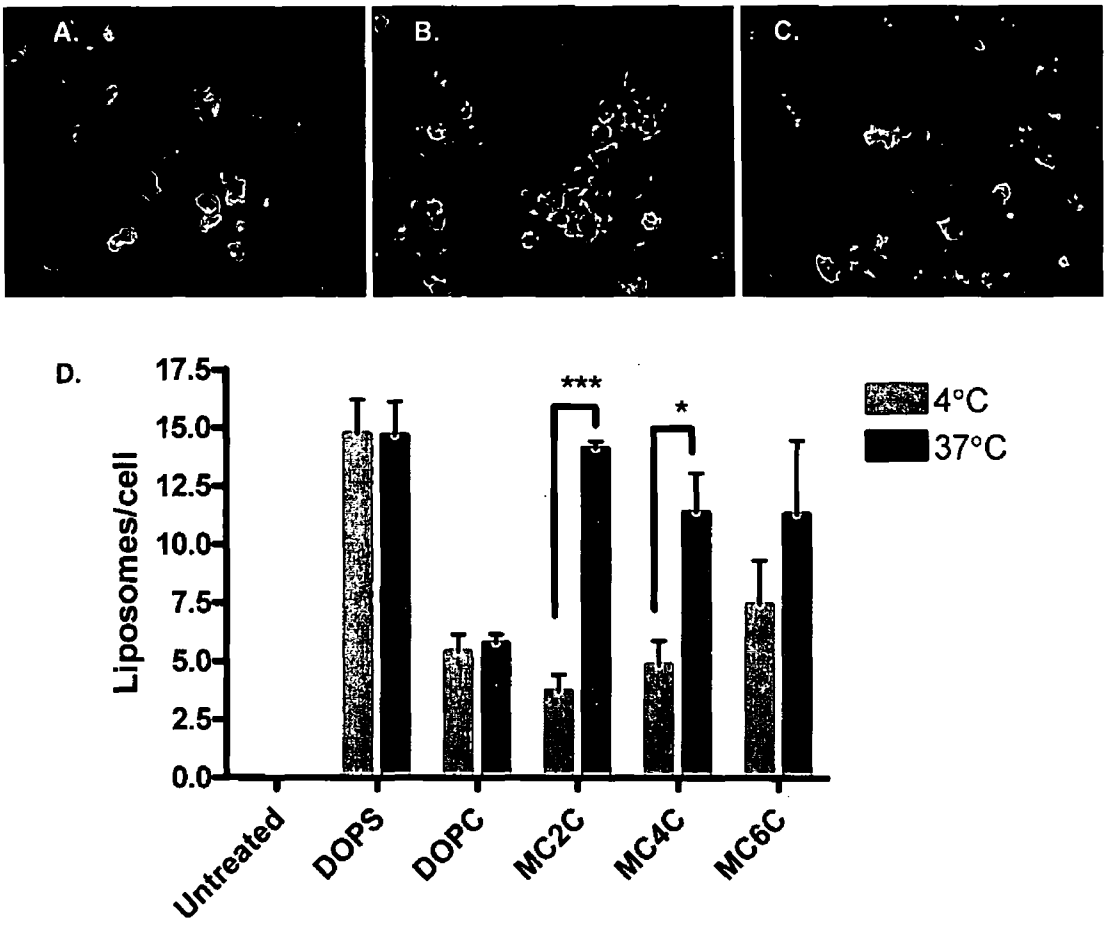


Figure 6.5: High content cell analysis of liposome uptake by RAW 264.7 cells at **4** and 37°C. RAW 264.7 cells were treated with 0, 100, 200 or 300μM of fluorescently tagged liposomes and incubated at either 4°C or 37°C for 2 hours, fixed and counterstained. HCA was used to acquire images in 3 channels and 5 fields per well. (A) shows untreated cells, (B) cells treated with 100μM MC2C liposomes and incubated for 2 hours at 4°C and (C) 37°C and (D) uptake of 100μM liposomes.
Statistical significance determined by two-way ANOVA with Bonferrini's post-hoc tests. * $p < 0.05$, ** $p < 0.01$ and *** $p < 0.0001$
Data represented as means ± SD (n = 6)

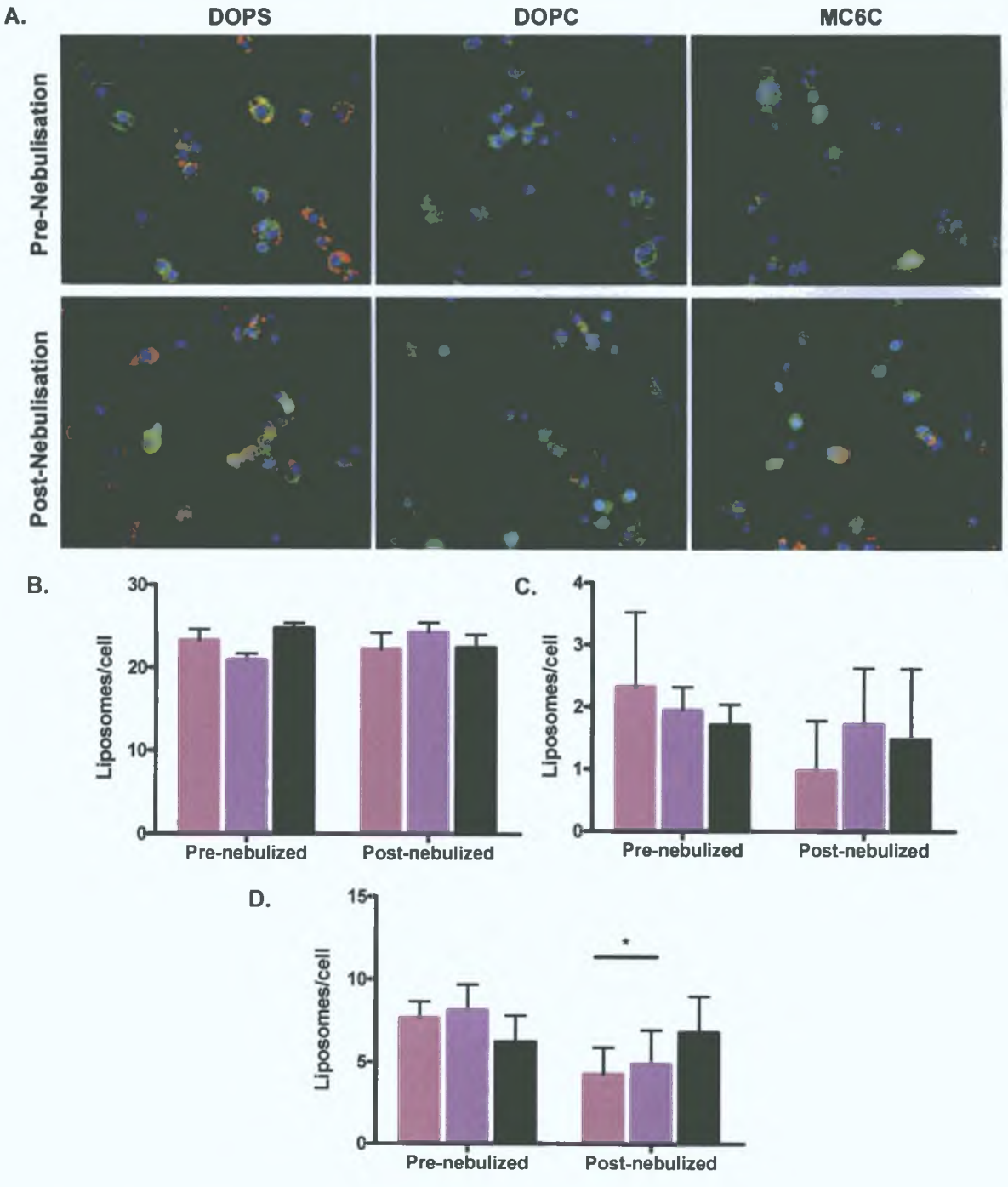


Figure 6.6: High content cell analysis of liposome uptake into RAW 264.7 cells pre- and post-nebulisation. Fluorescently labelled lipsomes were nebulised by an AeroNeb Pro nebuliser. Pre-nebulised and post-nebulised liposomes were incubated at 37°C for 2 hours with RAW 264.7 cells followed by fixation and staining of nuclei (hoescht; blue) and cells (phalloidin-FITC; green). Images (A) were acquired in 5 fields per well and analysed by an INCELL 1000 cell analyser for uptake of (B) DOPS, (C) DOPC and (D) MC6C liposomes (100 μM, 200μM and 300μM) Statistical differences were determined by two-way ANOVA with Bonferrini's post-hoc test (* $p < 0.05$, ** $p < 0.01$) vs. un-nebulised liposome treated counterparts. Data represented as means ± SD (n = 3)

### 6.4.2 *In vitro* Assessment of Liposome Toxicity

A major limitation of *in vivo* drug delivery is toxicity. A novel method for predicting *in vivo* airway toxicology was used combining HCA and cellomics cytotoxicity kits. RAW 264.7 cells were treated for 24 hours with liposome DOPS, DOPC, MC2C, MC4C and MC6C preparations and compared to untreated cells (negative control) and cells treated with DOTAP liposomes or 120μM valinomycin (positive controls). Cell viability, permeability, nuclear intensity, nuclear size and mitochondrial membrane potential were measured using a Cellomics multiparameter cytotoxicity kit and HCA. All preparations were found to be non-toxic at both 100 and 300μM concentrations except 300μM DOTAP and DOPS treatments (Figures 6.7 – 6.10).

In all cases positive control valinomycin showed high levels of toxicity (Figure 6.7) compared to untreated healthy cells validating this method for assessing toxicity. Significant toxic effects were also observed in the liposome positive control preparation consisting of 50% DOTAP. Due to toxicity cell count decreased, nuclei condensed reducing nuclear size and increasing the fluorescent intensity detected, cells became more permeable and mitochondrial membrane potential decreased. DOPS (at 100μM only) and all concentrations of DOPC (neutral) and mannosylated liposomes showed levels of cell viability consistent with untreated negative control cells. Toxicity induced by liposomes was assessed at two different concentrations 100μM (Figure 6.8) and 300μM (Figure 6.9) as concentrations required for *in vitro* transfection are within this range. Cells were stained for nuclei, permeability and MMP and images acquired (Figure 6.7 – 6.9). Images clearly show differences in cell number between 300μM DOTAP and DOPS liposome treatments (Figure 6.9) and healthy control cells (Figure 6.7).

Images were analysed using INCELL 1000 multi-target analysis mode of 5 fields per well. Cell loss, nuclear size, total nuclear intensity, cell permeability and MMP measurements per treatment were determined (Figure 6.10). In comparison to healthy untreated RAW 264.7 cells substantial cell loss was observed following treatment with 120μM valinomycin (positive control), 100μM and 300μM DOTAP liposomes and most significantly 300μM DOPS liposomes ($p < 0.001$). Only marginal decrease in cell viability was observed following neutral and mannosylated liposome treatments at both concentrations (Figure 6.10A). Hallmarks of apoptosis and necrosis include chromatin condensation and increased cell permeability or leakiness respectively. Additionally, MMP collapse is a mark of apoptosis and related to cytochrome c release.

Chromatin condensation was detected by a decrease in nuclear size and increase in total nuclear intensity. Valinomycin ($p < 0.05$) and 300μM DOPS liposome treatments showed similar nuclear shrinkage while DOTAP liposomes at both concentrations also decreased nuclear size but not to the same extent (Figure 6.10B). 100μM DOPS liposomes and DOPC and mannosylated liposomes at 100μM and 300μM showed nuclear sizes equivalent to healthy cells (Figure 6.10B). Total nuclear intensity was also increased by positive control treatment

valinomycin ($p < 0.001$) and DOTAP liposomes while cell nuclear intensities remained at healthy levels following all other liposome treatments at both concentrations (Figure 6.10C).

Necrosis can lead to cells becoming leaky and therefore the permeability of RAW 264.7 cells was assessed. Increased uptake of a fluorescent (Ex/Em 480/535nm) dye indicated an increase in permeability as demonstrated by the positive control valinomycin (Figure 6.10D). DOTAP liposomes at both concentrations also caused RAW 264.7 cells to become more permeable with 300μM DOTAP liposome treatment resulting in greater cell permeability than valinomycin. Again all other liposome treatments at both concentrations showed levels equivalent to untreated healthy control cells. This included DOPS liposomes of 300μM which by other parameters showed to induce substantial decrease in cell viability perhaps indicating induction of apoptosis as opposed to necrosis. MMP collapse associated with apoptosis was observed following treatment with positive control valinomycin, DOTAP and DOPS liposomes at 300μM. All other liposome treatments including DOPC and mannosylated liposomes at both concentrations and DOTAP and DOPS liposomes at 100μM maintained healthy cell MMPs. Overall this indicated apoptotic and necrotic cell death induced by 120μM valinomycin, DOTAP liposomes at both concentrations but more significantly at the higher 300μM concentration and apoptosis following 24 hour treatment with 300μM DOPS liposomes. DOPC (neutral) and mannosylated liposomes showed no significant changes in cell health compared to untreated negative control RAW 264.7 cells.

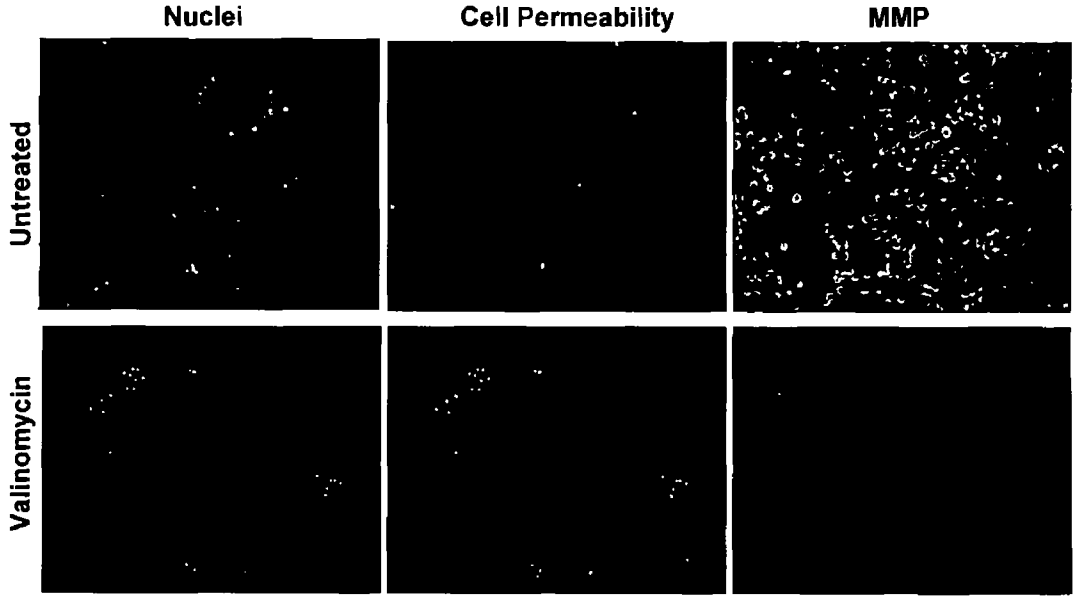


Figure 6.7: High content cell assessment of liposome associated cytotoxicity in RAW 264.7 cells. Fluorescent images were acquired by an INCELL 1000 analyser in 3 channels and show control treatments with cells treated with complete media as a negative control or 120μM valinomycin as a positive control.

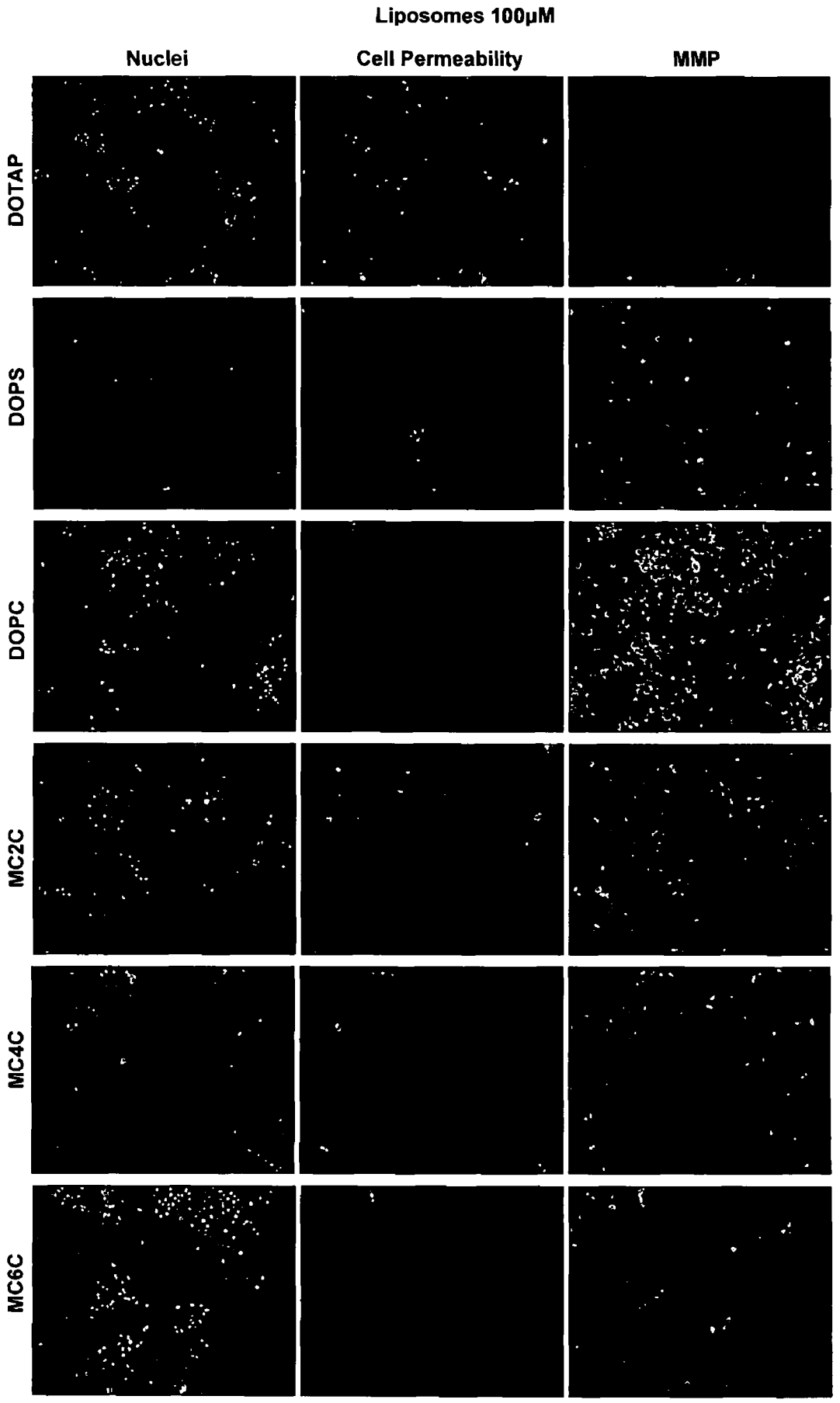


Figure 6.8: High content cell assessment of liposome associated cytotoxicity in RAW 264.7 cells. Fluorescent images were acquired in 3 channels by an INCELL 1000 analyser and show cells treated with 100μM liposomes in complete media for 24 hours.

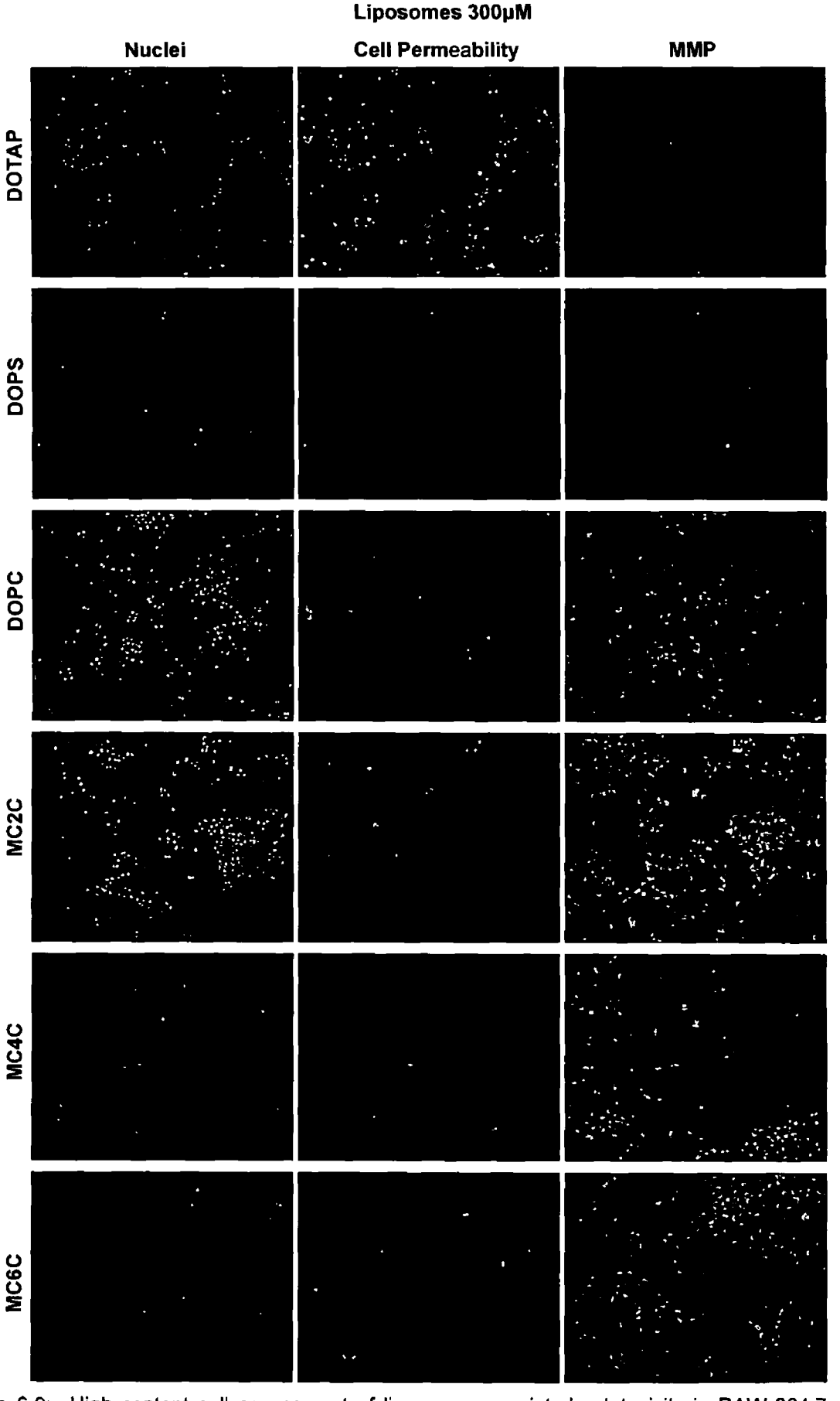


Figure 6.9: High content cell assessment of liposome associated cytotoxicity in RAW 264.7 cells. Fluorescent images were acquired in 3 channels by an INCELL 1000 analyser and show cells treated with 300µM liposomes in complete media for 24 hours.

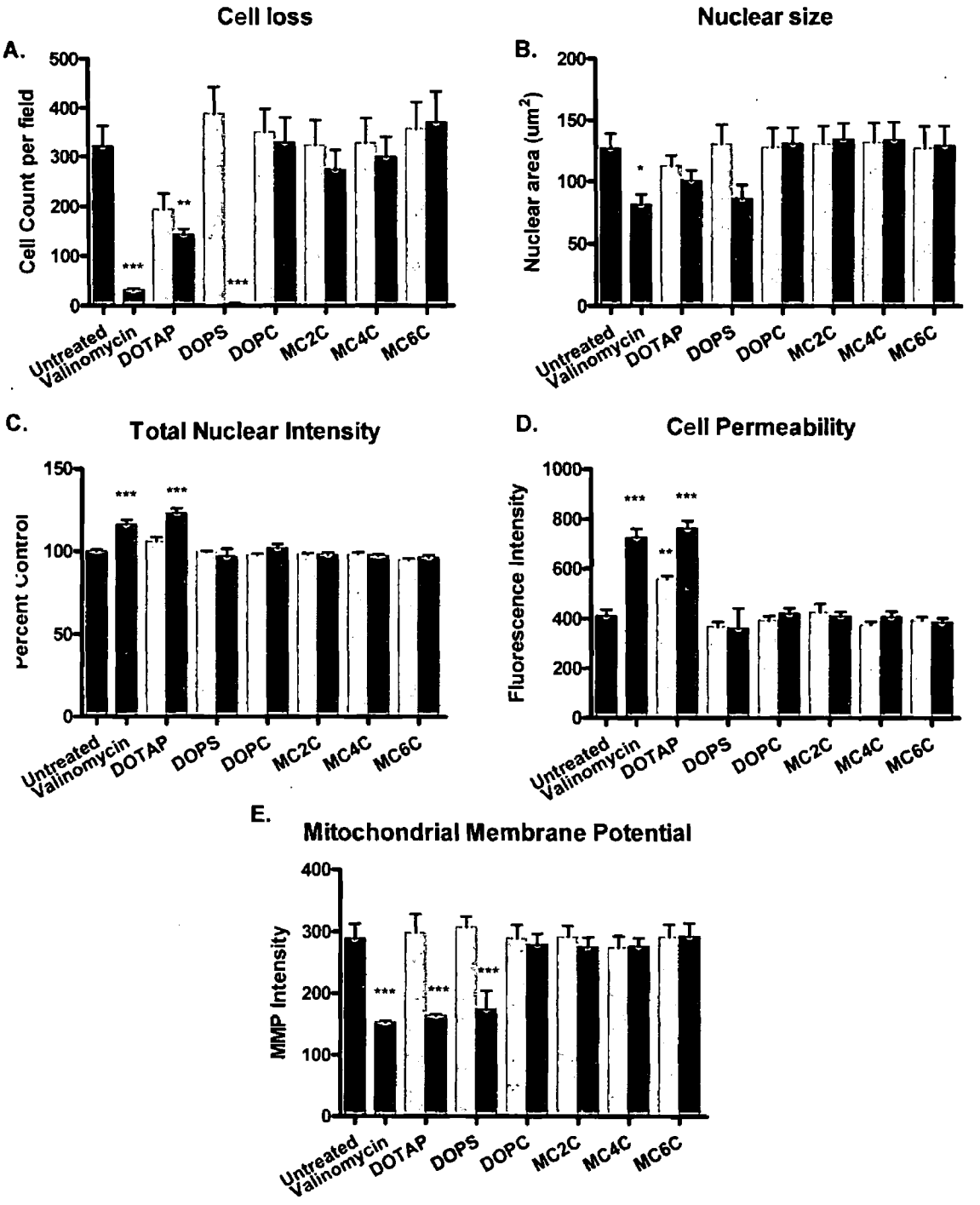


Figure 6.10: High content cell assessment of liposome toxicity in RAW 264.7 cells. RAW 264.7 cells were treated with complete media alone (negative control), 120μM valinomycin (positive control) or liposomes at ☐ 100μM or ▬ 300μM for 24 hours at 37°C. Cells were stained for nuclei (hoescht; blue), cell permeability (green) and mitochondrial membrane potential (MMP; red). Images were acquired and analysed using an INCELL 1000. Cell loss, nuclear size, nuclear intensity, cell permeability and MMP were measured (A - E). Data presented as means ± SD (n = 6). Statistical significance was determined by a two-way ANOVA. * $p < 0.05$, ** $p < 0.01$, *** $p < 0.001$ vs. healthy untreated groups (Bonferrioni's test)

### 6.4.3 *In vitro* Toxicity Assessment of siRNA Encapsulating Liposomes

Toxicity associated with siRNA loaded liposomes was also assessed in RAW 264.7 cells prior to formulation of liposomes for *in vivo* transfection. siRNA was complexed with cationic reagents DOTAP, PEI and protamine each being associated with toxicity [301-304] to improve siRNA encapsulation efficiency. Consequently cytotoxicity of siRNA complex loaded liposomes was also monitored as complexation can dramatically affect the physicochemical properties of a formulation. RAW 264.7 cells were untreated (negative control) or treated with 120μM valinomycin (positive control) or liposomes at 300μM for 24 hours at 37°C. DOPS, DOPC and mannosylated liposomes were either empty or encapsulated non-target siRNA complexed with DOTAP (N/P 4), protamine (weight ratio 4) or 25kDa PEI (N/P 7). DOTAP liposomes were also used as a cationic liposome control. Cells were stained for nuclei, cell permeability and MMP. Images were acquired of controls (Figure 6.7), DOPS liposomes (Figure 6.11), DOPC liposomes (Figure 6.12) and mannosylated liposomes (Figure 6.13) and analysed using an INCELL 1000. Cell loss, nuclear size, nuclear intensity, MMP and cell permeability were determined (Figure 6.14)

300μM DOPS liposomes showed high levels of toxicity with almost complete cell loss. Cell loss was greater than that of the positive control 120μM valinomycin and cationic DOTAP liposomes. Additionally an increase in nuclear size and drop in mitochondrial membrane potential was observed corresponding to a toxic event. The encapsulation of siRNA/DOTAP, siRNA/protamine and siRNA/PEI complexes in DOPS liposomes lessened the degree of toxicity compared to empty DOPS liposomes however DOPS liposomes encapsulating siRNA/PEI complexes exhibited cell loss almost equivalent to DOTAP liposome treatment (Figure 6.11 and 6.14).

Neutral DOPC liposomes showed little toxicity, although a small decrease in mitochrondrial membrane potential was found (Figure 6.12 and 6.14). Additionally a small proportion of cell loss was detected following 24 hour treatment with DOPC liposomes encapsulating siRNA/DOTAP and siRNA/PEI complexes and a decrease in nuclear size following DOPC siRNA/protamine liposomes. Toxic effects were however minimal following DOPC liposome treatment whether empty or encapsulating siRNA complexes.

Overall mannosylated (MC6C) liposomes show similar toxicity profiles to the neutral DOPC liposomes (Figure 6.13 and 6.14). Some cell loss was observed with mannosylated liposomes encapsulating siRNA/protamine and siRNA/PEI complexes with a marginally higher cell loss using protamine as the complexing reagent. This cell loss however is similar to that found in neutral liposome formulation counterparts. Minimal changes are found in nuclear size and intensity with a minor decrease in mitochondrial membrane potential following treatment with siRNA/protamine complex loaded mannosylated liposomes.

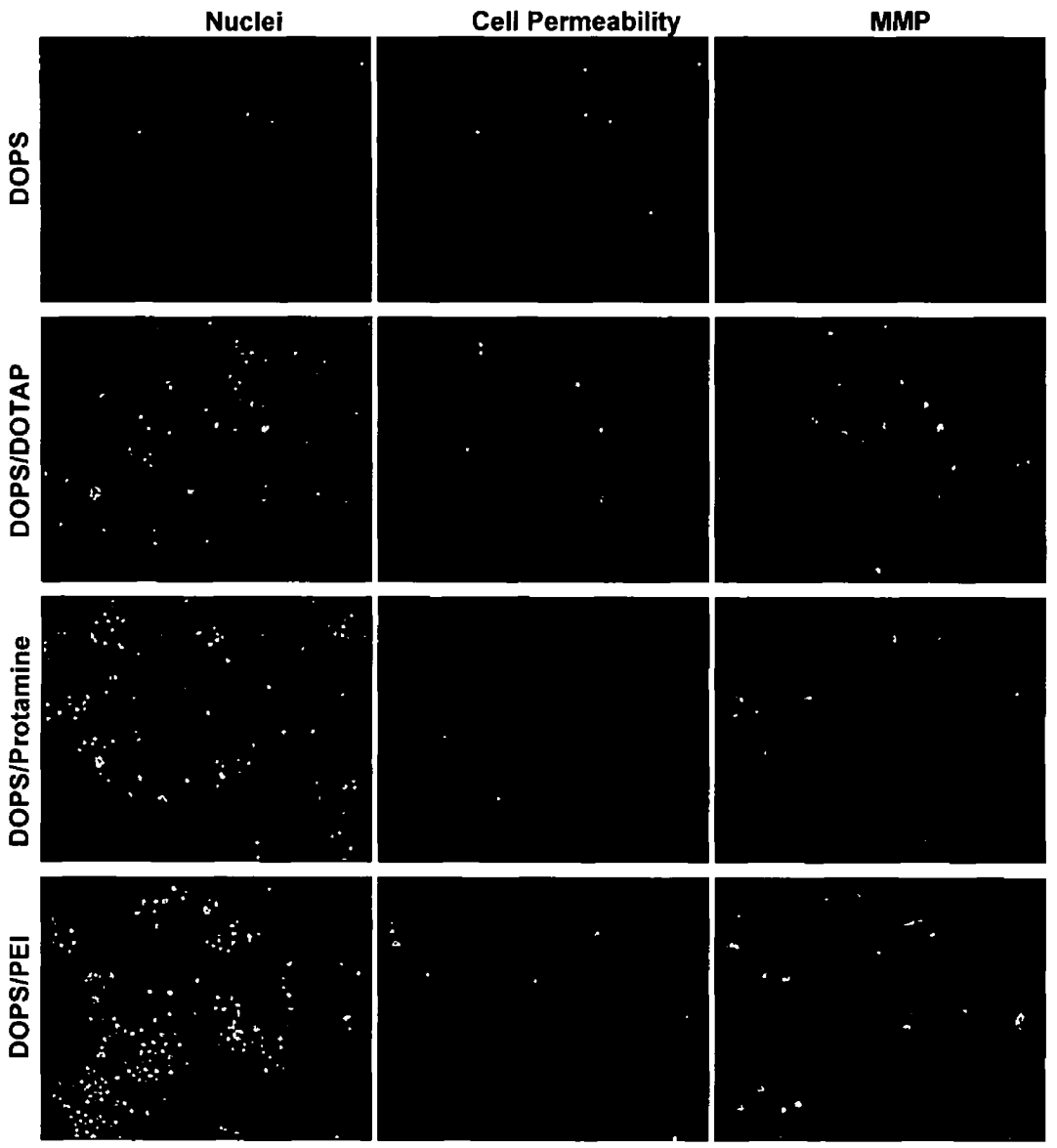


Figure 6.11: High content cell assessment of toxicity in RAW 264.7 cells induced by DOPS liposomes encapsulating siRNA complexes. RAW 264.7 cells were treated with 300μM empty DOPS liposomes or DOPS liposomes encapsulating siRNA complexed with DOTAP (N/P 4), protamine (weight ratio 4) or PEI (N/P 7) for 24 hours. Cells were stained for nuclei (hoescht), cell permeability and mitochondrial membrane potential (MMP). Images were acquired and analysed using an INCELL 1000.

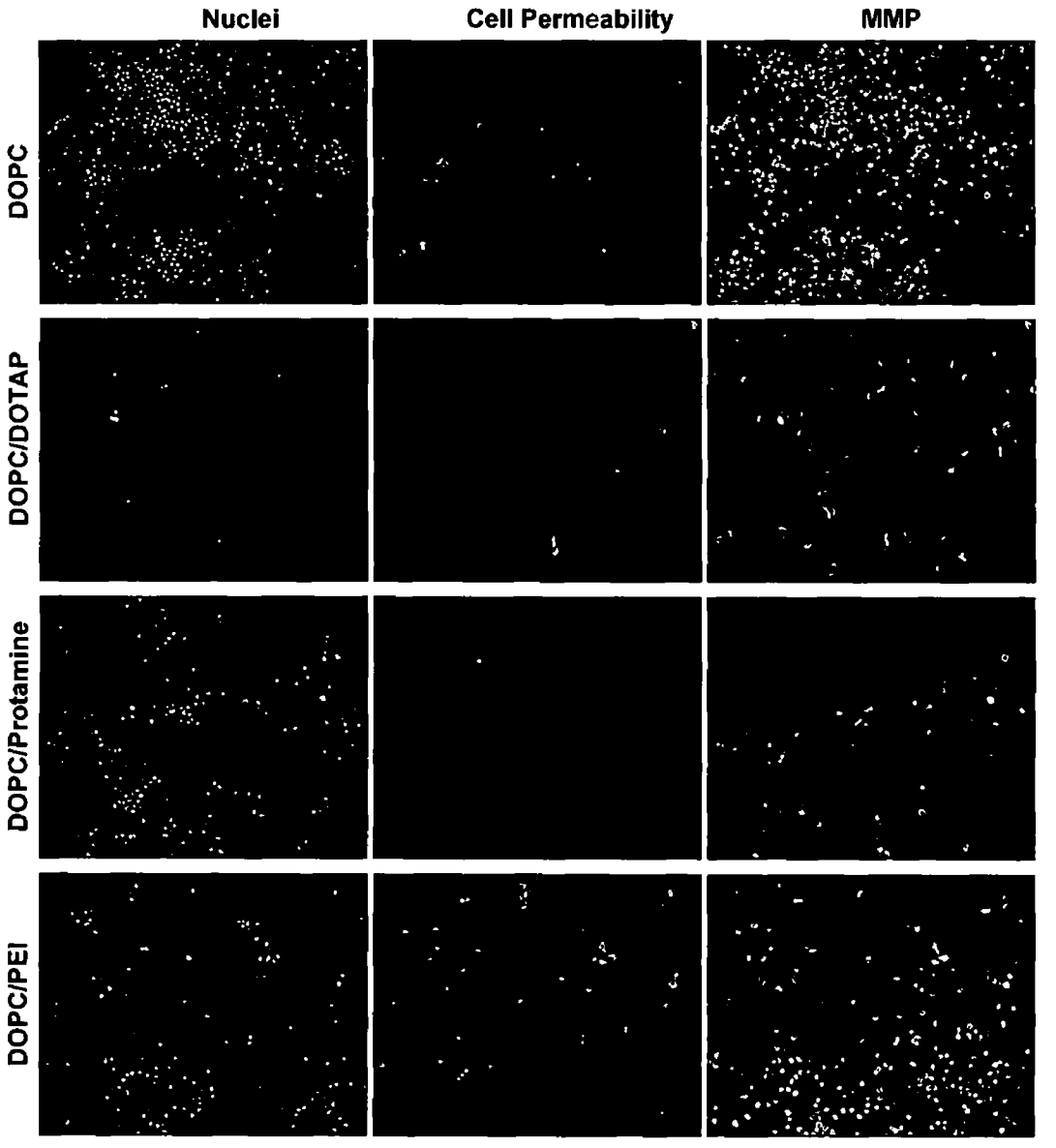


Figure 6.12: High content cell assessment of toxicity in RAW 264.7 cells induced by DOPC liposomes encapsulating siRNA complexes. RAW 264.7 cells were treated with 300μM empty DOPC liposomes or DOPC liposomes encapsulating siRNA complexed with DOTAP (N/P 4), protamine (weight ratio 4) or PEI (N/P 7) for 24 hours at 37°C. Cells were stained for nuclei (hoescht), cell permeability and mitochondrial membrane potential (MMP). Images were acquired and analysed using an INCELL 1000 at 100x magnification.

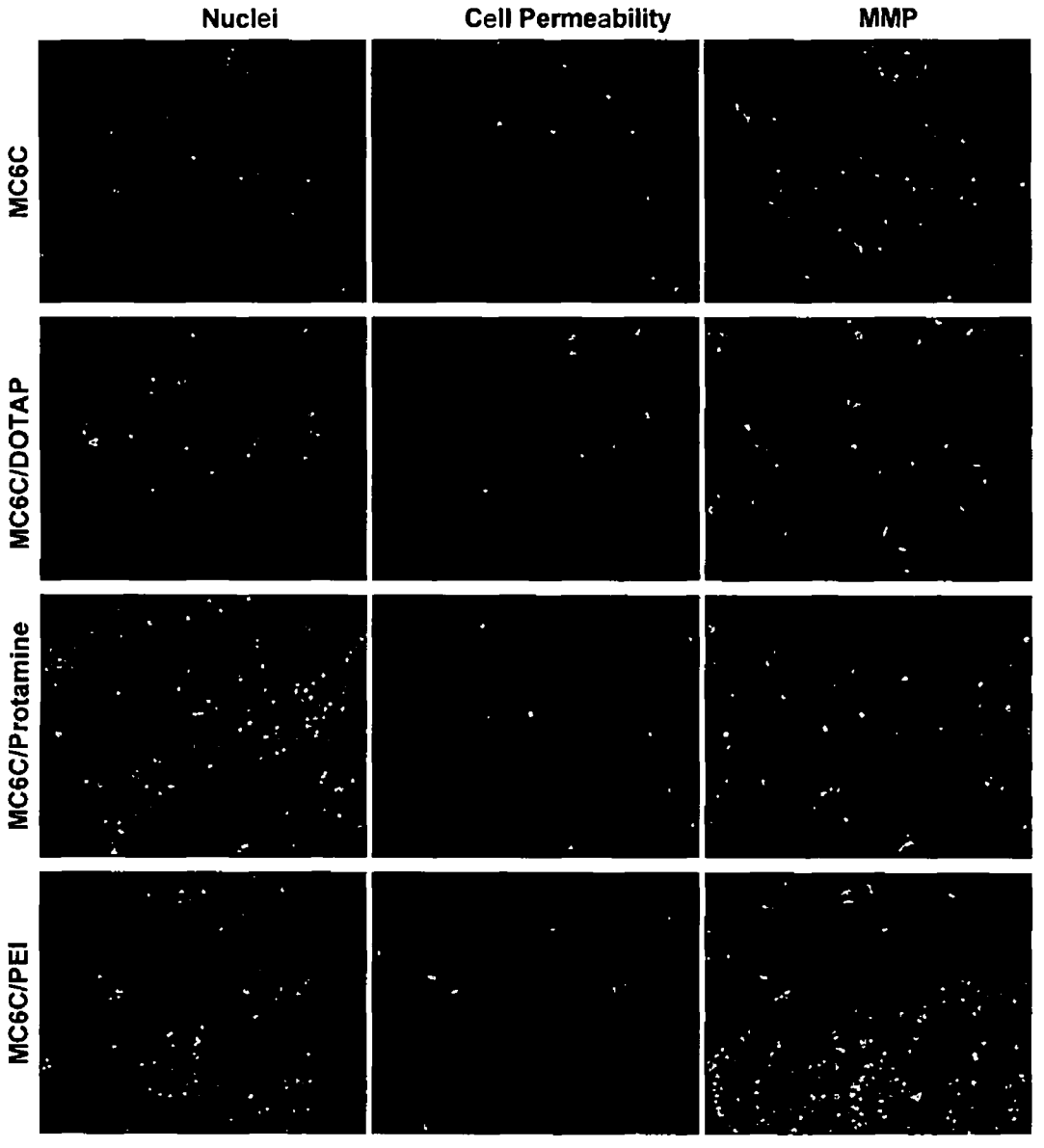


Figure 6.13: High content cell assessment of toxicity in RAW 264.7 cells induced by mannosylated (MC6C) liposomes encapsulating siRNA complexes. RAW 264.7 cells were treated with 300μM empty MC6C liposomes or MC6C liposomes encapsulating siRNA complexed with DOTAP (N/P 4), protamine (weight ratio 4) or PEI (N/P 7) for 24 hours at 37°C. Cells were stained for nuclei (hoescht), cell permeability and mitochondrial membrane potential (MMP). Images were acquired and analysed using an INCELL 1000 at 100x magnification.

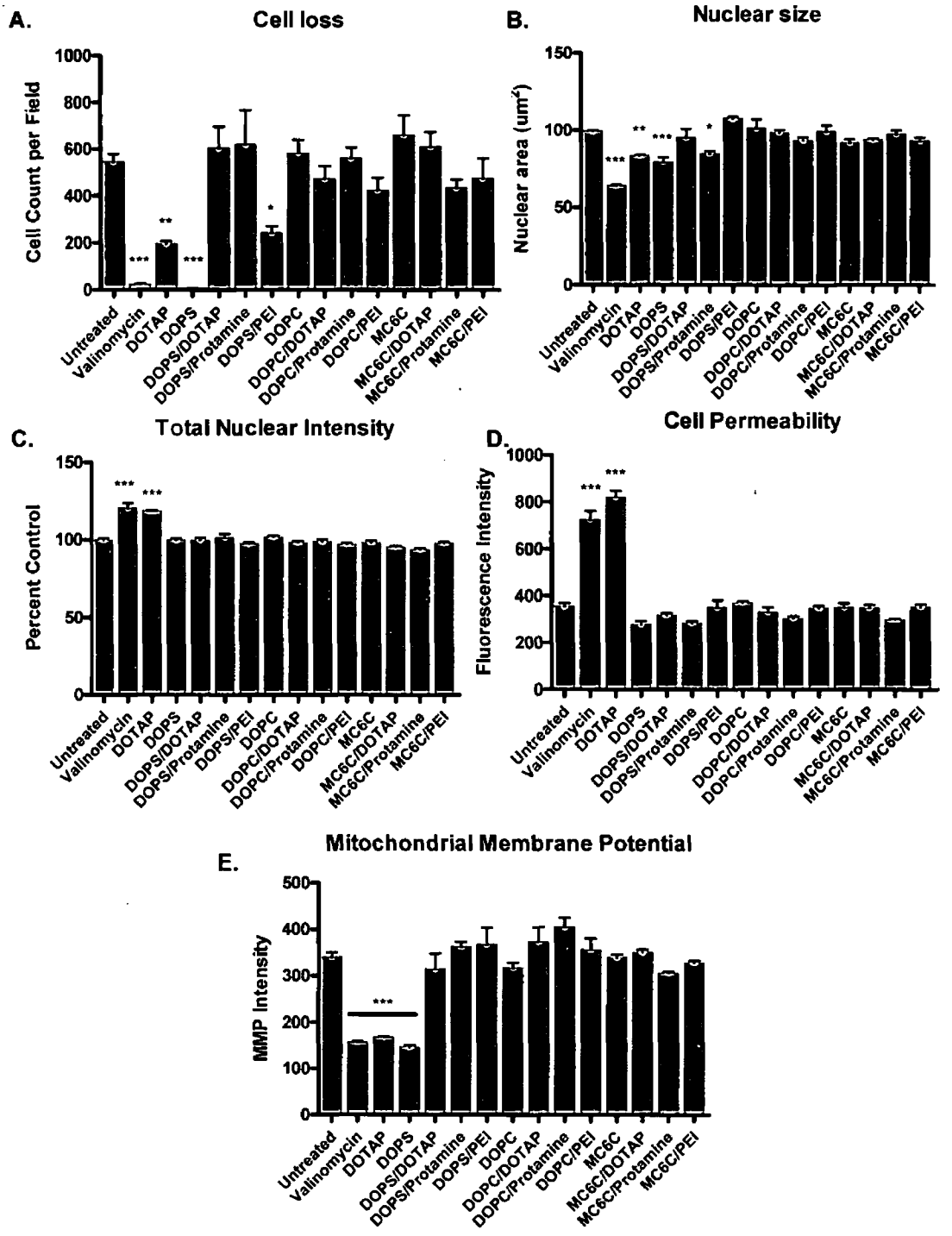


Figure 6.14: High content cell assessment of liposome toxicity in RAW 264.7 cells. RAW 264.7 cells were untreated (negative control), 120μM valinomycin (positive control) or liposomes at 300μM for 24 hours at 37°C. Liposomes were either empty or encapsulated non-target siRNA complexed with DOTAP (N/P 4), protamine (weight ratio 4) or 25kDa PEI (N/P 7). Cells were stained for nuclei (hoescht), cell permeability and mitochondrial membrane potential (MMP). Images were acquired and analysed using an INCELL 1000. Cell loss, nuclear size, nuclear intensity, cell permeability and MMP were measured (A - E). Data presented as means ± SD (n = 3). Statistical significance was determined by one-way ANOVA. * $p < 0.05$, ** $p < 0.01$, *** $p < 0.001$ vs. healthy untreated groups (Dunnetts test)

### 6.4.4 TNFα siRNA Sequence Comparisons

Prior to *in vivo* studies knockdown of TNFα was assessed *in vitro* using three commercially available siRNA sequences targeted to mouse TNFα in order to determine the optimal sequence for *in vivo* use. Transfections were carried out using HiPerFect transfection reagent in mouse RAW 264.7 cells which is suitable for macrophage transfection with protocols optimised for RAW 264.7 cell siRNA transfections. Initially knockdown was assessed 24, 48 and 72 hours post-transfection however an effect was only detected after 24 hours (Figure 6.15). TNFα1 and TNFα2 sequences lead to knockdown of TNFα expression after 24hours whilst TNFα3 siRNA enhanced TNFα secretion following LPS stimulation. Subsequent induced TNFα expression was determined 24 hours post-transfection.

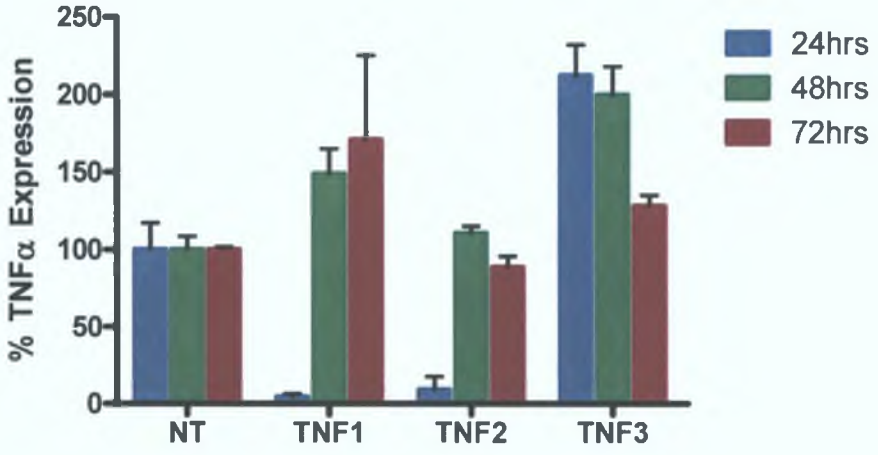


Figure 6.15: *In vitro* modulation of TNFα expression in RAW 264.7 cells using HiPerFect transfection reagent and three TNFα targeted siRNA sequences. RAW 264.7 cells were transfected with 375ng of non-target siRNA or one of three TNFα targeted siRNAs (TNFα1, TNFα2 or TNFα3). 24, 48 and 72 hours post-transfection cells were stimulated with 100ng/ml LPS for 3 hours and TNFα expression determined. Expression is represented as % of non-target siRNA transfected controls. Data is represented as means ± SD (n = 3)

HiPerFect mediated transfection of RAW264.7 cells was determined at 24 hours. Cells were stimulated with LPS for 3 hours and TNFα expression measured. As was previously seen in Figure 6.15 TNFα1 and TNFα2 siRNAs decreased TNFα induction while TNFα3 increased TNFα expression. TNFα expression was decreased to 34 ± 32.8% and 52.7 ± 55.6% following HiPerFect mediated transfection of TNFα1 and TNFα2 siRNA respectively compared to non-target siRNA transfected cells (Figure 6.16). TNFα expression by cells transfected with TNFα3 siRNA was increased 2-fold compared to non-target siRNA transfected controls. This validates TNFα1 siRNA together with a 24 hour transfection optimal for subsequent *in vivo* transfections.

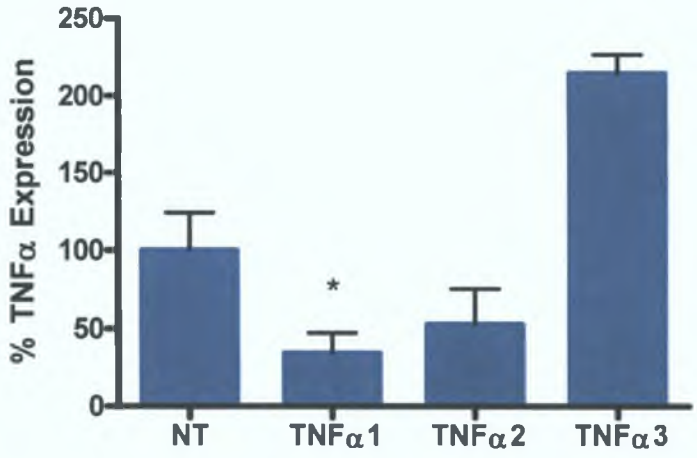


Figure 6.16: *In vitro* modulation of TNFα expression in RAW 264.7 cells using HiPerFect transfection reagent and three TNFα targeted siRNA sequences. RAW 264.7 cells were transfected with 375ng of non-target siRNA or one of three TNFα targeted siRNAs (TNFα1, TNFα2 or TNFα3). 24 hours post-transfection cells were stimulated with 100ng/ml LPS for 3 hours and TNFα expression determined. Expression is represented as % of non-target (NT) siRNA transfected controls.
Data is represented as means ± SD (n = 6).
Statistical significance was determined by unpaired students t-test. * $p < 0.05$ vs. NT siRNA transfected control

### 6.4.5 *In Vivo* Testing of siRNA Liposomes

#### 6.4.5.1 Size and Zeta Potential of siRNA Mannosylated (MC6C) Liposomes

Each batch of liposomes for *in vivo* use was characterised to ensure reproducibility. Mannosylated liposomes for *in vivo* administration showed post-extrusion diameter sizes of 280.4 ± 62 nm, 214.4 ± 3 nm and 188 ± 4 nm for empty, NT siRNA and TNFα siRNA encapsulating liposomes respectively (Table 6.4). Zeta potentials for siRNA complex encapsulating liposomes were less than empty liposomes. Overall zeta potentials were very positive and less than +65mV (Table 6.4). Prior to extrusion zeta potentials were above +70mV.

**Table 6.4 *In Vivo* Mannosylated liposome sizes and zeta potentials (Means ± SD)**

| Liposome | Size (d.nm) | PDI | Zeta Potential (mV) |
|---|---|---|---|
| Empty Mannosylated Liposomes | 280.4 ± 62 | 0.304 | 64.1 ± 3 |
| Non-target siRNA/PEI Mannosylated Liposomes | 214.4 ± 3 | 0.244 | 58.9 ± 2 |
| TNFα siRNA/PEI Mannosylated Liposomes | 188 ± 4 | 0.166 | 56 ± 1 |

#### 6.4.5.2 Validation of *In Vivo* Pulmonary Administration

Evan's blue is frequently used to measure vascular permeability for example across the blood brain barrier and in the lungs but also to determine the accuracy of delivery [286]. Initially, 2% Evan's blue dye was used to establish the effectiveness of the intratracheal method used in delivery of liquid formulations to the lungs prior to immunogenicity and knockdown studies. This showed a good distribution of the dye throughout the lungs and confirmed delivery to the lungs via the trachea as opposed to the stomach via the oesophagus. Intratracheal administration is a difficult procedure and therefore it was important for the technique to be as accurate and reproducible as possible before siRNA experiments were carried out. Mice were instilled with saline, siRNA or liposomes and after 24 hours received saline or LPS via the trachea followed 3 hours later by euthanasia. For day two saline treated groups' immunogenicity screens to naked siRNA and mannosylated liposomes were acquired. Although this was only an acute study, weights of mice were closely monitored and treatments did not cause any observable changes in animal health.

### 6.4.6 *In Vivo* Mannosylated Liposome Transfection

#### 6.4.6.1 Bronchoalveolar Lavage (BAL)

Mice received saline, siRNA or siRNA/liposomes by intratracheal administration followed by LPS after 24 hours. BAL was collected 3 hours following LPS instillation and BAL cells were counted and identified. Differences in total cell counts per treatment group were non-significant. In general LPS increased the number of BAL cells compared to saline however mannosylated liposomes both empty and encapsulating NT siRNA showed higher cell counts without LPS than with LPS treatment. Although a decrease in cell number was observed in NT siRNA and all mannosylated liposome treated groups particularly mice treated with mannosylated liposomes encapsulating TNFα siRNA (37.5 ± 13 ($10^4$) cells/ml) compared to saline/LPS treated controls (63.3 ± 49 ($10^4$) cells/ml). Additionally a decrease in cell number was observed following treatment with liposomes encapsulating TNFα siRNA compared to naked TNFα siRNA in LPS treated groups.

Neutrophils and macrophages were the only cell types identified in BAL (Figure 6.17). Macrophages were the predominant cell type identified and were found in abundance even in saline controls. Neutrophil presence was highest in groups receiving saline followed by LPS with low numbers counted in all other treatment groups. Treatment with liposomes encapsulating TNFα siRNA showed reduced levels of macrophages compared to naked and liposome encapsulated NT siRNA and naked TNFα siRNA treated groups. Furthermore neutrophil presence was lower following mannoyslated liposome encapsulated TNFα siRNA administration compared to naked TNFα siRNA.

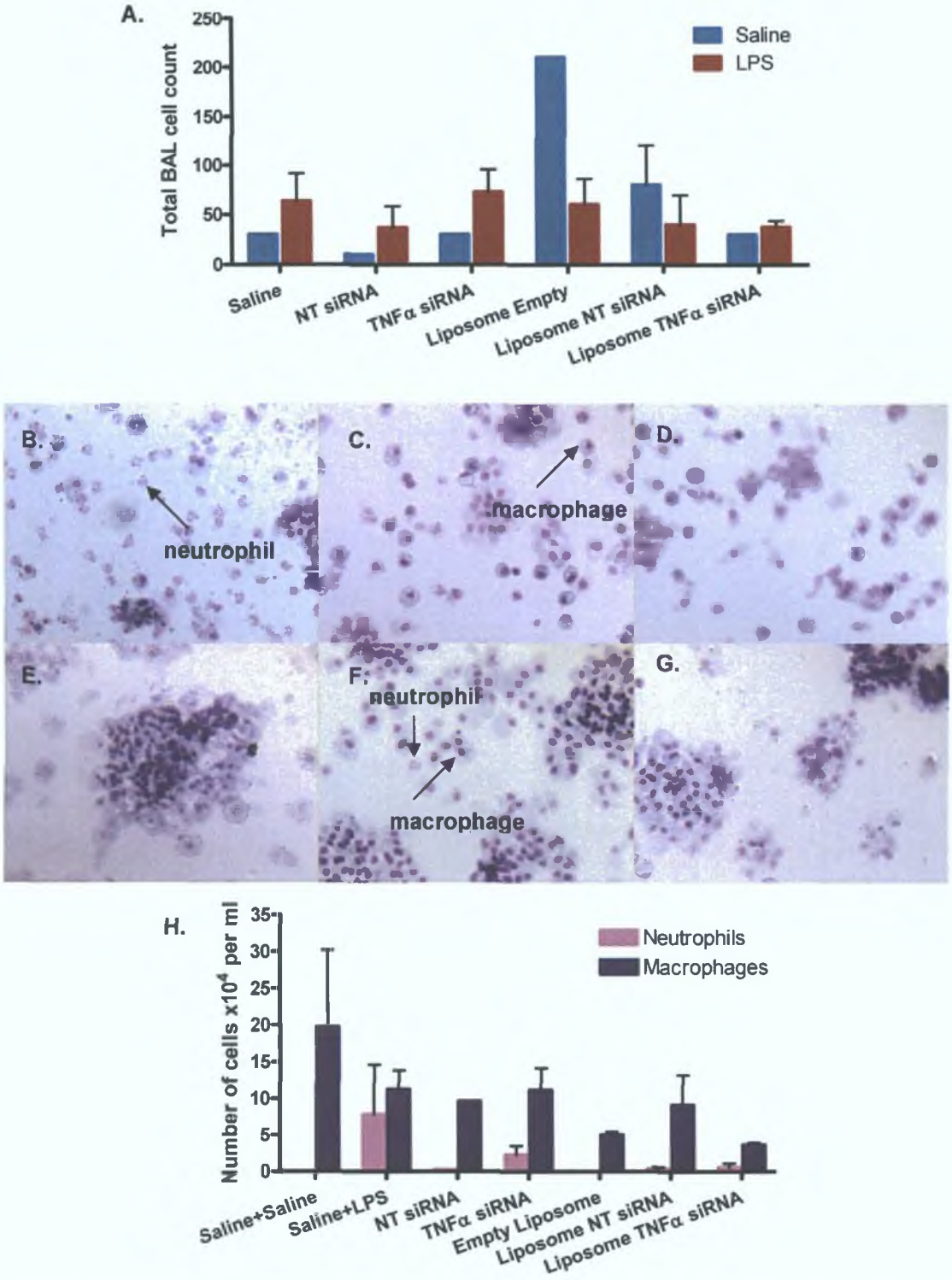


Figure 6.17: Bronchoalveolar lavage (BAL) cell differentiation from LPS stimulated mice. Total BAL cell counts were taken from saline and LPS (Day 2) treated groups using a haemocytometer (A). BAL cells were fixed in methanol and stained with Eosin Y and azur/methylene blue. Bright field images were acquired at 20x from C57BL/6 mice treated for 24 hours (Day 1) with (B) saline, (C) non-target (NT) siRNA, (D) TNFα targeted siRNA, (E) empty mannosylated liposomes, (F) mannosylated liposomes encapsulating NT/PEI complexes and (G) mannosylated liposomes encapsulating TNFα/PEI complexes (N/P ratio 7) followed by 3 hour (Day 2) LPS treatment. Macrophages and neutrophils were identified and counted (H).

### 6.4.6.2 TNFα knockdown and Cytokine Expression

Following siRNA or mannosylated liposome treatment mice were also treated with LPS. This was to stimulate an inflammatory response in the lung and assess the effectiveness of TNFα targeted siRNA to specifically suppress TNFα expression. In addition a comparision between the effectiveness of naked TNFα siRNA to liposome encapsulated siRNA could be made. To date there have been very few *in vivo* studies delivering siRNA to the lungs (Table 6.1 shows *in vivo* studies to date using intratracheal administration). Doses of siRNA have ranged from 1.33μg to 665μg via intratracheal administration. Our study was limited by the maximum tolerable volume that could be administered which was 50μl. Liposomes prepared in chapter 3 for *in vitro* experiments encapsulated a maximum of 1μM siRNA or almost 0.7μg per μi of liposome formulation. A starting dose of 30μg was selected as a similar dose had been used most frequently in previous studies. For these *in vivo* studies liposomes were prepared 2.5 times more concentrated than for *in vitro* studies in order to compensate for a higher siRNA loading. Additionally liposome preparations this concentrated had been administered previously *in vivo*.

Mice received either saline, siRNA or liposomes (day 1) and 24 hours later LPS for 3 hours (day 2) intratracheally. BALF cytokine levels were variable within treatment groups but similar between groups. siRNA naked or encapsulated in mannosylated liposomes was targeted to the pro-inflammatory cytokine TNFα with controls of non-target siRNA. TNFα expression levels were decreased following administration of naked TNFα siRNA and all liposome treatments most notably TNFα siRNA loaded mannosylated liposomes (Figure 6.18A). The decrease in expression was not significant due to a large variability with the treatment groups. It should be noted that the longer the time between preparation of liposomes and administration the less effective the formulation was in lowering TNFα protein levels. Figure 6.18E shows the percentage knockdown of TNFα in the various treatment groups with TNFα siRNA and mannosylated liposomes encapsulating TNFα siRNA yielding the most apparent TNFα knockdown.

The secretion of other major markers of inflammation including IL-1β, KC and MIP-2 not targeted by siRNA were measured in BALF (Figure 6.18). IL-1β induction was lessened following siRNA and mannosylated liposome administration compared to the control saline treatment (Figure 6.18B). Empty liposomes and liposomes encapsulating TNFα siRNA/PEI complexes showed a marginally higher IL-1β level than other siRNA and liposome treated groups.

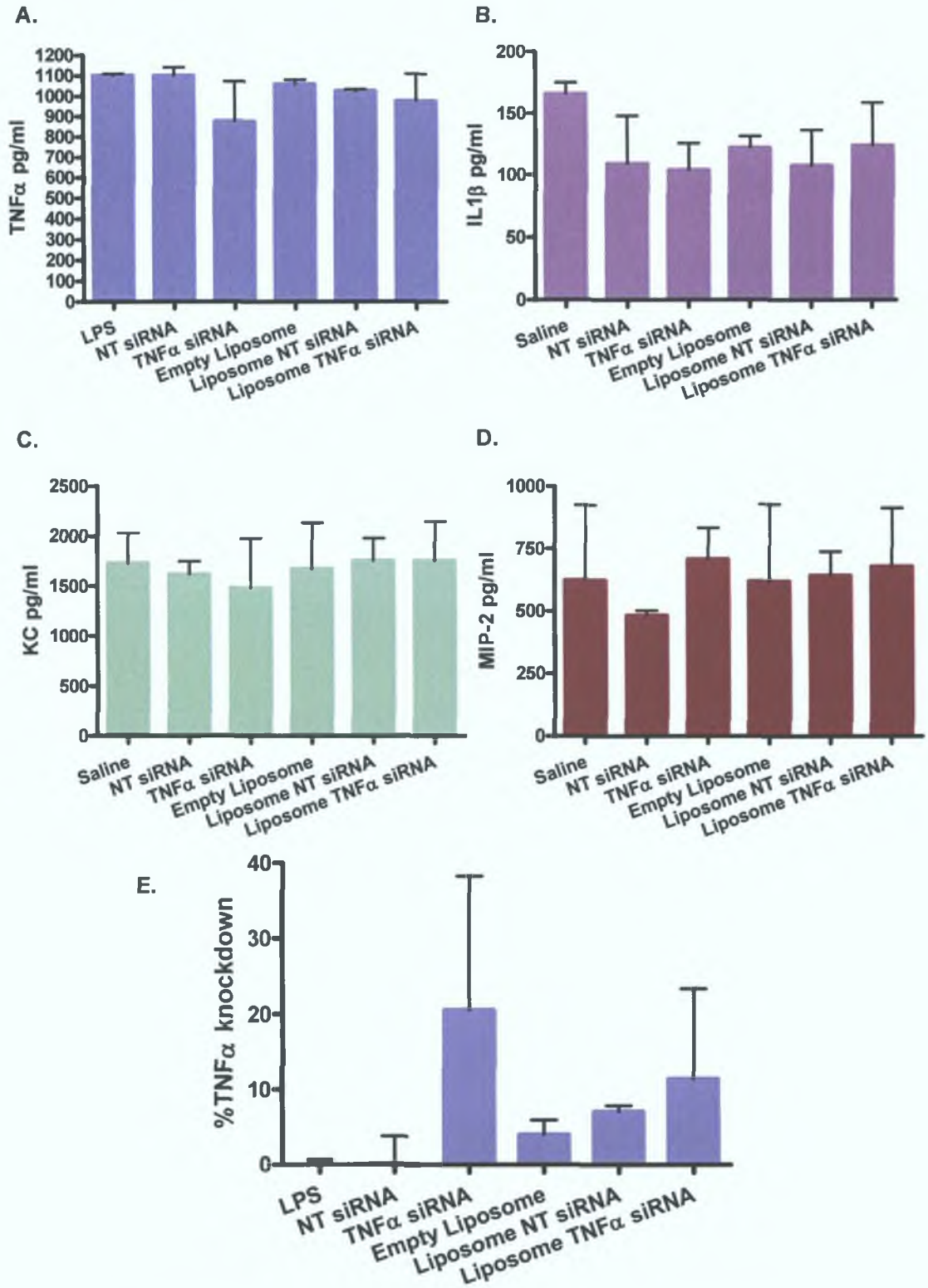


Figure 6.18: Bronchoalveolar lavage (BAL) cytokine expression in mice following 3 hour LPS treatment. C57 mice received saline, non-target siRNA (NT siRNA), TNFα targeting siRNA, empty mannoslyated liposomes or mannosylated liposomes encapsulating either NT siRNA or TNFα siRNA complexed with PEI (N/P 7) via intratracheal administration. After 24 hours 0.4mg/ml LPS was intratracheally administered for 3 hours and BAL was collected. Proinflammatory cytokine expression was determined of TNFα (A), IL-1β (B), KC (C) and MIP-2 (D). The percentage of TNFα knockdown was determined (F).

#### 6.4.6.3 Histopathology

Haemotoxylin and eosin stained lung sections from C57 mice were semi-quantitatively scored as shown in Table 6.5 and Figure 6.19. Mice received LPS via intrachael administration following 24 hour treatment with saline, siRNA or siRNA mannosylated liposomes. Histopathology showed the degree of inflammation through structural changes such as cell infiltration and blood vessel leakage. The effect of TNFα targeted siRNA on overall LPS induced lung inflammation could therefore be evaluated. Mild neutrophil-rich inflammation was observed following LPS administration with saline control showing an absence of inflammation and mannosylated liposomes encapsulating non-target siRNA complexed with PEI exhibiting very mild inflammation.

**Table 6.5 Histopathology Semi-quantitative scores**

| Treatment Group | | Degree of Neutrophil-rich Inflammation |
|---|---|---|
| Day 1 (24hrs) | Day 2 (3hrs) | |
| Saline | Saline | - |
| Saline | LPS | + |
| Non-target siRNA | LPS | + |
| TNFα siRNA | LPS | + |
| Non-target siRNA/PEI Mannosylated Liposomes | LPS | -/+ |
| TNFα siRNA/PEI Mannosylated Liposomes | LPS | + |

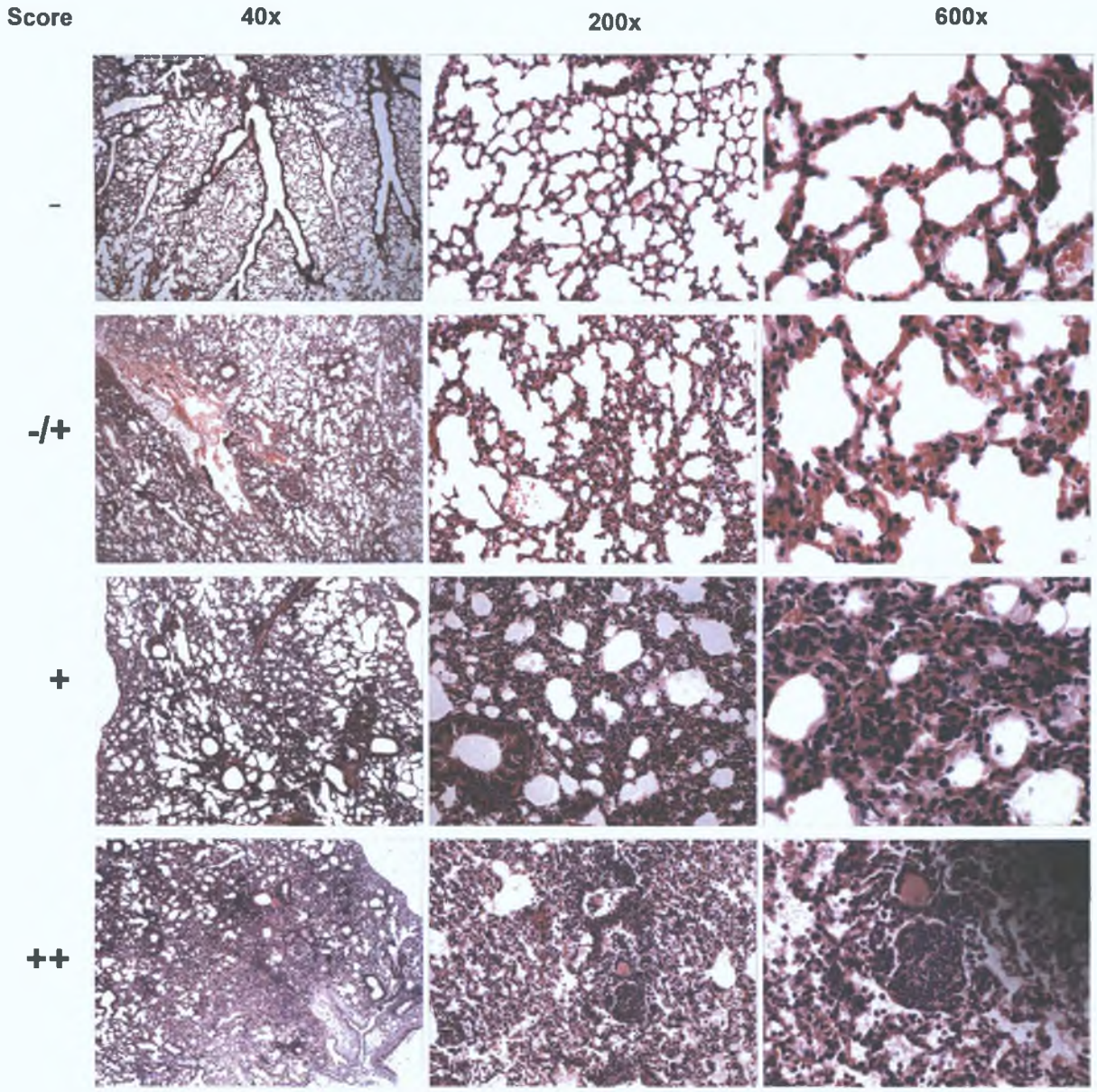


Figure 6.19: Photomicrographs representative of pulmonary histolopathology semi-quantitative scoring of neutrophil-rich inflammation. Haemotoxylin and eosin stained lung sections from saline, siRNA and mannoyslated liposome treated mice were scored based on the degree of neutrophil-rich inflammation observed (- absent, -/+ very mild, + mild and ++ moderate). Images were acquired at 40x, 200x and 600x magnification.

### 6.4.7 Effect of Mannosylated Liposomes on Immune Responses in the Lung

#### 6.4.7.1 Bronchoalveolar Lavage (BAL) cells

BAL cells were counted and total cell counts per ml calculated (Figure 6.20E) from mice treated for 24 hours with saline, saline followed by LPS (3 hours), non-target siRNA, TNFα siRNA, empty mannosylated (MC6C) liposomes, liposomes encapsulating non-target siRNA/PEI complexes and mannosylated liposomes encapsulating TNFα siRNA/PEI complexes. A marked increase in cell number was found following empty mannosylated liposome treatment. This increase was far greater than 24 hour saline followed by a 3 hour LPS treatment (the positive control).

The majority of BAL cells identified were macrophages (Figure 6.20A). A notable increase in macrophage presence was found following 24 hour treatment with empty mannosylated liposomes (Figure 6.20B). Neutrophils were also present mainly following LPS treatment and treatment with empty mannosylated liposomes.

Treatment groups of 30μg siRNA alone were n = 1 for some analysis methods and therefore a more accurate representation of the immunological response would require an increase in the n number. Liposome treatments were in general n = 2 -3 however for total cell count of the empty liposome treated group a lot of debris was collected in BALF from one animal. It was difficult to distinguish cells accurately and therefore data for this sample was omitted. Additionally a number of cell differential slides did not stain optimally and cells were not easily identifiable which reduced n numbers for these counts in some groups.

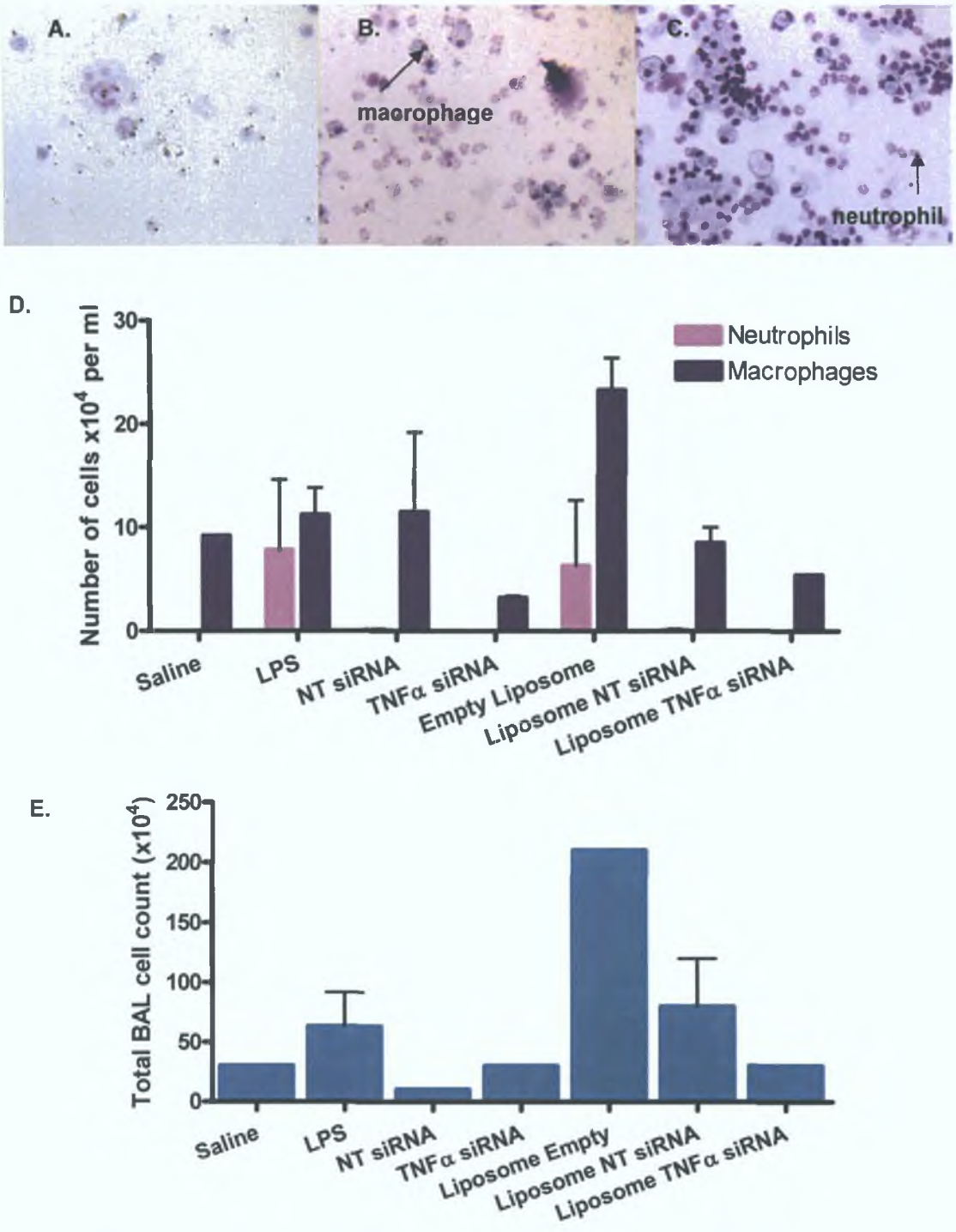


Figure 6.20: *Bronchoalveolar* lavage (BAL) cell differentiation collected from siRNA and liposome treated mice. Total BAL cell counts were taken using a haemocytometer (*E*). BAL cells were fixed in methanol and stained with Eosin Y and azur/methylene blue. Representative bright field images were acquired at 20x from C57 mice treated for 24 hours with (A) saline, (B) saline followed by 3 hour LPS treatment and (C) empty mannosylated liposomes. Macrophages and neutrophils were identified and counted (D).

### 6.4.7.2. Local and Systemic TH1/TH2 Response to siRNA and Mannosylated Liposomes

A range of cytokines and chemokines involved in TH1 and TH2 immune responses were detected by a multi-spot ultrasensitive assay in mouse BALF and plasma. Mice were intratrachaelly instilled with saline, non-target siRNA, TNFα targeted siRNA, empty mannosylated (MC6C) liposomes, non-targeted siRNA/PEI complexes encapsulated in mannosylated liposomes or TNFα siRNA/PEI complexes encapsulated in mannosylated liposomes and sacrificed 24 hours later. A summary of treatments and TH1/TH2 responses are shown in Table 6.6. LPS was intratracheally administered for 3 hours to show an acute TH1/TH2 response. Figure 6.21 shows the cytokine profiles in BALF and plasma following saline treatment for 24hour followed either by saline or LPS for 3hrs. Following saline administration cytokine concentrations are very low with BALF and plasma KC and IL-12 having the highest expression levels. LPS induced TNFα production in BALF but not in plasma therefore validating the animal model. KC, IL-10 and IL-12 expression was increased in BALF and plasma following the 3 hour LPS challenge. These immune mediators are mainly produced by macrophages.

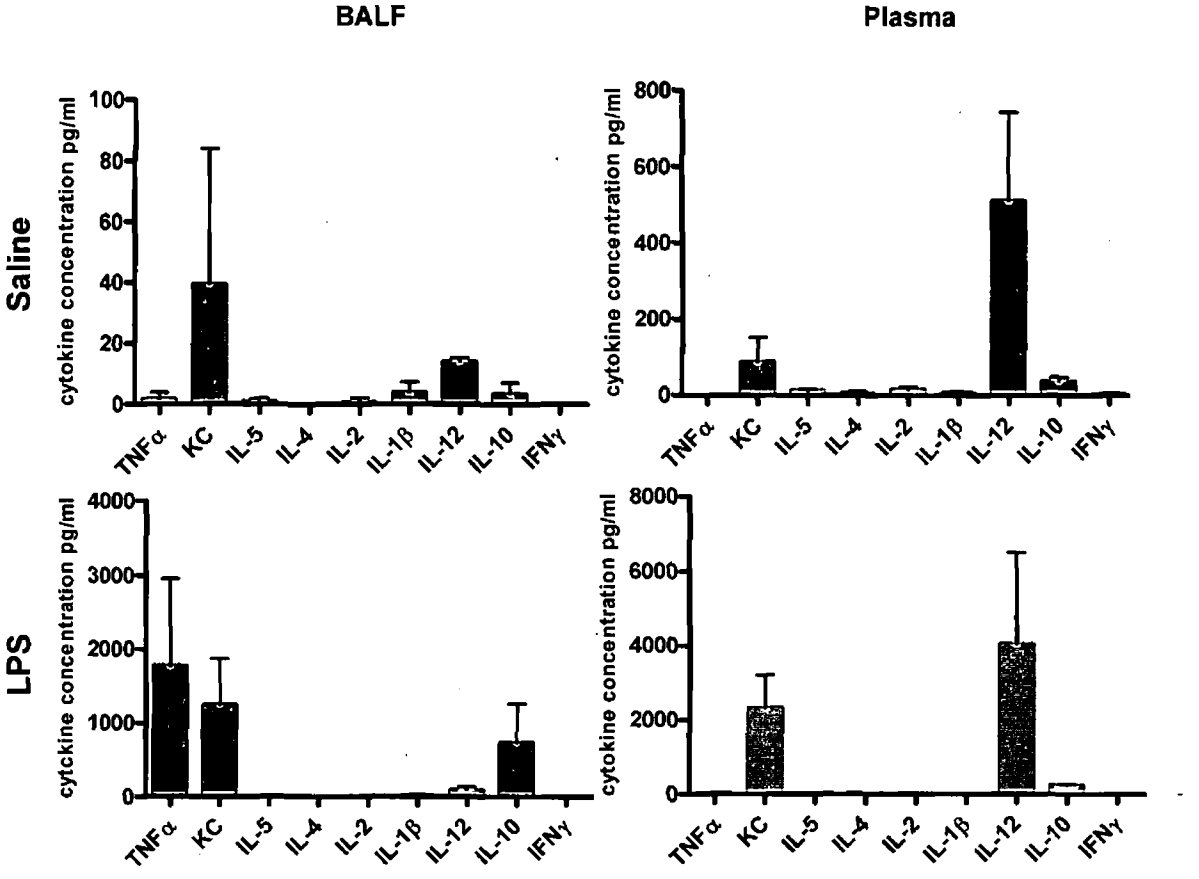


Figure 6.21: TH1/TH2 response in mice following saline and/or LPS intratracheal instillation. Saline was administered for 24 hours followed by saline or LPS for 3 hours. BALF and plasma cytokine profiles were determined using a Th1/Th2 cytokine 9-plex multi spot assay. Data represented as means ± SD (n = 3)

An acute 3 hour LPS challenge to the lungs produced a balanced Th1/Th2 response with all measured cytokines induced in the lung when compared to saline alone. The negative control saline treated groups set the baseline or normal lung cytokine levels and allow the effect of treatments on cytokine levels to be established. IFNγ, IL-2 and IL-5 were not increased systemically. However, as blood was stored on ice haemolysis occurred and therefore lipids present in the plasma samples due to haemolysis could interfere with the assay. Additionally, only siRNA alone and liposomes encapsulating TNFα siRNA treatment groups were n = 1 for Th1/Th1 immunogenic studies. Proteins particularly in BALF can adhere to labware and so MSD recommend adding a carrier protein such as BSA upon sample collection to reduce any protein loss. A carrier protein had not been added until immediately prior to analysis by the MSD multispot assay.

Non-target (NT) siRNA caused IFNγ induction in the lung while increasing levels of IFNγ, IL-4, IL-5 and IL-10 in the plasma (Table 6.6 and Figure 6.22). This shows a predominantly Th2 response systemically. TNFα siRNA on the other hand showed no effect on cytokine levels in BALF or plasma. Empty mannosylated liposomes delivered to the lungs induced all measured cytokines in the lungs after 24 hours however systemic expression was unaltered when compared to saline negative control. Mannosylated liposomes encapsulating NT siRNA/PEI complexes showed a similar response to NT siRNA inducing lung IFNγ, IL-4 and IL-5 and systemic IFNγ, IL-4 and IL-10. Induction of IL-5 was confined to the lung when NT siRNA was encapsulated in the mannosylated liposome. TNFα siRNA encapsulated in liposomes also showed a similar induction profile to TNFα alone whereby little or no Th1/Th2 response was detected. Only a moderate increase in lung IL-4 was measured. Both naked TNFα siRNA and TNFα siRNA/PEI complexes encapsulated in mannosylated liposomes showed no induction of lung IFNγ while NT siRNA and empty or NT siRNA loaded mannosylated liposomes showed increased IFNγ production compared to negative saline controls.

**Table 6.6: Summary of TH1/TH2 Response in Mice Following Saline, siRNA and Mannosylated Liposome Administration** (Data represented as means ± SD)

| Treatment | | | TH1 | | | | | | TH2 | | |
|---|---|---|---|---|---|---|---|---|---|---|---|
| *Day 1 (24hrs)* | *Day 2 (3hrs)* | | TNFα | IL-1β | IL-2 | IL-12 | IFNγ | KC | IL-4 | IL-5 | IL-10 |
| Saline | Saline | *BALF* | 1.8 ± 2.2 | 4.0 ± 3.3 | 0.7 ± 1.5 | 13.9 ± 1.3 | 0 ± 0 | 39.5 ± 44.5 | 0.0 ± 0.1 | 1.0 ± 0.9 | 3.4 ± 3.6 |
| | | *Plasma* | 1.3 ± 1.4 | 7.3 ± 1.6 | 15.5 ± 6.6 | 511.1 ± 232.2 | 5.4 ± 2.8 | 87.4 ± 65.1 | 7.3 ± 4.3 | 12.6 ± 3.5 | 36.8 ± 10.7 |
| Saline | LPS | *BALF* | 1775.9 ± 1179.9 | 17.9 ± 9.6 | 8.5 ± 6.2 | 90.9 ± 40.6 | 1.0 ± 0.8 | 1240.8 ± 627.1 | 1.3 ± 1.0 | 2.6 ± 1.3 | 734.5 ± 528.6 |
| | | *Plasma* | 34.5 ± 1.0 | 16.2 ± 5.4 | 19.8 ± 3.1 | 4056.2 ± 2456.3 | 9.9 ± 8.9 | 2323.9 ± 895.6 | 22.1 ± 13.2 | 15.9 ± 5.5 | 239.9 ± 34.8 |
| NT siRNA | Saline | *BALF* | 0.3 ± 0.3 | 5.1 ± 1.1 | 0.7 ± 1.0 | 21.8 ± 4.6 | 0.2 ± 0.1 | 6.7 ± 1.0 | 0.1 ± 0.2 | 1.2 ± 1.7 | 0 ± 0 |
| | | *Plasma* | 1.3 ± 1.8 | 4.3 ± 2.2 | 18.3 ± 2.5 | 465.1 ± 37.5 | 52.3 ± 8.1 | 59.6 ± 7.4 | 86.1 ± 14.6 | 27.8 ± 2.6 | 182.9 ± 11.7 |
| TNFα siRNA | Saline | *BALF* | 5.6 ± 2.9 | 2.0 ± 0.8 | 0.5 ± 0.7 | 21.48 ± 0.6 | 0 ± 0 | 15.0 ± 0.3 | 0 ± 0 | 1.0 ± 0.2 | 5.4 ± 7.7 |
| | | *Plasma* | 0 ± 0 | 5.0 ± 0.6 | 15.7 ± 7.6 | 440.5 ± 13.7 | 1.9 ± 2.1 | 268.8 ± 0.4 | 5.1 ± 0.2 | 7.8 ± 0.6 | 46.2 ± 2.5 |
| Empty MC6C Liposomes | Saline | *BALF* | 198.3 ± 212.6 | 11.2 ± 1.0 | 3.6 ± 2.3 | 48.4 ± 20.3 | 1.1 ± 0.6 | 427.1 ± 481.4 | 1.4 ± 0.5 | 2.7 ± 2.1 | 100.4 ± 112.5 |
| | | *Plasma* | 2.7 ± 2.2 | 5.8 ± 0.7 | 14.4 ± 6.2 | 290.7 ± 102.6 | 3.7± 0.9 | 109.1 ± 109.9 | 5.0 ± 2.2 | 9.7 ± 3.2 | 37.2 ± 10.2 |
| NT siRNA Liposome | Saline | *BALF* | 0.8 ± 1.2 | 1.4 ± 1.2 | 1.0 ± 1.9 | 17.7 ± 4.4 | 0.8 ± 0.7 | 2.7 ± 1.4 | 0.3 ± 0.6 | 2.6 ± 0.3 | 1.9 ± 1.6 |
| | | *Plasma* | 3.7 ± 2.7 | 4.2 ± 1.9 | 13.6 ± 4.4 | 460.5 ± 9.6 | 17.0 ± 18.1 | 65.1 ± 24.8 | 34.0 ± 34.3 | 15.5 ± 7.9 | 93.1 ± 72.8 |
| TNFα siRNA Liposome | Saline | *BALF* | 0.8 ± 0.5 | 1.9 ± 0.1 | 0 ± 0 | 12.2 ± 0.5 | 0 ± 0 | 8.1 ± 1.2 | 0.5 ± 0.7 | 0.4 ± 0.2 | 0 ± 0 |
| | | *Plasma* | 2.2 ± 3.2 | 3.1 ± 1.2 | 14.0 ± 7.5 | 462.4 ± 33.7 | 6.0 ± 1.9 | 71.6 ± 0.0 | 7.7 ± 2.0 | 10.9 ± 1.0 | 45.3 ± 3.8 |

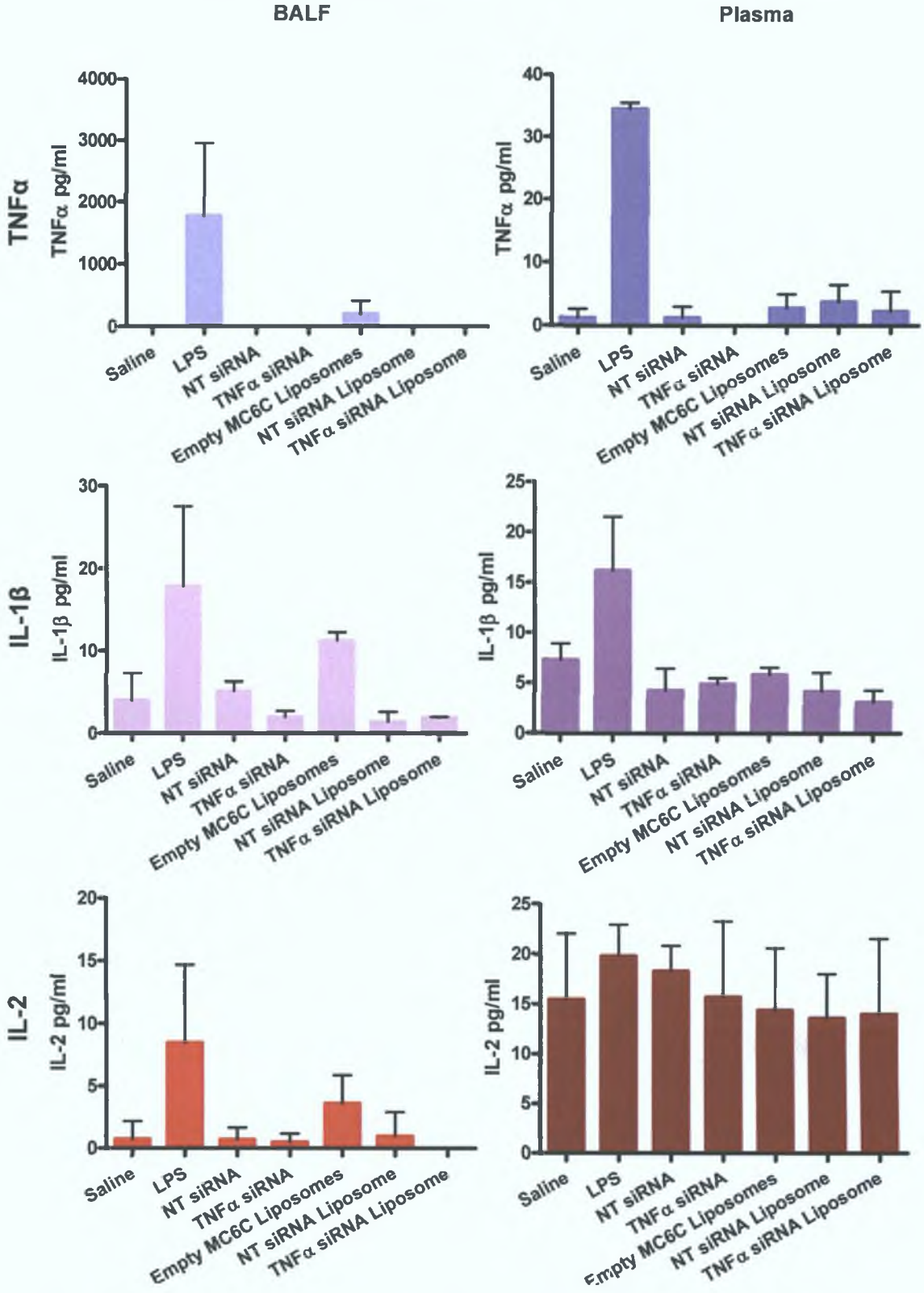


Figure 6.22: TH1/TH2 response in mice following saline, siRNA or mannosylated liposomes by intratracheal instillation. Saline, non-target (NT) siRNA, TNFα targeted siRNA, mannoslyated liposomes empty or encapsulating NT or TNFα siRNA complexed with PEI were administered for 24 hours. As a positive control a saline group were challenged with intratracheal administered LPS for 3 hours. BALF and plasma TNFα, IL-1β and IL-2 were determined using a Th1/Th2 cytokine 9-plex multi spot assay. Data represented as means ± SD (n = 1 – 4). Continued.

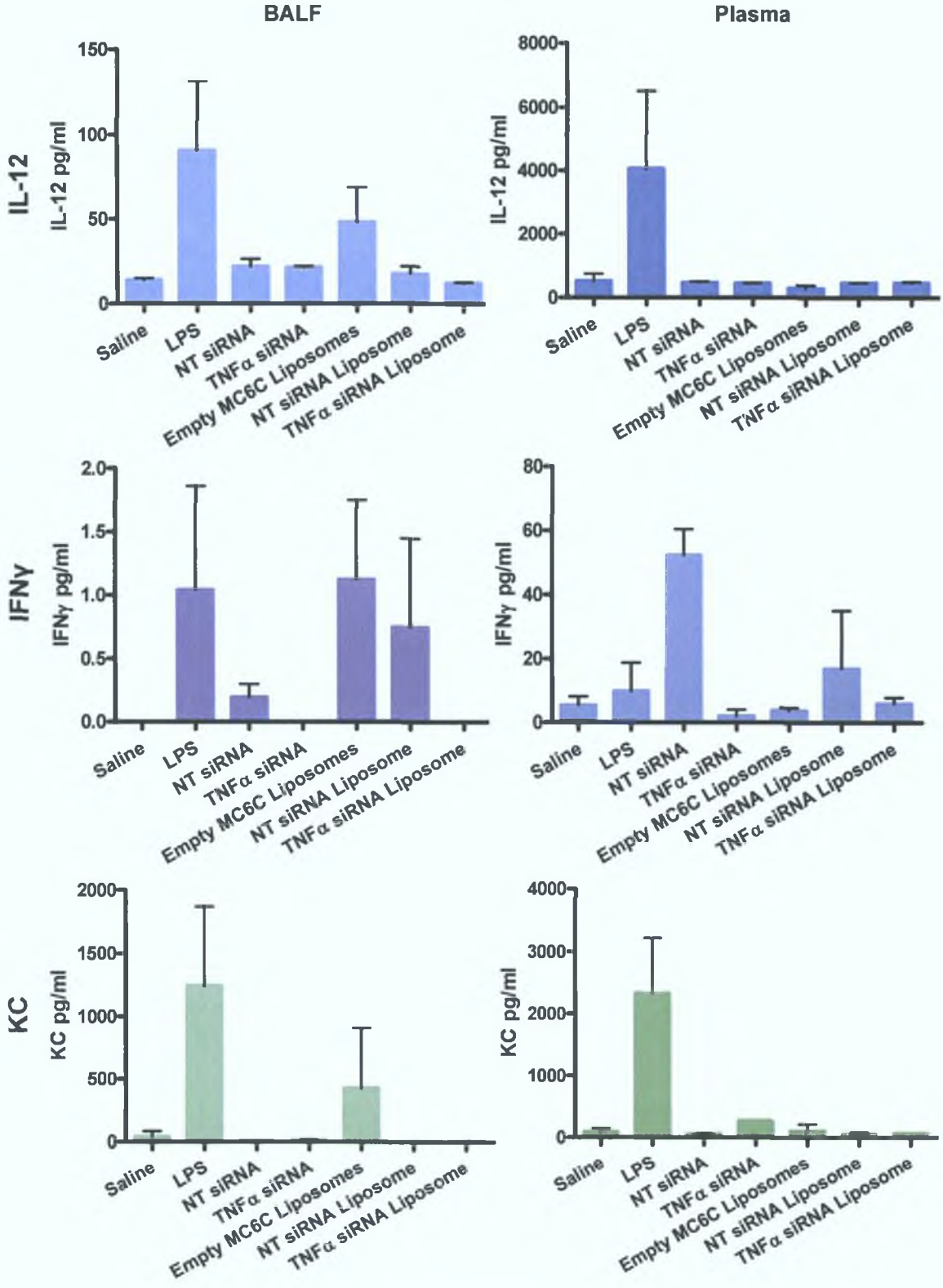


Figure 6.22: Continued. TH1/TH2 response in mice following saline, siRNA or mannosylated liposomes by intratracheal instillation. Saline, non-target (NT) siRNA, TNFα targeted siRNA, mannoslyated liposomes empty or encapsulating NT or TNFα siRNA complexed with PEI were administered for 24 hours. As a positive control a saline group were challenged with intratracheal administered LPS for 3 hours. BALF and plasma IL-12, IFN-γ and KC were determined using a Th1/Th2 cytokine 9-plex multi spot assay. Data represented as means ± SD (n = 1 – 4). Continued.

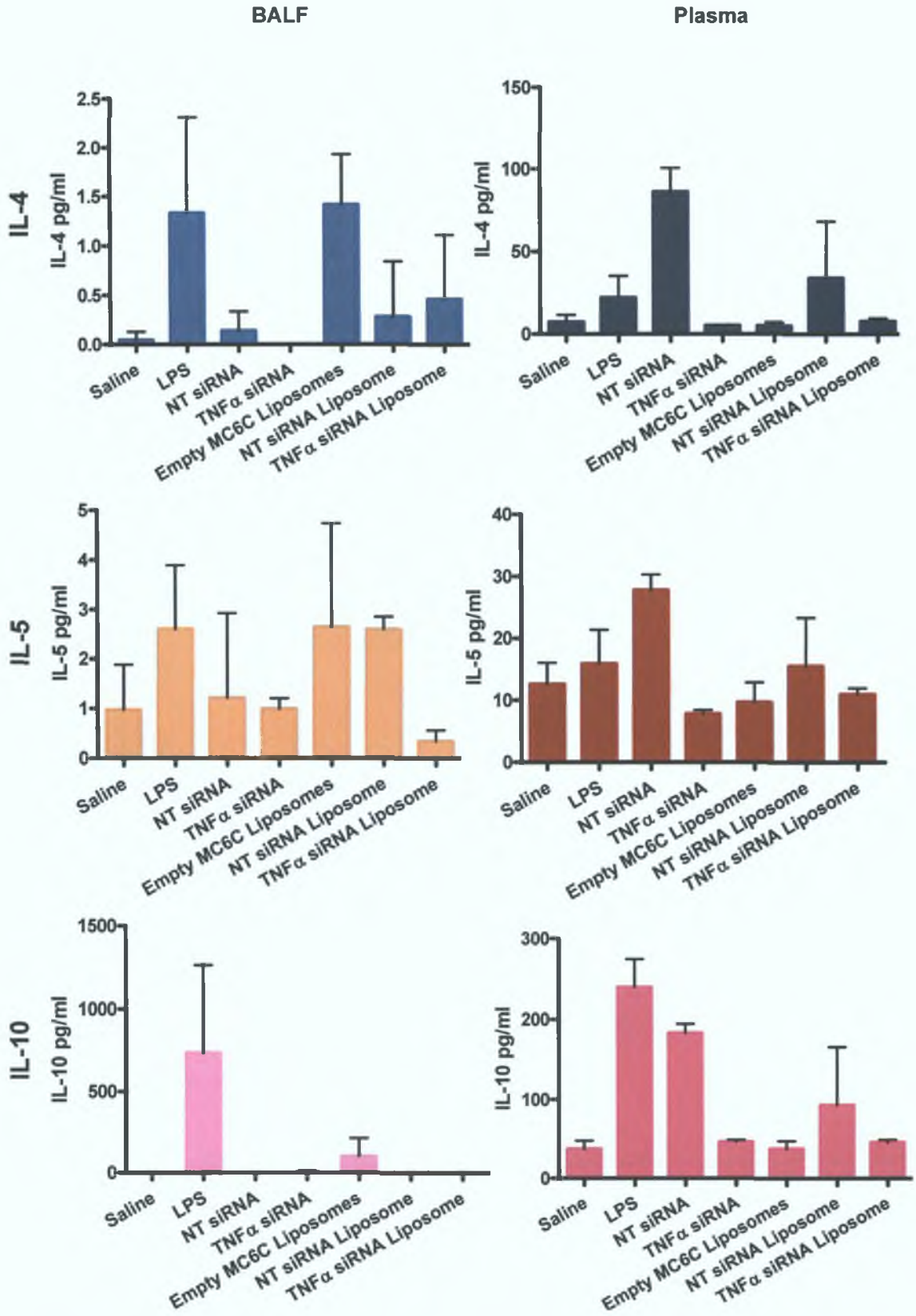


Figure 6.22: Continued. TH1/TH2 response in mice following saline, siRNA or mannosylated liposomes by intratracheal instillation. Saline, non-target (NT) siRNA, TNFα targeted siRNA, mannoslyated liposomes empty or encapsulating NT or TNFα siRNA complexed with PEI were administered for 24 hours. As a positive control a saline group were challenged with intratracheal administered LPS for 3 hours. BALF and plasma IL-4, IL-5 and IL-10 were determined using a Th1/Th2 cytokine 9-plex multi spot assay. Data represented as means ± SD (n = 1 – 4).

### 6.4.7.3 Histopathology following siRNA and Mannosylated Liposome Administration

Haemotoxylin and eosin stained lung sections from C57 mice intratracheally administered saline, siRNA or mannosylated liposomes were semi-quantitatively scored as shown in Table 6.7. The most apparent feature of inflammation was the presence of infiltrating neutrophils. An absent or very mild response was observed in this acute study to NT siRNA and mannosylated liposomes encapsulating siRNA/PEI complexes. Mild neutrophil-rich inflammation was found following 24 hour treatment with TNFα siRNA and also in groups treated with saline followed by an acute 3 hour LPS treatment. Empty mannosylated liposomes showed the greatest degree of inflammation scoring as moderate (++). In addition inflammatory features such as pavementing of neutrophils and the presence of neutrophils in the interstitium were observed following 24 hour empty liposome treatment.

**Table 6.7: Histopathology Semi-quantitative scores**

| Treatment Group | Degree of Neutrophil-rich Inflammation |
|---|---|
| Saline | - |
| Saline + LPS (3hrs) | + |
| Non-target siRNA | - |
| TNFα siRNA | + |
| Empty Mannosylated Liposomes | ++ |
| Non-target siRNA/PEI Mannosylated Liposomes | -/+ |
| TNFα siRNA/PEI Mannosylated Liposomes | -/+ |

## 6.5 Discussion

Through the use of inhalable biocompatible nanoparticles siRNA therapies for conditions including COPD, asthma and CF can be developed. Inhalable therapies offer an opportunity to delivery a drug directly to the target organ and thereby improve delivery, efficiency and avoid off-target effects. siRNA targeting pro-inflammatory mediators such as TNFα encapsulated in non-immungenic biocompatible targeted liposomes are one such therapeutic approach. TNFα siRNA has never been delivered directly to the lungs and therein we harnessed mannosylated liposomes for the first time to target alveolar macrophages.

The MR is highly expressed by macrophages and its expression has been measured by western blot analysis, immunocytochemistry, flow cytometry [305, 306], immunoprecipitation and PCR [307]. In a recent study by Kraus *et al.* (2010) MR expression of BV-2 cells, a mouse microglial cell line, was determined by high content screening [308]. Immunofluoresence confirmed MR expression by RAW 264.7 cells. Uptake of anionic, neutral and mannosylated liposomes also showed a similar pattern to that determined in differentiated THP-1 cells (chapter 3) but nebulised liposomes were also assessed. Comparison in uptake of liposomes pre- and post-nebulisation by a vibrating-mesh nebuliser (AeroNeb) revealed a significant decrease in uptake of mannosylated (MC6C) liposomes at 100 and 200μM post-nebulisation. This suggests these targeted systems may be less stable following nebulisation.

Propidium iodide and MTT assays are generally used to assess toxicity or cell viability *in vitro*. More recently high throughput screening techniques have been used to measure these effects *in vitro* whilst providing more detailed information on the effects of drugs or particles as well as images. Cellomics mulitparameter cytotoxicity assay allows the measurement of 7 parameters of cell death simultaneously. Before *in vivo* studies the most suitable, that is the least toxic, liposome formulation was determined. Cell loss, size and intensity of nuclei, cell permeability and mitochondrial membrane potentials in RAW 264.7 cells could be measured. Cytochrome c detection was determined using a mouse monoclonal cytochrome c primary antibody and DyLight™ 649 conjugated goat anti-mouse IgG secondary antibody and did not successfully bind under the conditions used.

Both DOPS and mannosylated liposomes were prepared as the targeting carriers to macrophages with DOPC liposomes as the neutral controls. On the whole, DOPS liposomes at high concentrations exhibited high levels of toxicity. These high concentrations would be necessary for transfection both *in vitro* and *in vivo*. The majority of the parameters measured were at an equivalent level to the positive toxic controls (valinomycin and DOTAP liposomes [93, 178, 179]). Valinomycin is a highly toxic potassium ionophor. DOTAP is a cationic lipid frequently used in the formulation of liposomes and lipoplexes for transfection. Although it is a more convenient lipid for transfection with high transfection efficiency it has been shown to interact with proteoglycans on the cell surface leading to toxicity as has been discussed in chapter 3. Consequently mannosylated liposomes were considered more suitable for *in vivo*

use. Mannosylated liposomes at both concentrations showed non-significant toxic effects. Liposomes composed with Mann-C6-Chol were the most biocompatible. Therefore, toxicity was assessed of MC6C liposomes empty or encapsulating siRNA. Some toxic effects were seen but were only minor. These effects were generally highest with siRNA complexed with protamine followed by PEI and the least pronounced effects seen when siRNA/DOTAP complexes were assessed. siRNA/DOTAP complexes were the least reproducible complexes with variability in size, zeta potential and most importantly encapsulation efficiency (Chapter 2). Also *in vitro* experiments indicated when siRNA/protamine and siRNA/PEI complexes were added to liposome formulations they improved transfection efficiency. Hence mannosylated (MC6C) liposomes encapsulating siRNA/PEI complexes were deemed the most suitable formulation for *in vivo* studies.

Additionally, Mann-C4-Chol containing liposomes, having positive zeta potentials [297], have previously been shown to be well tolerated *in vivo* [115]. Zeta potentials of *in vivo* MC6C liposomes encapsulating siRNA and empty ranged from 56 to 64 mV. This surface charge decreased from over +65mV following extrusion possibly due to neutral lipids masking or enveloping the positively charged siRNA/PEI complexes. PEI may also offer other advantages in siRNA delivery. PEI perhaps acts as a "proton sponge" [309] and can be protonated to a higher degree at lower pH. Thus within endosomes or lysosomes PEI will buffer the lower environmental pH causing osmotic swelling, possible lysosome rupture and release of the complex into the cell cytoplasm. Consequently PEI could assist in cytoplasmic delivery of siRNA while also protecting siRNA from lysosomal degradation. Toxic effects associated with this polymer is also most likely masked by liposome encapsulation.

A range of commercially available siRNAs against TNFα were compared using HiPerFect transfection reagent which is optimised for macrophage transfection. Transfections with these sequences revealed TNFα1 and TNFα2 to knockdown TNFα expression while TNFα3 enhanced TNFα expression particularly when compared to non-target siRNA transfected controls. TNFα1 siRNA was the most potent inhibitor of TNFα expression in RAW 264.7 cells and therefore was used for *in vivo* mannosylated liposome formulations encapsulating TNFα siRNA/PEI complexes. It has previously been shown that synthetic siRNA can induce a sequence dependent immune response [310]. Sioud *et al.* (2005) assessed 32 different siRNA sequences, 8 of which targeted TNFα [311]. One particular siRNA sequence targeting mouse TNFα induced high levels of TNFα and IL-6 in adherent PBMCs. Sequence homology between immune stimulating siRNAs was not significant but the presence of GU dinucleotides appeared to be involved in immune activation [311]. GU dinucleotides occur once in TNFα2 and twice in TNFα3 but not in TNFα1. This could explain the differences in TNFα expression between the three sequences.

It was not known whether LPS would interact with the liposome preparations and due to this and volume per dose constraints it was decided to administer siRNA or liposomes and LPS separately. It has previously been shown that intracellularly siRNA degrades after 24 hours.

Also recovery time for the mice was necessary from anaesthetic and the procedure itself, thus a recovery time of 24 hours was chosen. This allowed another 50µl liquid dose (either saline or LPS) to be safely administered and well tolerated. siRNA could then be delivered intracellularly prior to LPS challenge. Since the induction of a cytokine TNFα was to be determined, mice were sacrificed 3 hours following LPS administration. Lefort *et al.* (2001) showed a dose dependent increase in BALF TNFα concentration in C56BL/6 mice treated with aerosolised LPS (*E. coli* 055:B5) after 3 hours. TNFα was undetected in BALF after 24 hours [291]. A temporal transcriptional profile from C57BL/6 mouse lung post-treatment with aerosolised LPS (*E. coli* O111:B4) from 1 to 24 hours was generated in a study by Jeyaseelan *et al.* (2004). TNFα expression was 53.3-fold greater than controls 2 hours following LPS treatment and with only a 2-fold increase at 24 hours [293]. Therefore this time point maximises the amount of cytokines present in the BALF.

Although not significant, TNFα expression was marginally decreased in groups administered with TNFα siRNA and mannosylated liposomes encapsulating TNFα siRNA. The more freshly prepared the liposomes the more effective the siRNA was, as formulations administered over a week following preparation had little or no effect on TNFα expression compared to saline/LPS treated controls. This suggests degradation of siRNA over time and that preparations must be used immediately. Assessment of further doses was planned however time constraints did not permit this. Other pro-inflammatory cytokines and chemokines were elevated due to LPS stimulation of TLR-4 but were more variable with little difference between groups. This was a preliminary study and could be extensively optimised in terms of time points, dosing and formulation. Many of the *in vitro* liposome knockdown studies were carried out in parallel to the *in vivo* work but early experiments indicated 24 hour liposome treatment followed by a 3 hour LPS stimulation was optimal. It should also be noted that liposomes were targeted to alveolar macrophages but although the predominant mediators of inflammation these are not the only cell type present. Endothelial cells present would also be involved in the inflammatory response boosting cytokine and chemokine levels.

*In vivo* NT siRNA treatment in non-LPS challenged mice was associated with a low presence of neutrophils and histology revealed inflammation equivalent to the negative control group in the BAL while IFNγ was induced in the lung and IFNγ, IL-4, IL-5 and IL-10 were increased in the plasma. Additionally total BAL cell counts were on par with negative controls. This shows an absence of immunological response in the lung with a systemic mainly Th2 response. TNFα siRNA on the other hand showed little cytokine response in the lung or systemically but histology revealed mild inflammation. Additionally total BAL cell counts were similar to negative controls and neutrophils were not present. It has been postulated that synthetic siRNA could be recognised within the endosomes by TLR-7 and TLR-8 and thus elicit a sequence dependent immune response [310, 311].

A large increase in total BAL cell count was found following treatments with mannosylated liposomes particularly empty liposomes. Empty liposome treatments also lead to neutrophil

infiltration into alveolar spaces as indicated by the presence of neutrophils in BAL almost equivalent to acute LPS challenge. Liposome presence also induced a wide range of cytokines in the lung including TNFα, IFNγ, IL-12, KC, IL-1β, IL-2, IL-4, IL-5 and IL-10 but not systemically. This effect was induced by empty liposomes but not by liposomes encapsulating siRNA which only altered IFNγ, IL-4 and IL-5 in the lung. Liposome encapsulation of NT siRNA/PEI complexes also increased systemic levels of IFNγ, IL-4 and IL-10. Histological analysis revealed neutrophil rich inflammation following liposome treatments scored as moderate and mild following empty liposome and siRNA encapsulating liposome treatments respectively. Overall this shows empty mannosylated liposomes inducing an inflammatory response after 24 hours similar to that of an acute LPS challenge. This response involved the recruitment of neutrophils and the upregulation of all immune mediators measured but was localised in the lung. Liposomes encapsulating siRNA caused a far lesser degree of inflammation but an effect was detected in the plasma. Interestingly groups administered NT siRNA and liposomes encapsulating NT siRNA showed increased plasma levels of the same immune mediators (IFNγ, IL-4 and IL-10) but NT siRNA unencapsulated induced these mediators to a much greater extent.

*In vitro* screening of a range of liposomes and TNFα targeted siRNA sequences for toxicity and efficacy respectively were used to optimise formulations for *in vivo* transfection. *In vitro* liposomes showed low toxicity at 100 and 300μM with DOPS (300μM) the exception. Mannosylated liposomes containing Mann-C6-Chol were developed for *in vivo* administration. This shows the first time Mann-C6-Chol containing liposomes have been administered *in vivo* and siRNA has been incorporated into mannosylated liposomes. Although toxicity in RAW 264.7 cells was negligible following 24 hour empty mannosylated liposome treatment *in vivo* an immune response was elicited in the lung only. Loaded liposomes did not have such an exaggerated effect. Additionally, siRNA induction of systemic immune mediators was reduced following liposome encapsulation. Previously liposomes have been shown to maintain localised effects of drugs following pulmonary administration and avoid systemic or off-target effects [154]. Although a clear knockdown of TNFα was not observed following administration of naked TNFα siRNA or mannoslyated liposomes encapsulating TNFα siRNA a decrease in TNFα expression was observed in these treatment groups particularly following the administration of freshly prepared liposomes. In general the mannosylated liposomes prepared are non-toxic and well tolerated.

**Key Findings**

- Optimal liposome formulation and TNFα siRNA sequence determined *in vitro*
- TNFα knockdown was observed in the mouse lung following naked and mannosylated liposome encapsulated TNFα siRNA treatment in LPS challenged mice
- Mannosylated liposomes induced an immune response *in vivo* but were well tolerated and effects were localised to the lung

# Chapter 7

## Discussion

## 7.1 General Discussion and Conclusions

Macrophages play a key role in inflammatory lung diseases such as COPD, asthma and CF and consequently represent an important therapeutic target. To date the majority of clinical therapies provide relief from the immediate symptoms associated with these diseases with no long term or curative therapies available. Gene therapy could open a new avenue in the treatment of inflammatory lung disease. RNAi via siRNA can provide potent and specific targeting of inflammatory genes but requires biocompatible and safe delivery vectors [223, 312]. Viral vectors for gene therapies have been harnessed for RNA delivery producing high transfection efficiencies [312]. However, serious side-effects have ensued following viral-based transfection including immunogenicity and oncogenicity [249, 253, 312] calling for alternative vector systems for delivery. Non-viral vectors such as liposomes and polymeric systems are widely investigated for this purpose and can be modified to enable RNA targeting, slow RNA release and improved stability *in vivo*. The combination of RNAi with biocompatible, targeted delivery systems offers the potential to develop potent, gene and cell specific therapeutic agents.

In this thesis, a range of non-viral vectors for targeted siRNA delivery to alveolar macrophages were developed and compared including anionic and mannosylated liposomes and uncoated and gelatin-coated PLGA microparticles. These vector systems were developed to avoid the use of cationic lipids and polymers for intracellular delivery which can induce cytotoxicity. Anionic liposomes were composed of DOPS (a synthetic phosphatidylserine) and mannosylated liposomes incorporated mannosylated cholesterols into their bilayer in order to target macrophage SR and MRs. Uptake of PLGA microparticles by macrophages is optimal when the microparticles are manufactured in the size range 2 – 3μm in diameter [313] and has a hydrophobic surface which is readily opsonised [314]. Methods were developed to effectively encapsulate siRNA into liposome and microparticle formulations. siRNA liposomal and polymeric carrier systems were evaluated based on physicochemical properties and *in vitro* cell uptake, toxicity, immunogenicity and knockdown efficiency in macrophage cell models. Mannosylated siRNA liposomes were further developed for *in vivo* testing of both siRNA efficacy by direct delivery to the mouse lungs; liposomes induced local and systemic immunogenic effects. There is a growing need to deliver shRNA to monocytes and macrophages for research purposes and also as a potential means of eliciting therapeutic RNAi for clinical applications and the PLGA microparticle platforms were harnessed for delivery of shRNA.

Encapsulation methods were optimised for siRNA loading into anionic and mannosylated liposomes and PLGA microparticles. Both systems are generally associated with poor encapsulation efficiencies therefore siRNA encapsulation presents a considerable challenge. Cationic lipids are conventionally used for gene delivery because of their efficiency in encapsulation of nucleic acids and transfection of cells *in vitro*. Unfortunately cationic lipids such as DOTAP can be cytotoxic and lipoplex formulations are not as effective *in vivo* [92].

Several studies have encapsulated siRNA into anionic and neutral liposomes using a number of techniques such as freeze dried lipid matrix [94], pre-condensation of siRNA [96, 98] and repeated freeze thaw cycles [99, 105]. Pre-condensation of siRNA with cationic reagents, such as PEI and octa-arginine, has achieved encapsulation efficiencies of >80% in non-cationic liposomes [98]. Another challenge lay in the determination of encapsulation efficiency particularly when siRNA was condensed prior to encapsulation and in fact many published studies omit siRNA encapsulation efficiency determinations. Methods described in the literature used ribogreen or fluorescence assays to detect free siRNA removed by centrifugation or following liposome disruption by detergents [105, 169]. Using these techniques it was found that >95% siRNA was encapsulated in the prepared DOPS and mannosylated liposomes but this did not take into account the siRNA complexed with the cationic complexing agent which is undetectable by the quantitation method used. Similarly pre-condensation of siRNA has previously been used as a strategy for improved siRNA loading into PLGA particles with encapsulation efficiencies up to 80% and 32% with PEI and DOTAP respectively [156, 218, 219]. Percentage encapsulation efficiencies using DOTAP/siRNA complexes was better than reported in the literature with 56.5 ± 12.9% while siRNA appeared to leach out of the microparticles during the gelatin coating process reducing the encapsulation efficiency to 12.3 ± 7%.

Liposomes and microparticles were developed for both anatomical and cellular targeting to alveolar macrophages, i.e. they were designed for inhalation and cell targeting. Nebulisation of liposomes has been assessed with a variety of nebulisers including air jet, ultrasonic and vibrating mesh technologies and cargos such as DNA, proteins and peptides [119, 140-145, 148]. Although anionic liposomes have previously been aerosolised [119, 121], mannosylated liposomes and siRNA loaded liposomes have not been evaluated following nebulisation. Liposome formulations were nebulised using an air jet (PARI) or vibrating mesh (AeroNeb) nebuliser coupled with a glass twin impinger and characterised by size, zeta potential, deposition pattern and *in vitro* macrophage uptake. The AeroNeb device was more efficient than the air jet PARI device for all liposome formulations although there were differences in deposition patterns in a TSI between anionic, neutral and mannosylated liposomes. Furthermore, mannosylated liposomes showed a dramatic fall in zeta potential from positive to negative following nebulisation particularly those reaching TSI Stage B. Uptake of nebulised mannosylated liposomes was also significantly decreased in comparison to pre-nebulised liposomes, together suggesting an unstable system and possible damage to the mannose coating of the liposomes during nebulisation. Studies have been published using the PARI [140, 146] and AeroNeb [146, 147, 315-317] devices for liposome nebulisation. Gaspar *et al.* (2010) compared the size, zeta-potential and drug retention of a range of liposome preparations encapsulating a fluorescent model compound calcein following nebulisation by an AeroNeb nebuliser [315]. Size and surface charge of liposomes remained relatively stable post-nebulisation however nebulised liposomes were collected directly and not impinged so direct comparisons with our results cannot be made. Similarly other studies reported minimal change in liposome properties post-nebulisation however the presence of PEG on the liposome surface

resulted in decreased stability [316, 317]. Elhissi *et al.* (2007) nebulised liposome formulations into a TSI using a PARI LC Plus air-jet and a customised AeroNeb Pro nebuliser and observed nebulisation by the AeroNeb device was less disruptive to liposomes, completed nebulization in a much shorter time and lead to a greater mass output rate than the PARI nebulizer [146]. Although following size reduction to 400nm by extrusion liposomes were less stable post-nebulisation most likely due to the reduced liposome lammellarity [146].

Microparticles mean geometric diameters were ~2μm, an ideal size for deep lung deposition. PLGA microparticles are generally prepared as dry powder systems and therefore particle size is critical for efficient pulmonary delivery [9] whereas liposomes are typically in suspension which can be delivered via nebulisation in which droplet size is the important factor. For efficient alveolar deposition an aerodynamic diameter, which depends on geometric size and particle density, of 1 – 5μm is optimal [7]. Work from our lab has determined MMAD of 2.25μm for these PLGA microparticles using an Anderson cascade impactor [278].

Cell targeting was determined *in vitro* in a human macrophage cell model, differentiated THP-1 cells, monocytes/macrophages isolated from peripheral donor blood and mouse macrophages, RAW 264.7 cells. THP-1 cells are a monocytic cell line that can be differentiated by phorbol esters into macrophage like cells which express both SRs and MRs upon differentiation [318, 319]. Uptake assays were developed using HCA technology which combines imaging with quantification and gives a more precise measure of uptake than methods such as flow cytometry with liposomes or microparticles counted per cell [154, 198]. Uptake of liposomes in differentiated THP-1 cells corresponded with levels determined in RAW 264.7 cells confirming DOPS and MC6C liposomes as the leading delivery platforms. Kawakami *et al.* (1998) compared DNA/liposome complex transfection efficiency using galactosylated liposomes prepared with Gal-C2-Chol, Gal-C4-Chol and Gal-C6-Chol [173]. Similarly, the liposome incorporating the derivative with longer spacer length mediated the greatest gene transfer, most likely, associated with higher MR recognition [173] as previously spacer length of liposome surface ligands has been shown to be important in receptor binding [320, 321].

Both liposome and PLGA based systems successfully delivered siRNA for mediation of gene suppression *in vitro*. Transfection was more successful in primary monocytes/macrophages derived from peripheral blood than differentiated THP-1 cells, the macrophage-like cell line. THP-1 cells are notoriously difficult to transfect with approaches including viral transfection and nucleofection the most frequently used to date [274]. Non-viral methods for transfection, mainly nucleofection, with differentiation of THP-1 cells have been associated with a loss in cell viability and function [274]. At the concentrations required for our delivery systems (MPs and liposomes) to effect efficient knockdown toxicity was not evident. However the efficiency of transfection was variable between experiments particularly with isolated human blood monocytes/macrophages which could be due to donor dependent variation. Anti-TNFα siRNA complexed with either PEI or protamine and encapsulated in DOPS and MC6C liposomes showed the most efficient knockdown of TNFα expression in LPS stimulated cells.

Mannoylated liposomes have previously been used to deliver DNA and oligodeoxynucleotides (ODNs) but not siRNA [116], so this is the first proof of principle for this application. Similarly DOPS liposomes have not previously been used for siRNA delivery. PLGA nanoparticles and microparticles have previously been used for TNFα siRNA delivery [156, 223] but not for pulmonary use. Microparticles have also been used for pDNA transfection [215] which led to the development of shRNA loaded PLGA microparticles. shRNA microparticles were used to effectively knockdown expression of target genes IRF3 and TRIM68 in PBMCs and NK92NI cells respectively. This emphasised the versatility of this gene delivery platform.

MC6C liposomes were further tested for preliminary *in vivo* studies in a mouse inflammatory lung model. Pulmonary delivery of Mann-C6-Chol composed liposomes or anti-TNFα siRNA has not previously been reported in the literature. MC6C liposomes encapsulating PEI/anti-TNFα siRNA complexes were selected based on *in vitro* uptake and toxicity screens in mouse RAW 264.7 macrophage cells and knockdown and immune screens in human macrophage cell models. *In vitro* cell uptake screens strongly indicated DOPS and MC6C liposomes as forerunners for siRNA delivery with both systems achieving highly significant uptake by mouse and human macrophages. DOPS liposomes mediated significant knockdown of TNFα in LPS stimulated cells *in vitro* but also showed significant cytotoxicity. On the other hand MC6C liposomes knocked down TNFα but not significantly and did not induce significant toxicity in RAW 264.7 cells. *In vivo*, although not significant anti-TNFα siRNA decreased TNFα levels in BALF following a LPS challenge. Howard *et al.* (2009) achieved 44.3% knockdown of TNFα in peritoneal macrophages following I.P. administration of chitosan/TNFα siRNA nanoparticles compared to chitosan/control siRNA nanoparticle treatment in C57BL/6J mice [322]. It should also be noted that our liposomes were targeted to alveolar macrophages the predominant mediators of inflammation; however, these are not the only cell type present. Epithelial cells present would also be involved in the inflammatory response boosting cytokine and chemokine levels. Furthermore, Howard *et al.* (2009) harvested peritoneal macrophages from mice shortly after I.P. nanoparticle administration and cultured the cells *ex vivo* for 24 and 48 hours before determining TNFα expression [322].

In order to determine any adverse effects induced by these carrier systems, toxicity and immune screens were established. Anionic, neutral and mannosylated liposome *in vitro* toxicity and immune effects were compared to cationic DOTAP liposomes. Overall, treatment with DOTAP liposomes lead to highly significant levels of cell toxicity and induced the pro-inflammatory cytokine IL-1β in macrophage cells. Previously, DOTAP has been shown to cause high levels of toxicity in macrophages along with down regulation of TNFα and nitric oxide (NO) [93, 199, 200]. Moreover cationic liposomes can induce apoptosis in macrophages [178-181, 323]. In comparison, DOPS, DOPC and mannosylated liposomes tended to cause minimal or no toxic effects. However, anionic DOPS liposomes showed significant concentration dependent toxicity, particularly at 300μM following 24 hour treatment of RAW 264.7 cells. In differentiated THP-1 cells DOPS liposomes also caused significant activation of NFκB and induction of pro-inflammatory cytokines including IL-1β, IL-8 and TNFα. This targeting strategy

harnesses the endogenous processes of macrophages to recognise phosphatidylserine (PS) exposed on apoptotic cells followed by their phagocytosis. Kurosaka *et al.* (1998) found that differentiated THP-1 cells and monocyte-derived macrophages produced pro-inflammatory cytokines most notably IL-8 following exposure to apoptotic cells which were deemed apoptotic by size and PS exposure [324]. Perhaps DOPS therefore triggers a pro-inflammatory response in macrophages by a similar mechanism to PS of apoptotic cells. Uncoated PLGA microparticles exhibited some signs of toxicity in differentiated THP-1 cells but did not induce significant cell loss. PLGA microparticles also induced IL-1β and IL-8 and NFκB activation in differentiated THP-1 cells most significantly with gelatin coating.

Cell toxicity and immunogenic effects caused by neutral and mannosylated liposomes were far less significant than cationic and anionic liposomes. Mannosylated liposomes *in vitro* did produce a slight anti-inflammatory effect compared to untargeted DOPC liposomes that was concentration and linker dependent. Mannosylated liposomes significantly reduced NFκB activity and marginally decreased IL-8, IFNγ and TNFα production in differentiated THP-1 cells. Longer mannosylated cholesterol spacers reduced NFκB activity more significantly along with enhancing cell uptake. The longer the linker length the greater the availability of mannose to interact with the macrophage MR and thus cause MR activation and enhance mannosylated liposome uptake. Previously, MR activation has been shown to induce immunosuppression and NFκB inhibition *in vitro* [188, 189]. Nonetheless, significant induction of IL-13 ($p < 0.05$) was observed. IL-13 has been linked to asthma and COPD pathogenesis; macrophages being the predominant cellular source [325]. However, IL-13 inhibits the production of pro-inflammatory mediators such as ROS and prostaglandins in monocytes and macrophages possibly due to NFκB suppression while having the opposite effect on many other inflammatory cells [325]. Hence, mannosylated liposomes appear to activate MRs on macrophages to suppress NFκB activation and inflammation.

Conversely, empty MC6C liposomes *in vivo* strongly induced an inflammatory response in the mouse lung which was significantly dampened following encapsulation of PEI/siRNA complexes. Empty mannosylated liposomes after 24 hours increased neutrophil and macrophage presence in BALF as well as induction of a wide range of cytokines and chemokine most notably TNFα, IL-1β, KC, IL-4, IL-5 and IFNγ. Histopathology also revealed neutrophil-rich inflammation. Again it has to be highlighted that macrophages are not the only cell type present and although an inflammatory response was observed it may not be representative of the macrophage response but due to off-target effects. Cytokine and chemokine levels have been determined in rat lungs following administration of dex encapsulated in mannosylated liposomes [130]. However this study focused on the anti-inflammatory effects of dex and liposome encapsulated dex and did not examine the effects of the empty liposomes [130].

Liposome encapsulation of proteins and nucleic acids such as rSLPI and siGLO siRNA for *in vivo* pulmonary delivery has been reported to induce local effects while avoiding systemic effects and increasing lung retention [84, 154]. Cytokine and chemokine induction was detected

following NT naked or liposome encapsulated siRNA and empty MC6C liposomes in BALF. Synthetic siRNA within the endosomes may be recognised by TLR-7 and TLR-8 and induce a sequence dependent immune response [310, 311]. Mannosylated liposome encapsulation of NT siRNA reduced systemic immune mediator induction such as IFNγ and no systemic effects induced by empty MC6C were detected. Therefore intratracheallly administered mannosylated liposomes act locally with minimal systemic effects.

When comparing the two technologies described herein as potential platforms for clinical treatment a number of issues aside from those described above need to be considered including their stability and scalability. Microparticle formulations could sustain functional siRNA for longer periods than liposomes. DOPS mediated TNFα knockdown was very significant ($p < 0.01$) at 24 and 48 hours while MC6C liposomes mediated TNFα suppression 48 hours following transfection only. Microparticles on the other hand reduced TNFα expression after 48 and 72 hours. Previous studies have achieved TNFα knockdown ranging from 27 to 70% [102, 204] delivered via anionic liposomes with knockdown observed 24 to 96 hours following transfection [102] in LPS stimulated macrophages. Microparticles could be freeze dried, stored as powders and resuspended when required. Liposome formulations however had to be used as soon as possible to avoid loss of siRNA function.

### 7.2 Future Work

This project has explored many aspects of siRNA delivery to the lungs with the intention of developing safer more efficient carrier systems for targeting siRNA to alveolar macrophages in the lungs *in vivo*. Mannosylated liposomes represent promising siRNA carriers for therapeutic roles but a disadvantage is the poor siRNA stability over extended periods. Liposomes can be successfully lyophilised to improve long term storage stability but numerous variables are involved for optimisation including choice of lyoprotectant, methods of lyophilisation and liposome characteristics [326].

At a cellular level there are still many areas to be investigated such as an understanding of the uptake mechanisms and intracellular trafficking of the various carriers. Liposome and siRNA intracellular fate could be monitored over time using microscopy techniques [279]. Other inflammatory gene targets such as IL-1β and IL-6 [327] could be investigated and it is also possible to target multiple genes [282] potentially even within the same carrier system.

*In vivo* studies described were only preliminary and therefore require further optimisation including most importantly comprehensive dose-response studies. PCR analysis of the tissue would give a clearer understanding of the inflammatory response of the entire lung and give a more detailed and quantitative result than histopathological scoring provides. This would help distinguish the effects of siRNA/liposome treatments on alveolar macrophages and the lung epithelial cells and infiltrating neutrophils. It would also be interesting to isolate alveolar macrophages and assess knockdown as well as examine different time points and doses.

Additionally the use of fluorescently labelled siRNA and/or liposomes could be used to assess uptake and biodistribution within the lung tissue. As another leading siRNA carrier platform an obvious next step is the *in vivo* delivery of siRNA-microparticles and this is currently underway. The inflammatory lung model used represented an acute inflammatory response however a more appropriate model of chronic inflammatory lung disease such as models established with ovalbumin (OVA) or bleomycin [328] could be used to look at the ability of these systems to mediate gene silencing and/or affect inflammation long term [229, 322].

### 7.3 Conclusion

The major aim of this project was to develop non-toxic efficient vectors for siRNA delivery to alveolar macrophages and to mediate an anti-inflammatory effect via RNAi. A range of non-viral siRNA carriers were assessed for biocompatibility and ability to mediate gene silencing in alveolar macrophages under inflammatory conditions. Methods were developed to maximise siRNA encapsulation in targeted liposomes and microparticles and screen these carriers for uptake, toxicity and immunogenicity. HCA screening methods were developed to compare the siRNA carriers in human and mouse macrophage cells and hence determine optimal formulations for macrophage gene knockdown. High levels of knockdown via siRNA and shRNA delivery by microparticles were achieved with significant concentration- and time-dependent knockdown seen in a range of cell types for a number of cargoes. These platforms were capable of high RNA loading and prolonged RNA interference using both shRNA and siRNA, demonstrating the versatility of microparticles as both a research tool and a potential therapeutic carrier. Anionic DOPS liposomes induced very significant TNFα knockdown in monocytes/macrophages from human peripheral blood but at certain concentrations initiated a pro-inflammatory response and cell death in macrophages. Mannosylated liposomes showed optimal uptake, toxicity and immunogenic profiles with extended spacer length *in vitro.* Additonally, known anti-inflammatory effects of MR activation were observed in macrophage cells following mannosylated liposome treatment. MC6C liposomes also mediated successful TNFα knockdown *in vitro* and *in vivo* and the siRNA-MC6C liposomes were well tolerated in C57BL/6 mice. Therefore, a number of platforms for RNA delivery to macrophage cells were developed that offer an effective method of delivering RNA for research and therapeutic applications.

# Chapter 8

## Appendix

## 8.1 Mannosylated Cholesterol Characterisation

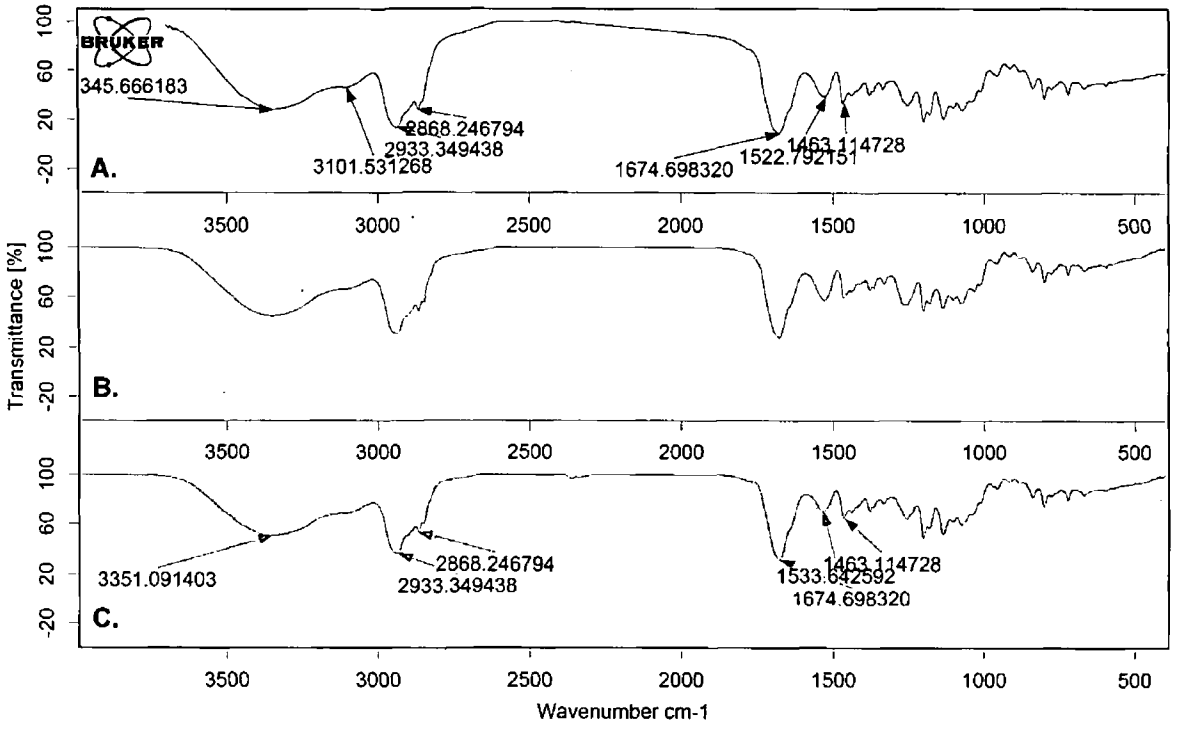


Figure 8.1: Infra-Red spectra of (A) Mann-C2-Chol, (B) Mann-C4-Chol and (C) Mann-C6-Chol

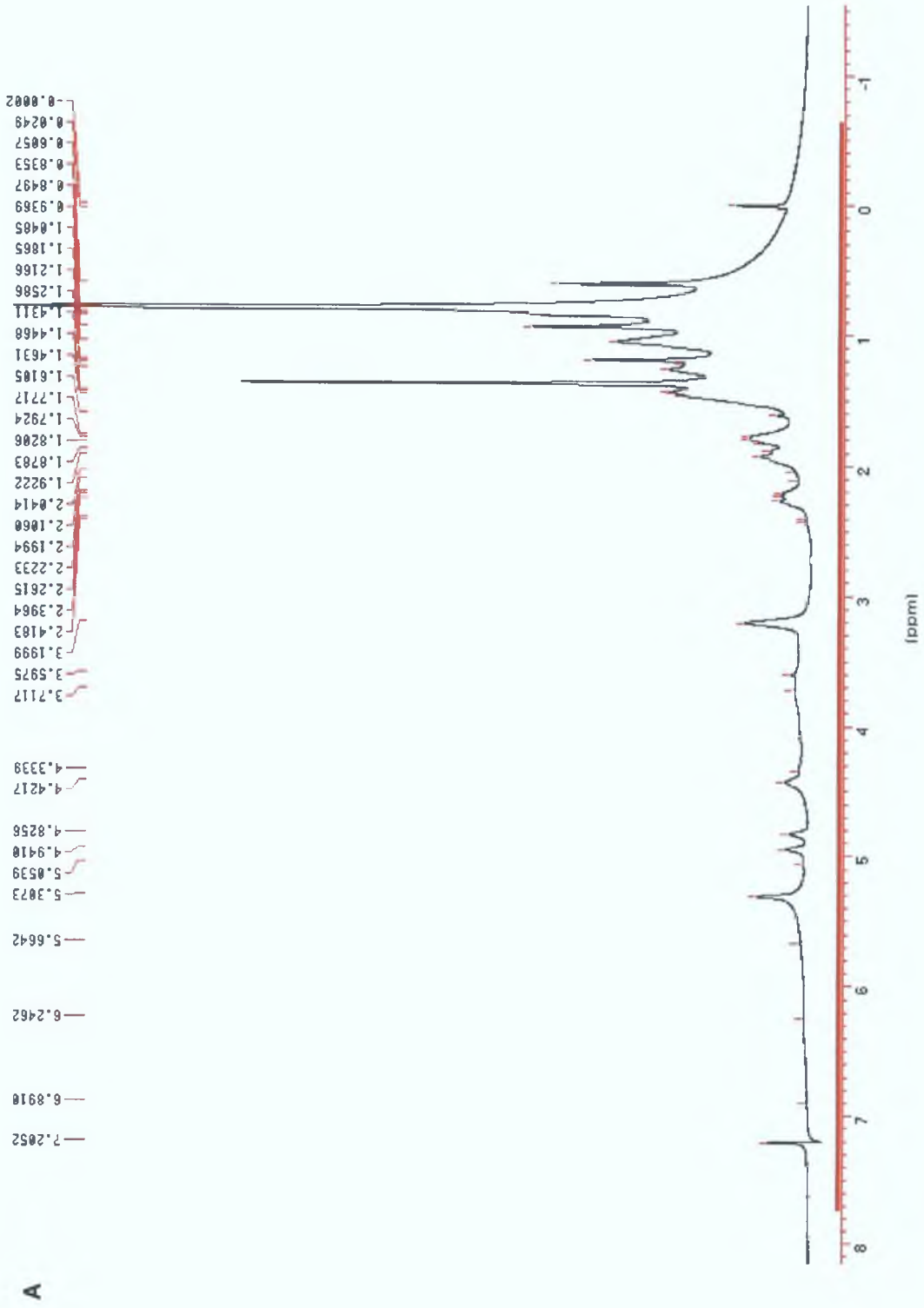
A
(ppm)

B
8.6164
7.8838
7.8650
7.7214
7.7019
7.1976
5.2727
4.7490
4.6769
4.5696
4.3294
3.9781
3.7053
3.5974
3.5648
3.5485
3.4513
3.3183
3.2920
3.2775
3.2619
3.0580
2.7005
2.5155
2.1981
2.1059
2.0526
1.9215
1.8789
1.7591
1.4618
1.4455
1.4298
1.3401
1.3307
1.2717
1.2585
1.1039
1.1507
1.0440
0.9337
0.8841
0.8509
0.8364
0.6658
0.6062
0.0254
0.0091
-0.0003
15
10
5
0
(ppm)

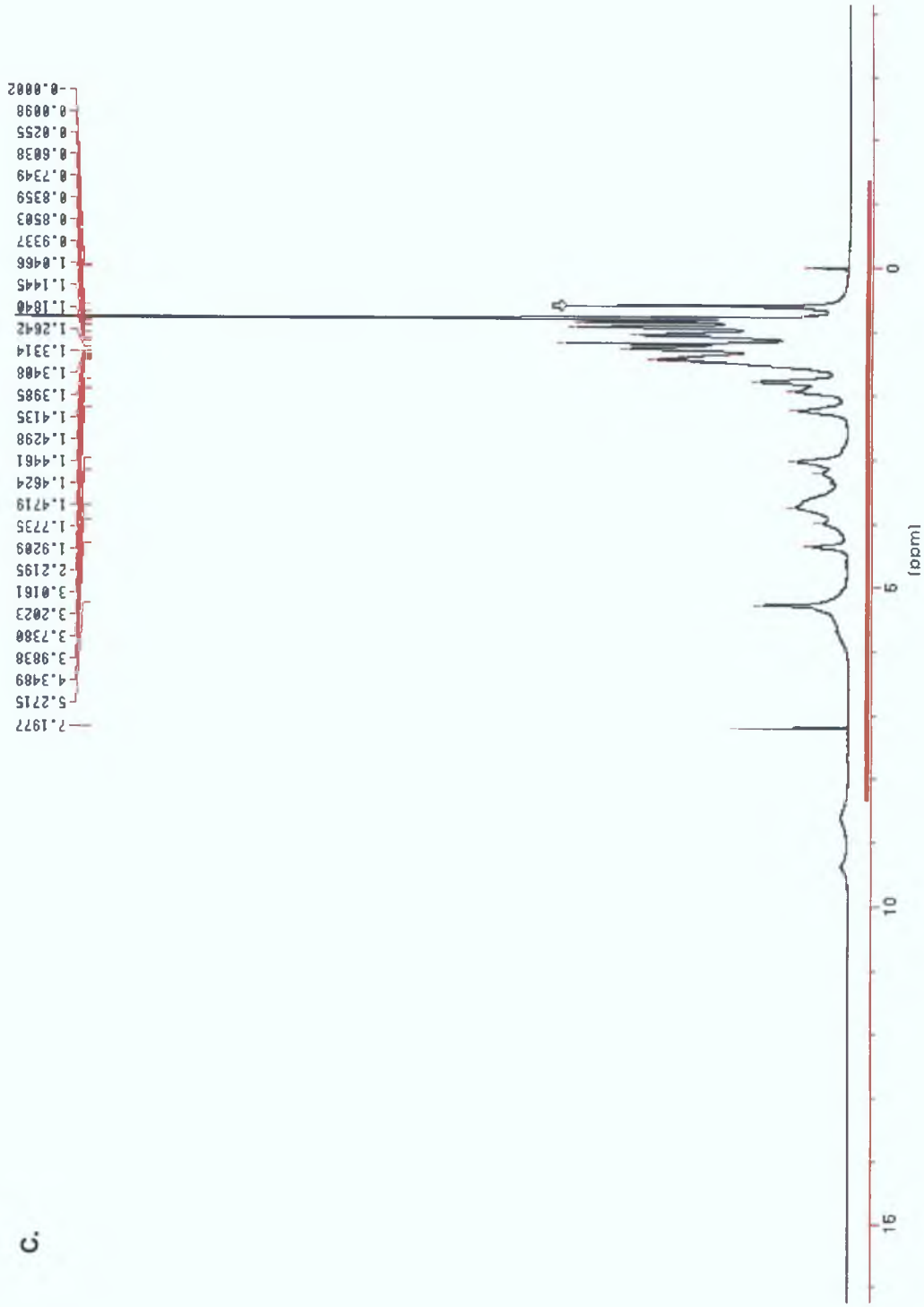


Figure 8.2: Nuclear Magnetic Resonance (NMR) spectra of (A) Mann-C2-Chol, (B) Mann-C4-Chol and (C) Mann-C6-Chol

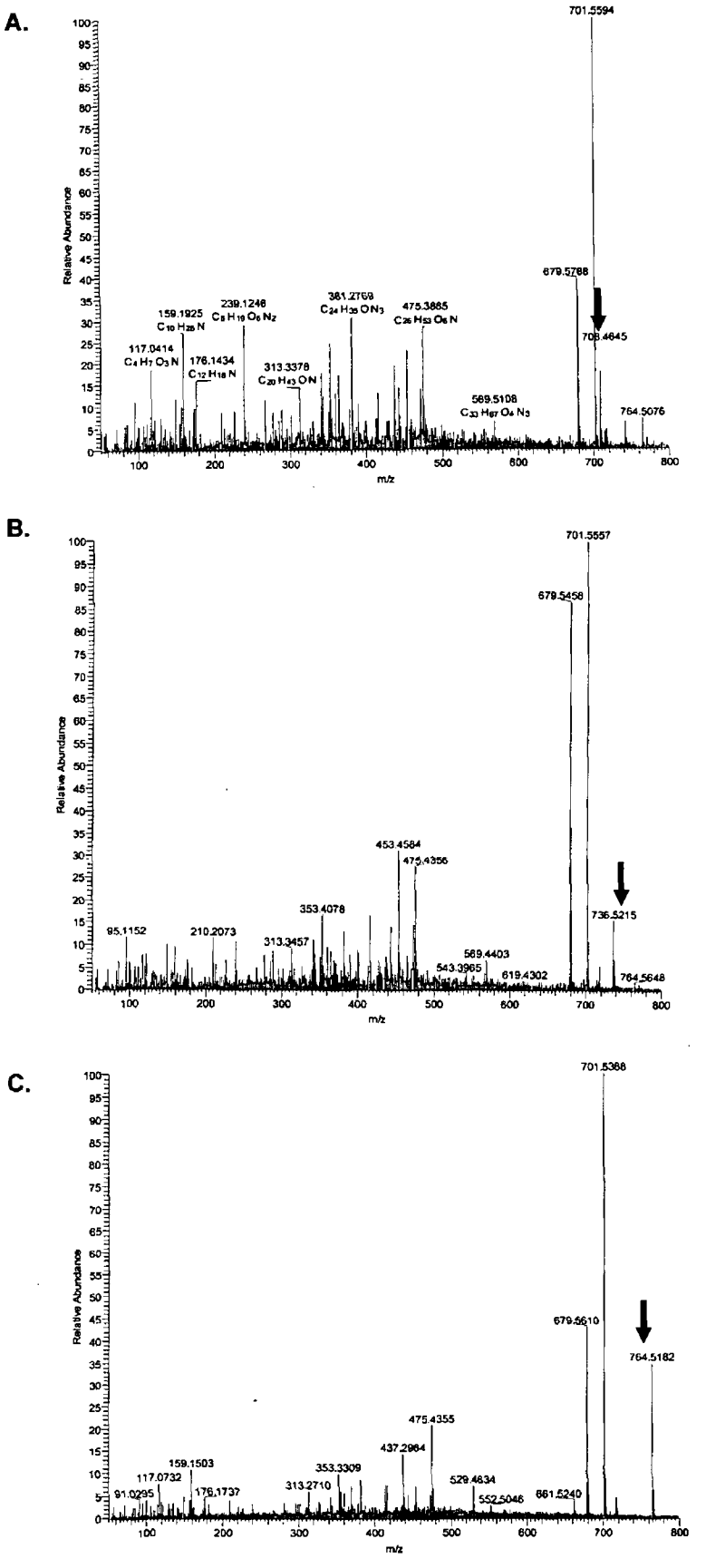


Figure 8.3: Mass spectrometry spectra of (A) Mann-C2-Chol, (B) Mann-C4-Chol and (C) Mann-C6-Chol

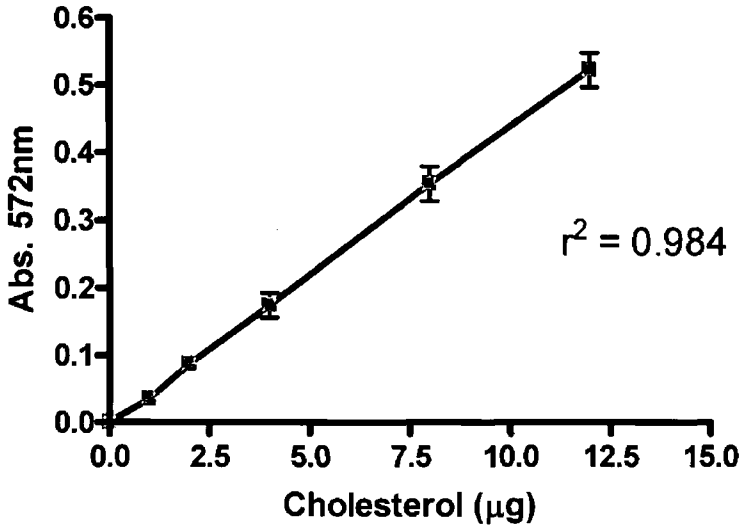


Figure 8.4: Representative cholesterol assay standard curve

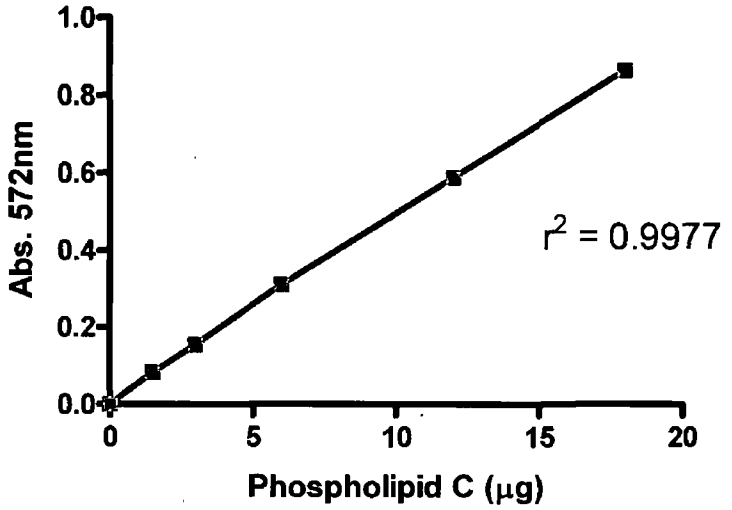


Figure 8.5: Representative phospholipid assay standard curve

A

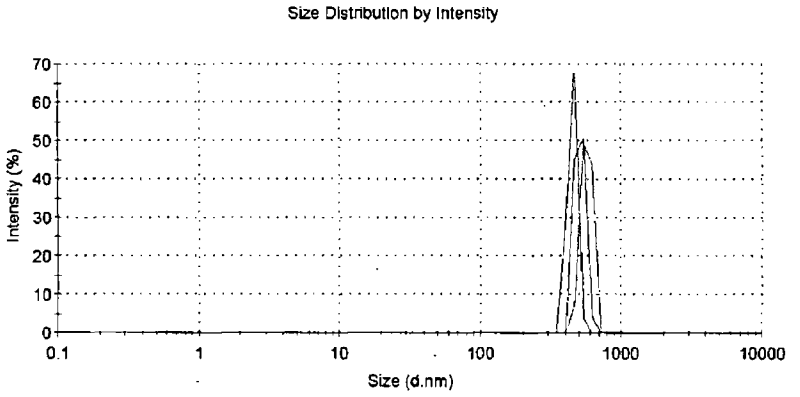


B

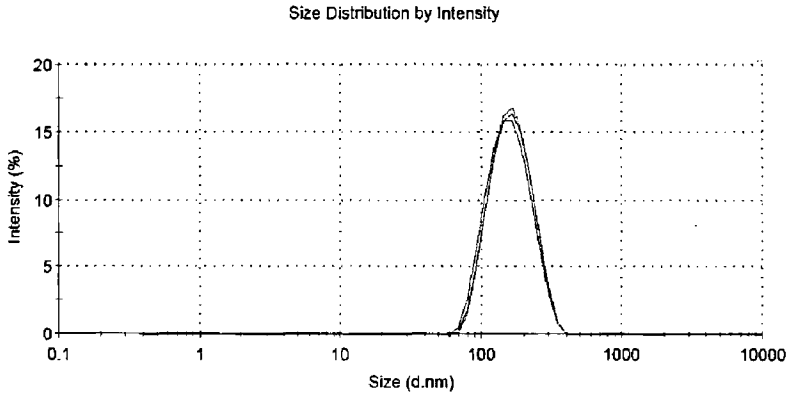


Figure 8.6: Size distribution by intensity before and after extrusion of DOPS:Chol 7:3 liposomes. Average size before extrusion was 1579 nm (PDI 0.776) and after extrusion was 148.4nm (PDI 0.096).

**Table 8.1: Liposome Stability**

| Liposome | Week 0 | | Week 1 | | Week 3 | | Week 4 | |
|---|---|---|---|---|---|---|---|---|
| | Average Size (nm) | PDI | Average Size (nm) | PDI | Average Size (nm) | PDI | Average Size (nm) | PDI |
| ***DOPS*** | 148.6 | 0.115 | 153.7 | 0.088 | 157.2 | 0.122 | 151.2 | 0.103 |
| ***DSPC*** | 186.4 | 0.289 | 170.0 | 0.151 | 168.2 | 0.138 | 168.6 | 0.147 |
| ***DOTAP*** | 135.8 | 0.060 | 164.1 | 0.086 | 174.1 | 0.088 | 179.7 | 0.107 |

### 8.3 Supplemental siRNA Data

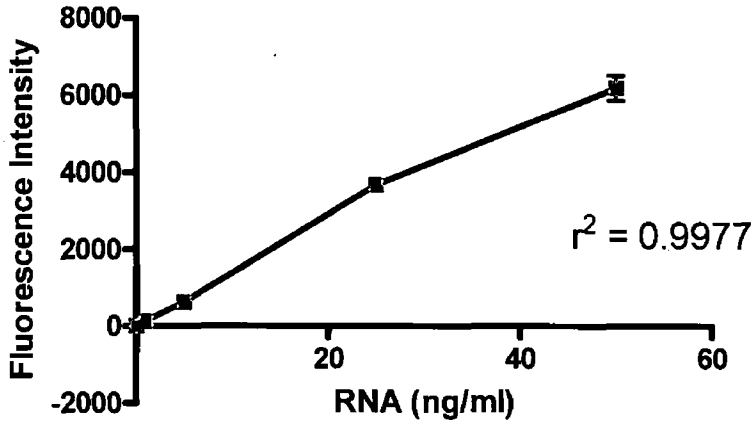


Figure 8.7: Representative Ribogreen Assay standard curve

**Table 8.2: NanoDrop siRNA limits of detection**

| Dilution Concentration (ng/pl) | Detected Concentration (ng/µl) | STDEV FROM THEORETICAL | 260/280 |
|---|---|---|---|
| 266 | 265 ± 3.7 | 0.70 | 2.1 |
| 100 | 101.4 ± 2.5 | 0.98 | 2.1 |
| 50 | 46.8 ± 0.2 | 2.24 | 2.2 |
| 25 | 22.3 ± 0.9 | 1.86 | 2.1 |
| 12.5 | 10.4 ± 1 | 1.51 | 2.1 |
| 6.25 | 5.3 ± 1.2 | 0.71 | 1.7 |
| 3.125 | 1.5 ± 0.6 | 1.18 | 1.8 |
| 2 | 0.5 ± 0.4 | 1.09 | 1.2 |
| 1 | -0.3 ± 0.2 | 0.93 | 1.5 |

## 8.4 Supplemental *In Vitro* Liposome Data

### 8.4.1 siRNA Cell Uptake Via a Commericial Tranfection Reagent

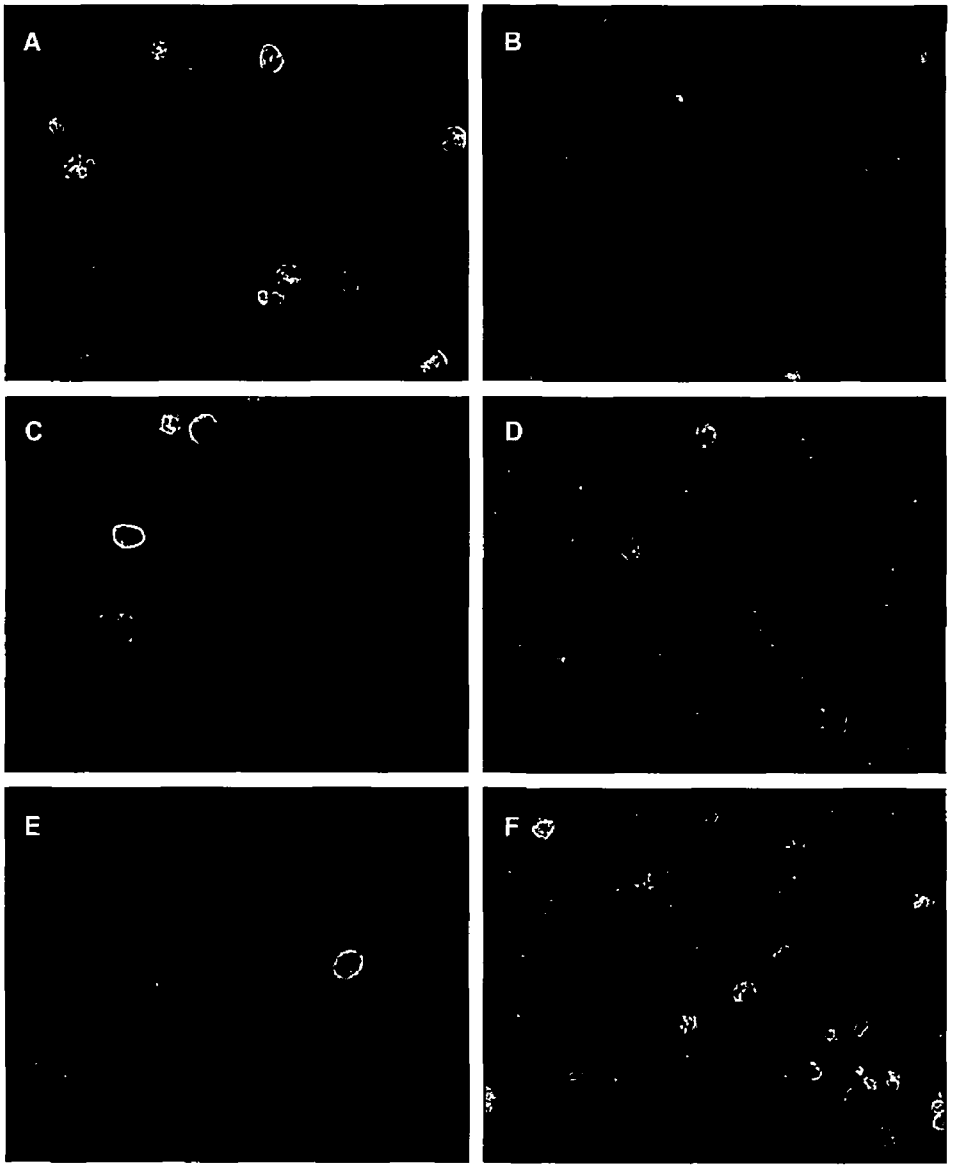


Figure 8.8: Fluorescent microscopy images (20x) of differentiated THP-1 cells treated as follows (A) media (control), (B) Dharmafect 2 transfection reagent only, (C) siGLO/Dharmafected 2 incubated for 1 hour, (D) siGLO/Dharmafected 2 incubated for 2 hours, (E) siGLO/Dharmafected 2 incubated for 3 hours and (F) siGLO/Dharmafected 2 incubated for 4 hours. siGLO is a fluorescently tagged siRNA (red). Cells were counter stained with Hoescht (blue; nuclei) and phalloidin-FITC (green; F-Actin).

### 8.4.2 Mannoylated Liposome Mediated TNFα Knockdown in Differentiated THP-1 Cells

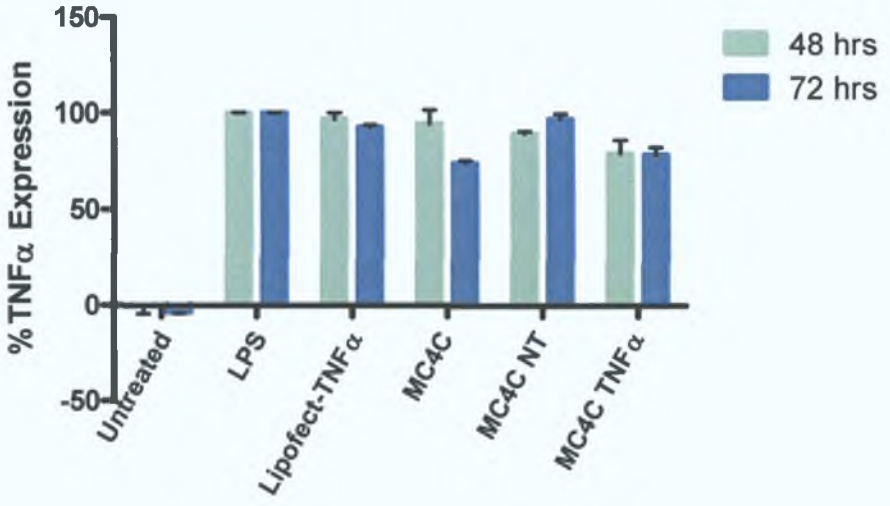


Figure 8.9: TNFα knockdown in differentiated THP-1 cells via 7.5% MC4C mannosylated liposomes (incorporating 10% DOTAP into the formulation) (n = 2)

### 8.4.3 Liposome Induced Toxicity

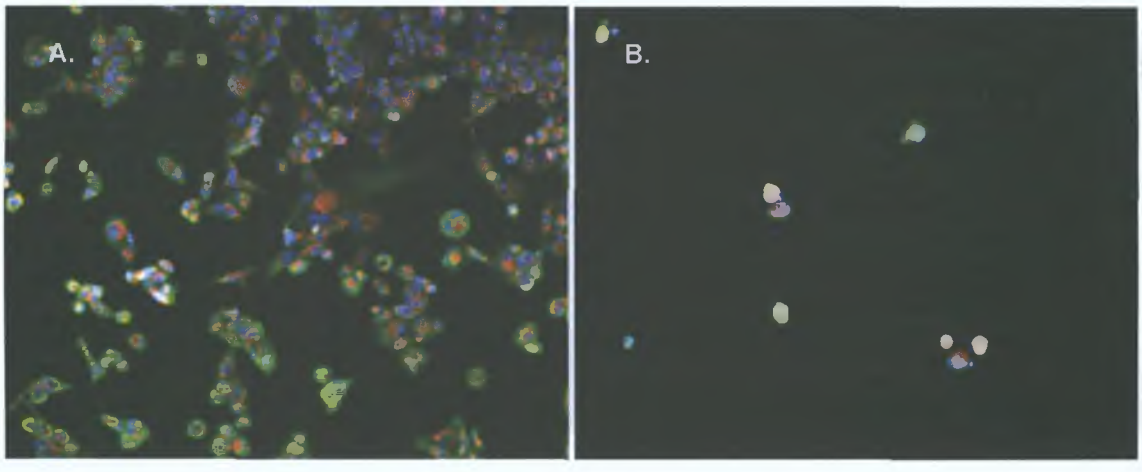


Figure 8.10: Toxicity screening determined by high content cell analysis. Differentiated THP-1 cells were treated with either (A) media alone (negative control) or (B) 120μM valinomycin (positive control). Cells were treated for 24 hours, fixed and stained for nuclei (hoescht; blue), cell permeability (green), mitochondrial membrane potential (MMP; red), and cytochrome c (cytochrome c antibody). Fused images were acquired using an INCELL 1000 (GE Healthcare).

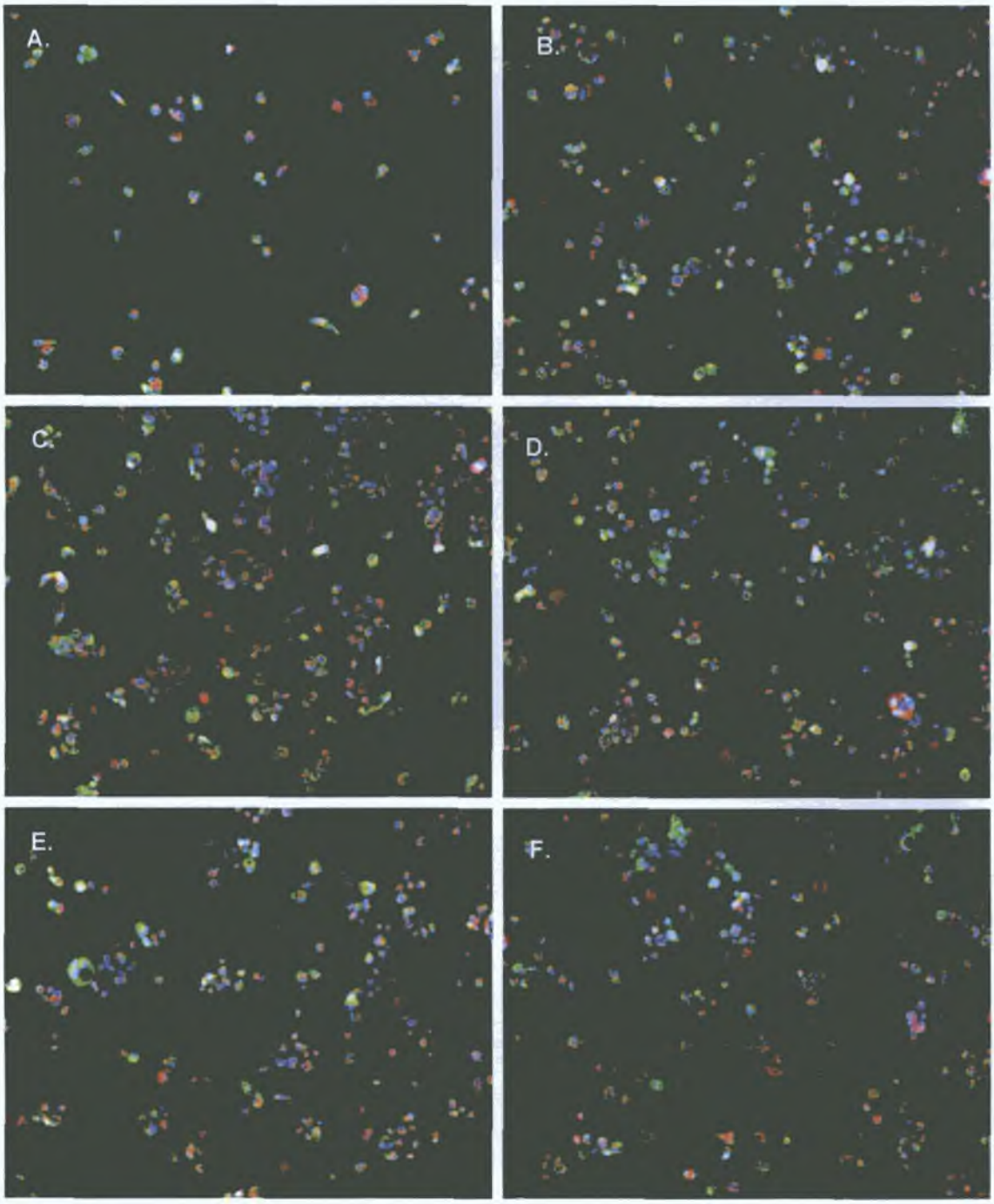


Figure 8.11: Liposome toxicity screening determined by high content cell analysis. Differentiated THP-1 cells were treated with 100μM (A) DOTAP, (B) DOPS, (C) DOPC, (D) MC2C, (E) MC4C and (F) MC6C liposomes for 24 hours, fixed and stained for nuclei (hoescht; blue), cell permeability (green), mitochondrial membrane potential (MMP; red), and cytochrome c (cytochrome c antibody). Fused images were acquired using an INCELL 1000 (GE Healthcare).

## 8.5 Supplemental *In Vitro* siRNA-Microparticle Toxicity Data

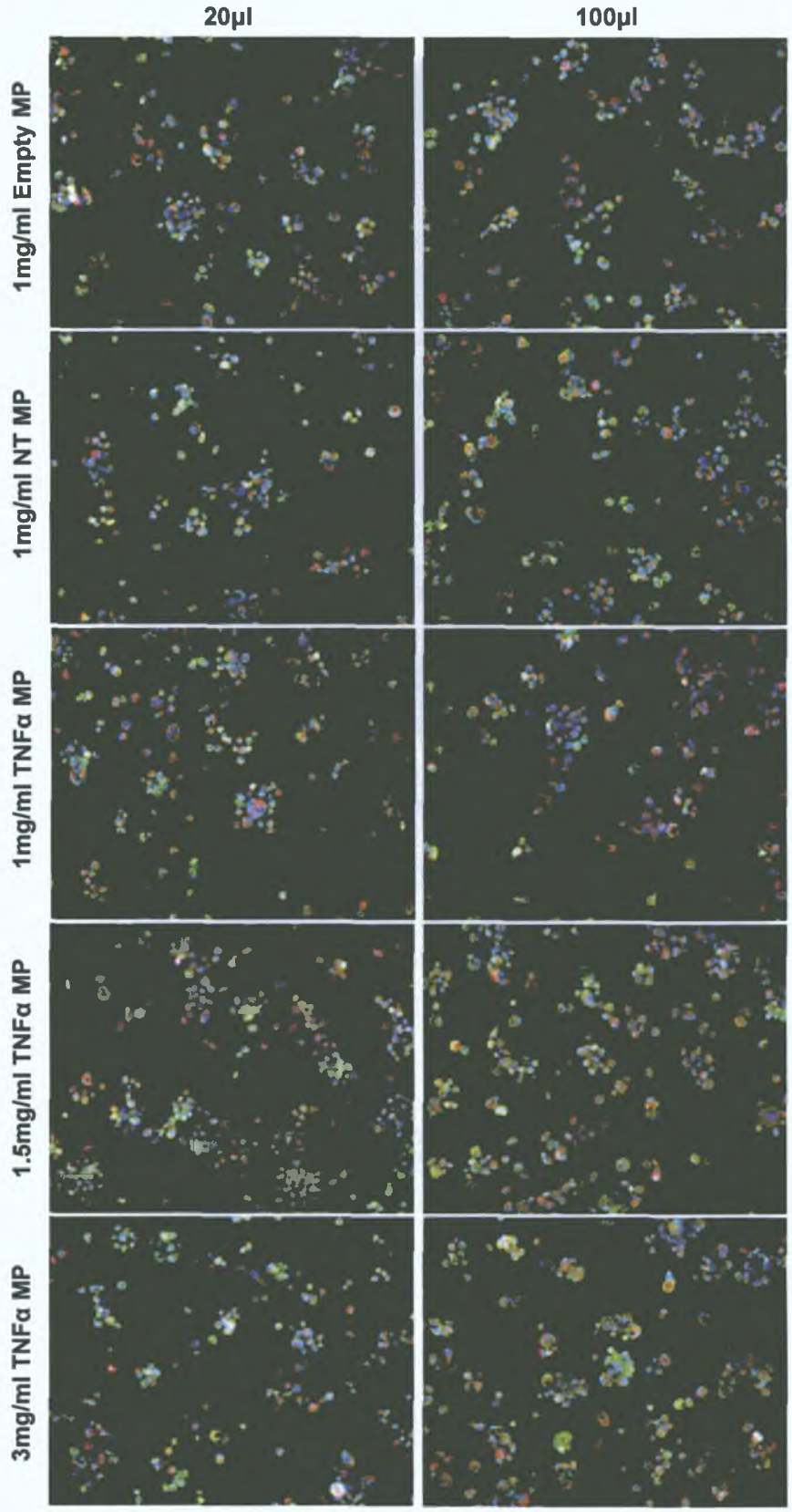


Figure 8.12: Microparticle toxicity screening determined by high content cell analysis. Differentiated THP-1 cells were treated with either 20 or 100µg empty microparticles (MP) or microparticles encapsulating non-target siRNA (NT MP). Cells were treated for 24 hours, fixed and stained for nuclei (hoescht; blue), cell permeability (green), mitochondrial membrane potential (MMP; red), and cytochrome c (cytochrome c antibody). Fused images were acquired using an INCELL 1000 (GE Healthcare). (controls Figure 8.10)

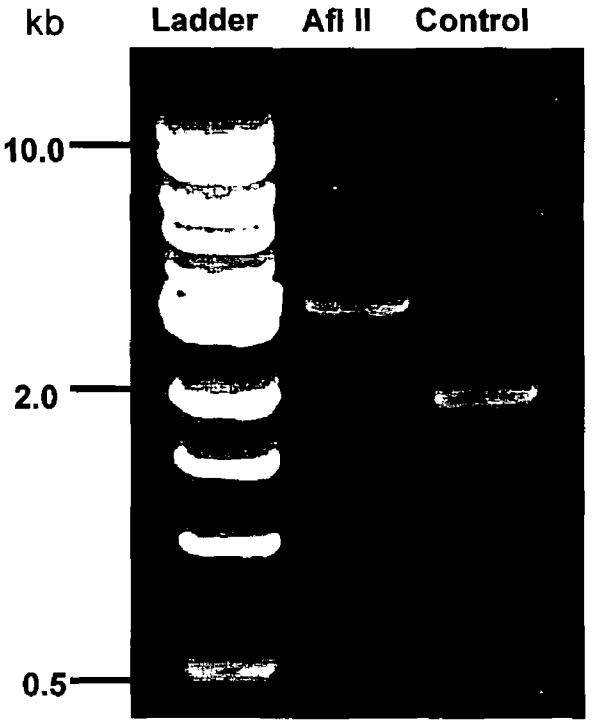


Figure 8.13: DNA digest of pmaxGFP with Afl II restriction enzyme.

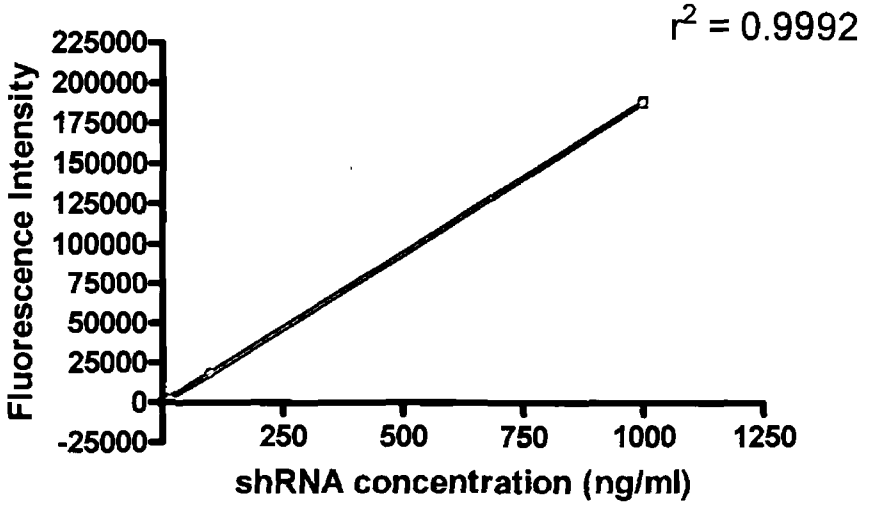


Figure 8.14: Representative shRNA standard curve by Quant iT picogreen assay

## References

1. Cotrim, A.P. and B.J. Baum, *Gene therapy: some history, applications, problems, and prospects.* Toxicol Pathol, 2008. **36**(1): p. 97-103.
2. Martini, F. and W.C. Ober, *Fundamentals of anatomy and physiology.* 4th ed. ed. 1998, Upper Saddle River, N.J.: Prentice Hall ; London : Prentice Hall International. 1 v. (various pagings).
3. Weibel, E.R. and D.M. Gomez, *Architecture of the human lung. Use of quantitative methods establishes fundamental relations between size and number of lung structures.* Science, 1962. **137**: p. 577-85.
4. Patton, J.S. and P.R. Byron, *Inhaling medicines: delivering drugs to the body through the lungs.* Nat Rev Drug Discov, 2007. **6**(1): p. 67-74.
5. Kleinstreuer, C., Z. Zhang, and J.F. Donohue, *Targeted drug-aerosol delivery in the human respiratory system.* Annu Rev Biomed Eng, 2008. **10**: p. 195-220.
6. Fahy, J.V. and B.F. Dickey, *Airway mucus function and dysfunction.* N Engl J Med, 2010. **363**(23): p. 2233-47.
7. Rogueda, P.G. and D. Traini, *The nanoscale in pulmonary delivery. Part 1: deposition, fate, toxicology and effects.* Expert Opin Drug Deliv, 2007. **4**(6): p. 595-606.
8. Agu, R.U. and M.I. Ugwoke, *In vitro and in vivo testing methods for respiratory drug delivery.* Expert Opin Drug Deliv, 2011. 8(1): p. 57-69.
9. Carvalho, T.C., J.I. Peters, and R.O. Williams, 3rd, *Influence of particle size on regional lung deposition--what evidence is there?* Int J Pharm, 2011. **406**(1-2): p. 1-10.
10. Heyder, J., *Deposition of inhaled particles in the human respiratory tract and consequences for regional targeting in respiratory drug delivery.* Proc Am Thorac Soc, 2004. **1**(4): p. 315-20.
11. Chow, A.H., et al., *Particle engineering for pulmonary drug delivery.* Pharm Res, 2007. **24**(3): p. 411-37.
12. Morjaria, J.B., M. Malerba, and R. Polosa, *Biologic and pharmacologic therapies in clinical development for the inflammatory response in COPD.* Drug Discov Today, 2010. **15**(9-10): p. 396-405.
13. Chmiel, J., M. Berger, and M. Konstan, *The role of inflammation in the pathophysiology of CF lung disease.* Clinical Reviews in Allergy and Immunology, 2002. **23**(1): p. 5-27.
14. Murdoch, J.R. and C.M. Lloyd, *Chronic inflammation and asthma.* Mutation Research/Fundamental and Molecular Mechanisms of Mutagenesis, 2010. **690**(1-2): p. 24-39.
15. Kita, H., *Eosinophils: multifaceted biological properties and roles in health and disease.* Immunological Reviews, 2011. **242**(1): p. 161-177.
16. Holgate, S.T., *The sentinel role of the airway epithelium in asthma pathogenesis.* Immunological Reviews, 2011. **242**(1): p. 205-219.
17. Proud, D. and R. Leigh, *Epithelial cells and airway diseases.* Immunological Reviews, 2011. **242**(1): p. 186-204.
18. Moiseeva, E.P. and P. Bradding, *Mast Cells in Lung Inflammation*
*Mast Cell Biology*, A.M. Gilfillan and D.D. Metcalfe, Editors. 2011, Springer US. p. 235-269.
19. Molfino, N.A. and P.K. Jeffery, *Chronic obstructive pulmonary disease: histopathology, inflammation and potential therapies.* Pulm Pharmacol Ther, 2007. **20**(5): p. 462-72.
20. Koziol-White, C.J. and R.A. Panettieri Jr, *Airway smooth muscle and immunomodulation in acute exacerbations of airway disease.* Immunological Reviews, 2011. **242**(1): p. 178-185.
21. Barnes, P.J., *Small airways in COPD.* N Engl J Med, 2004. **350**(26): p. 2635-7.
22. Martinez, F.J., J.F. Donohue, and S.I. Rennard, *The future of chronic obstructive pulmonary disease treatment—difficulties of and barriers to drug development.* The Lancet, 2011. **378**(9795): p. 1027-1037.
23. Rabe, K.F., et al., *Global Strategy for the Diagnosis, Management, and Prevention of Chronic Obstructive Pulmonary Disease: GOLD Executive Summary.* Am. J. Respir. Crit. Care Med., 2007. **176**(6): p. 532-555.
24. Farrell, P., et al., *Diagnosis of cystic fibrosis in the Republic of Ireland: epidemiology and costs.* Vol. 100. 2007. 557-60.
25. Kawada, N., et al., *Towards developing new strategies to reduce the adverse side-effects of nonsteroidal anti-inflammatory drugs.* Clin Exp Nephrol, 2011.
26. Bhakta, N.R. and P.G. Woodruff, *Human asthma phenotypes: from the clinic, to cytokines, and back again.* Immunological Reviews, 2011. **242**(1): p. 220-232.
27. Brightling, C., M. Berry, and Y. Amrani, *Targeting TNF-α: A novel therapeutic approach for asthma.* Journal of Allergy and Clinical Immunology, 2008. **121**(1): p. 5-10.

28. Naito, M., *Macrophage differentiation and function in health and disease.* Pathol Int, 2008. **58**(3): p. 143-55.
29. Varol, C., S. Yona, and S. Jung, *Origins and tissue-context-dependent fates of blood monocytes.* Immunol Cell Biol, 2009. **87**(1): p. 30-8.
30. Barnes, P.J., *Alveolar macrophages as orchestrators of COPD.* COPD, 2004. **1**(1): p. 59-70.
31. Benoit, M., B. Desnues, and J.L. Mege, *Macrophage polarization in bacterial infections.* J Immunol, 2008. **181**(6): p. 3733-9.
32. Mantovani, A., A. Sica, and M. Locati, *Macrophage polarization comes of age.* Immunity, 2005. **23**(4): p. 344-6.
33. Martinez, F.O., et al., *Macrophage activation and polarization.* Front Biosci, 2008. **13**: p. 453-61.
34. Van Rooijen, N. and A. Sanders, *Manipulation of Kupffer cells by liposome encapsulated clodronate and propamidine--synergistic and antagonistic effects of liposomal phospholipids and drugs.* International Journal of Pharmaceutics, 1998. **162**(1-2): p. 51-58.
35. Burke, B., et al., *Macrophages in gene therapy: cellular delivery vehicles and in vivo targets.* J Leukoc Biol, 2002. **72**(3): p. 417-28.
36. Gazi, U. and L. Martinez-Pomares, *Influence of the mannose receptor in host immune responses.* Immunobiology, 2009. **214**(7): p. 554-61.
37. Taylor, P.R., S. Gordon, and L. Martinez-Pomares, *The mannose receptor: linking homeostasis and immunity through sugar recognition.* Trends Immunol, 2005. **26**(2): p. 104-10.
38. McGreal, E.P., J.L. Miller, and S. Gordon, *Ligand recognition by antigen-presenting cell C-type lectin receptors.* Curr Opin Immunol, 2005. **17**(1): p. 18-24.
39. Gordon, S., *Pattern recognition receptors: doubling up for the innate immune response.* Cell, 2002. **111**(7): p. 927-30.
40. Apostolopoulos, V. and I.F. McKenzie, *Role of the mannose receptor in the immune response.* Curr Mol Med, 2001. **1**(4): p. 469-74.
41. Martinez-Pomares, L., et al., *Binding properties of the mannose receptor.* Immunobiology, 2001. **204**(5): p. 527-35.
42. Le Cabec, V., et al., *The human macrophage mannose receptor is not a professional phagocytic receptor.* J Leukoc Biol, 2005. **77**(6): p. 934-43.
43. McGreal, E.P., L. Martinez-Pomares, and S. Gordon, *Divergent roles for C-type lectins expressed by cells of the innate immune system.* Mol Immunol, 2004. **41**(11): p. 1109-21.
44. Stahl, P.D. and R.A. Ezekowitz, *The mannose receptor is a pattern recognition receptor involved in host defense.* Curr Opin Immunol, 1998. **10**(1): p. 50-5.
45. Hehlgans, T. and K. Pfeffer, *The intriguing biology of the tumour necrosis factor/tumour necrosis factor receptor superfamily: players, rules and the games.* Immunology, 2005. **115**(1): p. 1-20.
46. Murugan, V. and M.J. Peck, *Signal transduction pathways linking the activation of alveolar macrophages with the recruitment of neutrophils to lungs in chronic obstructive pulmonary disease.* Exp Lung Res, 2009. **35**(6): p. 439-85.
47. Parameswaran, N. and S. Patial, *Tumor necrosis factor-alpha signaling in macrophages.* Crit Rev Eukaryot Gene Expr, 2010. **20**(2): p. 87-103.
48. Ernandez, T. and T.N. Mayadas, *Immunoregulatory role of TNFalpha in inflammatory kidney diseases.* Kidney Int, 2009. **76**(3): p. 262-76.
49. Matera, M.G., L. Calzetta, and M. Cazzola, *TNF-alpha inhibitors in asthma and COPD: we must not throw the baby out with the bath water.* Pulm Pharmacol Ther. **23**(2): p. 121-8.
50. Fire, A., et al., *Potent and specific genetic interference by double-stranded RNA in Caenorhabditis elegans.* Nature, 1998. **391**(6669): p. 806-11.
51. Elbashir, S.M., et al., *Duplexes of 21-nucleotide RNAs mediate RNA interference in cultured mammalian cells.* Nature, 2001. **411**(6836): p. 494-8.
52. de Fougerolles, A., et al., *Interfering with disease: a progress report on siRNA-based therapeutics.* Nat Rev Drug Discov, 2007. **6**(6): p. 443-53.
53. Carthew, R.W. and E.J. Sontheimer, *Origins and Mechanisms of miRNAs and siRNAs.* Cell, 2009. **136**(4): p. 642-55.
54. Grimm, D., *Small silencing RNAs: state-of-the-art.* Adv Drug Deliv Rev, 2009. **61**(9): p. 672-703.
55. Sledz, C.A. and B.R. Williams, *RNA interference in biology and disease.* Blood, 2005. **106**(3): p. 787-94.

56. Akhtar, S. and I.F. Benter, *Nonviral delivery of synthetic siRNAs in vivo.* J Clin Invest, 2007. **117**(12): p. 3623-32.
57. Orban, T.I. and E. Izaurralde, *Decay of mRNAs targeted by RISC requires XRN1, the Ski complex, and the exosome.* RNA, 2005. **11**(4): p. 459-69.
58. Manjunath, N., et al., *Lentiviral delivery of short hairpin RNAs.* Adv Drug Deliv Rev, 2009. **61**(9): p. 732-45.
59. Wolff, J.A., et al., *Direct gene transfer into mouse muscle in vivo.* Science, 1990. **247**(4949 Pt 1): p. 1465-8.
60. Miyazaki, S. and J. Miyazaki, *In vivo DNA electrotransfer into muscle.* Dev Growth Differ, 2008. **50**(6): p. 479-83.
61. Pringle, I.A., et al., *Electroporation enhances reporter gene expression following delivery of naked plasmid DNA to the lung.* J Gene Med, 2007. **9**(5): p. 369-80.
62. Herweijer, H. and J.A. Wolff, *Progress and prospects: naked DNA gene transfer and therapy.* Gene Ther, 2003. **10**(6): p. 453-8.
63. Seow, Y. and M.J. Wood, *Biological gene delivery vehicles: beyond viral vectors.* Mol Ther, 2009. **17**(5): p. 767-77.
64. Yamane, I., M. Nishikawa, and Y. Takakura, *Cellular uptake and activation characteristics of naked plasmid DNA and its cationic liposome complex in human macrophages.* Int J Pharm, 2005. **305**(1-2): p. 145-53.
65. Behlke, M.A., *Chemical modification of siRNAs for in vivo use.* Oligonucleotides, 2008. **18**(4): p. 305-19.
66. Judge, A.D., et al., *Design of noninflammatory synthetic siRNA mediating potent gene silencing in vivo.* Mol Ther, 2006. **13**(3): p. 494-505.
67. Bramsen, J.B., et al., *A large-scale chemical modification screen identifies design rules to generate siRNAs with high activity, high stability and low toxicity.* Nucleic Acids Res, 2009. **37**(9): p. 2867-81.
68. Soutschek, J., et al., *Therapeutic silencing of an endogenous gene by systemic administration of modified siRNAs.* Nature, 2004. **432**(7014): p. 173-8.
69. Bumcrot, D., et al., *RNAi therapeutics: a potential new class of pharmaceutical drugs.* Nat Chem Biol, 2006. **2**(12): p. 711-9.
70. Gao, S., et al., *The effect of chemical modification and nanoparticle formulation on stability and biodistribution of siRNA in mice.* Mol Ther, 2009. **17**(7): p. 1225-33.
71. Shim, M.S. and Y.J. Kwon, *Efficient and targeted delivery of siRNA in vivo.* FEBS J, 2010. **277**(23): p. 4814-27.
72. de Martimprey, H., et al., *Polymer nanocarriers for the delivery of small fragments of nucleic acids: oligonucleotides and siRNA.* Eur J Pharm Biopharm, 2009. **71**(3): p. 490-504.
73. Gary, D.J., N. Puri, and Y.Y. Won, *Polymer-based siRNA delivery: perspectives on the fundamental and phenomenological distinctions from polymer-based DNA delivery.* J Control Release, 2007. **121**(1-2): p. 64-73.
74. Abrams, M.T., et al., *Evaluation of Efficacy, Biodistribution, and Inflammation for a Potent siRNA Nanoparticle: Effect of Dexamethasone Co-treatment.* Mol Ther, 2009. **18**(1): p. 171-180.
75. Durcan, N., C. Murphy, and S.-A. Cryan, *Inhalable siRNA: Potential as a Therapeutic Agent in the Lungs.* Molecular Pharmaceutics, 2008. **5**(4): p. 559-566.
76. Tokatlian, T. and T. Segura, *siRNA applications in nanomedicine.* Wiley Interdisciplinary Reviews: Nanomedicine and Nanobiotechnology, 2010. **2**(3): p. 305-315.
77. Quesada Calvo, F., et al., *Potential Therapeutic Target Discovery by 2D-DIGE Proteomic Analysis in Mouse Models of Asthma.* Journal of Proteome Research, 2011: p. null-null.
78. Kim, T.H., et al., *Blockade of the Wnt/β-Catenin Pathway Attenuates Bleomycin-Induced Pulmonary Fibrosis.* The Tohoku Journal of Experimental Medicine, 2011. **223**(1): p. 45-54.
79. Rosas-Taraco, A.G., et al., *Intrapulmonary Delivery of XCL1-Targeting Small Interfering RNA in Mice Chronically Infected with Mycobacterium tuberculosis.* Am. J. Respir. Cell Mol. Biol., 2009. **41**(2): p. 136-145.
80. Merkel, O.M., et al., *Nonviral siRNA Delivery to the Lung: Investigation of PEG−PEI Polyplexes and Their In Vivo Performance.* Molecular Pharmaceutics, 2009. **6**(4): p. 1246-1260.
81. Perl, M., et al., *Silencing of Fas, but Not Caspase-8, in Lung Epithelial Cells Ameliorates Pulmonary Apoptosis, Inflammation, and Neutrophil Influx after Hemorrhagic Shock and Sepsis.* The American Journal of Pathology, 2005. **167**(6): p. 1545-1559.

82. Beyerle, A., et al., *Comparative in vivo study of poly(ethylene imine)/siRNA complexes for pulmonary delivery in mice.* Journal of Controlled Release, 2011. **151**(1): p. 51-56.
83. Wang, J.-C., et al., *Attenuation of fibrosis in vitro and in vivo with SPARC siRNA.* Arthritis Research & Therapy, 2010. **12**(2): p. R60.
84. Garbuzenko, O., et al., *Intratracheal versus Intravenous Liposomal Delivery of siRNA, Antisense Oligonucleotides and Anticancer Drug.* Pharmaceutical Research, 2009. **26**(2): p. 382-394.
85. Gutbier, B., et al., *RNAi-mediated suppression of constitutive pulmonary gene expression by small interfering RNA in mice.* Pulmonary Pharmacology & Therapeutics, 2010. **23(4)**: p. 334-344.
86. Puri, A., et al., *Lipid-based nanoparticles as pharmaceutical drug carriers: from concepts to clinic.* Crit Rev Ther Drug Carrier Syst, 2009. **26**(6): p. 523-80.
87. Malmsten, M., *Surfactants and polymers in drug delivery.* 2002, New York: Marcel Dekker. vii, 348 p.
88. Maurer, N., D.B. Fenske, and P.R. Cullis, *Developments in liposomal drug delivery systems.* Expert Opin Biol Ther, 2001. **1**(6): p. 923-47.
89. Gregoriadis, G., *Liposome technology: Liposome Preparation and Related Techniques.* 3rd ed. ed. Vol. 1. 2007, New York ; London: Informa Healthcare. 3 v.
90. Labiris, N.R. and M.B. Dolovich, *Pulmonary drug delivery. Part II: the role of inhalant delivery devices and drug formulations in therapeutic effectiveness of aerosolized medications.* Br J Clin Pharmacol, 2003. **56**(6): p. 600-12.
91. Lasic, D.D., *Liposomes in gene delivery.* 1997, Boca Raton: CRC Press. 295p.
92. MacLachlan, I., *Liposomal Formulations for Nucleic Acid Delivery*, in *Antisense Drug Technology: Principles, Strategies, and Applications, Second Edition*, S.T. Crooke, Editor. 2007, Taylor & Francis Group. p. 237 - 270.
93. Lv, H., et al., *Toxicity of cationic lipids and cationic polymers in gene delivery.* J Control Release, 2006. **114**(1): p. 100-9.
94. Landen, C.N., Jr., et al., *Therapeutic EphA2 gene targeting in vivo using neutral liposomal small interfering RNA delivery.* Cancer Res, 2005. **65**(15): p. 6910-8.
95. Li, C. and Y. Deng, *A novel method for the preparation of liposomes: freeze drying of monophase solutions.* J Pharm Sci, 2004. **93**(6): p. 1403-14.
96. Chen, Y., et al., *Multifunctional nanoparticles delivering small interfering RNA and doxorubicin overcome drug resistance in cancer.* J Biol Chem, 2010. **285**(29): p. 22639-50.
97. Peer, D., et al., *Systemic leukocyte-directed siRNA delivery revealing cyclin D1 as an anti-inflammatory target.* Science, 2008. **319**(5863): p. 627-30.
98. Nakamura, Y., et al., *Octaarginine-modified multifunctional envelope-type nano device for siRNA.* J Control Release, 2007. **119**(3): p. 360-7.
99. Zheng, X., et al., *A novel in vivo siRNA delivery system specifically targeting dendritic cells and silencing CD40 genes for immunomodulation.* Blood, 2009. **113**(12): p. 2646-54.
100. Meng, J., et al., *Novel anion liposome-encapsulated antisense oligonucleotide restores susceptibility of methicillin-resistant Staphylococcus aureus and rescues mice from lethal sepsis by targeting mecA.* Antimicrob Agents Chemother, 2009. **53**(7): p. 2871-8.
101. Sun, P., et al., *Anionic LPD complexes for gene delivery to macrophage: preparation, characterization and transfection in vitro.* J Drug Target, 2008. **16**(9): p. 668-78.
102. Jing, Y., A. Shishkov, and B.C. Ponnappa, *Inhibition of tumor necrosis factor alpha secretion in rat Kupffer cells by siRNA: in vivo efficacy of siRNA-liposomes.* Biochim Biophys Acta, 2008. **1780**(1): p. 34-40.
103. Ko, Y.T., R. Bhattacharya, and U. Bickel, *Liposome encapsulated polyethylenimine/ODN polyplexes for brain targeting.* J Control Release, 2009. **133**(3): p. 230-7.
104. Yamauchi, M., et al., *Development of wrapped liposomes: novel liposomes comprised of polyanion drug and cationic lipid complexes wrapped with neutral lipids.* Biochim Biophys Acta, 2006. **1758**(1): p. 90-7.
105. Auguste, D.T., et al., *Triggered release of siRNA from poly(ethylene glycol)-protected, pH-dependent liposomes.* J Control Release, 2008. **130**(3): p. 266-74.
106. Pichu, S., et al., *Dicer-substrate siRNA inhibits tumor necrosis factor alpha secretion in Kupffer cells in vitro: In vivo targeting of Kupffer cells by siRNA-liposomes.* Pharmacol Res, 2011.
107. Ahsan, F., et al., *Targeting to macrophages: role of physicochemical properties of particulate carriers--liposomes and microspheres--on the phagocytosis by macrophages.* J Control Release, 2002. **79**(1-3): p. 29-40.

108. Chono, S., et al., *Influence of particle size on drug delivery to rat alveolar macrophages following pulmonary administration of ciprofloxacin incorporated into liposomes.* J Drug Target, 2006. **14**(8): p. 557-66.
109. Chono, S., Y. Tauchi, and K. Morimoto, *Influence of particle size on the distributions of liposomes to atherosclerotic lesions in mice.* Drug Dev Ind Pharm, 2006. **32**(1): p. 125-35.
110. Chono, S., et al., *Uptake characteristics of liposomes by rat alveolar macrophages: influence of particle size and surface mannose modification.* J Pharm Pharmacol, 2007. **59**(1): p. 75-80.
111. Ravichandran, K.S. and U. Lorenz, *Engulfment of apoptotic cells: signals for a good meal.* Nat Rev Immunol, 2007. **7**(12): p. 964-74.
112. Hafez, I.M. and P.R. Cullis, *Roles of lipid polymorphism in intracellular delivery.* Adv Drug Deliv Rev, 2001. **47**(2-3): p. 139-48.
113. Kamps, J.A. and G.L. Scherphof, *Receptor versus non-receptor mediated clearance of liposomes.* Adv Drug Deliv Rev, 1998. **32**(1-2): p. 81-97.
114. Wileman, T.E., M.R. Lennartz, and P.D. Stahl, *Identification of the macrophage mannose receptor as a 175-kDa membrane protein.* Proc Natl Acad Sci U S A, 1986. **83**(8): p. 2501-5.
115. Wijagkanalan, W., et al., *Efficient targeting to alveolar macrophages by intratracheal administration of mannosylated liposomes in rats.* J Control Release, 2008. **125**(2): p. 121-30.
116. Irache, J.M., et al., *Mannose-targeted systems for the delivery of therapeutics.* Expert Opin Drug Deliv, 2008. **5**(6): p. 703-24.
117. Kelly, C., C. Jefferies, and S.A. Cryan, *Targeted liposomal drug delivery to monocytes and macrophages.* J Drug Deliv, 2011. **2011**: p. 727241.
118. Chono, S., et al., *Efficient drug delivery to atherosclerotic lesions and the antiatherosclerotic effect by dexamethasone incorporated into liposomes in atherogenic mice.* J Drug Target, 2005. **13**(4): p. 267-76.
119. Gibbons, A.M., et al., *Delivery of rSLPI in a liposomal carrier for inhalation provides protection against cathepsin L degradation.* J Microencapsul, 2009. **26**(6): p. 513-22.
120. Epstein-Barash, H., et al., *Physicochemical parameters affecting liposomal bisphosphonates bioactivity for restenosis therapy: Internalization, cell inhibition, activation of cytokines and complement, and mechanism of cell death.* J Control Release, 2010.
121. Vyas, S.P., et al., *Design of liposomal aerosols for improved delivery of rifampicin to alveolar macrophages.* Int J Pharm, 2004. **269**(1): p. 37-49.
122. Oussoren, C., et al., *Liposomes as carriers of the antiretroviral agent dideoxycytidine-5'-triphosphate.* Int J Pharm, 1999. **180**(2): p. 261-70.
123. Salem, II and N. Duzgunes, *Efficacies of cyclodextrin-complexed and liposome-encapsulated clarithromycin against Mycobacterium avium complex infection in human macrophages.* Int J Pharm, 2003. **250**(2): p. 403-14.
124. Nardin, A., et al., *Liposomal muramyl tripeptide phosphatidylethanolamine: Targeting and activating macrophages for adjuvant treatment of osteosarcoma.* Curr Cancer Drug Targets, 2006. **6**(2): p. 123-33.
125. Jain, S., et al., *RGD-anchored magnetic liposomes for monocytes/neutrophils-mediated brain targeting.* Int J Pharm, 2003. **261**(1-2): p. 43-55.
126. Homem de Bittencourt, P.I., Jr., et al., *LipoCardium: endothelium-directed cyclopentenone prostaglandin-based liposome formulation that completely reverses atherosclerotic lesions.* Atherosclerosis, 2007. **193**(2): p. 245-58.
127. Koning, G.A., et al., *Interaction of differently designed immunoliposomes with colon cancer cells and Kupffer cells. An in vitro comparison.* Pharm Res, 2003. **20**(8): p. 1249-57.
128. Koning, G.A., J.A. Kamps, and G.L. Scherphof, *Interference of macrophages with immunotargeting of liposomes.* J Liposome Res, 2002. **12**(1-2): p. 107-19.
129. van Broekhoven, C.L., et al., *Targeting dendritic cells with antigen-containing liposomes: a highly effective procedure for induction of antitumor immunity and for tumor immunotherapy.* Cancer Res, 2004. **64**(12): p. 4357-65.
130. Wijagkanalan, W., et al., *Enhanced anti-inflammation of inhaled dexamethasone palmitate using mannosylated liposomes in an endotoxin-induced lung inflammation model.* Mol Pharmacol, 2008. **74**(5): p. 1183-92.
131. Espuelas, S., et al., *Influence of ligand valency on the targeting of immature human dendritic cells by mannosylated liposomes.* Bioconjug Chem, 2008. **19**(12): p. 2385-93.

132. Kole, L., L. Das, and P.K. Das, *Synergistic effect of interferon-gamma and mannosylated liposome-incorporated doxorubicin in the therapy of experimental visceral leishmaniasis.* J Infect Dis, 1999. **180**(3): p. 811-20.
133. Chono, S., et al., *Efficient drug targeting to rat alveolar macrophages by pulmonary administration of ciprofloxacin incorporated into mannosylated liposomes for treatment of respiratory intracellular parasitic infections.* J Control Release, 2008. **127**(1): p. 50-8.
134. Ishii, M. and N. Kojima, *Mucosal adjuvant activity of oligomannose-coated liposomes for nasal immunization.* Glycoconj J. **27**(1): p. 115-23.
135. Matsui, M., et al., *Targeted delivery of oligomannose-coated liposome to the omental micrometastasis by peritoneal macrophages from patients with gastric cancer.* Cancer Sci.
136. Dolovich, M.B. and R. Dhand, *Aerosol drug delivery: developments in device design and clinical use.* Lancet, 2011. **377**(9770): p. 1032-45.
137. Mitchell, J., S. Newman, and H.K. Chan, *In vitro and in vivo aspects of cascade impactor tests and inhaler performance: a review.* AAPS PharmSciTech, 2007. **8**(4): p. E110.
138. Hofmann, W., *Modelling particle deposition in human lungs: modelling concepts and comparison with experimental data.* Biomarkers, 2009. **14 Suppl 1**: p. 59-62.
139. Kim, C.S., *Deposition of aerosol particles in human lungs: in vivo measurement and modelling.* Biomarkers, 2009. **14 Suppl 1**: p. 54-8.
140. Birchall, J.C., I.W. Kellaway, and M. Gumbleton, *Physical stability and in-vitro gene expression efficiency of nebulised lipid-peptide-DNA complexes.* Int J Pharm, 2000. **197**(1-2): p. 221-31.
141. Densmore, C.L., et al., *Gene transfer by guanidinium-cholesterol: dioleoylphosphatidyl-ethanolamine liposome-DNA complexes in aerosol.* J Gene Med, 1999. **1**(4): p. 251-64.
142. Guillaume, C., et al., *Aerosolization of cationic lipid-DNA complexes: lipoplex characterization and optimization of aerosol delivery conditions.* Biochem Biophys Res Commun, 2001. **286**(3): p. 464-71.
143. Pillai, R., et al., *Ultrasonic nebulization of cationic lipid-based gene delivery systems for airway administration.* Pharm Res, 1998. **15**(11): p. 1743-7.
144. Stern, M., et al., *The effects of jet nebulisation on cationic liposome-mediated gene transfer in vitro.* Gene Ther, 1998. **5**(5): p. 583-93.
145. Chimote, G. and R. Banerjee, *In vitro evaluation of inhalable isoniazid-loaded surfactant liposomes as an adjunct therapy in pulmonary tuberculosis.* J Biomed Mater Res B Appl Biomater. **94**(1): p. 1-10.
146. Elhissi, A.M., et al., *Physical stability and aerosol properties of liposomes delivered using an air-jet nebulizer and a novel micropump device with large mesh apertures.* Int J Pharm, 2007. **334**(1-2): p. 62-70.
147. Elhissi, A.M., et al., *Formulations generated from ethanol-based proliposomes for delivery via medical nebulizers.* J Pharm Pharmacol, 2006. **58**(7): p. 887-94.
148. Hajos, F., et al., *Inhalable liposomal formulation for vasoactive intestinal peptide.* Int J Pharm, 2008. **357**(1-2): p. 286-94.
149. Huang, Y.Y. and C.H. Wang, *Pulmonary delivery of insulin by liposomal carriers.* J Control Release, 2006. **113**(1): p. 9-14.
150. Zaru, M., et al., *Liposomes for drug delivery to the lungs by nebulization.* Eur J Pharm Biopharm, 2007. **67**(3): p. 655-66.
151. Steele, T.W., et al., *Factors influencing polycation/siRNA colloidal stability toward aerosol lung delivery.* Eur J Pharm Biopharm, 2011.
152. Nielsen, E.J., et al., *Pulmonary gene silencing in transgenic EGFP mice using aerosolised chitosan/siRNA nanoparticles.* Pharm Res, 2010. **27**(12): p. 2520-7.
153. Nguyen, J., et al., *Fast degrading polyesters as siRNA nano-carriers for pulmonary gene therapy.* J Control Release, 2008. **132**(3): p. 243-51.
154. Gibbons, A., et al., *The effect of liposome encapsulation on the pharmacokinetics of recombinant secretory leukocyte protease inhibitor (rSLPI) therapy after local delivery to a guinea pig asthma model.* Pharm Res, 2011. **28**(9): p. 2233-45.
155. Jones, L.J., et al., *RNA quantitation by fluorescence-based solution assay: RiboGreen reagent characterization.* Anal Biochem, 1998. **265**(2): p. 368-74.
156. Mountziaris, P.M., et al., *Controlled release of anti-inflammatory siRNA from biodegradable polymeric microparticles intended for intra-articular delivery to the temporomandibular joint.* Pharm Res, 2011. **28**(6): p. 1370-84.
157. Moret, I., et al., *Stability of PEI-DNA and DOTAP-DNA complexes: effect of alkaline pH, heparin and serum.* J Control Release, 2001. **76**(1-2): p. 169-81.

158. Merkel, O.M., et al., *Nonviral siRNA delivery to the lung: investigation of PEG-PEI polyplexes and their in vivo performance.* Mol Pharm, 2009. **6**(4): p. 1246-60.
159. Dunne, M., et al., *Encapsulation of protamine sulphate compacted DNA in polylactide and polylactide-co-glycolide microparticles.* J Control Release, 2003. **92**(1-2): p. 209-19.
160. Van Rompaey, E., et al., *Interactions between oligonucleotides and cationic polymers investigated by fluorescence correlation spectroscopy.* Pharm Res, 2001. **18**(7): p. 928-36.
161. Turner, J.J., et al., *MALDI-TOF mass spectral analysis of siRNA degradation in serum confirms an RNAse A-like activity.* Mol Biosyst, 2007. **3**(1): p. 43-50.
162. Geusens, B., et al., *Ultradeformable cationic liposomes for delivery of small interfering RNA (siRNA) into human primary melanocytes.* J Control Release, 2009. **133**(3): p. 214-20.
163. Raemdonck, K., et al., *In situ analysis of single-stranded and duplex siRNA integrity in living cells.* Biochemistry, 2006. **45**(35): p. 10614-23.
164. Hasanovic, A., et al., *Improvement in physicochemical parameters of DPPC liposomes and increase in skin permeation of aciclovir and minoxidil by the addition of cationic polymers.* Eur J Pharm Biopharm, 2010. **75**(2): p. 148-53.
165. Kawakami, S., et al., *Biodistribution characteristics of mannosylated, fucosylated, and galactosylated liposomes in mice.* Biochim Biophys Acta, 2000. **1524**(2-3): p. 258-65.
166. Barenholz, Y., Lasic, D.D, *Handbook of Nonmedical Applications of Liposomes: v. 3: From Design to Microreactors.* 1996: CRC Press.
167. Hattori, Y., et al., *The role of dioleoylphosphatidylethanolamine (DOPE) in targeted gene delivery with mannosylated cationic liposomes via intravenous route.* J Control Release, 2005. **108**(2-3): p. 484-95.
168. Torchilin, V.P., et al., *Cell transfection in vitro and in vivo with nontoxic TAT peptide-liposome-DNA complexes.* Proc Natl Acad Sci U S A, 2003. **100**(4): p. 1972-7.
169. Huang, Z. and M.R. King, *An immobilized nanoparticle-based platform for efficient gene knockdown of targeted cells in the circulation.* Gene Ther, 2009. **16**(10): p. 1271-82.
170. Li, S.D. and L. Huang, *Surface-modified LPD nanoparticles for tumor targeting.* Ann N Y Acad Sci, 2006. **1082**: p. 1-8.
171. Hirsch, M., et al., *Preparation of small amounts of sterile siRNA-liposomes with high entrapping efficiency by dual asymmetric centrifugation (DAC).* J Control Release, 2009. **135**(1): p. 80-8.
172. Kleemann, E., et al., *Modified polyethylenimines as non-viral gene delivery systems for aerosol gene therapy: investigations of the complex structure and stability during air-jet and ultrasonic nebulization.* J Control Release, 2004. **100**(3): p. 437-50.
173. Kawakami, S., et al., *Asialoglycoprotein receptor-mediated gene transfer using novel galactosylated cationic liposomes.* Biochem Biophys Res Commun, 1998. **252**(1): p. 78-83.
174. Engel, A., et al., *Influence of spacer length on interaction of mannosylated liposomes with human phagocytic cells.* Pharm Res, 2003. **20**(1): p. 51-7.
175. Immordino, M.L., F. Dosio, and L. Cattel, *Stealth liposomes: review of the basic science, rationale, and clinical applications, existing and potential.* Int J Nanomedicine, 2006. **1**(3): p. 297-315.
176. Zuhorn, I.S., J.B. Engberts, and D. Hoekstra, *Gene delivery by cationic lipid vectors: overcoming cellular barriers.* Eur Biophys J, 2007. **36**(4-5): p. 349-62.
177. Wiethoff, C.M., et al., *The potential role of proteoglycans in cationic lipid-mediated gene delivery. Studies of the interaction of cationic lipid-DNA complexes with model glycosaminoglycans.* J Biol Chem, 2001. **276**(35): p. 32806-13.
178. Iwaoka, S., et al., *Cationic liposomes induce apoptosis through p38 MAP kinase-caspase-8-Bid pathway in macrophage-like RAW264.7 cells.* J Leukoc Biol, 2006. **79**(1): p. 184-91.
179. Aramaki, Y., S. Takano, and S. Tsuchiya, *Cationic liposomes induce macrophage apoptosis through mitochondrial pathway.* Arch Biochem Biophys, 2001. **392**(2): p. 245-50.
180. Arisaka, M., et al., *Involvement of protein kinase Cdelta in induction of apoptosis by cationic liposomes in macrophage-like RAW264.7 cells.* FEBS Lett, 2010. **584**(5): p. 1016-20.
181. Takano, S., Y. Aramaki, and S. Tsuchiya, *Physicochemical properties of liposomes affecting apoptosis induced by cationic liposomes in macrophages.* Pharm Res, 2003. **20**(7): p. 962-8.
182. Adler-Moore, J.P. and R.T. Proffitt, *Amphotericin B lipid preparations: what are the differences?* Clin Microbiol Infect, 2008. **14 Suppl 4**: p. 25-36.

183. Fidler, I.J., et al., *Design of liposomes to improve delivery of macrophage-augmenting agents to alveolar macrophages.* Cancer Res, 1980. **40**(12): p. 4460-6.
184. Moghimi, S.M. and A.C. Hunter, *Recognition by macrophages and liver cells of opsonized phospholipid vesicles and phospholipid headgroups.* Pharm Res, 2001. **18**(1): p. 1-8.
185. Tonges, L., et al., *Stearylated octaarginine and artificial virus-like particles for transfection of siRNA into primary rat neurons.* RNA, 2006. **12**(7): p. 1431-8.
186. Shepherd, V.L., et al., *L-Fucose-terminated glycoconjugates are recognized by pinocytosis receptors on macrophages.* Proc Natl Acad Sci U S A, 1981. **78**(2): p. 1019-22.
187. Stahl, P.D., et al., *Evidence for receptor-mediated binding of glycoproteins, glycoconjugates, and lysosomal glycosidases by alveolar macrophages.* Proc Natl Acad Sci U S A, 1978. **75**(3): p. 1399-403.
188. Chieppa, M., et al., *Cross-linking of the mannose receptor on monocyte-derived dendritic cells activates an anti-inflammatory immunosuppressive program.* J Immunol, 2003. **171**(9): p. 4552-60.
189. Xu, X., et al., *Involvement of mannose receptor in the preventive effects of mannose in lipopolysaccharide-induced acute lung injury.* Eur J Pharmacol, 2010. **641**(2-3): p. 229-37.
190. Chono, S., et al., *Effect of surface-mannose modification on aerosolized liposomal delivery to alveolar macrophages.* Drug Dev Ind Pharm, 2009.
191. Takagi, H., et al., *Cooperation of specific ICAM-3 grabbing nonintegrin-related 1 (SIGNR1) and complement receptor type 3 (CR3) in the uptake of oligomannose-coated liposomes by macrophages.* Glycobiology, 2009. **19**(3): p. 258-66.
192. Un, K., et al., *Enhanced transfection efficiency into macrophages and dendritic cells by a combination method using mannosylated lipoplexes and bubble liposomes with ultrasound exposure.* Hum Gene Ther, 2010. **21**(1): p. 65-74.
193. Kawakami, S., et al., *Mannose receptor-mediated gene transfer into macrophages using novel mannosylated cationic liposomes.* Gene Ther, 2000. **7**(4): p. 292-9.
194. Nakamura, K., et al., *Enhanced gene transfection in macrophages by histidine-conjugated mannosylated cationic liposomes.* Biol Pharm Bull, 2009. **32**(9): p. 1628-31.
195. Kuramoto, Y., et al., *Use of mannosylated cationic liposomes/ immunostimulatory CpG DNA complex for effective inhibition of peritoneal dissemination in mice.* J Gene Med, 2008. **10**(4): p. 392-9.
196. Tsuchiya, S., et al., *Induction of maturation in cultured human monocytic leukemia cells by a phorbol diester.* Cancer Res, 1982. **42**(4): p. 1530-6.
197. Cryan, S.A., et al., *Increased intracellular targeting to airway cells using octaarginine-coated liposomes: in vitro assessment of their suitability for inhalation.* Mol Pharm, 2006. **3**(2): p. 104-12.
198. Lawlor, C., et al., *The application of high-content analysis in the study of targeted particulate delivery systems for intracellular drug delivery to alveolar macrophages.* Mol Pharm, 2011. **8**(4): p. 1100-12.
199. Filion, M.C. and N.C. Phillips, *Toxicity and immunomodulatory activity of liposomal vectors formulated with cationic lipids toward immune effector cells.* Biochim Biophys Acta, 1997. **1329**(2): p. 345-56.
200. Filion, M.C. and N.C. Phillips, *Major limitations in the use of cationic liposomes for DNA delivery.* International Journal of Pharmaceutics, 1998. **162**(1-2): p. 159-170.
201. Tak, P.P. and G.S. Firestein, *NF-kappaB: a key role in inflammatory diseases.* J Clin Invest, 2001. **107**(1): p. 7-11.
202. Kidd, P., *Th1/Th2 balance: the hypothesis, its limitations, and implications for health and disease.* Altern Med Rev, 2003. **8**(3): p. 223-46.
203. Hibbitts, A., et al., *Screening of siRNA nanoparticles for delivery to airway epithelial cells using high-content analysis.* Therapeutic Delivery, 2011. **2**(8): p. 987-999.
204. Khoury, M., et al., *Efficient new cationic liposome formulation for systemic delivery of small interfering RNA silencing tumor necrosis factor alpha in experimental arthritis.* Arthritis Rheum, 2006. **54**(6): p. 1867-77.
205. Ai, J., et al., *Nanotoxicology and nanoparticle safety in biomedical designs.* Int J Nanomedicine, 2011. **6**: p. 1117-27.
206. Mayhew, E., M. Ito, and R. Lazo, *Toxicity of non-drug-containing liposomes for cultured human cells.* Exp Cell Res, 1987. **171**(1): p. 195-202.
207. Ravi Kumar, M., et al., *Nanoparticle-mediated gene delivery: state of the art.* Expert Opin Biol Ther, 2004. **4**(8): p. 1213-24.

208. Jain, R.A., *The manufacturing techniques of various drug loaded biodegradable poly(lactide-co-glycolide) (PLGA) devices.* Biomaterials, 2000. **21**(23): p. 2475-90.
209. Mundargi, R.C., et al., *Nano/micro technologies for delivering macromolecular therapeutics using poly(D,L-lactide-co-glycolide) and its derivatives.* J Control Release, 2008. **125**(3): p. 193-209.
210. Sivadas, N., et al., *A comparative study of a range of polymeric microspheres as potential carriers for the inhalation of proteins.* Int J Pharm, 2008. **358**(1-2): p. 159-67.
211. Rytting, E., et al., *Biodegradable polymeric nanocarriers for pulmonary drug delivery.* Expert Opin Drug Deliv, 2008. **5**(6): p. 629-39.
212. Cieslik, M., et al., *The evaluation of the possibilities of using PLGA co-polymer and its composites with carbon fibers or hydroxyapatite in the bone tissue regeneration process - in vitro and in vivo examinations.* Int J Mol Sci, 2009. **10**(7): p. 3224-34.
213. Allison, S.D., *Analysis of initial burst in PLGA microparticles.* Expert Opin Drug Deliv, 2008. **5**(6): p. 615-28.
214. Basarkar, A., et al., *Preparation, characterization, cytotoxicity and transfection efficiency of poly(DL-lactide-co-glycolide) and poly(DL-lactic acid) cationic nanoparticles for controlled delivery of plasmid DNA.* Int J Pharm, 2007. **343**(1-2): p. 247-54.
215. Abbas, A.O., M.D. Donovan, and A.K. Salem, *Formulating poly(lactide-co-glycolide) particles for plasmid DNA delivery.* J Pharm Sci, 2008. **97**(7): p. 2448-61.
216. Zambaux, M.F., et al., *Influence of experimental parameters on the characteristics of poly(lactic acid) nanoparticles prepared by a double emulsion method.* J Control Release, 1998. **50**(1-3): p. 31-40.
217. Sahoo, S.K., et al., *Residual polyvinyl alcohol associated with poly (D,L-lactide-co-glycolide) nanoparticles affects their physical properties and cellular uptake.* J Control Release, 2002. **82**(1): p. 105-14.
218. Alshamsan, A., et al., *STAT3 Silencing in Dendritic Cells by siRNA Polyplexes Encapsulated in PLGA Nanoparticles for the Modulation of Anticancer Immune Response.* Mol Pharm, 2010.
219. Jensen, D.K., et al., *Design of an inhalable dry powder formulation of DOTAP-modified PLGA nanoparticles loaded with siRNA.* J Control Release, 2011.
220. Lee, S.H., et al., *Self-assembled siRNA-PLGA conjugate micelles for gene silencing.* J Control Release, 2011. **152**(1): p. 152-8.
221. Jensen, D.M., et al., *Spray drying of siRNA-containing PLGA nanoparticles intended for inhalation.* J Control Release, 2010. **142**(1): p. 138-45.
222. Cun, D., et al., *High loading efficiency and sustained release of siRNA encapsulated in PLGA nanoparticles: quality by design optimization and characterization.* Eur J Pharm Biopharm, 2010. **77**(1): p. 26-35.
223. Wilson, D.S., et al., *Orally delivered thioketal nanoparticles loaded with TNF-alpha-siRNA target inflammation and inhibit gene expression in the intestines.* Nat Mater, 2010. **9**(11): p. 923-8.
224. Tahara, K., et al., *Chitosan-modified poly(D,L-lactide-co-glycolide) nanospheres for improving siRNA delivery and gene-silencing effects.* Eur J Pharm Biopharm, 2010. **74**(3): p. 421-6.
225. Murata, N., et al., *Anti-tumor effects of anti-VEGF siRNA encapsulated with PLGA microspheres in mice.* J Control Release, 2008. **126**(3): p. 246-54.
226. Khan, A., et al., *Sustained polymeric delivery of gene silencing antisense ODNs, siRNA, DNAzymes and ribozymes: in vitro and in vivo studies.* J Drug Target, 2004. **12**(6): p. 393-404.
227. Young, S., et al., *Gelatin as a delivery vehicle for the controlled release of bioactive molecules.* J Control Release, 2005. **109**(1-3): p. 256-74.
228. Wu, S.Y., et al., *Development of a novel method for formulating stable siRNA-loaded lipid particles for in vivo use.* Pharm Res, 2009. **26**(3): p. 512-22.
229. Lee, S., et al., *Solid polymeric microparticles enhance the delivery of siRNA to macrophages in vivo.* Nucleic Acids Res, 2009. **37**(22): p. e145.
230. Kissel, T., *Microencapsulation: Methods and industrial applications.* 2 ed. 2005: Informa Healthcare.
231. Sioud, M., *Induction of inflammatory cytokines and interferon responses by double-stranded and single-stranded siRNAs is sequence-dependent and requires endosomal localization.* J Mol Biol, 2005. **348**(5): p. 1079-90.
232. Sioud, M., *RNA interference and innate immunity.* Adv Drug Deliv Rev, 2007. **59**(2-3): p. 153-63.

233. Morjaria, J.B., M. Malerba, and R. Polosa, *Biologic and pharmacologic therapies in clinical development for the inflammatory response in COPD.* Drug Discov Today. **15**(9-10): p. 396-405.
234. Yu, J.-Y., S.L. DeRuiter, and D.L. Turner, *RNA interference by expression of short-interfering RNAs and hairpin RNAs in mammalian cells.* Proceedings of the National Academy of Sciences, 2002. **99**(9): p. 6047-6052.
235. McIntyre, G.J. and G.C. Fanning, *Design and cloning strategies for constructing shRNA expression vectors.* BMC Biotechnol, 2006. **6**: p. 1.
236. Wang, S.L., H.H. Yao, and Z.H. Qin, *Strategies for short hairpin RNA delivery in cancer gene therapy.* Expert Opin Biol Ther, 2009. **9**(11): p. 1357-68.
237. Yi, R., et al., *Exportin-5 mediates the nuclear export of pre-microRNAs and short hairpin RNAs.* Genes & Development, 2003. **17**(24): p. 3011-3016.
238. Rao, D.D., et al., *siRNA vs. shRNA: similarities and differences.* Adv Drug Deliv Rev, 2009. **61**(9): p. 746-59.
239. Cullen, B.R., *RNAi the natural way.* Nat Genet, 2005. **37**(11): p. 1163-5.
240. McAnuff, M.A., G.R. Rettig, and K.G. Rice, *Potency of siRNA versus shRNA mediated knockdown in vivo.* J Pharm Sci, 2007. **96**(11): p. 2922-30.
241. Siolas, D., et al., *Synthetic shRNAs as potent RNAi triggers.* Nat Biotechnol, 2005. **23**(2): p. 227-31.
242. Chung, K.H., et al., *Polycistronic RNA polymerase II expression vectors for RNA interference based on BIC/miR-155.* Nucleic Acids Res, 2006. **34**(7): p. e53.
243. Sano, M., et al., *Expression of long anti-HIV-1 hairpin RNAs for the generation of multiple siRNAs: advantages and limitations.* Mol Ther, 2008. **16**(1): p. 170-7.
244. Lechardeur, D. and G.L. Lukacs, *Nucleocytoplasmic transport of plasmid DNA: a perilous journey from the cytoplasm to the nucleus.* Hum Gene Ther, 2006. **17**(9): p. 882-9.
245. Rossi, J.J., *Expression strategies for short hairpin RNA interference triggers.* Hum Gene Ther, 2008. **19**(4): p. 313-7.
246. Robbins, M.A., et al., *Stable expression of shRNAs in human CD34+ progenitor cells can avoid induction of interferon responses to siRNAs in vitro.* Nat Biotechnol, 2006. **24**(5): p. 566-71.
247. Grimm, D., et al., *Fatality in mice due to oversaturation of cellular microRNA/short hairpin RNA pathways.* Nature, 2006. **441**(7092): p. 537-41.
248. Aigner, A., *Transkingdom RNA interference (tkRNAi) as a new delivery tool for therapeutic RNA.* Expert Opin Biol Ther, 2009. **9**(12): p. 1533-42.
249. Zhang, C., et al., *Inhibitory efficacy of hypoxia-inducible factor 1[alpha] short hairpin RNA plasmid DNA-loaded poly (D, L-lactide-co-glycolide) nanoparticles on choroidal neovascularization in a laser-induced rat model.* Gene Ther, 2010. **17**(3): p. 338-351.
250. Schaffer, D.V., J.T. Koerber, and K.I. Lim, *Molecular engineering of viral gene delivery vehicles.* Annu Rev Biomed Eng, 2008. **10**: p. 169-94.
251. De Silva, D., M.D. Mitchell, and J.A. Keelan, *Inhibition of choriodecidual cytokine production and inflammatory gene expression by selective I-kappaB kinase (IKK) inhibitors.* Br J Pharmacol, 2010. **160**(7): p. 1808-22.
252. Riviere, C., O. Danos, and A.M. Douar, *Long-term expression and repeated administration of AAV type 1, 2 and 5 vectors in skeletal muscle of immunocompetent adult mice.* Gene Ther, 2006. **13**(17): p. 1300-8.
253. Morris, K.V. and J.J. Rossi, *Lentiviral-mediated delivery of siRNAs for antiviral therapy.* Gene Ther, 2006. **13**(6): p. 553-8.
254. Itaka, K. and K. Kataoka, *Recent development of nonviral gene delivery systems with virus-like structures and mechanisms.* Eur J Pharm Biopharm, 2009. **71**(3): p. 475-83.
255. Abbas, A.O., M.D. Donovan, and A.K. Salem, *Formulating poly(lactide-co-glycolide) particles for plasmid DNA delivery.* Journal of Pharmaceutical Sciences, 2008. **97**(7): p. 2448-2461.
256. Hassani, Z., et al., *A hybrid CMV-H1 construct improves efficiency of PEI-delivered shRNA in the mouse brain.* Nucleic Acids Res, 2007. **35**(9): p. e65.
257. Misra, S., et al., *Delivery of CD44 shRNA/nanoparticles within cancer cells: perturbation of hyaluronan/CD44v6 interactions and reduction in adenoma growth in Apc Min/+ MICE.* J Biol Chem, 2009. **284**(18): p. 12432-46.
258. Liu, Y., et al., *Targeting hypoxia-inducible factor-1alpha with Tf-PEI-shRNA complex via transferrin receptor-mediated endocytosis inhibits melanoma growth.* Mol Ther, 2009. **17**(2): p. 269-77.

259. Wang, S.L., et al., *Selection of optimal sites for TGFB1 gene silencing by chitosan-TPP nanoparticle-mediated delivery of shRNA.* Cancer Genet Cytogenet, 2009. **190**(1): p. 8-14.
260. Lu, J.M., et al., *Current advances in research and clinical applications of PLGA-based nanotechnology.* Expert Rev Mol Diagn, 2009. **9**(4): p. 325-41.
261. Jilek, S., H.P. Merkle, and E: Walter, *DNA-loaded biodegradable microparticles as vaccine delivery systems and their interaction with dendritic cells.* Adv Drug Deliv Rev, 2005. **57**(3): p. 377-90.
262. Sun, C., et al., *Efficient inhibition of ovarian cancer by short hairpin RNA targeting claudin-3.* Oncol Rep, 2011. **26**(1): p. 193-200.
263. Cohen, H., et al., *Sustained delivery and expression of DNA encapsulated in polymeric nanoparticles.* Gene Ther, 2000. **7**(22): p. 1896-905.
264. Perry, A.K., et al., *The host type I interferon response to viral and bacterial infections.* Cell Res, 2005. **15**(6): p. 407-22.
265. Ostuni, R., I. Zanoni, and F. Granucci, *Deciphering the complexity of Toll-like receptor signaling.* Cellular and Molecular Life Sciences, 2010. **67**(24): p. 4109-4134.
266. Duvallet, E., et al., *Interleukin-23: A key cytokine in inflammatory diseases.* Annals of Medicine, 2011. **0**(0): p. 1-9.
267. Meroni, G. and G. Diez-Roux, *TRIM/RBCC, a novel class of 'single protein RING finger' E3 ubiquitin ligases.* BioEssays, 2005. **27**(11): p. 1147-1157.
268. Baek Sorensen, R., et al., *Melanoma inhibitor of apoptosis protein (ML-IAP) specific cytotoxic T lymphocytes cross-react with an epitope from the auto-antigen SS56.* J Invest Dermatol, 2009. **129**(8): p. 1992-9.
269. Billaut-Mulot, O., et al., *SS-56, a novel cellular target of autoantibody responses in Sjogren syndrome and systemic lupus erythematosus.* J Clin Invest, 2001. **108**(6): p. 861-9.
270. Miyajima, N., et al., *TRIM68 regulates ligand-dependent transcription of androgen receptor in prostate cancer cells.* Cancer Res, 2008. **68**(9): p. 3486-94.
271. Wither, J., et al., *Reduced proportions of natural killer T cells are present in the relatives of lupus patients and are associated with autoimmunity.* Arthritis Research & Therapy, 2008. **10**(5): p. R108.
272. Hervier, B., et al., *Phenotype and function of natural killer cells in systemic lupus erythematosus: Excess interferon-γ production in patients with active disease.* Arthritis & Rheumatism, 2011. **63**(6): p. 1698-1706.
273. Zhang, L., et al., *Lentiviral vector-mediated siRNA knockdown of SR-PSOX inhibits foam cell formation in vitro.* Acta Pharmacol Sin, 2008. **29**(7): p. 847-52.
274. Schnoor, M., et al., *Efficient non-viral transfection of THP-1 cells.* J Immunol Methods, 2009. **344**(2): p. 109-15.
275. Walter, E., et al., *Microencapsulation of DNA using poly(DL-lactide-co-glycolide): stability issues and release characteristics.* J Control Release, 1999. **61**(3): p. 361-74.
276. Shedlock, D.J. and D.B. Weiner, *DNA vaccination: antigen presentation and the induction of immunity.* J Leukoc Biol, 2000. **68**(6): p. 793-806.
277. Benita, S., *Microencapsulation : methods and industrial applications.* 2nd ed. ed. 2006, New York ; London: Taylor & Francis. xviii, 756 p.
278. Dillon, P., et al. *Bioengineered Microparticles For Tuberculosis (Mtb) Treatment Via Inhalation:Aerosol Performance And Efficacy In An In Vitro Model Of Mtb.* in *18th Congress of International Society for Aerosols in Medicine.* 2011. Rotterdam.
279. Watson, P., A.T. Jones, and D.J. Stephens, *Intracellular trafficking pathways and drug delivery: fluorescence imaging of living and fixed cells.* Advanced Drug Delivery Reviews, 2005. **57**(1): p. 43-61.
280. Kaiser, P.K., et al., *RNAi-based treatment for neovascular age-related macular degeneration by Sirna-027.* Am J Ophthalmol, 2010. **150**(1): p. 33-39 e2.
281. Roy, I. and N. Vij, *Nano-delivery in Airway Diseases: Challenges and Therapeutic Applications.* Nanomedicine, 2009.
282. Bitko, V., et al., *Inhibition of respiratory viruses by nasally administered siRNA.* Nat Med, 2005. **11**(1): p. 50-5.
283. Lam, J.K.-W., W. Liang, and H.-K. Chan, *Pulmonary delivery of therapeutic siRNA.* Advanced Drug Delivery Reviews, 2011. **In Press, Corrected Proof**.
284. Bivas-Benita, M., et al., *Non-invasive pulmonary aerosol delivery in mice by the endotracheal route.* European Journal of Pharmaceutics and Biopharmaceutics, 2005. **61**(3): p. 214-218.

285. Moschos, S.A., et al., *Lung Delivery Studies Using siRNA Conjugated to TAT(48-60) and Penetratin Reveal Peptide Induced Reduction in Gene Expression and Induction of Innate Immunity.* Bioconjugate Chemistry, 2007. **18**(5): p. 1450-1459.
286. Lomas-Neira, J.L., et al., *In vivo gene silencing (with siRNA) of pulmonary expression of MIP-2 versus KC results in divergent effects on hemorrhage-induced, neutrophil-mediated septic acute lung injury.* Journal of Leukocyte Biology, 2005. **77**(6): p. 846-853.
287. Heine, H., E. Rietschel, and A. Ulmer, *The biology of endotoxin.* Molecular Biotechnology, 2001. **19**(3): p. 279-296.
288. Wang, H.M., M. Bodenstein, and K. Markstaller, *Overview of the pathology of three widely used animal models of acute lung injury.* Eur Surg Res, 2008. **40**(4): p. 305-16.
289. Matute-Bello, G., C.W. Frevert, and T.R. Martin, *Animal models of acute lung injury.* American Journal of Physiology - Lung Cellular and Molecular Physiology, 2008. **295**(3): p. L379-L399.
290. Knapp, S., *LPS and bacterial lung inflammation models.* Drug Discovery Today: Disease Models, 2009. **6**(4): p. 113-118.
291. Lefort, J., L. Motreff, and B.B. Vargaftig, *Airway administration of Escherichia coli endotoxin to mice induces glucocorticosteroid-resistant bronchoconstriction and vasopermeation.* Am J Respir Cell Mol Biol, 2001. **24**(3): p. 345-51.
292. Schnyder-Candrian, S., et al., *Dual effects of p38 MAPK on TNF-dependent bronchoconstriction and TNF-independent neutrophil recruitment in lipopolysaccharide-induced acute respiratory distress syndrome.* J Immunol, 2005. **175**(1): p. 262-9.
293. Jeyaseelan, S., et al., *Transcriptional Profiling of Lipopolysaccharide-Induced Acute Lung Injury.* Infect. Immun., 2004. **72**(12): p. 7247-7256.
294. Grommes, J. and O. Soehnlein, *Contribution of neutrophils to acute lung injury.* Mol Med, 2011. **17**(3-4): p. 293-307.
295. Chaudhuri, N. and I. Sabroe, *Basic science of the innate immune system and the lung.* Paediatr Respir Rev, 2008. **9**(4): p. 236-42.
296. Singodia, D., et al., *Investigations into an alternate approach to target mannose receptors on macrophages using 4-sulfated N-acetyl galactosamine more efficiently in comparison with mannose-decorated liposomes: An application in drug delivery.* Nanomedicine: Nanotechnology, Biology and Medicine, 2011. **In Press, Uncorrected Proof**.
297. Dinh, T., et al., *Evaluation of Osteoclastogenesis via NFκB Decoy/mannosylated Cationic Liposome-Mediated Inhibition of Pro-inflammatory Cytokine Production from Primary Cultured Macrophages.* Pharmaceutical Research, 2011. **28**(4): p. 742-751.
298. Wijagkanalan, W., et al., *Intratracheally instilled mannosylated cationic liposome/NF[kappa]B decoy complexes for effective prevention of LPS-induced lung inflammation.* Journal of Controlled Release, 2011. **149**(1): p. 42-50.
299. Zhao, Y. and H. Yan, *Preparation of Mannosylated Oligoribonucleotides.* Nucleic Acids Symposium Series, 2008. **52**(1): p. 89-90.
300. Kim, N., et al., *Synthesis and characterization of mannosylated pegylated polyethylenimine as a carrier for siRNA.* International Journal of Pharmaceutics, 2011. **In Press, Uncorrected Proof**.
301. Florea, B., et al., *Transfection Efficiency and Toxicity of Polyethylenimine in Differentiated Calu-3 and Nondifferentiated COS-1 Cell Cultures.* AAPS PharmSci, 2002. 4(2): p. article 12.
302. Beyerle, A., et al., *Toxicity Pathway Focused Gene Expression Profiling of PEI-Based Polymers for Pulmonary Applications.* Molecular Pharmaceutics, 2010. **7**(3): p. 727-737.
303. Horrow, J.C., *Protamine.* Anesthesia & Analgesia, 1985. **64**(3): p. 348-361.
304. Vighi, E., et al., *Nuclear localization of cationic solid lipid nanoparticles containing Protamine as transfection promoter.* European Journal of Pharmaceutics and Biopharmaceutics, 2010. **76**(3): p. 384-393.
305. Engel, A., et al., *Influence of Spacer Length on Interaction of Mannosylated Liposomes with Human Phagocytic Cells.* Pharmaceutical Research, 2003. **20**(1): p. 51-57.
306. Noorman, F., et al., *Monoclonal antibodies against the human mannose receptor as a specific marker in flow cytometry and immunohistochemistry for macrophages.* Journal of Leukocyte Biology, 1997. **61**(1): p. 63-72.
307. Lane, K., et al., *Characterization of a rat alveolar macrophage cell line that expresses a functional mannose receptor.* Journal of Leukocyte Biology, 1998. **64**(3): p. 345-350.
308. Kraus, B., et al., *Hyperforin is a modulator of inducible nitric oxide synthase and phagocytosis in microglia and macrophages.* Naunyn-Schmiedeberg's Archives of Pharmacology, 2010. **381**(6): p. 541-553.

309. Boussif, O., et al., *A versatile vector for gene and oligonucleotide transfer into cells in culture and in vivo: polyethylenimine.* Proceedings of the National Academy of Sciences, 1995. **92**(16): p. 7297-7301.
310. Sioud, M., *RNA interference and innate immunity.* Advanced Drug Delivery Reviews, 2007. **59**(2-3): p. 153-163.
311. Sioud, M., *Induction of Inflammatory Cytokines and Interferon Responses by Double-stranded and Single-stranded siRNAs is Sequence-dependent and Requires Endosomal Localization.* Journal of Molecular Biology, 2005. **348**(5): p. 1079-1090.
312. Akhtar, S. and I. Benter, *Toxicogenomics of non-viral drug delivery systems for RNAi: potential impact on siRNA-mediated gene silencing activity and specificity.* Adv Drug Deliv Rev, 2007. **59**(2-3): p. 164-82.
313. Champion, J.A., A. Walker, and S. Mitragotri, *Role of particle size in phagocytosis of polymeric microspheres.* Pharm Res, 2008. **25**(8): p. 1815-21.
314. Fu, J., et al., *New polymeric carriers for controlled drug delivery following inhalation or injection.* Biomaterials, 2002. **23**(22): p. 4425-33.
315. Gaspar, M.M., O. Gobbo, and C. Ehrhardt, *Generation of liposome aerosols with the Aeroneb Pro and the AeroProbe nebulizers.* J Liposome Res, 2010. **20**(1): p. 55-61.
316. Kleemann, E., et al., *Iloprost-containing liposomes for aerosol application in pulmonary arterial hypertension: formulation aspects and stability.* Pharm Res, 2007. **24**(2): p. 277-87.
317. Anabousi, S., et al., *Effect of PEGylation on the stability of liposomes during nebulisation and in lung surfactant.* J Nanosci Nanotechnol, 2006. **6**(9-10): p. 3010-6.
318. Kohro, T., et al., *A comparison of differences in the gene expression profiles of phorbol 12-myristate 13-acetate differentiated THP-1 cells and human monocyte-derived macrophage.* J Atheroscler Thromb, 2004. **11**(2): p. 88-97.
319. Liao, H.S., et al., *De novo expression of the class-A macrophage scavenger receptor conferring resistance to apoptosis in differentiated human THP-1 monocytic cells.* Cell Death Differ, 1999. **6**(3): p. 245-55.
320. Kirpotin, D., et al., *Sterically stabilized anti-HER2 immunoliposomes: design and targeting to human breast cancer cells in vitro.* Biochemistry, 1997. **36**(1): p. 66-75.
321. Sasaki, A., et al., *Syntheses of novel galactosyl ligands for liposomes and the influence of the spacer on accumulation in the rat liver.* Biol Pharm Bull, 1995. **18**(5): p. 740-6.
322. Howard, K.A., et al., *Chitosan/siRNA nanoparticle-mediated TNF-alpha knockdown in peritoneal macrophages for anti-inflammatory treatment in a murine arthritis model.* Mol Ther, 2009. **17**(1): p. 162-8.
323. Arisaka, M., et al., *Involvement of lipid rafts in macrophage apoptosis induced by cationic liposomes.* Arch Biochem Biophys, 2011. **508**(1): p. 72-7.
324. Kurosaka, K., N. Watanabe, and Y. Kobayashi, *Production of proinflammatory cytokines by phorbol myristate acetate-treated THP-1 cells and monocyte-derived macrophages after phagocytosis of apoptotic CTLL-2 cells.* J Immunol, 1998. **161**(11): p. 6245-9.
325. Brightling, C.E., S. Saha, and F. Hollins, *Interleukin-13: prospects for new treatments.* Clin Exp Allergy, 2010. **40**(1): p. 42-9.
326. Chen, C., et al., *An overview of liposome lyophilization and its future potential.* J Control Release, 2010. **142**(3): p. 299-311.
327. Jorgensen, C. and F. Apparailly, *Prospects for gene therapy in inflammatory arthritis.* Best Pract Res Clin Rheumatol, 2010. **24**(4): p. 541-52.
328. Niese, K.A., et al., *The cationic amino acid transporter 2 is induced in inflammatory lung models and regulates lung fibrosis.* Respir Res, 2010. **11**: p. 87.